

***Research reactor  
core conversion guidebook***

***Volume 3: Analytical verification  
(Appendices G and H)***



INTERNATIONAL ATOMIC ENERGY AGENCY

IAEA

**RESEARCH REACTOR CORE CONVERSION GUIDEBOOK  
VOLUME 3: ANALYTICAL VERIFICATION (APPENDICES G AND H)  
IAEA, VIENNA, 1992  
IAEA-TECDOC-643  
ISSN 1011-4289**

Printed by the IAEA in Austria  
April 1992

## FOREWORD

In view of the proliferation concerns caused by the use of highly enriched uranium (HEU) and in anticipation that the supply of HEU to research and test reactors will be more restricted in the future, this guidebook has been prepared to assist research reactor operators in addressing the safety and licensing issues for conversion of their reactor cores from the use of HEU fuel to the use of low enriched uranium (LEU) fuel.

Two previous guidebooks on research reactor core conversion have been published by the IAEA. The first guidebook (IAEA-TECDOC-233) addressed feasibility studies and fuel development potential for light-water-moderated research reactors and the second guidebook (IAEA-TECDOC-324) addressed these topics for heavy-water-moderated research reactors. This guidebook, in five volumes, addresses the effects of changes in the safety-related parameters of mixed cores and the converted core. It provides an information base which should enable the appropriate approvals processes for implementation of a specific conversion proposal, whether for a light or for a heavy water moderated research reactor, to be greatly facilitated.

This guidebook has been prepared and coordinated by the International Atomic Energy Agency, with contributions volunteered by different organizations. The IAEA is grateful for these contributions and thanks the experts from the various organizations for preparing the detailed investigations and for evaluating and summarizing the results.

## **EDITORIAL NOTE**

*In preparing this material for the press, staff of the International Atomic Energy Agency have mounted and paginated the original manuscripts as submitted by the authors and given some attention to the presentation.*

*The views expressed in the papers, the statements made and the general style adopted are the responsibility of the named authors. The views do not necessarily reflect those of the governments of the Member States or organizations under whose auspices the manuscripts were produced.*

*The use in this book of particular designations of countries or territories does not imply any judgement by the publisher, the IAEA, as to the legal status of such countries or territories, of their authorities and institutions or of the delimitation of their boundaries.*

*The mention of specific companies or of their products or brand names does not imply any endorsement or recommendation on the part of the IAEA.*

*Authors are themselves responsible for obtaining the necessary permission to reproduce copyright material from other sources.*

*This text was compiled before the unification of Germany in October 1990. Therefore the names German Democratic Republic and Federal Republic of Germany have been retained.*

**PLEASE BE AWARE THAT  
ALL OF THE MISSING PAGES IN THIS DOCUMENT  
WERE ORIGINALLY BLANK**

## PREFACE

Volume 3 consists of Appendix G which contains detailed results of a safety-related benchmark problem for an idealized reactor and Appendix H which contains detailed comparisons of calculated and measured data for actual cores with MEU and LEU fuels. The results of the benchmark calculations in Appendix G are summarized in Chapter 7 of Volume 1 (SUMMARY) and the results of the comparisons between calculations and measurements are summarized in Chapter 8 of Volume 1.

Both of the approaches described in these appendices are very useful in ensuring that the calculational methods employed in the preparation of a Safety Report are accurate. As a first step, it is recommended that reactor operators/physicists use their own methods and codes to first calculate the benchmark problem, and then compare the results of calculations with measurements in their own reactor or in one of the reactors for which measured data is available in Appendix H.

<u>Topic</u>	<u>VOLUME 3 APPENDIX</u>	<u>VOLUME 1 SUMMARY Chapter</u>
Benchmark Calculations	G	7
Comparison of Calculations with Measurements	H	8

## CONTRIBUTING ORGANIZATIONS

Argonne National Laboratory	ANL	United States of America
Australian Atomic Energy Commission	AAEC	Australia
Comisión Chilena de Energía Nuclear	CChEN	Chile
Comisión Nacional de Energía Atómica	CNEA	Argentina
Commissariat à l'Énergie Atomique	CEA	France
Eidg. Institut für Reaktorforschung	EIR	Switzerland
Internationale Atomreaktorbau GmbH	INTERATOM	Federal Republic of Germany
Japan Atomic Energy Research Institute	JAERI	Japan
Junta de Energía Nuclear	JEN	Spain
Kyoto University Research Reactor Institute	KURRI	Japan
Oak Ridge National Laboratory	ORNL	United States of America
Risø National Laboratory	RISØ	Denmark
University of Michigan - Ford Nuclear Reactor	FNR	United States of America

The IAEA is grateful for the contributions volunteered by these organizations and thanks their experts for preparing the detailed investigations and for evaluating and summarizing the results presented in this Guidebook.

## CONTENTS

### APPENDIX G. BENCHMARK CALCULATIONS

G-0. Specifications for the safety-related benchmark problem .....	11
G-1. ANL: Safety-related benchmark calculations for MTR-type reactors with HEU, MEU and LEU fuels .....	15
<i>J.E. Matos, E.M. Pennington, K.E. Freese, W.L. Woodruff</i>	
G-2. INTERATOM: Benchmark calculations .....	65
G-3. JAERI: IAEA safety-related benchmark calculations .....	91
<i>Y. Naito, M. Kurosawa, Y. Komuro, R. Oyamada, Y. Nagaoka</i>	
G-4. EIR: Safety-related benchmark calculations for MTR reactors .....	107
<i>H. Amato, H. Winkler, J. Zeis</i>	
G-5. JEN: Calculations for the safety-related benchmark problem .....	125
G-6. AAEC: Self-limiting transients in heavy water moderated reactors .....	149
<i>J.W. Connolly, B.V. Harrington, D.B. McCulloch</i>	

### APPENDIX H. COMPARISON OF CALCULATIONS WITH MEASUREMENTS

H-1. CEA: Critical experiments in the ISIS reactor with the Caramel fuel element .....	159
H-2. Kyoto University Critical Assembly (KUCA) critical experiments using MEU fuel	
H-2.1. KURRI: KUCA critical experiments using medium enriched uranium fuel .....	169
<i>K. Kanda, S. Shiroya, M. Hayashi, K. Kobayashi, Y. Nakagome, T. Shibata</i>	
H-2.2. KURRI/ANL: Analysis of the KUCA MEU experiments using the ANL code system .....	183
<i>S. Shiroya, M. Hayashi, K. Kanda, T. Shibata, W.L. Woodruff, J.E. Matos</i>	
H-2.3. JAERI: Analysis of KUCA MEU cores by the JAERI SRAC code system .....	193
<i>T. Mori, K. Tsuchihashi</i>	
H-2.4. KURRI: Measurements of neutron flux distributions in a medium enriched uranium core .....	201
<i>S. Shiroya, H. Fukui, Y. Senda, M. Hayashi, K. Kobayashi</i>	
H-2.5. KURRI: Effect of reducing fuel enrichment on the void reactivity	
Part I. Experimental study ( <i>Abstract</i> ) .....	211
<i>H. Fukui, K. Mishima, S. Shiroya, M. Hayashi, K. Kanda, Y. Senda</i>	
Part II. Analytical study ( <i>Abstract</i> ) .....	213
<i>Y. Senda, S. Shiroya, M. Hayashi, K. Kanda</i>	
H-2.6. KURRI: Study on temperature coefficients of MEU and HEU cores in the KUCA .....	215
<i>K. Kanda, S. Shiroya, M. Mori, M. Hayashi, T. Shibata</i>	
H-2.7. KURRI: Study on temperature coefficient of reactivity in KUCA light-water moderated and reflected core — Effect of M/F ratio and core shape on this quantity .....	225
<i>K. Kanda, S. Shiroya, M. Mori, T. Shibata</i>	
H-3. JAERI: Critical experiments of the JMTRC MEU cores: Part I .....	237
<i>Y. Nagaoka, K. Takeda, S. Shimakawa, S. Koike, R. Oyamada</i>	
Critical experiments of the JMTRC MEU cores: Part II .....	247
<i>S. Shimakawa, Y. Nagaoka, S. Koike, K. Takeda, B. Komukai, R. Oyamada</i>	

H-4. Comparison of calculations with measurements	
H-4.1. FNR/ANL: Comparison of calculations with measurements in the FNR full-core LEU demonstration reactor .....	255
H-4.2. JAERI: Analysis of critical experiments of FNR LEU cores .....	275
<i>K. Arigane, K. Tsuchihashi</i>	
H-5. Comparison of calculations with measurements in the ORR whole-core LEU demonstration reactor	
H-5.1. ANL: Analytical support for the ORR whole-core LEU U <sub>3</sub> Si <sub>2</sub> -Al fuel demonstration .....	285
<i>M.M. Bretscher</i>	
H-5.2. ANL/ORNL: Comparison of calculated and measured irradiated wire data for HEU and mixed HEU/LEU cores in the ORR .....	297
<i>R.J. Cornella, M.M. Bretscher, R.W. Hobbs</i>	
H-6. ANL/ORNL: Measurements and analysis of critical assemblies for research reactors with mixed enrichments .....	305
<i>J.R. Deen, J.L. Snelgrove, R.W. Hobbs</i>	
H-7. EIR: Comparison of calculations and measurements of MEU fuel in the SAPHIR reactor .....	333
<i>H. Winkler, J. Zeis</i>	
H-8. RISØ: Comparisons between calculated and measured flux and reactivity in HEU, MEU and LEU fuel elements in DR-3 at Risø .....	341
<i>K. Haack</i>	
H-9. CNEA: Part I. Comparison of calculations with measurements of control rod worths in the HEU RA-2 reactor;	
<i>A. Gómez, A. M. Lerner, J. Testoni, R. Waldman</i>	
Part II. Uses of the method of computing control rod worths in the RA-3 reactor with HEU and LEU fuels .....	349
<i>A.M. Lerner, J. Testoni</i>	
H-10. CChEN: Measurements and analysis of critical experiments in the 'La Reina' reactor using medium enrichment uranium fuel .....	361
<i>J. Klein, R. Venegas, O. Mutis</i>	

## **Appendix G**

# **BENCHMARK CALCULATIONS**

### **Abstract**

Safety-related benchmark calculations for an idealized, light-water, pool-type reactor were performed (Appendices G-1 through G-5) to compare the computational methods used by various organizations. The calculations include control rod worths, power peaking factors, kinetics parameters, temperature and void coefficients, and postulated transients initiated by loss-of-flow and reactivity insertions. Appendix G-6 contains analyses of self-limiting transients for heavy water moderated reactors. Only limited conclusions for actual core conversions from HEU to LEU fuel should be drawn from the results in Appendix G.

## Appendix G-0

### SPECIFICATIONS FOR THE SAFETY-RELATED BENCHMARK PROBLEM

#### Abstract

Detailed specifications are described for a safety-related benchmark problem to compare calculational methods used in various research centres. The reactor description is the same one utilized for the benchmark problem solved in IAEA-TECDOC-233, except for a change in the description of the central flux trap. Parameters specified to be calculated include kinetics parameters, reactivity feedback coefficients, power peaking factors, control rod worths, and several transients.

- Reactor Description - 10 MW Reactor used for neutronics benchmark calculations in IAEA - TECDOC-233 (1980).
- Change in Description - Replace water in central flux trap with a 77 mm x 81 mm block of aluminum containing a square hole 50 mm on each side in order to compute more realistic radial and local power peaking factors for the limiting standard fuel element.
- Cores - HEU (93%) and LEU (20%).
- Burnup Status of Cores - BOL, based on equal % burnup.

#### Static Calculations

1. Prompt Neutron Generation Time and Delayed Neutron Fraction
  - a). HEU Core
  - b). LEU Core
2. Isothermal Reactivity Feedback Coefficients
  - a). Change of Water Temperature Only - 38°C, 50°C, 75°C, 100°C
  - b). Change of Water Density Only - 0.993, 0.988, 0.975, 0.958 g/cm<sup>3</sup>
  - c). Change of <sup>238</sup>U Temperature Only - 38°C, 50°C, 75°C, 100°C, 200°C
  - d). Core Void Coefficient - Change Water Density Only - 10%, 20% Void
  - e). Local Void Coefficient - Change Water Density Only - 5%, 10% Void separately in SFE-2, SFE-3, and SFE-4.  
e) is optional.
3. Radial and Local Power Peaking Factors

In HEU BOL Core:

  - a). Replace burned HEU CFE-1 with fresh HEU CFE and fresh LEU CFE.
  - b). Replace burned HEU SFE-1 with fresh HEU SFE and fresh LEU SFE.

In LEU BOL Core:

  - c). Replace burned LEU CFE-1 with fresh LEU CFE.

- d). Replace burned LEU SFE-1 with fresh LEU SFE.
  - e). Note reactivity changes for all cases.
- c) and d) are optional.

SFE = Standard Fuel Element; CFE = Control Fuel Element.  
 BOL cores contain fission products.  
 Fresh SFE and CFE contain no fission products.

#### 4. Control Rod Worths

- a). Reactivity worth of four fully-inserted control rods with Ag/In/Cd absorber in HEU core.
  - b). Repeat a) with B<sub>4</sub>C absorber using natural boron.
  - c). Repeat a) with Hafnium absorber.
  - d). Repeat a), b), and c) for LEU core.
- Cases with B<sub>4</sub>C and Hafnium absorbers are optional.

Control Rod Geometry : Fork-Type with blades fitting into guides described in IAEA - TECDOC-233 benchmark problem.

Length - 600 m  
 Thickness - 3.18 mm; 3.1 mm-thick absorber with a 0.04 mm layer of nickel on each surface of Ag/In/Cd and B<sub>4</sub>C blades.  
 - 3.1 mm-thick absorber for Hf blades (no nickel layer).  
 Width - 66 mm

#### Absorber Materials

- i). Ag/In/Cd  
 80.5 w/o Ag, 14.6 w/o In, 4.9 w/o Cd  
 Density of Ag-In-Cd : 9.32 g/cm<sup>3</sup>  
 Densities of Ag = 7.50 g/cm<sup>3</sup>, In = 1.36 g/cm<sup>3</sup>,  
 Cd = 0.46 g/cm<sup>3</sup>, Ni = 8.90 g/cm<sup>3</sup>.
- ii). Boron Carbide (B<sub>4</sub>C)  
 Density of B<sub>4</sub>C = 2.52 g/cm<sup>3</sup>.
- iii). Hafnium  
 Density of Hf = 13.3 g/cm<sup>3</sup>.

#### Transient Calculations

- Hot Channel Factors: Radial x Local Power Peaking Factor: 1.4  
 Axial Power Peaking Factor: 1.5  
 Engineering Factor: 1.2  
 Overpower Factor: 1.2
- Nominal Flow Rate: 1000 m<sup>3</sup>/hr
- Coolant Inlet Temperature: 38°C
- Coolant Inlet Pressure: 1.7 bar absolute
- Thermal Conductivity of UAl<sub>x</sub>-Al Fuel: 1.58 W/cm K (HEU)  
 0.5 W/cm K (LEU)

W	G	G	G	G	W
W	5Z	25Z	25Z SFE-2	5Z SFE-1	W
5Z	25Z CFE	45Z	45Z SFE-3	25Z CFE-1	5Z SFE-4
25Z	45Z	45Z	H <sub>2</sub> O + A1	45Z	25Z
5Z	25Z CFE	45Z	45Z	25Z CFE	5Z
W	5Z	25Z	25Z	5Z	W
W	G	G	G	G	W

W - Water      G - Graphite      SFE (CFE) - Standard (Control) Fuel Element

BOL Core Showing  $^{235}\text{U}$  Burnup in Each Fuel Element and Fuel Element Identification (see IAEA-TECDOC-233, p.445).

1. Fast Loss-of-Flow Transient

- Flow is reduced as  $e^{-t/T}$ , with  $T = 1$  second.
- Reactor scram initiated at 85% of nominal flow, with a 200 ms delay before linear shutdown reactivity insertion of  $-\$10$  in 1/2 s.

Compute time histories for HEU and LEU cores of reactor power, peak fuel temperature, peak clad temperature, and coolant exit temperature.

2. Slow Loss-of-Flow Transient

- Repeat (1) for HEU and LEU cores with  $T = 25$  seconds.

3. Slow Reactivity Insertion Transient

- Reactor critical at an initial power of 1 Watt
- Ramp reactivity insertion rates: 10  $\$/s$  (HEU)  
9  $\$/s$  (LEU)
- Safety system trip point:  $1.2 P_0 = 12$  MW
- Time delay of 25 ms before linear shutdown reactivity insertion of  $-\$10$  in 1/2 s.
- Hot channel factor: Radial x Local x Axial x Engineering

No overpower factor is included since safety system trip point is set at  $1.2 P_0 = 12$  MW.

Compute time histories for HEU and LEU cores of reactor power, input and net reactivity, peak fuel temperature, peak clad temperature, and coolant exit temperature. Also indicate total energy release beyond 12 MW.

4. Fast Reactivity Insertion Transient

Repeat (3) for HEU and LEU cores with:

- Ramp reactivity insertions: \$1.5 in 1/2 s (HEU)  
\$1.5 in 1/2 s (LEU)  
\$1.35 in 1/2 s (LEU)

Compute time histories for HEU and LEU cores of same variables specified in (3). Also indicate initial inverse period, peak power, time to peak power, and energy release to time of peak power.

## Appendix G-1

### SAFETY-RELATED BENCHMARK CALCULATIONS FOR MTR-TYPE REACTORS WITH HEU, MEU AND LEU FUELS

J.E. MATOS, E.M. PENNINGTON,  
K.E. FREESE, W.L. WOODRUFF  
RERTR Program,  
Argonne National Laboratory,  
Argonne, Illinois,  
United States of America

#### Abstract

Results are provided for the safety-related benchmark problem with HEU, MEU, and LEU fuels. Additional results include reactivity worths and power peaking factors with partially-inserted control rods. Comparisons of calculations and measurements for selected SPERT I transients are given along with results for self-limiting transients in the HEU and LEU benchmark cores.

A safety-related benchmark problem was specified in order to compare calculational methods used in various research centers. Detailed specifications for this problem are shown in the Appendix G-0. The reactor and fuel loading specifications are identical with those of the 10 MW neutronics benchmark problem defined in IAEA-TECDOC-233.<sup>1</sup> The single exception is that the central flux trap filled with water in Ref. 1 has been replaced by a 77 mm x 81 mm block of aluminum containing a square, water-filled hole 50 mm on each side in order to compute more realistic power peaking factors in the surrounding fuel elements. The models used and the results obtained for these calculations are described in the following sections.

#### 1. MODELS

##### 1.1 Cross Sections

Cross sections in ten energy groups (Table 1) for core materials as a function of  $^{235}\text{U}$  burnup were generated using the EPRI-CELL code<sup>2</sup>. Time intervals were adjusted to burn 5% of the initial  $^{235}\text{U}$  in each interval up to 50% burnup. The unit cell (Fig. 1) used in the infinite slab geometry consisted of fuel, clad, and water regions having their actual thicknesses, and an extra region with the appropriate thickness and composition to include the remaining water and aluminum in the same proportions as in the physical fuel element. Calculations were done in the  $B_1$  approximation with a fixed buckling of  $0.007837 \text{ cm}^{-2}$ . In addition, shielding factors generated using an integral transport option in the MC<sup>2</sup>-2 code<sup>3</sup> and the unit cell shown in Fig. 1 were input at the fine group level in the EPRI-CELL calculations in order to obtain a more accurate treatment of the resonance absorption in  $^{238}\text{U}$ . The shielding factors for  $^{238}\text{U}$  are most important in the 20% enriched lattice, followed by those in the 45% enriched lattice.

Ten-group cross sections were also generated for water and for graphite using EPRI-CELL with a fission spectrum source and zero buckling. These cross sections were used in the reflector and flux trap regions of the reactor.

TABLE 1. Energy Boundaries of 10-Group Cross Sections Used for Reactivity Coefficients,  $\beta_{eff}$ ,  $\lambda$ , and  $\Lambda$

Group	$E_U, \text{ev}$	$E_L, \text{ev}$	Group	$E_U, \text{ev}$	$E_L, \text{ev}$
1	$1.0 \times 10^7$	$6.393 \times 10^5$	6	1.166	0.6249
2	$6.393 \times 10^5$	$9.119 \times 10^3$	7	0.6249	0.4170
3	$9.119 \times 10^3$	$5.531 \times 10^3$	8	0.4170	0.1457
4	$5.531 \times 10^3$	1.855	9	0.1457	0.05693
5	1.855	1.166	10	0.0569	$2.53 \times 10^{-4}$

Energy Boundaries of 5-Group Cross Sections Used for Control Rod Worths and Power Peaking Factors

Group	$E_U, \text{ev}$	$E_L, \text{ev}$	Group	$E_U, \text{ev}$	$E_L, \text{ev}$
1	$1.0 \times 10^7$	$8.209 \times 10^5$	4	1.855	0.6249
2	$8.209 \times 10^5$	$5.531 \times 10^3$	5	0.6249	$2.53 \times 10^{-4}$
3	$5.531 \times 10^3$	1.855			

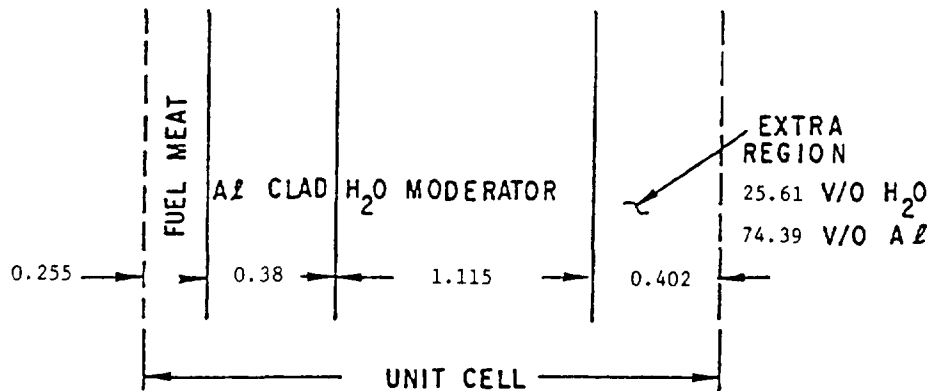
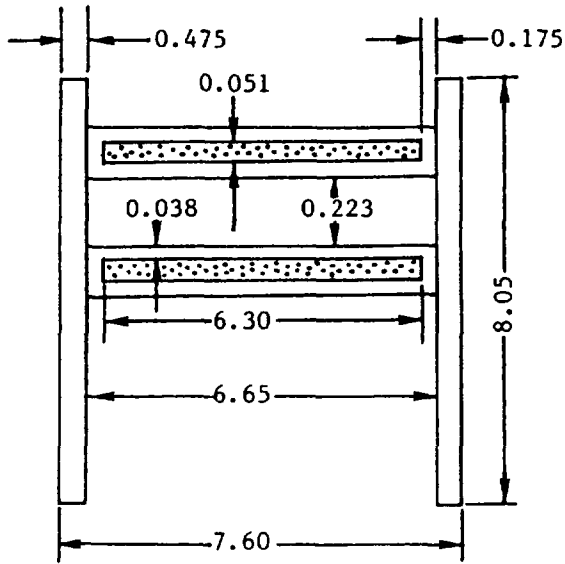


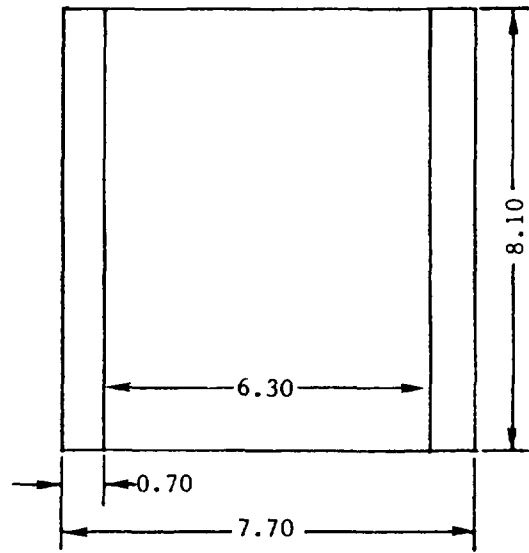
Figure 1. Geometry of Unit Cell Used for Calculation of Core Cross Sections (All Dimensions in mm).

## 1.2 Fuel Elements for Core Calculations

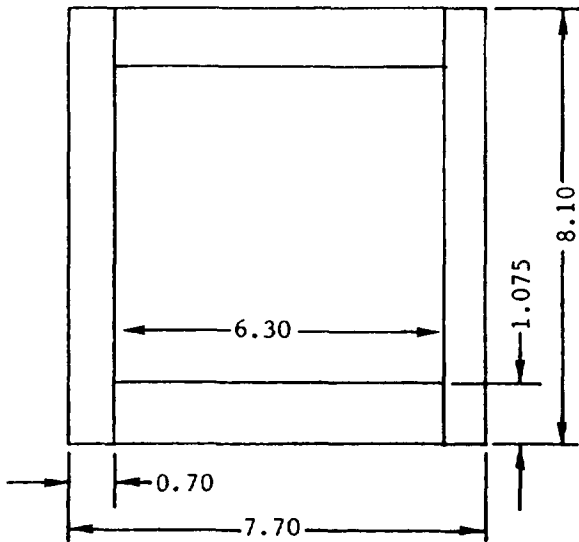
The planar models that were used to represent the standard and control elements in the diffusion theory calculations are shown in Fig. 2. Each standard element was modeled as three separate regions - one region (6.3 cm x 8.1 cm) representing the fueled portion of the element and two regions (each 0.7 cm x 8.1 cm) representing the sideplates and the other non-fueled portions of the element. Each control element without absorber blades was modeled in a similar manner, except that two additional separate regions were included to represent the aluminum guide plates and their associated water channels. Further additional regions were added to model the control elements with the absorber blades inserted.



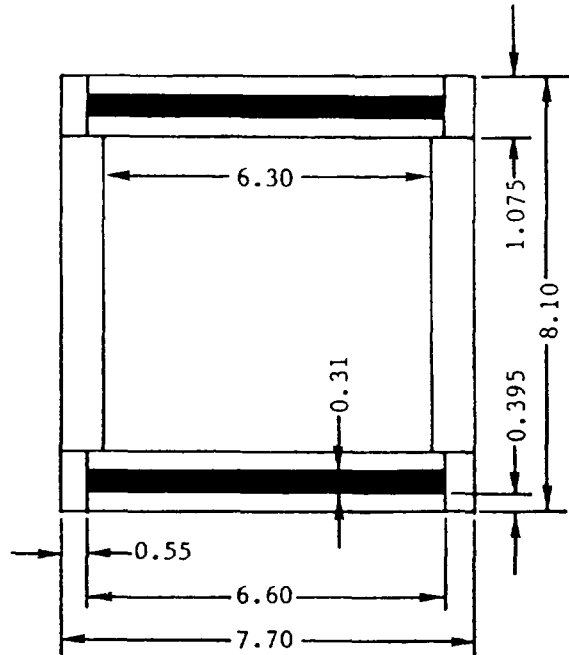
Standard Element: 23 Fuel Plates  
 Control Element : 17 Fuel Plates  
 4 Al Plates



Model for Standard Element



Model for Control Element  
 Without Absorber Blades



Model for Control Element  
 With Absorber Blades

Fig. 2. Models for Standard Element and for Control Element With and Without Absorber Blades. (Dimensions in cm.)

## 2. PROMPT NEUTRON GENERATION TIME AND DELAYED NEUTRON FRACTION

Two-dimensional diffusion-theory problems were run using the 10-group EPRI-CELL cross sections in DIF2D<sup>4</sup> to yield both real and adjoint fluxes, and were followed by diffusion-perturbation-theory calculations of delayed neutron fraction, prompt neutron lifetime ( $\ell$ ), and prompt neutron generation time ( $\Lambda$ ). The velocities used were computed in EPRI-CELL by flux-weighting  $1/v$ , using the fluxes and velocities for the fine groups making up the broad groups. Velocities of the fine groups correspond to the mid-point energies. The delayed neutron data are based on ENDF/B-IV. Table 2 gives the results for  $k_{\text{eff}}$ ,  $\beta_{\text{eff}}$ ,  $\ell$  and  $\Lambda$  for all three <sup>235</sup>U enrichments in the BOL cores. Table 3 presents the corresponding decay constants and delayed neutron fractions by family.

TABLE 2. Delayed-Neutron-Dependent Parameters

<u>Designation</u>	<sup>235</sup> U		<u><math>k_{\text{eff}}</math></u>	<u><math>\beta_{\text{eff}}</math></u>	<u><math>\ell, \mu\text{sec}^a</math></u>	<u><math>\Lambda, \mu\text{sec}^a</math></u>
	Enrichment(%)					
HEU	93		1.02839	0.007607	57.55	55.96
MEU	45		1.02422	0.007456	51.96	50.73
LEU	20		1.01796	0.007275	44.53	43.74

<sup>a</sup>  $\ell = \Lambda k_{\text{eff}}$ , where  $\ell$  is prompt neutron lifetime, and  $\Lambda$  is prompt neutron generation time

TABLE 3. Delayed Neutron Parameters  $\lambda$  and  $\beta$  by Families

<u>Family</u>	<u>HEU</u>		<u>MEU</u>		<u>LEU</u>	
	<u><math>\lambda, \text{sec}^{-1}</math></u>	<u><math>\beta</math></u>	<u><math>\lambda, \text{sec}^{-1}</math></u>	<u><math>\beta</math></u>	<u><math>\lambda, \text{sec}^{-1}</math></u>	<u><math>\beta</math></u>
1	0.0127	$2.9648 \times 10^{-4}$	0.0127	$2.8937 \times 10^{-4}$	0.0127	$2.7926 \times 10^{-4}$
2	0.0317	$1.5822 \times 10^{-3}$	0.0317	$1.5543 \times 10^{-3}$	0.0317	$1.5178 \times 10^{-3}$
3	0.1160	$1.4352 \times 10^{-3}$	0.1163	$1.4077 \times 10^{-3}$	0.1167	$1.3731 \times 10^{-3}$
4	0.3110	$3.1144 \times 10^{-3}$	0.3114	$3.0462 \times 10^{-3}$	0.3121	$2.9627 \times 10^{-3}$
5	1.3999	$9.7969 \times 10^{-4}$	1.3992	$9.6175 \times 10^{-4}$	1.3985	$9.4536 \times 10^{-4}$
6	3.8689	$1.9914 \times 10^{-4}$	3.8602	$1.9705 \times 10^{-4}$	3.8521	$1.9716 \times 10^{-4}$

### 3. ISOTHERMAL REACTIVITY FEEDBACK COEFFICIENTS

#### 3.1 Change of Water Temperature Only

Values of  $k_{eff}$  were computed for water temperatures of 38°C, 50°C, 75°C, and 100°C. The EPRI-CELL library contains the following hydrogen temperatures in the range of interest: 23°C, 77°C, 127°C, and 227°C. Therefore, EPRI-CELL problems were run at the four temperatures of the library for 45%, 25%, and 5% burnup, since these are the burnups in the various elements of the BOL core. After repeating these calculations for each enrichment, DIF2D problems for the BOL reactor were run for each of the four available temperatures. Coefficients were then derived for a cubic giving  $k_{eff}$  as a function of the temperature, T, which would pass through the four points of the  $k_{eff}$  vs. T curve. These coefficients were then used to give  $k_{eff}$  and hence reactivity differences at the specified temperatures. Table 4 presents  $k_{eff}$  and reactivity changes relative to the 38°C case for the BOL cores with all three enrichments.

TABLE 4. Reactivity Coefficients For Change of Water Temperature Only

<u>T(°C)</u>	<u>HEU</u>		<u>MEU</u>		<u>LEU</u>	
	<u><math>k_{eff}</math></u>	<u><math>\Delta\rho\times 1000</math></u>	<u><math>k_{eff}</math></u>	<u><math>\Delta\rho\times 1000</math></u>	<u><math>k_{eff}</math></u>	<u><math>\Delta\rho\times 1000</math></u>
20	1.02878	+ 2.150	1.02455	+ 1.842	1.01823	+ 1.478
38	1.02651	--	1.02262	--	1.01670	--
50	1.02501	- 1.426	1.02135	- 1.216	1.01570	- 0.968
75	1.02193	- 4.366	1.01874	- 3.724	1.01366	- 2.950
100	1.01893	- 7.247	1.01620	- 6.178	1.01168	- 4.881

#### 3.2 Change of Water Density Only and Whole-Core Void Coefficient

Values of  $k_{eff}$  were computed for water densities of 0.993, 0.988, 0.975, and 0.958 g/cm<sup>3</sup>, which correspond to the temperatures of 38°C, 50°C, 75°C, and 100°C, and for densities of 0.9 and 0.8, which are void conditions. Cross sections were generated for the six water densities at the three required burnups. The Dancoff factors input to EPRI-CELL for the resonance calculations were also a function of water density. The resulting cross sections were then used in running the six DIF2D problems for the BOL core with each enrichment. Table 5 lists  $k_{eff}$  and reactivity changes relative to the  $\rho(H_2O) = 0.993$  g/cm<sup>3</sup> case. Temperatures corresponding to the densities are also given, although the calculations were all done at the same temperature (23°C) in order to obtain coefficients for change of water density only. It should be noted that the axial reflector savings for the benchmarks is given to be 80 mm at both top and bottom of the core for all enrichments. Actually, the changes in axial reflector savings as a function of water density in the fuel elements might have a significant effect on the reactivity coefficients. However, this effect was not investigated here since no composition is given for the axial reflectors.

TABLE 5. Reactivity Coefficients For Change of Water Density Only

$\rho$ (H <sub>2</sub> O)		HEU		MEU		LEU	
(g/cm <sup>3</sup> )	T(°C)	$k_{eff}$	$\Delta\rho \times 1000$	$k_{eff}$	$\Delta\rho \times 1000$	$k_{eff}$	$\Delta\rho \times 1000$
1.0	4	1.02840	+ 1.714	1.02419	+ 1.843	1.01793	+ 2.011
0.9982	20	1.02794	+ 1.279	1.02370	+ 1.376	1.01740	+ 1.500
0.993	38	1.02659	--	1.02226	--	1.01585	--
0.988	50	1.02528	- 1.245	1.02085	- 1.351	1.01433	- 1.475
0.975	75	1.02180	- 4.566	1.01709	- 4.972	1.01028	- 5.427
0.958	100	1.01709	- 9.098	1.01204	- 9.879	1.00487	- 10.76
0.900	100	0.99965	- 26.25	0.99342	- 28.40	0.98511	- 30.72
0.800	100	0.96387	- 63.39	0.95591	- 67.90	0.94603	- 72.65

### 3.3 Change of Fuel Temperature Only

Values of  $k_{eff}$  were computed for fuel temperatures of 38°C, 50°C, 75°C, 100°C and 200°C. EPRI-CELL problems were run with resonance calculations being done at all of the desired temperatures and the three burnup stages. The temperatures for the thermal scattering calculations in the fuel materials were not changed, since the effect of fuel temperature changes is almost entirely a resonance absorption effect in <sup>238</sup>U. After the cross sections were generated, DIF2D problems were run to give  $k_{eff}$  for the specified fuel temperatures in the BOL cores for the three enrichments. Resulting values of  $k_{eff}$  and reactivity changes relative to the 38°C case are presented in Table 6. It is seen that the Doppler effect for the HEU case is very small compared to that for the LEU case.

TABLE 6. Reactivity Coefficients For Change of Fuel Temperature Only

T(°C)	HEU		MEU		LEU	
	$k_{eff}$	$\Delta\rho \times 1000$	$k_{eff}$	$\Delta\rho \times 1000$	$k_{eff}$	$\Delta\rho \times 1000$
20	1.028400	+ 0.0104	1.02423	+ 0.305	1.01797	+ 0.473
38	1.028389	--	1.02391	--	1.01748	--
50	1.028382	- 0.0066	1.02370	- 0.200	1.01716	- 0.309
75	1.028371	- 0.0170	1.02329	- 0.592	1.01650	- 0.948
100	1.028364	- 0.0236	1.02289	- 0.974	1.01586	- 1.567
200	1.028343	- 0.0435	1.02145	- 2.352	1.01345	- 3.908

TABLE 7. Slopes of Reactivity Components (38°C + 50°C)

<u>Effect</u>	<u>HEU</u>	<u>MEU</u>	<u>LEU</u>
	$\delta\rho/\delta T \times 10^3 / ^\circ\text{C}$	$\delta\rho/\delta T \times 10^3 / ^\circ\text{C}$	$\delta\rho/\delta T \times 10^3 / ^\circ\text{C}$
Water Temperature	0.1188	0.1013	0.0807
Water Density	<u>0.1038</u>	<u>0.1126</u>	<u>0.1229</u>
Sum	0.2226	0.2139	0.2036
Fuel Temperature	0.0006	0.0167	0.0258

Table 7 compares the slope of the three reactivity coefficients for a temperature change from 38°C to 50°C. The MEU and LEU cores have slightly larger feedback slopes than the HEU core because of the significant Doppler effect in these cores.

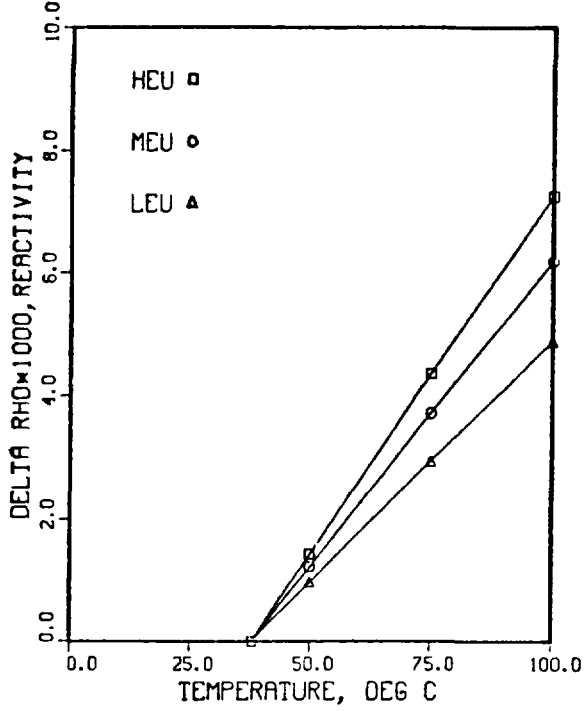
Figures 3 and 4 are plots showing the various feedback coefficients.

### 3.4 Local Void Coefficient

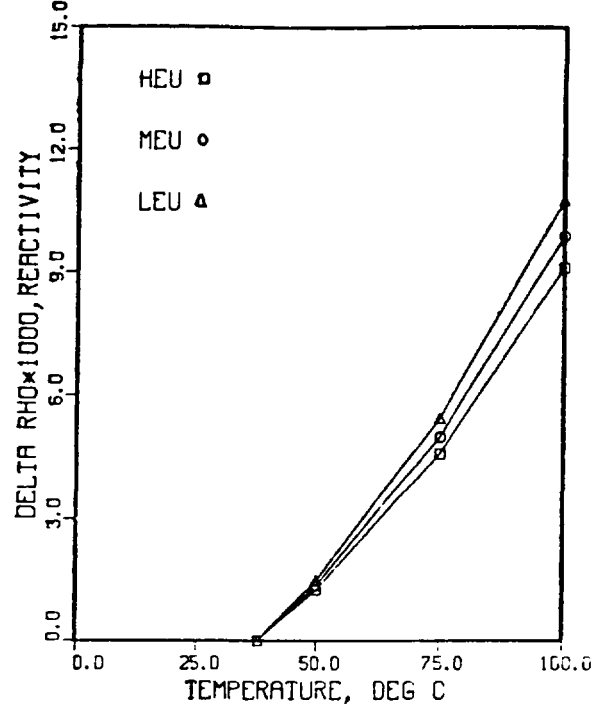
Local void coefficients were computed for changes in the water density from 0.993 to 0.95 and to 0.90 g/cm<sup>3</sup> separately in the elements denoted by SFE-2, SFE-3, and SFE-4 in the specifications. Since there was no longer quarter-core symmetry, calculations were performed for the entire core. In order to obtain smaller core storage and execution time, 5-group cross sections (see Table 1) rather than 10-group cross sections were used for these calculations. Thus, EPRI-CELL cross sections were generated for water densities of 0.993, 0.95, and 0.90 g/cm<sup>3</sup> at the three burnups involved, as described in Section 1 above.

Results of the local void coefficient calculations are shown in Table 8. Also shown are the reactivity coefficients for a change of water density from 0.993 to 0.90 in all elements for comparison with the corresponding 10-group values in Table 5. Since the 5-group values are smaller than the 10-group values by a factor of only 1.016 for all three enrichments, the 5-group calculations are considered to have adequate accuracy. Table 8 indicates that the local void coefficients are larger with MEU and LEU fuels than with HEU fuel. The reason is that the neutron spectrum is harder in the MEU and LEU cases since the <sup>235</sup>U and <sup>238</sup>U loadings are larger, and the neutron spectrum affects the leakage.

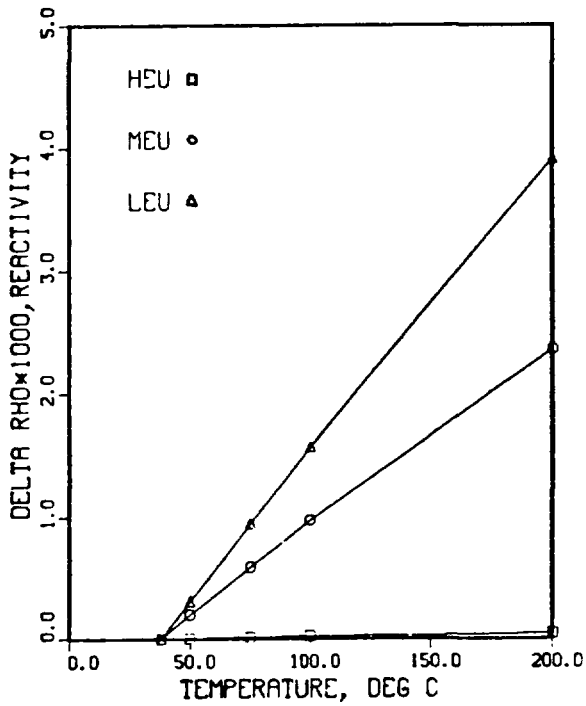
WATER TEMPERATURE EFFECT ONLY



WATER DENSITY EFFECT ONLY



DOPPLER EFFECT ONLY



WATER VOID EFFECT ONLY

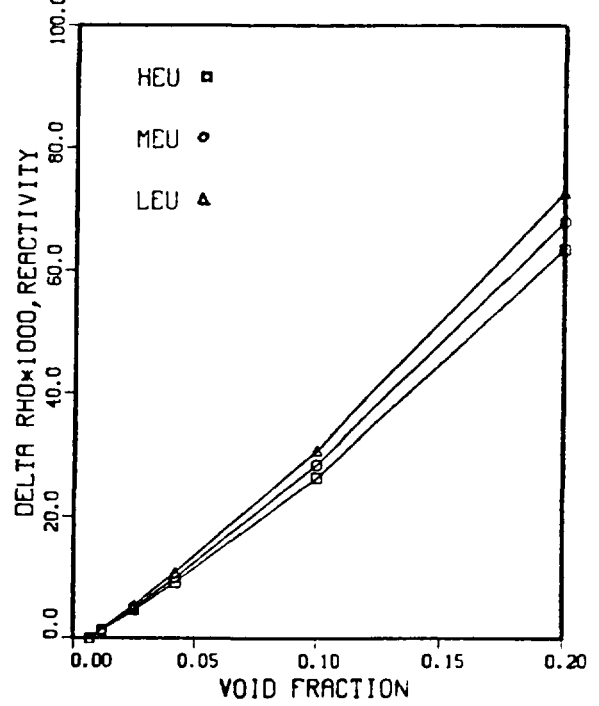
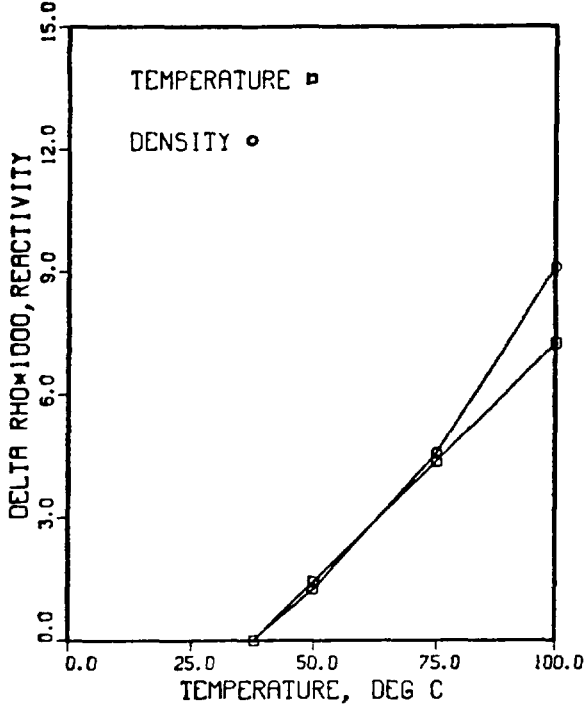
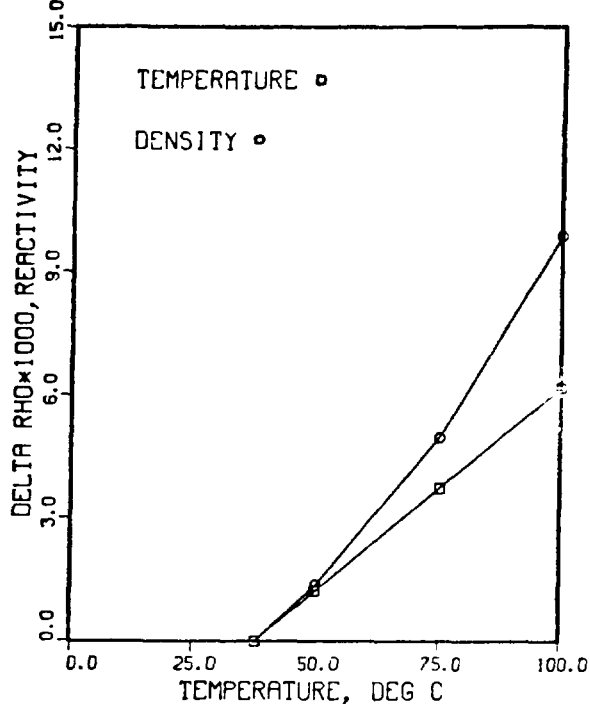


Figure 3. Isothermal Reactivity Feedback Data Corresponding to Changes in Water Temperature Only, Water Density Only, Doppler Effect Only and Water Voidage Only for HEU, MEU and LEU Cores

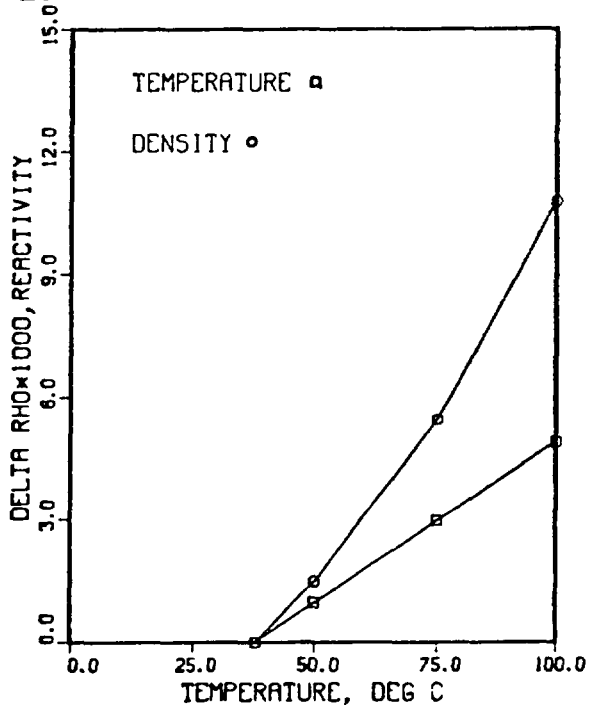
HEU WATER TEMP. AND DENSITY



MEU WATER TEMP. AND DENSITY



LEU WATER TEMP. AND DENSITY



WATER TEMPERATURE VS. DENSITY

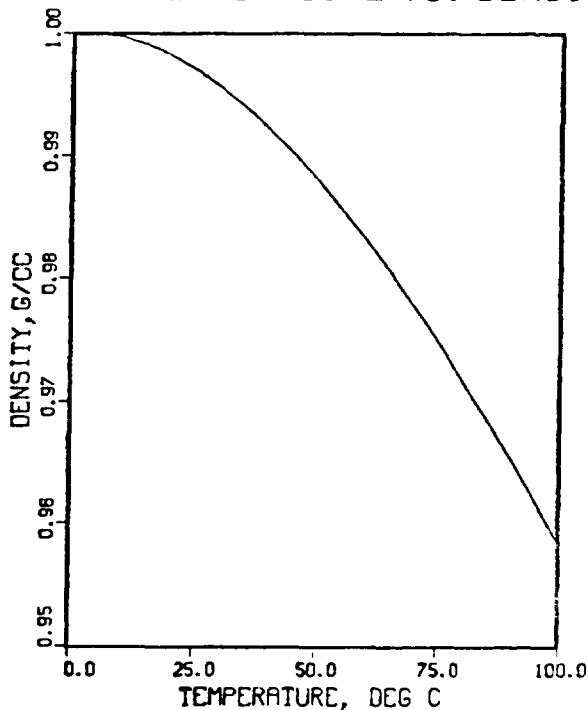


Figure 4.

Isothermal Reactivity Feedback Data for HEU, MEU and LEU Cores Comparing Reactivity Changes Due to Water Temperature Only and Water Density Only. Also shown is Water Temperature vs. Water Density up to 100°C.

TABLE 8. Reactivity Coefficients for Local Voids

$\rho_{H_2O}$ , g/cm <sup>3</sup>	Element Voided	<u>HEU</u>		<u>MEU</u>		<u>LEU</u>	
		$k_{eff}$	$-\Delta\rho \times 1000$	$k_{eff}$	$-\Delta\rho \times 1000$	$k_{eff}$	$-\Delta\rho \times 1000$
0.993	None	1.03155	-	1.02749	-	1.02143	-
0.95	SFE-2	1.03103	0.489	1.02694	0.521	1.02086	0.547
	SFE-3	1.03113	0.395	1.02699	0.474	1.02086	0.547
	SFE-4	1.03116	0.367	1.02709	0.379	1.02102	0.393
0.90	SFE-2	1.03041	1.073	1.02629	1.138	1.02019	1.190
	SFE-3	1.03061	0.884	1.02640	1.034	1.02018	1.200
	SFE-4	1.03069	0.809	1.02662	0.825	1.02055	0.844
	All	1.00477	25.84	0.99880	27.96	0.99082	30.25

#### 4. RADIAL AND LOCAL POWER PEAKING FACTORS

Radial and local power peaking factors were computed when selected fuel elements in the specified BOC core (containing equilibrium concentrations of Xe, Sm, and lumped fission products) were replaced with elements having fresh fuel (no Xe, no Sm, and no lumped fission products).

In the original neutronics benchmark problem (IAEA-TECDOC-233<sup>1</sup>, p. 445), the burnup of the fuel elements was chosen to simulate an outside-in shuffling pattern, but the "fresh elements" in the BOC quarter-core (SFE-1 and SFE-4) were arbitrarily chosen to have 5% burnup in order to include equilibrium fission product concentrations in all fuel elements. In a normal BOC core, these standard elements would contain fresh fuel without fission products.

Since the benchmark cores no longer had quarter-core symmetry after a single element was replaced, the diffusion calculations were performed for the entire core. In order to reduce computer storage requirements and execution times, these calculations were performed using 5-group rather than 10-group cross sections (Table 1). Separate EPRI-CELL cross sections were generated with five energy groups using the methods described in Section 1. Preliminary calculations indicated that element SFE-1 adjacent to the graphite reflector had a larger total power peaking factor than element SFE-4 adjacent to the water reflector.

In these 2D calculations without control absorbers, the radial power peaking factor is defined as the ratio of the average midplane power in a specific element to the average midplane power in all fuel elements. The local power peaking factor is defined as the ratio of the maximum midplane

power to the average midplane power in the specific element. The axial peaking factor is fixed as the peak-to-average ratio (1.31) of a chopped cosine with an extrapolation length of 8.0 cm for a fuel height of 60 cm. In Section 5.3, it is shown that the axial power peak will be increased by an additional factor of about 1.15 due to the power bulge toward the bottom of the core when the control absorbers are inserted 50%.

It is important to note that the maximum midplane power in the fuel of each element quoted in this section is the value at the edge of the mesh interval with highest power, and not the value at the center of the mesh interval with highest power. (There is a simple relationship between fluxes calculated at the centers of mesh intervals and the corresponding values at the edges of mesh intervals that can be built into computer codes). Normally, there is a sharp rise in power density near one corner of the fueled region in the limiting element. Local power peaking factors based on power densities computed at the centers of mesh intervals depend on the mesh spacing that is selected and underestimate the peaking.

The effect of the number of mesh intervals utilized and power peaking factors computed at the center and edge of the mesh intervals are illustrated in the table below for element SFE-1 in the HEU BOC reference core with no fresh element substitutions (i.e. SFE-1 with 5% burnup and equilibrium fission product concentrations). Models used for the standard fuel elements and control fuel elements (without absorbers) had separate fueled and non-fueled regions (see Fig.2).

HEU BOC Reference Core - No Fresh Element Substitutions

Mesh for Fueled Regions		Radial Power Peaking Factor in SFE-1	Maximum Local Power Peaking Factor in SFE-1 Based on		Radial × Local Power Peaking Factor in SFE-1 Based on	
Standard El. (6.3 × 8.1 cm <sup>2</sup> )	Control El. (6.3 × 5.95 cm <sup>2</sup> )		Center of Mesh Int.	Edge of Mesh Int.	Center of Mesh Int.	Edge of Mesh Int.
8 × 5	8 × 3	1.015	1.284	1.450	1.303	1.472
8 × 10	8 × 6	1.020	1.342	1.435	1.369	1.464
8 × 20	8 × 12	1.022	1.382	1.431	1.412	1.463

The table shows that the Local and Radial × Local power peaking factors based on power densities computed at the edges of the mesh intervals are nearly independent of the mesh spacing for the cases studied.

Table 9 shows the results of the specified calculations (using an 8 × 10 mesh in the 6.3 × 8.1 cm<sup>2</sup> fueled region of each standard element and an 8 × 6 mesh in the 6.3 × 5.95 cm<sup>2</sup> fueled region of each control element) for (1) no fresh elements substituted in the BOC cores, (2) specified fresh elements substituted in CFE-1 and SFE-1, and (3) a fresh element substituted in SFE-3 (for information only). For elements CFE-1 and SFE-1, the radial × local power peaking factor was larger for replacement of the control fuel element both in the equilibrium cores and in the mixed HEU-LEU core since the control elements in each case contain a larger volume fraction of water, but the same <sup>235</sup>U loading per fuel plate as the standard elements. Among the control fuel element cases for the HEU, MEU, and LEU equilibrium cores, the peaking factor was smallest for the LEU equilibrium core. However, the largest peaking factor was obtained when a burned HEU control element was replaced with a fresh LEU control element in the HEU equilibrium core.

The case in Table 9 for replacement of the standard fuel element with the largest power fraction (SFE-3) with a fresh fuel element may be of interest to some reactor operators. It shows the power peaking factors that would result for a hypothetical loading error in which fresh fuel was placed in SFE-3 rather than in SFE-1.

Since a number of participants in this benchmark problem are expected to have modeled the standard and control elements using homogenized fuel and non-fuel regions, the calculations shown in Table 9 were repeated with fuel element materials homogenized over their  $7.7 \times 8.1 \text{ cm}^2$  cross section.

TABLE 9. Radial and Local Power Peaking Factors  
Standard and Control Elements Modeled with  
Separate Fuel and Non-Fuel Regions (see Fig. 2)

<u>Element Substituted</u>	<u>Radial</u>	<u>Local</u>	<u>Radial × Local</u>	<u>k<sub>eff</sub></u>	<u>Δρ × 1000</u>
<u>HEU Core</u>					
None <sup>a</sup>	1.020	1.435	1.464	1.03335	-
CFE-1	1.358	1.336	1.814	1.03893	5.20
SFE-1	1.110	1.432	1.590	1.03567	2.17
SFE-3 <sup>b</sup>	1.496	1.362	2.038	1.04876	14.22
<u>MEU Core</u>					
None <sup>a</sup>	1.017	1.483	1.508	1.02944	-
CFE-1	1.337	1.335	1.785	1.03468	4.92
SFE-1	1.105	1.480	1.635	1.03168	2.11
SFE-3 <sup>b</sup>	1.470	1.390	2.043	1.04381	13.37
<u>LEU Core</u>					
None <sup>a</sup>	1.015	1.558	1.581	1.02354	-
CFE-1	1.314	1.332	1.750	1.02848	4.69
SFE-1	1.101	1.552	1.709	1.02568	2.04
SFE-3 <sup>b</sup>	1.440	1.427	2.055	1.03698	12.66
<u>LEU Substitutions in HEU Core</u>					
None <sup>a</sup>	1.020	1.435	1.464	1.03335	-
CFE-1	1.491	1.449	2.160	1.03885	5.12
SFE-1	1.209	1.548	1.872	1.03587	2.35
SFE-3 <sup>b</sup>	1.637	1.527	2.500	1.04859	14.06

<sup>a</sup>Limiting element is SFE-1 with 5% burnup.

<sup>b</sup>Information only.

The resulting power peaking factors (using power densities computed at the edges of the mesh intervals) are shown in Table 9a and are slightly smaller than those in Table 9. Note that a comparison of the  $k_{eff}$  values for the same cases in the two tables shows that fuel element models with separate fuel and non-fuel regions yield excess reactivities that are smaller than the values for their homogenized counterparts by about 0.6%  $\delta k/k$ .

TABLE 9a. Radial and Local Power Peaking Factors  
Standard and Control Elements Modeled with  
Homogenized Fuel and Non-Fuel Regions

<u>Element Substituted</u>	<u>Radial</u>	<u>Local</u>	<u>Radial × Local</u>	<u><math>k_{eff}</math></u>	<u><math>\Delta\rho \times 1000</math></u>
<u>HEU Core</u>					
None <sup>a</sup>	1.030	1.397	1.439	1.03952	-
CFE-1	1.349	1.310	1.767	1.04509	5.13
SFE-1	1.120	1.397	1.565	1.04188	2.18
SFE-3 <sup>b</sup>	1.508	1.384	2.087	1.05521	14.30
<u>MEU Core</u>					
None <sup>a</sup>	1.027	1.445	1.484	1.03585	-
CFE-1	1.326	1.308	1.734	1.04108	4.85
SFE-1	1.115	1.446	1.612	1.03813	2.12
SFE-3 <sup>b</sup>	1.481	1.415	2.096	1.05047	13.44
<u>LEU Core</u>					
None <sup>a</sup>	1.025	1.522	1.560	1.03020	-
CFE-1	1.301	1.309	1.703	1.03512	4.61
SFE-1	1.112	1.522	1.692	1.03237	2.04
SFE-3 <sup>b</sup>	1.450	1.458	2.114	1.04385	12.69
<u>LEU Substitutions in HEU Core</u>					
None <sup>a</sup>	1.030	1.397	1.439	1.03952	-
CFE-1	1.490	1.414	2.107	1.04502	5.06
SFE-1	1.227	1.468	1.801	1.04216	2.44
SFE-3 <sup>b</sup>	1.663	1.549	2.576	1.05522	14.31

<sup>a</sup>Limiting element is SFE-1 with 5% burnup.

<sup>b</sup>Information only.

## 5. CONTROL ROD CALCULATIONS

### 5.1 Worth of Fully-Inserted Rods

The worths of four fully-inserted control rods with Ag-In-Cd absorber, B<sub>4</sub>C absorber, and Hf absorber were computed in both the HEU and LEU equilibrium cores at BOL. The rods are fork-type with blades fitting between the first and third and the 21st and 23rd plates of the control fuel elements. The Ag-In-Cd and B<sub>4</sub>C blades are 600 mm long, 66 mm wide, and 3.18 mm thick, having a 3.1 mm thick absorber with a 0.04 mm thick layer of nickel on each surface. The hafnium blades are similar except that they are 3.1 mm thick and have no nickel plating. The Ag-In-Cd rods are 80.5% w/o Ag, 14.6% w/o In and 4.9% w/o Cd, while the B<sub>4</sub>C rods contain natural boron, and the Hf rods contain natural hafnium.

In order to validate the methods to be used for calculating control rod worths with diffusion theory, both Monte Carlo (using the VIM code<sup>5</sup>) and diffusion theory problems were run for the fresh HEU and LEU cores with no control rods and with four fully-inserted rods utilizing the specified absorbers. In the three-dimensional geometry used in the continuous-energy Monte Carlo calculations, each standard element, control element, and absorber blade were modeled in explicit detail. Axial reflectors 300 mm thick were assumed at the top and bottom of the core with the first 150 mm being a mixture of 80% water and 20% aluminum to represent the composition of the fuel element end boxes, and the second 150 mm being water only. Each problem consisted of 100,000 neutron histories. Five-group edits were obtained with the groups having the energy boundaries shown in Table 1. The  $k_{eff}$  values from the Monte Carlo calculations, and the reactivity changes obtained are presented in Table 10.

The cross section edits over the control rods in the Monte Carlo problems were used to calculate extrapolation distances,  $\lambda$ , for each group using the formula

$$a = \lambda \sum_{tr} = 0.7104 \left[ \frac{1 + 3 E_4 (\sum_a \cdot t)}{1 - 2 E_3 (\sum_a \cdot t)} \right] \quad (1)$$

where  $\sum_a$  is the macroscopic absorption cross section of the absorber blade calculated from the Monte Carlo edits,  $t = 3.1$  mm is the blade thickness,  $E_3$  and  $E_4$  are exponential integrals, and  $\sum_{tr}$  is the macroscopic transport cross section of the surrounding medium. Note that the extrapolation distance,  $\lambda$ , equals  $0.7104/\sum_{tr}$  in the black absorber limit. Two-dimensional diffusion problems were then run in 5 groups for the fresh-fuel cores using EPRI-CELL cross sections for all regions outside the control blades, and the condition

$$D\phi' + \frac{\phi}{3a} = 0 \quad (2)$$

at the surfaces of the blades, where  $D$  is the diffusion coefficient for the medium outside the blades and  $\phi$  and  $\phi'$  are the flux and its derivative. The  $k_{eff}$  values from the diffusion-theory calculations for fresh-fuel cores are given in Table 11, along with reactivity changes and comparisons with the corresponding Monte Carlo reactivity changes. Note that the Monte Carlo and diffusion-theory problems are not completely identical, since the Monte Carlo problems have actual axial reflectors, while the diffusion-theory problems are two-dimensional with assumed axial reflector savings of 80 mm at both ends of the core. However, Table 11 shows that the reactivity changes as calculated by Monte Carlo and by diffusion-theory calculations with extrapolation boundary conditions agree rather well.

Methods Comparison - Monte Carlo vs Diffusion Theory  
 Reactivity Worths for Four Fork-Type Control Rods  
 Inserted into HEU and LEU Cores with Fresh Fuel

TABLE 10. Monte Carlo Results - Four Inserted Rods - Fresh Fuel Cores

Enrichment	Absorber	$k_{eff}$	$-\Delta\rho, \%$	$-\Delta\rho, \$$
HEU	None	1.20165 ± 0.00315	-	-
	Ag-In-Cd	1.03462 ± 0.00331	13.43 ± 0.38	17.65 ± 0.50
	B <sub>4</sub> C	0.99957 ± 0.00308	16.82 ± 0.38	22.11 ± 0.50
	Hf	1.04260 ± 0.00311	12.70 ± 0.36	16.70 ± 0.47
LEU	None	1.17404 ± 0.00314	-	-
	Ag-In-Cd	1.03720 ± 0.00328	11.24 ± 0.38	15.45 ± 0.52
	B <sub>4</sub> C	0.99873 ± 0.00329	14.95 ± 0.40	20.55 ± 0.55
	Hf	1.03900 ± 0.00305	11.07 ± 0.36	15.22 ± 0.49

TABLE 11. Diffusion Theory Results - Four Inserted Rods - Fresh Fuel Cores

Enrichment	Absorber	$k_{eff}$	$-\Delta\rho, \%$	$-\Delta\rho, \$$	$\frac{\Delta\rho_D/\Delta\rho^a}{MC}$
HEU	None	1.19372	-	-	-
	Ag-In-Cd	1.03370	12.97	17.05	0.966
	B <sub>4</sub> C	0.99236	17.00	22.35	1.011
	Hf	1.03771	12.59	16.55	0.991
LEU	None	1.16954	-	-	-
	Ag-In-Cd	1.03054	11.53	15.85	1.026
	B <sub>4</sub> C	0.99110	15.39	21.15	1.029
	Hf	1.03407	11.20	15.40	1.012

a:  $\Delta\rho$  From Diffusion Theory/  $\Delta\rho$  From Monte Carlo

Table 12 presents diffusion-theory values of  $k_{eff}$  and reactivity changes for the BOC cores. The same values of "a" calculated from Eq (1) were used in the calculations as were used for the corresponding fresh-fuel cores. These values are not expected to be very sensitive to burnup. Also there is little difference in the "a" values for a given absorber for the HEU and LEU fresh-fuel cores.

Tables 13 through 15 present the relative neutron absorption rates (%) in the Ag-In-Cd,  $B_4C$ , and Hf control rod materials for both the HEU and LEU fresh-fuel cores. The data were obtained from the Monte Carlo edits.

Table 13 shows that all three of the materials in the Ag-In-Cd rod have considerable absorption with cadmium being a strong thermal absorber and silver and indium being strong resonance absorbers. When the spectrum is hardened in going from the HEU to the LEU core, the increased resonance absorption in silver and indium tends to compensate for the decreased thermal absorption in cadmium. It is seen from Table 14 that almost all of the absorption in the  $B_4C$  rods is in  $^{10}B$ . There is considerable epithermal as well as thermal absorption, since the rods are black at thermal energies, but gray at higher energies. Table 16 shows that about 70% of the absorption in the hafnium control rods is in  $^{177}Hf$ , although its abundance in natural hafnium is only 18.5%.

For convenience of potential users, microscopic absorption cross sections for the materials in the Ag-In-Cd,  $B_4C$ , and Hf control blades obtained from the Monte Carlo calculations are shown in Tables 16, 17, and 18. In addition, the Monte Carlo values of the parameter  $a = \lambda_{tr}^{\sum}$  that were used in the diffusion theory calculations are shown in Table 19 for all three types of absorber blades in the fresh HEU and LEU cores. There are only small differences between the values of "a" in the HEU and LEU cores.

TABLE 12. Control Rod Worths - BOC Cores Four Fully-Inserted Fork-Type Rods; Diffusion Theory

<u>Enrichment</u>	<u>Absorber</u>	<u><math>k_{eff}</math></u>	<u><math>-\Delta\rho, \%</math></u>	<u><math>-\Delta\rho, \\$</math></u>
HEU	None	1.03334	-	-
	Ag-In-Cd	0.87872	17.03	22.39
	$B_4C$	0.84376	21.74	28.58
	Hf	0.88370	16.39	21.55
LEU	None	1.02353	-	-
	Ag-In-Cd	0.89149	14.47	19.89
	$B_4C$	0.85752	18.91	25.99
	Hf	0.89552	13.97	19.20

TABLE 13. Relative Neutron Absorption Rates (%) in Ag-In-Cd Control Rod Materials for HEU and LEU Fresh-Fuel Cores

<u>HEU Core</u>						
<u>Group<sup>a</sup></u>	<u><sup>107</sup>Ag</u>	<u><sup>109</sup>Ag</u>	<u><sup>113</sup>In</u>	<u><sup>115</sup>In</u>	<u>Cd</u>	<u>Ni</u>
1+2	1.238	0.709	0.019	0.288	0.059	0.020
3+4	6.538	15.477	0.404	13.382	0.669	0.025
5	<u>3.434</u>	<u>8.287</u>	<u>0.016</u>	<u>7.286</u>	<u>42.028</u>	<u>0.120</u>
Total	11.210	24.473	0.439	20.956	42.756	0.166

<u>LEU Core</u>						
<u>Group<sup>a</sup></u>	<u><sup>107</sup>Ag</u>	<u><sup>109</sup>Ag</u>	<u><sup>113</sup>In</u>	<u><sup>115</sup>In</u>	<u>Cd</u>	<u>Ni</u>
1+2	1.431	0.818	0.023	0.334	0.068	0.024
3+4	6.795	17.300	0.399	14.157	0.844	0.028
5	<u>3.179</u>	<u>7.714</u>	<u>0.015</u>	<u>6.918</u>	<u>39.843</u>	<u>0.113</u>
Total	11.406	25.830	0.437	21.408	40.755	0.165

a - See Table 1 For Group Boundaries

TABLE 14. Relative Neutron Absorption Rates (%) in B<sub>4</sub>C Control Rod Materials For HEU and LEU Fresh-Fuel Cores

<u>HEU Core</u>				
<u>Group<sup>a</sup></u>	<u><sup>10</sup>B</u>	<u><sup>11</sup>B</u>	<u>C</u>	<u>Ni</u>
1+2	3.375	0.0002	0.002	0.016
3+4	52.221	0.0003	~0.0	0.014
5	<u>44.295</u>	<u>0.0002</u>	<u>~0.0</u>	<u>0.076</u>
Total	99.891	0.001	0.002	0.106

<u>LEU Core</u>				
<u>Group<sup>a</sup></u>	<u><sup>10</sup>B</u>	<u><sup>11</sup>B</u>	<u>C</u>	<u>Ni</u>
1+2	3.912	0.0002	0.003	0.018
3+4	56.622	0.0003	~0.0	0.014
5	<u>39.368</u>	<u>0.0002</u>	<u>~0.0</u>	<u>0.064</u>
Total	99.800	0.001	0.003	0.096

a - See Table 1 For Group Boundaries.

TABLE 15. Relative Neutron Absorption Rates in Hafnium Control Rod Materials for HEU and LEU Fresh-Fuel Cores

HEU Core						
Group <sup>a</sup>	<u><sup>174</sup>Hf</u>	<u><sup>176</sup>Hf</u>	<u><sup>177</sup>Hf</u>	<u><sup>178</sup>Hf</u>	<u><sup>179</sup>Hf</u>	<u><sup>180</sup>Hf</u>
1+2	0.005	0.122	0.885	0.385	0.485	0.368
3+4	0.188	0.850	32.778	5.772	6.209	0.744
5	<u>0.292</u>	<u>0.965</u>	<u>36.016</u>	<u>9.104</u>	<u>2.791</u>	<u>2.038</u>
Total	<u>0.486</u>	<u>1.937</u>	<u>69.679</u>	<u>15.262</u>	<u>9.486</u>	<u>3.150</u>

LEU Core						
Group <sup>a</sup>	<u><sup>174</sup>Hf</u>	<u><sup>176</sup>Hf</u>	<u><sup>177</sup>Hf</u>	<u><sup>178</sup>Hf</u>	<u><sup>179</sup>Hf</u>	<u><sup>180</sup>Hf</u>
1+2	0.006	0.144	1.045	0.463	0.579	0.438
3+4	0.231	0.933	35.210	6.359	6.808	0.808
5	<u>0.266</u>	<u>0.878</u>	<u>33.151</u>	<u>8.289</u>	<u>2.539</u>	<u>1.852</u>
Total	<u>0.503</u>	<u>1.954</u>	<u>69.407</u>	<u>15.111</u>	<u>9.926</u>	<u>3.099</u>

a - See Table 1 For Group Boundaries.

TABLE 16 - Microscopic Absorption Cross Sections (barns)  
 Edited from the Monte Carlo Calculation for  
 Ag-In-Cd Control Rod Materials in the Fresh HEU Core

Group	<u>Cd</u>	<u><sup>113</sup>In</u>	<u><sup>115</sup>In</u>
1	0.0309 ± 0.0002	0.2327 ± 0.0009	0.1166 ± 0.0007
2	0.2451 ± 0.0034	0.5286 ± 0.0041	0.3790 ± 0.0035
3	3.2594 ± 0.2187	20.148 ± 1.761	10.297 ± 0.359
4	27.098 ± 0.648	48.177 ± 4.803	440.90 ± 16.49
5	2053.8 ± 31.2	6.1700 ± 0.0532	127.52 ± 0.69

Group	<u><sup>107</sup>Ag</u>	<u><sup>109</sup>Ag</u>
1	0.0806 ± 0.0003	0.0432 ± 0.0002
2	0.5760 ± 0.0066	0.3600 ± 0.0046
3	4.8383 ± 0.1548	11.961 ± 0.345
4	6.2099 ± 0.0261	22.602 ± 0.029
5	18.916 ± 0.189	49.097 ± 0.439

TABLE 17 - Microscopic Absorption Cross Sections (barns)  
 Edited from the Monte Carlo Calculation for  
 B<sub>4</sub>C Control Rod Materials in the HEU Core

Group	<u><sup>10</sup>B</u>	<u><sup>11</sup>B</u>	<u>C</u>
1	0.3293 ± 0.0013	9.8063-6 ± 2.0593-6	1.3605-3 ± 1.5510-4
2	2.1033 ± 0.0215	2.6125-5 ± 6.5835-6	0.0 ± 0.0
3	59.850 ± 0.850	7.8338-5 ± 1.0889-6	5.1090-5 ± 7.6635-7
4	583.19 ± 3.38	7.5446-4 ± 4.4287-6	5.1730-4 ± 2.9848-6
5	1807.4 ± 19.9	2.3516-3 ± 2.5868-5	1.5954-3 ± 1.7390-5

TABLE 18 - Microscopic Absorption Cross Sections (barns)  
 Edited from the Monte Carlo Calculation for  
 Hf Control Rod Materials in the HEU Core

<u>Group</u>	<u><math>^{174}\text{Hf}</math></u>	<u><math>^{176}\text{Hf}</math></u>	<u><math>^{177}\text{Hf}</math></u>
1	0.0741 ± 0.0003	0.0740 ± 0.0003	0.0740 ± 0.0003
2	0.7314 ± 0.0097	0.5211 ± 0.0064	1.1220 ± 0.0155
3	43.572 ± 4.061	6.5209 ± 0.4493	46.175 ± 0.9743
4	60.150 ± 0.470	6.7231 ± 0.0478	661.05 ± 18.91
5	216.32 ± 1.48	23.366 ± 0.159	245.09 ± 1.11

<u>Group</u>	<u><math>^{178}\text{Hf}</math></u>	<u><math>^{179}\text{Hf}</math></u>	<u><math>^{180}\text{Hf}</math></u>
1	0.0740 ± 0.0003	0.0740 ± 0.0003	0.0740 ± 0.0003
2	0.2915 ± 0.0028	0.8090 ± 0.0101	0.2008 ± 0.0016
3	8.2012 ± 0.3059	18.395 ± 0.596	0.8008 ± 0.0750
4	15.023 ± 0.050	7.6642 ± 0.0468	1.9461 ± 0.0166
5	42.138 ± 0.276	25.466 ± 0.172	7.3101 ± 0.0504

TABLE 19 - Values of  $a = \lambda \sum_{tr}$  Based on Monte Carlo Calculations for the  
 Three Control Blade Types in the Fresh HEU and LEU Cores

<u>HEU</u>			
<u>Group</u>	<u>Ag-In-Cd</u>	<u>B<sub>4</sub>C</u>	<u>Hf</u>
1	663.38	323.84	709.85
2	101.38	51.119	105.02
3	6.0516	2.2576	4.2948
4	1.0549	0.7198	0.8457
5	0.7834	0.7104	1.2304

<u>LEU</u>			
<u>Group</u>	<u>Ag-In-Cd</u>	<u>B<sub>4</sub>C</u>	<u>Hf</u>
1	657.23	323.84	702.82
2	102.71	51.081	104.86
3	6.1855	2.2945	4.4897
4	1.0406	0.7200	0.8683
5	0.7899	0.7104	1.2452

## 5.2 Worth of Partially-Inserted Rods

Calculations (not included in the benchmark specifications) of the reactivity worths of partially-inserted control rods with Ag-In-Cd absorber in the HEU and LEU BOL cores (with no fresh element substitutions) were also performed since the results are of interest to reactor operators.

Three-dimensional diffusion theory models of the HEU and LEU BOL cores were first set up with quarter-core symmetry and a homogeneous axial distribution of the  $^{235}\text{U}$  in the standard and control element planar geometries shown in Fig. 2. The end boxes on the top and bottom of each fuel element were represented using a homogenized mixture of 25 v/o Al and 75 v/o  $\text{H}_2\text{O}$  extending 15 cm above the fuel. A thickness of 20 cm of water was added above the axial end boxes. The calculations were done using five energy groups (Table 1) and the same internal boundary conditions (i.e. asymptotic current-to-flux ratios at the surface of the absorber slab) that were used in calculating the reactivity worths of fully-inserted rods described in the previous section.

The calculated absolute reactivities in %  $\delta k/k$  and in  $\$$  for eight positions of the four control rods in the HEU and LEU BOL cores are listed in Table 20. The corresponding reactivity values relative to the rods 100% withdrawn are shown in Table 21. The tips of the rods were at the bottom of the fuel meat (height = 0.0 cm) in the fully-inserted position and at the top of the fuel meat (height = 60.0 cm) in the fully-withdrawn position.

TABLE 20 - Absolute Values of Reactivity vs Rod Position  
for HEU and LEU BOL Benchmark Cores

Rod Position, %	Height of Rod Withdrawn	Tip, cm	HEU			LEU		
			$k_{\text{eff}}$	$\delta k/k, \%$	$\$^a$	$k_{\text{eff}}$	$\delta k/k, \%$	$\$^b$
0		0.0	0.88579	-12.89	-16.94	0.89729	-11.45	-15.74
10		6.0	0.89075	-12.26	-16.12	0.90179	-10.89	-14.97
20		12.0	0.90333	-10.70	-14.07	0.91236	-9.61	-13.21
33		19.8	0.93264	-7.22	-9.49	0.93664	-6.76	-9.29
50		30.0	0.97250	-2.83	-3.72	0.97055	-3.03	-4.16
67		40.2	1.00422	0.42	0.55	0.99827	-0.17	-0.23
85		51.0	1.02652	2.58	3.40	1.01769	1.74	2.39
100		60.0	1.03350	3.24	4.26	1.02341	2.29	3.15

TABLE 21 - Values of Reactivity vs Rod Position  
Relative to 100% Withdrawn for HEU and  
LEU BOL Benchmark Cores

Rod Position, % Withdrawn	Height of Rod Tip, cm	HEU			LEU		
		$k_{eff}$	$\delta k/k, \%$	$\$^a$	$k_{eff}$	$\delta k/k, \%$	$\$^b$
0	0.0	0.88579	16.13	21.20	0.89729	13.74	18.89
10	6.0	0.89075	15.50	20.38	0.90179	13.18	18.12
20	12.0	0.90333	13.94	18.33	0.91236	11.90	16.36
33	19.8	0.93264	10.46	13.75	0.93664	9.05	12.44
50	30.0	0.97250	6.07	7.98	0.97055	5.32	7.31
67	40.2	1.00422	2.82	3.71	0.99827	2.46	3.38
85	51.0	1.02652	0.66	0.86	1.01769	0.55	0.76
100	60.0	1.03350	0.0	0.0	1.02341	0.0	0.0

$${}^a\beta_{HEU} = .007607; \quad {}^b\beta_{LEU} = .007275$$

It is interesting to compare the reactivity data in Table 12 and those in Table 20 for the cases with the rods fully-inserted and fully-withdrawn. The rod worths in Table 20 were obtained using the 3D model described above and those in Table 12 were obtained using the specified 2D model with an extrapolation length of 80 mm in the core and reflectors. The results are summarized below:

Comparison of Control Rod (Ag-In-Cd) Reactivity Worths  
Between Specified 2D Benchmark Model and 3D Model

Position of 4 Rods	Reactivity Worth, \$			
	HEU		LEU	
	2D	3D	2D	3D
100% Out	4.25	4.26	3.16	3.15
100% In	-18.14	-16.94	-16.73	-15.74
\$ (Out-In)	22.39	21.20	19.89	18.89

With the rods 100% out, the 2D and 3D data are almost identical for the HEU and LEU cases, indicating that the 80 mm extrapolation length was an excellent choice. However, with the rods fully-inserted, the reactivity differential between the 2D and 3D models was \$1.19 for the HEU core and \$1.00 for the LEU core. This effect may be important in calculating shutdown margins in real reactors. The effect on rod worths of the actual  $^{235}\text{U}$  axial burnup distribution may be important as well.

The reactivity data (in \$) from Table 20 are plotted in Fig. 5 as a function of the percentage that the four rods are withdrawn. The S-shaped curves for the two cases have the same general shape and display the smaller rod worth in the LEU core. Both cases have the same reactivity worth in the range of 35-40% withdrawn. The HEU core would be critical with the rods withdrawn about 64% and the LEU core would be critical with the rods withdrawn about 68%.

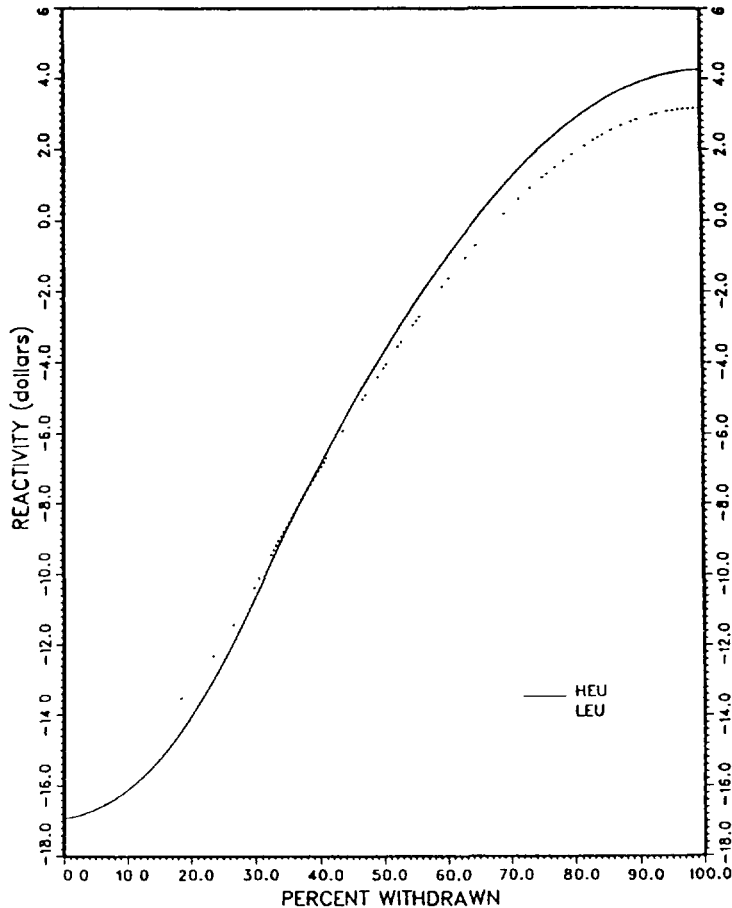


Fig. 5  
Reactivity (\$) vs. Rod Position  
for HEU and LEU BOL Benchmark Cores.

### 5.3 Axial Power Peaking with Partially-Inserted Rods

Axial power peaking effects due to partially-inserted control rods are also of interest to reactor operators. Using the calculations described in Section 5.2, the axial power densities at the midplane mesh point with peak power in CFE-1 and in SFE-1 for the HEU BOL core are plotted in Figs. 6 and 7, respectively, for the full-out, full-in, and four partially-withdrawn rod positions. The corresponding curves for CFE-1 and SFE-1 for the LEU BOL core are shown in Figs. 8 and 9, respectively.

In all four cases, the peak axial power density was obtained when the control rods were withdrawn 50%, and the peak was located at a height of about 20 cm from the bottom of the active core (or about 1/3 of the way up from the bottom of the fuel).

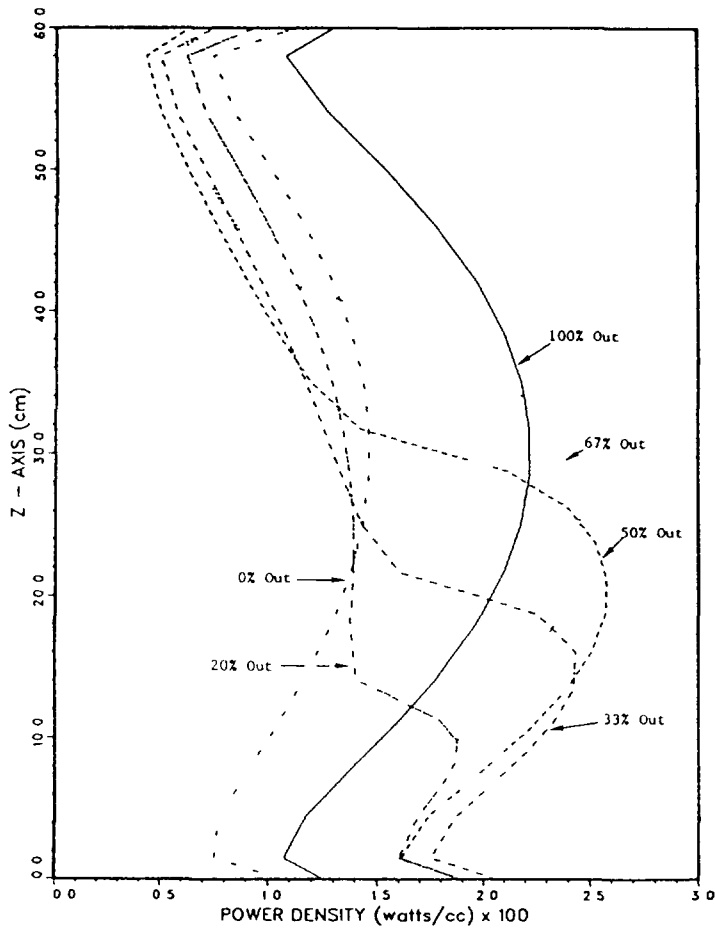


Fig. 6  
 HEU BOL CORE: CFE-1  
 Axial Power Densities at Midplane Power Peak  
 for Six Positions of the Four Control Rods

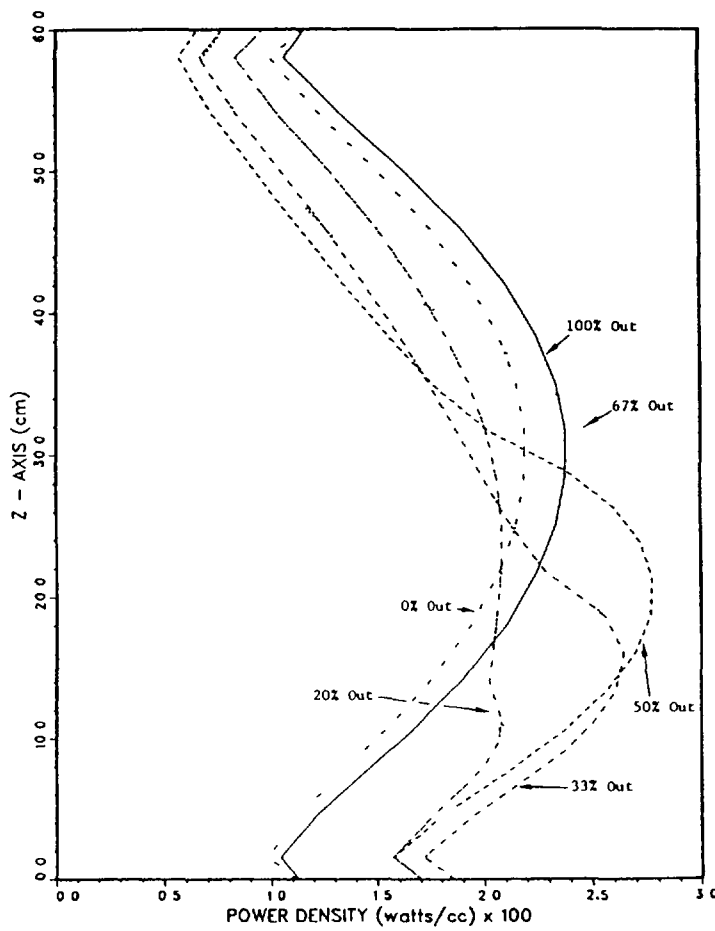


Fig. 7  
 HEU BOL CORE: SFE-1  
 Axial Power Densities at Midplane Power Peak  
 for Six Positions of the Four Control Rods

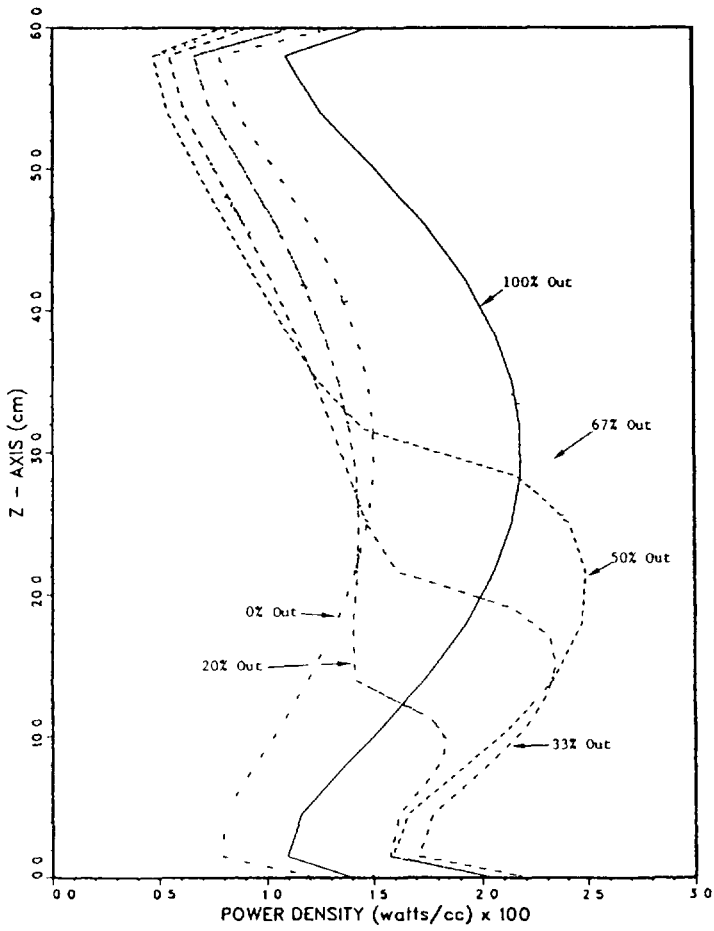


Fig. 8

LEU BOL CORE: CFE-1

Axial Power Densities at Midplane Power Peak for Six Positions of the Four Control Rods

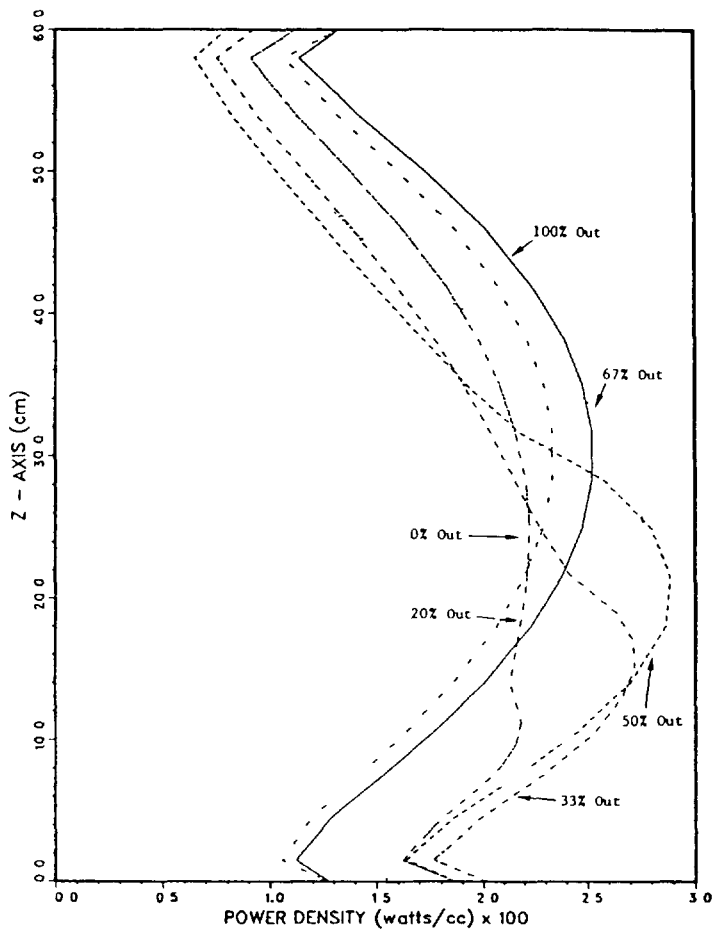


Fig. 9

LEU BOL CORE: SFE-1

Axial Power Densities at Midplane Power Peak for Six Positions of the Four Control Rods

Listed in the Table 22 are the peak values of the power densities in each of the four cases with the rods 50% withdrawn and 100% withdrawn.

TABLE 22 - Peak Power Densities ( $W/cm^3$ ) in CFE-1 and SFE-1 for HEU and LEU BOL Cores with Control Rods Withdrawn 50% and 100%

Control Rod Position	CFE-1			SFE-1		
	HEU	LEU	LEU/HEU	HEU	LEU	LEU/HEU
50% Out	258	249	0.97	277	289	1.04
100% Out	222	218	0.98	238	252	1.06
Ratio $\left(\frac{50\% \text{ Out}}{100\% \text{ Out}}\right)$	1.16	1.14		1.16	1.15	

The axial peak power densities in all four cases are about 15% larger with the rods 50% withdrawn rather than 100% withdrawn. In CFE-1, the peak power densities are 2-3% lower in the LEU core than in the HEU core for both rod positions. In SFE-1, they are about 5% larger in the LEU core.

In Figs. 6 and 8, it is interesting to note that the "kinks" in the power density profiles occur at higher axial locations than the tips of the control rods in these diffusion-theory calculations. Effects which occur around the tips of control rods are not addressed here, but would be the subject of another study using transport theory calculations.

Figure 10 shows the axial power density profiles in CFE-1 and SFE-1 in the HEU and LEU cores with the rods 50% withdrawn.

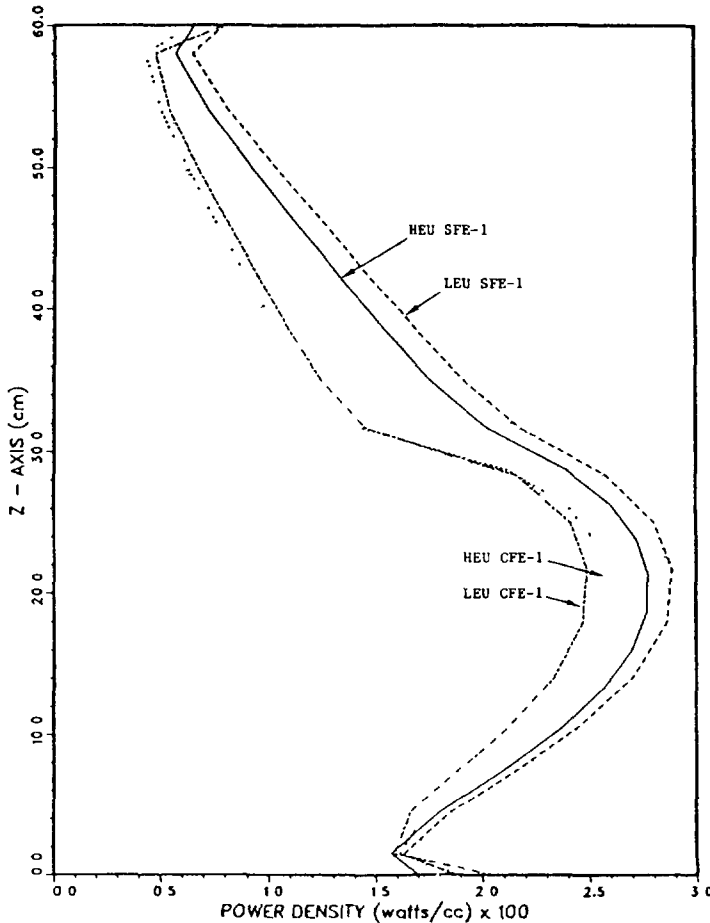


Fig. 10

HEU and LEU BOL CORES: CFE-1 and SFE-1  
Axial Power Densities at Midplane Power Peak  
with the Four Control Rods 50% Withdrawn

## 6. TRANSIENT CALCULATIONS

This section describes the models and methods used for the transient analysis of the HEU and LEU benchmark cores using the PARET code,<sup>6</sup> and provides a summary of the results.

### 6.1 PARET Code Description

The PARET code provides a coupled thermal, hydrodynamic, and point kinetics capability with continuous reactivity feedback. The core can be represented by one to four regions. Each region may have different power generation, coolant mass flow rate, and hydraulic parameters as represented by a single fuel pin or plate with its associated coolant channel. The heat transfer in each fuel element is computed on the basis of a one-dimensional conduction solution in each of up to 21 axial sections. The hydrodynamics solution is also one-dimensional for each channel at each time node. The heat transfer may take place by natural or forced convection, nucleate, transition, or stable film boiling, and the coolant is allowed to range from subcooled liquid, through the two-phase regime, and up to and including superheated steam and allows for coolant flow reversal. The code also has an optional "boiling model" which estimates the voiding produced by subcooled boiling. A description of the current PARET code and a comparison for the SPERT I experiments are provided in Ref. 7.

### 6.2 Models for Analysis of Benchmark Transients

Before computing the benchmark transients, several modeling variations were tested in order to determine the sensitivity of the results to the model employed. These variations included both the number of channels and the type and detail of the reactivity feedback coefficients. The choice of heat transfer correlations and models is also considered.

The benchmark problem specifies that isothermal reactivity feedback coefficients be used in the transient calculations. However, in order to assess the importance of the axial and radial reactivity feedback coefficient distributions, first order perturbation theory was used to calculate a pointwise feedback distribution in the HEU BOL benchmark core. The first order perturbation theory data was generated using an RZ model with four radial regions consisting of 1) the equivalent of three inner standard elements, 2) next three standard elements, 3) four control elements and next five standard elements, and 4) the outermost ten standard elements. The axial dimension included 21 (2.857 cm) equal intervals over the 60.0 cm active core. For the temperature (spectral) perturbation, the water temperature over the active core was increased from a base temperature of 23°C to a temperature of 77°C, and the water density was decreased by 1% at a temperature of 23°C for the density (void) component. The total overall reactivity coefficient from these perturbations was in good agreement with the isothermal coefficient from the XY computations described in Section 3. Normalized axial distributions for the coefficient were taken from the pointwise data at each region center. The axial power (source) shape was assumed to be a chopped cosine with a peak-to-average of 1.5 and having a radial component consistent with the region-average variation in the power density by region.

These four region data were used to define a four channel PARET model. These data were also reduced to single distributions for one and two channel models. The  $1.50/0.5$  s reactivity insertion transient (the most severe HEU case specified) was used for this analysis. Table 23 provides a comparison of the various models using both the RZ perturbation data and the XY isothermal data specified for the benchmark. Comparisons were first made

TABLE 23. Comparison of Results of Model and Reactivity Coefficient Distribution Variations for \$1.5/0.5 s Fast Reactivity Insertion Transient in HEU Benchmark Core

Model Data	No. of Channels	$\hat{P}(t_m, s)$ , MW	$E_{t_m}$ , MJ	$\hat{T}(t, s)$ , °C <sup>a</sup>		
				Fuel	Clad	Outlet
<u>Average Channel Comparisons</u>						
RZ Perturbation Data with Axial Distribution	4	133.1(0.656)	3.22	141.2(0.674)	132.3(0.675)	67.5(0.779)
RZ Perturbation Data with Axial Distribution	1	133.2(0.656)	3.22	133.1(0.680)	128.2(0.682)	62.1(0.794)
<u>Hot Channel Comparisons</u>						
RZ Perturbation Data with Axial Distribution	2	133.2(0.656)	3.22	158.6(0.666)	139.7(0.667)	88.1(0.759)
RX Perturbation Data with Uniform Distribtuion	2	135.2(0.657)	3.39	159.8(0.666)	140.1(0.667)	90.0(0.759)
XY Isothermal Data with Uniform Distribution	2	137.5(0.657)	3.40	160.2(0.666)	140.3(0.667)	90.8(0.759)

<sup>a</sup>The peak temperatures in the first two cases do not represent the hottest plate or flow channel, while the last three 2 channel cases include a hot channel model.

for average data with four channels and one channel using the same perturbation data. Comparisons were then made with different feedback data for a two channel model with one channel representing the hottest channel and the other channel representing the remainder of the active core.

For the average channel comparisons, the single channel model gives results for peak power and energy release that are almost identical to those for the more detailed four channel model. This suggests that the radial dependence of the source and reactivity coefficient is not important, and that multi-channel models are not necessary for an accurate prediction of power and energy release.

The two channel model with a distributed reactivity coefficient gives results identical to the single (average) channel model for power and energy release. However, since the two channel model includes a model for the hot channel, the peak temperatures predicted are those for the hottest channel. The second two channel model used the overall RZ perturbation theory reactivity coefficient collapsed to form a uniform distribution. This model gave a slightly higher prediction for peak power, energy release, and hot channel temperatures. The non-uniform distribution appears to enhance the negative reactivity feedback in the more important central region, but in this case has only a slight effect on the peak values predicted. The uniform distribution model predicts higher estimates of the peak values and gives more conservative results. The third two-channel case represents the model used for the analysis of the benchmark cores. This model used a uniform axial distribution for the XY isothermal reactivity coefficient data computed in Section 3. The predicted values are slightly higher due to a smaller reactivity feedback coefficient than that obtained from perturbation theory.

As a further test, the third two-channel model was found to give identical results to that of a two-step method where an average channel power trace was first obtained with a single channel model, and then a second power driven transient run with hot channel factors to compute the peak temperatures.

The original PARET code had only a provision for a void/density reactivity coefficient, while the modified version allows for a separate representation of the coolant temperature component. The effects of the choice of feedback model are shown in Table 24. Neither the perturbation theory case with separate axial weighting factors nor the case with uniform isothermal data show any significant differences. It should be noted, however, that only density and temperature changes are included. The Doppler reactivity coefficient remained fixed for these cases.

The variation in results that can be expected from the choice of correlations and two-phase models has also been considered. These cases give significant differences in the peak cladding temperature and ONB predictions as shown in Table 25. With the original two-phase scheme, the ONB and fully developed subcooled nucleate boiling are predicted by the same correlation. The transition two-phase scheme uses the Bergles-Rohsenow (B-R) correlation for the detection of ONB (its intended use) with a choice of correlations for fully developed nucleate boiling. These results include the choice of Dittus-Boelter (D-B) and Seider-Tate (S-T) correlations for single phase flow and the Jens-Lottes (J-L) and the McAdams two-phase correlations. Results are also provided which include the voiding model option.

In comparing the original two-phase scheme with the transition model, the B-R cases give almost identical results as expected (the B-R correlation is used for both ONB and fully developed nucleate boiling). With both the J-L and the McAdams correlation, the original two-phase scheme

TABLE 24. Comparison of Reactivity Coefficient Models for \$1.50/0.5 s Fast Reactivity Insertion in HEU Benchmark Core

Model and Data	$\hat{P}(t_{m,s}), \text{ MW}$	$E_{t_m}, \text{ MWs}$	$\hat{T}(t,s), \text{ }^\circ\text{C}$		
			Fuel	Clad	Outlet
"Equivalent" Void Coeff. <sup>a</sup> Perturbation Data	133.2(0.656)	3.22	158.6(0.666)	139.7(0.667)	88.1(0.759)
Void and Temperature Coeff. <sup>b</sup> Pertrubation Data	130.7(0.656)	3.20	157.7(0.666)	139.4(0.667)	86.8(0.760)
"Equivalent" Void Coeff. <sup>c</sup> Isothermal Data	137.5(0.657)	3.40	160.2(0.666)	140.3(0.667)	90.8(0.759)
Void and Temperature Coeff. <sup>d</sup> Isothermal Data	134.0(0.656)	3.24	159.0(0.666)	139.8(0.668)	88.9(0.759)

<sup>a</sup>The "Equivalent" void coefficient with perturbation data is -0.6807 \$/% void.

<sup>b</sup>For perturbation data the void coefficient is -0.2992 \$/% void, and the coolant temperature coefficient is -0.01646 \$/°C.

<sup>c</sup>The "Equivalent" void coefficient with isothermal data is -0.6370 \$/% void.

<sup>d</sup>For isothermal data the void coefficient is -0.3257 \$/% void, and the coolant temperature coefficient is -0.01537 \$/°C.

TABLE 25. HEU  $\$1.50/0.5\%$  Benchmark Core with Various Correlations and Two-Phase Schemes

	D-B Single Phase			S-T Single Phase			
	Original 2 $\phi$ Scheme	Transition 2 $\phi$ Scheme		Original 2 $\phi$ Scheme	Transition 2 $\phi$ Scheme		
	No Void Model	No Void Model	Void Model	No Void Model	No Void Model	Void Model	
P-R 2 $\phi$ Correlation	P, MW( $t_m, s$ )	130.7(0.656)	130.7(0.656)	130.7(0.656)	129.0(0.656)	129.0(0.656)	129.0(0.656)
	$t_{ONB}, s$	0.6545	0.6545	0.6545	0.6565	0.6565	0.6565
	T <sub>fuel</sub> , °C( $t$ )	157.7(0.666)	157.0(0.664)	157.3(0.665)	156.5(0.666)	156.6(0.666)	156.8(0.665)
	T <sub>clad</sub> , °C( $t$ )	139.4(0.666)	138.2(0.666)	138.4(0.667)	138.9(0.668)	138.8(0.666)	139.6(0.666)
	$t_{no NB}, s$	0.7005	0.7045	0.7048	0.6955	0.7005	0.7002
	T <sub>outlet</sub> , °C( $t$ )	86.8(0.760)	87.3(0.760)	87.1(0.762)	85.8(0.762)	86.0(0.764)	84.2(0.770)
J-L 2 $\phi$ Correlation	P, MW( $t_m, s$ )	130.7(0.656)	130.7(0.656)	130.7(0.656)	129.0(0.656)	129.0(0.656)	129.0(0.656)
	$t_{ONB}, s$	0.6595	0.6545	0.6545	0.6615	0.6565	0.6565
	T <sub>fuel</sub> , °C( $t$ )	169.7(0.668)	166.6(0.668)	166.3(0.668)	167.9(0.668)	165.1(0.668)	164.5(0.668)
	T <sub>clad</sub> , °C( $t$ )	152.9(0.668)	149.4(0.670)	149.3(0.670)	152.2(0.670)	149.1(0.670)	148.9(0.670)
	$t_{no NB}, s$	0.6965	0.7185	0.7195	0.6925	0.7115	0.7103
	T <sub>outlet</sub> , °C( $t$ )	84.3(0.766)	85.2(0.764)	83.7(0.762)	83.4(0.770)	84.2(0.768)	82.0(0.774)
McAdams 2 $\phi$ Correlation	P, MW( $t_m, s$ )	130.7(0.656)	130.7(0.656)	130.7(0.656)	129.0(0.656)	129.0(0.656)	129.0(0.656)
	$t_{ONB}, s$	0.6615	0.6545	0.6545	0.6635	0.6565	0.6565
	T <sub>fuel</sub> , °C( $t$ )	175.1(0.670)	172.1(0.670)	171.6(0.670)	172.8(0.670)	169.9(0.670)	169.0(0.670)
	T <sub>clad</sub> , °C( $t$ )	159.7(0.670)	156.4(0.672)	156.2(0.671)	158.7(0.672)	155.5(0.672)	155.0(0.672)
	$t_{no NB}, s$	0.6965	0.7235	0.7228	0.6915	0.7155	0.7134
	T <sub>outlet</sub> , °C( $t$ )	83.2(0.770)	84.1(0.768)	83.1(0.770)	82.3(0.774)	83.1(0.772)	81.3(0.772)

predicts ONB at a later time, and subsequently higher peak temperatures are predicted for the fuel and clad. Conversely, the peak outlet temperatures are slightly higher for the transition model (without the voiding model), and a longer subcooled nucleate boiling interval is observed.

The S-T single-phase correlation gives a slightly higher heat transfer coefficient and predicts a slightly lower peak power than the D-B correlation. The ONB is delayed with S-T, but the peak temperatures are slightly lower. The results for this transient are not strongly influenced by the choice of single-phase heat transfer correlation.

The voiding model also has only a slight effect on this transient. Since the ONB occurs only at or after the peak power, voiding does not influence the peak power predicted. The voiding model, however, can have a strong influence on faster transients with an earlier ONB.

It should be pointed out that a slightly different version of the PARET code was used for the early modeling comparisons described in this Section (6.2) than was used for the specified benchmark calculations reported in Section 6.3. However, the trends that are shown and the conclusions drawn are unchanged. For example, the results for the HEU \$1.50/0.5s transient case with the S-T Single-Phase, Transition 2 $\phi$  Scheme, Void Model, and the McAdams 2 $\phi$  Correlation give peak fuel, clad, and coolant outlet temperatures of 169.0°C, 155.0°C, and 81.3°C, respectively, in Table 25 and corresponding values of 170.9°C, 155.9°C, and 83.8°C for the same transient in Table 29. The data shown in Section 6.3 should be used for final comparisons.

### 6.3 Results for Analysis of Benchmark Transients

The PARET code two-channel model, as described above, uses one channel to represent the hottest plate and flow channel and the other "average" channel to represent the remaining 550 fuel plates in a volume weighted sense. The axial source distribution was represented by 21 axial regions and a chopped cosine shape which had an axial power peaking factor of 1.5 for both the "average" channel and the hot channel. For the hot channel, this axial distribution was multiplied by the other specified hot channel factors (1.4 Nuclear x 1.2 Engineering = 1.68). The 1.2 overpower factor was not included in the reactivity insertion transients. For the moderator heat source description, the assumption was made that 4.5% of the total energy is deposited directly in the moderator. This direct heating of the moderator by gamma radiation has only a small effect on the estimates for peak power and temperatures. A linear approximation was used for all of the reactivity feedback coefficients. The Bergles-Rohsenow correlation was selected for detecting onset of nucleate boiling, the transition model with the McAdams correlation was included for fully developed two-phase flow, and the Seider-Tate correlation was used for the single-phase forced convection regime.

#### 6.3.1 Fast Loss-of-Flow Transients

Figure 11 shows the relative power and flow and the resulting peak temperatures at the fuel centerline, clad surface, and coolant outlet for the exponential loss-of-flow transient with a time constant of 1.0 s in the HEU and LEU cores. This loss-of-flow transient is characterized quantitatively in Table 26. The flow coast-down was initiated after 1.0 s at a power of 12 MW. Thus, a 1.2 overpower factor was included. The fast loss-of-flow transients for both the HEU and LEU cores show a peak in the fuel and clad temperatures after about 1.4 seconds. The peak temperatures at the fuel center-

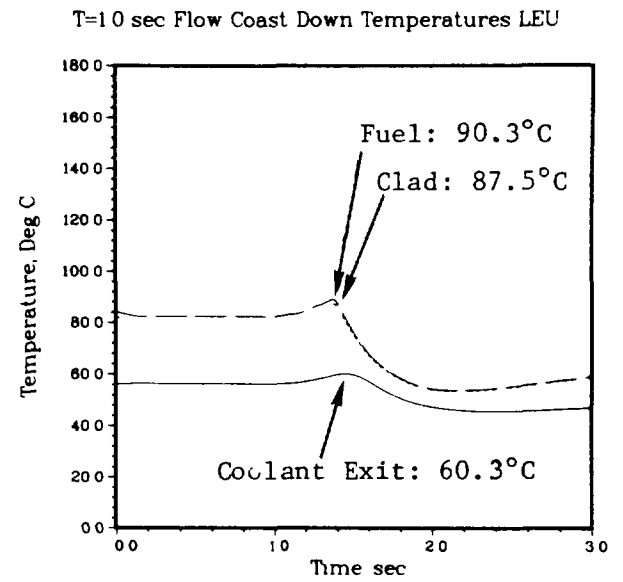
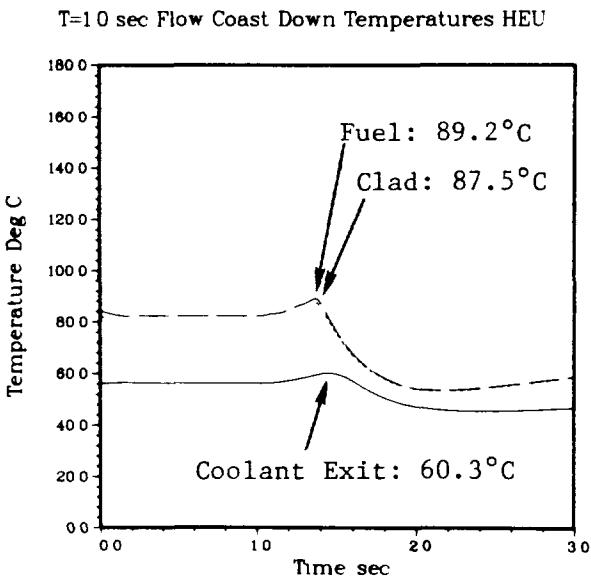
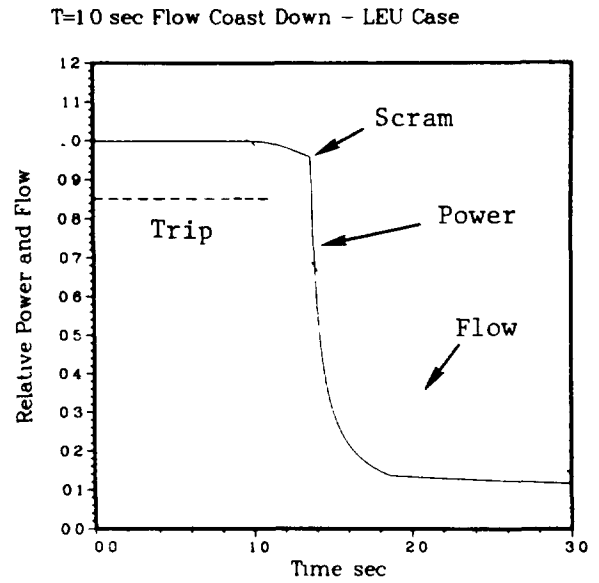
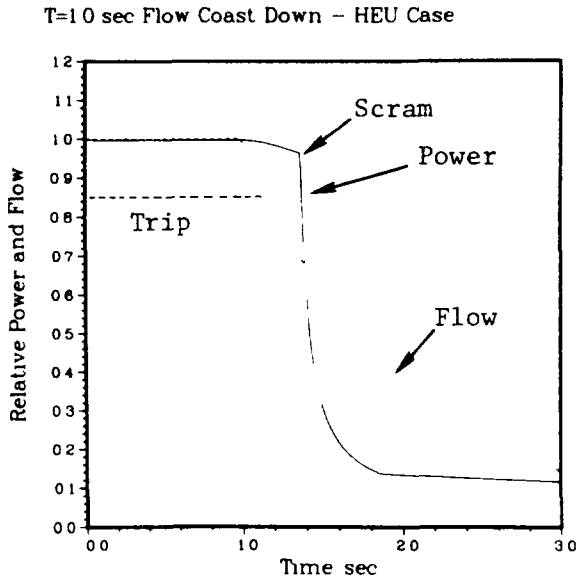


Fig. 11. Transient Responses of HEU and LEU Benchmark Cores to a Loss-of-Coolant Flow with a Decay Time of 1.0 sec, a Scram Trip at 85% Flow and a 200 ms Delay.

TABLE 26. Tabulated Results for Transient Response of HEU and LEU Benchmark Cores to a Loss-of-Coolant Flow with a Decay Time of 1.0 s, a Scram Trip at 85% Flow, and a 200 ms Delay

Trip Time at 85% of Nominal Flow		1.16 s	
		<u>T, °C (t, s)</u>	
<u>"Peak Temperatures"</u>	<u>HEU</u>	<u>LEU</u>	
Fuel Center Line	89.2 (0.371)	90.3 (0.371)	
Clad Surface	87.5 (0.376)	87.5 (0.371)	
Coolant Outlet	60.3 (0.451)	60.3 (0.446)	
<u>At 2.9 s (15% Nominal Flow)</u>		<u>T, °C</u>	
	<u>HEU</u>	<u>LEU</u>	
Fuel Center Line	58.3	58.5	
Clad Surface	58.1	58.2	
Coolant Outlet	46.6	46.5	

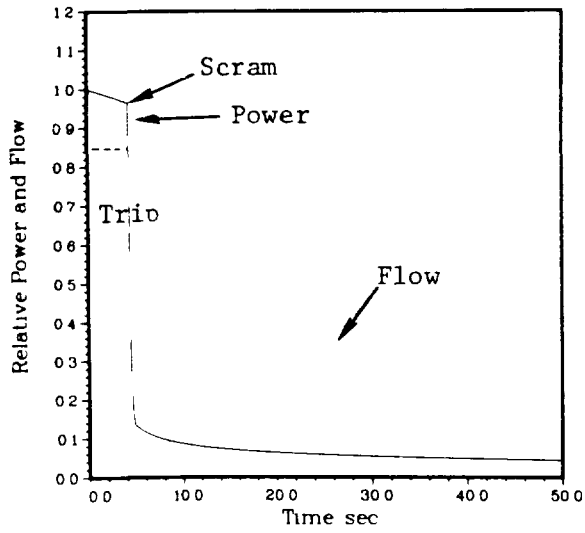
line, clad surface, and coolant exit were 89.2°C, 87.5°C, and 60.3°C, respectively in the HEU core. In the LEU core, the corresponding peak temperatures were 90.3°C, 87.5°C, and 60.3°C, respectively.

The transient was terminated at 15% of nominal flow. Realistically, the flow would be expected to reverse direction and establish a natural convection flow rate which should be adequate to cool the core. It should also be noted that at low flow rates the peak temperature in the coolant may occur upstream from the outlet (the heated slug has not yet reached the outlet). The LEU fuel temperature is slightly higher due to the lower thermal conductivity of the fuel meat, but the coolant temperatures for the LEU and HEU cases are virtually the same.

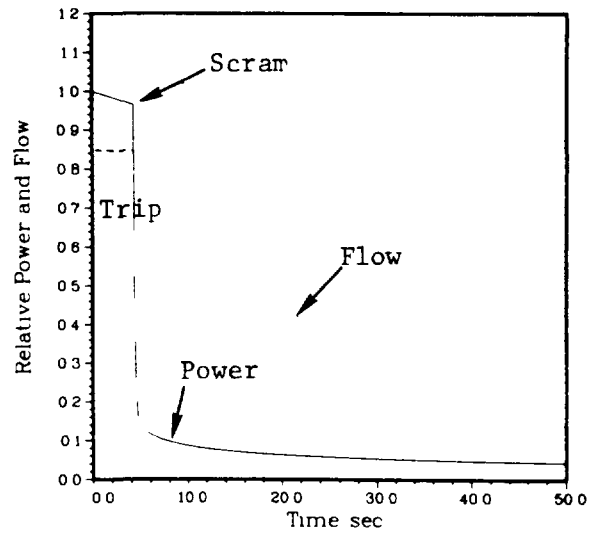
### 6.3.2 Slow Loss-of-Flow Transients

The results for the slow loss-of-flow transients are shown in Fig. 12 and in Table 27. The calculations were performed in the same manner as for the fast loss-of-flow transient, but with a time constant of 25.0 s. The peak temperatures at the fuel centerline, clad surface, and coolant exit were 85.8°C, 83.9°C, and 58.9°C in the HEU core. In the LEU core, the corresponding peak temperatures were 86.8°C, 83.7°C, and 58.8°C, respectively.

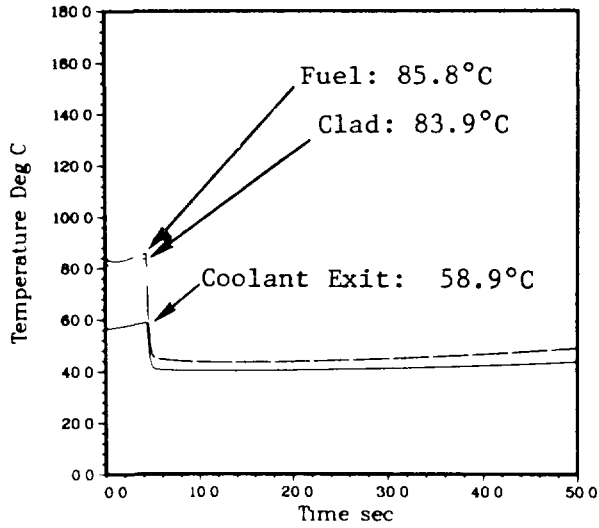
T=250 sec Flow Coast Down - HEU Case



T=250 sec Flow Coast Down - LEU Case



T=250 sec Flow Coast Down Temperatures HEU



T=250 sec Flow Coast Down Temperatures LEU

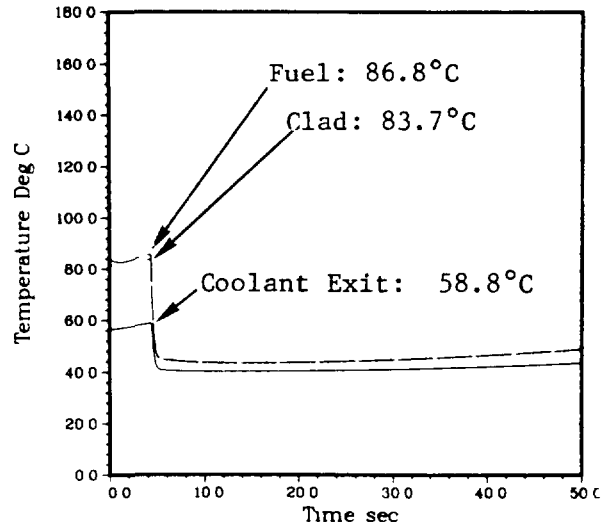


Fig. 12. Transient Responses of HEU and LEU Benchmark Cores to a Loss-of-Coolant Flow with a Decay Time of 25.0 sec, a Scram Trip at 85% and a 200 ms Delay.

TABLE 27. Tabulated Results for Transient Response of HEU and LEU Benchmark Cores to a Loss-of-Coolant Flow with a Decay Time of 25.0 s, a Scram Trip at 85% Flow, and a 200 ms Delay

Trip Time at 85% of Nominal Flow		5.08 s	
		<u>T, °C (t, s)</u>	
<u>"Peak Temperatures"</u>	<u>HEU</u>	<u>LEU</u>	
Fuel Center Line	85.8 (4.29)	86.8 (4.29)	
Clad Surface	83.9 (4.29)	83.7 (4.29)	
Coolant Outlet	58.9 (4.29)	58.8 (4.29)	
<u>At 48.0 s (15% Nominal Flow)</u>		<u>T, °C</u>	
	<u>HEU</u>	<u>LEU</u>	
Fuel Center Line	48.3	48.4	
Clad Surface	48.2	48.3	
Coolant Outlet	43.3	43.3	

### 6.3.3 Slow Reactivity Insertion Transients

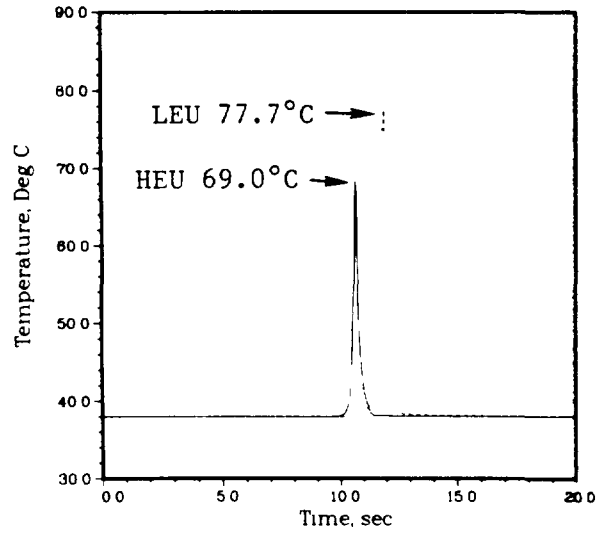
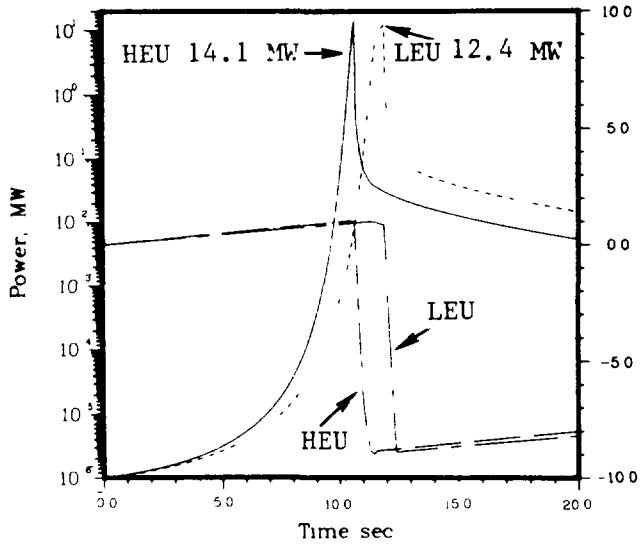
The slow reactivity insertion results are provided in Fig. 13 and Table 28. The faster HEU transient rises quickly to the 12 MW reactor trip setting and shows a sharp narrow power burst. The peak power is 14.1 MW. The slower LEU case shows a stronger prompt feedback from the Doppler component. The result is a much broader burst, and even though the peak power just exceeds the 12 MW trip point (12.4 MW) the energy released is larger for the LEU core. As a consequence, the peak temperature at the clad surface reached 77.7°C in the LEU core and 69.0°C in the HEU core. The peak temperatures are well below any critical values, and no boiling occurred in either case.

### 6.3.4 Fast Reactivity Insertion Transients

Figure 14 and Table 29 show the results for the fast reactivity insertion transients. The HEU and LEU cores with a  $\beta$ 1.50/0.5 s ramp have very similar behaviors. Since the LEU core has a shorter prompt neutron generation time and thus a smaller minimum period, the peak power is reached slightly earlier. The power burst for the LEU core is slightly narrower than for the HEU case, and even though the peak power is slightly higher for LEU core the energy release is lower. The peak temperature at the fuel centerline is about 13°C higher for the LEU core, largely due to the smaller thermal conductivity of the fuel meat. The clad surface temperature is about 1°C higher for the LEU core, and the maximum coolant outlet temperature is about 2°C lower for the LEU core. A brief period of localized nucleate boiling is predicted for the hot channel in both cores.

0.10 Dollars/sec HEU - 0.09 Dollars/sec LEU

Clad Temperature For HEU and LEU Cases



Coolant Outlet Temperature - HEU and LEU

Fuel Center Line Temperature - HEU and LEU

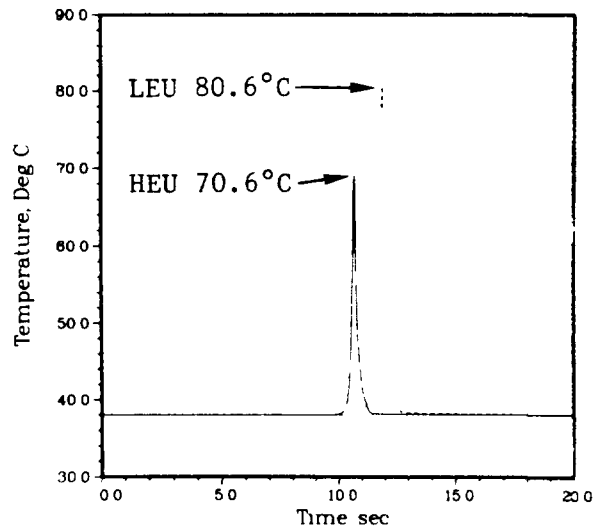
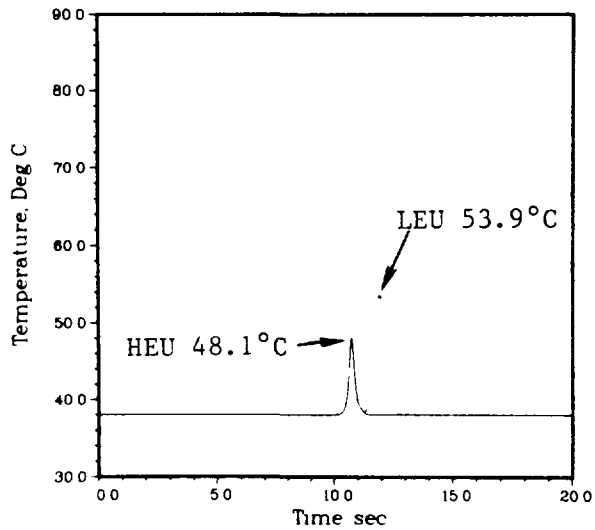


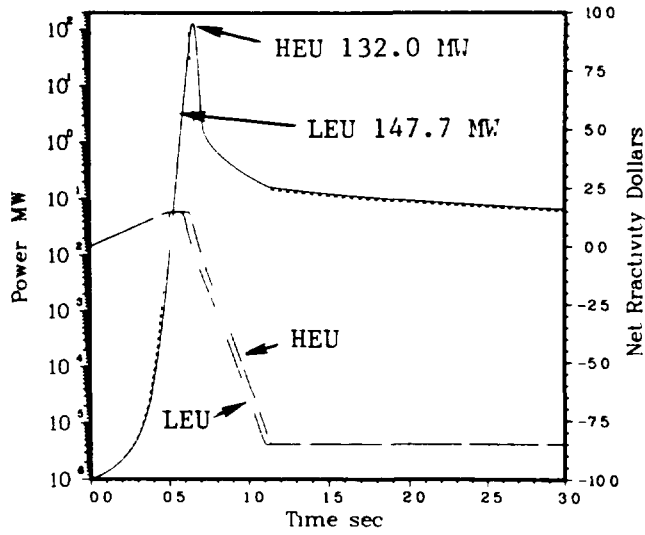
Fig. 13. Transient Responses of Benchmark Cores to Reactivity Insertions of  $0.1/\text{sec}$  for HEU and  $0.09/\text{sec}$  for LEU with an Overpower Scram Trip at 12 MW and a 25 ms Delay.

TABLE 28. Tabulated Results for Slow Reactivity Insertion Transients in HEU and LEU Benchmark Cores

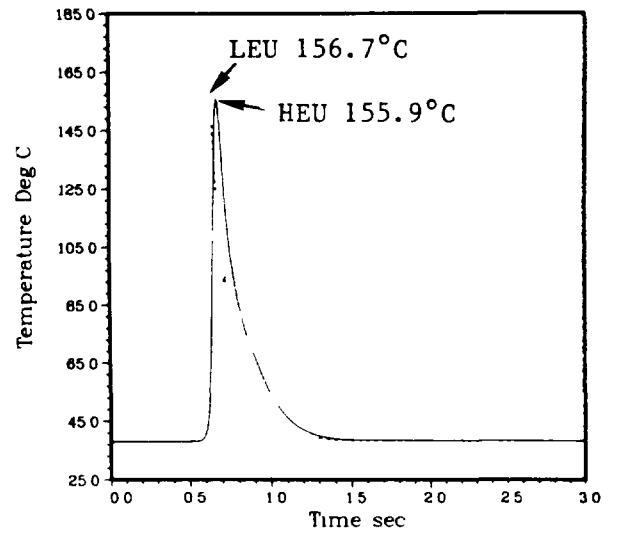
Ramp	HEU	LEU
	$\$0.10/s$	$\$0.09/s$
Trip Time @ 12 MW, s	10.62	11.87
Min. Period, s	0.10	0.11
$\hat{P}(t_m)$ , MW	14.1 (10.64)	12.4 (11.89)
$\hat{T}_{\text{fuel}}(t)$ , °C	70.6 (10.66)	80.6 (11.90)
$\hat{T}_{\text{clad}}(t)$ , °C	69.0 (10.66)	77.7 (11.90)
$\hat{T}_{\text{outlet}}(t)$ , °C	48.1 (10.74)	53.9 (11.93)
$E_{\text{trip}}$ , MJ	1.370	4.239
$E_{t_m}$ , MJ	1.743	4.549
<u>20.0 s</u>		
P, MW	0.0054	0.0146
E, MJ	2.288	5.299
All T, °C	38.0	

$t_m$  = time to peak power;  $E_{t_m}$  = energy release to time of peak power.

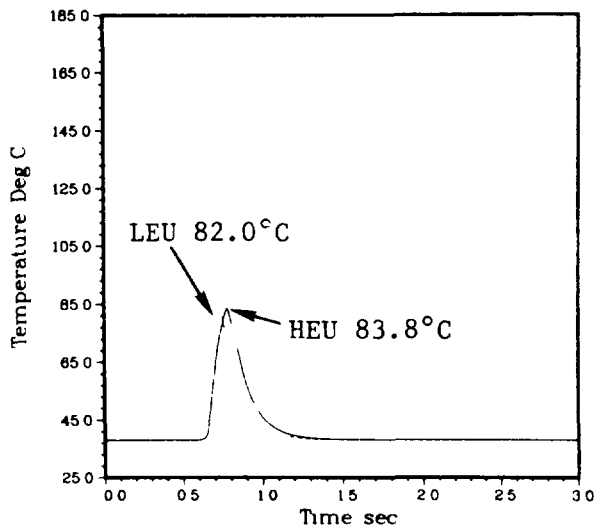
150 Dollars/0.5 sec HEU - 150 Dollars/0.5 sec LEU



Clad Temperature For HEU and LEU Cases



Coolant Outlet Temperature - HEU and LEU



Fuel Center Line Temperature - HEU and LEU

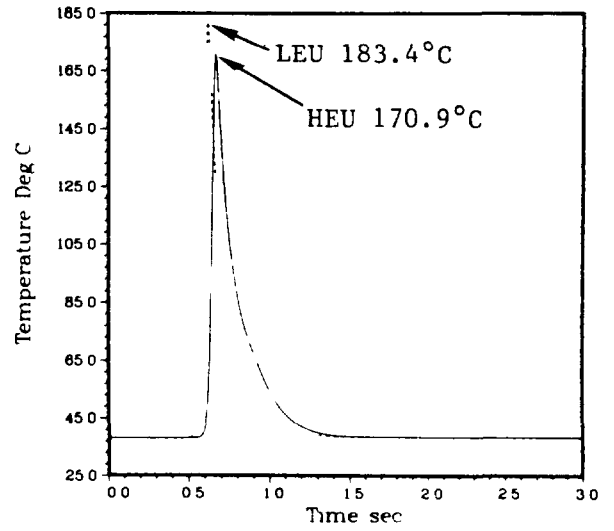


Fig. 14. Transient Responses of HEU and LEU Benchmark Cores to a Reactivity Insertion of  $\$1.50/0.5$  s with an Overpower Scram Trip at 12 MW and a 25 ms Delay.

TABLE 29. Tabulated Results for Fast Reactivity Insertion Transients in HEU and LEU Benchmark Cores

Ramp	HEU	LEU	
	\$1.50/ 0.5 s	\$1.50/ 0.5 s	\$1.35/ 0.5 s
Trip Time @ 12 MW, s	0.609	0.573	0.656
Min. Period, ms	15	12	17
$\hat{P}(t_m)$ , MW	132.0 (0.660)	147.7 (0.613)	63.2 (0.693)
$E_{t_m}$ , MJ	3.26	2.95	1.54
$\hat{T}_{fuel}(t, s)$ , °C	170.9 (0.670)	183.4 (0.626)	114.8 (0.714)
$\hat{T}_{clad}(t, s)$ , °C	155.9 (0.672)	156.7 (0.628)	108.0 (0.717)
$\hat{T}_{outlet}(t, s)$ , °C	83.8 (0.780)	82.0 (0.735)	58.2 (0.826)

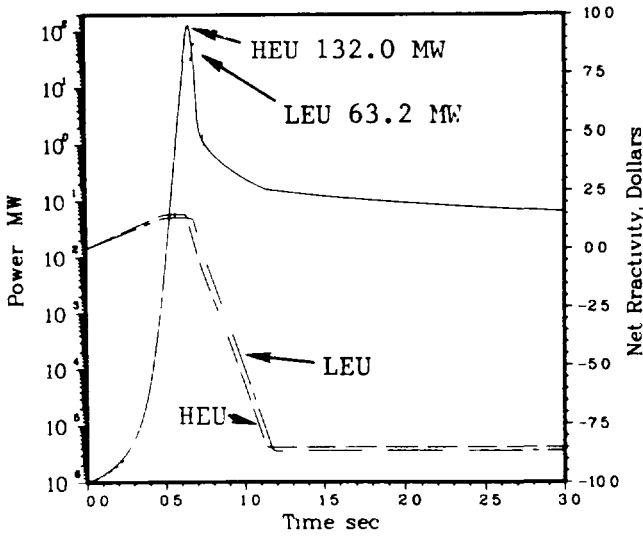
A comparison (Fig. 15 and Table 29) was also made between the HEU core with a reactivity insertion of \$1.5/0.5 s and the LEU core with a \$1.35/0.5 s insertion since absorber worths are generally lower in the LEU core due to its harder neutron spectrum. The LEU core with a \$1.35/0.5 s ramp shows a characteristically slower rise to the peak values. The peak power and the energy released to the time of peak power are less than half the values reached in the HEU core with a \$1.50/0.5 s ramp, and the peak temperatures are correspondingly lower. No boiling is predicted for this LEU case.

For completeness, the HEU core was also run with the \$1.35/0.5 s ramp. These HEU and LEU results are compared in Fig. 16 and Table 30. The behavior is very similar to the \$1.50/0.5 s transients. Nucleate boiling is not predicted for either of these cases.

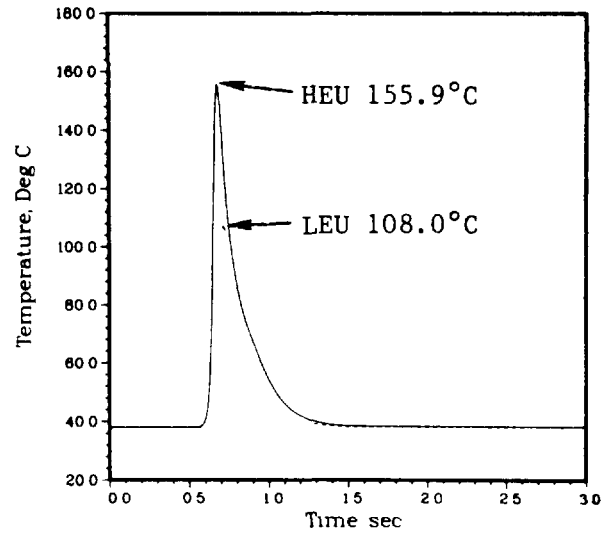
### 6.3.5 Comments on Results

The prompt Doppler feedback from the LEU fuel does not play a strong role in the fast transients, and the LEU and HEU burst shapes are quite similar. The rate of increase in power is primarily determined by the reactivity insertion rate with only slight secondary differences due to the prompt neutron generation time. The rate of decrease after scram is likewise determined by the worth and rate at which the rods are inserted. The Doppler feedback for slow reactivity insertion transients, however, can be a significant factor in determining the shape and peak power in the LEU core. The HEU core with \$0.10/s ramp insertion shows a shape similar to the fast transients, while the shape before scram for the \$0.09/s insertion in the LEU core indicates that this transient is already limited by the feedback reactivity.

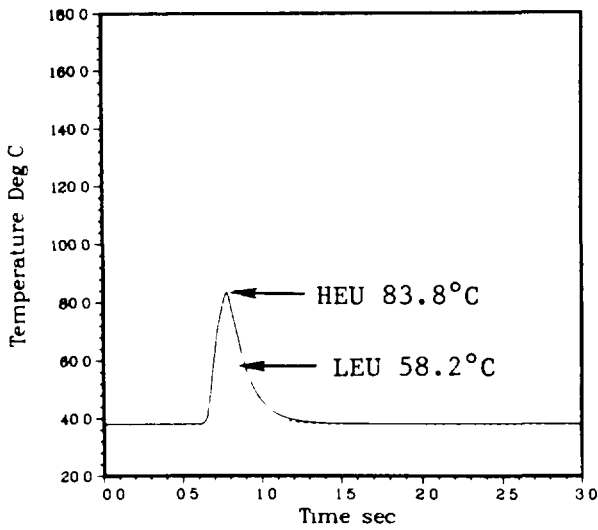
150 Dollars/0.5 sec HEU - 135 Dollars/0.5 sec LEU



Clad Temperature For HEU and LEU Cases



Coolant Outlet Temperature - HEU and LEU



Fuel Center Line Temperature - HEU and LEU

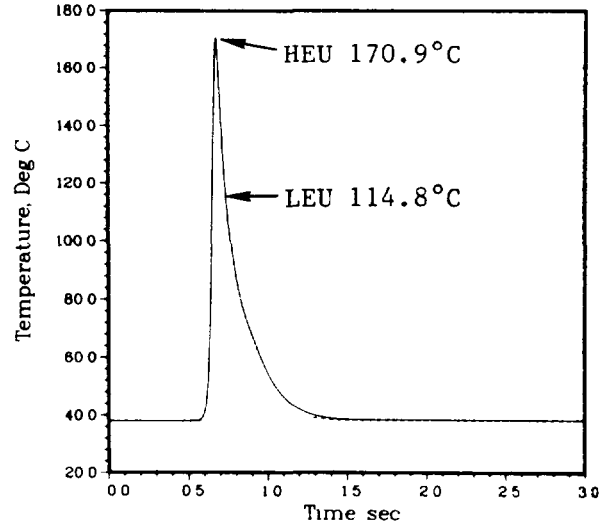
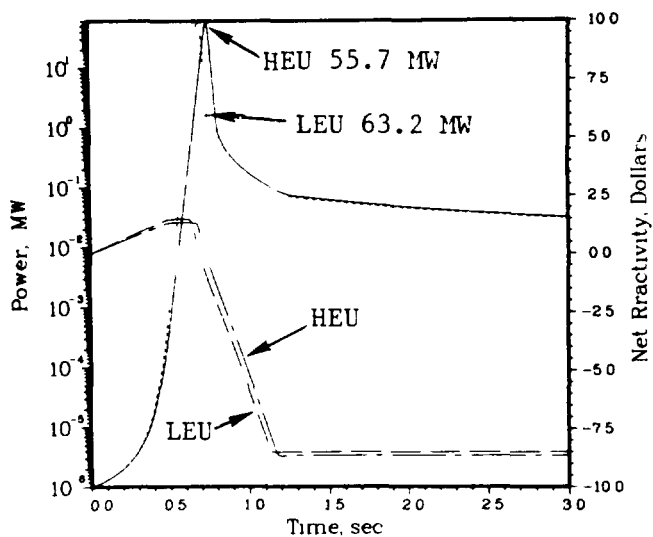
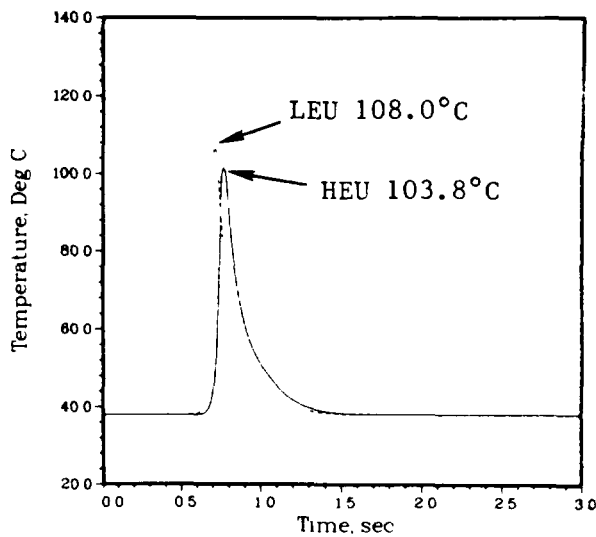


Fig. 15. Transient Responses of Benchmark Cores to Reactivity Insertions of \$1.50/0.5 s for HEU and \$1.35/0.5 s for LEU with an Overpower Scram Trip at 12 MW and a 25 ms Delay.

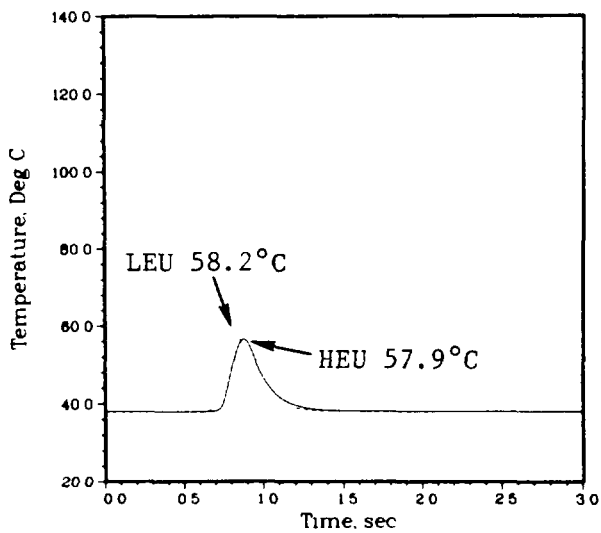
135 Dollars/0.5 sec HEU - 135 Dollars/0.5 sec LEU



Clad Temperature For HEU and LEU Cases



Coolant Outlet Temperature - HEU and LEU



Fuel Center Line Temperature - HEU and LEU

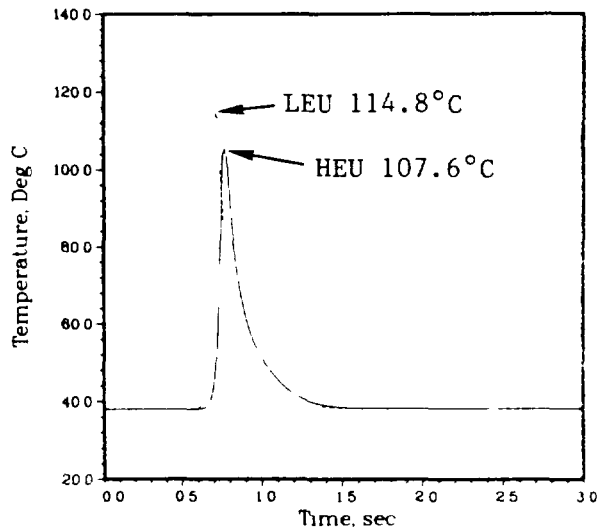


Fig. 16. Transient Responses of HEU and LEU Benchmark Cores to a Reactivity Insertion of  $\$1.35/0.5$  s with an Overpower Scram Trip at 12 MW and a 25 ms Delay.

TABLE 30. Tabulated Results—Comparison of Fast Reactivity Insertion Transients at \$1.35/0.5 s in HEU and LEU Benchmark Cores

	<u>HEU</u>	<u>LEU</u>
Trip Time @12MW, s	0.707	0.656
Min. Period, ms	20	17
$\hat{P}(t_m)$ , MW	55.7 (0.747)	63.2 (0.693)
$E_{t_m}$ , MJ	1.58	1.54
$\hat{T}_{\text{Fuel}}(t,s)$ , °C	107.6 (0.772)	114.8 (0.714)
$\hat{T}_{\text{Clad}}(t,s)$ , °C	103.8 (0.774)	108.0 (0.717)
$\hat{T}_{\text{Outlet}}(t,s)$ , °C	57.9 (0.880)	58.2 (0.826)

It should also be noted that these results do not include the effect of the lower control rod worths predicted for the LEU core in Section 5, but the differences in control rod worths for scram in the HEU and LEU cores are not expected to significantly change the results of this study.

These results are also influenced by the methods, models, and correlations used for the computations, as noted in Section 6.2. The fast transient results are probably most strongly influenced by the choice of models and correlations chosen for the predicted two-phase regime. The use of other choices of correlations for these cases would suggest peak clad temperatures 15–20°C lower than those predicted. The correlation chosen gives more conservative estimates for the peak clad temperature, and the hot channel peaking factors already include conservatism for uncertainties. The estimated peak cladding temperatures are all well below the melting point of the clad, and no film boiling is predicted.

#### 6.4 Sensitivity of Results to Variations in Kinetics Parameters and Thermal Conductivity

In this section, the influence of variations in some of the kinetics and thermal parameters is considered. The thermal properties of the HEU fuel are considered to be well established, and variations are considered only in the thermal conductivity of the LEU fuel. The kinetics parameter variations are limited to the prompt neutron generation time ( $\Lambda$ ), the effective delayed neutron fraction ( $\beta$ ), and the moderator reactivity feedback coefficients. Again, the \$1.50/0.5 s transient for the benchmark cores is used as a base case.

The results of changing the thermal conductivity of the LEU fuel from the benchmark specification of 0.5 W/cmK to a maximum value of 1.50 W/cmK in steps of 0.25 W/cmK are shown in Table 31. The largest change, as expected,

occurs in the peak fuel temperature, and the smallest change is noted in the peak clad temperature. The energy release to the time of peak power (not shown) was virtually unchanged over this range. The differential change decreases as the conductivity is increased. Any uncertainties in the thermal conductivity would not have a significant impact on the LEU benchmark results.

Variations in the kinetics parameters  $\Lambda$  and  $\beta$  were assessed by changing the base values (Section 2) by 10% in the HEU benchmark core. This degree of change should not be taken as a reflection of the expected uncertainty in these parameters. The results of these changes are shown in Table 32. It can be noted that for super prompt critical insertions the inverse period is approximately  $(\rho-1)\beta/\Lambda$ , where  $\rho$  is the reactivity insertion in dollars. Thus, increasing  $\beta$  is approximately equivalent to decreasing  $\Lambda$  by the same amount. This approximate equivalence is confirmed in Table 32. These changes in  $\Lambda$  (or  $\beta$ ) might also be interpreted as variations in the reactivity insertion rate. The largest changes are reflected in the peak power and energy release values. A decrease in  $\Lambda$  (or increase in reactivity insertion) results in a much larger increase in the peak power than a corresponding increase in  $\Lambda$  produces.

Table 31. Changes with the Thermal Conductivity of the LEU Benchmark Fuel for the \$1.50/0.5s Insertion

Thermal Conductivity, W/cmK	Relative Changes, %*			
	$\hat{P}$	$\hat{T}_{Fuel}$	$\hat{T}_{Clad}$	$\hat{T}_{outlet}$
0.75	+0.63	-3.1	+0.14	+0.44
1.00	+0.96	-4.7	+0.22	+0.68
1.25	+1.17	-5.7	+0.26	+0.82
1.50	+1.30	-6.3	+0.29	+0.91

\*Base case with thermal conductivity of 0.50 W/cmK

Table 32. Changes with the Prompt Neutron Generation Time (and Effective Delayed Neutron Fraction) in the HEU Benchmark \$1.50/0.5s Insertion

Parameter	Relative Changes, %				
	$\hat{P}$	$E_{tm}$	$\hat{T}_{Fuel}$	$\hat{T}_{Clad}$	$\hat{T}_{outlet}$
$\Lambda + 10\%$	-19.0	-11.3	-5.1	-2.2	-10.3
$\Lambda - 10\%$	+27.8	+21.2	+6.6	+2.7	+13.3
$\beta + 10\%$	+24.3	+19.1	+5.7	+2.4	+11.6

The results of changing the moderator reactivity feedback by  $\pm 10\%$  for the HEU benchmark core are shown in Table 33. These changes produce a much smaller effect than that produced by corresponding changes in  $\Lambda$ . Again the changes introduced do not necessarily represent the expected uncertainty in the reactivity coefficients, but the choice is useful for comparisons. This degree of uncertainty, however, is probably not unreasonable in these coefficients.

Table 33. Changes with the Moderator Reactivity Feedback in the HEU Benchmark \$1.50/0.5s Insertion

Feedback Coeff. Change, %	Relative Changes, %				
	$\hat{P}$	$E_{tm}$	$\hat{T}_{Fuel}$	$\hat{T}_{Clad}$	$\hat{T}_{outlet}$
+ 10%	-1.4	-1.2	-0.43	-0.19	-1.3
- 10%	+1.4	+4.2	+0.44	+0.19	+1.4

### 6.5 Self-Limited Transients

Although the transients specified for the benchmark cores do not include self-limiting cases, it is of interest to consider cases where the specified scram is removed.

Table 34 provides a comparison of both the HEU and LEU benchmark cores for both protected and unprotected transients of \$1.50/0.5 s. This table also provides a comparison of some of the reactivity feedback coefficients and parameters for the HEU and LEU cases. Uniform (isothermal) coefficients with a uniform weighting were assumed. The prompt neutron generation time,  $\Lambda$ , and the Doppler coefficient show the largest changes with enrichment, and these differences are largely responsible for the observed differences in the transient results.

In the cases with scram, the influence of the larger Doppler coefficient for the LEU core is overshadowed by the negative reactivity from the insertion of control rods. The shorter  $\Lambda$  for the LEU core produces a smaller initial period and a faster rise in power. Consequently, the LEU case with scram shows a slightly higher peak power than the HEU case. However, the peak temperatures reached at the clad surface are very similar in both cases.

In the unprotected (self-limited) transients, the strong influence of the large Doppler feedback in the LEU core is quite apparent. All of the values recorded are substantially lower for this LEU case. The larger void/density coefficient with LEU also contributes to the differences noted. The prompt Doppler feedback in the LEU case dominates during the early stages of the transient. The maximum clad surface temperature in all cases is substantially below the melting point of 582°C for 6061 alloy. The LEU case shows a margin to melting of about 320°C, while the HEU peak clad temperature is about 275°C below the melting point.

TABLE 34. Self-Limited Transients: \$1.50/0.5 s Cases  
With and Without Scram for HEU and LEU Cores

Case	Period, ms	$\hat{P}$ , MW ( $t_m$ , s)	$E_{t_m}$ , MWh	$\hat{T}_{clad}$ , °C		
				at $t_m$	Max. (t, s)	
HEU	With Specified Scram	14.5	132 (0.656)	3.26	131	156 (0.672)
	Self-limited	14.5	371 (0.667)	7.30	220	308 (0.685)
LEU	With Specified Scram	11.9	148 (0.613)	2.95	126	157 (0.628)
	Self-limited	11.9	283 (0.622)	5.56	181	263 (0.642)

Reactivity Coefficients and Parameters

	$\lambda$ , $\mu$ s	$\beta_{eff}$	Coolant Temperature \$/°C	Void/density, \$/% Void	Doppler, \$/°C
HEU	55.96	7.607-3	1.537-2	0.3257	3.6-5
LEU	43.74	7.275-3	1.082-2	0.4047	3.31-3

Thermal Properties of Fuel Meat and Clad

	Thermal Conductivity, W/cmK		Specific Heat, J/gK	
	<u>Fuel Meat</u>	<u>Clad</u>	<u>Fuel Meat</u>	<u>Clad</u>
HEU	1.58	1.80	0.728	0.892
LEU	0.50	1.80	0.340	0.892

6.6 Clad Temperature Limitations Compared with  
SPERT I Experiments

The PARET code has also been used to determine the reactivity insertion limits imposed by the clad melting temperature. A comparison of the characteristics and parameters for the HEU benchmark core and for two SPERT I cores (B-24/32 and D-12/25) are shown in Table 35. All of the results described in this section are taken directly from Ref. 7.

The PARET options and parameters are identical to those derived from the SPERT I comparisons in Ref. 7. These include the S-T correlation for single-phase, the transition model with the B-R correlation for ONB, the McAdams correlation for fully developed two-phase, the original Tong correlation for departure from nucleate boiling, and the voiding model option. Based on the favorable results from the SPERT I comparisons, this model should give reasonable estimates for the peak clad temperature for the benchmark cores. The clad melting temperature is taken as 582°C for 6061 alloy.

TABLE 35. A Comparison of the Characteristics and Parameters of the HEU Benchmark Core and Two SPERT I Cores

Parameter	SPERT I Cores		HEU Benchmark Core
	B-24/32	D-12/25	
Plates/Fuel Element, Std. (Contl.)	24	12(6)	23(17)
Number of Standard Fuel Elements	32	20	21
Number of Contro Fuel Elements	0	5	4
Fuel Meat Thickness, mm	0.51	0.51	0.51
Clad Thickness, mm	0.51	0.51	0.38
Water Channel Thickness, mm	1.65	4.55	2.23
$^{235}\text{U}/\text{plate}$ , g	7.0	14.0	12.2
Temperature (spectrum)* Coeff., $\$/^\circ\text{C}$	-2.528-2	-2.801-2	-1.537-2
Void Coefficient, $\$/\%$ Void	-0.3571	-0.4214	-0.3257
Neutron Generation Time, $\mu\text{s}$	50.0	60.0	56.0
$\beta_{\text{eff}}$	0.007	0.007	0.0076
Peak/Ave. Power in Core	2.5	2.4	2.52

\*Doppler Coefficient is negligible for all cases.

For the HEU benchmark core, a step insertion of  $\sim \$2.35$  is the limiting case, i.e. for step reactivity insertions larger than this limit the peak surface temperature of the clad is predicted to exceed the clad melting temperature. The results from the  $\$2.35$  step at the time of peak power are compared with results obtained for the SPERT I D-12/25 core in Fig. 17. The D-12/25 core included destructive tests which indicated extensive plate melting for inverse periods greater than  $\sim 166\text{s}^{-1}$  ( $\sim \$2.36$  insertion). The agreement with experiment is remarkably good even though the two cores have somewhat different characteristics. This similarity of behavior was also noted in the diversity of cores considered in the SPERT I series of experiments (Ref. 8). The damage line indicated in Fig. 17 ( $\sim 140\text{s}^{-1}$ ) shows the threshold for clad damage from thermal stress. The PARET code does not have the capability of assessing any damages from thermal stress, but the threshold for clad melting can serve as a useful indicator for the limits on reactivity insertions.

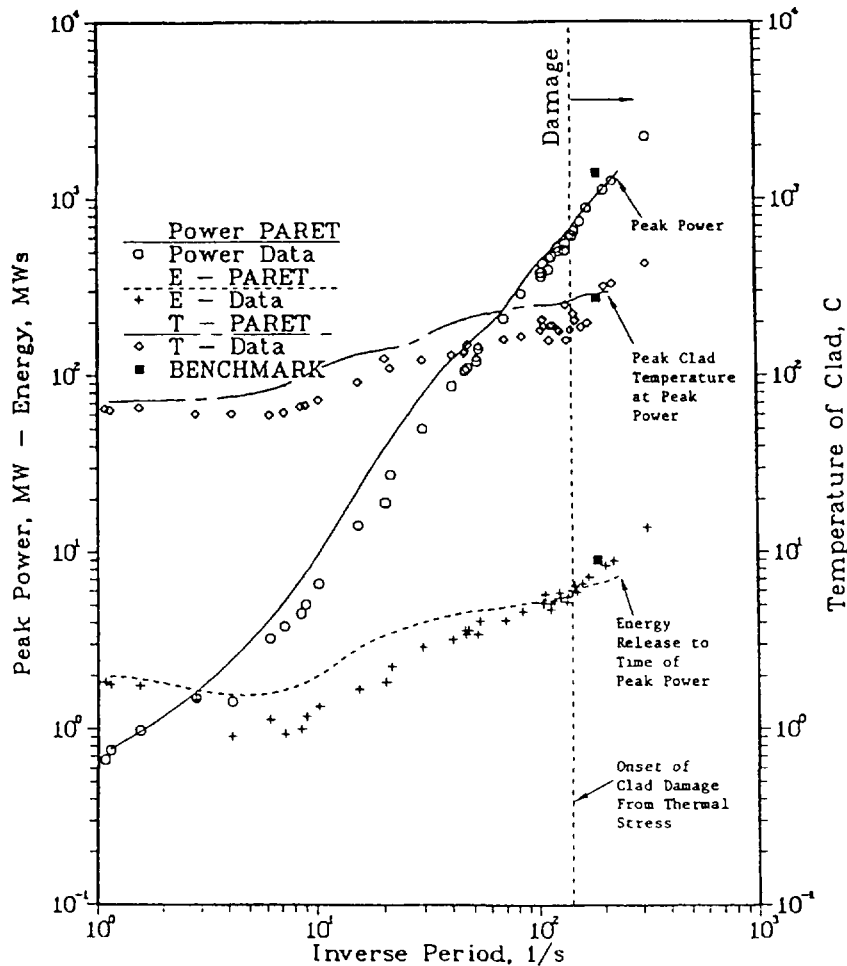


Fig. 17. Comparison of PARET Calculations with Measurements in the SPERT I D-12/25 Core.

The results for the SPERT I B-24/32 core are provided in Fig. 18. Although this core did not include destructive tests, the HEU benchmark core limiting case is included for comparison purposes. An extrapolation of the data for the B-24/32 core would suggest that the benchmark core would also agree well with this SPERT I data.

Figure 19 provides a comparison of the HEU and LEU benchmark cores showing the clad melting threshold for reactivity insertions over a range of ramp durations (from a step to 0.75 s). The areas above the curves indicate where clad melting would be expected. Also shown in this figure is the corresponding maximum net reactivity inserted (the difference between the external reactivity inserted and the reactivity from feedback). This maximum generally occurs at the same time in the transient as the minimum period.

While the two curves in Fig. 19 for HEU and LEU fuel show some similarities, they also show substantial differences. The LEU core can clearly tolerate a larger reactivity insertion before clad melting than the HEU core. The maximum step insertion is  $\sim 2.80$  for the LEU core compared to  $\sim 2.35$  for the HEU core. Both curves show the same general shape. The ramp insertions of short duration are equivalent to a step insertion. The entire ramp is inserted before the power, temperatures, and feedback have increased substan-

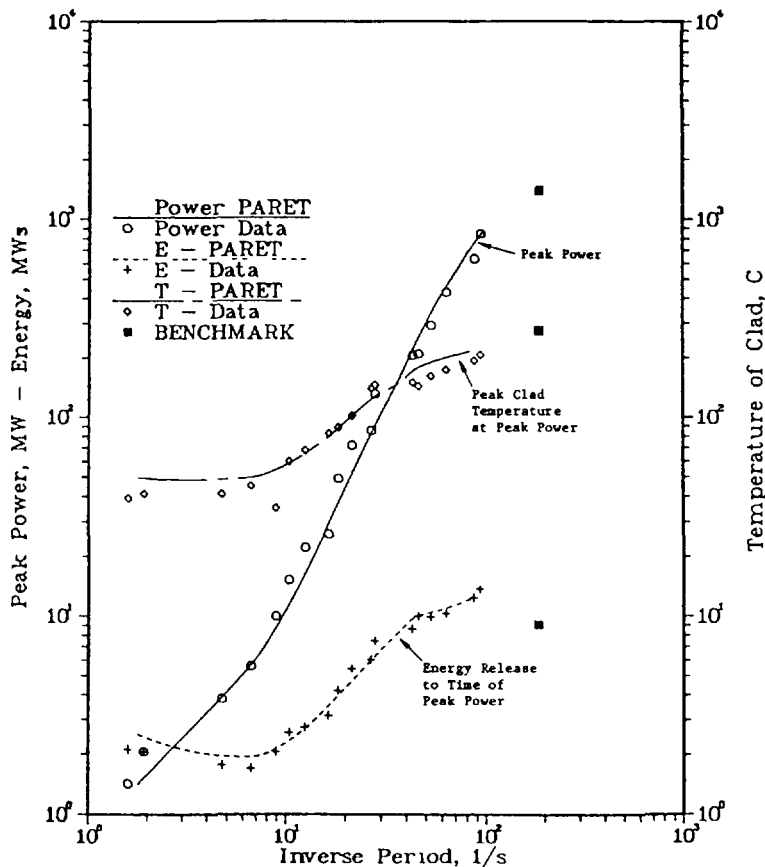


Fig. 18. Comparison of PARET Calculations with Measurements in the SPERT I B-24/32 Core.

tially, and the limiting reactivity insertion remains constant. For ramps of longer duration, the feedback reactivity limits the net reactivity and turns over the transient before the maximum of the ramp is reached. A limiting ramp rate (constant slope) is reached, and a constant maximum net reactivity is observed for each case. The limiting ramp rate for the LEU core,  $\sim 14.8$   $\$/s$ , is more than double that for the HEU core,  $\sim 6.4$   $\$/s$ . The LEU core also shows an earlier transition from the limiting step portion of the curve to the limiting ramp rate range.

Table 36 shows the limiting cases for the LEU core with a 0.5 s ramp as the Doppler and the larger void coefficient are eliminated to approximate the HEU case. The Doppler contributes about 2/3 of the difference noted between the LEU and the HEU limits, the larger void coefficient contributes another 28% of the difference, and the remaining 5% difference can be attributed to other unresolved differences such as the prompt neutron generation time, for example. The benefits of a prompt Doppler coefficient with LEU fuel are clearly demonstrated by these results.

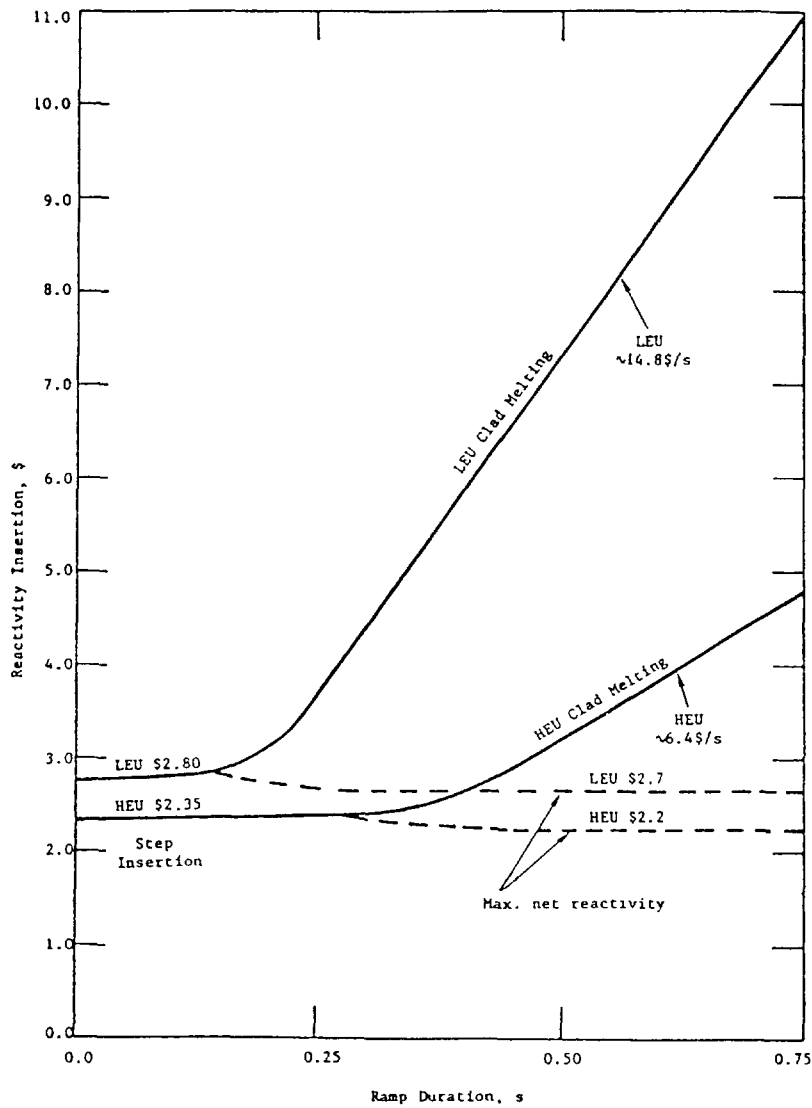


Fig. 19. Reactivity Insertion Limits for Clad Melting in the HEU and LEU Benchmark Cores.

TABLE 36. Feedback Components with 0.5 s Limiting Ramp

Case	Limiting Ramp, \$	Relative Change (% of Total)
LEU Base	7.40	-
LEU without Doppler	4.60	-2.80 (67)
LEU without Doppler and with HEU void Coefficient	3.40	-4.00 (95)
HEU	3.20	4.20 (100)

## References

1. "Research Reactor Core Conversion from the Use of Highly Enriched Uranium to the Use of Low Enriched Uranium Fuels Guidebook", IAEA-TECDOC-233. Prepared by a Consultants Group, Coordinated and Edited by the Physics Section, IAEA. Vienna, (1980).
2. EPRI-CELL Code provided to Argonne National Laboratory by Electric Power Research Institute, Palo Alto, California (1977).
3. H. Henryson II, B. J. Toppel and C. G. Stenberg, "MC<sup>2</sup>-2: A Code to Calculate Fast Neutron Spectra and Multigroup Cross Sections", ANL-8144 (ENDF239) (June, 1976)
4. T. A. Daley, G. K. Leaf and A. S. Kennedy, "The ARC System Two-Dimensional Diffusion Theory Capability, DARC2D, "ANL-7716 (May, 1972).
5. R. E. Prael and L. J. Milton, "A User's Manual for the Monte Carlo Code VIM," FRA-TM-84 (February 20, 1976).
6. C. F. Obenchain, "PARET - A Program for the Analysis of Reactor Transients," IDO-17282 (1969).
7. W. L. Woodruff, "A Kinetics and Thermal-Hydraulics Capability for the Analysis of Research Reactors", Nuclear Technology, 64, 196 (1984).  
  
W. L. Woodruff, "The PARET Code and the Analysis of the SPERT I Transients," ANL/RERTR/TM-4, Proceedings of the International Meeting on Research and Test Reactor Core Conversions from HEU to LEU Fuels, Argonne National Laboratory, Argonne, Illinois, November 8-10, 1982.
8. S. G. Forbes, et al, "Analysis of Self-shutdown Behavior in the SPERT I Reactor," IDO-16528 (1959).

## BENCHMARK CALCULATIONS

## INTERATOM\*

Bergisch Gladbach,  
Federal Republic of Germany

## Abstract

Results are provided for the safety-related benchmark problem with HEU and LEU fuels. Additional results include a comparison of decay heat power versus shutdown time in the HEU and LEU cores and a comparison of the reactivity worths of an oval absorber and a fork-type absorber.

- 1 The results presented in the German Contribution to the Safety-Related Benchmark are based on the 10 MW-Reactor Core defined for Neutronic Benchmark Calculations in IAEA-TECDOC-233(1980) with the only alteration within the central flux trap as described above. All calculations are carried out for the core status BOC with xenon equilibrium. The fuel used was HEU (93 w/o U 235) and LEU (20 w/o U 235), resp.

2 Static Calculations2.1 Prompt Neutron Lifetime

The prompt neutron lifetime was determined by calculating the eigenvalue of the perturbed system in xy-geometry and four energy groups. A perturbation of  $1/v$ -behaviour was inserted for the whole arrangement representing the core plus reflector. In discrete energy groups the following equation is valid

$$\left\{ -\nabla^2 D^g + \Sigma_a^g + \Sigma_r^g + \frac{1}{v^g} s \right\} \phi^g = \frac{\chi^g}{k} \sum_{g'} \nu \Sigma_f^{g'} \phi^{g'} + \phi^{g-1} \cdot \Sigma_r^{g-1}$$

The multiplication factors got when solving the above equation with and without perturbation lead to

$$\bar{l} = \frac{1}{k} \cdot \frac{\Delta k}{\Delta s}$$

Carrying out the calculations for HEU- and LEU-fuel, resp. one gets

$$\bar{l}_{HEU} = 54.5 \mu s$$

$$\bar{l}_{Leu} = 42.2 \mu s$$

Calculations with different xenon status result in deviations of the order of  $1 \mu s$  for the prompt neutron lifetime. The core state was BOC for all calculations.

---

\* Work performed on behalf of the Minister of Research and Technology of the Federal Republic of Germany.

## 2.2 Delayed Neutron Fraction

From calculations with prompt neutron fission spectra the delayed neutron fractions result as given below

$$\beta_{\text{eff}}^{\text{HEU}} = 7.62 - 3$$

$$\beta_{\text{eff}}^{\text{LEU}} = 7.32 - 3$$

## 2.3 Reactivity Feed-Back Coefficients

Reactivity Feed-Backs were calculated using the following method:

First the INTERATOM burnup code MONSTRA was used to calculate burnup-dependent cross-sections for the different parameters such as fuel temperature, water temperature and water density. These cross-sections are obtained by taking over the burnup-dependent isotopic concentrations from the MONSTRA-calculations with the nominal values of the said parameters.

Secondly the cross-sections generated are used in two dimensional diffusion calculations of the core with the INTERATOM-code IAMADY in xy-geometry to get the reactivity differences to the basic core calculation. The codes used are described in more detail within IAEA-TECDOC-233, p. C-68/69.

### 2.3.1 Change of Water Density Only

The set of water density values used for the calculations is presented in table 2.3-1. The range used is between 1.0 and .8 g/cm<sup>3</sup>. The reactivity differences are adjusted against the reactivity at  $\rho_w = .9984$  g/cm<sup>3</sup> which is the nominal value for the core and which is used during the work for IAEA-TECDOC-233. Up to  $\rho_w = .9485$  there is a relation between water density and water temperature. The two  $\rho_w$ -values beyond can only be reached by partial voiding of the coolant.

Table 2.3-1: Reactivity Coefficients for Change of Water Density  
 $\rho_w$  Only

$\rho_w$	$T_w$	HEU		LEU	
		$\Delta\rho \times 1000$	$\frac{\Delta\rho}{\Delta T_w} \times 10^5 / K^{-1}$	$\Delta\rho \times 1000$	$\frac{\Delta\rho}{\Delta T_w} \times 10^5 / K^{-1}$
1.0	0.	+ 0.371	+ 1.9	+ 0.430	+ 2.1
.9984	20.	0.	0.0	0.000	0.0
.9924	40.	- 1.361	- 6.8	- 1.584	- 10.1
.9777	70.	- 4.825	- 11.5	- 5.679	- 13.5
.9485	113.	-12.043	- 16.8	- 13.971	- 19.5
.8986	-	-25.796		- 29.647	
.7987	-	-59.233		- 66.890	

To simplify the overview over the results figure 2.3-1 (upper right part) supplies a comparison of the reactivity feed-back of water density only when using HEU- and LEU-fuel, resp. The abszissa was scaled in the water saturation temperature corresponding to the density used. The figure demonstrates that this reactivity feed-back is distinctly greater in case of LEU-fuel than for the HEU-fuel.

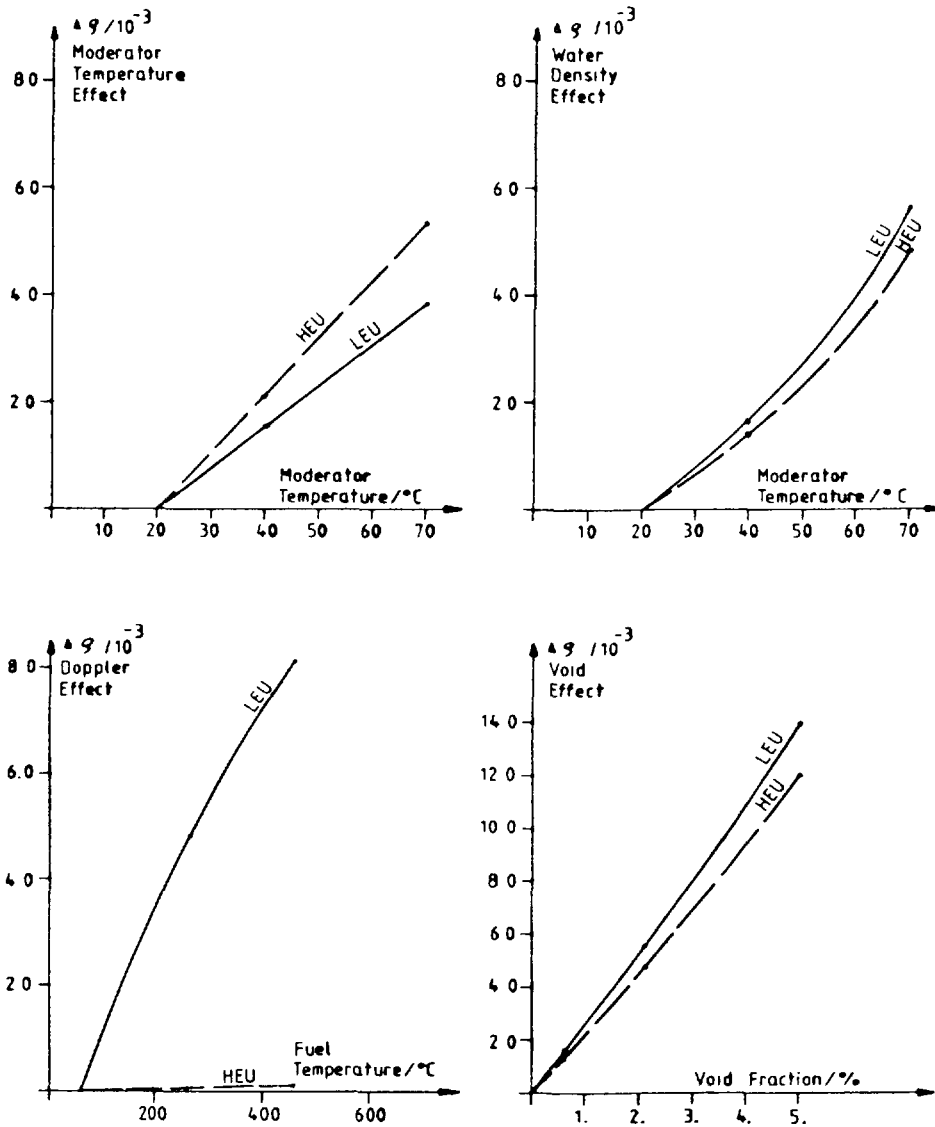


FIG. 2.3-1. Isothermal reactivity feedbacks for HEU and LEU fuels:  
 changes in moderator temperature only  
 fuel temperature only  
 water density only  
 water voidage only.

### 2.3.2 Change of Moderator Temperature Only

The split up of the moderator feed-back into density effect and temperature effect means that the physical effect taken into account under moderator temperature only is the different movement of the hydrogen atoms at different temperatures whereas the moderator density was .9984 g/cm<sup>3</sup> throughout these calculations. The calculational way used here is based on the work done by Nelkin and Kappel & Young, i. e. on a theoretical model rather than measured cross-sections. The results are presented in table 2.3-2 for three water temperatures (20, 40, 70 °C). The resulting feed-backs are somewhat less negative for the LEU-fuel than for HEU. Figure 2.3-1 (upper left part) compares the results for both fuels under consideration.

Table 2.3-2: Reactivity Coefficients for Change of Water Temperature T<sub>w</sub> Only

T <sub>w</sub> °C	HEU		LEU	
	Δρx1000	$\frac{\Delta\rho}{\Delta T_w} \times 10^5 / K^{-1}$	Δρx1000	$\frac{\Delta\rho}{\Delta T_w} \times 10^5 / K^{-1}$
20	0.		0.	
40	- 2.093	- 10.47	- 1.569	- 7.85
70	- 5.389	- 10.98	- 3.863	- 7.65

### 2.3.3 Change of Fuel Temperature Only

The third variable to take into account is the fuel temperature. It is well known that the so-called Doppler-effect of HEU-fuel is rather small as may be seen from table 2.3-3. For LEU-fuel the coefficient for the fuel temperature is of the same order as the other two effects discussed above, which is indeed a favourable effect of the LEU-fuel especially as the Doppler-effect is prompt. On the other hand the favourable Doppler-coefficient enlarges the cold-hot swing in case of the use of LEU-fuel, but this effect is still relatively small.

The fuel temperatures which were calculated by the MONSTRA-IAMADY-way are 60, 260, and 460 °C. Figure 2.3-1 (lower left part) compares results for LEU and HEU. The water density within these calculations was fixed to .9984 g/cm<sup>3</sup>.

### 2.3.4 Void Reactivity Feed-Back

It is quite obvious that the results of table 2.3-1 for the water density effect only can also be used to get the so-called void coefficient. When following this line the results can be composed as in table 2.3-4 as well as in figure 2.3-1 (lower right part) versus the parameter voidage, i. e. the relative void fraction based on the nominal water density of .9984 g/cm<sup>3</sup>. Here again we get the somewhat higher feed-back for the LEU-fuel corresponding to the density effect described above.

Table 2.3-3: Reactivity Coefficients for Change of Fuel Temperature T<sub>F</sub> Only

T <sub>F</sub> °C	T <sub>F</sub> K	HEU		LEU	
		Δρx1000	$\frac{\Delta\rho}{\Delta T_B} \times 10^7 / K^{-1}$	Δρx1000	$\frac{\Delta\rho}{\Delta T_B} \times 10^7 / K^{-1}$
60	333	0.	-	0.	-
260	533	-.0725	- 3.62	- 3.96	- 198.
460	733	-.1178	- 2.27	- 7.28	- 166.

Table 2.3-4: Void Reactivity Coefficients

ρ <sub>w</sub> g/cm <sup>3</sup> g/cm <sup>3</sup>	Voidage % %	HEU		LEU	
		Δρx1000	$\frac{\Delta\rho}{\Delta\rho_w} \times 10^3 / \%^{-1}$	Δρx1000	$\frac{\Delta\rho}{\Delta\rho_w} \times 10^3 / \%^{-1}$
1.0	-.160	+ 0.371	- 2.32	+ 0.430	- 2.69
.9984	-	0.	-	0.	-
.9924	.601	- 1.361	- 2.27	- 1.584	- 2.64
.9777	2.073	- 4.825	- 2.35	- 5.629	- 2.75
.9485	4.998	- 12.043	- 2.47	-13.971	- 2.85
.8986	9.996	- 25.796	- 2.75	-29.647	- 3.14
.7987	20.002	- 59.233	- 3.34	-66.890	- 3.72

In extension of the global void reactivity feed-backs local void feed-backs were calculated reducing the density in specific fuel elements of the different core zones. For the inner core zone the fuel element SFE-3 was inserted with reduced moderator density; the outer core zone is represented by fuel element SFE-3 which is neighboured to the graphite reflector, as well as by fuel element SFE-4 which is surrounded by water on two sides. All core calculations were carried out using homogeneous xenon-equilibrium at the begin of the cycle. Two percentages of voidage were calculated in each case, 5 % and 10 %. Table 2.3-5 presents the results for the reactivity feed-backs. These results reflect the overall tendency got for the global void feed-back, somewhat higher values for LEU-fuel and nearly doubling the values when changing from 5 to 10 % voidage. The differences between inner and outer zone are comparatively small.

Table 2.3-5: Local Void Feed-Backs

Enrichment	Fuel Element Voided	Reactivity Step at 5 %-Voidage	Reactivity Step at 10 %-Voidage
HEU	SFE-3	Δρ = - 0.54 o/oo	Δρ = - 1.11 o/oo
	SFE-2	Δρ = - 0.46 o/oo	Δρ = - 0.96 o/oo
	SFE-4	Δρ = - 0.40 o/oo	Δρ = - 0.81 o/oo
LEU	SFE-3	Δρ = - 0.60 o/oo	Δρ = - 1.22 o/oo
	SFE-2	Δρ = - 0.63 o/oo	Δρ = - 1.28 o/oo
	SFE-4	Δρ = - 0.42 o/oo	Δρ = - 0.84 o/oo

## 2.4 Power Peaking Factors

The radial power peaking factors for the benchmark core as specified in IAEA-TECDOC-233 (including the small alteration at the flux trap mentioned above) are calculated in xy-diffusion calculation by code IAMADY.

### 2.4.1 Radial Fuel Element Power Peaking Factors

One of the basic outputs of xy-core calculations are the power peaking factors computed element-wise. To check the calculational methods there is a definite list of different calculations needed with different replacements in the nominal core. So the radial fuel element power peaking factors are composed in table 2.4-1.

### 2.4.2 Local Power Peaking Factors

Whereas method and results are obtained straightforward for the element-wise factors the local power peaking factors caused some problems. This is due to the fact that the height of the local value depends on the mesh-width in the core calculation, as the local peaking factors (mesh peaking factors) are calculated by the code IAMADY using the power in the respective mesh interval.

In case one has a clear flux gradient across one fuel element especially in the thermal energy region, it is quite obvious that the local power peaking factor will be enlarged when reducing the mesh up to almost a point. That may be interpreted as the maximum local power peak. A good approximation in calculating the local peaking factor is to take the value at the edge of the mesh interval with the highest power. As such edge values are not calculated for the power or power peaking factor by IAMADY the local power peaking factor (edge value) was determined via the thermal flux by the ratio of the maximum flux at the edge of the mesh interval with the highest power and the average flux of the fueled part of the respective element.

Beside the radial fuel element power peaking factors in table 2.4-1 the mesh peaking factors as well as the local peaking factors and the total peaking factors are indicated.

### 2.4.3 Remark on the Results

It must be mentioned that all calculations on power peaking factor in the way and the philosophy they are calculated here are not binding for a licensing procedure in the Federal Republic of Germany. The results serve the task of comparing methods mainly. In this specific sense they are of great interest for the different calculators.

Table 2.4-1 Radial Fuel Element Power Peaking Factors  
 (Substitution by Fresh Fuel Elements in Core with  
 Xenon-Equilibrium)

Core Status	Element	Radial Peaking Factor	Mesh** Peaking Factor	Local Peaking Factor	Total* Peaking Factor
HEU no substitution	SFE-1	1.031	1.268	1.508	1.555
CFE-1 substituted	CFE-1	1.327	1.173	1.295	1.718
SFE-1 substituted	SFE-1	1.122	1.272	1.506	1.690
LEU no substitution	SFE-1	1.022	1.293	1.664	1.700
CFE-1 substituted	CFE-1	1.268	1.148	1.281	1.624
SFE-1 substituted	SFE-1	1.112	1.349	1.661	1.847
LEU in HEU no substitution	SFE-1	1.031	1.268	1.508	1.555
CFE-1 substituted	CFE-1	1.492	1.217	1.417	2.114
SFE-1 substituted	SFE-1	1.255	1.324	1.597	2.004

\* Total Peaking Factor = Radial Peaking Factor x Local Peaking Factor

\*\* Dependent on the Actual Mesh Choice

## 2.5 Decay Heat Power

For both the fuels under investigation (HEU-fuel with 280 g U 235, LEU-fuel with 390 g U 235) the decay heat power was calculated according to the draft of the German Standard DIN 25463, dated April 1980 which is very similar to the US-Standard ANSI/ANS-5.1-1979.

Figure 2.5-1 presents the decay heat power of the defined core configuration for both fuels not including the contribution of the delayed neutrons. Whereas for very short shutdown-times the deviation between the two curves of figure 2.5-1 is rather small, for longer periods of shutdown the differences grow up to 10 % after 30 days approx. and beyond 40 % after more than 1000 days. This will be demonstrated more clearly by figure 2.5-2 which presents the deviation of the overall decay heat power of the LEU-case from the HEU-case.

Moreover it was checked, which contributions are responsible for the overall deviations:

- figure 2.5-3 presents the relative deviation of the contribution of the fission products which is responsible for the 40 %-deviation in the area of 1000 days shutdown-time.
- figure 2.5-4 adds the absolute deviation of the contribution of the actinides. The main contribution of the actinides to the deviation in decay heat power is in the area of short shutdown-times.

- the relative maximum in figure 2.5-2 in the area of  $2 \cdot 10^5$  s is an effect of a correction of the contribution of the fission products due to the neutron capture in fission products excluding Cs 133. This correction determines the differences between the curves of figure 2.5-2 and 2.5-3 mainly.
- the contribution of CS 133 calculated separately is such a small one that any deviation of it does not influence the overall result even though this contribution is enlarged by a factor 2 approx. when changing from HEU to LEU.

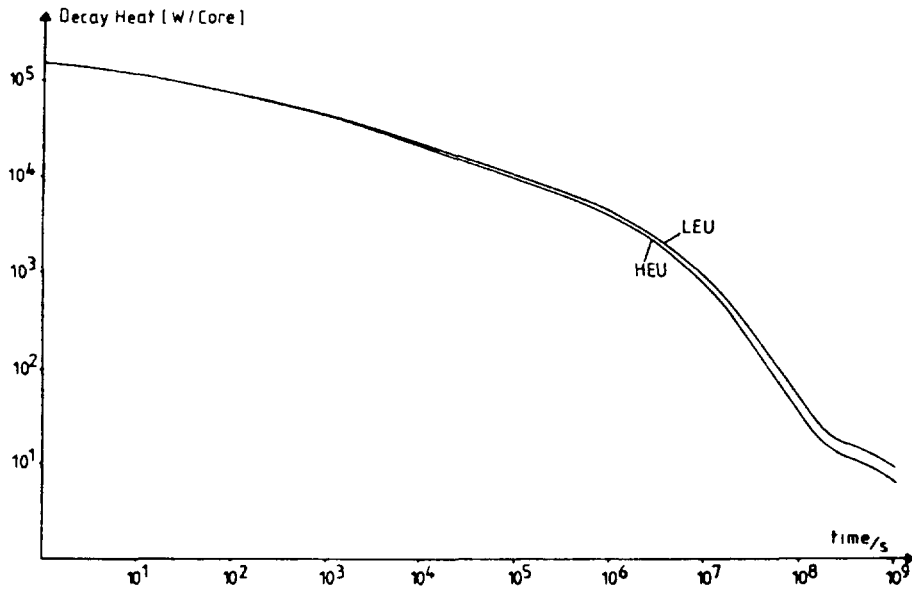


FIG. 2.5-1. Decay heat versus shutdown time for 10 MW benchmark core with HEU and LEU loading, respectively.

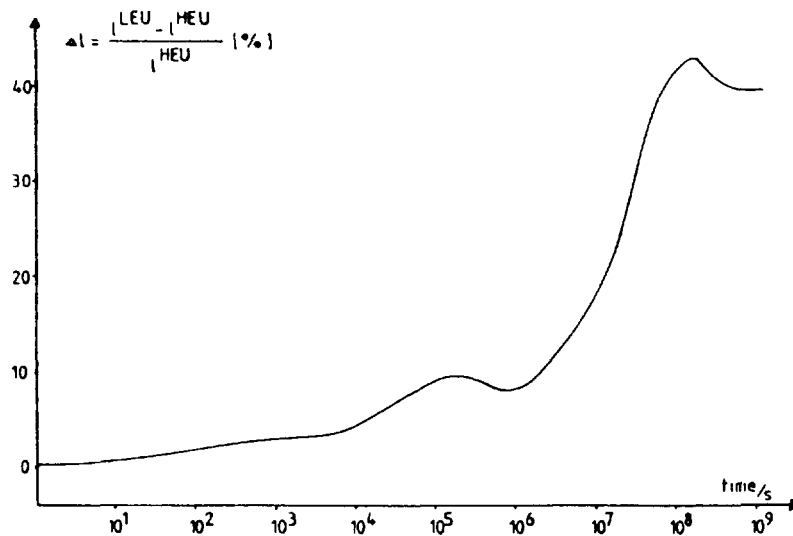


FIG. 2.5-2. Decay heat deviation  $\Delta I$ .

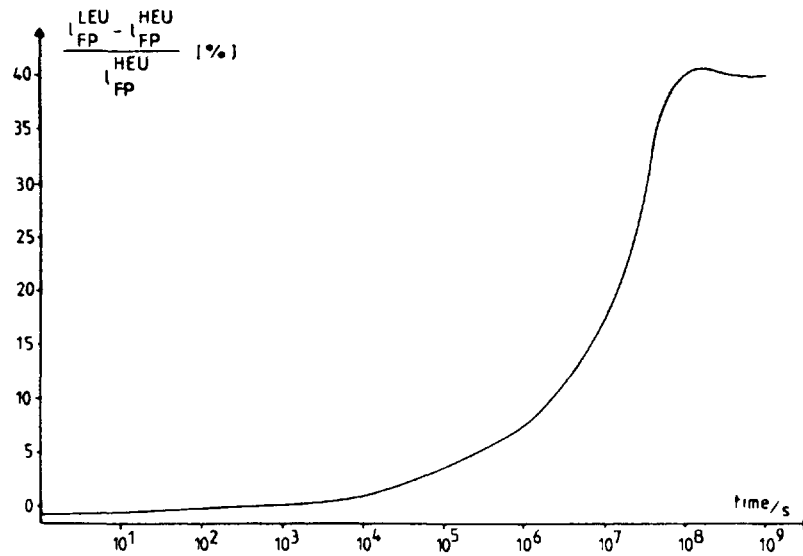


FIG. 2.5-3. Deviation of fission products contribution  $I_{FP}$  to decay heat from HEU to LEU.

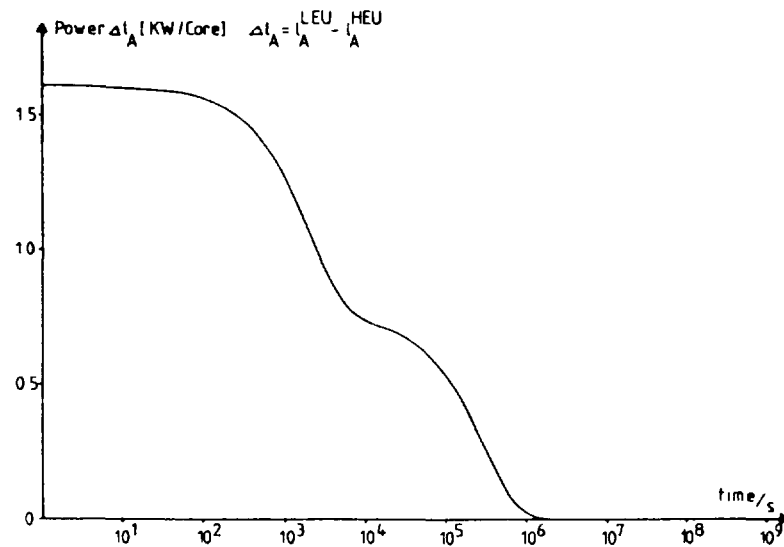


FIG. 2.5-4. Difference of actinides contribution to decay heat  $I_A$ .

For the calculations the following model was used:

- for the incore time of the different fuel elements the burnup was transferred to full power hours; no shutdown periods were taken into account.
- the local power peaking factors of the different fuel elements were not taken into account, i. e. a uniform power distribution was assumed.

This somewhat simplified modelling will not influence the principal result when comparing the two fuels under the decay heat aspect.

All calculations needed to obtain the control rod worths for the 10 MW-core loaded with different fuels are based on the method of adjusting absorption rates. How to use this method properly was extensively checked outside the calculations needed for the defined benchmark. These tests used one-dimensional (Program IANSN) as well as two-dimensional (Programs DOT 2 and DOT 4/2) transport calculations to take all heterogenities into account for the basic fixation of the absorption rate in the absorber cell. This cell comprises the area of those three fuel plates omitted to bring in the absorber blade and its guiding plates. In the opposite direction the cell is extended such to include the structure parts of the fuel element (comb plate) up to the measures of the grid plate area the control element is put into. By a transport diffusion absorption rate adjustment the four group macroscopic cross-sections were obtained for the core diffusion calculation in the xy-model. The detailed investigations carried out have set clear that a separate consideration of the inner part and the outer part of the absorber cell in the diffusion calculations improves the results insomuch as this separation of areas with different heterogenity reflect much better the results of the 2-dimensional transport calculations. Whereas the absorption rate adjustment was carried out in a one dimensional model, the effectiveness calculations were performed in two dimensions. The 10 MW-benchmark cores were calculated in two states. The first state uses only fresh fuel in the core set-up instead of the burnup-distribution originally specified. The second state takes into account the different burn-ups of the different fuel elements.

Table 2.6-1 composes the results got for the HEU- and the LEU-fuel, resp. Two types of absorber materials were calculated, the AgInCd-blades and the boron-blades. It is a clear outcome of these calculations that the absorber effectiveness of the 4 absorbers in the HEU-case is higher than in the LEU-case and, moreover, that calculations with fresh fuel underestimate this difference between HEU- and LEU-shutdown margin.

Tests were also carried out by changing the burnup state of the fuel surrounding the absorber cell when calculating the macroscopic absorber cross-sections. Such influences are rather small. Corresponding changes in the absorber effectiveness are .1 % maximum.

If one compares this reduction with the differences in burn-up reactivity loss during cycle (see for example IAEA-TECDOC-233, table 2-19:  $\Delta\rho = 2.18\%$  in the HEU-case and  $\Delta\rho = 1.03\%$  in the LEU-case, if equal MWD per cycle are assumed) the consequence is that the reduction of absorber effectiveness will not be compensated by the reduction in reactivity loss due to burn-up. In case of equal percentage of loss of U 235 during cycle the cited table reflects an even more disadvantageous relation.

Table 2.6-1: Control Rod Worths

	HEU-fuel	LEU-fuel	Difference HEU-LEU
AgInCd-Absorber			
fresh fuel in core	$\Delta\rho = 13.3 \%$	$\Delta\rho = 11.7 \%$	1.6 %
core with specified burnup	$\Delta\rho = 16.9 \%$	$\Delta\rho = 14.2 \%$	2.7 %
B-Absorber			
fresh fuel in core	$\Delta\rho = 17.2 \%$	$\Delta\rho = 15.3 \%$	1.9 %
core with specified burnup	$\Delta\rho = 21.3 \%$	$\Delta\rho = 18.3 \%$	3.0 %

So the total control rod worth available specifically in case one rod sticks may influence the decision about the fuel for the core conversion as well as the cycle length possible for a specific reactor. Case by case calculations are needed to assess the potential available.

## 2.7 Comparison of the oval absorber and fork-type absorber

Somewhat outside the basic benchmark calculations investigations were performed to compare the effectiveness of different absorber design. Figure 2.7-1 shows typical oval absorber and fork-type absorber designs, respectively both based on the 23 fuel plate elements.

The absorber blade consists of an AgInCd-alloy with a steel canning, the guide plates are made out of Al. The material of which the oval absorber consists is natural boron carbide ( $B_4C$ ) with a layer of cadmium.

These absorbers were compared with each other with regard to their shutdown efficiency which is defined by

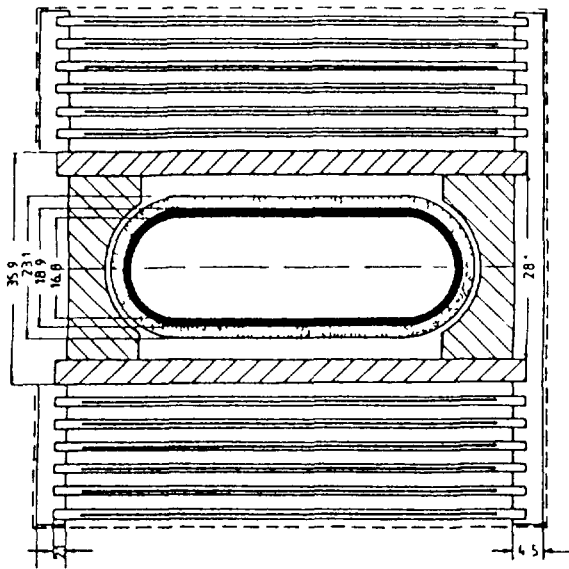
$$= (k_1 - k_2) / (k_1 \cdot k_2)$$

where  $k_1, k_2$  are the effective multiplication factors of the free-of-rod status and the shutdown status, resp.

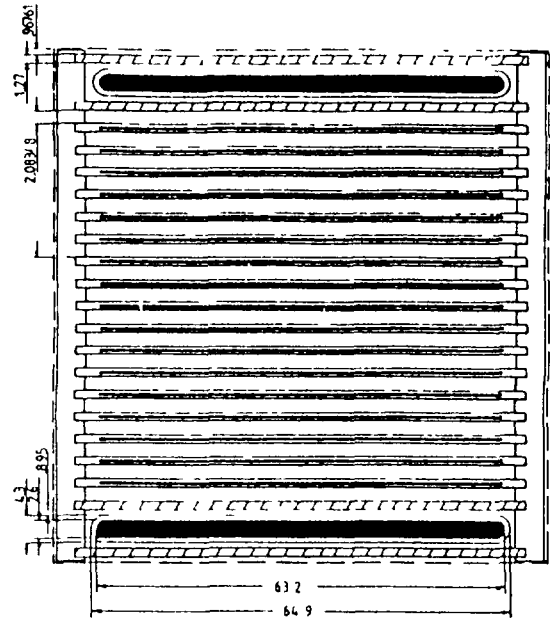
The calculations the comparison is based on are carried out with the DOT-4-code in S-4 approximation and 4 energy groups.

For the fuel we chose a typical fresh HEU-fuel with 180 g U5 in 23 plates per FE. The core was modelled by an infinite lattice made up out of 5 FE and 1 CE regularly (Figure 2.7 - 2).

Cross Section of the Oval Absorber



Cross Section of the Fork Type Absorber



fuel thickness 0.51      cladding thickness 0.39  
all dimensions in mm      23 plates

FIG. 2.7-1. Absorber types.

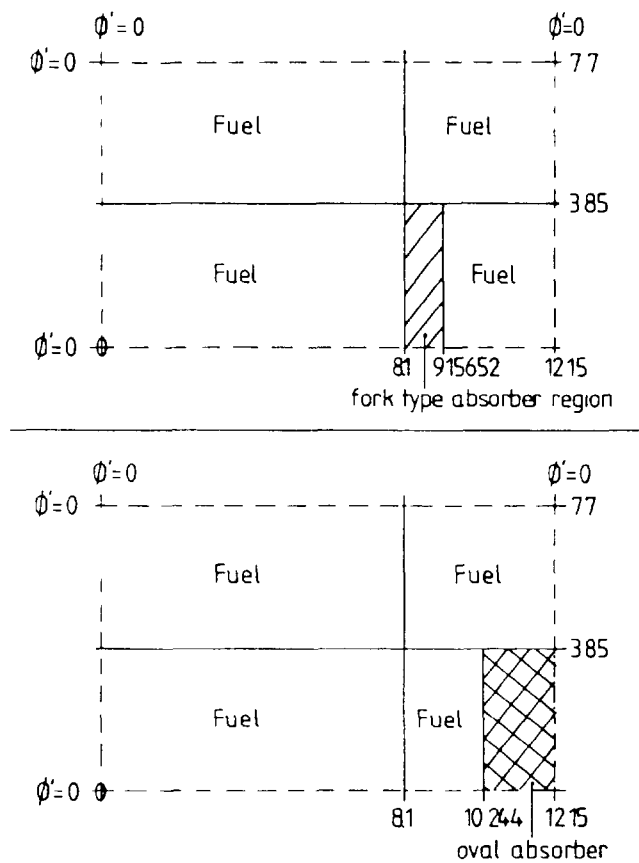


FIG. 2.7-2. Model of the infinite lattice for calculations.

Form the homogeneous DOT-4-calculations we found the following k:

Oval absorber: shutdown case  $k_{eff} = 1.21629$   
follower case  $*k_{eff} = 1.38361$   
 $= 9.94 \%$

Fork-type absorber: shutdown case  $k_{eff} = 1.17680$   
follower case  $*k_{eff} = 1.40025$   
 $= 13.56 \%$

This shows an improvement of the shutdown efficiency by the fork-type absorber of about 36 %. The result corresponds to measurements performed in Germany.

### 3 Dynamic Calculations

#### 3.1 Method of Analysis

The calculations were performed with the INTERATOM version of the thermal hydraulic code COBRA IIIC (1). The following modifications in the original code were necessary in order to apply it to the steady-state and transient analysis of plate-type fuel elements:

- the cross flow calculations will be bypassed if laterally closed coolant channels are specified
- at steady state and at each time step the flow distribution at the core inlet will be corrected iteratively requiring that the pressure drop across each coolant channel is equal to the core pressure drop. The iteration will be terminated if the inlet flow distribution changes by less than a specified amount.
- suitable heat transfer correlations were added which handle forced convection and boiling heat transfer
- weighted average values for fuel temperature, coolant density and coolant temperature in the core are calculated at steady state and at each time step
- different time steps can be chosen in the course of a transient

The major modification was the addition of a point kinetics module to COBRA IIIC which calculates at the end of each time step the power which is produced in the meat during the following time step. Besides specified external reactivities the module takes into account feedback effects caused by changes in the fuel

---

\* fully withdrawn absorbers, with followers

- (1) D. S. Rowe: "COBRA" IIIC: A Digital Computer Program for Steady-State and Transient Termal-Hydraulic Analysis of Rod Bundle Nuclear Fuel Elements", BNWL-1695, 1973

and coolant temperature. The time step is initially imposed by COBRA IIIC. The module subdivides this time step for the kinetics calculations if necessary and feeds back the energy released in the fuel during the desired COBRA IIIC time step. In case a scram or trip occurs within such a time interval the module overrules the specified time step and initiates an additional thermal hydraulic calculation.

### 3.2 Calculational Model

The core is represented by two coolant channels. One channel describes the thermal hydraulic behaviour of the core and the other channel represents the hot channel in the core. The core height is divided into 25 axial intervals of equal length, the fuel plate is modelled by 7 nodes in the lateral direction. For the analysis of the reactivity insertion transients the size of the COBRA IIIC time steps was adjusted depending on the rate of change of the variables to be fed back into the kinetics module. For the loss of flow transients the time step was not changed in the course of the transient. In each case, however, it was made sure that the results obtained were independent of the size of the time step.

### 3.3 Reactor Description

The calculations were performed for the 10 MW core used for neutronics bench mark calculations as described in IAEA-TECDOC-233. A radial nuclear hot channel factor of 1.4 and an axial nuclear hot channel factor of 1.5 has been chosen. The axial flux shape has been approximated by a chopped cosine distribution. For the engineering hot spot factor and the engineering hot channel factor values of 1.095 have been applied. The following reactivity coefficients for the HEU/LEU core have been used (see chapter 2.3): change of fuel temperature  $-3.6 \times 10^{-7} / -1.98 \times 10^{-5}$  1/K, change of moderator temperature  $-1.05 \times 10^{-4} / -0.78 \times 10^{-4}$  1/K and change of moderator density  $2.27 \times 10^{-4} / 2.64 \times 10^{-4}$  m<sup>3</sup>/kg.

### 3.4 Results

The four transients specified in (2) were analysed for the HEU and LEU core:

1. Fast Loss-of-Flow Transient
2. Slow Loss-of-Flow Transient
3. Slow Reactivity Insertion Transient
4. Fast Reactivity Insertion Transient

---

(2) Letter dated April 15, 1981 from Dr. Matos/ANL to participants of Vienna-meeting (March 9 - 11, 1981)

### 3.4.1 Fast Loss-of-Flow Transient

The most important results are listed in Table 3-1. Figure 3-1 shows the thermal power generated in the fuel as a function of time. In Figure 3-2 the coolant outlet temperature and the maximum meat and clad temperature for the hot channel are plotted vs. time. Fig. 3-3 presents the minimum bubble detachment parameter  $\eta$  defined by

$$\eta(z) = \frac{V(z) \cdot (T_S(z) - T_B(z))}{q''(z)}$$

where

V	coolant velocity
$T_S$	saturation temperature
$T_B$	bulk coolant temperature
$q''$	heat flux
z	distance from channel inlet

at different times. The bubble detachment parameter  $\eta$  is a measure for the safety margin against occurrence of excursive flow instability in a coolant channel. The stability threshold may be set at  $\eta \sim 40 \text{ cm}^3 \text{ K/Ws}$  for the purpose of this evaluation.

Table 3-1: Fast Loss of Flow Transient

Fuel	HEU	LEU
Initial Power, MW	12	12
Initial Flow Rate, m <sup>3</sup> /h	1000	1000
Time Constant for Flow Delay, s	1	1
Flow Trip Point, %	85 (0.163)*	85 (0.163)
Time Delay, s	0.2	0.2
Power Level at Scram, %	115.4 (0.363)	114.0 (0.363)
Peak Fuel Temperature, °C	91.0 (0.363)	91.9 (0.363)
Peak Clad Temperature, °C	89.5 (0.380)	89.3 (0.363)
Peak Outlet Temperature, °C	56.5 (0.460)	56.4 (0.460)
Min. Bubble Detachment Parameter, cm <sup>3</sup> K/Ws	256.7 (0.380)	258.1 (0.380)

\*) Quantities in parentheses indicate time (in seconds) at which values occur

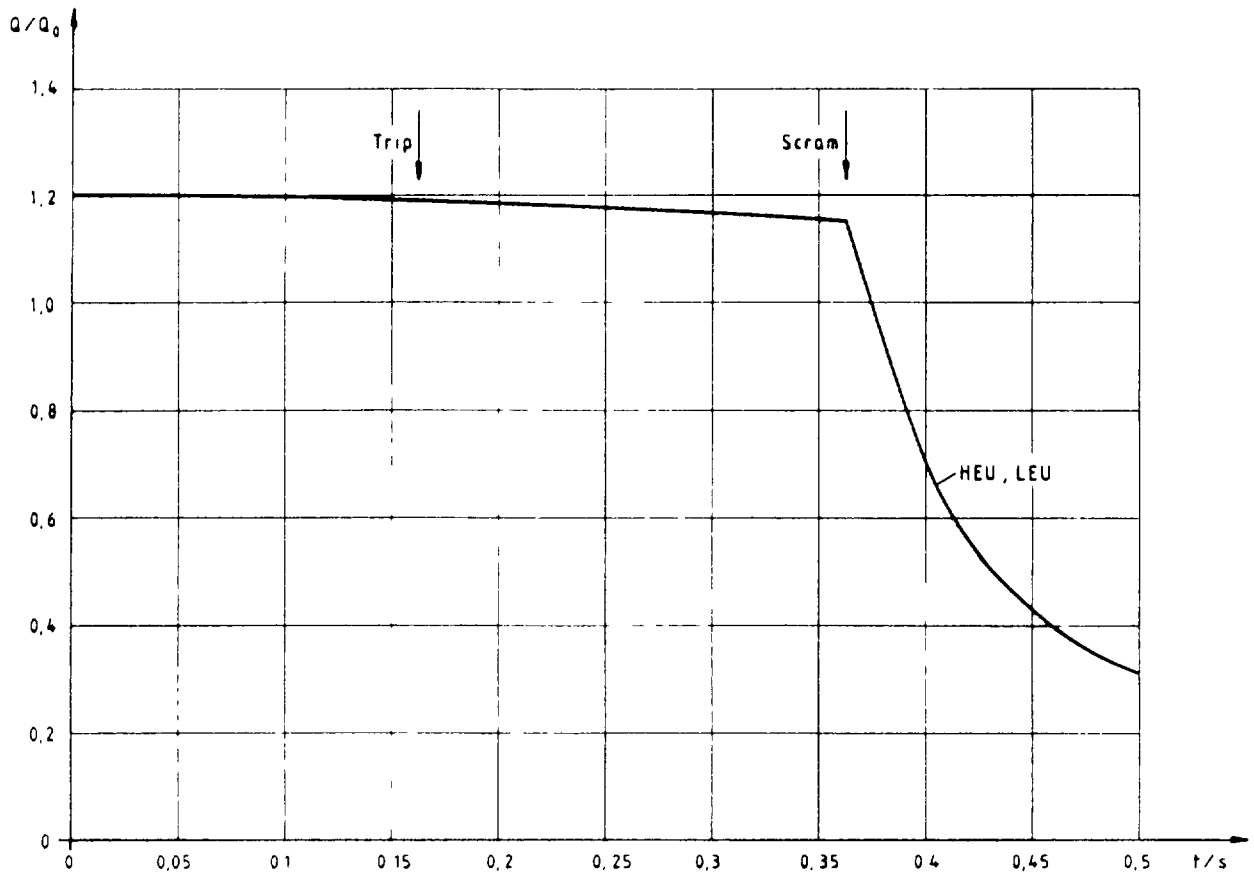


FIG. 3-1. Fast loss of flow transient: relative power generated in the fuel.

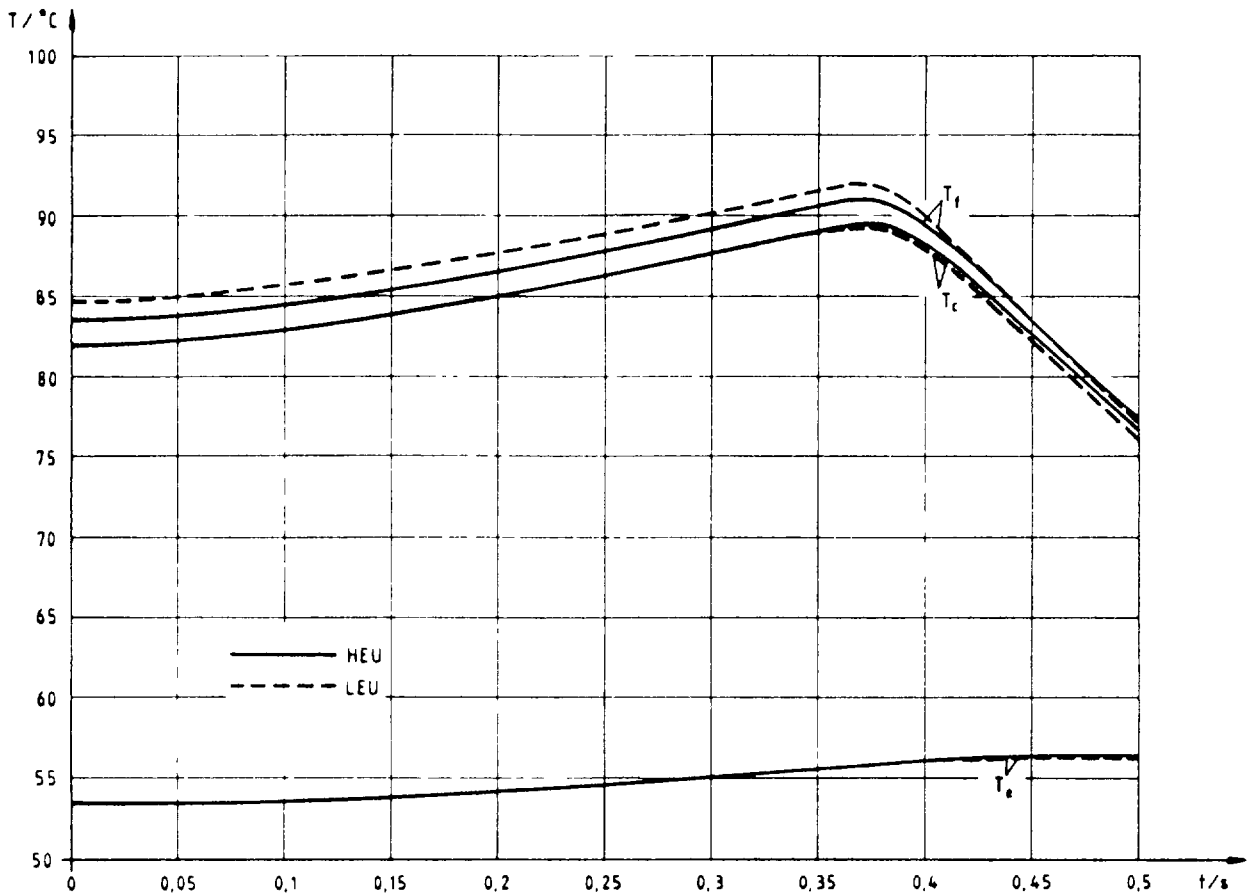


FIG. 3-2. Fast loss of flow transient: maximum fuel and clad temperatures, hot channel coolant exit temperature.

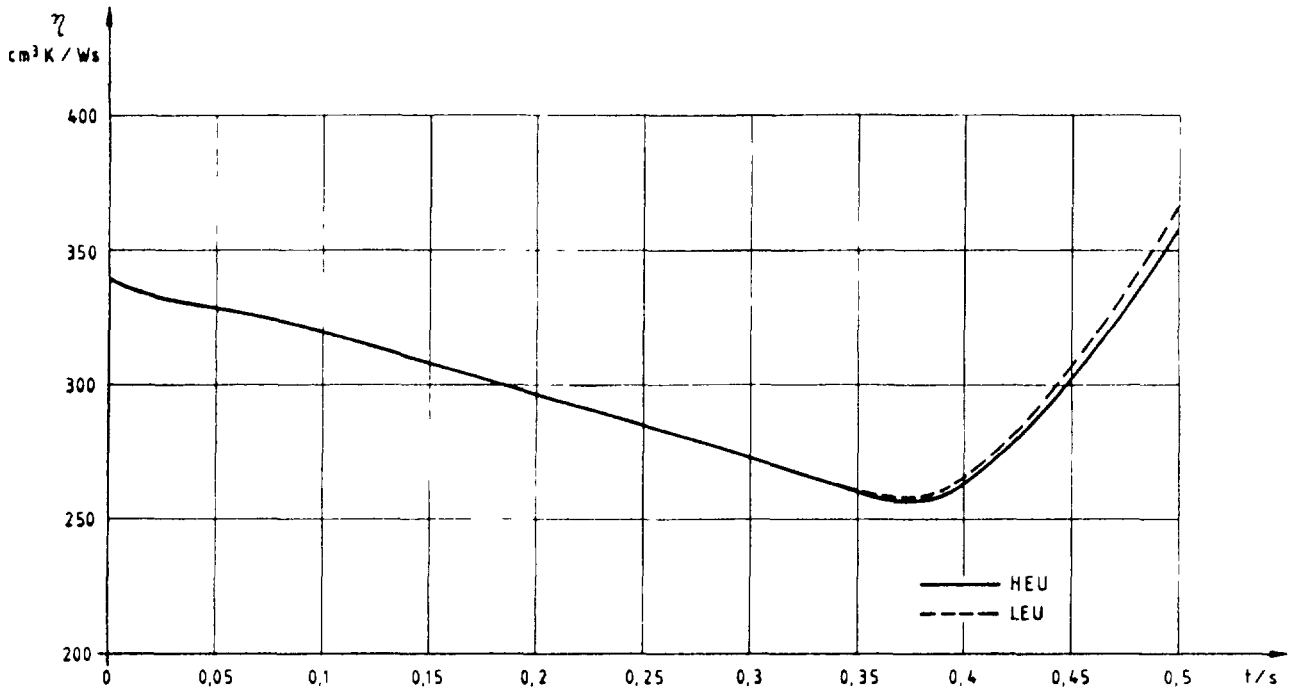


FIG. 3-3. Fast loss of flow transient: minimum bubble detachment parameter.

#### 3.4.2 Slow Loss-of-Flow Transient

The relevant information on these transients is given in Table 3-2. Figure 3-4 is a plot of the power generated in the fuel as a function of time. The maximum coolant outlet temperature and the fuel plate temperatures are shown in Figure 3-5 and the bubble detachment parameter in Figure 3-6 for various times.

#### 3.4.3 Slow Reactivity Insertion Transient

The results of these analyses are summarized in Table 3-3. Figure 3-7 presents the power generated in the fuel plates as a function of time. The maximum coolant outlet temperature and fuel plate temperatures are plotted in Figure 3-8 and the bubble detachment parameter  $\eta$  in Figure 3-9 vs. time.

#### 3.4.4 Fast Reactivity Insertion Transient

A summary of the results for these transients is presented in Table 3-4. In Figures 3-10 to 3-12 the transient behaviour of the power, the maximum coolant outlet and fuel plate temperatures and the bubble detachment parameter  $\eta$  is shown.

*Text cont. on p. 88.*

Table 3-2: Slow Loss of Flow Transient

Fuel	HEU	LEU
Initial Power, MW	12	12
Initial Flow Rate, m <sup>3</sup> /h	1000	1000
Time Constant for Flow Decay, s	25	25
Flow Trip Point, %	85 (4.063)*	85 (4.063)
Time Delay, s	0.2	0.2
Power Level at Scram, %	115.5 (4.263)	114.6 (4.263)
Peak Fuel Temperature, °C	87.4 (4.263)	88.2 (4.263)
Peak Clad Temperature, °C	85.8 (4.263)	85.5 (4.263)
Peak Outlet Temperature, °C	55.6 (4.263)	55.4 (4.263)
Min. Bubble Detachment Parameter, cm <sup>3</sup> K/Ws	293.2 (4.263)	295.4 (4.263)

\*) Quantities in parentheses indicate time (in seconds) at which values occur

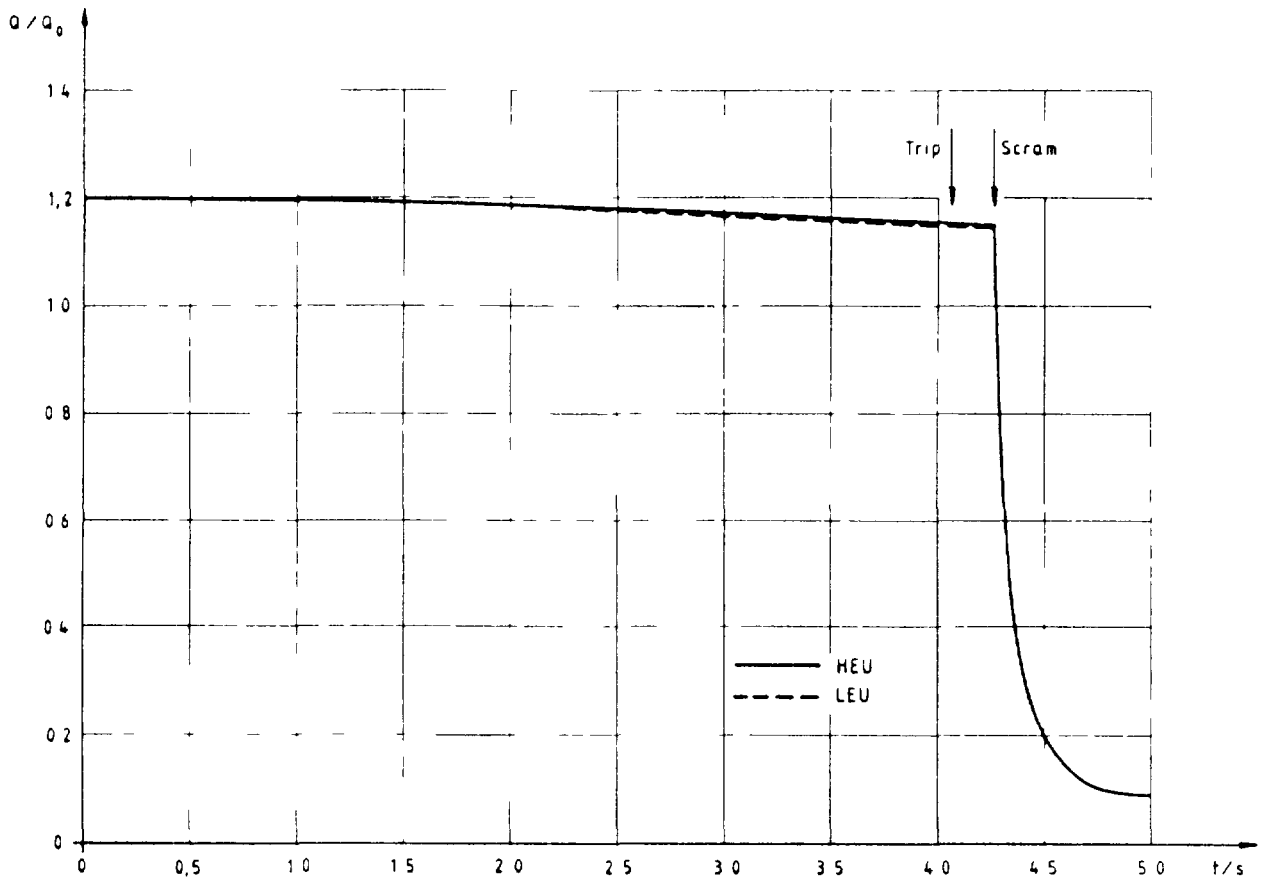


FIG. 3-4. Slow loss of flow transient: relative power generated in the fuel.

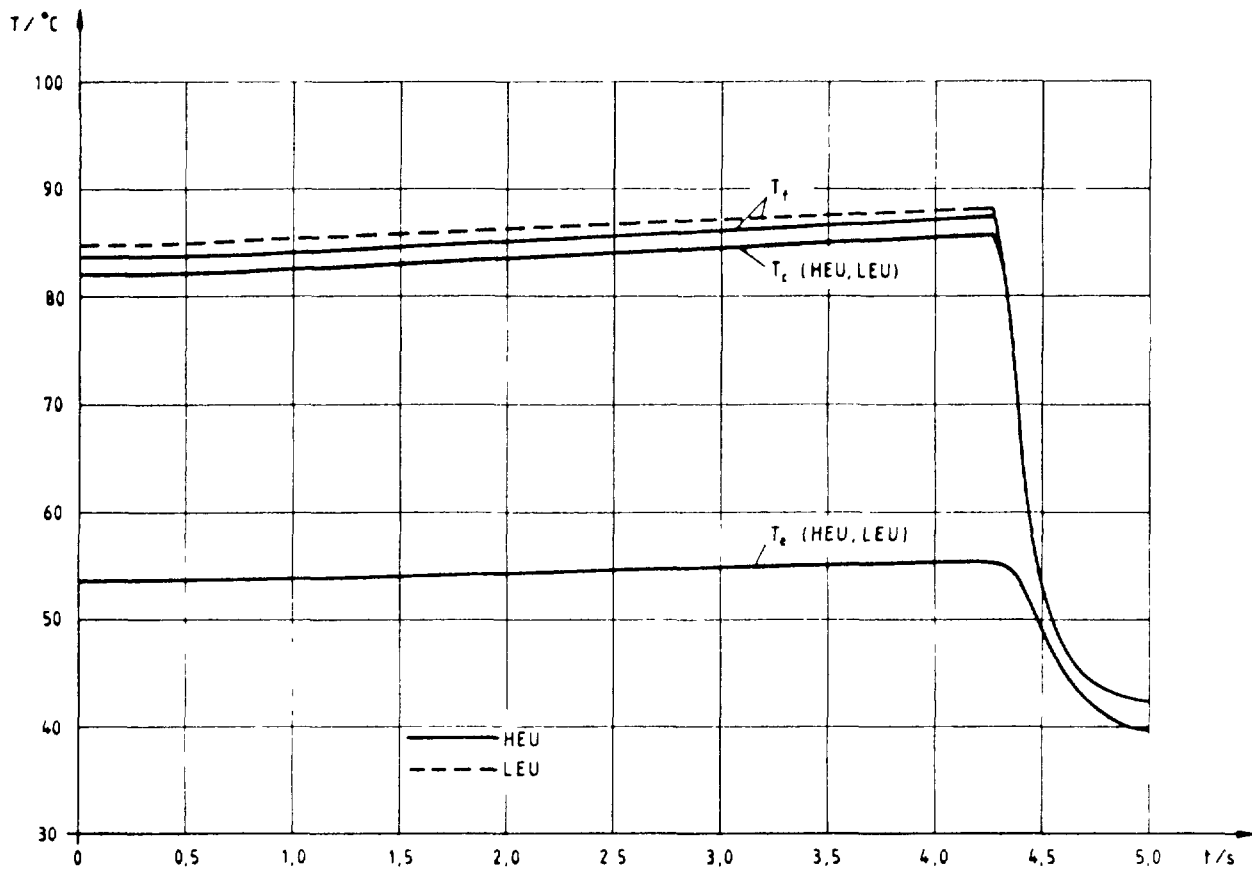


FIG. 3-5. Slow loss of flow transient: maximum fuel and clad temperatures, hot channel coolant exit temperature.

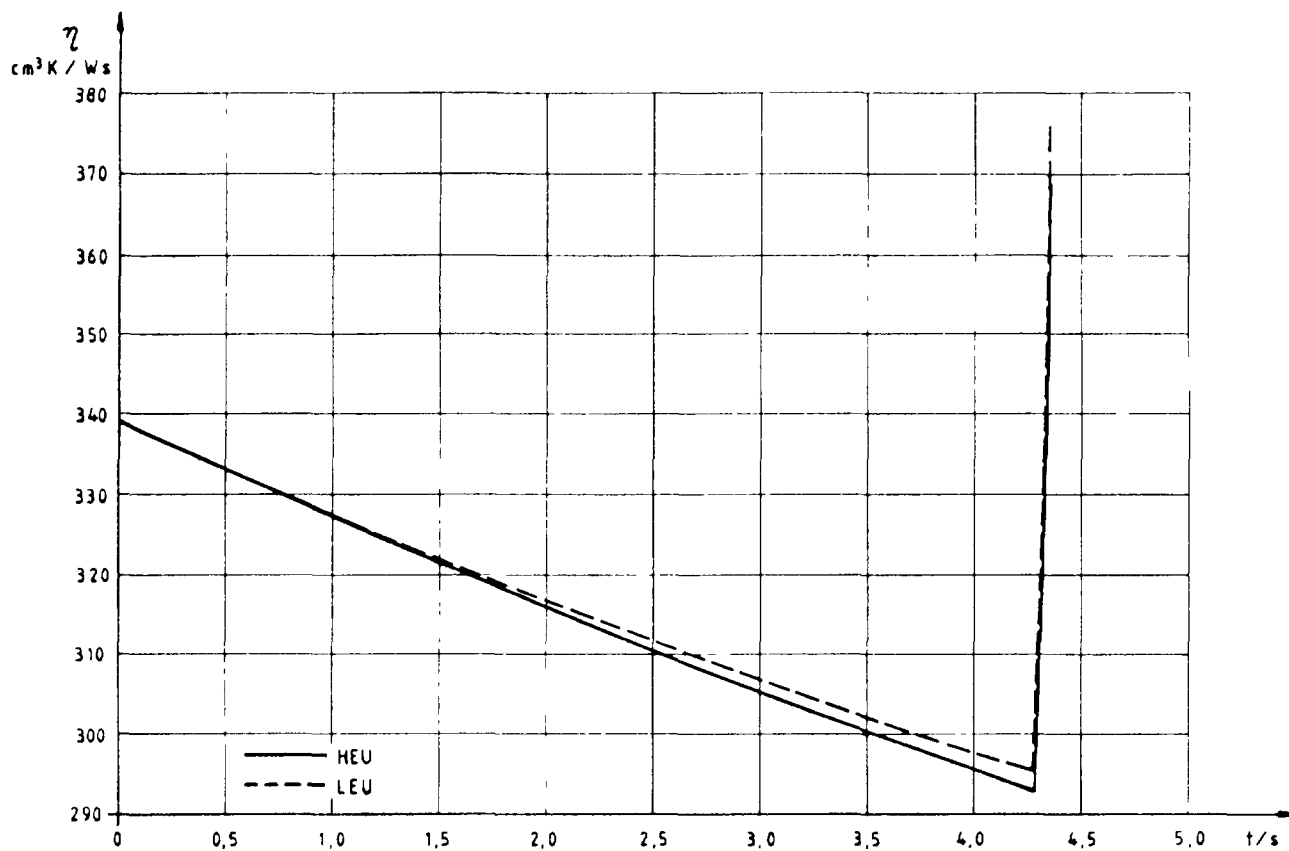


FIG. 3-6. Slow loss of flow transient: minimum bubble detachment parameter.

Table 3-3: Slow Reactivity Insertion Transient

Fuel	HEU	LEU
Reactivity Insertion Rate, c/s	10	9
Initial Power, W	1	1
Trip Point, MW	12 (10.569) *	12 (12.028)
Flow Rate, m <sup>3</sup> /h	1000	1000
Time Delay, s	0.025	0.025
Minimal Period, s	0.10 (10.520)	0.11 (11.300)
Peak Power, MW	14.36 (10.594)	12.18 (12.053)
Total Energy Release to Time of Peak Power, Ws	1.526 x 10 <sup>6</sup>	5.936 x 10 <sup>6</sup>
Total Energy Release beyond 12 MW, Ws	5.0 x 10 <sup>4</sup>	1.9 x 10 <sup>3</sup>
Peak Fuel Temperature, °C	70.5 (10.61)	80.8 (12.06)
Peak Clad Temperature, °C	69.2 (10.62)	78.1 (12.06)
Peak Outlet Temperature, °C	45.2 (10.70)	51.1 (12.10)
Min. Bubble Detachment Parameter, cm <sup>3</sup> K/Ws	483.0 (10.62)	373.6 (12.06)

\*) Quantities in parentheses indicate time (in seconds) at which values occur

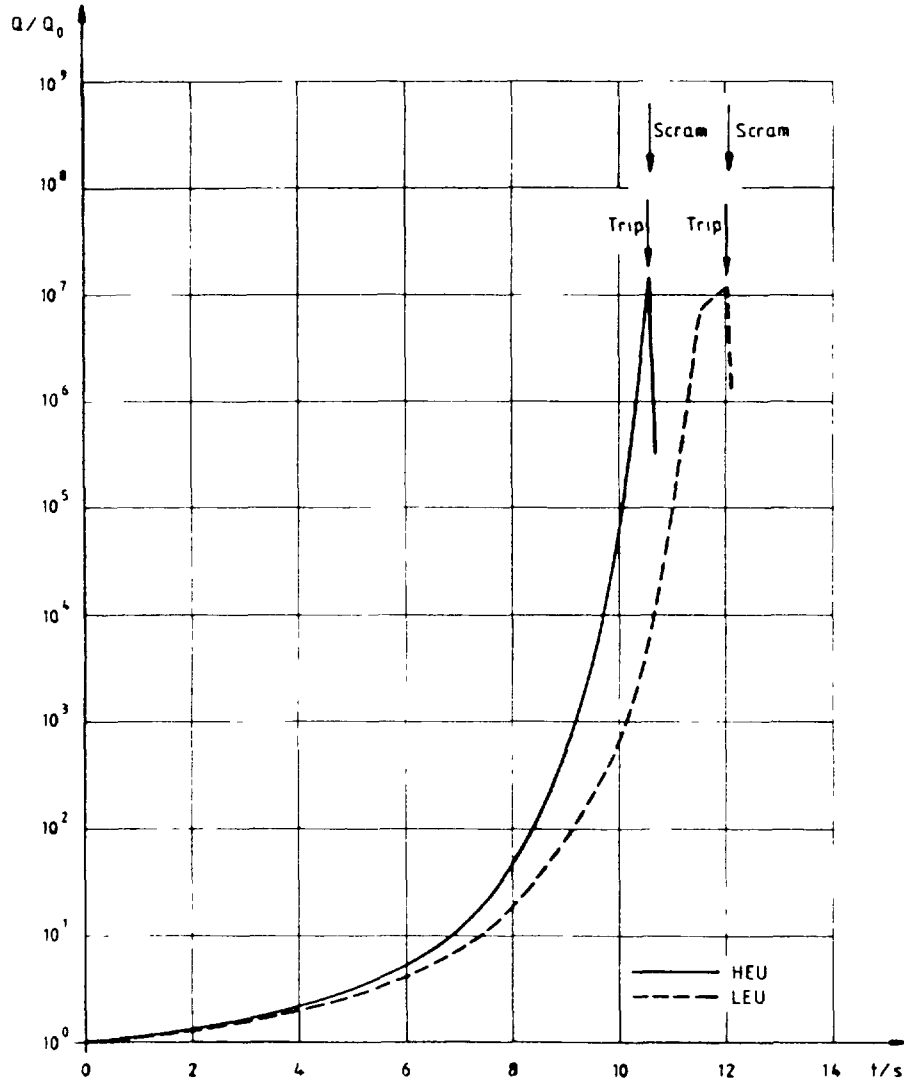


FIG. 3-7. Slow reactivity insertion transient: relative power generated in the fuel.

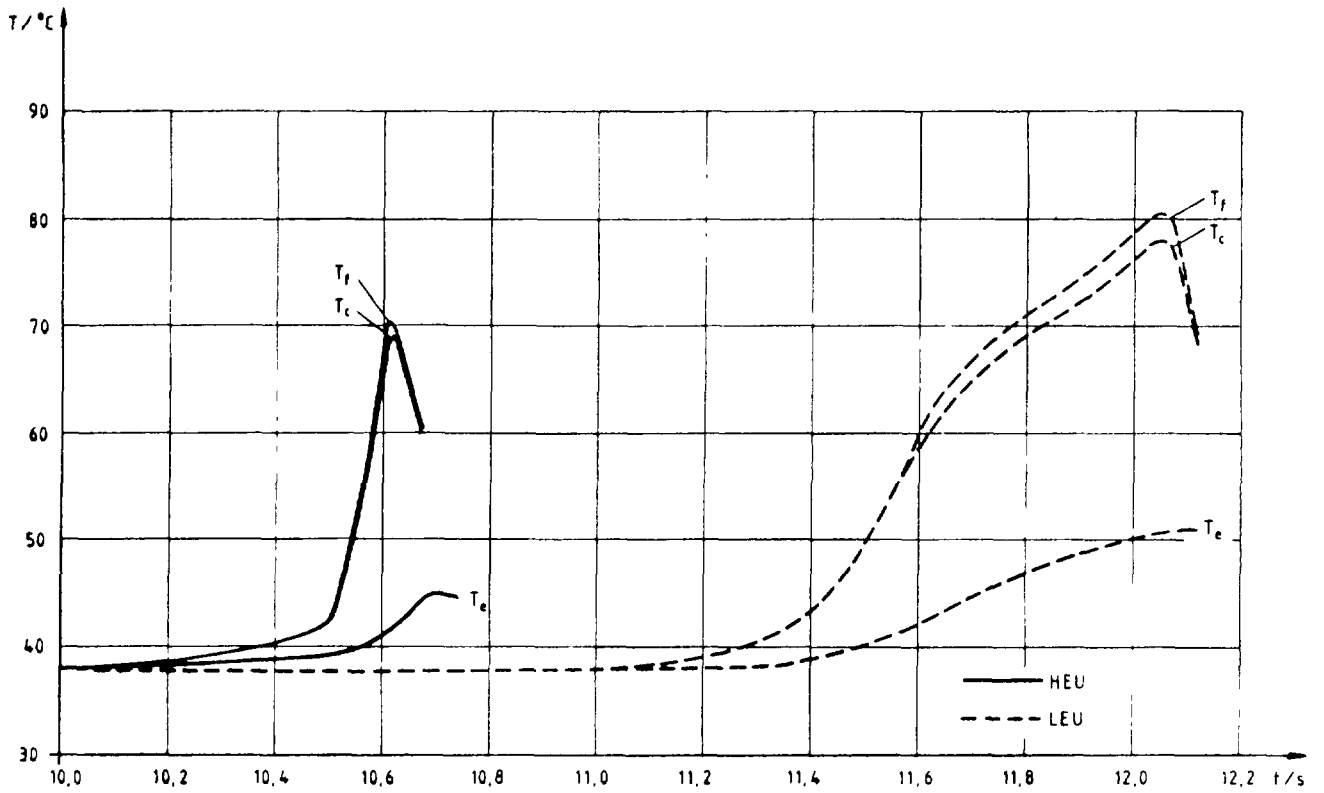


FIG. 3-8. Slow reactivity insertion transient: maximum fuel and clad temperatures, hot channel coolant exit temperature.

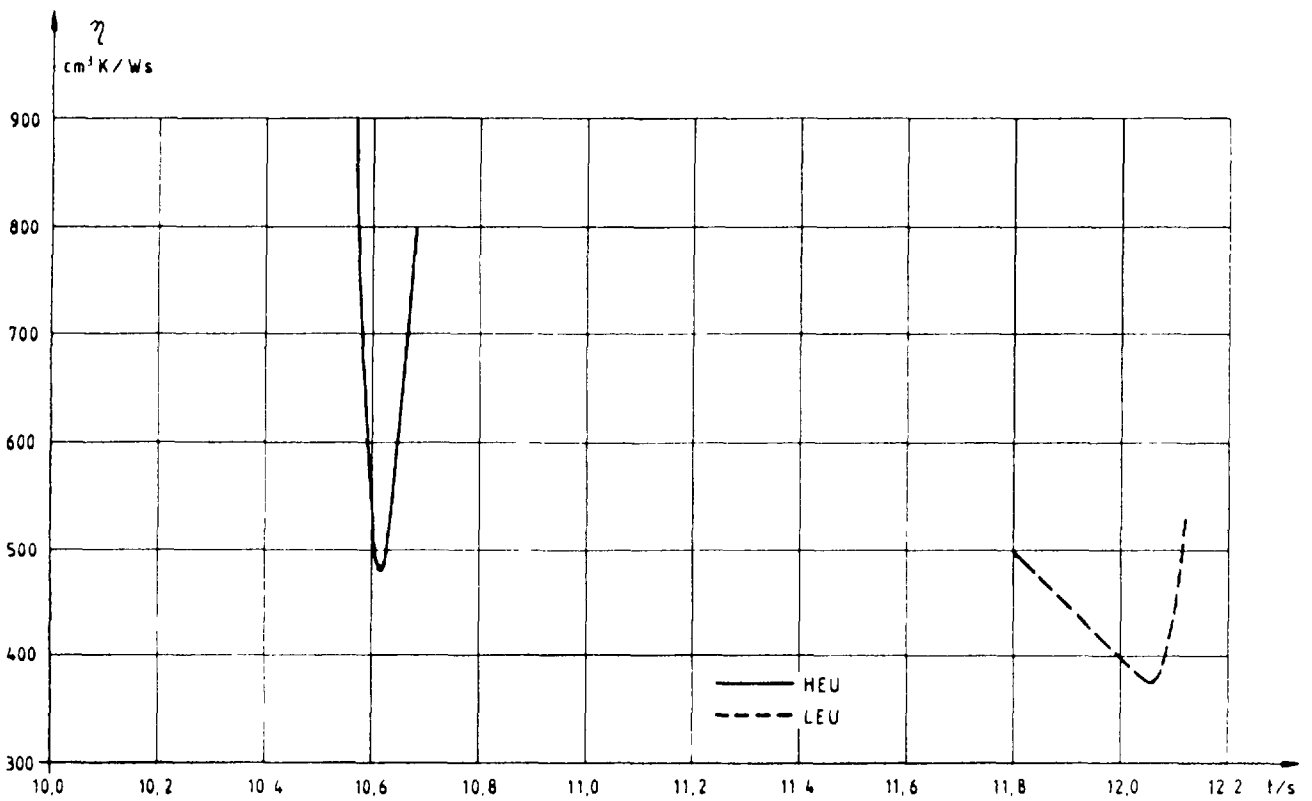


FIG. 3-9. Slow reactivity insertion transient: minimum bubble detachment parameter.

Table 3-4: Fast Reactivity Insertion Transient

Fuel	HEU	LEU	LEU
Reactivity Insertion Rate, $\$/s$	3	2.7	3
Max. Reactivity, $\$$	1.5	1.35	1.5
Initial Power, W	1	1	1
Trip Point, MW	12 (0.6047)*	12 (0.6497)	12 (0.5686)
Flow Rate, $m^3/h$	1000	1000	1000
Time Delay, s	0.025	0.025	0.025
Minimal Period, s	0.014	0.017	0.012
Peak Power, MW	135.1 (0.650)	62.9 (0.688)	143.9 (0.608)
Total Energy Release to Time of Peak Power, Ws	$3.14 \times 10^6$	$1.59 \times 10^6$	$2.83 \times 10^6$
Peak Fuel Temperature, $^{\circ}C$	173.4 (0.665)	111.0 (0.708)	185.8 (0.625)
Peak Clad Temperature, $^{\circ}C$	160.0 (0.665)	105.1 (0.710)	168.2 (0.625)
Peak Outlet Temperature, $^{\circ}C$	70.7 (0.783)	52.0 (0.840)	63.2 (0.740)
Min. Bubble Detachment Parameter, $cm^3 K/Ws$	33.8 (0.670)	206.2 (0.710)	45.8 (0.635)

\* Quantities in parentheses indicate time (in seconds) at which values occur

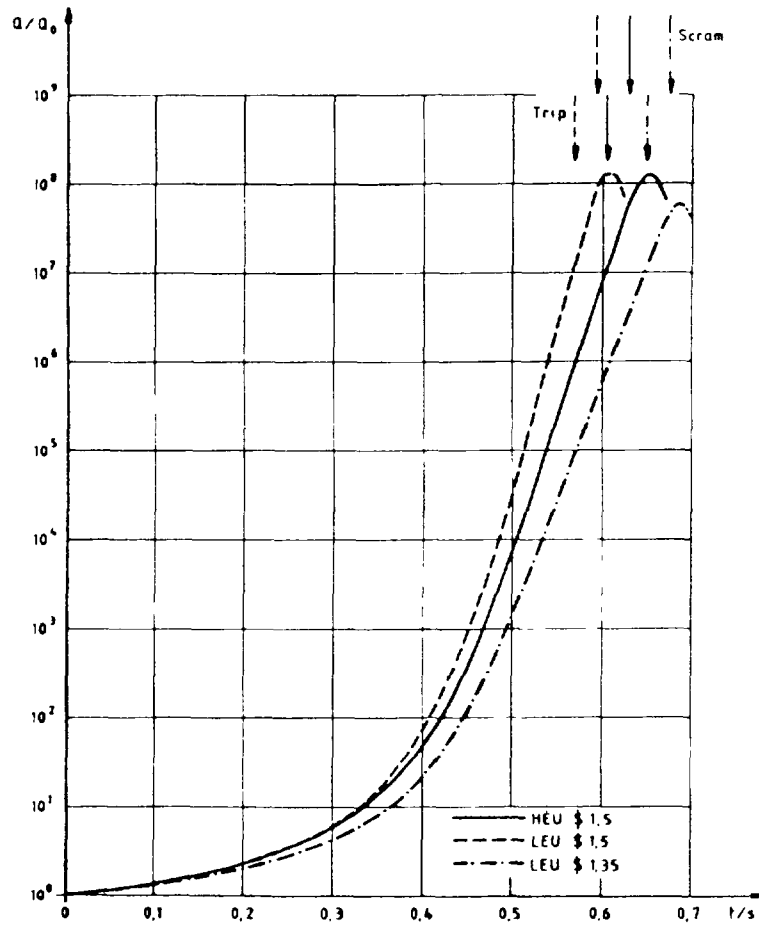


FIG. 3-10. Fast reactivity insertion transient: relative power generated in the fuel.

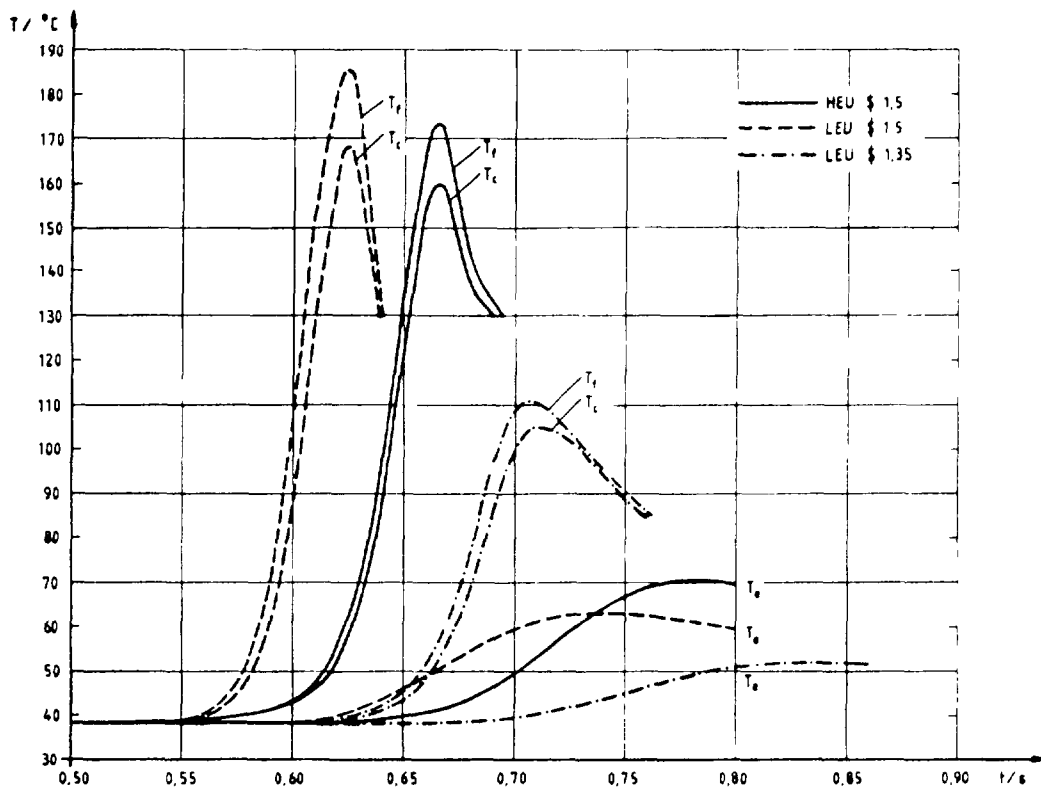


FIG. 3-11. Fast reactivity insertion transient: maximum fuel and clad temperatures, hot channel coolant exit temperature.

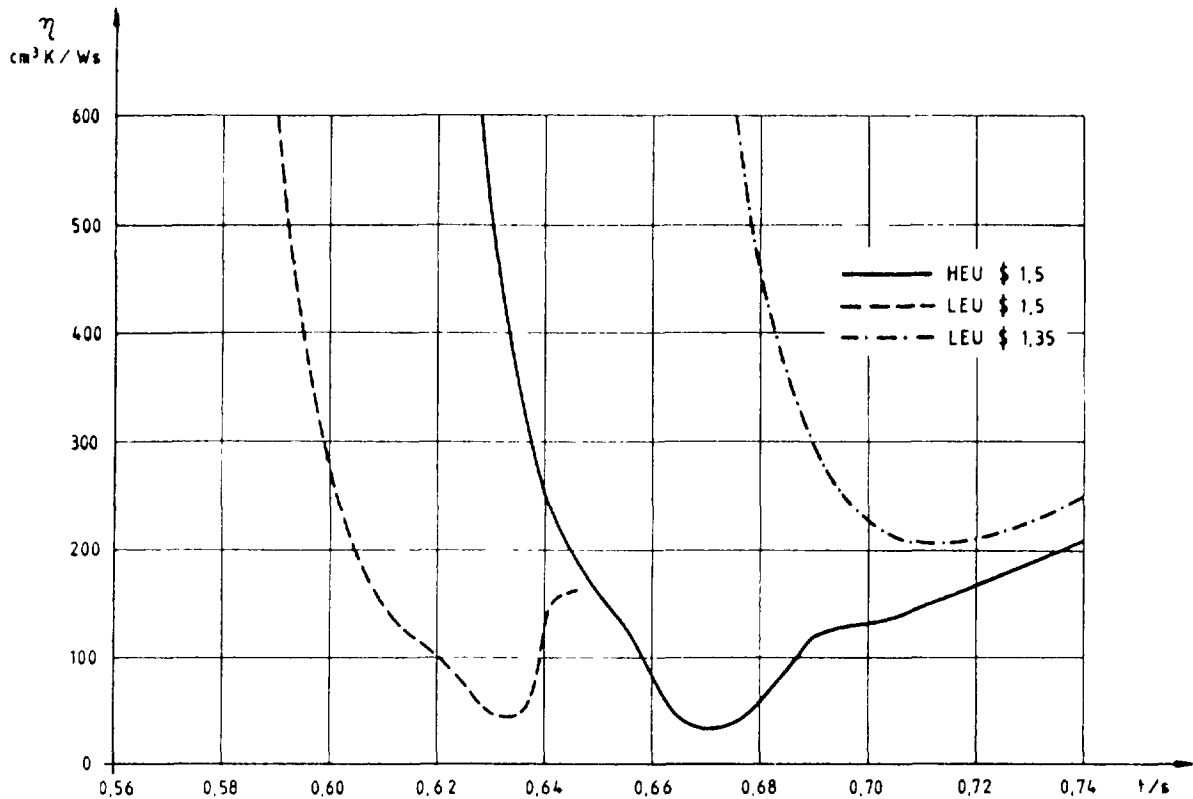


FIG. 3-12. Fast reactivity insertion transient: minimum bubble detachment parameter.

### 3.5 Discussion and Conclusions

#### 3.5.1 Fast Loss-of-Flow Transient

It is evident from Table 3-1 and Figures 3-1 to 3-3 that the transients are almost identical for HEU and LEU fuel. Though the negative net reactivity due to the increase in coolant and fuel temperature is slightly larger for LEU fuel this doesn't affect the power level at scram very much. The temperature increase stays below 8 K and the safety margin against excursive flow instability reduces by 25 % compared to steady-state conditions. Since there is still a factor of about 6 between the acceptable and the actual minimum safety margin against flow instability this transient doesn't endanger the core for both types of fuel.

#### 3.5.2 Slow Loss-of-Flow Transient

Table 3-2 and Figures 3-4 to 3-6 show that again the transient behaviour of the core for both types of fuel is almost identical. The temperature increase is less than 4 K and the stability safety margin is reduced by 14 % but still amounts to about 7. As for the fast flow coastdown we conclude that this transient doesn't cause any problems for HEU and LEU cores.

### 3.5.3 Slow Reactivity Insertion Transient

As can be seen in Table 3-3 and Figures 3-7 to 3-10 the HEU and LEU cores behave markedly different. In the HEU case the trip point is reached earlier because the reactivity feedback is less than for the LEU core. Consequently the peak power is higher too. On the other hand the total energy released to the time of peak power is by a factor of 3.9 higher for LEU than for HEU. Therefore the coolant and fuel plate temperatures for the LEU core are above the ones for the HEU core. In line with this behaviour the safety margin against flow instability is lower for the LEU core than for the HEU core. It is interesting to note, however, that even for the LEU core the peak coolant and fuel plate temperatures are slightly below and the flow stability safety margin is about 10 % above the values reached at steady state under overpower conditions.

Thus we conclude that the transition from HEU to LEU aggravates this type of transient somewhat, but that the consequences are still less severe than that one encountered during steady-state operation of the core at overpower.

### 3.5.4 Fast Reactivity Insertion Transient

First the different behaviour of the HEU- and LEU-core after the ramp insertion of 1.5 \$ will be discussed. The trip point is reached somewhat earlier and the peak power is slightly higher for LEU than for HEU. The total energy release for time of peak power is marginally lower for LEU than for HEU but more energy is stored in the fuel plates for LEU and thus these temperatures are a few degrees above the HEU-case. The flow stability margin is 36 % higher for LEU than for HEU. In conclusion we can say that this type of transient has comparable consequences for the HEU- and LEU-core.

The reduced reactivity insertion for a LEU-core, i. e. 1.35 \$ in 0.5 s, causes a much less severe transient than the 1.5 \$ transients discussed above.

**IAEA SAFETY-RELATED BENCHMARK CALCULATIONS**

Y. NAITO, M. KUROSAWA, Y. KOMURO,  
R. OYAMADA, Y. NAGAOKA  
Japan Atomic Energy Research Institute,  
Tokai-mura, Naka-gun, Ibaraki-ken,  
Japan

**Abstract**

The results of static and transient calculations are provided for the IAEA safety-related benchmark problem.

**1. Static Calculations for a 10 MW Light Water Research Reactor**

by Y.Naito, M. Kurosawa, and Y.Komuro

**1.1 Calculation Method**

The neutronic calculations have been performed with the computer code system RETER-ACE which was used for solving the previous IAEA benchmark problems for light water research reactors (IAEA-TECDOC-233, 1980). Treatment of fission products is different from the previous one where only three lumped fission products are assumed. In the present calculations important decay chains are selected and the birth and decay of individual isotopes which belong to the chains are calculated without lumping the fission products. The less-important fission products are lumped into one pseudo nuclide. In the RETER-ACE system, 26 energy cross sections (MGCL 26) are applied for cell burn-up calculation and collapsed to 3 or 4 group constants with burn-up dependent neutron energy spectrum for succeeding diffusion calculations. The cut off energies for 3 groups are 5.53 Kev and 0.68256 ev. For cell calculation, one dimensional Sn transport routine ANISN-JR is used, and for core calculation two dimensional diffusion routine 2DFEM with finite element method is used. With this 2DFEM, not only an effective multiplication factor of a core is calculated but also neutron generation time, effective delayed neutron fraction and so on are obtained with both real and adjoint fluxes.

**1.2. Computed Results**

The reactor cores for this calculations are same as the 10 MW reactor used for the previous neutronics benchmark calculations except the more realistic structure of central irradiation channel box.

**1.2.1 Prompt Neutron Generation Time and Delayed Neutron Fraction**

Delayed neutron energy spectra and fraction data are derived from Keepin (Physics of Nuclear Kinetics by G.R. Keepin). The computed results of prompt neutron generation time and delayed neutron fraction at the BOL core are shown in Table 1.

Table 1 Prompt Neutron Generation Time and Delayed Neutron Fraction at BOL

	HEU	LEU
$\Lambda(\mu s)$	57.60	44.39
$\beta_{eff}(\%)$	0.744	0.7219

### 1.2 2 Isothermal Reactivity Feedback Coefficients

Changing water temperature, water density, and fuel temperature, effective multiplication factors  $k_{eff}$  at the BOL core are computed. With these computed results, isothermal reactivity feedback coefficients are obtained.

Change of water temperature only  
 \*\*\*\*\*

Values of  $k_{eff}$  were computed for water temperature of 27°C, 50°C, and 100°C taking into consideration of the different movement of the hydrogen atoms at different temperature where the moderator density was assumed to be 1.0 g/cm<sup>3</sup> throughout these calculations. The results are presented in Table 2

Table 2 Reactivity Coefficient for Change of Water Temperature  
 $T_W$  Only ( $\rho_W = 1.0$  g/cm<sup>3</sup>, BOL)

$T_W$ °C	HEU		LEU	
	$\Delta\rho \times 10^3$	$\frac{\Delta\rho}{\Delta T_W} \times 10^5$	$\Delta\rho \times 10^3$	$\frac{\Delta\rho}{\Delta T_W} \times 10^5$
27	---	---	---	---
50	-2.32	-10.09	-2.15	-9.35
100	-8.23	-11.82	-6.26	-8.22

Change of water density only  
 \*\*\*\*\*

Values of  $k_{eff}$  were computed for water densities of 1.0, 0.993, 0.975, 0.958, 0.900 and 0.800 where the moderator temperature was assumed to be 27°C throughout these calculations. The results are presented in Table 3.

Change of fuel temperature only  
 \*\*\*\*\*

Values of  $K_{eff}$  were computed for fuel temperature of 27°C, 100°C, 200°C and 287°C where the moderator temperature and density were assumed to be 27°C and 1.0 g/cm<sup>3</sup> respectively throughout these calculations. The results are presented in Table 4.

Table 3 Reactivity Coefficients for Change of Water Density

$\rho_w$  Only (T = 27°C, BOL)

$\rho_w$	$T_w$	HEU			LEU		
		$\Delta\rho \times 10^3$	$\frac{\Delta\rho}{\Delta\rho_w} \times 10^3$	$\frac{\Delta\rho}{\Delta T_w} \times 10^5$	$\Delta\rho \times 10^3$	$\frac{\Delta\rho}{\Delta\rho_w} \times 10^3$	$\frac{\Delta\rho}{\Delta T_w} \times 10^5$
1.0	4.	1.37	195.7	4.03	1.53	218.6	4.50
.993	38.	---	---	---	---	---	---
.975	75.	-3.42	-190.0	-10.82	-4.18	-232.2	-11.80
.958	100.	-6.95	-207.6	-14.12	-8.30	-242.4	-16.48
.900		-19.80	-221.6		-21.73	-231.6	
.800		-45.99	-261.9		-53.10	-313.7	

Table 4 Reactivity Coefficients for Change of Fuel Temperature  $T_F$  Only ( $\rho_w = 1.0 \text{ g/cm}^3$ , BOL)

$T_F$	HEU		LEU	
	$\Delta\rho \times 10^3$	$\frac{\Delta\rho}{\Delta T_F} \times 10^5$	$\Delta\rho \times 10^3$	$\frac{\Delta\rho}{\Delta T_F} \times 10^5$
27	---	---	---	---
100	- 0.068	- 0.093	- 1.390	- 1.904
200	- 0.125	- 0.056	- 3.210	- 1.820
287	- 0.160	- 0.040	- 4.708	- 1.722

Table 5 compares the initial slope of the above three reactivities as coefficients for a temperature change from 27°C to 100°C. The LEU core has slightly large initial feedback slopes than the HEU core.

### 1.2.3 Control Rod Worths

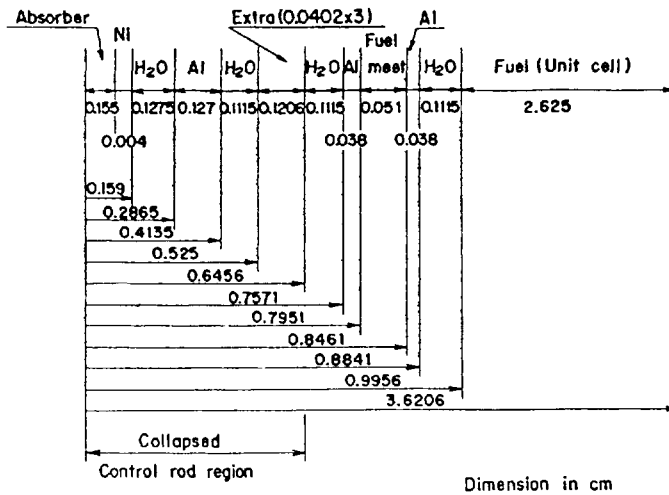
The averaged cross sections of control elements were obtained by a one-dimensional Sn routine ANISN-JR. The model for cell calculation is shown in Fig. 1. Reactivity worths of four control elements in the core are shown in Table 6.

Table 5 Initial Slopes of Reactivity Components  
(27°C → 100°C)

Effect	HEU	LEU
	$\Delta\rho/\Delta T \times 10^5 / ^\circ\text{C}$	$\Delta\rho/\Delta T \times 10^5 / ^\circ\text{C}$
Water Density	-11.210	-13.387
Water Temperature	-11.274	- 8.575
Fuel Temperature	- 0.093	- 1.904
Total	-22.577	-23.866

Table 6 Control Rod Worth at BOL

Absorber	HEU	LEU	HEU-LEU
	Control Rod Worth $\Delta\rho_H (\% \Delta K / K)$	Control Rod Worth $\Delta\rho_L (\% \Delta K / K)$	$\Delta\rho_H - \Delta\rho_L$ (% $\Delta K / K$ )
Ag-In-Cd	17.47	13.94	3.53
B <sub>4</sub> C	23.08	19.03	4.05



Al	Al-27 $6.0260 \times 10^{-2}$	Ag / In / Cd	Ag-107 $2.150 \times 10^{-2}$ Ag-109 $2.037 \times 10^{-2}$ In-113 $3.017 \times 10^{-4}$ In-115 $6.832 \times 10^{-3}$ Nat Cd $2.465 \times 10^{-3}$
H <sub>2</sub> O	H-1 $6.6856 \times 10^{-2}$ O-16 $3.3428 \times 10^{-2}$		
Extra	H-1 $1.7122 \times 10^{-2}$ O-16 $8.5609 \times 10^{-3}$ Al-27 $4.4827 \times 10^{-2}$	B <sub>4</sub> C	B-10 $2.056 \times 10^{-2}$ B-11 $8.938 \times 10^{-2}$ C-12 $2.744 \times 10^{-2}$
NI	Nat Ni $9.130 \times 10^{-2}$		

Fig.1 Calculation model for a control rod cell

## 2. Transient Calculations

by R. Oyamada, Y. Nagaoka

### 2 1 Common Input Data

Common input data for the loss-of-flow transient and the reactivity insertion transient analysis are as follows :

- Hot Channel Factors
  - Radial \* Local Power Peaking Factor : 1.4
  - Axial Power Peaking Factor : 1.5
  - Engineering Factor : 1.2
- Normal Flow Rate : 1000 m<sup>3</sup>/hr
- Coolant Inlet Temperature : 38°C
- Coolant Inlet Pressure : 1.7 bar absolute
- Thermal Conductivity
  - UAlx-Al Meat : 1.58 W/cm.°C (HEU)
  - : 0.5 W/cm °C (LEU)
  - Al Clad : 2.034 W/cm.°C
- Heat Capacity
  - UAlx-Al Meat : 0.176 cal/g.°C (HEU)
  - : 0.080 cal/g.°C (LEU)
  - Al Clad : 0.215 cal/g.°C
- Density
  - UAlx-Al Meat : 3 233 g/cm<sup>3</sup> (HEU)
  - : 6 108 g/cm<sup>3</sup> (LEU)
  - Al Clad : 2 7 g/cm<sup>3</sup>

(Following data are the values calculated as described in the static calculations)

- Prompt Neutron Generation Time : 55 96  $\mu$ s (HEU)
- : 44 39  $\mu$ s (LEU)
- Delayed Neutron Fraction : 0 007444 (HEU)
- : 0 007219 (LEU)
- Isothermal Reactivity Feedback Coefficients
  - Change of Water Temperature : -0 01515  $\$/^{\circ}$ C (HEU)
  - (20°C -100°C) : -0 01188  $\$/^{\circ}$ C (LEU)
  - Change of Water Density : -2 844 \$ (HEU)
  - (1 0- 0 9) : -3 222 \$ (LEU)
  - Change of Fuel Temperature : -1 249 E-4  $\$/^{\circ}$ C (HEU)
  - : -2 637 E-3  $\$/^{\circ}$ C (LEU)

### 2 2 Loss-of-Flow Transient

#### 2 2 1 Calculation Method

Loss-of-Flow Transient was calculated using RELAP 4/MOD 5 Ref 1 which is a program to analyze transient thermal-hydraulics of nuclear reactor

Temperature rise along axial direction was calculated in small length increments for both of average and hot channels. The axial power distribution was represented by distribution factors at 17 axial mesh points based on a chopped cosine shape with a 15 mm extrapolation length, which gives the peak-to-average ratio to be 1.5

In calculation of feedback reactivities, only the average channel was taken for simplicity. That is, the core was assumed to consist of one region with average channels. For axial direction, weight functions proportional to square of neutron flux were taken into account.

Dittus and Boelter heat transfer correlation Ref 2) for subcooled liquid forced convection was used.

Decay heat model used was one provided in RELAP-4, which is similar to the proposed ANS-standard model Ref 3). Infinite operating time prior to shutdown was assumed in obtaining the decay heat.

Calculation conditions were as follows :

- Initial reactor power : 12 MW
- Flow is reduced as  $\exp(-t/T)$ , with  $T = 1$  second and  $T = 25$  seconds.
- Reactor scram initiated at 85% of normal flow, with a 200 ms delay before linear shutdown reactivity insertion of  $-\$10$  in 1/2 sec.

TABLE 7 Results for Transient Response of HEU and LEU Benchmark Cores to a Loss-of-Coolant Flow with a Decay Time of 1.0 s.

<u>Peak</u>	<u>T, °C (t, s)</u>	
	<u>HEU</u>	<u>LEU</u>
Clad Surface	98.4 (0.40)	97.1 (0.40)
Coolant Exit	58.4 (0.48)	58.1 (0.48)
<u>At 10.0 s</u>	<u>T, °C</u>	
	<u>HEU</u>	<u>LEU</u>
Clad Surface	106.0	95.2
Coolant Exit	48.4	49.3

### 2.2.2 Computed Results

The results for the case with flow decay of  $T = 1$  second are shown in Table 8 and in Fig. 2.

The results for the case with flow decay of  $T = 25$  seconds are shown in Table 9 and in Fig. 3.

As can be seen in these tables and figures the HEU and the LEU cores show almost identical transient.

TABLE 8 Results for Transient Response of HEU and LEU Benchmark Cores to a Loss-of-Coolant Flow with a Decay Time of 25.0 s.

<u>Peak</u>	<u>T, °C (t, s)</u>	
	<u>HEU</u>	<u>LEU</u>
Clad Surface	96.4 (4.2)	96.1 (4.2)
Coolant Exit	57.7 (4.3)	57.5 (4.3)

<u>At 10.0 s</u>	<u>T, °C</u>	
	<u>HEU</u>	<u>LEU</u>
Clad Surface	41.1	41.1
Coolant Exit	39.0	39.0

TABLE 9 Results for Slow Reactivity Insertion Transients in HEU and LEU Benchmark Cores

<u>Ramp</u>	<u>HEU</u>	<u>LEU</u>
	<u>10¢/s</u>	<u>9¢/s</u>
Trip Time		
12 MW, s	10.643	11.900
P (t <sub>m</sub> ), MW	13.75 (10.668)	12.35 (11.923)
T <sub>feul</sub> (t), °C	70.5 (10.688)	81.2 (11.933)
T <sub>clad</sub> (t), °C	69.2 (10.693)	78.5 (11.933)
T <sub>exit</sub> (t), °C	47.7 (10.773)	52.8 (11.978)
E <sub>t<sub>m</sub></sub> , MJ	1.75	4.69

<u>20.0 s</u>		
P, MW	0.006	0.015
E, MJ	2.35	5.48

t<sub>m</sub> = time to peak power; E<sub>t<sub>m</sub></sub> = energy release to time of peak power.

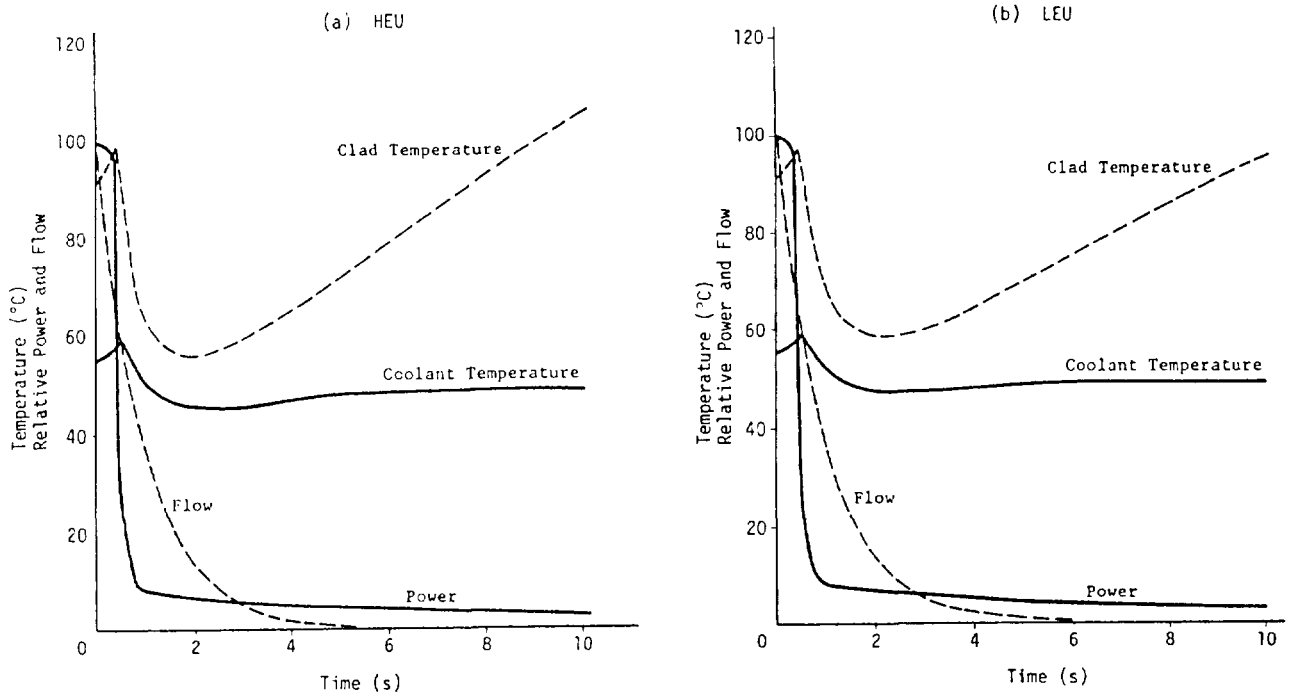


Fig. 2 Transient Responses of HEU and LEU Benchmark Cores to a Loss of Coolant Flow with Decay Time of 1.0 Sec.

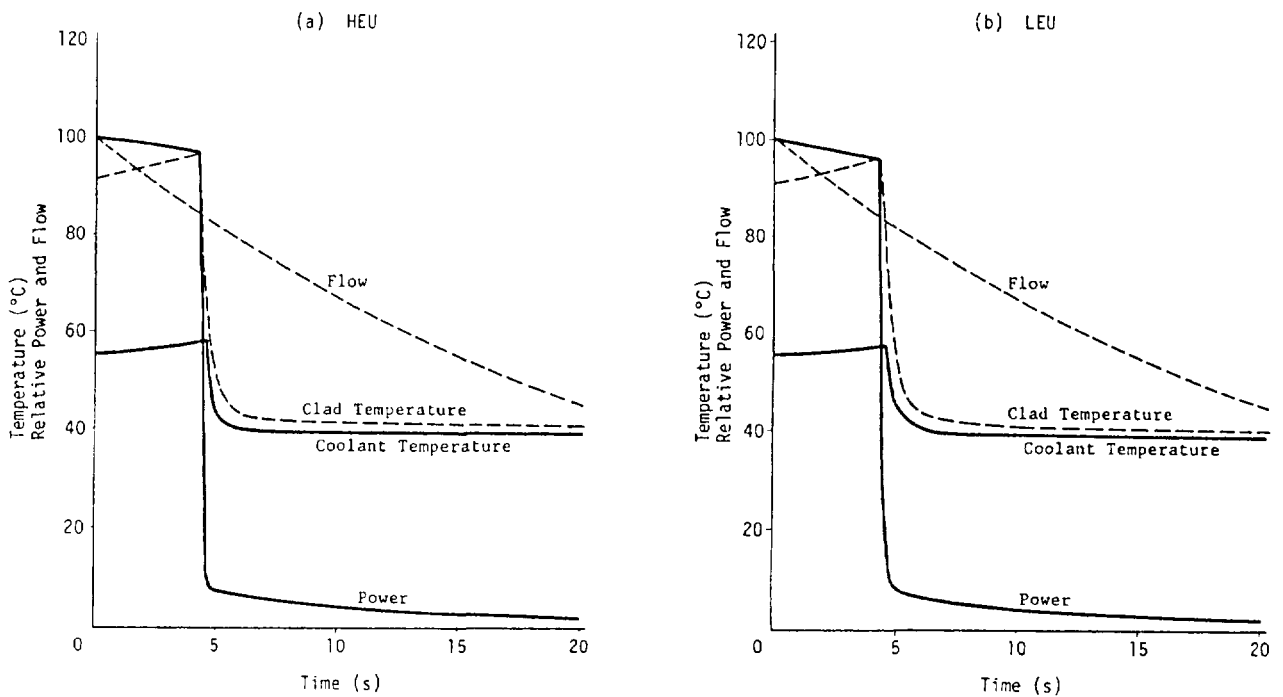


Fig. 3 Transient Responses of HEU and LEU Benchmark Cores to a Loss of Coolant Flow with Decay Time of 25 Secs.

## 2.3 Reactivity Insertion Transient Calculations

### 2.3.1 Calculation Method

Reactivity insertion transient analyses were performed using the code EUREKA-PT, which was developed by modifying EUREKA Ref 4) for plate-type reactors, and its reliability has been demonstrated through the SPERT-III C core experiment analyses. The code provides a coupled thermal, hydrodynamic, and point kinetics capability with continuous reactivity feedback.

The calculation model used is similar to that used in the loss-of-flow transient calculations described in 2.2.1, except that the EUREKA-PT code uses one channel to represent the hottest plate and the other 'average' channel to represent the remaining 550 fuel plates in a volume weight sense.

As described in 2.2.1, weight functions proportional to square of neutron flux were taken into account for regionwise reactivity feedback coefficients. In order to assess the importance of the regionwise reactivity feedback coefficients, a transient calculation for the LEU core with reactivity of  $1.5\$/0.5\text{sec}$  insertion were also carried out on the case without treating the weight function i.e. with isothermal reactivity feedback coefficients. The results show the peak power is only at most 2% higher than that of the case with treating the weight functions. This suggests that taking the regionwise reactivity coefficient is not so important.

Calculation conditions were as follows :

#### Slow Reactivity Insertion Transient

- Reactor critical at an initial power of 1 Watt
- Ramp reactivity insertion rates : 10 cent/sec (HEU)  
: 9 cent/sec (LEU)
- Safety system trip point : 1.2 Po = 12 MW
- Time delay of 25 ms before linear shutdown reactivity insertion of - \$10 in 1/2 sec.
- Hot channel factor : Radial \* Local \* Axial \* Engineering  
No overpower factor is included since safety system trip point is set at 1.2 Po = 12 MW.

#### Fast Reactivity Insertion Transient

Repeated above for HEU and LEU cores with :

- Ramp reactivity insertions : \$1.5 in 1/2 sec (HEU)  
: \$1.5 in 1/2 sec (LEU)  
: \$1.35 in 1/2 sec (LEU)

### 2.3.2 Computed Results

The results of calculations for the case of the slow reactivity insertion transients are shown in Table 9 and Fig. 4.

In the LEU case the effect of the Doppler feedback is represented explicitly. Consequently the energy released is larger in the LEU core than in the HEU core, though the peak power is smaller in the former case.

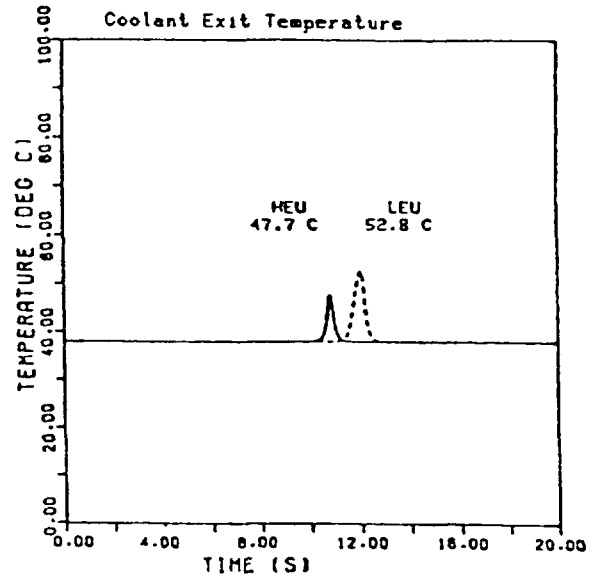
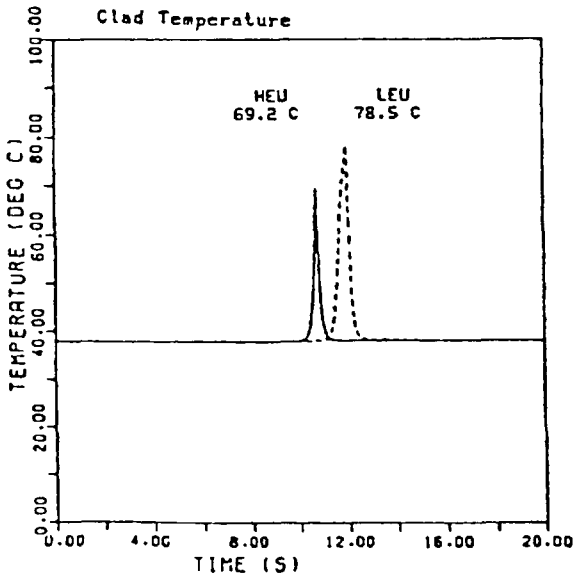
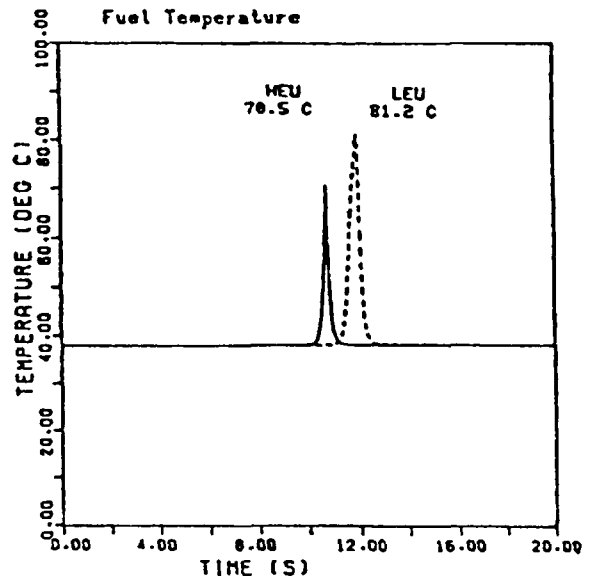
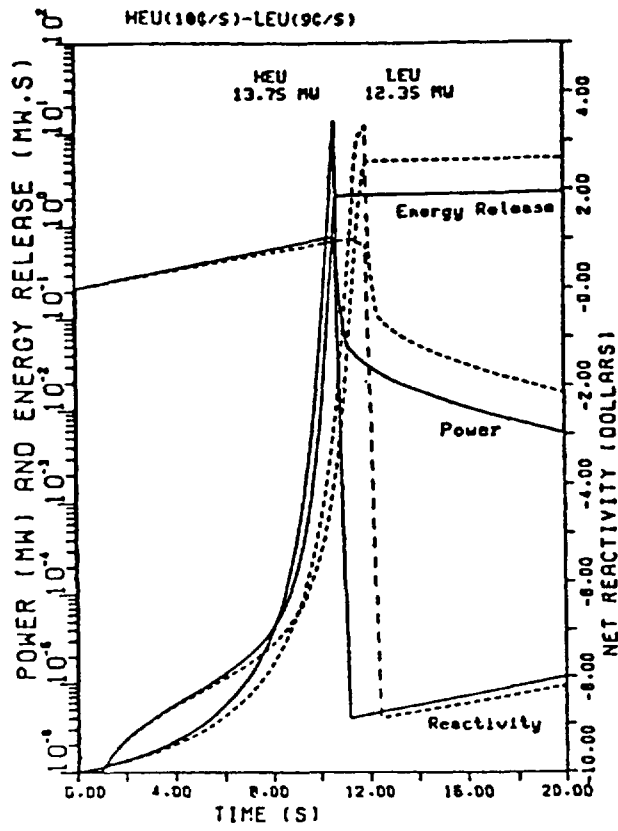


Fig. 4 Transient Responses of Benchmark Cores to Reactivity Insertion of 10  $\rho$ /s for HEU and 9  $\rho$ /s for LEU

The results of calculations for the case of the fast reactivity insertion transients are shown in Tables 10 and 11 and Fig.5 through 7.

The power, released energy, and temperature are lower in the HEU core than in the LEU core for both 1.5\$/0.5sec and 1.35\$/0.5sec cases. This is attributed to large prompt neutron generation time of the HEU core.

TABLE 10 Results for Fast Reactivity Insertion Transients in HEU and LEU Benchmark Cores

Ramp	HEU		LEU	
	\$1.50/ 0.5 s	\$1.50/ 0.5 s	\$1.35/ 0.5 s	\$1.35/ 0.5 s
Trip Time				
12 MW, s	0.619	0.576	0.660	
Min. Period, ms	15.2	12.2	17.1	
P (t <sub>m</sub> ), MW	114.8 (0.664)	143.8 (0.616)	61.5 (0.697)	
E <sub>t<sub>m</sub></sub> , MJ	2.86	2.95	1.53	
T <sub>fuel</sub> (t, s), °C	155.4 (0.678)	171.0 (0.625)	112.4 (0.719)	
T <sub>clad</sub> (t, s), °C	147.3 (0.678)	149.2 (0.627)	107.2 (0.722)	
T <sub>exit</sub> (t, s), °C	62.3 (0.820)	62.7 (0.762)	55.1 (0.827)	

TABLE 11 Results-Comparison of Fast Reactivity Insertion Transients at \$1.35/0.5 s in HEU and LEU Benchmark Cores

	HEU	LEU
Trip Time		
12 MW, s	0.720	0.660
Min. Period, ms	21.3	17.1
P (t <sub>m</sub> ), MW	50.7 (0.760)	61.5 (0.697)
E <sub>t<sub>m</sub></sub> , MJ	1.53	1.53
T <sub>fuel</sub> (t, s), °C	102.5 (0.786)	112.4 (0.719)
T <sub>clad</sub> (t, s), °C	99.8 (0.787)	107.2 (0.722)
T <sub>exit</sub> (t, s), °C	53.9 (0.891)	55.1 (0.827)

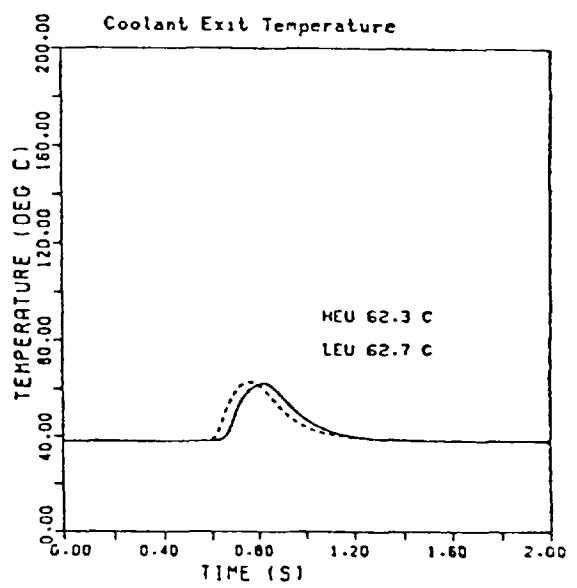
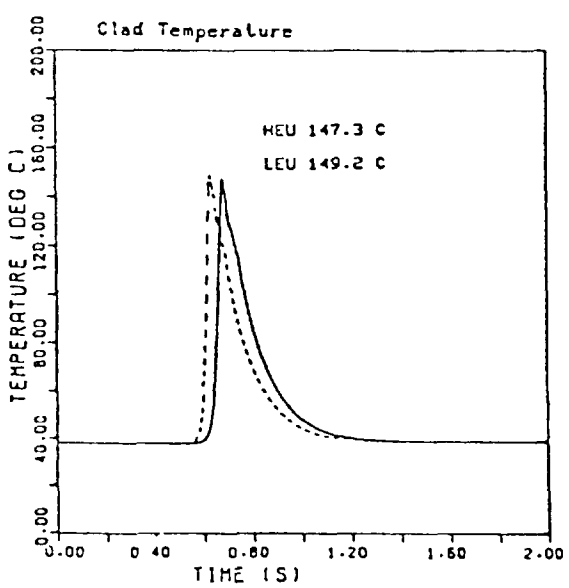
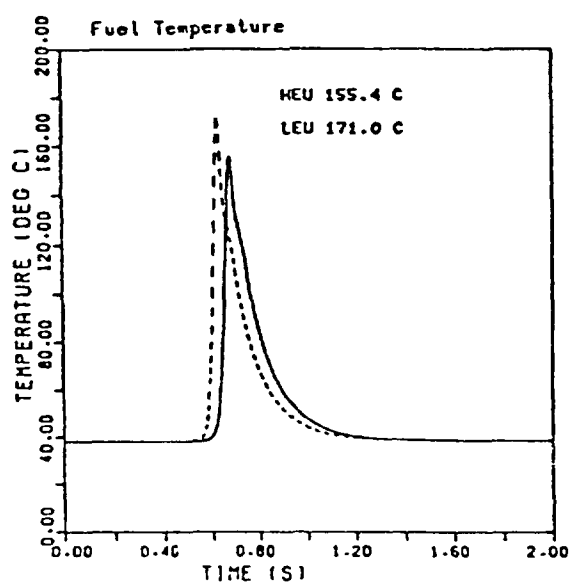
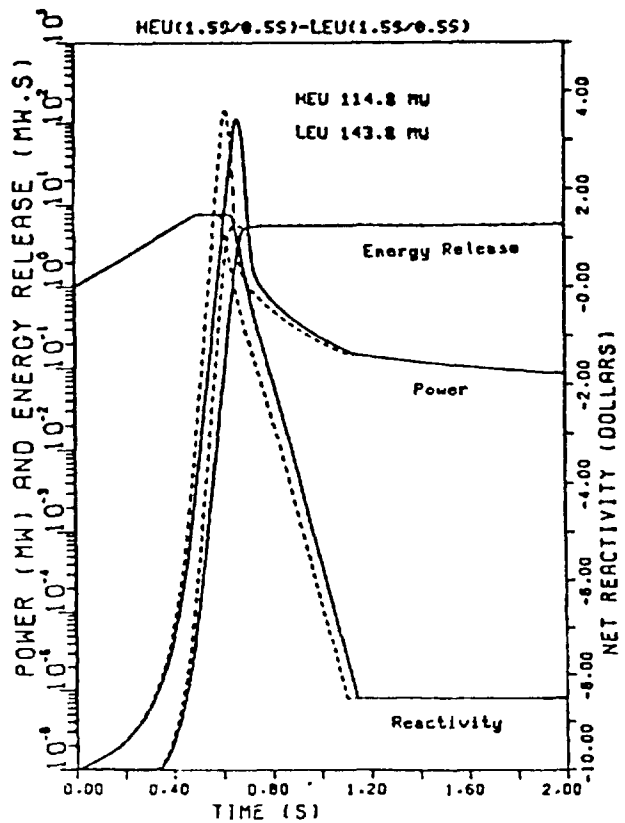


Fig. 5 Transient Responses of HEU and LEU Benchmark Cores to a Reactivity Insertion of \$ 1.5/0.5 s

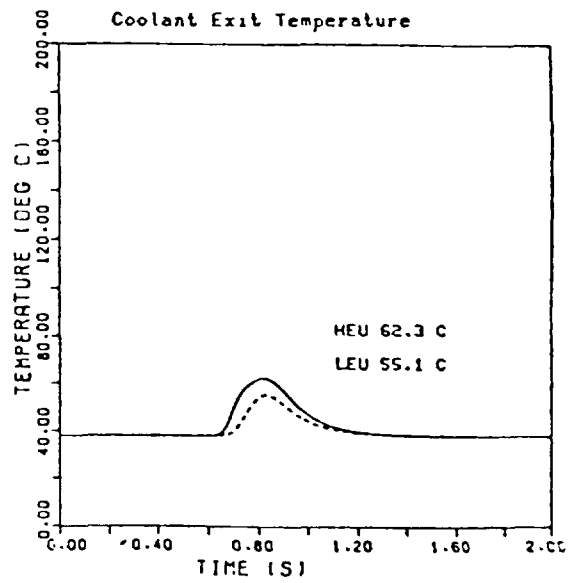
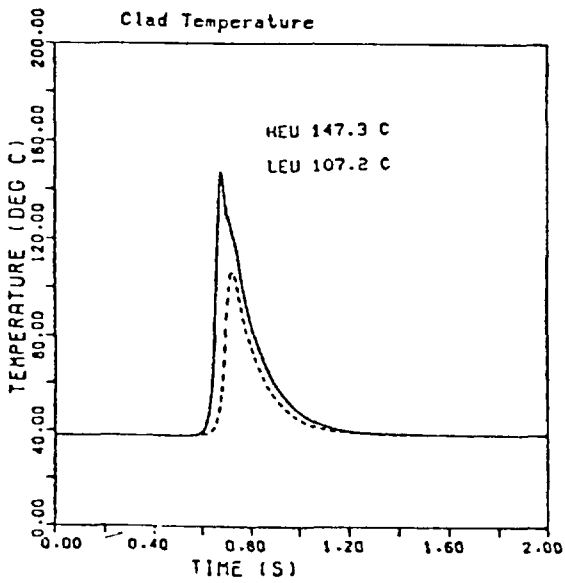
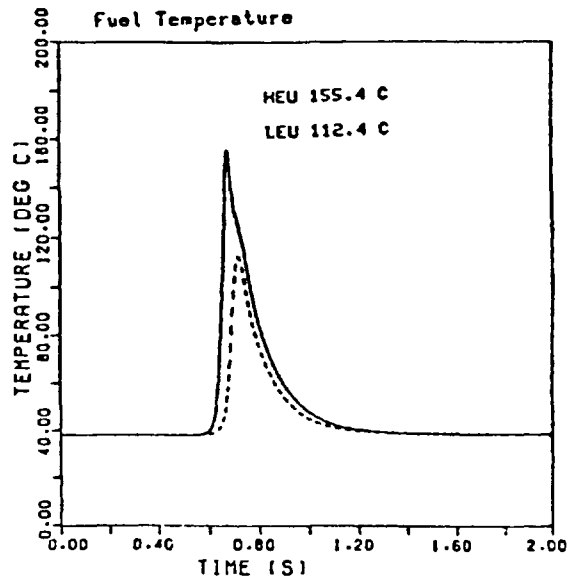
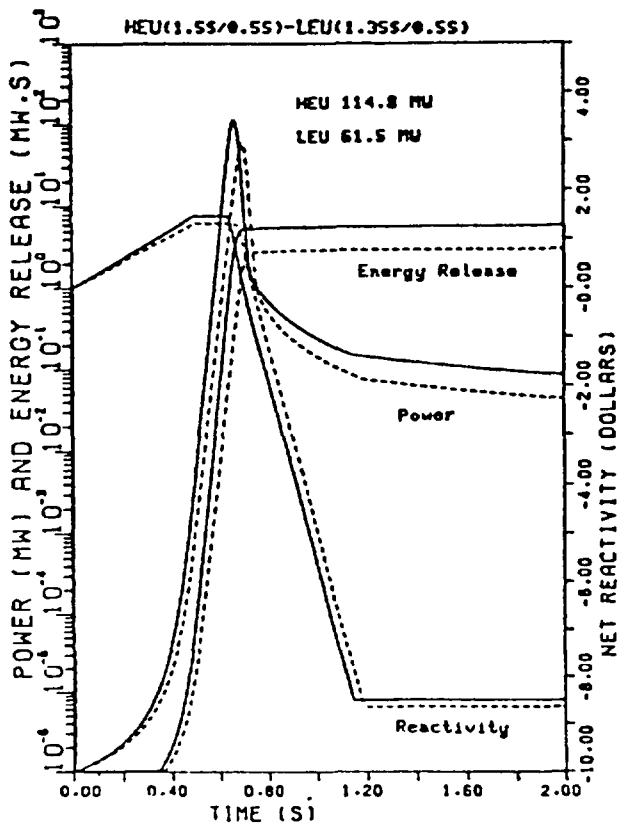


Fig. 6 Transient Responses of Benchmark Cores to Reactivity Insertion of  $\$ 1.5/0.5$  s for HEU and  $\$ 1.35/0.5$  s for LEU

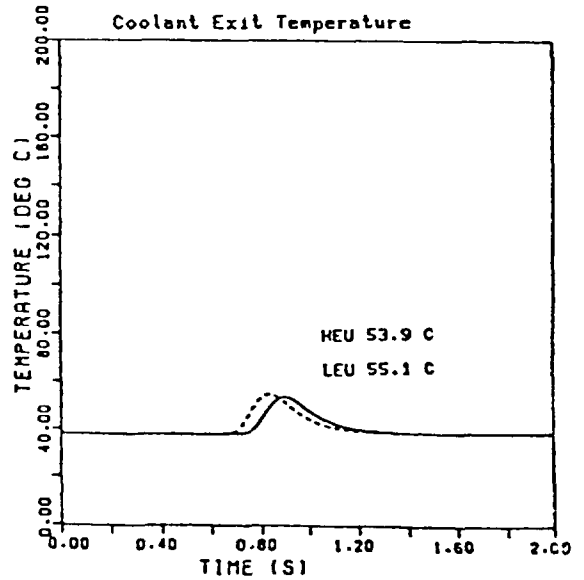
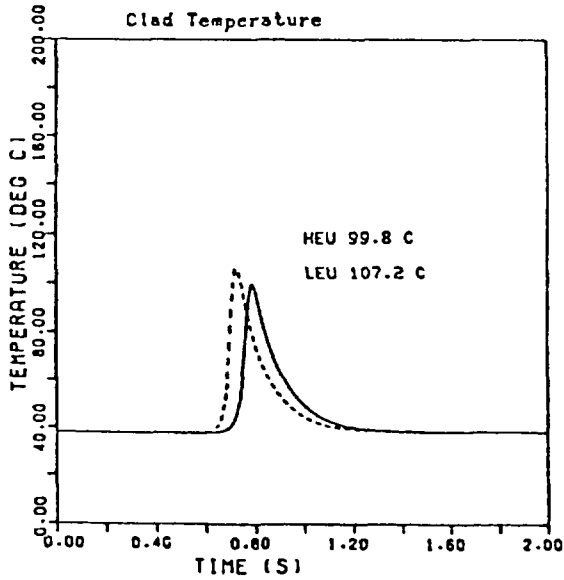
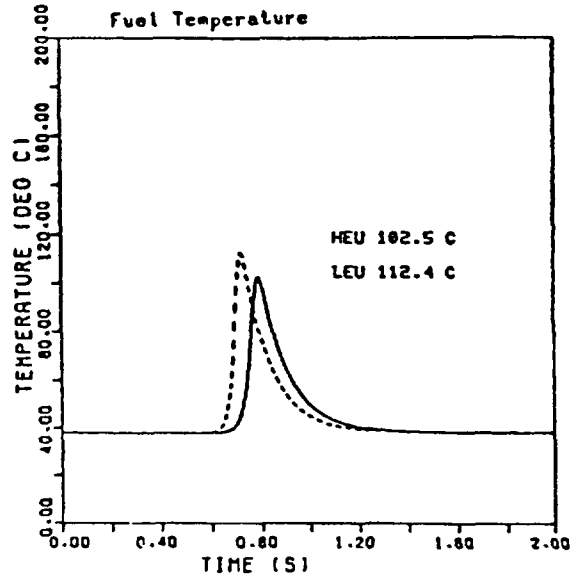
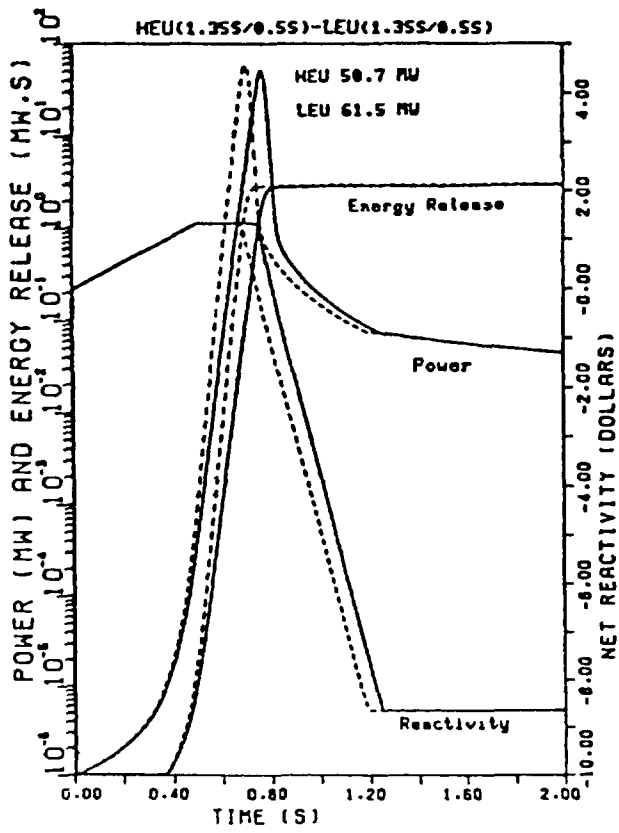


Fig. 7 Transient Responses of HEU and LEU Benchmark Cores to a Reactivity Insertion of  $\beta$  1.35/0.5 s

## REFERENCES

- 1) RELAP-4 /MOD 5 A Computer Program for Transient Thermal-Hydraulic Analysis of Nuclear Reactors and Related Systems, User's Manual, Vol. 1, 2 and 3, ANCR-NUREG-1335 (September, 1976)
- 2) F. W. Dittus and L. M. K. Boelter, Heat Transfer in Automobile Radiators of the Tubular Type, University of California Publications, 2(1930) pp 443 - 461.
- 3) Proposed ANS Standard Decay Energy Release Rates Following Shutdown of Uranium-Fueled Thermal Reactors, ANS-5-1 (October 1971)
- 4) M. Ishikawa, Y. Kuge, N. Ohnishi, E. Takeuchi and Y. Kanbayashi, 'EUREKA : A Computer Code for Uranium-Oxide Fueled, Water Cooled Reactor Kinetic Analysis', JAERI 1235 (September 1974).

**SAFETY-RELATED BENCHMARK CALCULATIONS  
FOR MTR REACTORS**

H. AMATO, H. WINKLER, J. ZEIS  
Eidgenössisches Institut für Reaktorforschung,  
Würenlingen, Switzerland

**Abstract**

Results of the calculated temperature coefficients and dynamic parameters for the IAEA benchmark core are given for HEU, MEU and LEU fuels. Some comparison of the calculated values with experimental data is also presented.

**1. INTRODUCTION**

In connection with the first IAEA-Guidebook on Research Reactor Core conversion from HEU to LEU (Ref.1 ) further safety related BENCHMARK problems have been specified at an IAEA-Meeting in 1981.

This report describes, as a first part, the calculation methods used for the SAPHIR reactor and gives the results of different reactivity coefficients.

The core configuration is the defined BENCHMARK core (Ref. 2) based on a 6 x 5 element core reflected on two sides by graphite.

The calculation results indicate that for the HEU fuel the moderator temperature coefficient dominates, whereas for MEU and especially for LEU fuel the fuel Doppler coefficient becomes dominating for the normal operating conditions. This should give an advantage in certain power excursion cases, because the fuel coefficient is very fast.

**2. Cross Section Data**

The WIMS-D1 Code (Ref. 3) has been used to create the cross section data for the different temperature and water densities. They have been calculated for 5, 25 and 45% burnup for the standard element and 25% burnup for the control element.

The calculations are based on the same homogenized fuel cell as defined in (Ref.4) and have been carried out for 5 neutron energy groups. Table 1 to 3 gives the calculated  $k_{\infty}$  of the different cases for high enriched (HEU, 93%) medium enriched (MEU, 45%) and low enriched (LEU, 20%) fuel elements of the 23 plate MTR type.

Table 1:  $k_{\infty}$  for Change of Water Temperature Only

Burn up %	T(°C)	Infinite Multiplication Factor		
		HEU	MEU	LEU
5	20	1.647994	1.612017	1.561967
	38	1.646455	1.610620	1.560757
	50	1.645482	1.609740	1.559990
	75	1.643573	1.608012	1.558491
	100	1.641822	1.606426	1.557115
25	20	1.558427	1.527404	1.479451
	38	1.556706	1.525850	1.478098
	50	1.555618	1.524869	1.477241
	75	1.553479	1.522941	1.475568
	100	1.551513	1.521177	1.474049
45	20	1.439852	1.419623	1.381651
	38	1.437911	1.417923	1.380213
	50	1.436683	1.4616850	1.379310
	75	1.434261	1.414756	1.377564
	100	1.432033	1.412856	1.375992
KE 25	20	1.452730	1.471622	1.487519
	38	1.451453	1.470426	1.486377
	50	1.450664	1.469691	1.485677
	75	1.449147	1.468293	1.484365
	100	1.447806	1.467079	1.483247

Table 2:  $k_{\infty}$  for Change of Water Density

Burn up %	Density or Void fraction g/cm <sup>3</sup> , %	Corresp. Temp. (°C)	Infinite Multiplication Factor		
			HEU	MEU	LEU
5	0.9982	20	1.647994	1.612017	1.542961
	0.993	38	1.648569	1.612321	1.542971
	0.988	50	1.649106	1.612604	1.542980
	0.975	75	1.650524	1.613338	1.542979
	0.958	100	1.652351	1.614266	1.542942
	5%	20	1.653386	1.514781	1.542902
	10%	20	1.658616	1.617244	1.542438
	20%	20	1.668468	1.621059	1.540058
25	0.9982	20	1.558427	1.527505	1.461206
	0.993	38	1.559058	1.527725	1.461178
	0.988	50	1.559648	1.528024	1.461150
	0.975	75	1.561204	1.528799	1.461051
	0.958	100	1.563209	1.529774	1.460877
	5%	20	1.564342	1.530312	1.460755
	10%	20	1.570064	1.532864	1.459819
	20%	20	1.580774	1.536648	1.456197
45	0.9982	20	1.439852	1.419623	1.363883
	0.993	38	1.440596	1.420010	1.363856
	0.988	50	1.441290	1.420370	1.363828
	0.975	75	1.443126	1.421307	1.363727
	0.958	100	1.445493	1.422487	1.363545
	5%	20	1.446833	1.423142	1.363415
	10%	20	1.453625	1.426277	1.362403
	20%	20	1.466461	1.431112	1.358413
KE 25	0.9982	20	1.452730	1.471622	1.438147
	0.993	38	1.453848	1.472530	1.438534
	0.988	50	1.454894	1.473380	1.438894
	0.975	75	1.457672	1.475627	1.439829
	0.958	100	1.461280	1.478533	1.441007
	5%	20	1.463336	1.480183	1.441660
	10%	20	1.473933	1.488589	1.444773
	20%	20	1.495017	1.504773	1.449557

Table 3:  $K_{\infty}$  for Change of Fuel Temperature Only  
(WIMS - Calculations)

Burn up &	T(°C)	Infinite Multiplication Factor		
		HEU	MEU	LEU
5	20	1.647994	1.612017	1.561967
	38	1.647988	1.611451	1.561000
	50	1.647983	1.611083	1.560371
	75	1.647975	1.610337	1.559098
	100	1.647967	1.609618	1.557870
	200	1.647938	1.606962	1.553339
25	20	1.558427	1.527404	1.479451
	38	1.558421	1.526865	1.478526
	50	1.558417	1.526515	1.477925
	75	1.558410	1.525806	1.476707
	100	1.558402	1.525121	1.475533
	200	1.558374	1.522592	1.471194
45	20	1.439852	1.419623	1.381651
	38	1.439847	1.419117	1.380766
	50	1.439843	1.418788	1.380191
	75	1.439835	1.418120	1.379025
	100	1.439828	1.417476	1.377901
	200	1.439800	1.415095	1.373741
KE 25	20	1.452730	1.471622	1.487519
	38	1.452712	1.471485	1.487309
	50	1.452700	1.471396	1.487172
	75	1.452676	1.471215	1.486894
	100	1.452652	1.471040	1.486626
	200	1.452566	1.470394	1.485631

### 3. Core Calculations

For the calculation of the homogenous reactivity feed back coefficients the two dimensional diffusion code CODIFF of the programme system BOXER (Ref. 5) is used. The BOL-BENCHMARK configuration (Fig. 1a) is the basis of the calculations.

Datenblatt für LADUNG - Nr.		$P_{max, nom.}$ : 10 MW																																																																																																																				
Ladung für: IAEA-BENCHMARK		VA-Nr.: _____																																																																																																																				
<b>LADUNGSANORDNUNG</b>	<b>IA: Burn up distribution</b>																																																																																																																					
<table style="width: 100%; border-collapse: collapse;"> <tr><td style="width: 5%; border: 1px solid black;">Nr.</td><td style="border: 1px solid black;">Normalelement</td></tr> <tr><td style="border: 1px solid black;">Nr.</td><td style="border: 1px solid black;">Kontrollelement</td></tr> <tr><td style="border: 1px solid black;">Nr.</td><td style="border: 1px solid black;">GA-Kontrollelement</td></tr> <tr><td style="border: 1px solid black;">Be</td><td style="border: 1px solid black;">Reflektorelement</td></tr> <tr><td style="border: 1px solid black;">Q</td><td style="border: 1px solid black;">Neutronenquelle</td></tr> <tr><td style="border: 1px solid black;"> </td><td style="border: 1px solid black;"> </td></tr> <tr><td style="border: 1px solid black;"> </td><td style="border: 1px solid black;"> </td></tr> </table>	Nr.	Normalelement	Nr.	Kontrollelement	Nr.	GA-Kontrollelement	Be	Reflektorelement	Q	Neutronenquelle					<table style="width: 100%; border-collapse: collapse; text-align: center;"> <tr><td></td><td>1</td><td>2</td><td>3</td><td>4</td><td>5</td><td>6</td><td>7</td><td>8</td><td>9</td></tr> <tr><td style="border: 1px solid black;">1</td><td style="border: 1px solid black;">" "</td><td style="border: 1px solid black;"> </td><td style="border: 1px solid black;"> </td></tr> <tr><td style="border: 1px solid black;">2</td><td style="border: 1px solid black;"> </td><td style="border: 1px solid black;"> </td><td style="border: 1px solid black;"> </td><td style="border: 1px solid black;">5</td><td style="border: 1px solid black;">25</td><td style="border: 1px solid black;">5</td><td style="border: 1px solid black;"> </td><td style="border: 1px solid black;"> </td><td style="border: 1px solid black;"> </td></tr> <tr><td style="border: 1px solid black;">3</td><td style="border: 1px solid black;"> </td><td style="border: 1px solid black;">C</td><td style="border: 1px solid black;">5</td><td style="border: 1px solid black;">25</td><td style="border: 1px solid black;">45</td><td style="border: 1px solid black;">25</td><td style="border: 1px solid black;">5</td><td style="border: 1px solid black;">C</td><td style="border: 1px solid black;"> </td></tr> <tr><td style="border: 1px solid black;">4</td><td style="border: 1px solid black;"> </td><td style="border: 1px solid black;">C</td><td style="border: 1px solid black;">25</td><td style="border: 1px solid black;">45</td><td style="border: 1px solid black;">45</td><td style="border: 1px solid black;">45</td><td style="border: 1px solid black;">25</td><td style="border: 1px solid black;">C</td><td style="border: 1px solid black;"> </td></tr> <tr><td style="border: 1px solid black;">5</td><td style="border: 1px solid black;"> </td><td style="border: 1px solid black;">C</td><td style="border: 1px solid black;">25</td><td style="border: 1px solid black;">45</td><td style="border: 1px solid black;">45</td><td style="border: 1px solid black;">45</td><td style="border: 1px solid black;">25</td><td style="border: 1px solid black;">C</td><td style="border: 1px solid black;"> </td></tr> <tr><td style="border: 1px solid black;">6</td><td style="border: 1px solid black;"> </td><td style="border: 1px solid black;">C</td><td style="border: 1px solid black;">5</td><td style="border: 1px solid black;">25</td><td style="border: 1px solid black;">45</td><td style="border: 1px solid black;">25</td><td style="border: 1px solid black;">5</td><td style="border: 1px solid black;">C</td><td style="border: 1px solid black;"> </td></tr> <tr><td style="border: 1px solid black;">7</td><td style="border: 1px solid black;"> </td><td style="border: 1px solid black;"> </td><td style="border: 1px solid black;"> </td><td style="border: 1px solid black;">5</td><td style="border: 1px solid black;">25</td><td style="border: 1px solid black;">5</td><td style="border: 1px solid black;"> </td><td style="border: 1px solid black;"> </td><td style="border: 1px solid black;"> </td></tr> <tr><td style="border: 1px solid black;">8</td><td style="border: 1px solid black;"> </td><td style="border: 1px solid black;"> </td></tr> <tr><td style="border: 1px solid black;">9</td><td style="border: 1px solid black;">" "</td><td style="border: 1px solid black;"> </td><td style="border: 1px solid black;">" "</td></tr> </table>			1	2	3	4	5	6	7	8	9	1	" "									2				5	25	5				3		C	5	25	45	25	5	C		4		C	25	45	45	45	25	C		5		C	25	45	45	45	25	C		6		C	5	25	45	25	5	C		7				5	25	5				8										9	" "								" "		
Nr.	Normalelement																																																																																																																					
Nr.	Kontrollelement																																																																																																																					
Nr.	GA-Kontrollelement																																																																																																																					
Be	Reflektorelement																																																																																																																					
Q	Neutronenquelle																																																																																																																					
	1	2	3	4	5	6	7	8	9																																																																																																													
1	" "																																																																																																																					
2				5	25	5																																																																																																																
3		C	5	25	45	25	5	C																																																																																																														
4		C	25	45	45	45	25	C																																																																																																														
5		C	25	45	45	45	25	C																																																																																																														
6		C	5	25	45	25	5	C																																																																																																														
7				5	25	5																																																																																																																
8																																																																																																																						
9	" "								" "																																																																																																													
Bemerkungen: _____																																																																																																																						
<b>LADUNGSANORDNUNG</b>	<b>IB: Element Places</b>																																																																																																																					
<table style="width: 100%; border-collapse: collapse;"> <tr><td style="width: 5%; border: 1px solid black;">Nr.</td><td style="border: 1px solid black;">Normalelement</td></tr> <tr><td style="border: 1px solid black;">Nr.</td><td style="border: 1px solid black;">Kontrollelement</td></tr> <tr><td style="border: 1px solid black;">CFE</td><td style="border: 1px solid black;">GA-Kontrollelement</td></tr> <tr><td style="border: 1px solid black;">Be</td><td style="border: 1px solid black;">Reflektorelement</td></tr> <tr><td style="border: 1px solid black;">Q</td><td style="border: 1px solid black;">Neutronenquelle</td></tr> <tr><td style="border: 1px solid black;">SFX</td><td style="border: 1px solid black;">Standard fuel element x</td></tr> <tr><td style="border: 1px solid black;"> </td><td style="border: 1px solid black;"> </td></tr> <tr><td style="border: 1px solid black;"> </td><td style="border: 1px solid black;"> </td></tr> </table>	Nr.	Normalelement	Nr.	Kontrollelement	CFE	GA-Kontrollelement	Be	Reflektorelement	Q	Neutronenquelle	SFX	Standard fuel element x					<table style="width: 100%; border-collapse: collapse; text-align: center;"> <tr><td></td><td>1</td><td>2</td><td>3</td><td>4</td><td>5</td><td>6</td><td>7</td><td>8</td><td>9</td></tr> <tr><td style="border: 1px solid black;">1</td><td style="border: 1px solid black;">" "</td><td style="border: 1px solid black;"> </td><td style="border: 1px solid black;"> </td></tr> <tr><td style="border: 1px solid black;">2</td><td style="border: 1px solid black;"> </td><td style="border: 1px solid black;"> </td><td style="border: 1px solid black;"> </td><td style="border: 1px solid black;">SF4</td><td style="border: 1px solid black;"> </td><td style="border: 1px solid black;"> </td></tr> <tr><td style="border: 1px solid black;">3</td><td style="border: 1px solid black;"> </td><td style="border: 1px solid black;">C</td><td style="border: 1px solid black;">SF1</td><td style="border: 1px solid black;">CFE-1</td><td style="border: 1px solid black;"> </td><td style="border: 1px solid black;">CFE</td><td style="border: 1px solid black;"> </td><td style="border: 1px solid black;">C</td><td style="border: 1px solid black;"> </td></tr> <tr><td style="border: 1px solid black;">4</td><td style="border: 1px solid black;"> </td><td style="border: 1px solid black;">C</td><td style="border: 1px solid black;">SF2</td><td style="border: 1px solid black;">SF3</td><td style="border: 1px solid black;"> </td><td style="border: 1px solid black;"> </td><td style="border: 1px solid black;"> </td><td style="border: 1px solid black;">C</td><td style="border: 1px solid black;"> </td></tr> <tr><td style="border: 1px solid black;">5</td><td style="border: 1px solid black;"> </td><td style="border: 1px solid black;">C</td><td style="border: 1px solid black;"> </td><td style="border: 1px solid black;">C</td><td style="border: 1px solid black;"> </td></tr> <tr><td style="border: 1px solid black;">6</td><td style="border: 1px solid black;"> </td><td style="border: 1px solid black;">C</td><td style="border: 1px solid black;"> </td><td style="border: 1px solid black;">CFE</td><td style="border: 1px solid black;"> </td><td style="border: 1px solid black;">CFE</td><td style="border: 1px solid black;"> </td><td style="border: 1px solid black;">C</td><td style="border: 1px solid black;"> </td></tr> <tr><td style="border: 1px solid black;">7</td><td style="border: 1px solid black;"> </td><td style="border: 1px solid black;"> </td></tr> <tr><td style="border: 1px solid black;">8</td><td style="border: 1px solid black;"> </td><td style="border: 1px solid black;"> </td></tr> <tr><td style="border: 1px solid black;">9</td><td style="border: 1px solid black;">" "</td><td style="border: 1px solid black;"> </td><td style="border: 1px solid black;">" "</td></tr> </table>			1	2	3	4	5	6	7	8	9	1	" "									2				SF4						3		C	SF1	CFE-1		CFE		C		4		C	SF2	SF3				C		5		C						C		6		C		CFE		CFE		C		7										8										9	" "								" "
Nr.	Normalelement																																																																																																																					
Nr.	Kontrollelement																																																																																																																					
CFE	GA-Kontrollelement																																																																																																																					
Be	Reflektorelement																																																																																																																					
Q	Neutronenquelle																																																																																																																					
SFX	Standard fuel element x																																																																																																																					
	1	2	3	4	5	6	7	8	9																																																																																																													
1	" "																																																																																																																					
2				SF4																																																																																																																		
3		C	SF1	CFE-1		CFE		C																																																																																																														
4		C	SF2	SF3				C																																																																																																														
5		C						C																																																																																																														
6		C		CFE		CFE		C																																																																																																														
7																																																																																																																						
8																																																																																																																						
9	" "								" "																																																																																																													
Bemerkungen: _____																																																																																																																						
<b>LADUNGSANORDNUNG</b>																																																																																																																						
<table style="width: 100%; border-collapse: collapse;"> <tr><td style="width: 5%; border: 1px solid black;">Nr.</td><td style="border: 1px solid black;">Normalelement</td></tr> <tr><td style="border: 1px solid black;">Nr.</td><td style="border: 1px solid black;">Kontrollelement</td></tr> <tr><td style="border: 1px solid black;">Nr.</td><td style="border: 1px solid black;">GA-Kontrollelement</td></tr> <tr><td style="border: 1px solid black;">Be</td><td style="border: 1px solid black;">Reflektorelement</td></tr> <tr><td style="border: 1px solid black;">Q</td><td style="border: 1px solid black;">Neutronenquelle</td></tr> <tr><td style="border: 1px solid black;"> </td><td style="border: 1px solid black;"> </td></tr> <tr><td style="border: 1px solid black;"> </td><td style="border: 1px solid black;"> </td></tr> </table>	Nr.	Normalelement	Nr.	Kontrollelement	Nr.	GA-Kontrollelement	Be	Reflektorelement	Q	Neutronenquelle					<table style="width: 100%; border-collapse: collapse; text-align: center;"> <tr><td></td><td>1</td><td>2</td><td>3</td><td>4</td><td>5</td><td>6</td><td>7</td><td>8</td><td>9</td></tr> <tr><td style="border: 1px solid black;">1</td><td style="border: 1px solid black;">" "</td><td style="border: 1px solid black;"> </td><td style="border: 1px solid black;"> </td></tr> <tr><td style="border: 1px solid black;">2</td><td style="border: 1px solid black;"> </td><td style="border: 1px solid black;"> </td></tr> <tr><td style="border: 1px solid black;">3</td><td style="border: 1px solid black;"> </td><td style="border: 1px solid black;"> </td></tr> <tr><td style="border: 1px solid black;">4</td><td style="border: 1px solid black;"> </td><td style="border: 1px solid black;"> </td></tr> <tr><td style="border: 1px solid black;">5</td><td style="border: 1px solid black;"> </td><td style="border: 1px solid black;"> </td></tr> <tr><td style="border: 1px solid black;">6</td><td style="border: 1px solid black;"> </td><td style="border: 1px solid black;"> </td></tr> <tr><td style="border: 1px solid black;">7</td><td style="border: 1px solid black;"> </td><td style="border: 1px solid black;"> </td></tr> <tr><td style="border: 1px solid black;">8</td><td style="border: 1px solid black;"> </td><td style="border: 1px solid black;"> </td></tr> <tr><td style="border: 1px solid black;">9</td><td style="border: 1px solid black;">" "</td><td style="border: 1px solid black;"> </td><td style="border: 1px solid black;">" "</td></tr> </table>			1	2	3	4	5	6	7	8	9	1	" "									2										3										4										5										6										7										8										9	" "								" "		
Nr.	Normalelement																																																																																																																					
Nr.	Kontrollelement																																																																																																																					
Nr.	GA-Kontrollelement																																																																																																																					
Be	Reflektorelement																																																																																																																					
Q	Neutronenquelle																																																																																																																					
	1	2	3	4	5	6	7	8	9																																																																																																													
1	" "																																																																																																																					
2																																																																																																																						
3																																																																																																																						
4																																																																																																																						
5																																																																																																																						
6																																																																																																																						
7																																																																																																																						
8																																																																																																																						
9	" "								" "																																																																																																													
Bemerkungen: _____																																																																																																																						

FIG. 1.

In the vertical direction a buckling of  $B_z^2 = 1,6943 \cdot 10^{-3} \text{cm}^{-2}$ , corresponding to a extrapolated height of 76,3 cm where used. The vertical buckling, or the reflector saving, of course, is influenced by temperature and the water density and hence influences the  $k_{\text{eff}}$ . Cross check calculations indeed indicate that the reactivity differences are influenced in only a minor way by this effect (only a few percent of the value).

#### 4. Homogeneous Reactivity Feed-back Coefficients

##### 4.1 Change of Water Temperature Only

For the defined core configuration values of  $k_{\text{eff}}$  are calculated for water temperatures of 20, 38, 50, 75 and 100°C using the 5 group WIMS-cross section data for each corresponding burn up and enrichment.

The reactivity coefficients indicated are given by

$$\Delta\rho = \frac{K_0 - 1}{K_0} - \frac{K(T) - 1}{K(T)}$$

where  $K_0 = K(T)$  for 20°C  
 $K(T) = K$  for specified temperature

Table 4 presents  $k_{\text{eff}}$  and the reactivity differences at the specified temperatures, relative to the 20°C case for the BOL core with all three enrichments.

##### 4.2 Change of Water Density Only

Values of  $k_{\text{eff}}$  were computed for water densities of 0,9982, 0,993, 0,988, 0,975 and 0,958 g·cm<sup>-3</sup> which correspond to the temperatures given in Section 4.1, using the corresponding WIMS-data. In supplement homogeneous void coefficients for 5, 10 and 20% void at a temperature of 20°C are calculated.

Table 5 presents  $k_{\text{eff}}$  and the corresponding reactivity differences at the specified temperature and void content respectively, relative to the 20°C case of the BOL core at all enrichments.

##### 4.3 Change of Fuel Temperature Only

Values of  $k_{\text{eff}}$  where computed for fuel temperatures of 20, 38, 50, 75 100 and 200°C for the BOL core and for all enrichments. As input data the WIMS five group cross sections are used as described in Sect. 2.

Table 4: Reactivity Coefficients For Change of Water Temperature Only

T(°C)	HEU		MEU		LEU	
	k <sub>eff</sub>	-Δρx1000	k <sub>eff</sub>	-Δρx1000	k <sub>eff</sub>	-Δρx1000
20	1.026918	-	1.028665	-	1.026385	-
38	1.024648	2.157	1.026691	1.869	1.024774	1.532
50	1.023185	3.553	1.025430	3.067	1.023746	2.512
75	1.020190	6.422	1.022839	5.537	1.021659	4.507
100	1.017331	9.177	1.020382	7.891	1.019688	6.399

Table 5: Reactivity Coefficients For Change of Water Density Only

(g/cm <sup>3</sup> )	TC(°C)	HEU		MEU		LEU	
		k <sub>eff</sub>	-Δρx1000	k <sub>eff</sub>	-Δρx1000	k <sub>eff*</sub>	-Δρx1000
0.9982	20	1.026918	-	1.028665	-	1.015604	-
0.993	38	1.025535	1.313	1.027184	1.443	1.014023	1.535
0.988	50	1.024222	2.563	1.025764	2.749	1.012586	2.935
0.975	75	1.020703	5.929	1.022029	6.312	1.008642	6.796
0.958	100	1.015974	10.490	1.016967	11.182	1.003375	12.001
5% (.948)	20	1.013197	13.187	1.013949	14.109	1.000314	15.050
10% (.898)	20	0.998039	28.177	0.997901	28.57	0.983737	31.896
20% (.799)	20	0.962808	64.841	0.960957	67.09	0.946321	72.098

\*) In this case k<sub>eff</sub> is slightly different from the other value due to changes in Zone definitions at WIMS-calculations. They have no influence on Δρ values.

1) Estimated from k<sub>∞</sub> at burn up of 25%.

For the creation of the WIMS cross sections, the fuel density has been maintained constant to the 20°C case and only the temperature has been changed. Thus, this temperature effect corresponds mainly to the U-238 resonance effect.

Table 6 represents the calculated values of k<sub>eff</sub> and the reactivity differences relative to the 20°C case for the BOL core with all three enrichments. The Δρ<sub>T<sub>f</sub></sub>-value of the HEU fuel has been estimated from the k<sub>∞</sub> at 25% burn up, because the accuracy of the CODIFF calculations has been insufficient. The error in this case is only a few percent, as can be shown by calculating the Δρ<sub>T<sub>f</sub></sub> for MEU and LEU fuels in the same manner. This indeed is only valuable for the fuel temperature coefficient and not for the moderator coefficient.

Table 6: Reactivity Coefficients for Change of Fuel Temperature Only

T(°C)	HEU		MEU		LEU	
	k <sub>eff</sub>	-Δρx1000	k <sub>eff</sub>	-Δρx1000	k <sub>eff</sub>	-Δρx1000
20	1.026934		1.028665	-	1.026385	-
38	1.026930	0,004 <sup>1)</sup>	1.028412	0.2392	1.025936	0.426
50	1.026928	0,006 <sup>1)</sup>	1.028267	0.3763	1.025664	0.685
75	1.026923	0,011 <sup>1)</sup>	1.027944	0.6719	1.025082	1.238
100	1.026917	0,017 <sup>1)</sup>	1.027627	0.9819	1.024513	1.780
200	1.026895	0,039	1.026441	2.106	1.022412	3.786 (3.794) <sup>1)</sup>

\*) In this case k<sub>eff</sub> is slightly different from the other value due to changes in Zone definitions at WIMS-calculations. They have no influence on Δρ values.

<sup>1)</sup> Estimated from k<sub>∞</sub> at burn up of 25%.

In Figs. 2 to 5 the corresponding reactivity feedback coefficients are shown graphically for all three enrichments. This figures show that the main reactivity effect for the HEU core is given by the water (moderator) temperature effects. For the MEU and especially for the LEU core the fuel or Doppler coefficient dominates for the normal operating range. Fig. 5 gives the homogenous void coefficient for the BOL core relative to the water density of 20°C.

#### 4.4 Linear Temperatur Coefficient

In Figs. 2 to 5, it is shown that the reactivity feedback with respect to temperature is nearly linear. Thus a linear feedback coefficient ( $\alpha_T$ ) can be derived in practice.

Table 7 shows the corresponding linear feedback temperature coefficients for all three enrichments in the range of 38°C to 50°C.

#### 4.5 Local Void Coefficient

Local void coefficients were computed for changes in water density of 5 and 10% (which correspond to densities of 0,9483, 0,8984g·cm<sup>-3</sup>) relative to the water density at 20°C (0,0082g·cm<sup>-3</sup>) separately in the denoted elements SFE-2, SFE-3 and SFE-4 in Fig. 1B. The results of these calculations are shown in Table 8 for all three enrichments. These elements were introduced in the loading corresponding to a water density of 0,993g·cm<sup>-3</sup>, so the void coefficient is relative to the 38°C case. However, the water temperature still is 20°C, so the k<sub>eff</sub> is slightly higher in reality than for 38°C.

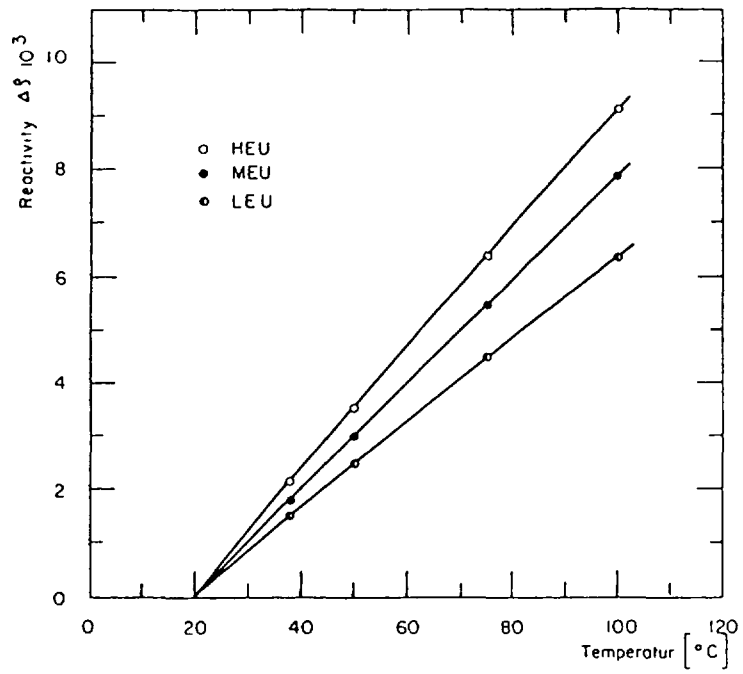


Fig. 2 Water Temperature Effect Only

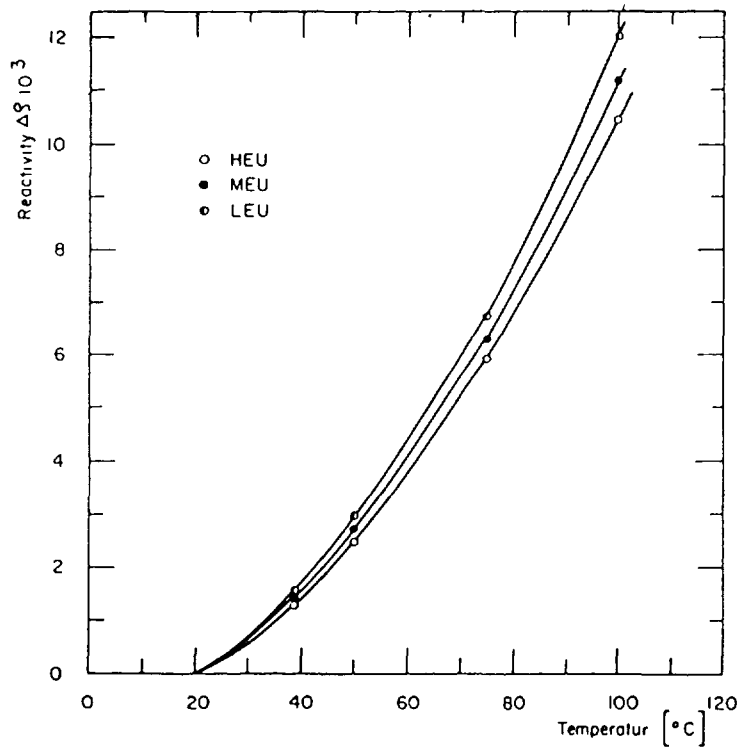


Fig. 3 Water Density Effect Only

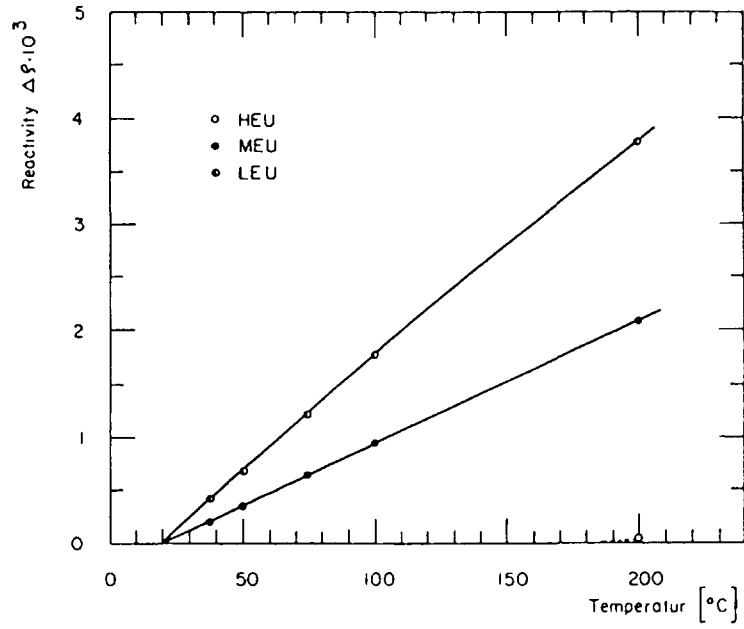


Fig. 4 Fuel Temperature Effect Only

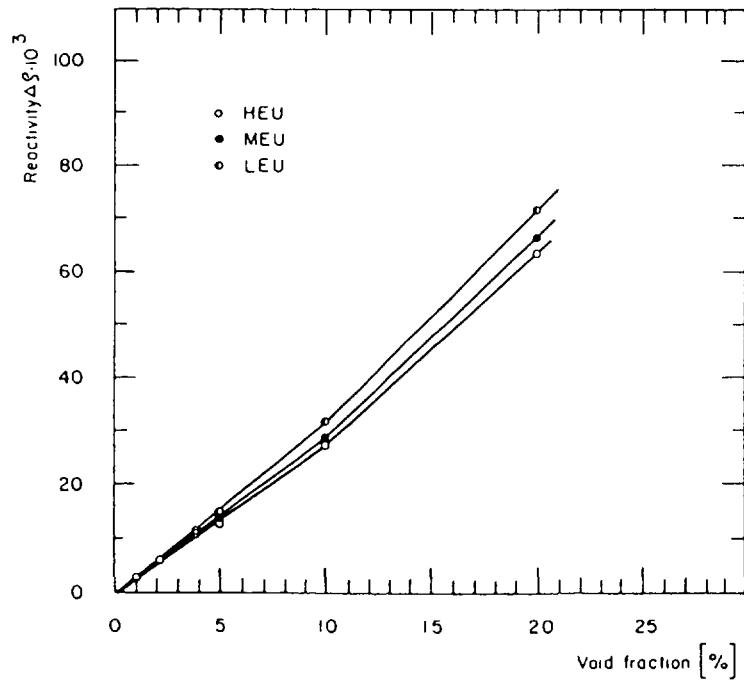


Fig. 5 Water Void Effect Only

Table 7: Slope of reactivity coefficient ( $\alpha$ ) in the range of 38°C + 50°C

Effect		HEU	MEU	LEU
		$\frac{d\rho}{dt} \times 10^{-3} (^{\circ}\text{C})^{-1}$	$\frac{d\rho}{dt} \times 10^{-3} (^{\circ}\text{C})^{-1}$	$\frac{d\rho}{dt} \times 10^{-3} (^{\circ}\text{C})^{-1}$
Water temperature	$\alpha_{T_W}$	0,116	0,100	0,082
Water density	$\alpha_{\rho_W}$	0,104	0,109	0,117
Fuel temp.	$\alpha_{T_f}$	0,0002	0,011	0,022

Table 8: Local Void reactivity coefficient

Void %	$\rho_{H_2O}$ g·cm <sup>-3</sup>		HEU		MEU		LEU	
			$k_{eff}$	$\Delta\rho \times 10^{-3}$	$k_{eff}$	$\Delta\rho \times 10^{-3}$	$k_{eff}$	$\Delta\rho \times 10^{-3}$
0	0,993	none	1,025535	--	1,027184	--	1,014023	--
5	0,9483	SFE-2	1,024980	0,528	1,026602	0,552	1,013443	0,564
		3	1,025149	0,367	1,026670	0,487	1,013527	0,483
		4	1,025104	0,410	1,026739	0,422	1,013589	0,422
10	0,8984	SFE2+3			1,026128	1,002		
		SFE-2	1,024371	1,108	1,025977	1,145	1,012818	1,173
		3	1,024609	0,881	1,026116	1,013	1,012836	1,156
		4	1,024608	0,882	1,026243	0,893	1,013104	0,895

#### 4.6 Total Reactivity Coefficient

In order to receive a feeling about the changes of total reactivity coefficient with the enrichment, normal operating conditions should be considered.

Supposing a normal startup procedure of an MTR-reactor from zero power to a thermal power of 10 MW, the following conditions exist (example SAPHIR):

	initial (zero power)	Full power	
Power	0,05 (fp)	10	MW
Flow rate	220	220	$l \cdot s^{-1}$
Water temperature inlet	20	20	$^{\circ}C$
Water temperature outlet	20	30	$^{\circ}C$
Mean moderator temperature $\bar{T}_M$	20	26	$^{\circ}C$
Mean fuel temperature $\bar{T}_f$	20,3	45	$^{\circ}C$

Taking into account the different temperature conditions, the loss of reactivity between zero and full power becomes:

$$\Delta\rho_p = \left( \alpha_{d_W} + \alpha_{T_W} \right) \cdot \Delta T_W + \alpha_{T_f} \cdot \Delta T_f$$

The results for this reference case are given in Table 9.

Measurements (Ref. 6) made at SAPHIR with HEU fuel at 5 and 10 MW and a flow rates of  $120 l \cdot s^{-1}$  and  $260 l \cdot s^{-1}$  give an extrapolated value for the reactivity difference at 10 MW and the BENCHMARK Core:

$$\Delta\rho_p = 16.5 \pm 0.8 \%$$

which is in very good agreement with the calculated value of 17.1%.

## 5. POWER PEAKING FACTOR

### 5.1 Introduction

The radial and local power peaking factors were calculated for the specified benchmark core in TECDOC-233 with the small alteration of a block of aluminum with a smaller water gap in the central irradiation position. The dimension of the water gap has in both directions two mesh intervals with (4.1 x 3.85cm) in order to have the same calculation scheme as for the other calculations.

Table 9: Effective temperature coefficient on power

	HEU $\Delta\rho \times 10^{-3}$	MEU $\Delta\rho \times 10^{-3}$	LEU $\Delta\rho \times 10^{-3}$
Moderator	1,320	1,254	1,194
Fuel	0,005	0,275	0,550
$\Delta\rho_{\text{Power}}$	1,325	1,529	1,744
$\Delta\rho_p [\beta]$	17,1	20,0	23,7

In grid positions CFE-1 and SFE-1 (see Fig. 1B), the burned fuel element (either HEU or LEU) has been replaced by a fresh control- or standard element and the power distribution has been calculated. Table 10 shows the determined specific power for the different cases. The calculations were carried out with the EIR-diffusion code CODIFF.

Table 10: Specific Power in different Elements [ $\text{W}\cdot\text{cm}^{-3}$ ]

Element Substitution	mean Power Element $\bar{P}_{\text{Elem}}$	max mesh Power $P_{\text{mesh}}$	max Power Edge of El. $P_{\text{max}}$	mean Core Power $\bar{P}_0$	
HEU Core (HEU-Substitution)					
none SFE1	115.5	136.5	157.	} $\bar{P}_0 = 106.9 \text{W}\cdot\text{cm}^{-3}$	
none CFE1	96.5	110.1			
SFE1 HEU	126.0	148.1	175.		
CFE2 HEU	119.9	137.8	142.		
HEU-Core (LEU-Substitution)					
SFE1 LEU	136.9	166.5	202.		
CFE1 LEU	137.1	162.3	167.		
LEU-Core (LEU-Substitution)					
none SFE1	113.2	136.8	210.		
none CFE1	98.5	108.4			
SFE1	123.3	148.4	228.		
CFE1	117.7	128.9	132.		

### 5.2 Radial Peaking Factor for a Fuel Element

The radial peaking factor is defined as the ratio of the mean power in a specific fuel element to the mean power of the whole core.

The mean power in the core has been determined for 10MW to be

$$\bar{P}_O = 106.9W \cdot cm^{-3}$$

Table 11 shows the calculated radial peaking factors.

Table 11: Radial and local power peaking factors

Element Substitution	radial fr	local mesh fm	local cell f <sub>max</sub>	total fr x f <sub>max</sub>	K <sub>eff</sub>	Δρx10 <sup>3</sup>
		HEU-core (HEU-substitution)				
none	1.080	1.182	1.36	1.47	1.026934	
SFE1	1.179	1.175	1.39	1.64	1.029234	2.18
CFE1	1.122	1.149	1.18	1.32	1.032775	5.51
		HEU-core (LEU-substitution)				
none	1.080	1.182	1.36	1.47	1.026934	
SFE1	1.281	1.216	1.48	1.90	1.029404	2.34
CFE1	1.283	1.184	1.22	1.57	1.034704	7.32
		LEU-core (LEU-substitution)				
none	1.059	1.208	1.85	1.97	1.026469	
SFE1	1.153	1.204	1.85	2.13	1.028709	2.12
CFE1	1.101	1.095	1.12	1.23	1.031934	5,16

### 5.3 Local Power Peaking Factor in a Specific Element

The local power peaking factor is defined as the ratio of the maximum power in the specified element to the mean power in this element.

The maximum calculated power in an element depends on the mesh width especially if strong power gradients exist in this element. So the calculated results for the choosen mesh with 1/4 of the element dimensions does not necessarily give the maximum power in this element. So a second calculation has been run with a small mesh in the critical outer regions of the specified element. This mesh has the dimension of one fuel cell, i.e. one fuel plate with one water gap.

The dimension of the inner mesh points of the element have been adapted in order to maintain the total mesh points.

In Table 10 the corresponding specific power is given as  $P_{\text{mesh}}$ , which means the calculated power for a mesh with of  $\sqrt[4]{4}$  element dimension and  $P_{\text{max}}$  for the mesh dimension of a fuel cell. Table 11 shows the corresponding power peaking factors.

#### 5.4 Total Power Peaking Factor

The total power peaking factor given in Table 11 is defined as the ratio of maximum cell power to the mean power of the core.

#### 5.5 Reactivity Differences

For each calculated case  $K_{\text{eff}}$  has also been determined. Table 11 gives the calculated  $K_{\text{eff}}$  and the reactivity difference  $\Delta\rho$  for the replacement of the burned fuel element by a fresh fuel element.

#### 5.6 Discussion of the Results

The maximum power peaking factors are clearly found for the element SFE-1 which is surrounded by water and graphite as reflector. The replacement of a corresponding fresh fuel element in the HEU-/LEU-core gives an increase of the power peaking of 9% for the mean power in the element and 13% for the maximum power. The replacement of the 5% burned HEU-element by a fresh LEU-element have corresponding increases of 18% and 29%, respectively. Thus a careful check of the safety margins is needed, if a core conversion with a stepwise replacement of the HEU fuel elements is considered.

The calculations also show that no real reactivity problem exists by replacing the HEU-element with LEU elements.

The calculated reactivity differences are of the same magnitude or even smaller than for the normal shuffling of HEU-elements.

### 6. BENCHMARK CALCULATION OF BASIC KINETIC PARAMETERS

#### 6.1 Introduction

The specifications of the problem are identical to those of the 10 MW benchmark defined in IAEA-TECDOC-233, except for the central flux trap, which includes an aluminum block with a central hole.

The results of the calculation of the basic kinetic parameters are presented in Table 12.

Table 12: Kinetic parameters

Transport calculations

Designation	Enrichment % U-235	$k_{eff}$	$\beta_{eff}$	$\lambda, [\mu\text{sec}]$	$\Lambda, [\mu\text{sec}]$
HEU	93	1.02639	$778.4 \cdot 10^{-5}$	60.36	58.81
MEU	45	1.02746	$765.2 \cdot 10^{-5}$	52.18	50.79
LEU	20	1.03039	$736.2 \cdot 10^{-5}$	46.12	44.76
<u>Diffusion calculations</u>					
HEU	93	1.02443	$777.2 \cdot 10^{-5}$	60.98	59.53
MEU	45	1.02624	$763.9 \cdot 10^{-5}$	52.68	51.33
LEU	20	1.02462	$735.1 \cdot 10^{-5}$	46.54	45.42

6.2 Short Description of the Calculation Method

The atomic densities of the isotopes existing in the irradiated fuel were taken from a WIMS burn-up calculation. These densities were fed into the code MICROX (7) to perform 2-region cell calculations and to obtain P0 and P1 microscopic cross sections and  $1/v$  constants in a five group structure. The cross sections for the reflector materials (C and H<sub>2</sub>O) were also produced through a MICROX calculation for an infinite water medium with a fixed source having an energy distribution corresponding to a fission spectrum.

The microscopic cross sections were converted to RSYST (8) format and mixed to obtain the macroscopic cross sections for the specified materials.

At this stage a 1-D calculation was performed using the code ANISN (9). The flux and current spectra from this 1-D modeling of the problem were used to collapse the cross sections to a standard 4 groups structure and to obtain diffusion cross sections using the weighted column sum correction for the fast groups and the row sum correction for the thermal group. The reactivity and flux distribution calculations were performed with the code DOT 3.5 (10) in S4-P1 approximation and with the diffusion code FINELM (11). The effective delayed neutron fraction and prompt neutron lifetime were obtained using the code BETAEFF (12).

## REFERENCES

- 1) Research Reactor Core Conversion from HEU to LEU Fuels Guidebook.  
IAEA-TEC DOC-233, 1980
- 2) Specification of Methodical BENCHMARK-Problems  
Appendix F-0.1, IAEA-TEC DOC-233
- 3) Report IBJ 1509/CYFRONET/PR/A  
The S-WIMS-Code for the CYBER-72 Computer  
Krystyna Kowalska, Warszawa, 1975
- 4) BENCHMARK Calculations for MTR-Reactors  
Appendix F-3 IAEA-TEC DOC-233  
(TM-SR-119, H. Winkler / J. Zeis, EIR, Würenlingen 1979)
- 5) J.M. Paratte, K. Foskolos, P. Grimm, C. Maeder  
TM-45-81-41, 12.10.1981  
Benützungsanleitung zum Code BOXER
- 6) Sicherheitsbericht für 10 MW des Forschungsreaktors SAPHIR  
M. Baggenstos / H. Winkler et al.  
TM-53-81-3 Oktober 1981
- 7) R. Wälti, P. Koch: GA-A10827 (1972)
- 8) R. Rühle, IKE-Bericht Nr. 4-12 (1973)
- 9) "Revised ANISN User's manual", WANL-TMI-1967 (1969)
- 10) F. Mynatt et al., ORNL-TM-5490 (1975)
- 11) C. Higgs, D. Davierwala, EIR-Bericht Nr. 442 (1981)
- 12) J. Hadermann, P. Wydler, EIR TM-PH-705 (1981)

**CALCULATIONS FOR THE SAFETY-RELATED BENCHMARK PROBLEM**

JUNTA DE ENERGIA NUCLEAR  
 Calculations and Models Division,  
 Madrid, Spain

**Abstract**

Results are provided for the safety-related benchmark problem with HEU and LEU fuels.

**1. INTRODUCTION**

The present paper represents the JEN/Spain contribution to a benchmark problem, selected for the IAEA Guidebook on Safety-related aspects of research-reactor core conversion. The calculations were made in accordance with the problem specifications, also included in the same appendix of the Guidebook. For better understanding, some information is repeated here; specifically, figures 1 and 2 show the core pattern, and fig. 3 presents the radial geometry of the standard fuel element; same does fig. 6 for the control fuel element.

As this contribution has been delivered at a rather late time, the authors have had access to other-laboratories contributions in draft form; for this reason, some differences or discrepancies have become apparent, and are mentioned or discussed in the text.

The work has been performed with the participation of several engineers, as follows:

Coordination: M. Gómez-Alonso;  
 Static Calculations: A. Brú, C. Ahnert;  
 Dynamic Calculations: E. Donoso, J.J. Sánchez-Miró,  
 R. Martínez-Fanegas.

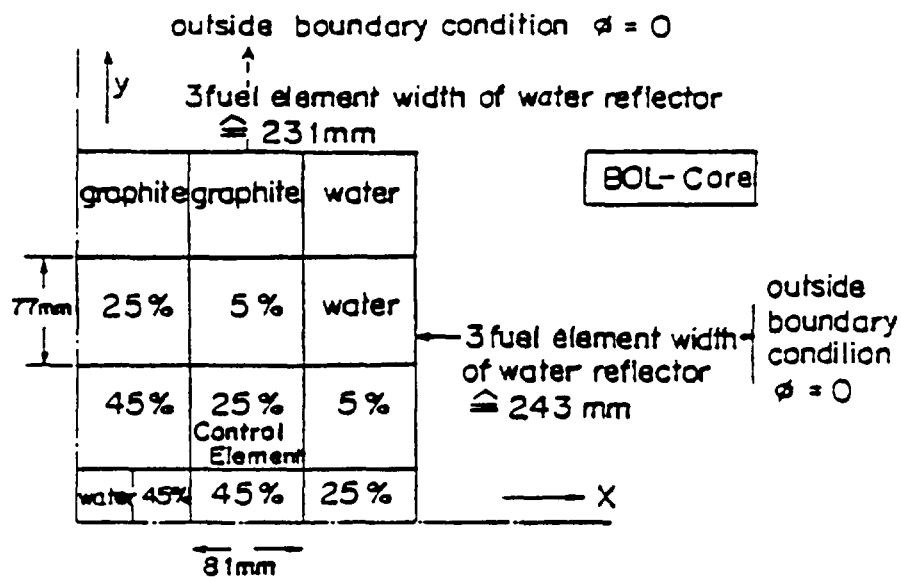


FIG. 1. Core configuration in previous (neutronic) benchmark problem (for central element, see Fig. 2).



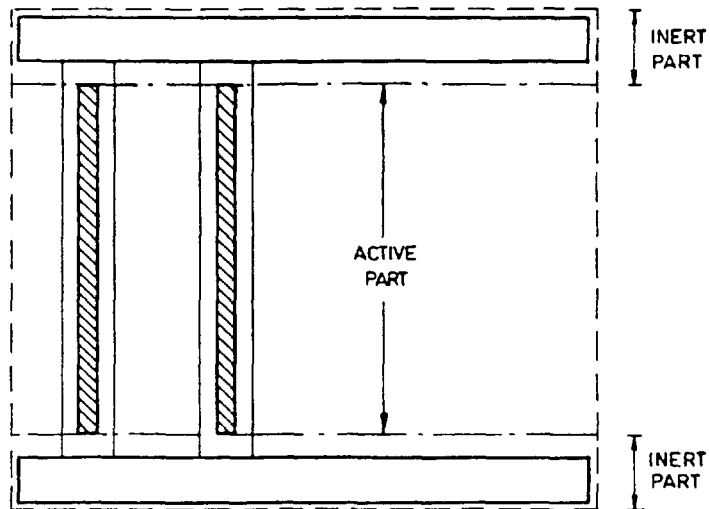


FIG. 5 x-y model for SFE.

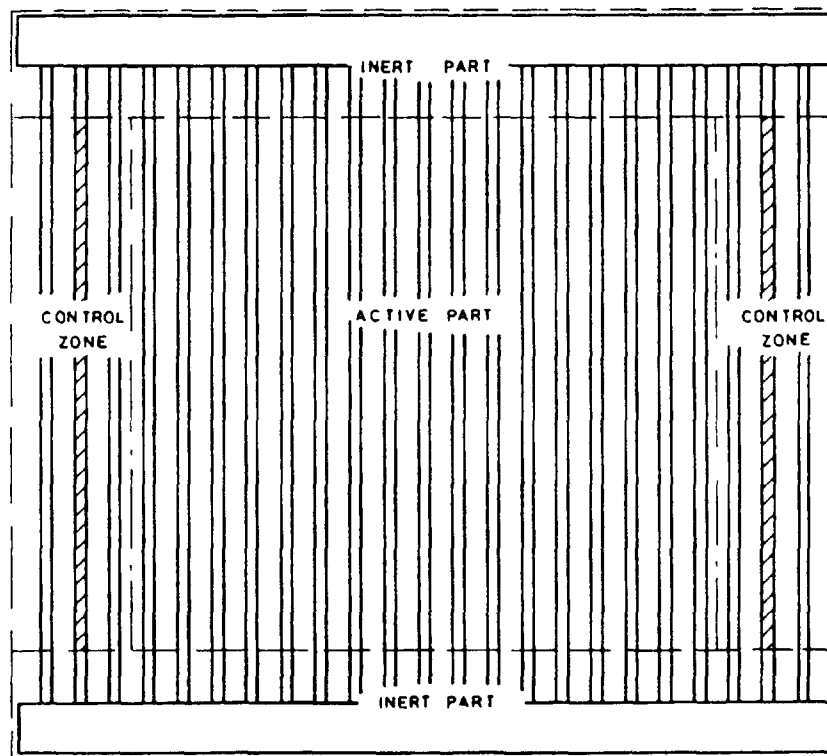


FIG. 6 Control fuel element (CFE) x-y model.

## 2. METHODS USED FOR STATIC CALCULATIONS

### 2.1. General

Neutronic models common to several calculations will be described here, while models specific to each calculation will appear in the corresponding sections. Fig. 7 shows this general scheme of a neutronic calculational method (3-5), developed for studies of MTR-



type reactors, using codes available at JEN. According to this method, we may distinguish the following steps in the calculation:

- a) determination of few-group cross sections for both fuel elements and other elements;
- b) preparation of a library of few-group constants in due format;
- c) X-Y diffusion calculation of the reactor core.

Due to the fact that, in step (c), the standard fuel element (SFE) is treated as two distinct regions (see fig. 5), the constants for these two regions have to be obtained independently in step (a). Similarly, as shown in fig. 6, at least three different sets of constants are necessary to describe the control fuel elements (CFE).

## 2.2. Cell spectral calculations

To obtain cross sections in few groups for some parts of fuel elements, cell calculations were performed with the spectral code WIMS-TRACA (1), a JEN version of the WIMS-D (2) code.

For the fueled or "active" part (fig. 5, fig. 6) of the fuel elements, "pure" cell calculations were performed, accounting for half the meat, clad and moderator in the unit cell (see fig. 4 for dimensions; for both inner and outer cells, an "average" channel width of 0.2252 cm is used). The burnup dependence was analysed, and 4-group constants were obtained for the different burnups present in the core (5 %, 25 % and 45 %). The group structure is shown in table 1. Other parameters were as follows, in general:  $T=38^{\circ}\text{C}$ , total buckling  $B^2=B_r^2+B_z^2=6.1(-3)+1.7(-3)=7.8\times 10^{-3}\text{ cm}^{-2}$ .

For the "inert" part (fig. 5, fig. 6) of both SFE and CFE, a "supercell" model of the standard fuel element was used, as shown in fig. 4; the "extra region" accounts for the two "inert" parts in SFE (fig. 5). No burnup dependence is considered.

## 2.3. One-dimensional spectral calculations

To obtain the constants of other elements in the core, one-dimensional multi-slab spectral calculations are performed, again using the WIMS code. The dimension considered is a traverse from a midplane of the core to the outer boundary (see fig. 2). The active parts of the fuel elements encountered, are given homogenized compositions, but corresponding resonance fine-group cross sections and disadvantage factors are input to the code, to have an adequate treatment. Those parameters are taken from the "pure" cell calculations of section 2.2; with little error, a unique set of parameters (corresponding to the average burnup of 25 %), is used for all fuel elements encountered.

As shown in fig. 2 three different one-dimensional calculations are needed; from line (1) calculation 4-group constants are obtained for the graphite reflector elements, the water reflector elements, and the water surrounding the core; line (2) calculation gives constants for the "control zone" (rods out) of the CFE(\*); from line (3) calculation, constants are obtained for the central element or trap.

---

(\*) For the "rods out" situation, instead of the absorber plates, aluminium ("follower") plates of the same dimensions are assumed.

This one-dimensional model is supposed to give better results than the alternative homogeneous cell calculations, because the spectrum in each element is affected by the neighboring elements, including fuel elements.

#### 2.4. Library preparation and diffusion calculations

As shown in fig. 7, an auxiliary program developed at JEN, WIMSEEDIT (6), is used for preparing a library of macroscopic cross sections, in the format of the diffusion code, CITATION. That WIMSEEDIT code also facilitates the transfer of disadvantage factors and resonance parameters, from the cell WIMS calculation to the one-dimensional WIMS calculation.

The X-Y diffusion calculations are performed using the finite-difference CITATION-2/2 computer code (7), to obtain  $k_{eff}$ , ordinary and adjoint fluxes, power densities, etc. The axial buckling is given its geometric value of  $1.7 \times 10^{-3} \text{ cm}^{-2}$ .

### 3. BASIC KINETIC PARAMETERS

#### 3.1. Prompt Neutron Generation Time

As a first approximation, this parameter has been hand-calculated, using data easily available from the neutronic codes used in other sections. Then, a few-group zero-dimensional expression for the generation time was needed; from the established theory (12), the following formula is derived:

$$\Lambda = \frac{\sum_{g=1}^n \phi_g^+ \cdot \frac{1}{v_g} \cdot \phi_g^I}{(\nu \Sigma_f \phi)^T \sum_{g=1}^n \phi_g^+ \chi_g} ,$$

where:  $\phi_g^+$  is core-average adjoint flux for group  $g$ ,

$v_g$  is core-average  $g$ -group neutron velocity,

$\phi_g^I$  is core-integrated  $g$ -group ordinary flux,

$\chi_g$  is  $g$ -group fraction of fission spectrum,

$(\nu \Sigma_f \phi)^T$  is total (core) source of fission neutrons.

In this analysis, parameters in  $n=4$  energy groups were used, obtained as follows:

a) from a supercell WIMS calculation, parameters  $\chi_g$  and  $v_g$  (flux-weighting of  $1/v$  absorber);

b) from an X-Y CITATION calculation, parameters  $\phi_g^+$ ,  $\phi_g^I$  and  $(\nu \Sigma_f \phi)^T$

The results are indicated below:

$$\Lambda \text{ (HEU)} = 51.7 \text{ } \mu\text{s} , \Lambda \text{ (LEU)} = 38.0 \text{ } \mu\text{s}.$$

### 3.2. Delayed Neutron Fraction

Similarly, the effective delayed neutron fraction,  $\beta_{\text{eff}}$ , has been calculated using core-average few-group constants, by means of the following expression:

$$\beta_{\text{eff}} = \frac{\sum_{g=1}^n \phi_g^+ \chi_g'}{\sum_{g=1}^n \phi_g^+ \chi_g} \cdot \frac{\sum_i \beta^i \sum_{j=1}^n (\nu \Sigma_f)_j^i \phi_j^I}{(\nu \Sigma_f \phi)^T}$$

where:  $i$  is an index for fissionable isotopes,  
 $\chi_g'$  is g-group fraction in typical delayed-neutron spectrum,  
 $\beta^i$  is i-nuclide delayed-neutron fraction.

Again, parameters in n=4 energy-groups were used; they were obtained as in the previous section, with several differences:

$(\nu \Sigma_f \phi)^T$  and  $(\Sigma_j (\nu \Sigma_f)_j^i \phi_j^I)$  were taken from WIMS,  $\beta^i$  and  $\chi_g'$  from the literature (13). The following results were obtained:

$$\beta_{\text{eff}} (\text{HEU}) = 0.00736, \quad \beta_{\text{eff}} (\text{LEU}) = 0.00713.$$

## 4. ISOTHERMAL REACTIVITY FEEDBACK COEFFICIENTS

### 4.1. Calculational models

As a first approximation, a 25 % - burned SFE supercell model (fig. 4) was selected as core representative for the calculation of the reactivity coefficients (see fig. 7). With this rough model, the reactivity values obtained for the reference cases (all T 38°C,  $\rho_w=0.993$  g/cc, no voids) were as follows:

$$k_{\text{eff}} (\text{HEU}) = 1.0733, \quad k_{\text{eff}} (\text{LEU}) = 1.0337.$$

Then, in WIMS, each specified feedback parameter,  $T_x$ , was varied, following the values given in the Problem Specifications. Then, a minor code, POLAJ, was used to fit the reactivity values to a second-degree polynomial in  $T_x$ ; the first derivative,  $d\rho/dT_x$ , is the desired  $\alpha_x$  coefficient.

Also, coefficient mean values  $\Delta\rho/\Delta T_x$  were obtained for a typical range of  $T_x$  values.

### 4.2. Change of water temperature only

Keeping constant the rest of the input data, WIMS problems were run for water temperatures (in moderator and extra region) of 20°C, 60°C and 100°C, for which a specific hydrogen scattering set was at WIMS library. By means of the polynomial fit mentioned above, the reactivity coefficient and defect were calculated for the temperatures given in the Specifications.

Table 2 presents these quantities for the HEU and LEU cores; fig. 8 shows the function  $-\Delta\rho(T_w)$  vs.  $T_w$ , and fig. 9 the function  $(-d\rho/dT_w)$  vs.  $T_w$ , also for both cores. Table 6 gives the average values in the range (38°C - 100°C). The functions  $(d\rho/dT_w)$ , for the temperature effect, are as follows ( $T_w$  in °C,  $d\rho/dT_w$  in pcm/°C or  $10^{-5} \Delta k/k/°C$ ):

$$\text{HEU: } (d\rho/dT_w)^T = -9.55 + 2.05 \times 10^{-2} T_w.$$

$$\text{LEU: } (d\rho/dT_w)^T = -7.74 + 2.13 \times 10^{-2} T_w.$$

TABLE 1  
Energy group structure

Group	Energy Limits	
	$E_U$	$E_L$
1	10.0 Mev	9.118 keV
2	9.118 keV	4.00 eV
3	4.00 eV	0.625 eV
4	0.625 eV	0

TABLE 2  
Reactivity Coefficients for Change of Water Temperature Only

$T_w$ (°C)	HEU		LEU	
	$-\Delta\rho$ (x1000)	$d\rho/dT_w$ (pcm/°C)*	$-\Delta\rho$ (x1000)	$d\rho/dT_w$ (pcm/°C)*
38	-	-8.77	-	-6.93
50	1.038	-8.53	0.816	-6.68
75	3.105	-8.01	2.420	-6.15
100	5.044	-7.50	3.890	-5.62

(\* ) 1 pcm =  $10^{-5} \Delta k/k$

TABLE 3  
Reactivity Coefficients for Change of Water Density Only

$T_w$ (°C)	$\rho_w$ (g/cm <sup>3</sup> )	HEU		LEU	
		$-\Delta\rho$ (x1000)	$d\rho/dT_w$ (pcm/°C)	$-\Delta\rho$ (x1000)	$d\rho/dT_w$ (pcm/°C)
38	0.993	-	-15.02	-	-16.55
50	0.988	2.104	-18.84	2.356	-20.87
75	0.975	7.732	-26.80	8.583	-29.89
100	0.958	15.468	-34.77	17.242	-38.90

TABLE 4

Reactivity Coefficients for Change of Fuel Temperature

$T_F$ (°C)	HEU		LEU	
	$-\Delta\rho$ (x1000)	$d\rho/dT_F$ (pcm/°C)	$-\Delta\rho$ (x1000)	$d\rho/dT_F$ (pcm/°C)
38	-	-.0201	-	-3.08
50	.0018	-.0197	.369	-3.03
75	.0072	-.0191	1.117	-2.95
100	.0117	-.0185	1.839	-2.86
200	.0289	-.0159	4.518	-2.50

TABLE 5

Void Reactivity Coefficients

Void fraction (%)	$\rho_w$ (g/cm <sup>3</sup> )	HEU		LEU	
		$-\Delta\rho$ (x1000)	$-d\rho/d\rho_w$ ( $\Delta k/k/(g/cc)$ )	$-\Delta\rho$ (x1000)	$d\rho/d\rho_w$ ( $\Delta k/k/(g/cc)$ )
0	0.993	-	0.366	-	0.413
5	0.9433	20.51	0.448	22.826	0.495
10	0.8937	44.40	0.530	49.042	0.576
20	0.7944	105.43	0.695	114.577	0.740

TABLE 6

Average reactivity coefficients

	Parameter and range	Feedb. Coeffic.		Units
		HEU	LEU	
Water temperature	$T_w$ (38-100°C)	-8.14	-6.27	pcm/°C
Water density	$T_w$ do.	-24.95	-27.81	do.
Fuel temperature	$T_F$ do.	-0.019	-2.97	do.
Subtotal	T do.	-36.94	-37.05	do.
Water voids	$\rho_w$ (0.94-0.89 g/cc)	0.482	0.529	$\Delta k/k/g.cm^3$

#### 4.3. Change of water density only

WIMS problems were run changing the water concentration in the moderator and extra regions, according to the densities in the Specifications. The temperatures were taken as 38°C.

The results are presented in table 3, figures 10 and 11, and again table 6. The functions  $d\rho/dT_w$ , for the density component, follow (same units as above):

$$\begin{aligned} \text{HEU: } (d\rho/dT_w)^D &= -2.91 - 0.3186 T_w. \\ \text{LEU: } (d\rho/dT_w)^D &= -2.85 - 0.3606 T_w. \end{aligned}$$

(It is observed that, for this reactivity coefficient component, the values encountered in this contribution are about double of the values obtained by other laboratories; it is not yet clear where is the origin of this discrepancy, either in the method or in the code used).\*

#### 4.4. Change of fuel temperature only

WIMS problems were run changing the "meat" temperature datum, according to the values in the Specifications. Water temperature and density were set at 38°C and 0.993 g/cc, respectively.

The results are presented in table 4, figures 12 and 13, and again table 6 (average values). It is very apparent that this Doppler coefficient is large for LEU fuel, and almost negligible for HEU fuel. The functions  $d\rho/dT_F$  are given below (same units as in Sect. 4.2):

$$\begin{aligned} \text{HEU: } d\rho/dT_F &= -0.021 + 2.57 \times 10^{-5} T_F. \\ \text{LEU: } d\rho/dT_F &= -3.21 + 3.57 \times 10^{-3} T_F. \end{aligned}$$

#### 4.5. Core void coefficient

To obtain whole-core void coefficients, the water concentration was varied only in the "moderator region" (representing the channel between plates), in several WIMS problems, corresponding to 5 %, 10 % and 20 % of void fraction in water. A common temperature of 38°C was assumed.

The results appear in table 5, figures 14 and 15, and table 6; like for the water-density coefficient, the LEU value is larger than the HEU one. The functions  $d\rho/d\rho_w$  are as follows:

$$\begin{aligned} \text{HEU: } d\rho/d\rho_w &= 2.013 - 1.659 \rho_w \\ \text{LEU: } d\rho/d\rho_w &= 2.049 - 1.647 \rho_w \end{aligned}$$

(Also as in Section 4.3, there is a remarkable discrepancy with results of other laboratories, which requires further investigation).\*

---

\* Note: Density-only coefficient has been recalculated using a two-dimensional X-Y model for the LEU case and the results (average value = 14.4 pcm/°C are in agreement with those of other laboratories. The same may occur for the other reactivity coefficients.

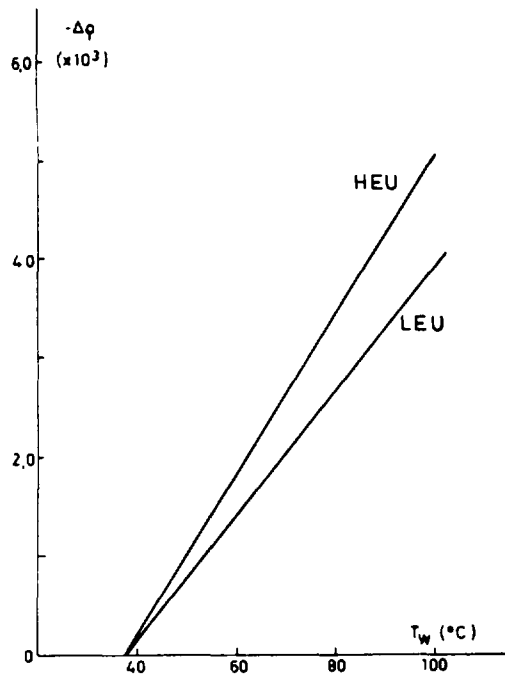


FIG. 8. Water-temperature effect changing  $T_W$  only.

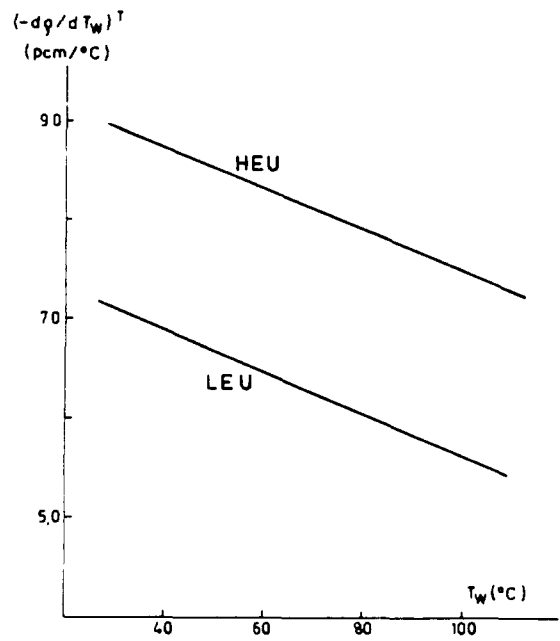


FIG. 9. Water-temperature reactivity coefficient changing  $T_W$  only.

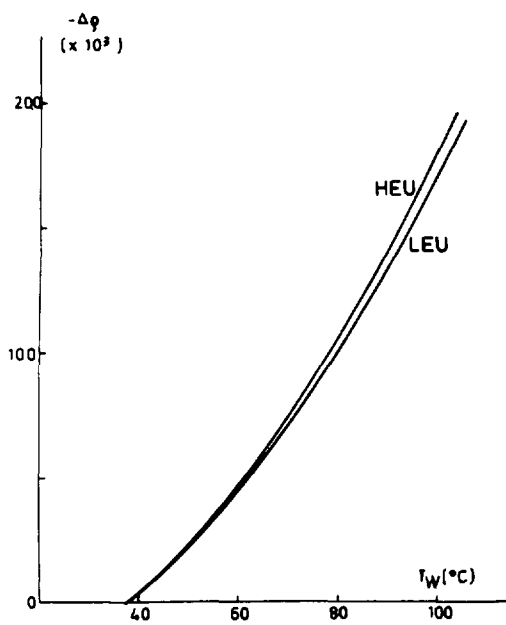


FIG. 10. Water-temperature effect: density component.

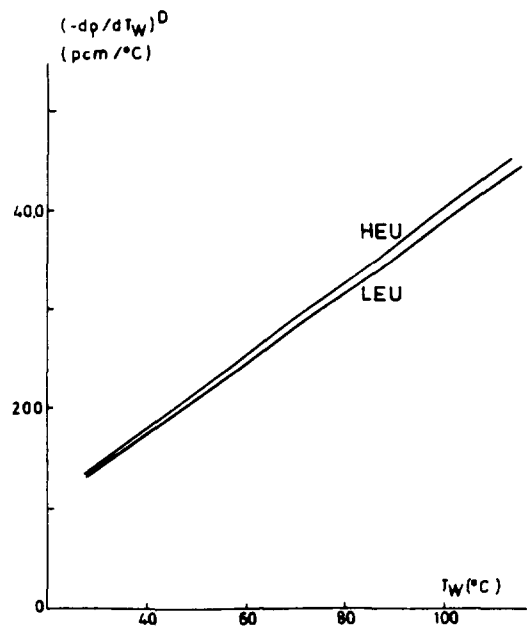


FIG. 11. Water-temperature reactivity coefficient: density component.

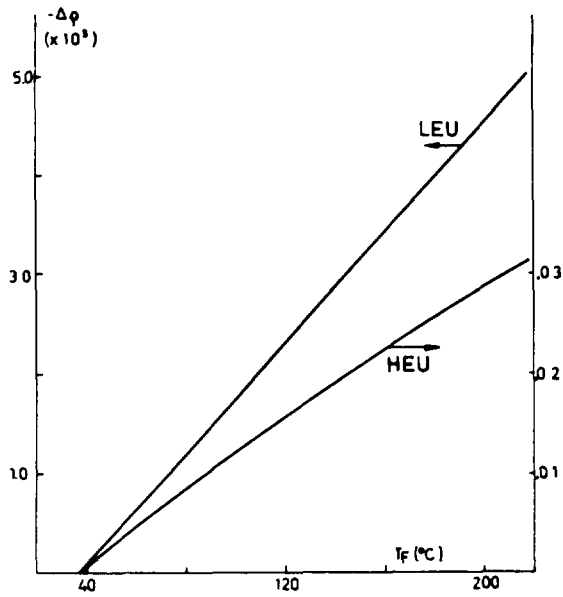


FIG. 12. Fuel-temperature effect on reactivity.

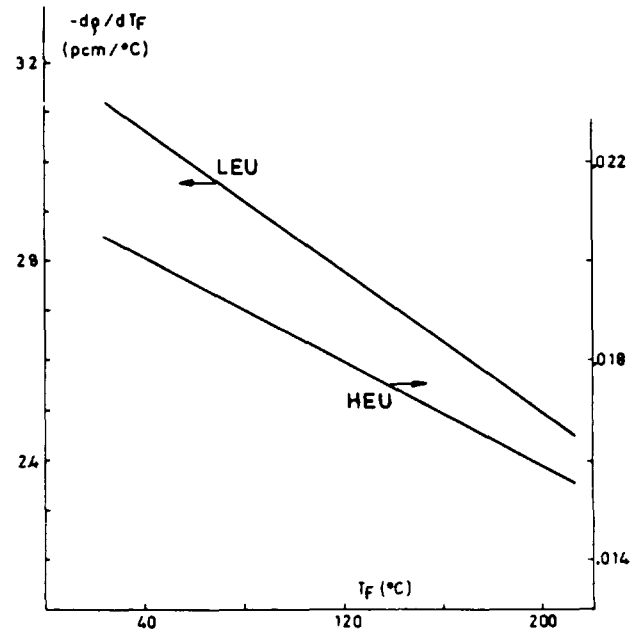


FIG. 13. Fuel-temperature reactivity coefficient.

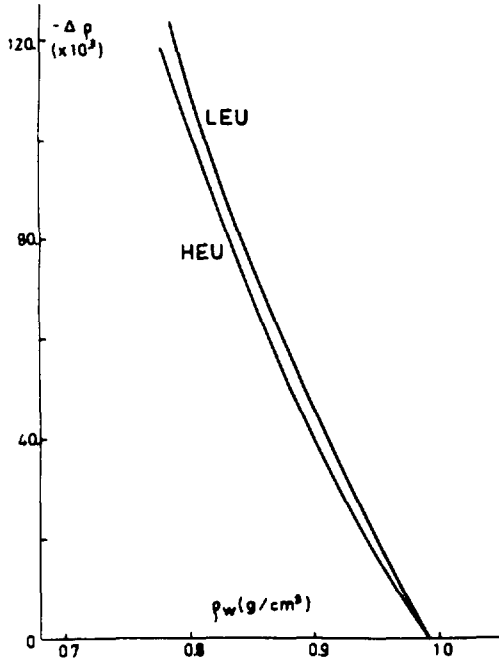


FIG. 14. Water-voids effect on reactivity.

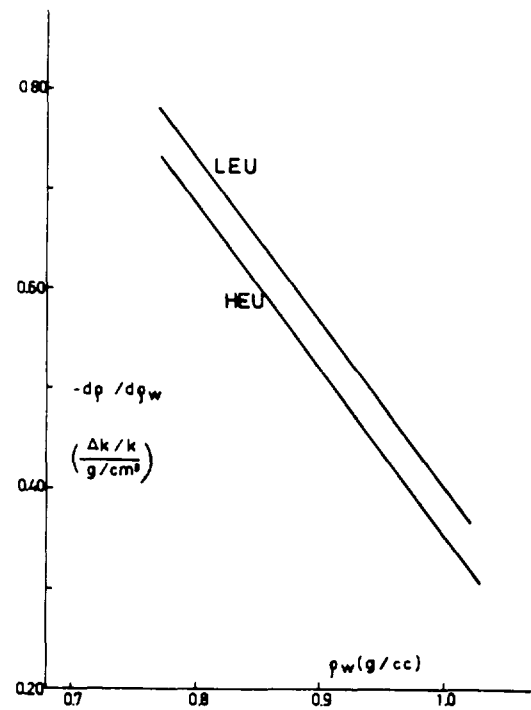


FIG. 15. Water-voids reactivity coefficient.

## 5. RADIAL AND LOCAL POWER PEAKING FACTORS

### 5.1. Calculational model

For the peaking factor calculations, several core configurations were analysed, generally including one fresh fuel element in a BOC core. As no longer quarter-core symmetry exists, whole-core X-Y CITATION cases were executed, in the usual way (see Sect. 2.4).

From the corresponding power-density edits, the various power peaking factors (radial, local and total) were obtained. The radial factor is defined as the average relative power density in a fuel element as compared to the core average. The local factor is defined as the quotient of the maximum power density inside the fuel element to the fuel-element average; instead of the continuous or point maximum, the X-Y mesh-element maximum is taken here (mesh spacing between 0.15 and 0.8 cm). Finally, the product radial x local is here called the total peaking factor.

### 5.2. Results

Table 7 presents the value of  $k_{eff}$  and the various peaking factors for the different cases in the Specifications.

It is observed that higher values of the radial peaking factors are obtained for the CFE-1 substitutions; this is not surprising, because a larger difference in burnup exists between the old and new fuel elements (25 % to 0 %).

The values of the local peaking factors are very dependent on the mesh width. On the other side, as expected, the local power peaks usually occur at one corner of the "active part" of the fuel element, mainly due to abundant water around.

TABLE 7  
Radial and Local Power Peaking Factors

Core	Fresh Element	Substituted Element	$K_{eff}$	Power peaking factors		
				Radial	Local	Rad. x Loc.
HEU	HEU	none*	1.0339	1.023	1.451	1.484
		CFE-1	1.0394	1.328	1.259	1.672
		SFE-1	1.0366	1.141	1.392	1.589
	LEU	CFE-1	1.0394	1.471	1.338	1.968
		SFE-1	1.0369	1.250	1.501	1.876
LEU	LEU	none*	1.0170	0.987	1.584	1.563
		CFE-1	1.0228	1.286	1.241	1.596
		SFE-1	1.0204	1.136	1.511	1.716

\* Relative power values in element SFE-1.

## 6. CONTROL ROD WORTHS

### 6.1. Calculational model

For control rod calculations, a remarkable computational effort have to be devoted to the determination of suitable diffusion-theory cross sections for the absorber regions of the control fuel elements, CFE. The procedure used here is schematically shown in fig. 7; a brief description of it follows. First, a WIMS one-dimensional calculation is performed along a core traverse (line 2 of fig.2) which perpedicularly crosses through the plates of a CFE; this spectral calculation is very detailed in energy and space, using the same input data (except for the absorber blade) as the corresponding WIMS cross-section calculation for the CFE "control zone" (rods out) mentioned in section 2.3. The reactivity difference  $\Delta\rho$  between both WIMS calculations is obtained.

Then, two similar one-dimensional problems (rods in and rods out) are analysed with the diffusion code CITATION 2/2, using ordinary flux-weighted constants, and the same group structure and mesh width as in further X-Y core calculations. Normally, the reactivity difference  $\Delta\rho$  between both CITATION calculations (with and without absorber) does not coincide with the WIMS value mentioned above; to match that reference value, the absorption cross section and the diffusion coefficient of the absorber region, in the thermal and epithermal groups, are adjusted accordingly.

Once diffusion-effective absorber constants are available, usual core calculations (see Sect. 2.4) are performed, for the two conditions (rods out and rods in). Separate few-group constants are used for the absorber and the remaining two regions of the "control zone" of CFE's.

### 6.2. Results

(The calculation procedure outlined above has been satisfactorily used at JEN for large blade-type control rods; however, it has not been validated for fork-type control rods. For this reason, no results are given).\*

## 7. METHODS USED FOR TRANSIENT CALCULATIONS

### 7.1. Computer codes

The model used for the different transient calculations, is mainly based in the computer code COSTAX-BOIL (8) (JEN version (9)). This program has a one-dimensional (axial) treatment of the core, both for the Neutron Kinetics and for the Thermal-hydraulics of the average channel.

Neutron Kinetics additional characteristics are as follows: 2 energy groups, up to 6 families of delayed neutrons, finite-difference space aproximation, temperature and void reactivity feedback, etc.

---

\* 'Table 8. Control rod worths' was not submitted for publication.

Other features of the Thermalhydraulics part are as follows: detailed cylindrical and plate-tipe geometries, the heat transfer to coolant may take place by forced convection, nucleate, transition, or stable film boiling, and the coolant is allowed to range from subcooled liquid, through the homogeneous model for two-phase flow, up to saturated steam. The Bergles-Rohsenow correlation is used for the subcooled nucleate boiling mode, and the Dittus-Boelter correlation is used for the single-phase forced convection regime.

The JEN version of COSTAX-BOIL is improved with the following additions:

- a) decay heat model, taken from the RELAP code (10);
- b) hot-channel model, which permits the analysis of an additional channel with a different power;
- c) the axial calculation of the bubble detachment parameter,  $\eta$  (see the contribution by INTERATOM, section 3.4.1).

Other code incidentally used has been LUCU-2, developed at JEN (11); see Section 8.4 for details.

### 7.2. General calculational model

This refers to the application of COSTAX-BOIL/JEN. As the specifications for the transients in the benchmark problem were mainly adapted to Point Kinetics codes, some additional questions arose, which were solved with the following assumptions, believed reasonable:

- a) Two-group constants were needed for the core; they were obtained with a "pure" cell model, using WIMS.
- b) For the axial reflector, a certain typical composition was assumed ( $\sim 30\%$  Al,  $\sim 70\%$  H<sub>2</sub>O, in volume); a one-dimensional WIMS supplied the two-group constants.
- c) Two-group neutron velocities are also needed; rough estimates were obtained using  $(1/v)$  weighting in WIMS (see (a) above); further adjustment is attained affecting the velocities by the adequate factor, in such a way that the value of the generation time,  $\Lambda$ , as calculated entering 2-group parameters in its definition (section 3.1, taking  $g=1,2$ ), should match the more precise value of  $\Lambda$  obtained from the Static Calculations.
- d) As the axial power distribution is explicitly obtained by the COSTAX code, provisions have to be taken in relation with the axial peaking factor  $F_z$ ; specifically, the  $\Sigma_a$  of an upper part of the core is incremented, and its height is adjusted to force  $F_z$  to have the specified value (1.5).

### 7.3. Main common data

Besides the data contained in the Problem Specifications, other important data were as follow:

- a) The 2-group structure has the energy boundary at 0.625 eV; the (adjusted) group velocities were:  $v_1=8.39 \times 10^6$  cm/s;  $v_2=1.62 \times 10^5$  cm/s (HEU), and  $v_1=7.85 \times 10^6$  cm/s.,  $v_2=1.42 \times 10^5$  cm/s (LEU).

- b) With the purpose of gaining time, some data were taken from other contributions to the Appendix, as indicated below:
  - i) from JAERI contribution, the density and heat capacity of the meat, the isothermal reactivity feedback coefficients, and the prompt neutron generation time (used indirectly, see section 7.2.c).
  - ii) from ANL contribution, the decay constants and fractions of the delayed neutrons.
- c) The reactor core was divided in 60 axial intervals.
- d) In each transient, the time step for integration was kept constant, its value being less than 1/15 of the minimum reactor period.
- e) The decay heat from fission products was assumed to amount to 7 % of total power at time zero (reactor at steady state).
- f) The number of active coolant channels was taken the same as the number of fuel plates, 551; consequently, the coolant flow per channel is  $1000/551=1.815 \text{ m}^3/\text{hr}$ .

## 8. LOSS-OF-FLOW TRANSIENTS

### 8.1. Specific calculational details

Because of the overpower factor, the initial or steady-state reactor power is taken to be  $1.2 \times 10^{12}$  MW. For consistency, the power peaking factor for the hot channel is the product radial  $\times$  local  $\times$  engineering, i.e.  $1.4 \times 1.2 = 1.68$ .

### 8.2. Fast transient

The coolant flow (or velocity) decreases exponentially with a 1-sec time constant. A scram is produced soon as indicated in the Specifications.

The main results for both HEU and LEU cores are presented in table 9, and figures 16 and 17. As expected, the differences between the HEU and LEU cases are irrelevant, due to the fact that the decay-heat part of the power dominates over the fission component.

The curves for the temperatures exhibit a moderate peak soon after the scram, then show a minimum for  $t \sim 1.5$  sec, and then rise again continuously. For  $t \sim 7$  sec, when the (downward) coolant velocity is very low, the code begins to fail; see section 8.4 for applicable comments.

TABLE 9 - Fast Loss-of-Flow Transient

	HEU	LEU
Flow Trip Point, %	85(0.16)*	85(0.16)
Power Level at Scram, MW	11.8(0.36)	11.7(0.36)
Peak Fuel Temperature, °C	94.5(0.37)	95.4(0.37)
Peak Clad Temperature, °C	94.0(0.38)	93.9(0.37)
Peak Coolant Outlet Temperature, °C	59.4(0.43)	59.3(0.43)
Min. Bubble Detachment Parameter, cm <sup>3</sup> K/Ws	268.0(0.38)	262.2(0.38)
<u>At 6.0 s</u>		
Fuel Temperature, °C	123.5	125.3
Clad Temperature, °C	123.5	125.2
Coolant Outlet Temperature, °C	64.8	65.65
Min. Bubble Detachment Parameter, cm <sup>3</sup> K/Ws	52.4	51.0

(\* ) Quantities in parentheses indicate time (in seconds) at which values occur

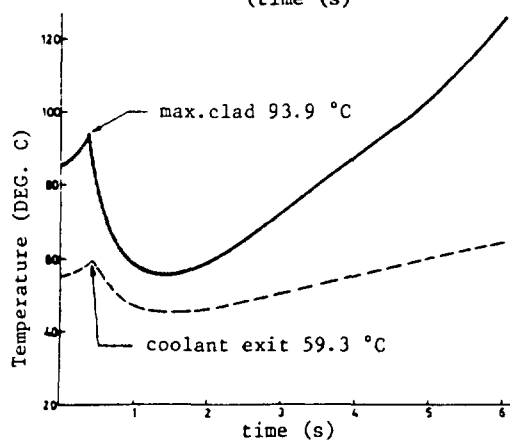
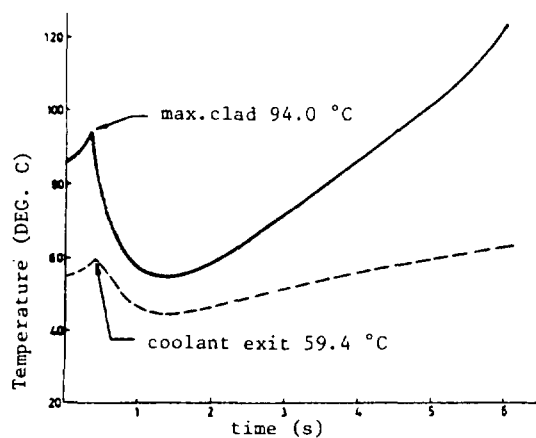
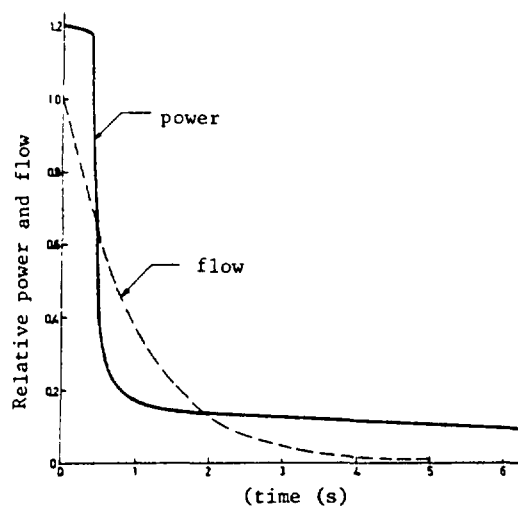
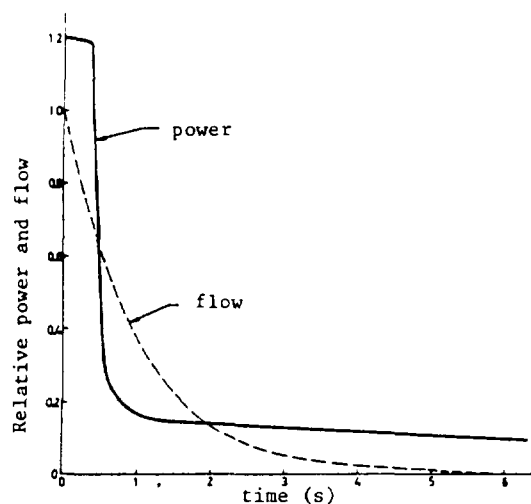


FIG. 16. Fast loss of flow transient for HEU core.

FIG. 17. Fast loss of flow transient for LEU core.

### 8.3. Slow transient

The coolant velocity at core inlet decreases exponentially with a 25-sec time constant.

The main results for both HEU and LEU cores are shown in table 10 and figures 18 and 19; as in the fast transient, there are no significant differences between the high and low-enriched cores. Again, similarly as in the fast case, in a particular transient, after a first peak and a subsequent minimum, the temperatures increase continuously. Of course, this situation would be unacceptable for a long time; one option could be that, at a certain coolant flow value, some device is actuated which favors natural convection through the reactor core. This is further discussed in the next section.

TABLE 10 - Slow Loss-of-Flow Transient

	HEU	LEU
Flow Trip Point, %	85(4.06) *	85(4.06)
Power Level at Scram, MW	11.8(4.26)	11.7(4.26)
Peak Fuel Temperature, °C	91.2(4.27)	91.9(4.27)
Peak Clad Temperature, °C	90.7(4.27)	90.3(4.27)
Peak Coolant Temperature, °C	58.3(4.27)	58.1(4.27)
Min. Bubble Detachment Parameter, cm <sup>3</sup> K/Ws	301(4.27)	304(4.27)
<u>At 45.0 s</u>		
Fuel Temperature, °C	43.9	44.1
Clad Temperature, °C	43.9	44.0
Coolant Outlet Temperature, °C	40.9	40.9

(\*) Quantities in parentheses indicate time (in seconds) at which values occur

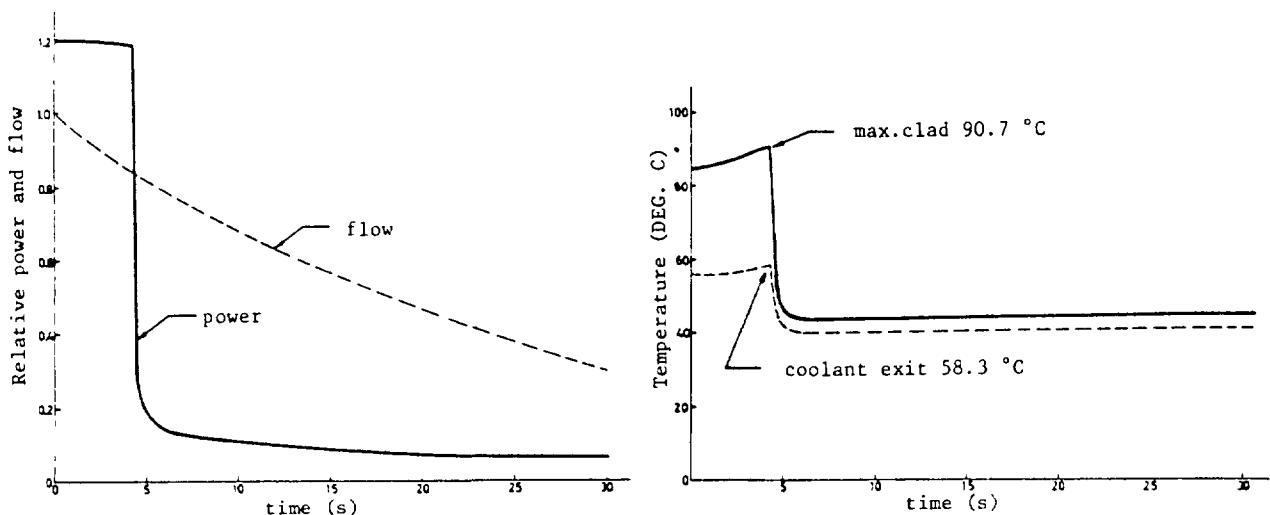


FIG. 18. Slow loss of flow transient for HEU core.

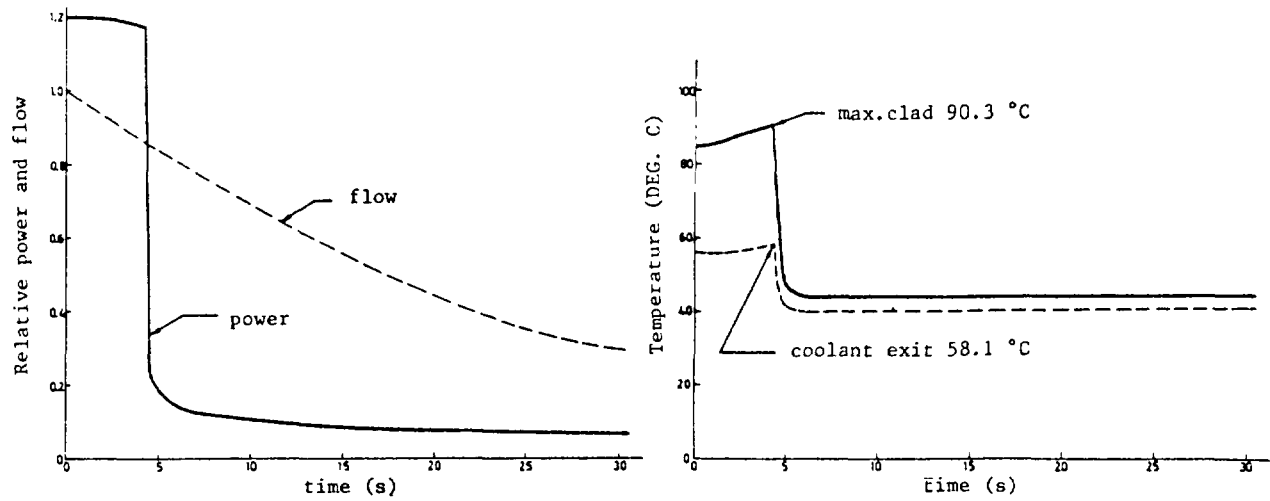


FIG. 19. Slow loss of flow transient for LEU core.

#### 8.4. Transient termination by natural convection

The assumption is made that, as the coolant flow reduces below 10 % of its nominal value, the water plenums below and above the core are put in free contact with the pool water.

Code LUCU-2 (11) has been used for the transient analysis (\*). This code has a one-dimensional (axial) modelling of the thermal-hydraulic behaviour of a MTR channel (either average or hot), solving the customary equations. Several regimes are considered: forced convection, mixed convection, flow reversal and natural convection; simple correlations for two-phase flow are included. The time-dependent power generation in the plate is an input datum, as are the initial values of the coolant velocity, the average plate temperature and the coolant outlet temperature.

For illustrative purposes, only one case has been analysed in this manner: the final part of the slow loss-of-flow transient, for the LEU core. The initial data for LUCU were taken from the output of COSTAX at time  $t=58$  sec (at which, flow is 10 % of nominal). Fig. 20 presents the corresponding results of transient evolution, showing a rapid flow reversal and subsequent natural convection. It is seen that a broad peak of the plate temperature occurs shortly after the flow reversal, followed by a lower peak of the coolant outlet temperature, and leading to a quasi-stable situation; the maximum temperatures are well below safety limits. Fig. 20 also presents the results already described in section 8.3 for the normal assumption of reducing forced flow, obtained with the COSTAX code; a conclusion that may be derived from this comparison, is that the increasing temperatures of the normal case would exceed the peaks of the natural convection case in less than 2 minutes from the beginning of the transient.

(\*) The code has not yet been checked against experimental results.

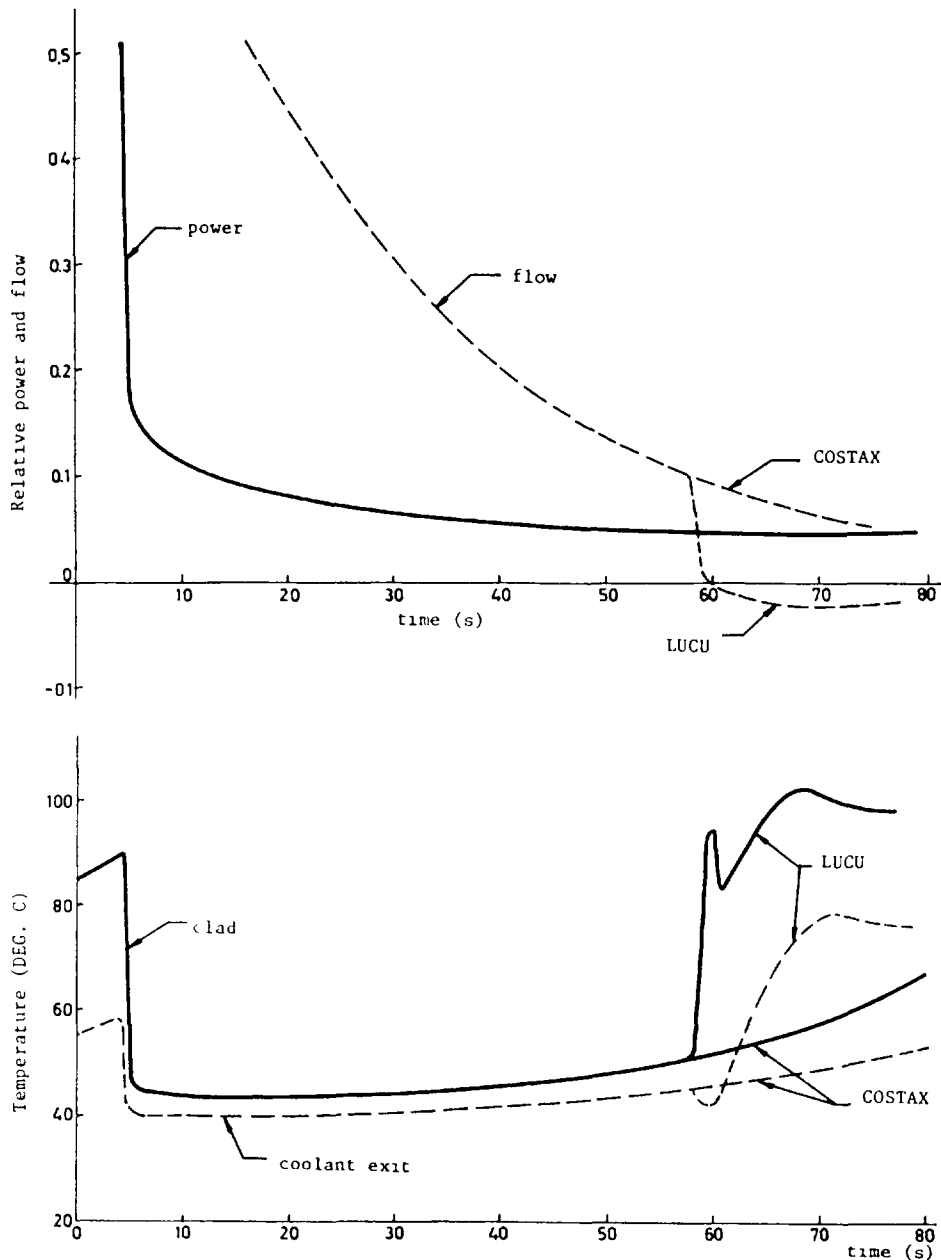


FIG. 20. Slow loss of flow transient: comparison with natural convection option (LUCU code).

## 9. REACTIVITY INSERTION TRANSIENTS

### 9.1. Calculational model

Any reactivity perturbation,  $\Delta\rho$ , is treated by the COSTAX code by applying a  $(1+\Delta\rho)$  factor to the  $(\nu\Sigma_f)$  constants of the different regions. No overpower factor is applied in any form; initial reactor power is 1 W. Trip and scram conditions are given in the Problem Specifications.

### 9.2. Slow ramps

For the HEU core, a reactivity addition rate of 0.10  $\$/\text{sec}$ , or  $7.61 \times 10^{-4} \Delta k/k/\text{sec}$ , is considered; for the LEU core, the rate is 0.09  $\$/\text{sec}$ , or  $6.55 \times 10^{-4} \Delta k/k/\text{sec}$ .

The main results for both cases are given in table 11 and figures 21 and 23. It is seen that the LEU transient is slower than the HEU one, but gives rise to more energy release and higher temperatures. In any case, there is no boiling, as expected for transients which are supposed not to be severe at all.

(The comparison with the results of other contributions, shows discrepancies for the LEU case; present analysis gives a higher peak power, a much lower energy release, and also lower temperatures. The origin for these differences seems to be in a slower power growth during the early part of the transient; no explanation exists yet for this discrepancy, which does not appear in the HEU case).

TABLE 11 - Slow Reactivity Insertion Transient

	HEU	LEU
Reactivity Insertion Rate, $\$/s$	0.10	0.09
Trip Point, MW	12(10.61)*	12(11.68)
Minimal Period, s	0.095(10.49)	0.11(11.42)
Peak Power, MW	14.93(10.64)	13.01(11.71)
Total Energy Release to Time of Peak Power, MJ	1.629	2.103
Total Energy Release beyond 12 MW, MJ	0.076	0.019
Peak Fuel Temperature, °C	69.9(10.66)	73.2(11.72)
Peak Clad Temperature, °C	69.5(10.66)	71.9(11.73)
Peak Coolant Outlet Temperature, °C	47.5(10.73)	48.8(11.78)
Min. Bubble Detachment Parameter, $cm^3K/Ws$	537(10.66)	502(11.73)
<u>At 20.0 s</u>		
Power, MW	0.007	0.0092
Energy, MJ	2.198	2.656
All Temperatures, °C	38.0	38.0

(\*) Quantities in parentheses indicate time (in seconds) at which values occur

TABLE 12 - Fast Reactivity Insertion Transients

	HEU	LEU	LEU
Max. Reactivity, $\$$	1.5	1.5	1.35
Trip Point, MW	12(0.611)*	12(0.597)	12(0.691)
Minimal Period, ms	14.5(0.500)	13.5(0.500)	19.2(0.500)
Peak Power, MW	132.7(0.659)	116.1(0.638)	51.8(0.729)
Total Energy Release to Time of Peak Power, MJ	3.465	2.624	1.44
Peak Fuel Temperature, °C	167.1(0.672)	166.4(0.654)	105.0(0.753)
Peak Clad Temperature, °C	162.3(0.675)	156.6(0.654)	102.1(0.756)
Peak Outlet Temperature, °C	108.7(0.747)	80.4(0.711)	54.9(0.840)
Min. Bubble Detachment Parameter, $cm^3K/Ws$	36.2(0.765)	58.2(0.657)	241(0.759)

(\*) Quantities in parentheses indicate time (in seconds) at which values occur

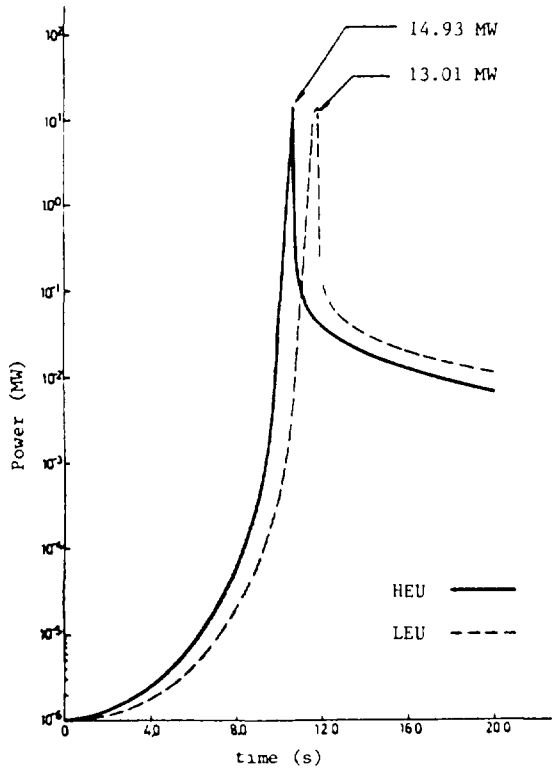


FIG. 21. Slow reactivity insertion transient for HEU and LEU cores.

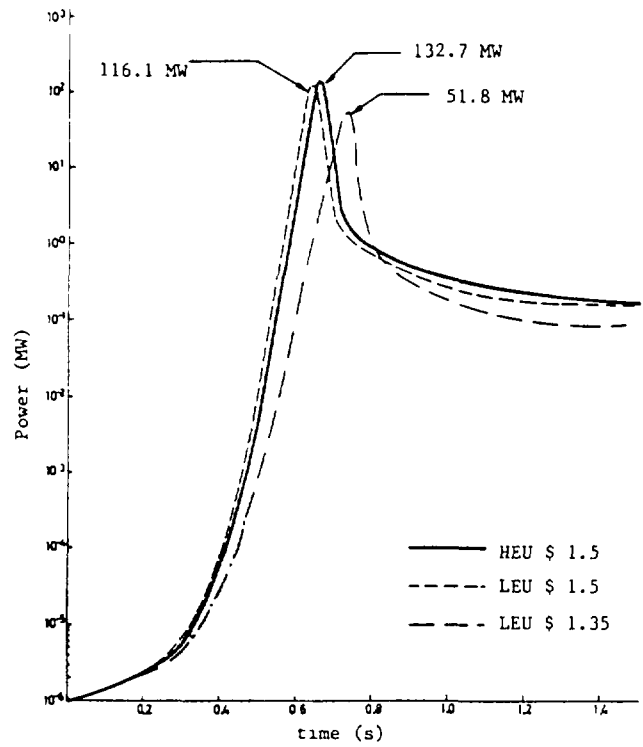


FIG. 22. Fast reactivity insertion transients for HEU and LEU cores.

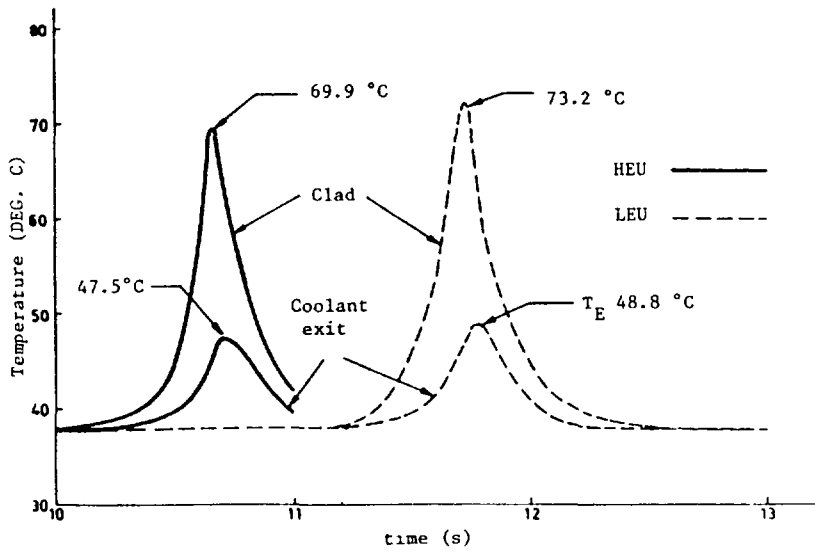


FIG. 23. Slow reactivity insertion transient for HEU and LEU cores: maximum temperatures.

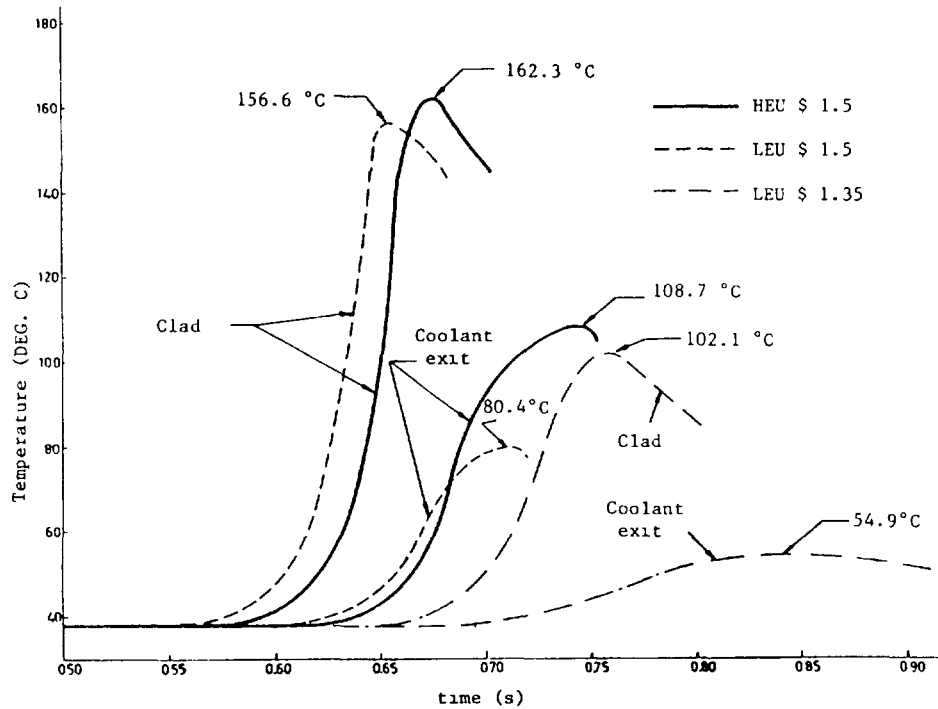


FIG. 24. Fast reactivity insertion transients for HEU and LEU cores: maximum temperatures.

### 9.3. Fast ramps

For the HEU core, a reactivity addition of 1.5 \$ (or 1.14 %  $\Delta k/k$ ) in 0.5 sec is considered; for the LEU core, two ramps are studied: 1.5 \$ (1.09 %  $\Delta k/k$ ) in 0.5 sec, and 1.35 \$ (0.98 %  $\Delta k/k$ ) in 0.5 sec.

The main results of these analyses are given in table 12 and figures 22 and 24. For the 1.5 \$ ramp, the comparison of results between the HEU and LEU cases is as follows: the transient is faster for the LEU core, but the power peak obtained is lower, and same are the energy release  $E(t_m)$  and the temperatures; a slight difference, in a similar direction, is also observed in the minimal value of the bubble detachment parameter:  $\eta_m=36$  for HEU,  $\eta_m=58$  for LEU. Consistent with these low values, the code outputs indicate that, after the power peak, boiling occurs in both cases; moreover, after some time of these low  $\eta$  values, the temperature calculation in the COSTAX code begins to fail; this fact is reflected in fig. 24, by cutting the corresponding curves.

The analysis of the 1.35 \$ ramp for the LEU core gives a much less severe behaviour; the peak clad temperature is below saturation temperature, and no boiling occurs.

(Again, a certain discrepancy, between this and other contributions, is observed in these fast ramp results for the LEU cases. Specifically, the peak power in present contribution, is lower and delayed, inducing a lower energy release, and delayed peaks of the fuel and clad temperatures. As in the case of the slow ramp (section 9.2), a slower rate of power increase, from the transient beginning to the peak, is in the origin of the differences. The possible causes of this discrepancy, which affects the LEU cases only, will need further investigation).

## REFERENCES

- 1) C. AHNERT. Programa WIMS-TRACA para el cálculo de elementos combustibles; manual de usuario y datos de entrada. Report JEN-461, 1980.
- 2) J.R. ASKEW et al. A General Description of the Lattice Code WIMS, Journal Brit. Nucl. Energy Soc., No. 5, p. 564, 1966.
- 3) M. GOMEZ-ALONSO et al. Diseño preliminar optimizado de reactores de piscina. Paper B-7, 6th Annual Meeting Sociedad Nuclear Española, Barcelona, 1980.
- 4) M. GOMEZ-ALONSO et al. Optimized Conversion from HEU to LEU for an intermediate-power swimming pool reactor. Paper IAEA-SR-77/20, Seminar on Research Reactor Operation and Use, Jülich (FRG), 1981.
- 5) E. MINGUEZ, M. GOMEZ-ALONSO. Cálculos de "bechmark" para el análisis neutrónico de un reactor con combustible tipo MTR. Paper 3.5, 8th Annual Meeting Sociedad Nuclear Española, Santander 1982.
- 6) J. PEÑA. WIMSEDIT: un programa para el manejo de la impresión de salida del código WIMS-TRACA. Internal report JEN/TCR/A-02/82, 1982.
- 7) T.B. FOWLER et al. Nuclear Reactor Core Analyses Code: CITATION, Revision 2. Report ORNL-TM-2496/Rev.2, 1971.
- 8) G. FORTI. COSTAX-BOIL: A computer programme of the COSTANZA series for the Axial Dynamics of BWR and PWR Nuclear Reactors. Report EUR-4497-e, 1970.
- 9) R. MARTINEZ-FANEGAS, M. GOMEZ-ALONSO. Mejoras en el código COSTAX-BOIL: versión JEN-01. Internal JEN Report, in preparation.
- 10) INEL. RELAP4/MOD5: A Computer Program for Transient Thermal-Hydraulic Analysis of Nuclear Reactors and Related Systems; User's Manual. Report ANCR-NUREG-1335, 1976.
- 11) J.J. SANCHEZ-MIRO, G. RESCO. Desarrollo de métodos de cálculo de convección natural y mixta, en estado transitorio, para un reactor de tipo piscina; aplicación al análisis de un LOFA. Paper 2.16, 9th Annual Meeting Sociedad Nuclear Española, Sevilla, 1983.
- 12) G.I. BELL, S. GLASSTONE. Nuclear Reactor Theory. Van Nostrand Reinhold Co., 1970.
- 13) R.J. TUTTLE. Delayed Neutron Data for Reactor-Physics Analysis. Nucl. Sci. Eng. 56, 37 (1975).

## Appendix G-6

### SELF-LIMITING TRANSIENTS IN HEAVY WATER MODERATED REACTORS

J.W. CONNOLLY, B.V. HARRINGTON, D.B. McCULLOCH

Lucas Heights Research Laboratories,  
Australian Atomic Energy Commission,  
Lucas Heights, New South Wales,  
Australia

#### Abstract

A brief description is provided of the methods and models for reactivity transient calculations in heavy water moderated research reactors as a supplement to the heavy water reactor benchmark problem discussed in IAEA-TECDOC-324. These methods and models were validated by comparison with experimental transient data from the SPERT II BD22/24 heavy water moderated core. Experimental and calculated transient parameters for this core are compared.

#### 1. INTRODUCTION

IAEA Tecdoc 233 defined generic 2 MW and 10 MW light water moderated research reactors for a series of benchmark calculations of specified reactor parameters with high and low enrichment cores. Subsequent to the publication of Tecdoc 233, a series of benchmark transient calculations, based on the same generic reactors, was defined (App.F0), and the results of these calculations constitute the major parts of Appendices F1 to F5 of the present document.

In a similar manner, a 10 MW generic heavy water moderated research reactor was defined for HEU/LEU benchmark comparison calculations for the Heavy Water Reactor Guidebook prepared as a supplement to Tecdoc 233. Because differences in transient behaviour with reduction in enrichment were in this case expected to be small and/or favourable, transient benchmarks were not considered essential, and none were defined for inclusion in the present document.

The benchmark heavy water moderated reactor is very closely similar to the AAEC's 10 MW HIFAR. Methods of transient calculation broadly similar to those reported in Appendix F1 have been developed independently at the AAEC's Lucas Heights Research Laboratories over a number of years in the context of HIFAR safety assessment. They have been validated by comparison with a range of light and heavy water moderated SPERT core experimental programs, and have shown excellent agreement.

The brief account of this work which follows, and the results presented, are included in the 'Benchmark Appendices' of the present document for the sake of completeness. Although the studies do not relate specifically to the benchmark heavy water moderated research reactor, both the HIFAR and the SPERT BD22/24 cores resemble the benchmark very closely. The material presented therefore demonstrates that calculations of the change with core enrichment of the transient behaviour of heavy water moderated research reactors can be carried out with the same confidence as those for light water moderated reactors.

## 2. THE METHOD

The transient characteristics of D<sub>2</sub>O and H<sub>2</sub>O moderated reactors differ because the prompt neutron lifetime of the former is much longer than that of the latter, and because most D<sub>2</sub>O reactors have a large lattice pitch. In such reactors there are thus two distinct zones producing reactivity feedback; the first is the coolant within the fuel elements and the second, the bulk moderator between the fuel elements. For transients initiated under conditions of forced convection cooling, the subsequent power history is therefore partly determined by the fraction of coolant which flows to the bulk moderator region.

In the following sections, a summary is given of transient calculations for the DIDO class reactor HIFAR, which is essentially the same as the benchmark D<sub>2</sub>O moderated HEU core. To validate these calculations, the experimental data from the SPERT II program have also been analysed using the same methods.

The code used in the analysis was the one-dimensional conductive heat transfer-coupled neutron kinetics code ZAPP (Ref. 1). This code includes a simulation of boiling heat transfer and has been extensively tested against SPERT I data (Ref. 2,3). Comparison between PARET (Ref. 4) and ZAPP calculations of these SPERT I data shows that both codes yield rather similar results even though the thermohydraulic modelling used in the two codes is completely different.

ZAPP was developed further to enable calculations to be made under forced convection heat transfer conditions. This model was then tested against data from the SPERT II program for the close packed D<sub>2</sub>O moderated core (Ref. 5). An empirical voiding model for transients terminated by steam expulsion of coolant from the coolant channels of the expanded D<sub>2</sub>O core BD 22/24 was then developed. This composite model was applied to the H<sub>2</sub>O moderated core D12/25 of the SPERT I program and enabled experimental

burst parameters for transients characterised by initial inverse periods ( $\alpha_0$ ) up to the maximum induced ( $300 \text{ s}^{-1}$ ) to be satisfactorily reproduced.

### 2.1 Comparison between the Benchmark D<sub>2</sub>O Moderated HEU Reactor, HIFAR and SPERT II BD 22/24

Table 1 lists data pertinent to transient analysis for the three reactors. The major design difference is the flat plate geometry of the BD 22/24 fuel element, which results in a larger heat transfer area and a smaller volume of coolant within the fuel element than in the other two cores. The volume of coolant per fuel element in the benchmark is larger than that in HIFAR because the region of D<sub>2</sub>O within the inner fuel tube is specified as coolant; in HIFAR, this D<sub>2</sub>O is contained within an aluminium thimble and flow through the region is small.

### 3. CALCULATIONS OF TRANSIENTS IN BD 22/24 AND COMPARISON WITH EXPERIMENTAL RESULTS

During the SPERT II BD 22/24 program, measurements of the burst parameters peak power ( $P_{\text{max}}$ ), energy release to the time of peak power ( $E_{\text{tm}}$ ), central fuel plate temperature at the time of peak power ( $\theta_{\text{tm}}$ ) and maximum central fuel plate temperature ( $\theta_{\text{max}}$ ) were measured. These experiments were performed without forced convection coolant flow and at several values of reactor vessel pressure and initial D<sub>2</sub>O temperature.

Figure 1 compares calculated and measured burst parameters as a function of initial inverse period ( $\alpha_0$ ). The agreement is good. The effect on the calculated energy release of deleting the steam void growth model is also shown in this figure. The calculations produced nucleate boiling heat transfer conditions at or before peak power for values of  $\alpha_0 > 2 \text{ s}^{-1}$  and steam void growth contribution to reactor shutdown for values of  $\alpha_0 > 7 \text{ s}^{-1}$ .

#### 3.1 Calculated Burst Parameters in HIFAR without Coolant Flow

Transient calculations were performed for HIFAR using the cylindrical geometry version of ZAPP, under conditions of zero coolant flow and over a  $\alpha_0$  range similar to that for the SPERT II experiments. Figure 2 shows the computed burst characteristics as a function of  $\alpha_0$ . Because of the smaller heat transfer area of HIFAR compared with BD 22/24, nucleate boiling is established at or before peak power for values of  $\alpha_0 > 1 \text{ s}^{-1}$  and steam voidage contributes to shutdown for all  $\alpha_0 > 6 \text{ s}^{-1}$ . Otherwise the burst parameters calculated for HIFAR closely resemble those for BD 22/24, since the reactivity coefficient per unit energy release is about the same for both reactors.

TABLE 1

## COMPARISON OF CHARACTERISTICS OF REACTORS BD22/24, HIFAR AND BENCHMARK

PARAMETER	BD22/24	HIFAR	BENCHMARK
Number of fuel elements	24	25	26
Lattice pitch (mm)	152.4	152.4	152
Fuel plate geometry	parallel slab	annular slab	annular slab
Fuel alloy thickness (mm)	0.508	0.66	0.5
Cladding thickness (mm)	0.508	0.432	0.51
<sup>235</sup> U/fuel element (g)	154	150	150
Heat transfer area (m <sup>2</sup> )	40	29	29
Prompt neutron lifetime (μs)	660	500	460 (a)
Max./Ave. core power	1.5	1.6	
Clean cold critical mass (kg)	2.8	~1.0	
Coolant vol/fuel element (L)	1.5	2.5	3.9 (b)
Whole reactor temperature coefficient at 20°C ( $\frac{\delta k}{k} \text{ } ^\circ\text{C}^{-1}$ )	$-24 \times 10^{-5}$	$-34 \times 10^{-5}$	
Central void coefficient ( $\frac{\delta k}{k} \text{ cm}^{-3}$ )	$-1.9 \times 10^{-6}$	$-1.9 \times 10^{-6}$ (a)	$-1.7 \times 10^{-6}$ (a,b)
Total coolant void coefficient ( $\frac{\delta k}{k} / \%$ )	$-5.25 \times 10^{-4}$ $-5.47 \times 10^{-4}$ (a)	$-8.04 \times 10^{-4}$ (a)	
Coolant temperature coefficient ( $\frac{\delta k}{k} \text{ } ^\circ\text{C}^{-1}$ ) at 20°C	$-6.5 \times 10^{-5}$ (a)	$-10.3 \times 10^{-5}$ (a)	$-13.4 \times 10^{-5}$ (a,b,c)

(a) Calculated value

(b) Includes central thimble region

(c) Mean Value from 20 - 50°C

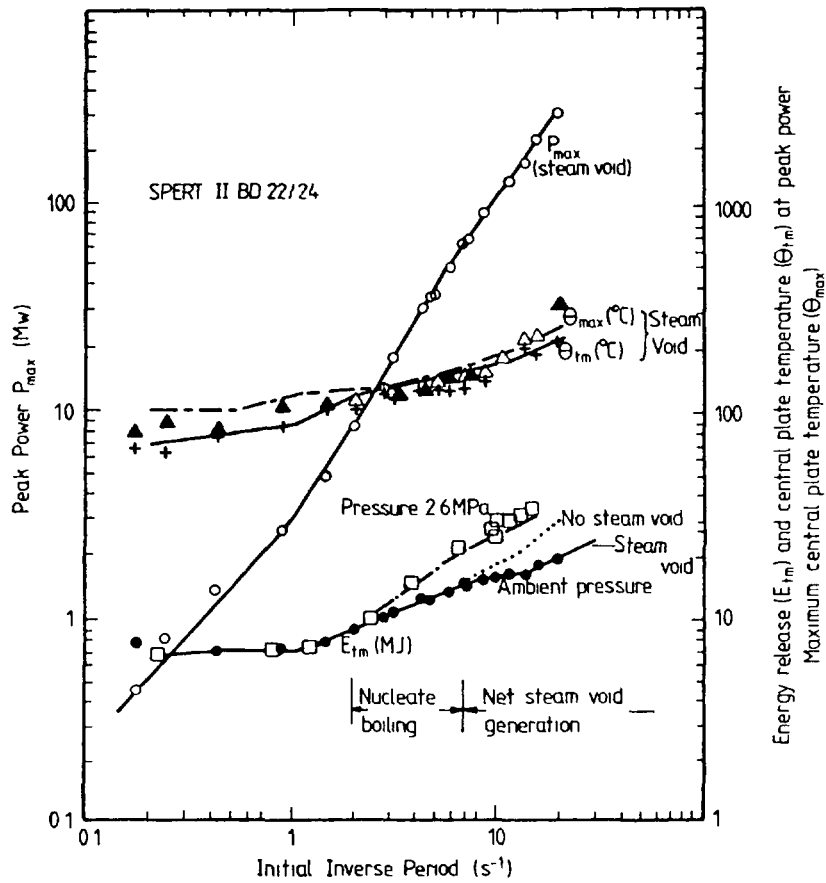


Figure 1 Comparison between measured and calculated transient parameters — SPERT II BD 22/24

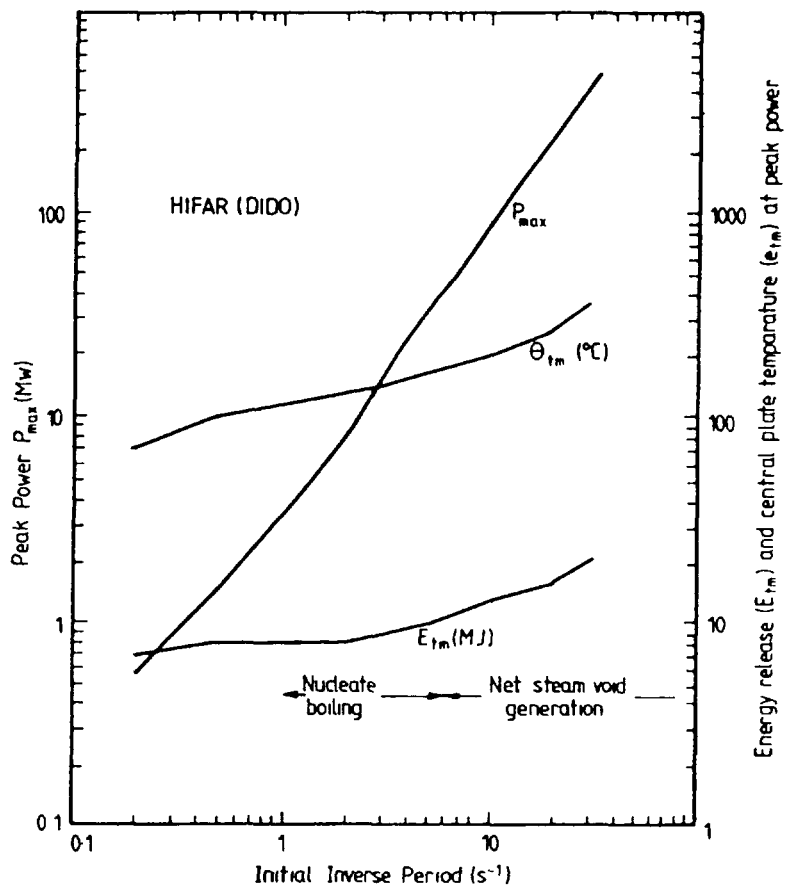


Figure 2 Calculated transient parameters for HIFAR (no coolant flow)

### 3.2 Calculations of Transients in HIFAR with Forced Coolant Flow

HIFAR operations are restricted to two modes. In the low power mode, with the shutdown pump operating, the power is restricted to 150 kW maximum and the core coolant flow is  $29 \text{ L s}^{-1}$ ; in the high power mode, the maximum permitted power is 10 MW with two main pumps delivering a coolant flow rate of  $364 \text{ L s}^{-1}$ .

Calculated peak and runout powers (equilibrium power attained after peak power) for the low power mode are shown as a function of step reactivity insertion in Fig. 3. Because these calculations were performed with a low (10 kW) initial reactor power, it was found that ramp additions of reactivity, to the same total reactivity injection as a step, produced the same peak power; this arises because the ramp is complete before the reactor power is high enough to generate appreciable reactivity feedback.

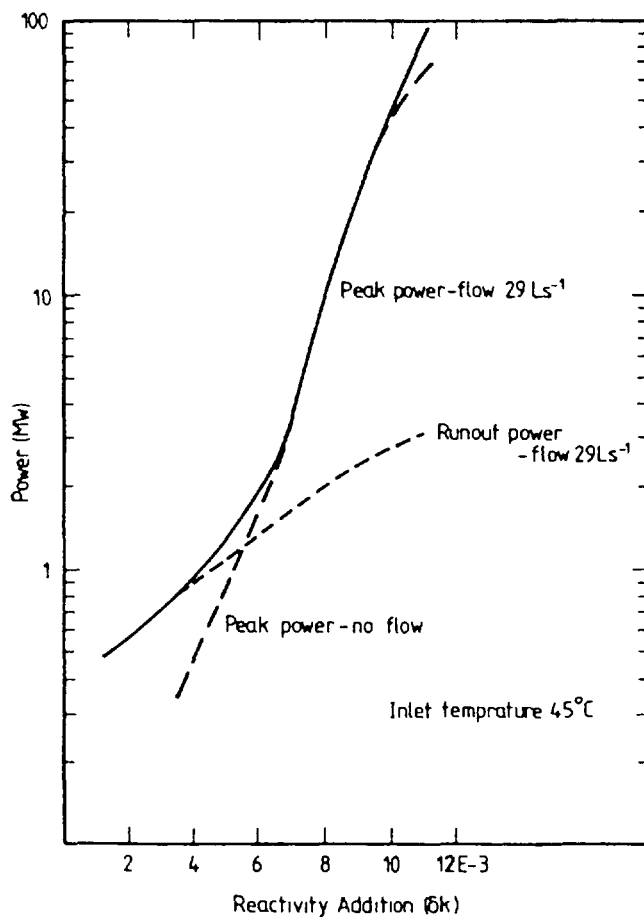


Figure 3 Calculated powers for HIFAR — initial power 10 kW

In the high power mode, the time for coolant to traverse the core is small ( $\sim 0.1$  s) and the initial power is high (10 MW). The former means that heated coolant flowing into the bulk moderator produces appreciable feedback and the coolant flow path partition between reflector and bulk moderator therefore needs to be known; the latter results in the immediate production of reactivity feedback and thus a dependence of peak power on ramp rate.

Evidence from experiments on HIFAR (Ref. 6) and on the similar reactor DR3 (Ref. 7) suggests that the fraction of coolant flow directed to the bulk moderator is large. For the calculated peak powers as a function of ramp rate and ramp height shown in Fig. 4, it has been assumed that all coolant flows directly into the bulk moderator. Subsidiary calculations suggest that the peak powers do not change greatly unless the fraction of flow to this region drops below  $\sim 0.4$ .

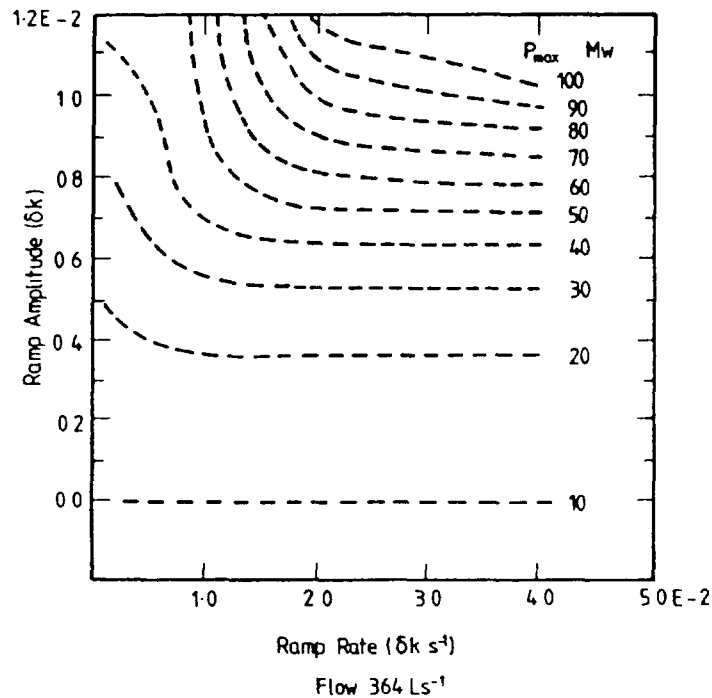


Figure 4 Calculated peak powers for HIFAR — initial power 10 MW

## REFERENCES

1. CLANCY, B.E. (1983) ZAPP - A computer program for the simulation of reactor power transients. AAEC/E568.
2. CLANCY, B.E., CONNOLLY, J.W. and HARRINGTON, B.V. (1975) - An analysis of power transients observed in SPERT I reactors. Part 1 - Transients in aluminium plate-type reactors initiated at ambient temperature. AAEC/ E345.
3. CLANCY, B.E., CONNOLLY, J.W. and HARRINGTON, B.V. (1976) - An analysis of power transients observed in SPERT I reactors. Part 2 - Dependence of burst parameters on initial temperature and core moderation. AAEC/E383.
4. WOODRUFF, W.L. (1982) - The PARET code and the analysis of the SPERT I transients. ANL/RETR/TM-4.
5. CONNOLLY, J.W. and HARRINGTON, B.V. (1977) - An analysis of power transients in THE SPERT II D<sub>2</sub>O moderated close packed core. AAEC/E418.
6. HARRIES, J.R. and WILSON, D.J. (1978) - Measurement of the dynamic response of the materials testing reactor HIFAR. AAEC/E428.
7. La COUR CHRISTENSEN (1963) - An experimental and theoretical investigation of the dynamic response of the nuclear reactor DR3. RISØ Report 56.

# **Appendix H**

## **COMPARISON OF CALCULATIONS WITH MEASUREMENTS**

### **Abstract**

Calculations are compared with measurements in several reactors in order to determine the accuracy of neutronics calculations for cores containing MEU and LEU fuels.

## Appendix H-1

### CRITICAL EXPERIMENTS IN THE ISIS REACTOR WITH THE CAMEL FUEL ELEMENT

COMMISSARIAT A L'ENERGIE ATOMIQUE

Centre d'études nucléaires de Saclay,

Gif-sur-Yvette, France

#### Abstract

Neutron tests of the caramel type  $UO_2$  fuel were conducted in Isis in 1979. The new fuel elements of this type have been used since 1980 in Osiris, where they replaced the highly enriched U-Al fuel.

The Isis tests were preceded by calculations, whose results are compared with those obtained by measurements.

#### 1.1 CALCULATION METHODS (NEUTRON)

##### 1.1.1 Effective macroscopic cross-sections

These are the result of unidimensional transport calculations, performed using the Apollo code <1>.

##### Library of effective cross-sections

The nuclear data base employed is ENDF B/4 of American origin. It is a multigroup library that gives the following characteristics for the elements and their chief isotopes:

- . microscopic diffusion cross-sections,
- . microscopic absorption cross-sections,
- . microscopic production ( $\nu\sigma_f$ ) " ,
- . elastic, inelastic transfer cross-sections etc.

Several thermal matrices generally appear for the same isotope, with different temperatures. In the case of self-protected cross-sections, the effective cross-sections are given for a series of temperature values.

##### Resolution of the transport equation

For a unidimensional environment, the Apollo code resolves the transport equation in its integral form, in the multigroup approximation. The number of groups used here is 99.

Since we are dealing with cells exhibiting considerable anisotropy, collision is assumed to be linearly anisotropic; this is the approximation B1.

### Calculation of self-protection of resonances

This is broken down into two steps. The first consists of calculating the effective cross-sections that are employed, and the second of calculating the self-protected cross-sections.

### Calculation of the diffusion and leakage coefficient

Calculation of the flux in the cell makes it possible to proceed with the calculation of a current. For any reaction, one can then define an effective cross-section, homogenized for each group, and find an eigenfunction of the multigroup transport equation. Even in the thermal part, the diffusion coefficient accounts for the collision anisotropy (approximation B1).

### Evolution calculation

It is possible to evoke evolution in heterogeneous fuel zones. In the case at hand, the fissile region can be treated as an infinite (plate/water) network.

The changes in heavy isotopes are calculated by successive iterations, taking account of the variation in effective cross-sections with the neutron spectrum and the fine structure of the fluxes in the cell.

This can be carried out at constant flux, or at constant mean power.

### Environmental absorption characteristics

The various environments are quite different with respect to their neutron properties:

- . the hafnium of the control rods acts as a black body to thermal neutrons,
- . the fissile region of fuel elements,
- . experimental mock-ups, structures, which are relatively non-absorbent,
- . the various reflectors and moderators (beryllium, water), which are very large and relatively non-absorbent.

These are treated differently for the calculation of their effective cross-sections.

### High absorption zone

#### Hafnium absorbent of control rods

The very high absorption of this material is a hindrance for diffusion calculations.

An Apollo one-dimensional transport calculation is carried out in the real geometry (structures, water channels), and in a fissile environment (neighbouring fuel elements).

#### Fissile region of fuel elements

The elementary unit consists of the fuel plate ( $\text{UO}_2$  fissile core and  $\bar{\Gamma}$  clad) and the water channel. A one-dimensional transport calculation is carried out for an infinite network of plates, with the adjustment of transverse leaks. The microscopic cross-section library employed has already been described. Due consideration is given to the fine structure of the fluxes, and also to the self-protection of resonances. The expected result is a set of microscopic effective cross-sections accurately representing the properties of the fissile region of the element. Microscopic effective cross-sections are also obtained (four groups), as well as the diffusion coefficients of the fissile region.

#### Geometric zoning for calculations

The media surrounding the core (core box, structures, light water) are considered as homogeneous for calculation of the neutron constants. Certain core constants, such as the beryllium reflector blocks, aluminium and experimental mock-ups, have several cooling water channels. These channels are also homogenized for the requirements of the neutron calculation on one location of the network.

Other constituents, like the standard and control elements, exhibit an excessively heterogeneous character for overall representation. For example, the fuel element consists of the juxtaposition of a fuel plates network with water and structures.

#### Zoning of standard and control elements

- . The standard fuel element is divided into two zones:
  - . fissile region (uranium plate/water) network ,
  - . edge plate region.
- . The fuel follower of the control element in:
  - . fissile region ,
  - . edge plate region ,
  - . peripheral region (aluminium/water).

The absorbing part of the control elements in:

- . central water cavity ,
- . hafnium absorbent and structures ,
- . peripheral medium .

## Energy groups employed

Distribution into macrogroups	interval	
	energy	lethargy
fast No.1	10 MeV to 907 keV	0 to 2.4
fast No.2	907 keV to 5 keV	2.4 to 7.6
epithermal	5 keV to 0.625 eV	7.6 to 16.588
thermal	0.625 eV to 0	16.588 to 25.233

### 1.1.2 xy two-dimensional diffusion calculations

Daixy diffusion code <2>.

The reactor is represented in rectangular coordinates, by a cross-section in the median plane of the fuel element.

Each core element is treated with the required level of detail, by zoning into several regions of different types (fissile region, edges etc). The microscopic effective cross-sections of these regions were calculated, in transport theory, during the previous cell calculations.

To account for axial leaks, a transverse Laplacian is introduced in the form of "extrapolated height". All the core constituents are represented, with the control elements in positions completely up or down.

Successive iterations supply a critical parameter, the value of the effective multiplication factor.

The essential results are concerned with the following:

- . the reactivity available for different loading states, the anti-reactivity of the experimental devices, the efficiency of the control elements,
- . distribution of sources in accordance with the different parameters (configuration of control rods, burnup of fuel elements etc),
- . value of neutron fluxes: the value of the thermal and fast neutron fluxes in the different core regions, and in particular in the experimental zones.

### 1.1.3 Isis/Osiris specific characteristics

The caramel fuel used in Osiris is enriched to 7%, and refuelling between two operating cycles ( $\approx 28$  EFPD) is partial. No burnable poison is used. In the first load the partly burnt elements constituting the core at equilibrium are replaced by fuel that is less rich in U235 (4.75% and 5.62%).

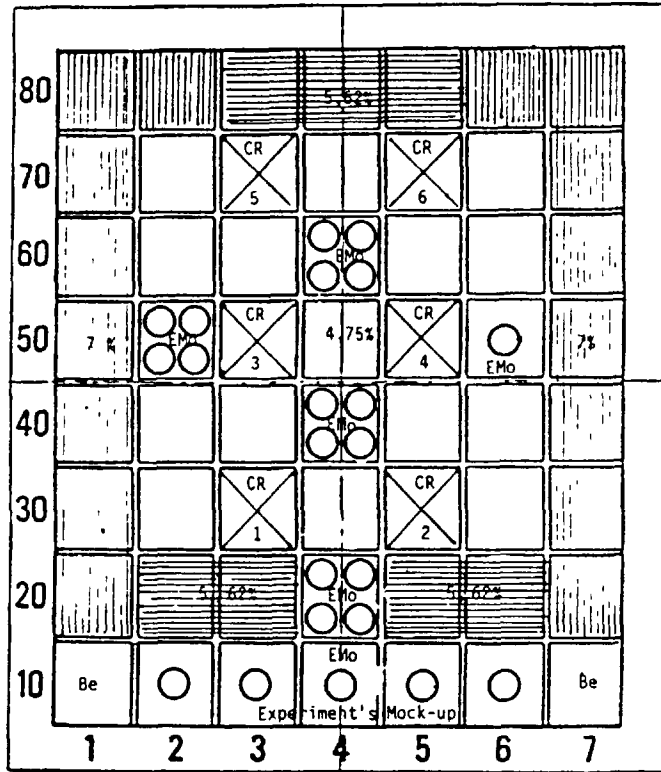
The control elements have an absorbent part (hafnium frame) and a caramel fuel follower.

Mock-ups placed in the fissile network and on a row serve to simulate the Osiris irradiation experiments. Reflector blocks (beryllium) are placed on one of on side of the core, in variable numbers.

Before the loading of the Osiris reactor, an experimental study of the core was carried out on the Isis neutron mock-up.

The large-scale configuration (7 × 7) planned for Osiris was built up progressively by proceeding from smaller cores, like the minimum compact core without the experimental mock-ups described below.

caramel 1.45 mm density UO <sub>2</sub> : 10.3 g/cm <sup>3</sup>	standard elements (17 plates)	control elements (14 plates)
caramel dimensions	17.1 x 17.1 x 1.45mm	17.1 x 17.1 x 1.45mm
spacing between caramels	1.58mm	1.58 mm
active width	72.9 mm	54.3 mm
active length	629 mm	
number of caramels per plate	136 (34 x 4)	99 (33 x 3)
UO <sub>2</sub> weight per plate	578.9 g	421.4 g
uranium weight per plate	510.3 g	371.5 g
<sup>235</sup> U weight per plate		
4.75 %	24.2 g	
5.62 %	28.7 g	
7 %	35.7 g	26 g
UO <sub>2</sub> weight per element	9 841 g	5 899 g
uranium weight per element	8 675 g	5 200 g
<sup>235</sup> U weight per element		
4.75 %	412 g	
5.62 %	487.5 g	
7 %	607.3 g	364.1 g
plate thickness	2.22 mm	2.22 mm
internal channel	2.63 mm	2.85 mm
end channels	2.29 mm	2.46 mm



ISIS FUEL LOADING 7x7  
Enrichment (4.75% ; 5.62% ; 7%)

## 1.2 AVAILABLE REACTIVITIES

### 1.2.1 Minimum compact core

This core has no irradiation experiment mock-ups. The control elements are in place in their final configuration. The minimum critical size is determined by progressively positioning the standard fuel elements (4.75%).

The critical configuration includes:

.	12 standard elements	4.75%	4972.7 g
.	6 control element followers	7%	2271.0 g
			<hr/>
			7244 g <sup>235</sup> U

As predicted by calculation, criticality is reached with twelve 4.75% elements with the six rods in the high position.

excess reactivity available	calculation 6 CR H	experiment
$\rho$ pcm	+25	$\epsilon$

## 1.2.2 Osiris type configuration (7 × 7)

### Loading

#### Standard fuel elements (38)

.	15 elements	enrichment 4.75%	6076g	<sup>235</sup> U
.	8 elements	" 5.62%	3891g	"
.	16 elements	" 7%	9143g	"

#### Control elements

	6 fuel followers	" 7%	2270g	"
--	------------------	------	-------	---

or 21 380 g <sup>235</sup>U

The absorbent part of the control elements consists of hafnium in the form of a hollow square tube (51 inner side × 58.2 outer side × 568 mm long, thickness 3.6 mm).

### Experimental mock-ups

Placed in the fissile network or in the free locations inside the rack, they are used to simulate Osiris irradiation experiments.

### Beryllium reflector blocks

#### Experimental mock-ups

- . Four in the network.
- . One in a slot.

### Beryllium reflector blocks

In row 10, two Be blocks in the corners.

#### Experimental mock-ups

In row 10, five others mock-ups.

### Excess initial reactivity

Criticality is reached with the two safety rods in the high position, by raising the next control rod CR No.1. The stabilization level is 130 mm.

The initial reactivity values are as follows:

.	calculated	10,800 pcm
.	measured	10,530 pcm

The measured value is obtained from anti-reactivity measurements of the control elements given below.

Anti-reactivity of control rods

The anti-reactivity of rods not selected as safety rods can be measured by using a reactimeter, or by the double criticality method with boronation of the core circuit water.

The anti-reactivity of the two rods selected as safety rods is measured by dropping, using a reactimeter.

The following table gives the results obtained.

anti-reactivity of rods raised in sequence 2,5,1,6,3,4 Osiris type large core pcm	measured anti-reactivities
2 + 5	5800
1	2100
6	2820
3	2810
4	3050
total anti-reactivity of six rods	16,600
$\beta_{\text{eff}} = 750 \cdot 10^{-5}$ effective proportion of delayed neutrons	

1 3 POWER DISTRIBUTION IN THE FUEL

The measurement system consists of three miniaturized fission chambers (deposit of  $^{235}\text{U}$ ), mounted on an aluminium support strip, that is inserted between the fissile plates of the fuel element. Measurements are taken for several rod configurations, in the horizontal plane of symmetry of the core, and are supplemented by vertical distributions in some fuel elements of the network.

Prior calibration of the chambers is performed by simultaneously irradiating a number of gold detectors, placed in several locations distributed in the core.

Since all the fuel elements of the first core are new, the indications of the fission chambers make it possible to determine the power distribution within the fuel elements, and the relative contribution of each element to the total power of the reactor.

### Comparison of calculations with measurements

Agreement is excellent with respect to the internal elements of the network. For the peripheral elements, the power peaking, due to the vicinity of the reflectors, is a little underestimated by the calculation.

This is due to the fact that the fuel's neutron characteristics are normally calculated for an infinite network. In the transport calculation, a more faithful representation of the real environment of the peripheral fuel elements provides a better picture of the variation in neutron spectrum, but lengthens the computer calculation time. It is very easy to adjust the calculation results such as to get good estimates of the power distribution and hot point factor.

#### 1.4 NEUTRON FLUX IN EXPERIMENTAL LOCATIONS

Miniature fission chambers are used to measure the thermal ( $^{235}\text{U}$ ) and fast ( $^{237}\text{Np}$ ) fluxes. Gamma heating is measured with calorimeters.

The flux values correspond to disturbed values for the core box locations where the experimental maquettes have been positioned, and to undisturbed fluxes in water, at the outer periphery of the core box.

### Comparison of calculations and measurements

Fluxes in irradiation places :

#### Thermal fluxes

Locations in network	deviations of 0 to 20%
Locations row 10	deviations of 0 to 20%
Locations first periphery	deviations -5 to +5%

#### Fission fluxes

Locations in network	deviations 20 to 25%
Locations row 10	deviations 20 to 25%
Locations first periphery	deviations 0 to 10%

The values calculated at the first periphery, in an undisturbed medium, show very good agreement with measurements.

As for the internal locations in the core box, occupied by generally rather absorbent experimental mock-ups, the calculated fission flux values are higher than the measured results.

## 1.5 CONTROL RODS ANTIREACTIVITY

We must adjust cross sections to obtain a good accuracy for reaction rates in the hafnium absorber. So the calculation results for the effectiveness of control rods will be in good accordance with measurements.

## 1.6 GAMMA HEATING

Gamma heating is measured in the irradiation locations of the network and at the first periphery, and were not subjected to calculation.

## CONCLUSION

The comparison of measurement results, obtained in Isis on the first caramel core, with the results of prior neutron calculations, shows the following:

- . excellent agreement of values relating to reactivity,
- . overestimate of neutron fluxes in the internal irradiation experiments in the core box, but good agreement for undisturbed fluxes at the first outer periphery of the core box.

## REFERENCES

- <1> Code de transport Apollo  
A. Kavenoky, M. Livolant, ...  
CEA/SERMA - T.1193
- <2> Code de diffusion Daixy  
R. Bruyère, A. Guillou, P. Quilichini and C. Vasseur  
CEA.R.2759 (1965)

## Appendix H-2

# KYOTO UNIVERSITY CRITICAL ASSEMBLY (KUCA) CRITICAL EXPERIMENTS USING MEU FUEL

### Appendix H-2.1

#### KUCA CRITICAL EXPERIMENTS USING MEDIUM ENRICHED URANIUM FUEL

K. KANDA, S. SHIROYA, M. HAYASHI,  
K. KOBAYASHI, Y. NAKAGOME, T. SHIBATA  
Research Reactor Institute,  
Kyoto University,  
Osaka, Japan

#### Abstract

In accordance with the joint ANL-KURRI program, the critical experiments using MEU fuel in the KUCA, a light-water-moderated and heavy-water-reflected single-core, were started in May, 1981. In advance of the critical experiments, the MEU fuel elements and the boron loaded side-plates were fabricated by CERCA in France.

The first critical state of the core using MEU fuel was achieved at 3:12 p.m., May 12, 1981. After that, several experiments were performed. The paper provides the results of measurements concerning the critical approach, the reactivity effects of side-plates containing boron burnable-poison, the space dependent effects of void reactivities and the temperature reactivity coefficients. These data will be used to examine the computer code systems in various countries and also used for core conversion of the KUHFR from HEU to MEU.

**Keywords:** *critical experiment, fuel fabrication, MEU fuel, critical mass, boron burnable-poison, void effect, temperature coefficient, KUCA, light-water moderator, heavy-water reflector, KUHFR*

### INTRODUCTION

Due to mutual concerns in the USA and Japan about the proliferation potential of highly-enriched uranium (HEU), a joint study program<sup>1)</sup> was initiated between Argonne National Laboratory (ANL) and Kyoto University Research Reactor Institute (KURRI) in 1978. In accordance with the reduced enrichment for research and test reactor (RERTR) program, the alternatives were studied for reducing the enrichment of the fuel to be used in the Kyoto University High Flux Reactor (KUHFR)<sup>2)</sup>. The KUHFR has a distinct feature in its core configuration: it is a coupled-core. Each annular shaped core is light-water-moderated and placed within a heavy water reflector with a certain distance between them. The phase A reports of the joint ANL-KURRI program independently prepared by two laboratories in February 1979<sup>3),4)</sup>, concluded that the use of medium-enrichment uranium (MEU, 45%) in the KUHFR is feasible, pending results of the critical experiments in the Kyoto University Critical Assembly (KUCA)<sup>5)</sup> and of the burnup test in the Oak Ridge Research Reactor (ORR)<sup>6)</sup>.

The fuel material used in this experiment is different from the former fuel in the following ways:

- (1) high density — the H/U ratio is decreased in order to be more undermoderated,
- (2) MEU — the  $U^{238}/U^{235}$  ratio content is increased.

We had no data on fission gas release from high density burnup fuel of MEU.

The main purposes of the critical experiments are as follows:

- (1) To examine our code system, which was used in the calculation of the Safety Review Report for HEU fuel. The core configuration of the KUHFR is so complicated that we have to confirm the feasibility of our computing technique in calculating the nuclear characteristics of high density MEU fuel core.
- (2) To supply standard criticality data using high density MEU fuel to various countries, which is requested by the Technical Committee of the International Atomic Energy Agency, and to examine the computer code systems in these countries.

Further, the fabrication technique itself is also to be checked, because (1) high density MEU fuel has not been fabricated in the world and (2) it is the first experience for us to order the fabrication to a foreign fabricator.

An application for a safety review (Reactor Installation License) of MEU fuel to be used in the KUCA was submitted to the Japanese Government in March 1980, and a license was issued in August 1980. Subsequently, the application for 'Authorization before Construction' was submitted and was approved in September 1980. Fabrication of MEU fuel elements for the KUCA experiments by CERCA in France was started in September 1980, and was completed in March 1981. The critical experiments using MEU fuel started in May 1981 utilizing the single core as a first step. Those on a coupled-core will follow.

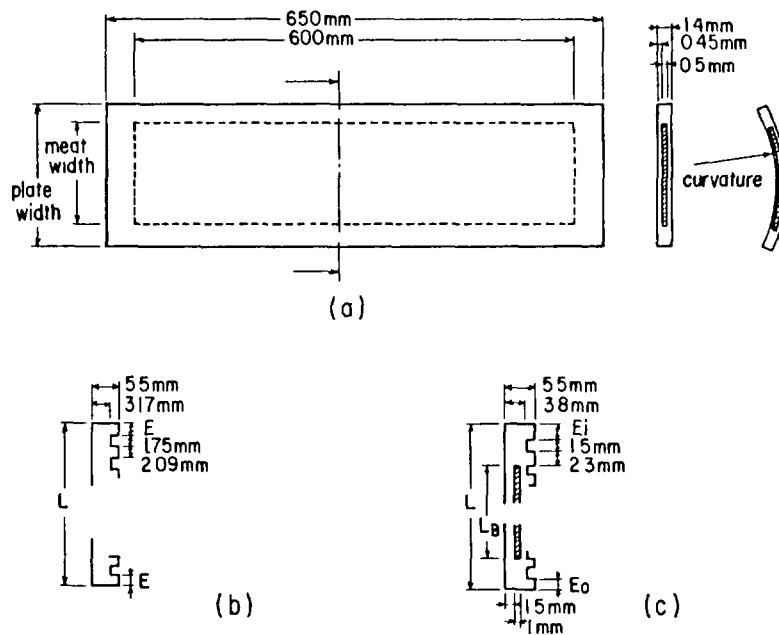
The first critical state of the core using MEU fuel was achieved at 3: 12 p. m., May 12, 1981. After that, several experiments were performed as follows: the reactivity effects of the side-plates containing boron burnable-poison, the void reactivities, the temperature coefficients.

## FABRICATION OF MEU FUEL ELEMENTS

MEU fuel elements for the KUCA critical experiments were fabricated by Compagnie pour l'Etude et la Réalisation de Combustibles Atomiques (CERCA) in France. One fuel element consists of two side-plates and either fifteen or seventeen curved fuel plates. The fuel plate, side-plates, and fuel elements are illustrated in Figs. 1 and 2. The total number of fuel plates fabricated is 294, of 32 different widths. The fuel plates were fabricated by the picture frame technique. The dimension and uranium content of each fuel plate are listed in Table 1.

MEU fuel was supplied from the United States Department of Energy (USDOE) to CERCA for Kyoto University. The nominal enrichment is  $45.0 \pm 0.4$  w/o. The chemical form of the meat (fuel core) is  $UAl_2$ -Al dispersion, and the density is about  $4.0$  g/cm<sup>3</sup>. The uranium density of the fuel core is  $1.69$  g/cm<sup>3</sup> and  $^{235}U$  density is  $0.7575$  g/cm<sup>3</sup>. For reference, these values of the former fuel with the 93% HEU are  $0.6357$  g/cm<sup>3</sup> and  $0.5918$  g/cm<sup>3</sup>, respectively.

The boron loaded side-plates were also fabricated by the picture frame technique. The purity of natural boron contained in the side-plates is more than 98%.



- (a): fuel plate (the width is tabulated in Table 1).
- (b): side-plate containing no burnable-poison,  
inner fuel element:  $L=59.34$  mm,  
outer fuel element:  $L=67.41$  mm.
- (c): side-plate containing boron burnable-poison,  
inner fuel element:  $L=59.40$  mm,  $L_B=47.1$  mm,  
outer fuel element:  $L=67.00$  mm,  $L_B=54.7$  mm.

Fig. 1. Illustration of the fuel plate and side-plates.

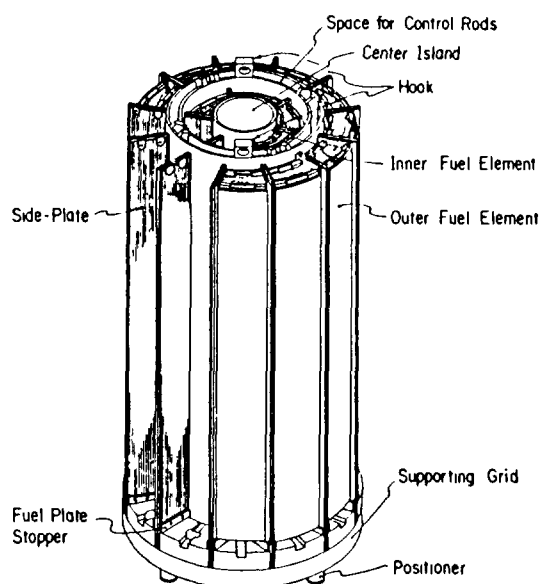


Fig. 2. View of the assembled fuel elements.

Table 1. Specifications of MEU fuel plates.

plate no.	inner fuel plate					outer fuel plate				
	width of fuel (mm)	width of meat (mm)	curvature radius (mm)	Uranium (gr)	U-235 (gr)	width of fuel (mm)	width of meat (mm)	curvature radius (mm)	Uranium (gr)	U-235 (gr)
1	48.70	39.50	54.4	20.00	8.99	61.16	51.96	133.3	25.96	11.67
2	52.68	43.48	58.2	21.64	9.72	63.15	53.95	137.1	26.94	12.11
3	56.66	47.46	62.0	23.67	10.64	65.14	55.94	140.9	28.51	12.81
4	60.64	51.44	65.8	25.67	11.54	67.13	57.93	144.7	28.99	13.00
5	64.62	55.42	69.6	27.57	12.39	69.12	59.92	148.5	30.12	13.54
6	68.60	59.40	73.4	29.57	13.29	71.11	61.91	152.3	31.04	13.91
7	72.58	63.38	77.2	31.87	14.21	73.10	63.90	156.1	31.92	14.36
8	76.56	67.36	81.0	34.26	15.41	75.09	65.89	159.9	32.85	14.76
9	80.54	71.34	84.8	36.18	16.24	77.08	67.88	163.7	33.89	15.23
10	84.51	75.31	88.6	38.27	17.16	79.07	69.87	167.5	35.55	15.99
11	88.49	79.29	92.4	40.34	18.10	81.06	71.86	171.3	36.49	16.41
12	92.47	83.27	96.2	43.09	19.26	83.05	73.85	175.1	37.10	16.61
13	96.45	87.25	100.0	44.49	19.98	85.04	75.84	178.9	38.25	17.10
14	100.43	91.23	103.8	46.74	20.89	87.03	77.83	182.7	39.68	17.76
15	104.41	95.21	107.6	48.30	21.64	89.02	79.82	186.5	40.69	18.27
16	—	—	—	—	—	91.01	81.81	190.3	41.45	18.63
17	—	—	—	—	—	93.00	83.80	194.1	42.69	19.11

enrichment = 44.87 w%, plate length = 650 mm, meat length = 600 mm

### 1. Fabrication Procedures

The fabrication process of the MEU fuel plates is shown in Fig. 3, and the fabrication procedure is as follows;

- (1) fabrication of U-Al alloy by melting uranium metal and aluminum,  
— uranium content of  $UAl_x$ :  $69 \pm 3$  w/o
- (2) crushing and grinding  $UAl_x$  into powder, and sieving,  
—  $UAl_x$  grain size:  $40 \mu\text{m}$  (40 w/o maximum) and  
 $40 - 125 \mu\text{m}$  (the rest)
- (3) weighing and blending the  $UAl_x$  and aluminum powders for each fuel compact,
- (4) compacting the blended powder,  
— uranium concentration in the fuel compacts: 42 w/o maximum
- (5) assembling the fuel compact into the aluminum frame and cover plates,
- (6) cladding by hot and cold rolling, and marking,
- (7) annealing at  $425^\circ\text{C}$  for 1 hour to test for blistering,
- (8) cold rolling to specified thickness,
- (9) cutting the plates to specified sizes,
- (10) chemically etching the plate surface,
- (11) curving the plates,
- (12) final cleaning and inspection,
- (13) packaging for shipment.

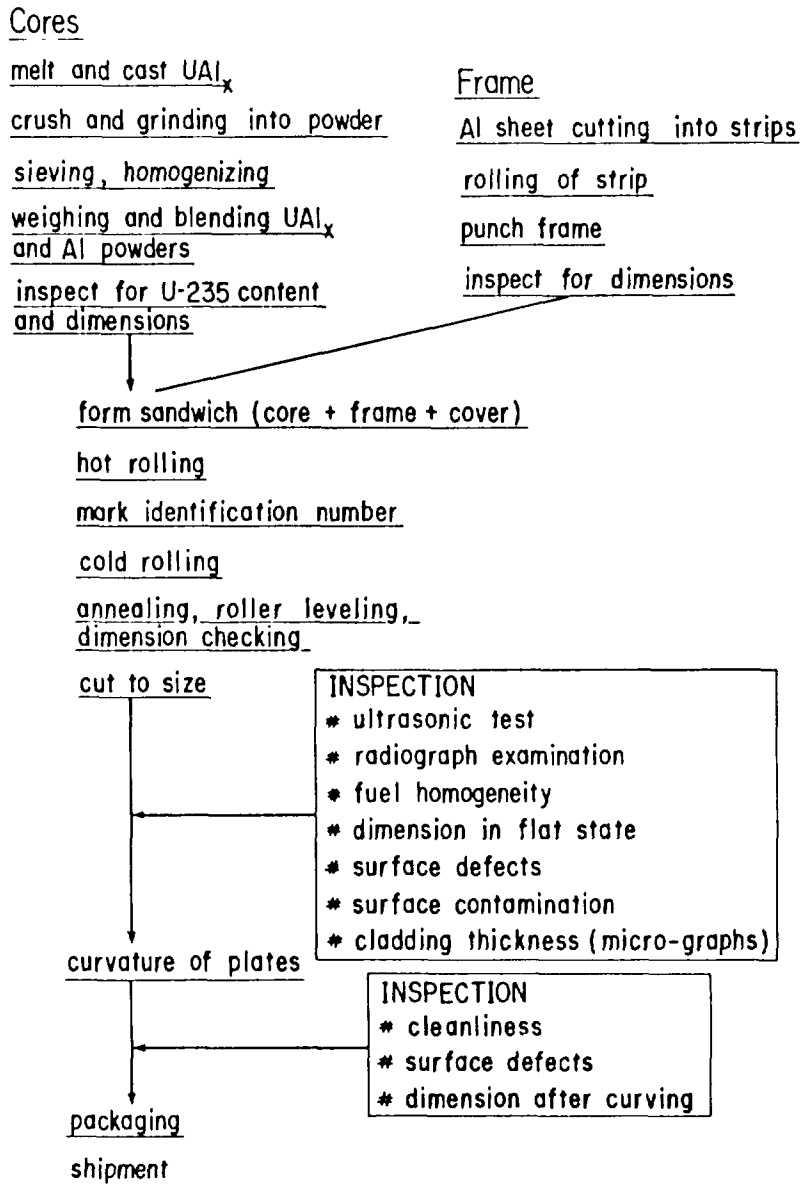


Fig. 3. Fabrication process of the MEU fuel plates.

The fabrication procedure of the boron loaded side-plates is as follows:

- (1) weighing and blending the natural boron and aluminum powders,  
 — weight of natural boron:  $640 \text{ mg} \pm 5 \%$  for outer elements and  
 $570 \text{ mg} \pm 5 \%$  for inner elements  
 boron grain size:  $80 \mu\text{m}$  maximum
- (2) assembling the blended powder and silver markers into the aluminum frame and cover plates,
- (3) cladding by rolling,
- (4) annealing at  $425^\circ\text{C}$  for 1 hour,
- (5) roller leveling to specified thickness,
- (6) cutting the plates and machining with grooves and engraving to specified sizes,
- (7) chemically etching the plate surface,
- (8) packaging for shipment.

## 2. *Inspection*

The actual inspection of the fabrication of MEU fuel elements was performed by Compagnie Générale des Matières Nucleaires (COGEMA) in France, which was chosen by Kyoto University to be the acting inspector. The inspectors of Kyoto University visited CERCA three times — at the beginning of fabrication, mid and final stages —, then Kyoto University authorized the inspection results reported by COGEMA. The Science and Technology Agency of the Japanese Government further inspected the MEU fuel elements in Japan.

The following items were considered in the inspection of the fuel plates: uranium enrichment from the supplier's report, uranium and aluminum purities by chemical analysis,  $^{235}\text{U}$  content in each fuel plate by the gamma-ray counting examination, fuel homogeneity by the X-ray absorption technique, cladding bond integrity by ultrasonic testing, cladding and dog bone thickness by destructive testing, dimension, surface defects, and surface contamination by the alpha counting method. Because of high density fuel, we especially examined the bonding between the aluminum cladding and the aluminate fuel meat.

The inspection items for the side-plates were as follows, boron and aluminum purities by chemical analysis, boron content in each side-plate by weighing natural boron, boron core location by radiograph examination, cladding bond integrity by ultrasonic testing, cladding and core thickness by destructive testing, dimension, surface condition, and surface contamination by the alpha counting method. The inspections for the side-plate were rather easy because the boron content was not so high.

The inspection report and records such as X-ray absorption diagrams, radiographs, ultrasonic test diagrams and micro-photographs taken in the destructive testing, were delivered to KURRI.

## 3. *Transport of MEU Fuel Elements*

MEU fuel elements were transported from CERCA in France to KURRI in Japan as a Type A Fissile Class II Package. Four FS-13 containers were used. These packages were certified to satisfy the IAEA requirements of the package design by Ministre des Transports (French Government), Department of Transportation (Government of the United States) and Science and Technology Agency (Japanese Government).

The transport between France and Japan was performed by a cargo plane via Alaska.

# EXPERIMENTAL

## 1. *Core Configuration*

Figure 4 shows the view of the heavy water tank made from aluminum for the single-core experiments. The fuel elements are assembled in a cylindrical form as shown in Fig. 2 and installed in the heavy water tank. The annular shaped core is light-water-moderated and placed within a heavy water reflector<sup>7)</sup>. The core has a cylindrical center island of light water. The fuel region is divided into two parts by the space for control rods, which are called the inner and outer fuel regions, respectively. The inner region consists of 6 fuel elements, while the outer region consists of 12 elements. Each fuel plate which has some curvature, can be inserted one by one between aluminum side-plates. The plane cross-section of the assembly looks like a Japanese fan or a kind of cake called Baumkuchen.

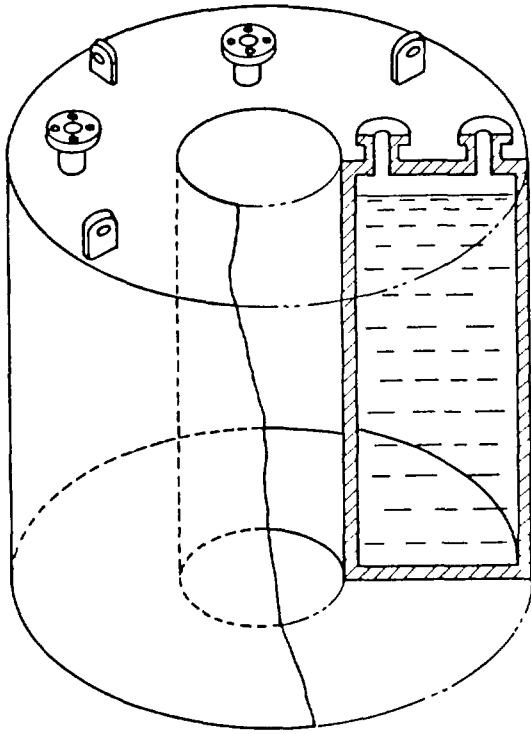


Fig. 4. View of the heavy water tank for a single-core.

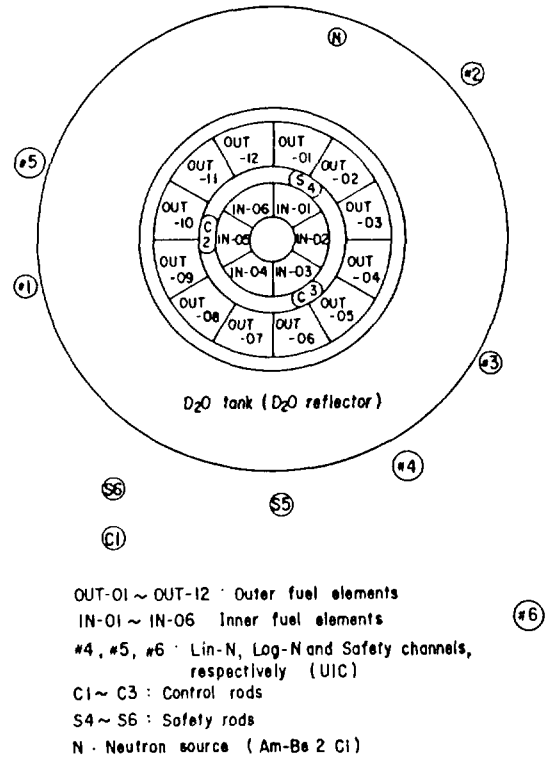


Fig. 5. Configuration of the C38R(BK D<sub>2</sub>O)MEU core.

The core configuration employed in this work was called C38R(BK D<sub>2</sub>O)MEU and is illustrated in Fig. 5. The outer fuel elements were numbered as OUT-01, OUT-02 and so on, while the inner as IN-01, IN-02 and so on. The maximum numbers of fuel plates which can be loaded in the outer and inner fuel elements are 17 and 15 per element, respectively. The core was mainly controlled by two rods, namely C2 and C3 rods, because all safety rods were withdrawn to the upper limit at each operation and C1 rod was apart from the core. The detectors were arranged around the heavy water tank. The neutron source was located under the heavy water tank.

## 2. Critical Approach

As a first step for the critical approach of the core, every one of the outer fuel elements was fully loaded with 17 fuel plates (204 fuel plates, 3135.24 g-<sup>235</sup>U). Then, the critical approach was performed by inserting fuel plates into the inner fuel elements from outside to inside in regular order. At that time, all side-plates contained no burnable poison and the pitch between fuel plates was 3.84 mm. The inverse multiplication method was adopted for the critical approach. The detectors used in this experiment were three fission chambers for the start-up channels, namely #1, #2 and #3. The first critical state was achieved at the 8th step of fuel loadings.

## 3. Reactivity Effects of Boron Burnable-Poison

After achieving the first critical state, the reactivity effects of the outer and inner side-plates containing boron burnable-poison were measured. The reason for using side plates with burnable-poison is attempt to obtain longer fuel life in the KUHFR. For the outer side-plates, the measurements were performed as follows: substituting fuel elements with burnable-poison for fuel elements without poison one by one from OUT-12

towards OUT-01 in order, the excess reactivity or subcriticality of the core was measured before and after each substitution. The excess reactivity was measured by the positive period method, and the subcriticality by the source multiplication method. The reactivity effect of the boron burnable-poison was obtained from the difference between two reactivities measured before and after the substitution.

For the inner side-plates, after achieving the critical state with full loading of outer side-plates which contained burnable-poison, the substitutions were made from IN-06 towards IN-01 by the same way as for the outer side-plates. After two steps of these substitutions, there remained no more space to insert any fuel plate for adjusting the criticality of the core. Then, another set of measurements was performed changing the loading pattern of fuel elements. All the inner fuel elements which contained burnable-poison and was filled to the capacity with 15 fuel plates, were loaded in the core, and the criticality was adjusted by the number of fuel plates inserted outside of the outer fuel elements. At that time, any outer element contained no burnable-poison. Then, substituting inner fuel elements with poison for those without poison one by one from IN-06 towards IN-01 in order, reactivity was measured for each case before and after the substitution.

The pitch between fuel plates in the side-plate containing burnable-poison was 3.80 mm. From the results of the above measurements, the mass reactivity coefficients of fuel plates were incidentally obtained.

#### 4. *Reactivity Effects of Voids*

The reactivity effects of void at four locations in the core were measured. The locations were (1) the middle of the cylindrical center island of light water, (2) the space for control rods, (3) the light water gap between the heavy water tank and the outer fuel region and (4) the middle of the heavy water reflector. In advance of the measurements, 294 fuel plates were fully loaded in the core. The criticality was adjusted by the number of side-plates containing burnable-poison. All of the inner and one half of the outer fuel elements contained poison. Aluminum void pipes of several diameters were employed to simulate the void. The excess reactivity was measured before and after pouring light- or heavy- water into the void pipe by the positive period method. The difference between two reactivities before and after the injection corresponded the effects of the voids.

#### 5. *Temperature Coefficients*

The temperature reactivity coefficients were measured for two core configurations. One had an acrylic void pipe at the center island of light water and the other had no such a void. The outer diameter of the acrylic void pipe was 100 mm and the inner diameter was 92 mm. The core configuration without void was the same as that arranged for the measurements of the void effects. While, in the core with the acrylic void pipe, all the fuel elements except only one outer element contained burnable-poison. The temperature of light and heavy water were raised simultaneously by the electric heater installed in both region and was adjusted to be the same in both region. The temperatures of several locations in the core were monitored by the thermocouples set there. The excess reactivities of the core at seven temperature points from 20°C to 70°C were measured by the positive period method and the temperature reactivity coefficients of the core were obtained from them.

## RESULTS AND DISCUSSION

### 1. Critical Mass

The inverse multiplication curves measured by the start-up channels are shown in Fig. 6. The first critical state of the C38R(BK D<sub>2</sub>O)MEU core was achieved with 262 fuel plates. The masses of <sup>235</sup>U and U were 4165.74 g and 9284 g, respectively. The excess reactivity measured by the positive period was 0.211 %Δk/k. Using the measured mass reactivity coefficient for the fuel plate (0.0198 %Δk/k/g-<sup>235</sup>U), the least critical mass of the core was estimated as 4155 g-<sup>235</sup>U or 9260 g-U.

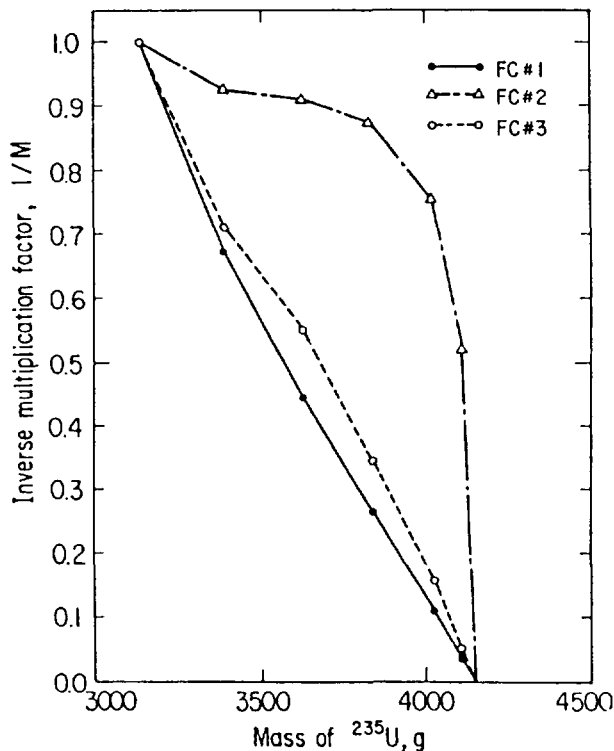


Fig. 6. Inverse multiplication curves measured by the start-up channels.

On the other hand, the critical state of the C38R(BK D<sub>2</sub>O)HEU core for which HEU (93 %) fuel was used, was formerly achieved with 276 fuel plates. The masses of <sup>235</sup>U and U were 3524.46 g and 3784 g, respectively. The excess reactivity was 0.468 %Δk/k. The increase of <sup>235</sup>U mass in MEU core was caused by the absorption of <sup>238</sup>U, whose density is increased more than twice.

A preliminary calculation for the MEU core using a two-dimensional diffusion code KR302DPT<sup>8)</sup> with 3 group constants gave the result that critical mass was 4347 g-<sup>235</sup>U (266 fuel plates). A more precise calculation is now being performed by means of a two-dimensional finite-element diffusion code 2D-FEM-KUR or a three-dimensional code 3D-FEDM-KUR<sup>7),9)</sup>.

## 2. Reactivity Effects of Side-Plates Containing Burnable-Poison

The reactivity effect caused by the substitution of burnable-poison for each fuel element without poison is shown in Figs 7-(a) and -(b). The measured reactivity of each element with burnable-poison was not constant. It is due to the reactivity interference effects with the side-plates containing burnable-poison already inserted in previous steps. The reactivity effects were approximately  $-0.4\% \Delta k/k$  per outer fuel element and  $-0.6\% \Delta k/k$  per inner element.

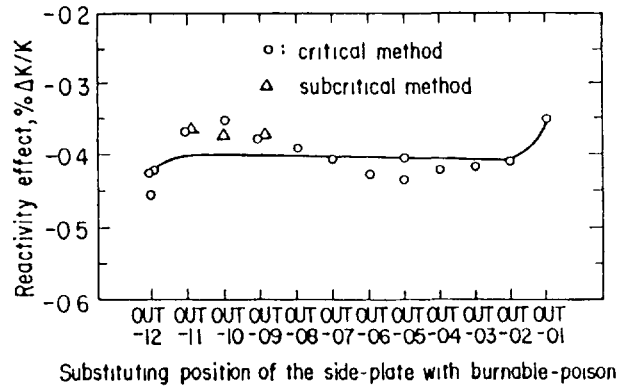


Fig. 7-(a). Reactivity effects caused by the substitution of burnable-poison for each outer fuel element without poison. (solid line shows a simple expectation on the qualitative tendency of the interference effect)

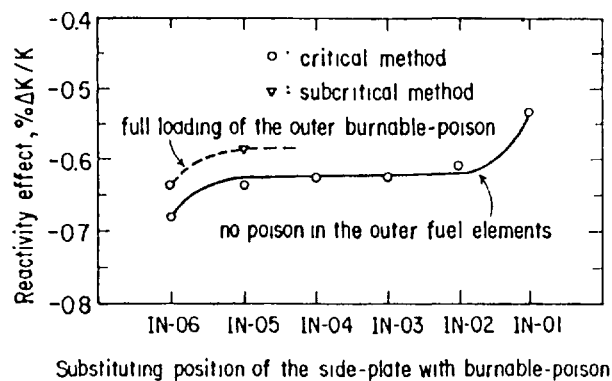


Fig. 7-(b). Reactivity effects caused by the substitution of burnable-poison for each inner fuel element without poison. (solid line shows a simple expectation on the qualitative tendency of the interference effect)

The integral effects for fuel elements containing poison are shown in Fig. 8. The total reactivity of the outer side-plates containing boron burnable-poison was measured as approximately  $-4.7\% \Delta k/k$ , while that of the inner was  $-3.7\% \Delta k/k$ . Taking account of the interference effects between the inner and outer side-plates with poison, the integral effects of burnable-poison would be about  $8\% \Delta k/k$ .

The critical state was achieved with 286 fuel plates, when all outer burnable-poison side-plates were loaded. The mass of  $^{235}\text{U}$  was 4438.62 g and the excess reactivity was  $0.133\% \Delta k/k$ . On the other hand, the critical state was achieved with 277 fuel plates under full loading of inner burnable-poison. The mass of  $^{235}\text{U}$  was 4189.53 g and the excess reactivity was  $0.057\% \Delta k/k$ .

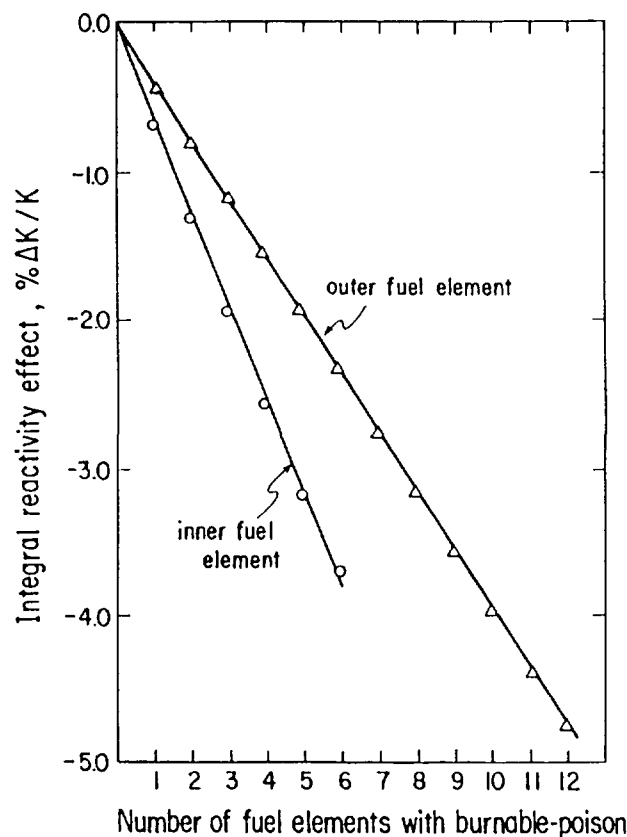


Fig. 8. Integral reactivity effects of the inner and outer fuel elements containing boron burnable-poison. (integrated values of Figs. 7-(a) and (b))

From these experiments, the mass reactivity coefficient of individual fuel plate was obtained for the inside part of the inner fuel region and for the outside of the outer region: (1) For the inner fuel plates, the values were in the range from 0.014 to 0.021  $\% \Delta k/k/g^{-235}\text{U}$ . The tendency was observed that the value was larger for fuel plates nearer to the center island of the core. This phenomenon corresponds to the fact that the neutron importance is higher at the inner part of the core. (2) For the outer fuel plates, the mass reactivity coefficients were approximately 0.0085  $\% \Delta k/k/g^{-235}\text{U}$ . That was roughly one half of the value for the inner fuel plate.

These measured values are very useful to examine the calculation method. It will be reflected to the final design of the KUHFRR fuel elements.

### 3. Reactivity Effects of Aluminum Void Pipes

The reactivity effects of voids measured at four locations using aluminum pipes are tabulated in Table 2. In the control rod space and at the middle of the heavy water reflector, the reactivity effects of voids were negative. While they were positive at the other locations. The void coefficient was estimated as approximately  $1 \times 10^{-5} \Delta k/k/\text{cm}^3$  at the middle of the center island of light water,  $-5 \times 10^{-6} \Delta k/k/\text{cm}^3$  at the space for control rods,  $2 \times 10^{-6} \Delta k/k/\text{cm}^3$  at the light water gap region between the outer fuel region and the heavy water tank and  $-2 \times 10^{-7} \Delta k/k/\text{cm}^3$  at the middle of the heavy water reflector, respectively. These values can be understood from the H/U ratio, that is, whether the moderation in these regions is undermoderated or wellmoderated.

Table 2. Reactivity Effects of Aluminum Void Pipes.

locations in the core	outer diameter (cm)	inner diameter (cm)	void reactivity (% $\Delta k/k$ )
middle of the center island of light water	1.0	0.7	0.0249
	2.5	1.9	0.171
	2.5	2.1	0.212
	2.5	2.2	0.231
	2.5	2.3	0.245
4.0	3.38	0.538	
space for control rods	1.0	0.7	-0.0109
light water gap between the outer fuel region and the heavy water tank	1.0	0.7	0.0042
	2.5	2.3	0.0632
middle of the heavy water reflector	3.5	2.9	-0.0096
	6.5	5.5	-0.0303
	9.0	8.4	-0.0781

4. Temperature Reactivity Coefficients

In Fig. 9, the temperature reactivity coefficients are shown. For the core without void, the temperature coefficient was positive below 70°C. On the other hand, it changed their sign from positive to negative at approximately 33°C for the core with acrylic void pipe at the center island of light water. Two curves of the temperature coefficients were almost parallel to each other and both curves tended to be linear beyond 35°C. The difference between two was approximately  $9 \times 10^{-5} \Delta k/k/^\circ\text{C}$ .

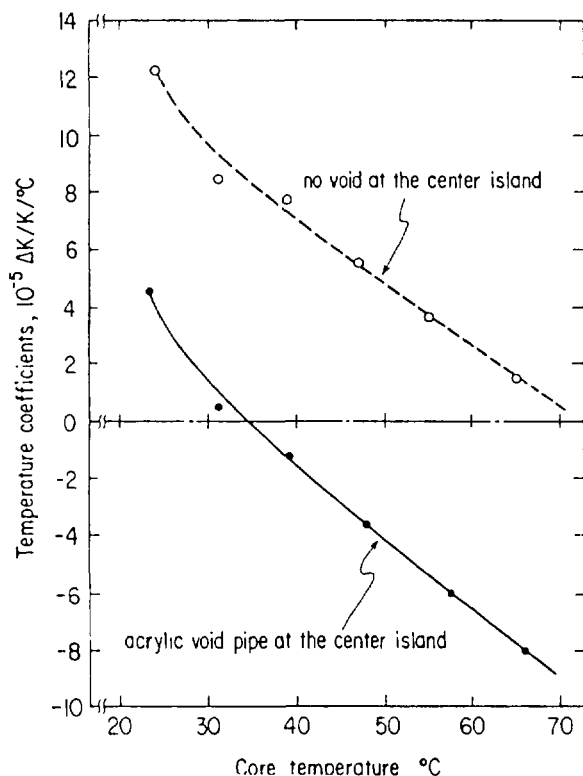


Fig. 9. Temperature reactivity coefficients for the cores with and without an acrylic void pipe at the center.

In general, at very high temperature the negative temperature coefficient due to Doppler effect of  $^{238}\text{U}$  absorption must be dominant, but it was not observed in the present temperature region.

### ACKNOWLEDGEMENTS

The authors wish to thank Mr. Toshimitsu Sagane and other members of the KUCA for their generous help and cooperation in the experiments. They are very grateful to Dr. Manuel M. Bretscher of ANL, Prof. Yuichi Ogawa's group of Hokkaido Univ., Prof. Shvozo Nakadoi and Prof. Shigeyasu Sakamoto's group of Tokai Univ., Prof. Otohiko Aizawa's group of Musashi Inst. of Technol., Prof. Kojiro Nishina's group of Nagoya Univ., Prof. Hiroshi Nishihara's group of Kyoto Univ., Prof. Kenji Sumita's group of Osaka Univ. and Prof. Kazuhiko Kudo's group of Kyushu Univ. for their cooperation in the experiments. They wish to thank the members of the Technical Committee of the KUCA chaired by Prof. Hiroshi Nishihara of Kyoto Univ., for their advice and support in this work.

### REFERENCES

- 1) "Research Reactor Using Medium-Enriched Uranium", (ed. K. Kanda and Y. Nakagome), KURRI-TR-192 (1979).
- 2) Shibata, T., "Construction of a High Flux Research Reactor and Conversion of Kyoto University Reactor KUR to a TRIGA Type Pulsed Reactor", Research Reactor Renewal and Upgrading Program, IAEA-214 (1978) 183.
- 3) Shibata, T. and K. Kanda, "ANL-KURRI Joint Study on the Use of Reduced Enrichment Fuel in KUHFR — Phase A Report —", (February 15, 1979).
- 4) Travelli, A., D. Stahl and T. Shibata, "The U. S. RERTR Program, Its Fuel Development Activities, and Application in the KUHFR", ANS Trans., 36 (1981) 92.
- 5) Kanda, K., K. Kobayashi, M. Hayashi and T. Shibata, "Reactor Physics Experiment Using Kyoto University Critical Assembly", J. At. Energy Soc. Japan, 21 (1979) 557, in Japanese.
- 6) Shibata, T. and A. Travelli, "ANL-KURRI Joint Study on the Use of Reduced Enrichment Fuel in KUHFR — Status Report on Phase B —", (December 12, 1980).
- 7) Hayashi, M. and S. Shiroya, "Few-Group for the HEU and MEU Cores in the KUCA", Annu. Rep. Res. Reactor Inst. Kyoto Univ., 14 (1981).
- 8) Tsuruta, H. and K. Kobayashi, "The Preparation of Input Data for KR302DPT -- A two-dimensional diffusion and perturbation code --", JAERI-memo 4775 (1972)
- 9) Naito, Y., S. Tsuruta and M. Hayashi, "A New Mixed Method with Finite Difference and Finite Element Method for Neutron Diffusion Calculation", J. Nucl. Sci. and Technol., 18 (8) (1981) 571.

## Appendix H-2.2

### ANALYSIS OF THE KUCA MEU EXPERIMENTS USING THE ANL CODE SYSTEM

S. SHIROYA, M. HAYASHI,  
K. KANDA, T. SHIBATA  
Research Reactor Institute,  
Kyoto University,  
Osaka, Japan

W.L. WOODRUFF, J.E. MATOS  
RERTR Program,  
Argonne National Laboratory,  
Argonne, Illinois,  
United States of America

#### Abstract

Critical experiments using MEU fuel in the KUCA, a light-water-moderated and heavy-water-reflected single-core, were started in May 1981. This paper provides some results on the analysis of the KUCA critical experiments using the ANL code system. The critical mass for HEU and MEU single-cores and the boron burnable-poison effects for MEU cores were analysed. Five-group constants were generated using the EPRI-CELL code and two dimensional diffusion calculations were performed using the DIF3D code. For the analysis on the critical mass, a two-dimensional finite-element diffusion code (2D-FEM-KUR) was also applied and the results compared with the DIF3D (2D) code.

#### Introduction

The joint ANL-KURRI program<sup>1</sup> was initiated in 1978 for reducing the enrichment of the fuel to be used in the KUHF<sup>2</sup>. The KUHF has a distinct feature in its core configuration, namely a coupled-core. The core consists of two annular shaped modules that are light-water moderated and placed within a heavy-water reflector with a specified distance between them. The phase A reports of the joint ANL-KURRI program, independently prepared by the two laboratories in February 1979,<sup>3,4</sup> concluded that MEU fuel is feasible for the KUHF.

In accordance with an ANL-KURRI joint study concerning the RERTR program, the critical experiments using MEU fuel in the KUCA<sup>5</sup> were started in May 1982. Thereafter, the KUCA experiments have been providing valuable data with regard to the RERTR Program.<sup>6,7,8</sup>

This paper provides some preliminary results on the analysis of the KUCA critical experiments using the ANL code system. Since this system was employed in the earlier neutronics calculations for the KUHF, it is important to assess its capabilities for the KUHF. The KUHF has a unique core configuration which is difficult to model precisely with current diffusion theory codes. The KUCA core employed in this series of critical experiments was similar to that of the KUHF, although it was not a coupled core (single core). Even for this simpler KUCA core, it is still difficult to model the geometry precisely with a finite-difference diffusion code.

This paper also provides some results from a finite-element diffusion code (2D-FEM-KUR),<sup>9,10</sup> which was developed in a cooperative research program between KURRI and JAERI. This code provides the capability for mockup of a complex core configuration as the KUHFRR. Using the same group constants generated by the EPRI-CELL code,<sup>11</sup> the results of the 2D-FEM-KUR code are compared with the finite difference diffusion code (DIF3D(2D))<sup>12</sup> which is mainly employed in this analysis.

### Description of the ANL Code System

Microscopic broad-group cross-section data at ANL is generated using the EPRI-CELL code. This code combines a heterogeneous P<sub>1</sub> GAM<sup>13</sup> type treatment for the epithermal spectra and resonances and a heterogeneous integral-transport treatment (THERMOS)<sup>14</sup> for the thermal range. The epithermal treatment includes (1) an interpolation over tabulated groupwise-resonance integrals as a function of temperature and potential scattering for the resonance self-shielding, (2) resonance overlap corrections, (3) an optional buckling search, and (4) many other refinements. The code also provides a cell depletion calculation based on the CINDER code for each of the THERMOS space points in a depletable zone. Cell-averaged cross-section data at preselected times in the depletion history can be obtained in either a 2, 3, 4 or 5 group structure. A flow diagram for the EPRI-CELL code is shown in Fig. 1.

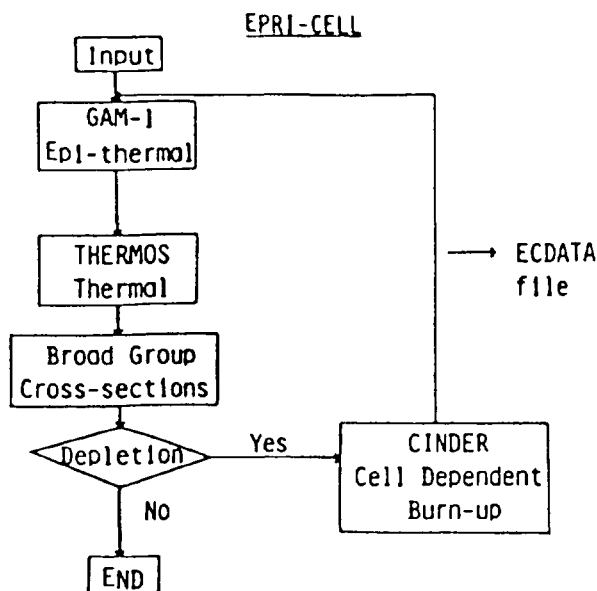


Figure 1. Flow Chart for the EPRI-CELL Code

The EPRI-CELL libraries at ANL are based mostly on ENDF/B-IV data. The 68 group epithermal, GAM, library is generated using MC<sup>2</sup>-2<sup>15</sup> and the integral transport RABANL option for the resonance self-shielding parameters. The 35-group thermal, THERMOS, library is generated using the AMPX<sup>16</sup> or NJOY codes with an S<sub>α,β</sub> treatment for hydrogen and deuterium.

The neutronics calculations are performed using the DIF3D code. This code has the capability for 1-D through 3-D diffusion theory calculations for several geometries based on the finite-difference method.

### Description of KUCA Fuel Assemblies

In this study, experimental results of critical mass for HEU and MEU cores and the boron burnable-poison effects were analyzed.

The specifications of HEU and MEU fuel plates are tabulated in Tables 1 and 2. An illustration of the fuel plates and side-plates is shown in Fig. 2. The HEU fuel plates were fabricated in Japan by Nuclear Fuel Industries, and the MEU fuel plates were fabricated in France by CERCA. Each fuel plate can be inserted one by one between aluminum side-plates. For MEU fuels, special side-plates containing boron burnable-poison were also fabricated (see Fig. 2).

Figure 3 shows the heavy water tank which is employed in the single core KUCA experiments. Figure 4 shows a view of the assembled fuel elements. This assembly is then installed in the center of the heavy-water tank and filled with light water. A typical core configuration is shown in Fig. 5.

TABLE 1. SPECIFICATIONS OF HEU (NFI)

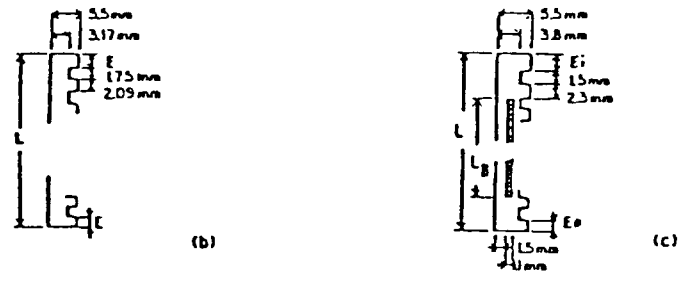
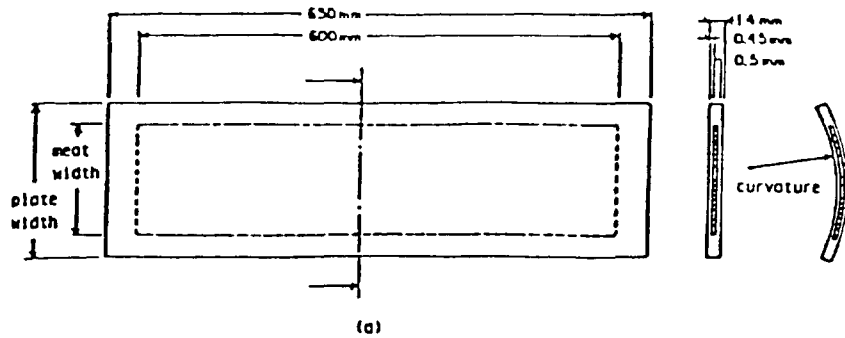
plate no.	inner fuel plate					outer fuel plate				
	width of fuel (mm)	width of meat (mm)	curvature radius (mm)	Uranium (gr)	U-235 (gr)	width of fuel (mm)	width of meat (mm)	curvature radius (mm)	Uranium (gr)	U-235 (gr)
1	51.71	42.95	56.17	8.10	7.54	62.60	53.84	133.83	10.22	9.52
2	55.74	46.98	60.01	8.83	8.22	64.61	55.85	137.67	10.54	9.82
3	59.76	51.00	63.85	9.70	9.03	66.62	57.86	141.51	10.97	10.22
4	63.78	55.02	67.69	10.49	9.77	68.63	59.87	145.35	11.33	10.55
5	67.80	59.04	71.53	11.22	10.45	70.64	61.88	149.19	11.83	11.02
6	71.82	63.06	75.37	12.06	11.23	72.65	63.89	153.03	12.13	11.30
7	75.84	67.08	79.21	12.84	11.96	74.66	65.90	156.87	12.57	11.71
8	79.86	71.10	83.05	13.60	12.67	76.67	67.91	160.71	12.98	12.09
9	83.88	75.12	86.89	14.37	13.38	78.69	69.93	164.55	13.54	12.61
10	87.91	79.15	90.73	15.07	14.04	80.70	71.94	168.39	14.03	13.07
11	91.93	83.17	94.57	15.68	14.60	82.71	73.95	172.23	14.17	13.20
12	95.95	87.19	98.41	16.46	15.33	84.72	75.96	176.07	14.73	13.72
13	99.97	91.21	102.25	17.41	16.22	86.73	77.97	179.91	14.90	13.88
14	103.99	95.23	106.09	18.32	17.06	88.74	79.98	183.75	15.28	14.23
15	108.01	99.25	109.93	18.96	17.66	90.75	81.99	187.59	15.54	14.47
16	—	—	—	—	—	92.76	84.00	191.43	15.91	14.82
17	—	—	—	—	—	94.77	86.01	195.27	16.42	15.29

enrichment 93.14 w%      plate length = 650 mm  
fuel plate pitch = 3.84 mm      meat length = 600 mm

TABLE 2. SPECIFICATIONS OF MEU (CERCA)

plate no.	inner fuel plate					outer fuel plate				
	width of fuel (mm)	width of meat (mm)	curvature radius (mm)	Uranium (gr)	U-235 (gr)	width of fuel (mm)	width of meat (mm)	curvature radius (mm)	Uranium (gr)	U-235 (gr)
1	48.70	39.50	54.4	20.00	8.99	61.16	51.96	133.3	25.96	11.67
2	52.68	43.48	58.2	21.64	9.72	63.15	53.95	137.1	26.94	12.11
3	56.66	47.46	62.0	23.67	10.64	65.14	55.94	140.9	28.51	12.81
4	60.64	51.44	65.8	25.67	11.54	67.13	57.93	144.7	28.99	13.00
5	64.62	55.42	69.6	27.57	12.39	69.12	59.92	148.5	30.12	13.54
6	68.60	59.40	73.4	29.57	13.29	71.11	61.91	152.3	31.04	13.91
7	72.58	63.38	77.2	31.87	14.21	73.10	63.90	156.1	31.92	14.36
8	76.56	67.36	81.0	34.26	15.41	75.09	65.89	159.9	32.85	14.76
9	80.54	71.34	84.8	36.18	16.24	77.08	67.88	163.7	33.89	15.23
10	84.51	75.31	88.6	38.27	17.16	79.07	69.87	167.5	35.55	15.99
11	88.49	79.29	92.4	40.34	18.10	81.06	71.86	171.3	36.49	16.41
12	92.47	83.27	96.2	43.09	19.26	83.05	73.85	175.1	37.10	16.61
13	96.45	87.25	100.0	44.49	19.98	85.04	75.84	178.9	38.25	17.10
14	100.43	91.23	103.8	46.74	20.89	87.03	77.83	182.7	39.68	17.76
15	104.41	95.21	107.6	48.30	21.64	89.02	79.82	186.5	40.69	18.27
16	—	—	—	—	—	91.01	81.81	190.3	41.45	18.63
17	—	—	—	—	—	93.00	83.80	194.1	42.69	19.11

enrichment 44.87 w%      plate length = 650 mm  
fuel plate pitch = 3.8 mm      meat length = 600 mm



- (a) : fuel plate
- (b) : side-plate containing no burnable-poison
  - inner fuel element :  $L = 59.34 \text{ mm}$
  - outer fuel element :  $L = 67.41 \text{ mm}$
- (c) : side-plate containing burnable-poison
  - inner fuel element :  $L = 59.40 \text{ mm}$ ,  $L = 47.1 \text{ mm}$
  - outer fuel element :  $L = 67.00 \text{ mm}$ ,  $L = 54.7 \text{ mm}$

Fig. 2. Illustration of the fuel plate and side-plates.

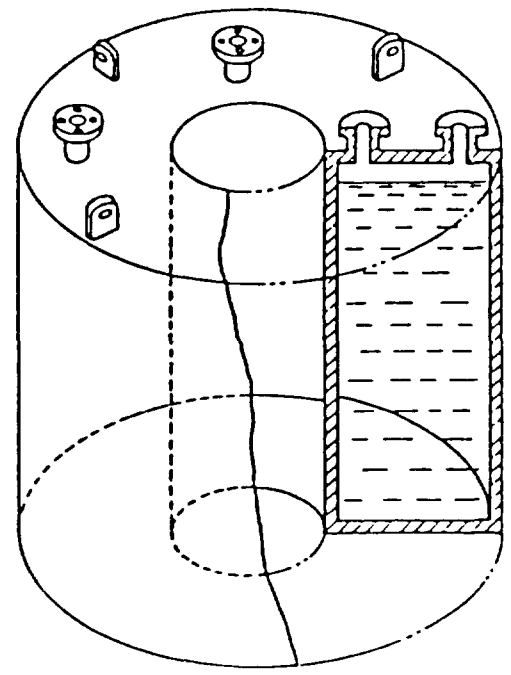


Fig. 3. View of the heavy water tank for a single-core.

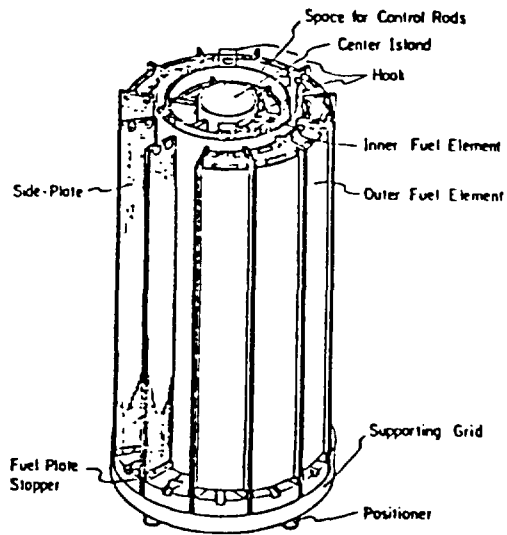
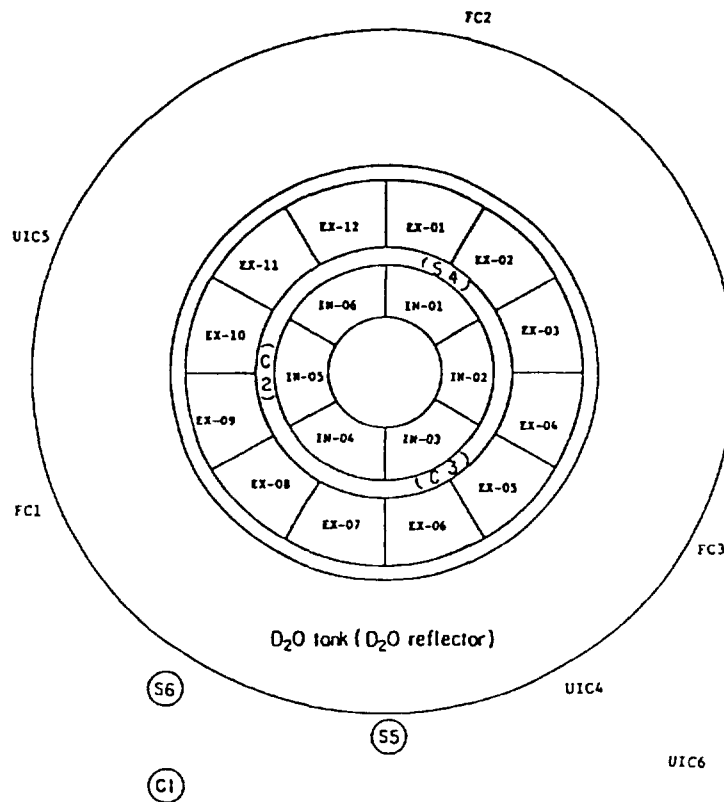


Fig. 4. View of the assembled fuel elements.



IN-01 - IN-06 : Inner fuel elements (containing no burnable-poison)  
 EX-01 - EX-12 : Outer fuel elements (containing no burnable-poison)  
 C1 - C3 : Control rods  
 S4 - S6 : Safety rods  
 FC1 - FC3 : Fission chambers  
 UIC4 - UIC6 : Uncompensated ionization chambers

EX-01 - EX-12 contain 17 fuel plates.  
 IN-01, -02, -05, -06 contain 10 fuel plates.  
 IN-03 - IN-04 contains 9 fuel plates.  
 Total 262 plates

Fig. 5. C38R(BK D<sub>2</sub>O)MEU core configuration using the side-plates with 3.8 mm pitch.

## The Generation of Group Constants

The single core employed in the KUCA critical experiments was divided into 10 regions for the MEU core and into 11 regions for the HEU core. For the MEU core, these regions are (1) the inner and (2) the outer fuel regions, (3) the inner and (4) the outer side-plate regions, (5) the light-water region in the center of core, (6) the control rod region, (7) the outer vessel region between the outer fuel elements and the heavy-water reflector including the inner wall of the annular shaped aluminum tank for containing the heavy-water, (8) the heavy-water reflector region, (9) the outer wall region of the aluminum heavy-water tank, and (10) the light-water reflector region outside of the heavy-water tank. For the HEU core, the inner vessel (11) which separates the fuel from the center island containing light water was also modeled.

In generating group constants, the EPRI-CELL code with slab geometry was used for each region. The upper energy boundaries of the five-group structure used at ANL are as follows: 10 MeV, 0.821 MeV, 5.53 KeV, 1.855 eV, and 0.625 eV.

For the inner (1) and outer (2) fuel regions, the materials between two side plates were modeled as a unit cell for full fuel loading (see Fig. 6). The fuel meat, aluminum clad, and light-water moderator were modeled as shown. The residual region between the edge of the fuel meat and the side-plate was taken into account as an extra-region. RABANL corrections were applied for resonance self-shielding.

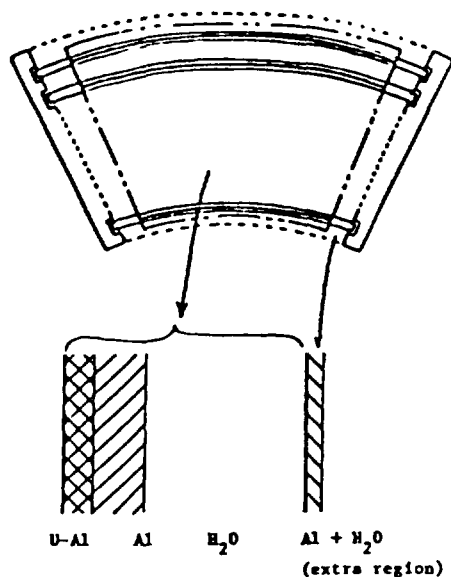


Fig. 6. Model of the unit cell used in the generation of group constants.

For the inner (3) and outer (4) side-plate regions in Fig. 7, the treatment of the side-plate with and without boron burnable-poison was different. In each case, the small portion of the light water in the grooves of the side-plate was ignored, but the light water in the gap between two side-plates was taken into account. For the side-plate without burnable-poison, a simple fission spectrum was assumed. With burnable-poison, the spectrum for collapsing cross sections was generated using a homogenized core source. For the side-plate with burnable-poison, all regions were represented explicitly. The end sections of the side-plate containing no poison were included as an extra-region.

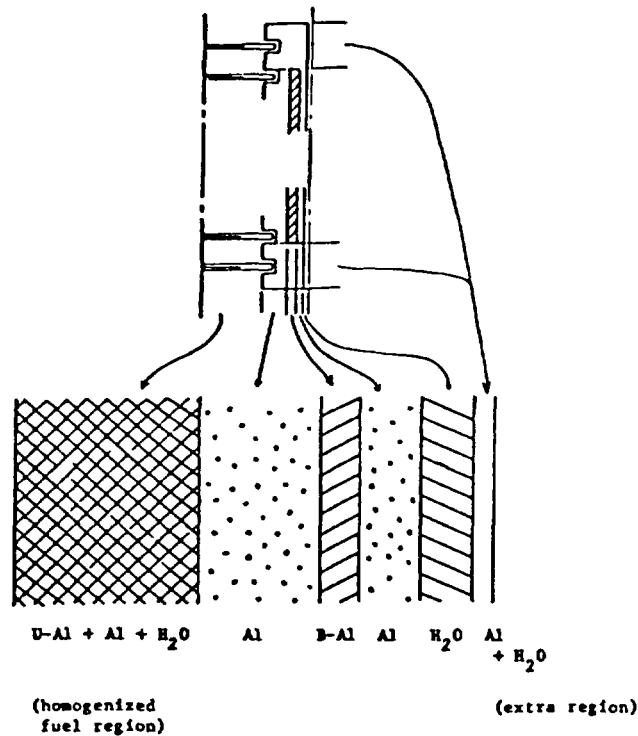


Fig. 7. Model for the side-plate with burnable-poison.

For the regions (5) through (11), a  $^{235}\text{U}$  fission spectrum was employed. In the control rod region (6), aluminum sheaths for control rod insertion, and aluminum spacers, and all other aluminum support structures were homogenized. The inner (11) and the outer (7) vessel regions consist of aluminum and light-water. In these regions, heterogenities were taken into account. For the outer tank wall region (9), the group constants prepared for aluminum in outer vessel region (7) were utilized. For the center light-water (5) region and the light-water reflector (10) regions, group constants were prepared using a  $^{235}\text{U}$  fission spectrum in the same thickness of light water.

### Neutronics Calculations

Using the DIF3D code, two dimensional diffusion calculations were performed. In the Phase B calculations<sup>17</sup> for the KUFR, extrapolation lengths were derived using fitted data from R-Z computations. These varied by region from ~10 cm in the center to >15 cm in the heavy-water reflector. On the other hand, the experimental results gives the extrapolation lengths as  $8.1 \pm 0.1$  cm in the center light-water region,  $7.8 \text{ cm} \pm 0.1$  cm in the outer fuel region and  $9.8 \pm 0.3$  cm in the heavy-water reflector, respectively. In this paper, the experimental values of the extrapolation lengths were adopted.

The core configuration was modeled in X-Y geometry (Fig. 8). In the inner part of the core, a mesh of approximatey  $0.25 \times 0.25$  cm was employed. In the heavy-water reflector and in the heavy-water tank regions, a  $1 \times 1$  cm mesh was used. In the light-water reflector region, a  $2 \times 2$  cm mesh was used.

For some cores, the 2D-FEM-KUR code was applied to compare results with the DIF3D(2D) code. Figure 9 shows the core configuration simulated by the 2D-FEM-KUR code.

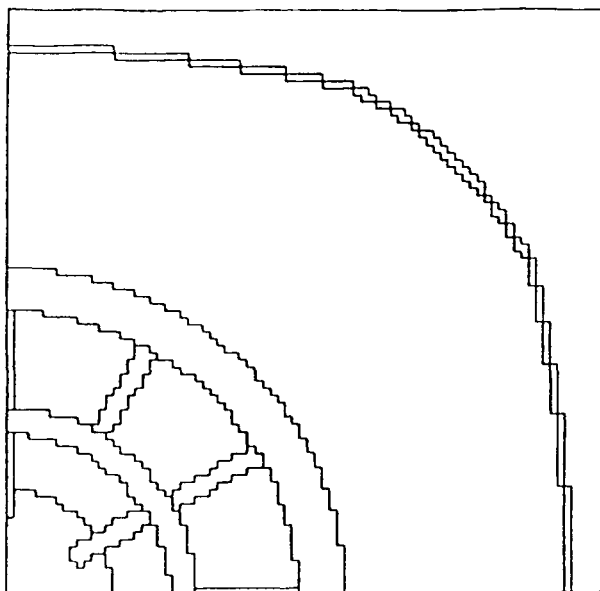


Fig. 8. Example of the core configuration (MEU) used in the DIF3D(2D) code.

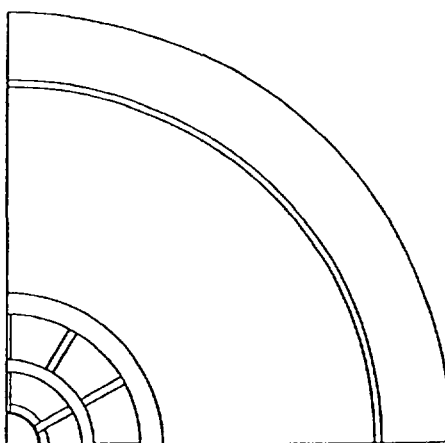


Fig. 9. Example of the core configuration (HEU) used in the 2D-FEM-KUR code.

### Results and Discussions

Preliminary results of calculations for the cores employed in the critical mass measurements are tabulated in Table 3. Results for the cores used in the burnable-poison effects measurements are tabulated in Table 4.

Tables 3 and 4 show that ratios between the results of calculations and experiments are less than 1.6%. Calculated eigenvalues are always higher than the experimental values. One reason for this tendency is due to the method employed in the fuel regions for generating group constants in this paper. The extra-region in Fig. 6 tends to increase the H/U ratio in the fuel meat region. This causes a shift from an under-moderated fuel region to a more well-moderated region and leads to the over-estimation of the eigenvalue. Calculations using group constants prepared without the extra region are currently in progress.

TABLE 3. CRITICAL CORES WITHOUT BURNABLE POISON

Fuel	Pitch (mm)	Number of Plates	$K_{exp}$	$K_{cal}$		C/E	
				DIF3D(2D)	2D-FEM-KUR	DIF3D(2D)	2D-FEM-KUR
HEU (44.87%)	3.80	262	1.0008	1.0112	1.0111	1.0104	1.0103
HEU (44.87%)	3.84	262	1.0021	1.0112	1.0122	1.0091	1.0101
HEU (93.14%)	3.84	267	1.0047	1.0198	1.0204	1.0150	1.0157

TABLE 4. CORES WITH BURNABLE POISON

	Pitch (mm)	Number of Plates	Eigenvalue			Reactivity Effect of BP		
			$K_{exp}$	$K_{cal}$	C/E	$\rho_{exp}$ ( $\Delta k/k$ )	$\rho_{cal}$ ( $\Delta k/k$ )	C/E
Outer SP with BP	3.80	288	1.0047	1.0188	1.0141	-4.7	-4.408	0.94
Inner SP without BP	3.84							
Outer SP without BP	3.84	277	1.0006	1.0130	1.0124	-3.6	-3.485	0.97
Inner SP with BP	3.80							
All SP with BP	3.80	294	<0.986	0.9939	>1.008	(-8)*	-7.666	(0.96)
All SP without BP	3.84	294	-	1.0759	-	-	-	-

SP: side-plate, BP: burnable-poison.

\*Estimated from experiment.

Although the core configuration was not simulated exactly in the diffusion calculations, and simple treatments were used in generating some of the group constants, the agreement between the calculations and the experiments is sufficient for design calculations of the KUFR. Even for burnable-poison effects, which are difficult to calculate accurately by means of the diffusion theory, the differences shown in Table 4 are less than 7%.

The agreement between the results obtained using the DIF3D(2D) code and the 2D-FEM-KUR code was quite good. Both the 2D-FEM-KUR code with its explicit geometrical representation and the DIF3D(2D) code with a jagged X-Y approximation for the core can be used with confidence for neutronic design calculations of the KUFR.

#### ACKNOWLEDGEMENTS

This study was performed as a part of the joint ANL-KURRI program. The authors wish to thank Mr. T. Naito of JAERI and Mr. S. Tsuruta of Japan Information Service who developed the 2D-FEM-KUR code. They are also grateful to Prof. K. Nishina of Nagoya University, Dr. K. Tsuchihashi and Dr. S. Matsuura of JAERI for valuable discussions.

## REFERENCES

1. K. Kanda and Y. Nakagome ed., "Research Reactor Using Medium-Enriched Uranium," KURRI-TR-192 (1972).
2. T. Shibata, "Construction of High Flux Research Reactor and Conversion of Kyoto University Reactor KUR to TRIGA Type Pulsed Reactor," IAEA-214, p. 183 (1978).
3. T. Shibata and K. Kanda, "ANL-KURRI Joint Study on the Use of Reduced Enrichment Fuel in KUHFR -- Phase A Report --," February 15, 1979.
4. A. Travelli, D. Stahl, and T. Shibata, "The US RERTR Program, Its Fuel Development Activities, and Application in the KUHFR," ANS Trans., <sup>36</sup>, p. 92 (1981).
5. K. Kanda, K. Kobayashi, M. Hayashi, and T. Shibata, "Reactor Physics Experiment Using Kyoto University Critical Assembly," J. At. Energy Soc. Japan, <sup>21</sup>, p. 557 (1979), in Japanese.
6. K. Kanda, S. Shiroya, M. Hayashi, Y. Nakagome, and T. Shibata, "KUCA Critical Experiments Using MEU Fuel," IAEA-SR-77/30 (1981).
7. K. Kanda, S. Shiroya, M. Hayashi, K. Kobayashi, Y. Nakagome, and T. Shibata, "KUCA Critical Experiments Using Medium Enriched Uranium Fuel," Annu. Rep. Res. Reactor Inst. Kyoto Univ., <sup>15</sup> (1982).
8. S. Shiroya, H. Fukui, Y. Senda, M. Hayashi, and K. Kobayashi, "Measurements of Neutron Flux Distributions in a Medium Enriched Uranium Core," Annu. Rep. Res. Reactor Inst. Kyoto Univ., <sup>15</sup> (1982).
9. M. Hayashi and S. Shiroya, "Few-Group Constants for the HEU and MEU Cores in the KUCA," Annu. Rep. Res. Reactor Inst. Kyoto Univ., <sup>14</sup>, p. 153 (1981).
10. Y. Naito, S. Tsuruta, and M. Hayashi, "A New Mixed Method with Finite Difference and Finite Element Method for Neutron Diffusion Calculation," J. Nucl. Sci. and Technol., <sup>18</sup>, p. 571 (1981).
11. B. A. Zolotar, et al., "EPRI-CELL Code Description," Advanced Recycle Methodology Program System Documentation, Part II, Chapter 5 (Oct. 1975).
12. D. R. Ferguson and K. L. Derstine, "Optimized Iteration Strategies and Data Management Considerations for Fast-Reactor Finite-Difference Diffusion Theory Codes," Nuc. Sci. Eng., <sup>64</sup>, pp. 593-604 (1977).
13. G. D. Joanu and J. S. Dudek, "GAM-1: A Consistent P<sub>1</sub> Multigroup Code for The Calculation of Fast Neutron Spectra and Multigroup Constants," GA-1850 (1961).
14. H. C. Honeck, "THERMOS, A Thermalization Transport Theory Code for Reactor Lattice Calculations," BNL 5826 (1961).
15. H. Henryson II, B. J. Toppel and C. G. Stenberg, "MC<sup>2</sup>-2: A Code to Calculate Fast Neutron Spectra and multigroup Cross Sections," ANL-8144 (1976).
16. N. M. Greene, et al., "AMPX: A Modular Code System For Generating Coupled Multigroup Neutron-Gamma Libraries from ENDF/B," ORNL/TM-3706 (1976).
17. T. Shibata and A. Travelli, "ANL-KURRI Joint Study on the Use of Reduced Enrichment Fuel in KUHFR -- Status Report on Phase B--," December 12, 1980.

## Appendix H-2.3

### ANALYSIS OF KUCA MEU CORES BY THE JAERI SRAC CODE SYSTEM

T. MORI, K. TSUCHIHASHI  
Japan Atomic Energy Research Institute,  
Tokai-mura, Naka-gun, Ibaraki-ken,  
Japan

#### Abstract

As part of the Japanese RERTR Program, a series of calculations using the JAERI SRAC code system were performed for the KUCA critical experiments with MEU fuel. Parameters studied include critical masses, the mass coefficient, boron plate reactivities, and the reactivities due to void pipes inserted in the central water island.

#### 1 Introduction

As a part of Japanese RERTR program, a series of calculations have been done for the KUCA critical experiments using MEU fuel by the code system SRAC (Ref. 1-5 ) which has been developed since 1978 as the nuclear design and analysis part of the JAERI standard thermal reactor code system.

This report describes a preliminary analysis of the data measured in the fiscal year of 1981 by the current data library of the SRAC.

#### 2 Calculational Method

##### Cross Sections

The optional data library is taken to use that based on ENDF/B-4 files except the scattering law for H<sub>2</sub>O and D<sub>2</sub>O which are stored only in ENDF/B-3.

The transport cross sections for P<sub>0</sub> transport calculations are calculated by the B<sub>1</sub> approximation which correspond to the diffusion coefficients as  $D = 1/(3 \Sigma_{tr})$ .

Resonance absorption of heavy nuclides is calculated by the table look-up method for  $E > 130.07$  eV, and the ultra-fine (about 4500 pts.) group collision probability method for  $130.07$  eV  $> E > 0.993$  eV (thermal cut off).

The energy group structure for this analysis is as shown in Table 1 composed of 22 fast groups and 31 thermal groups. This structure is chosen to have sufficient number of energy groups in the core calculations to consider the spatial variation of neutron spectrum which is foreseen by the heterogeneous disposition of H<sub>2</sub>O islands in the KUCA cores.

**Table 1 Energy Group Structure in Fast and Thermal Neutron Range**

Fine	Few	Energy Range (eV)		Lethargy Range	
1	1	0.10000E+08	0.60653E+07	0.0	0.5000
2		0.60653E+07	0.36788E+07	0.5000	1.0000
3		0.36788E+07	0.22313E+07	1.0000	1.5000
4		0.22313E+07	0.13534E+07	1.5000	2.0000
5		0.13534E+07	0.82085E+06	2.0000	2.5000
6	2	0.82085E+06	0.49787E+06	2.5000	3.0000
7		0.49787E+06	0.30197E+06	3.0000	3.5000
8		0.30197E+06	0.11109E+06	3.5000	4.5000
9		0.11109E+06	0.40868E+05	4.5000	5.5000
10		0.40868E+05	0.15034E+05	5.5000	6.5000
11	3	0.15034E+05	0.55308E+04	6.5000	7.5000
12		0.55308E+04	0.20347E+04	7.5000	8.5000
13		0.20347E+04	0.74852E+03	8.5000	9.5000
14		0.74852E+03	0.27536E+03	9.5000	10.5000
15		0.27536E+03	0.13007E+03	10.5000	11.2500
16		0.13007E+03	0.61442E+02	11.2500	12.0000
17	4	0.61442E+02	0.29023E+02	12.0000	12.7500
18		0.29023E+02	0.13710E+02	12.7500	13.5000
19		0.13710E+02	0.64760E+01	13.5000	14.2500
20		0.64760E+01	0.30590E+01	14.2500	15.0000
21		0.30590E+01	0.16374E+01	15.0000	15.6250
22		0.16374E+01	0.99312E+00	15.6250	16.1250
Fine	Few	Energy Range (eV)		Velocity Range (cm/sec)	
1	1	0.99312E+00	0.60236E+00	0.13784E+07	0.10735E+07
2		0.60236E+00	0.41399E+00	0.10735E+07	0.88996E+06
3		0.41399E+00	0.36528E+00	0.88996E+06	0.83597E+06
4		0.36528E+00	0.31961E+00	0.83597E+06	0.78196E+06
5		0.31961E+00	0.29792E+00	0.78196E+06	0.75496E+06
6		0.29792E+00	0.27699E+00	0.75496E+06	0.72796E+06
7	2	0.27699E+00	0.23742E+00	0.72796E+06	0.67396E+06
8		0.23742E+00	0.20090E+00	0.67396E+06	0.61996E+06
9		0.20090E+00	0.18378E+00	0.61996E+06	0.59296E+06
10		0.18378E+00	0.16743E+00	0.59296E+06	0.56597E+06
11		0.16743E+00	0.15183E+00	0.56597E+06	0.53896E+06
12		0.15183E+00	0.13700E+00	0.53896E+06	0.51196E+06
13	3	0.13700E+00	0.12293E+00	0.51196E+06	0.48496E+06
14		0.12293E+00	0.10963E+00	0.48496E+06	0.45797E+06
15		0.10963E+00	0.97080E-01	0.45797E+06	0.43096E+06
16		0.97080E-01	0.85397E-01	0.43096E+06	0.40420E+06
17		0.85397E-01	0.74276E-01	0.40420E+06	0.37696E+06
18		0.74276E-01	0.64017E-01	0.37696E+06	0.34996E+06
19	4	0.64017E-01	0.54520E-01	0.34996E+06	0.32296E+06
20		0.54520E-01	0.45785E-01	0.32296E+06	0.29596E+06
21		0.45785E-01	0.37813E-01	0.29596E+06	0.26897E+06
22		0.37813E-01	0.30602E-01	0.26897E+06	0.24196E+06
23		0.30602E-01	0.24154E-01	0.24196E+06	0.21497E+06
24		0.24154E-01	0.18467E-01	0.21497E+06	0.18796E+06
25	5	0.18467E-01	0.13543E-01	0.18796E+06	0.16097E+06
26		0.13543E-01	0.93805E-02	0.16097E+06	0.13396E+06
27		0.93805E-02	0.59804E-02	0.13396E+06	0.10696E+06
28		0.59804E-02	0.33423E-02	0.10696E+06	0.79965E+05
29		0.33423E-02	0.14663E-02	0.79965E+05	0.52965E+05
30		0.14663E-02	0.35238E-03	0.52965E+05	0.25965E+05
31		0.35238E-03	0.10010E-04	0.25965E+05	0.43761E+04

## Process

### Step 1 Primary cell calculation for single fuel plate cell

A one dimensional plane cell composed of a fuel plate, cladding, and coolant water is supposed as shown in Fig.1. In this step three linear equations are successively solved for (1) fast 15 groups (10 MeV - 130.07 eV), (2) resonance 4500 groups, (3) thermal 31 groups.

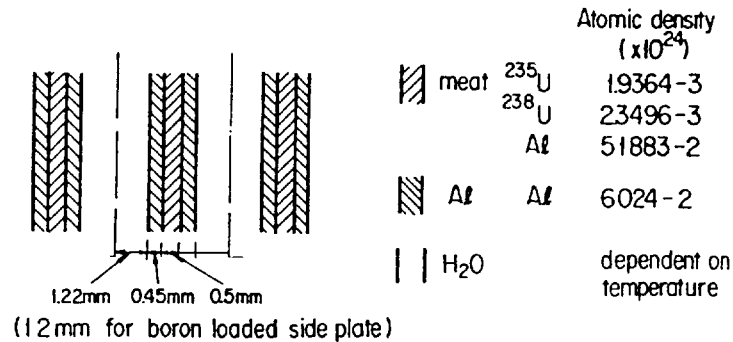


FIG. 1. Primary cell model.

### Step 2 Secondary cell calculation

To consider the neutron distribution in the azimuthal direction, a one dimensional plane cell of side plate, side water, and homogenized fuel region is supposed as shown in Fig. 2a. A similar cell is also supposed for the case where boron plate is inserted in the side plates as shown in Fig.2b. Because spreading side plate spacing is assumed as parallel, the plate to plate spacing is taken to keep the same volume of fuel region. Thus the spacing changes by fuel loading.

To compare the boron plate reactivity worth, both of collision probability method and one dimensional SN routine were used.

### Step 3 Core calculation

Using the 53 group cross sections obtained by the above process, one dimensional diffusion equation is solved in the R-geometry shown in Fig.3. The extrapolation distance in the axial direction is decided to meet the critical mass of unpoisoned core.

To estimate the axial leakage through the central void pipe, a series of two dimensional SN calculations in R-Z geometry are executed with 9 group energy cross sections which are condensed from the results of one dimensional diffusion calculation.

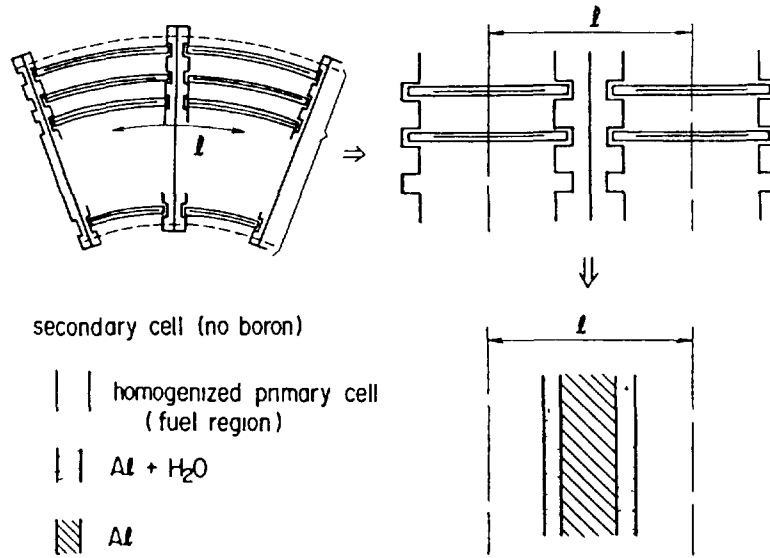


FIG. 2a. Secondary cell model (no boron).

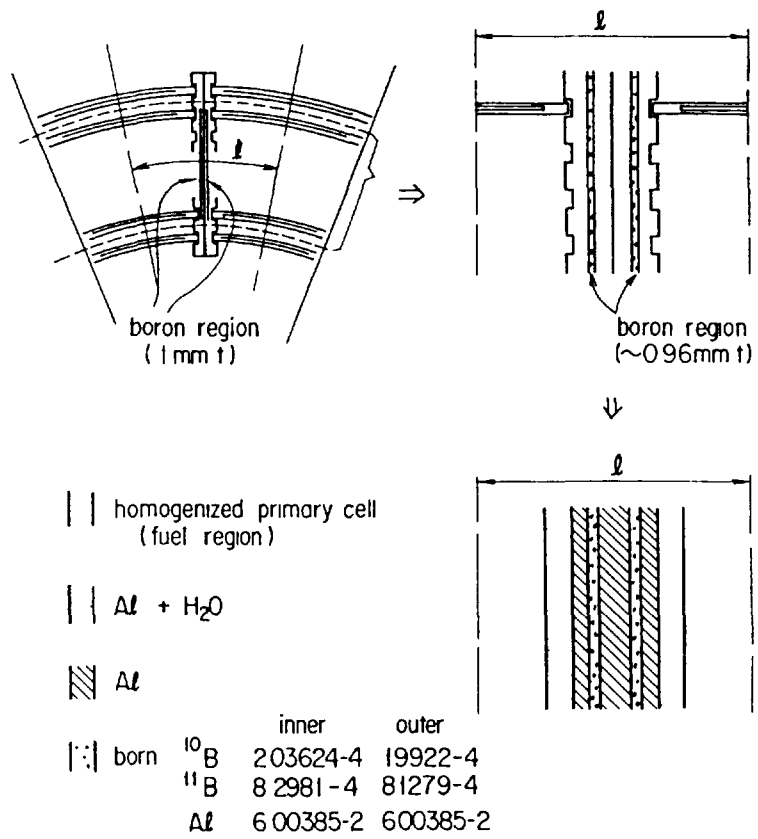


FIG. 2b. Secondary cell model (with boron).

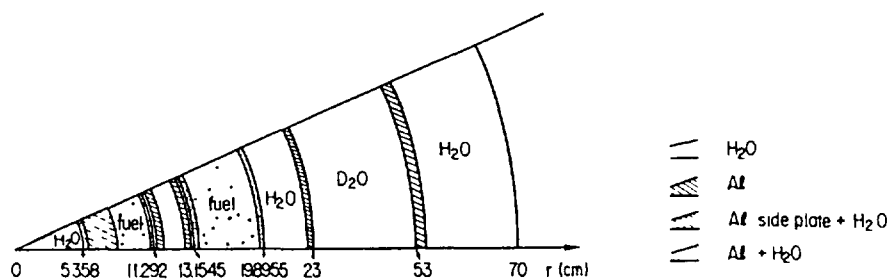


FIG. 3. Core model for 1-D diffusion.

### 3 Comparison of calculated results with measured ones

In Table 2, the calculated  $K_{eff}$  values to estimate the critical mass and boron worth are listed. The values on the first column of  $K_{eff}$  are the results of 1-D diffusion calculation where the secondary cell are treated by the collision probability method, those on the second column are  $K_{eff}$  values with 1-D SN routine in the treatment of the secondary cell. Those on the third column are to show the effect of axial buckling.

In Table 3, the mass coefficients are compared with experimental values. The results show that it is difficult to predict the coefficients which shows sharp position dependence due to the heterogeneous disposition of water islands by the diffusion approximation.

In Table 4, the reactivity worth of boron plates are compared. The underestimate of boron worth by the collision probability method are not improved by 1-D SN calculation. Any two dimensional analysis might be suitable to take account of H<sub>2</sub>O regions which are located at inner and outer radial direction of the secondary cell.

Table 2 Calculated effective multiplication factors

Case:	Outer	: Inner	: Temp	:	K <sub>eff</sub>		:
No.:	Nbr.	: Nbr.	:	:	PIJ*	ANISN**:	PIJ
:	Fuel B	: Fuel B	:	:	H=74.0cm	:	H=70.0cm:
1	: 17	: 9	: 300	:	0.99339	:	0.98210
2	: 17	: 10	: 300	:	1.00731	:	0.99594
3	: 17	: 15	: 300	:	1.06692	:	1.05501
4	: 17 B	: 15	: 300	:	1.02667	1.02782	:
5	: 17	: 15 B	: 300	:	1.03463	1.03543	:
6	: 17 B	: 15 B	: 300	:	0.99246	:	:
7	: 15	: 15 B	: 300	:	0.99978	:	:
8	: 16	: 15 B	: 300	:	1.01570	:	:
9	: 17 B	: 13	: 300	:	1.00327	:	:
10	: 17 B	: 14	: 300	:	1.01738	:	:

Note PIJ\* : The secondary cell solved by collision prob method  
 ANISN\*\* : The secondary cell solved by ANISN

Table 3 Mass coefficients

Case	Core (fuel plates)	Exp $\Delta k/k/g$ U-235	Calculated $\Delta k/k/g$ U-235
1 2	no B (inner)	0.0198%	0.0168%
5 7 8	inner B (outer)	0.0085%	0.0070-0.0078%
4 9 10	outer B (inner)	0.014% - 0.021%	0.0159-0.0227%

Table 4 Reactivity Worth of Boron Plate

Case	Core	Exp $\Delta k/k$	Exp Keff	Calculated $\Delta k/k$	Calculated Keff
1 2	no boron		1.002114		1.002671
7 8	outer boron	4.7%	1.001332	3.8%	1.009066
9 10	inner boron	3.7%	1.000570	3.0%	1.012678

The reactivity effects of the aluminum void pipes inserted in the core center as to remove H<sub>2</sub>O are shown in Table 5. Some competing effects i.e., the positive effect due to decreasing neutron absorption by H<sub>2</sub>O, the negative effect of decreasing of slowing power and increasing axial leakage result in the positive reactivity worth. Calculated values shows that both of 2-D SN calculations and 1-D diffusion calculations overestimate this effect.

Table 5 Reactivity effect by the central void tube

Case	Outer dia. (cm)	Inner dia. (cm)	Exp % $\Delta k/k$	Calculated *			
				Exp % $\Delta k/k$	TWOTRAN ** Keff	1-D Diffusion *** % $\Delta k/k$	1-D Diffusion *** Keff
6	0.				0.99111		0.99246
A	1.0	0.7	0.0249	*****	*****	*****	*****
B	2.5	1.9	0.171	0.271	0.99378	0.249	0.99492
C	2.5	2.1	0.212	0.282	0.99389	0.262	0.99504
D	2.5	2.2	0.231	0.288	0.99395	0.268	0.99510
E	2.5	2.3	0.245	0.294	0.99401	0.275	0.99517
F	4.0	3.38	0.538	0.665	0.99769	0.704	0.99944

Note \* Full insertion of boron plates is assumed

\*\* No upper, lower reflector considered

\*\*\* The void tube is homogenized with surrounding water in the central region ( $r < 5.358$  cm)

The measured temperature reactivity coefficients of the cores, with or without acrylic void pipe at the center island are integrated numerically assuming linear dependence on temperature of experimental values as plotted in Fig. 4. The experimental  $k_{eff}$  values are normalized to meet the calculational values at 300 °K. The calculated values at 350 °K seem to show fairly good agreement with the experimental ones. The calculations along the intermediate temperatures failed due to the improper interpolation formula for the thermal scattering law  $S(\alpha, \beta)$ .

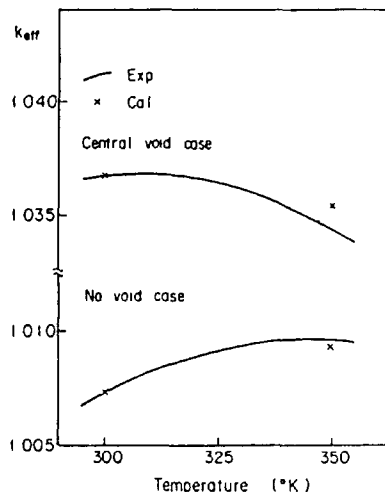


FIG. 4. Temperature effect on  $k_{eff}$ .

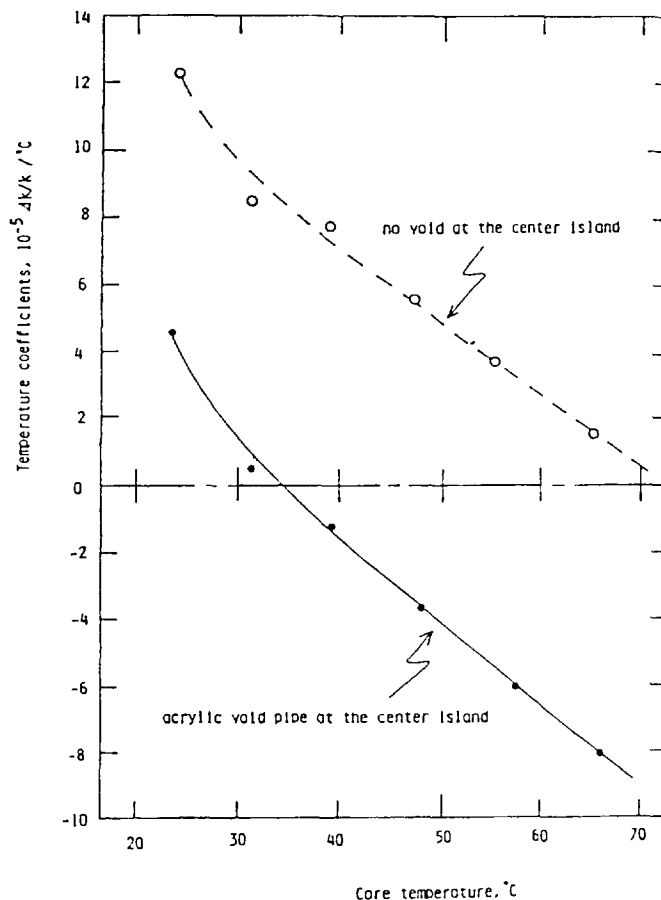


FIG. 5. Temperature reactivity coefficients.

#### 4 Discussion

We have not yet got the satisfactory results. The heterogenous core configuration such as the local existense of water islands seems to make difficult the analysis. Some approach using P1 coefficients of cross sections might be necessary.

Until publishing the final report, the 2-D analysis of the secondary cell for boron plate worth, the 2-D core analysis to predict the extrapolation distance, and the improvement of the interpolation formula of the thermal scattering law for the analysis of temperature coefficients will be done.

#### References

- 1 'Reactor Engineering Division Annual Report', Division of Reactor Engineering, JAERI-M 9032 (1980)
- 2 'Reactor Engineering Division Annual Report', Division of Reactor Engineering, JAERI-M 9672 (1981)
- 3 'Reactor Engineering Division Annual Report', Division of Reactor Engineering, JAERI-M 82-114 (1982)
- 4 'Benchmark Calculations by the Thermal Reactor Standard Nuclear Design Code System SRAC', K.Tsuchihashi, F Akino, Y.Nagaoka, and Y Ishiguro, JAERI-M 9781 (1981) (in Japanese)
- 5 'SRAC : JAERI Thermal Reactor Standard Code System for Reactor Design and Analysis', K Tsuchihashi, H Takano, K Horikami, Y Ishiguro, K Kaneko, and T Hara, JAERI- (to be published)

## Appendix H-2.4

### MEASUREMENTS OF NEUTRON FLUX DISTRIBUTIONS IN A MEDIUM ENRICHED URANIUM CORE

S. SHIROYA, H. FUKUI\*, Y. SENDA\*,  
M. HAYASHI, K. KOBAYASHI  
Research Reactor Institute,  
Kyoto University,  
Osaka, Japan

#### Abstract

Neutron flux distributions were measured using the foil activation technique as part of single-core experiments in the C-core of the KUCA with MEU fuel in order to validate a computer code system developed in cooperation with JAERI. The single cylindrical core was light-water-moderated and heavy-water-reflected. Relative flux distributions were obtained with and without a void in the light-water moderator at the center of the reactor. The values of reflector savings were obtained for a few positions in the core without the void. Comparisons of measured and calculated data are presented.

**Keywords:** *neutron flux distribution, reflector saving, critical experiments, activation technique, MEU fuel, light water moderator, heavy water reflector, KUCA, RERTR program*

#### INTRODUCTION

In accordance with the reduced enrichment for research and test reactor (RERTR) program, a joint study program was initiated between Argonne National Laboratory (ANL) and Kyoto University Research Reactor Institute (KURRI) in 1978<sup>1)</sup>. In the joint ANL-KURRI program, alternatives were studied for reducing the enrichment of the fuel to be used in the proposed Kyoto University High Flux Reactor (KUHFR)<sup>2)</sup>. The KUHFR has a distinct feature in its core configuration. It is a coupled-core. Two annular shaped cores are light-water-moderated and placed within a heavy-water reflector with a certain distance between them. To simulate such a complicated configuration for analytical purposes, a code system was developed in cooperation with Japan Atomic Energy Research Institute (JAERI)<sup>3)</sup>.

For test studies on the use of a code system, it is important to measure not only the multiplication factor but also neutron flux distributions. The measurement of neutron flux distributions provides detailed information which is useful for testing a code system. It is especially important to obtain the value of reflector savings at various positions in the reactor for use in two-dimensional calculations, since it is difficult to predict them precisely by calculations.

---

\* Engineering, Kyoto University, Yoshida-honmachi, Sakyo-ku, Kyoto 606, Japan.

As a part of the single-core critical experiments program using medium-enriched uranium (MEU 45%) fuel in the Kyoto University Critical Assembly (KUCA)<sup>4)</sup>, the neutron flux distributions were measured. The present paper provides experimental neutron flux distributions measured in the C38R(BK D<sub>2</sub>O)MEU core which was assembled in the C core<sup>5)</sup> of the KUCA. The C38R(BK D<sub>2</sub>O)MEU designation means a light-water-moderated, heavy-water-reflected cylindrical core using the MEU fuel of "Baumkuchen" type.

For the measurement of neutron flux distributions, the foil activation technique was employed. Gold wires, with and without a cadmium sheath, were activated. Relative neutron flux distributions were obtained for various positions in the core with and without a void in the light-water moderator at the center of the reactor. The values of reflector savings were obtained for a few positions in the core without the void.

## EXPERIMENTAL

### (1) Experimental Arrangement

The positions of foil irradiations in the C38R(BK D<sub>2</sub>O)MEU core are shown in Figs. 1 and 2 with its configuration. The differences between the cores shown in Figs. 1 and 2 are seen at the center H<sub>2</sub>O region and the outer fuel region. In Fig. 1, all fuel

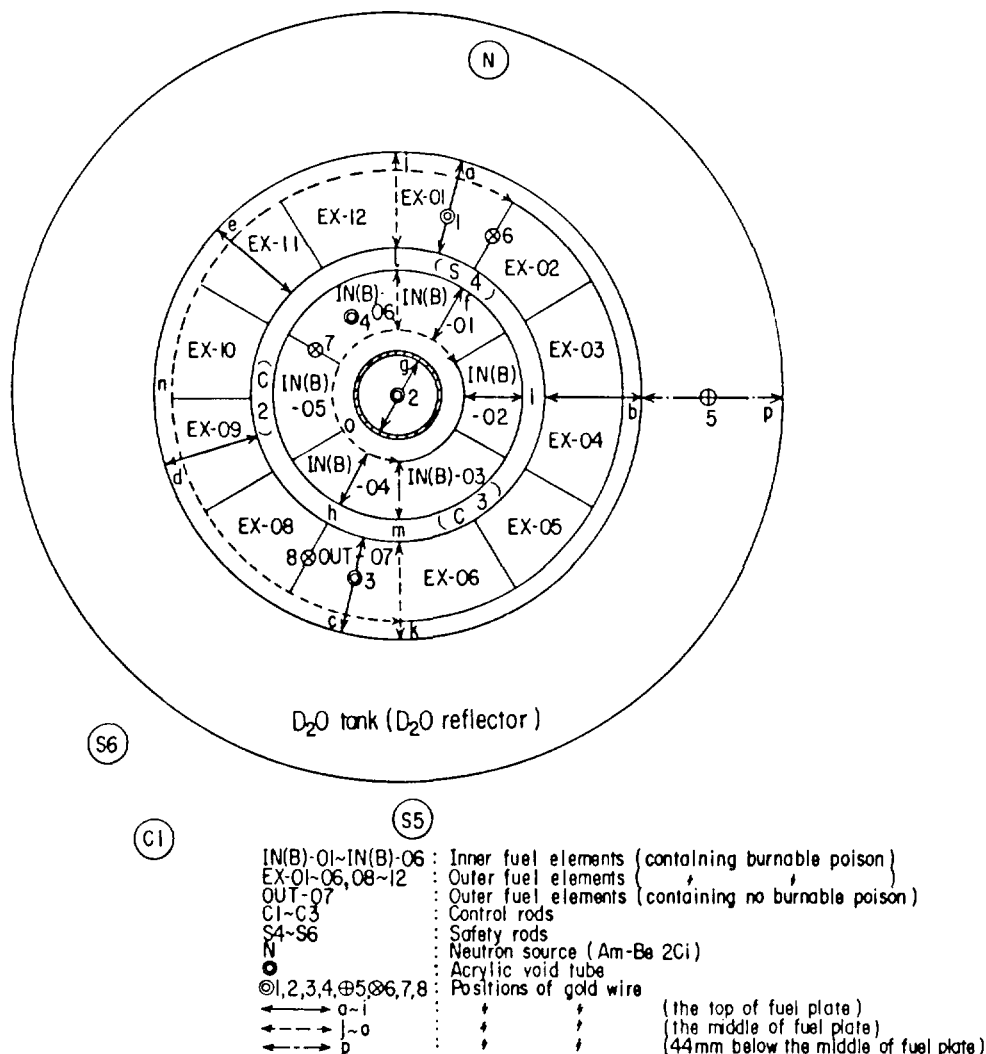


Fig. 1. Positions of wire irradiations in the C38R(BK D<sub>2</sub>O)MEU core with an acrylic void tube at the center.

elements except one outer element contain boron burnable-poison. An acrylic void tube of 10 cm o. d. and 9.2 cm i. d. is located at the center. In Fig. 2, one half of outer fuel elements contain no burnable-poison and there is no void at the center. Two hundred and ninety-four fuel plates are fully loaded in both cores. The pitch between fuel plates in the fuel element containing burnable-poison is 3.80 mm, while that in the fuel element without burnable-poison is 3.84 mm. The numerical symbols (1~11) in Figs. 1 and 2 indicate the positions where gold wires were set vertically. The alphabetical symbols (a~p) indicate gold wires set horizontally.

Bare gold wires (purity 99.999%) of 0.5 mm diameter were set at the all positions. To obtain thermal-neutron flux distributions, gold wires covered with cadmium sheath (0.5 mm thick and 1 mm i. d.) were set as shown in Fig. 2.

The gold wires were irradiated at approximately 1 W. Each irradiation time was 30 minutes. After the irradiations, gold wires were cut into small pieces (1~2 cm). The gamma-rays (0.412 MeV) emitted from the decay of  $^{198}\text{Au}$  ( $^{197}\text{Au}(n, \gamma)^{198}\text{Au}$ ) were counted with an automatic sample changer (OKEN model S-1023) in which a well-type NaI(Tl) scintillator of 2" dia.  $\times$  3" long is installed.

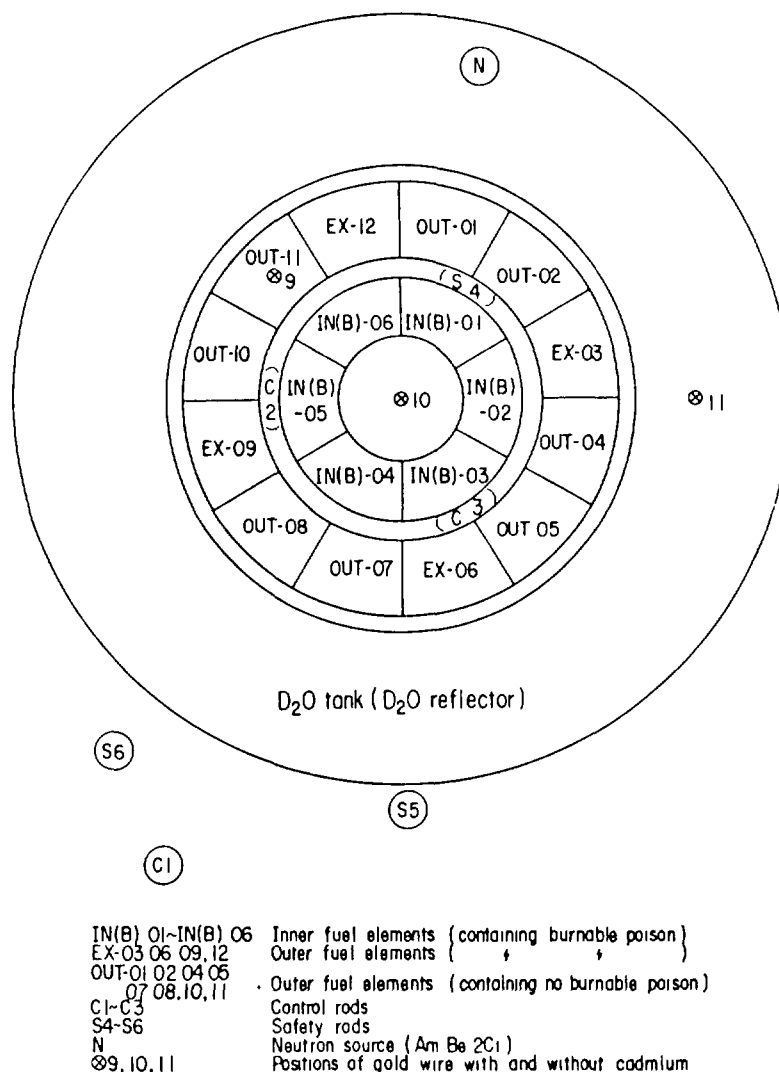


Fig. 2. Positions of wire irradiations in the C38R(BK D<sub>2</sub>O)MEU core without void at the center.

## (2) Data Processing

The saturated activity  $A_s$  (1/sec) is proportional to neutron flux and was obtained with  $^{199}\text{Au}$  decay corrections applied for irradiation time, waiting time and counting time.

$$A_s = \frac{\lambda T_c C}{(1 - \exp(-\lambda T_i)) \exp(-\lambda T_w) (1 - \exp(-\lambda T_c))},$$

where

$$\begin{aligned} \lambda &: \text{decay constant of } ^{199}\text{Au} \quad (2.975 \times 10^{-6}/\text{sec}), \\ T_i &: \text{irradiation time} \quad (\text{sec}), \\ T_w &: \text{waiting time} \quad (\text{sec}), \\ T_c &: \text{counting time} \quad (\text{sec}), \\ C &: \text{measured counting rate} \quad (1/\text{sec}). \end{aligned}$$

After weighing each piece of gold wire, the saturated activity  $A'_s$  per unit weight and per unit power level was obtained as follows:

$$A'_s = \frac{A_s}{W'P},$$

where

$$\begin{aligned} W &: \text{weight of a piece of gold wire} \quad (\text{mg}), \\ P &: \text{reactor power level} \quad (\text{W}). \end{aligned}$$

This value  $A'_s$  was regarded as the relative neutron flux.

To obtain the relative thermal neutron flux, the saturated activity of cadmium-covered gold wire was subtracted from that of bare gold wire. The axial neutron flux distributions were fitted by the least square technique to a cosine curve as follows:

$$y = A \cos(B(x - C)),$$

where

$$\begin{aligned} A, B, C &: \text{constants for a cosine fit,} \\ y &: \text{neutron flux,} \\ x &: \text{distance from the surface of grid plate (cm).} \end{aligned}$$

As the length of the fuel meat was 60 cm, the axial reflector saving  $\delta$  (cm) was obtained from the following equation,

$$\delta = \left( \frac{-\pi}{B} - 60 \right) / 2.$$

## RESULTS AND DISCUSSION

### (1) Horizontal neutron flux distributions

The horizontal neutron flux distributions are shown in Figs. 3, 4, 5 and 6. These neutron flux distributions were measured in the core with the acrylic void tube at the center.

Figures 3 and 4 show the neutron flux distributions in the fuel and heavy-water reflector regions, respectively. In Fig. 3, neutron flux distributions (j~m), measured at the middle height of fuel plates between the side-plates, have some depressions in the fuel

region The reason is that the side-plates contained boron burnable-poison In the void region, the flux distribution (g) is flat At the outside of the inner fuel region, the flux distribution (f) measured on the top of fuel plates was more depressed than that of (i)

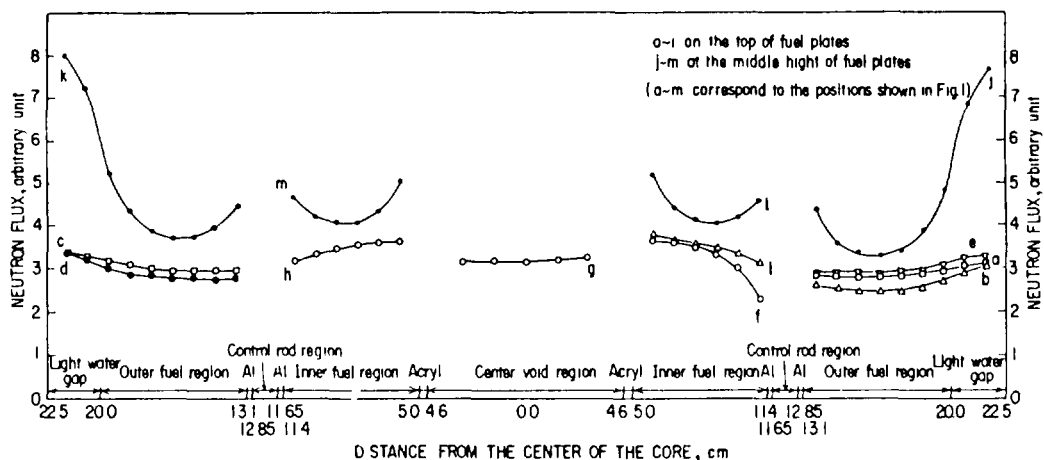


Fig 3 Horizontal flux distributions in the C38R(BK D<sub>2</sub>O)MFU core with an acrylic void tube at the center

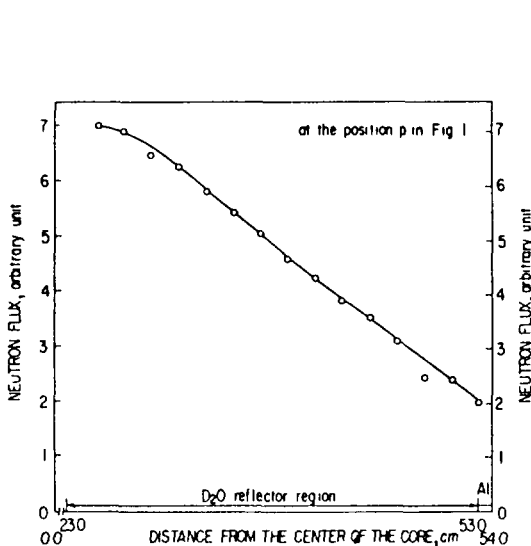


Fig 4 Horizontal flux distributions at D<sub>2</sub>O reflector in the C38R(BK D<sub>2</sub>O)MEU core with an acrylic void tube at the center

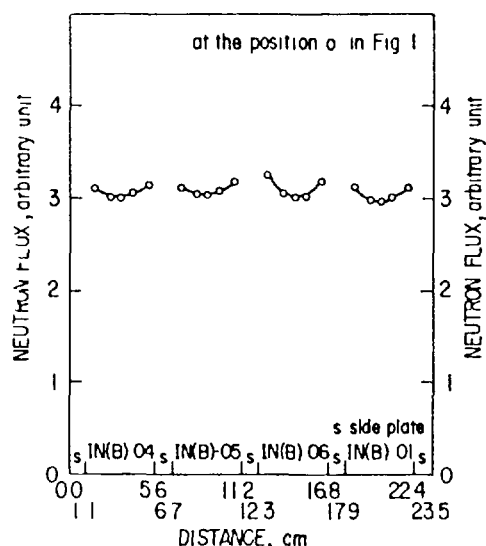


Fig 5 Horizontal flux distributions along the inner circular direction of inner fuel region in the C38R(BK D<sub>2</sub>O)MLU core with an acrylic void tube at the center

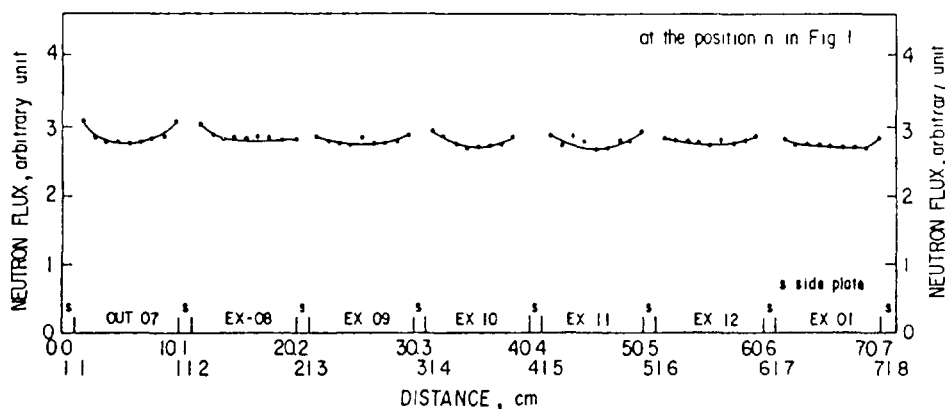


Fig 6 Horizontal flux distributions along the outer circular direction of outer fuel region in the C38R(BK D<sub>2</sub>O)MEU core with an acrylic void tube at the center

This is because the lower edge of the fully withdrawn safety rod S4 is near that position. In Fig. 4, the neutron flux in heavy-water reflector, measured at 44 mm below the middle height of fuel plates, has no peak and decreases rather rapidly with distance from the center of the core. This phenomenon reflects the facts that there is a light-water gap, approximately 2.5 cm thick, between the outer fuel region and the heavy-water tank and the 30 cm thick layer of heavy-water is not sufficient for a neutron reflector.

Figures 5 and 6 show the neutron flux distributions at the middle height of fuel plates along the inner circular direction of the inner fuel region and along the outer circular direction of the outer fuel region, respectively. In Figs. 5 and 6, there are peaks near the side-plate regions, though the regions contain boron burnable-poison.

(2) Vertical neutron flux distributions

The vertical neutron flux distributions in the core with a void at the center are shown in Figs. 7, 8 and 9, while those for the core without void are shown in Figs. 10 and 11.

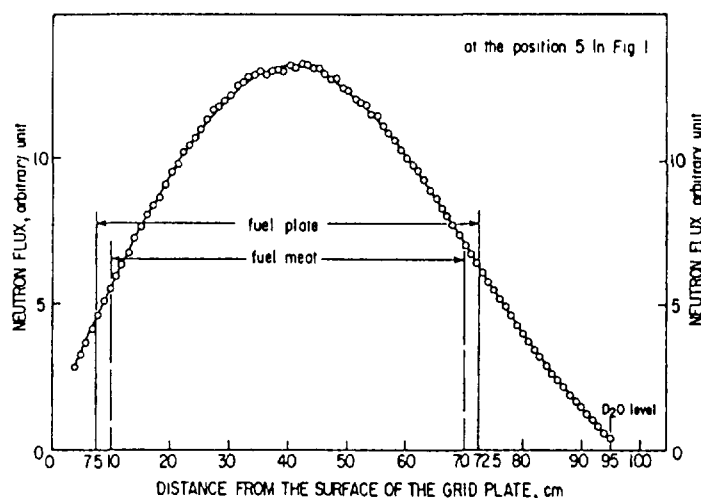


Fig. 7. Vertical flux distributions in the heavy-water reflector of the C38R(BK D<sub>2</sub>O) MEU core with an acrylic void tube at the center.

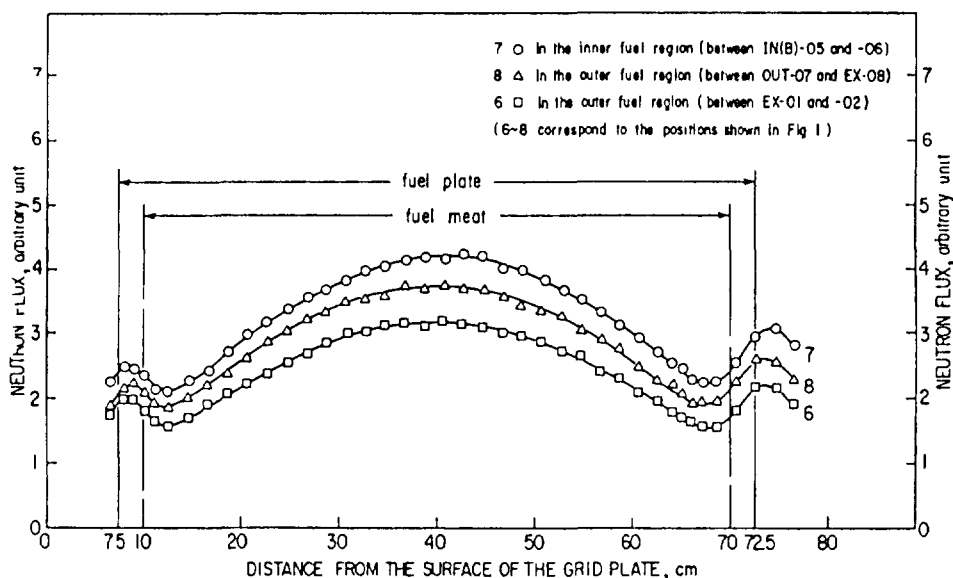


Fig. 8. Vertical flux distributions between side-plates in the C38R(BK D<sub>2</sub>O) MEU core with an acrylic void tube at the center.

Asymmetric features were observed in all of the vertical distributions. Namely, the neutron flux near the upper edge of fuel plates was higher than that near the lower edge. The reason was that the thickness of light- or heavy-water layer was not the same at the upper and lower site. At the upper site it was much thicker. In addition to that, there were layers of other materials such as aluminum and stainless-steel at the lower site. These materials are not favorable for the reflection of neutrons. In fact, neutrons are strongly absorbed in the stainless-steel layer.

Figure 7 shows the neutron flux distribution in heavy-water reflector. The irregular points near the peak in Fig. 7 might be caused by the horizontal aluminum pipe installed in the heavy-water tank for the measurement of neutron flux distributions.

Figure 8 shows the neutron flux distributions in the inner fuel region (between IN(B)-05 and -06) and outer fuel region (between EX-01 and -02, OUT-07 and EX-08). In Fig. 8, the neutron flux (7) in inner fuel region is larger than those of (6) and (8) in outer fuel region. The difference between (6) and (8) in outer fuel region was caused by the OUT-07 element which contains no boron burnable-poison.

Figure 9 shows the neutron flux distributions in the central void region, the inner fuel region (IN(B)-06), and the outer fuel region (EX-01, OUT-07). Figure 10 shows the neutron flux distributions in the center H<sub>2</sub>O region, the outer fuel region (OUT-11) and the heavy-water reflector. In Figs. 9 and 10, the neutron flux in the center is distinctly higher than anywhere else for either core with and without void.

The thermal neutron flux distributions are shown in Fig. 11 in the center H<sub>2</sub>O region, the outer fuel region (OUT-11) and heavy-water reflector.

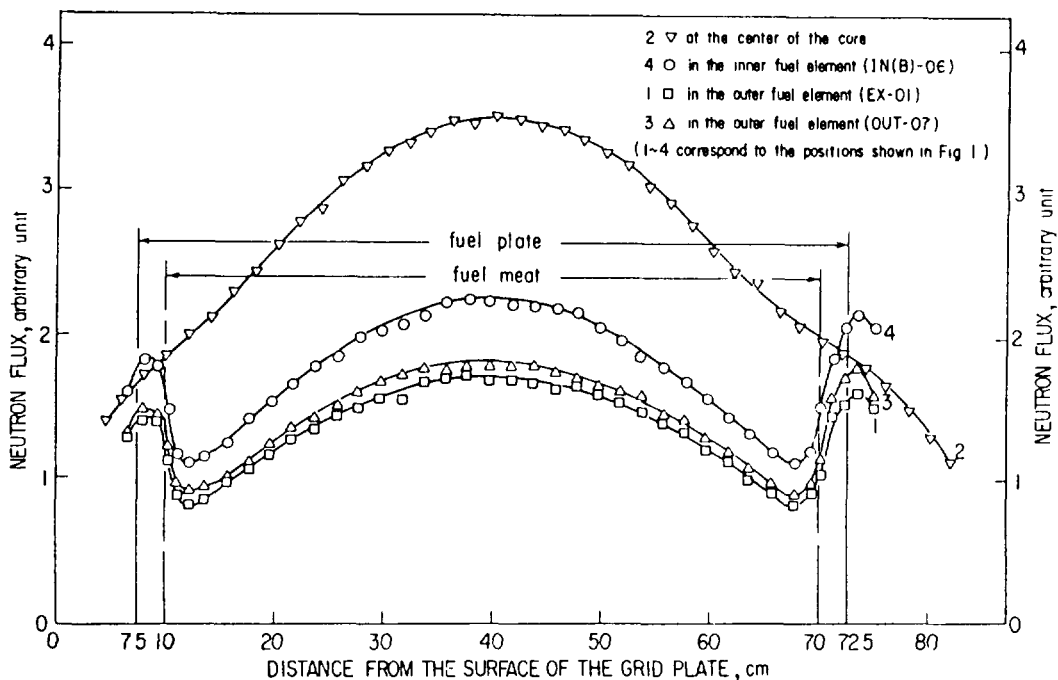


Fig. 9. Vertical flux distributions along center axis of the fuel element in the C38R(BK D<sub>2</sub>O) MEU core with an acrylic void tube at the center.

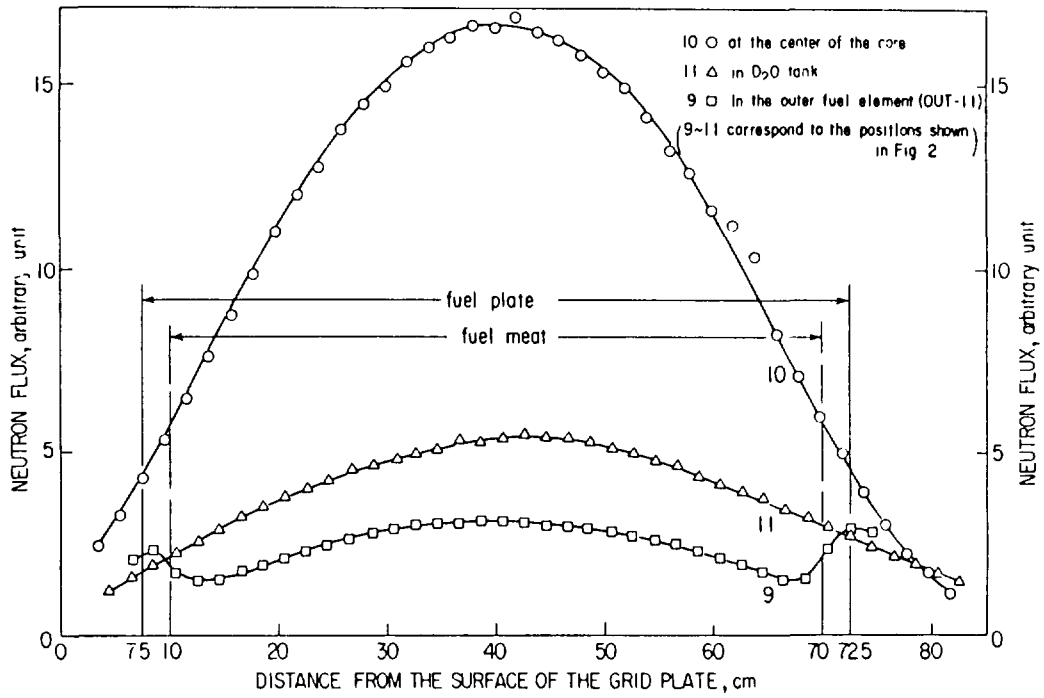


Fig. 10. Vertical flux distributions in the C38R(BK D<sub>2</sub>O)MEU core without void at the center.

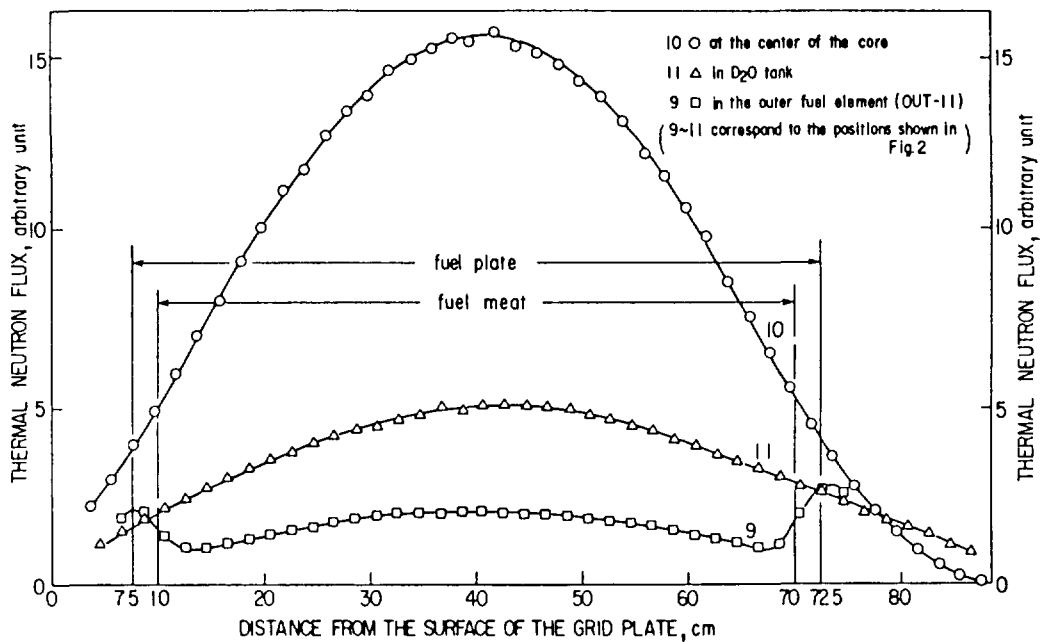


Fig. 11. Thermal-neutron flux distributions in the C38R(BK D<sub>2</sub>O)MEU core without void at the center.

### (3) Reflector savings

Measured neutron flux distributions, corrected for epi-cadmium neutrons, were fitted by the least square technique to a cosine curve to obtain axial reflector savings. These results are listed in Table 1. Table 1 shows that the extrapolation distance in the heavy-water reflector is larger than those in the fuel and the central light-water region, while the center position of the flux distribution,  $C$ , is the same in all regions.

Table 1. Axial reflector savings and extrapolation distance.

	A (n/sec cm <sup>2</sup> )	B (1/cm <sup>2</sup> )	C (cm)	$\delta$ (cm)
heavy-water reflector	0.27	$3.949 \times 10^{-2}$	40.4	$9.8 \pm 0.3$
outer fuel region	1.01	$4.158 \times 10^{-2}$	40.2	$7.8 \pm 0.1$
center region of light-water	1.01	$4.119 \times 10^{-2}$	40.0	$8.1 \pm 0.1$

### ACKNOWLEDGEMENTS

The authors express their thanks to the KUCA staff and to Mr T. Hamada for their assistance in carrying out the experiments. They express their thanks to Prof. Kojiro Nishina's group from Nagoya University for their cooperation in the experiments. They express their thanks to Prof. Keiji Kanda, Prof. Toshikazu Shibata of KUCA and Prof. Hiroshi Nishihara of Kyoto University for their encouragement and discussions. They express their thanks to the members of the Technical Committee of the KUCA chaired by Prof. Hiroshi Nishihara of Kyoto University for their advice and support in this work.

### REFERENCES

- 1) Shibata, T. and K. Kanda, "ANL-KURRI Joint Study on the Use of Reduced Enrichment Fuel in KUFR — Phase A Report —", (February 15, 1979).
- 2) Shibata, T., "Construction of a High Flux Research Reactor and Conversion of Kyoto University Reactor KUR to a TRIGA Type Pulsed Reactor", Research Reactor Renewal and Upgrading Program, IAEA-214 (1978) 183.
- 3) Hayashi, M. and S. Shiroya, "Few-Group Constants for the HEU and MEU Cores in the KUCA", Annu. Rep. Res. Reactor Inst. Kyoto Univ., 14 (1981).
- 4) Kanda, K., K. Kobayashi, M. Hayashi and T. Shibata, "Reactor Physics Experiment Using Kyoto University Critical Assembly", J. At. Energy Soc. Japan, 21 (1979) 557, in Japanese.
- 5) Sagane T. and T. Shibata, "Light-Water Moderator Core of Kyoto University Critical Assembly", KURRI-TR-178 (1978), in Japanese.

**EFFECT OF REDUCING FUEL ENRICHMENT  
ON THE VOID REACTIVITY\***

*Part I. Experimental study*

*(Abstract)*

H. FUKUI<sup>1</sup>

Department of Nuclear Engineering,  
Kyoto University,  
Kyoto

K. MISHIMA, S. SHIROYA, M. HAYASHI, K. KANDA

Research Reactor Institute,  
Kyoto University,  
Osaka

Y. SENDA<sup>2</sup>

Department of Nuclear Engineering,  
Kyoto University,  
Kyoto

Japan

Reactivity of void in the channels between the fuel plates is measured, and the impact of core conversion from using HEU to MEU fuel in the light-water-moderated cylindrical core with heavy water reflector is investigated on this quantity at the Kyoto University Critical Assembly. The void was generated in the flow channels by producing nitrogen gas bubbles through a small needle-like nozzle and the reactivity effect was measured. The void fraction was measured in an out-of-pile experiment. The results indicate that the void effect on reactivity is slightly larger (more negative) in the MEU core than in the HEU core. It is also shown that the interference effect of reactivity by bubbling in two adjacent channels simultaneously is within the experimental error.

---

\* The full text of this paper was published in Nuclear Technology, Vol. 70 (Sep. 1985).

Present addresses:

<sup>1</sup> Kobe Shipyard & Engine Works, Mitsubishi Heavy Industries, Ltd, 1-1-1 Wadasaki-cho, Hyogo-ku, Kobe 652, Japan.

<sup>2</sup> Mitsubishi Atomic Power Industries, Inc., 2-4-1 Shiba-kouen, Minato-ku, Tokyo 105, Japan.

**EFFECT OF REDUCING FUEL ENRICHMENT  
ON THE VOID REACTIVITY\***

*Part II. Analytical study*

*(Abstract)*

Y. SENDA<sup>1</sup>

Department of Nuclear Engineering,  
Kyoto University,  
Kyoto

S. SHIROYA, M. HAYASHI, K. KANDA

Research Reactor Institute,  
Kyoto University,  
Osaka

Japan

The results of analyses on the void reactivity measurements performed in the Kyoto University Critical Assembly using MEU fuel as well as HEU fuel are provided. In consideration of the heterogeneity of a complex core, four-group constants were generated by SRAC, a standard thermal reactor code system for reactor design and analysis at the Japan Atomic Energy Research Institute. The eigenvalue and perturbation calculations were subsequently performed by the 2D-FEM-KUR code, which is a two-dimensional diffusion code based on the finite element method. The calculated eigenvalue  $k_{\text{eff}}$  agreed with the measured value to within 0.5% in the calculated-to-experiment ratio. The void reactivity calculated by perturbation theory approximately reproduced the experimental data including the spatial dependence. The discrepancy between the calculated and measured void reactivity was  $<0.05 \times 10^{-3} \Delta k/k$  per voided flow channel.

---

\* The full text of this paper was published in Nuclear Technology, Vol. 70 (Sep. 1985).

<sup>1</sup> Present address: Mitsubishi Atomic Power Industries, Inc., 2-4-1 Shiba-kouen, Minato-ku, Tokyo 105, Japan.

## Appendix H-2.6

### STUDY ON TEMPERATURE COEFFICIENTS OF MEU AND HEU CORES IN THE KUCA

K. KANDA, S. SHIROYA, M. MORI,  
M. HAYASHI, T. SHIBATA  
Research Reactor Institute,  
Kyoto University,  
Osaka, Japan

#### Abstract

Recently, measurements of the temperature reactivity coefficients were performed in the KUCA in succession to the study on void reactivity effects. The objective cores of study were light-water-moderated and heavy-water reflected ones loaded with HEU or MEU fuel. The following effects on the temperature coefficients were investigated for the range from 20°C through 70°C: (1) the reduction in fuel enrichment, (2) the fuel loading pattern, and (3) the existence of boron burnable poison. The measured data were analyzed using the SRAC system to assess the computational technique for the temperature effects on reactivity. Through the present study, no remarkable difference was observed between the temperature effects in HEU and MEU cores. It was found that the difference in the core configuration causes a much greater effect on this quantity than the other differences including the fuel enrichment. The calculated results agree approximately with the experimental data.

#### INTRODUCTION

In accordance with the international Reduced Enrichment for Research and Test Reactors [RERTR] program, the critical experiments using medium-enriched-uranium [MEU] fuel was launched in 1981 using the Kyoto University Critical Assembly [KUCA]. Thereafter, the KUCA experiments have been providing useful data with regard to the RERTR program.<sup>1-15</sup>

Recently, measurements of the temperature effects on reactivity were performed in the KUCA in succession to the study on the void reactivity effects<sup>2,4,6,10,11,14,15</sup>, since the temperature coefficient as well as the void coefficient is a physical quantity closely related to the safety of liquid-moderated reactors. It is important to investigate the effects of reducing fuel enrichment on these quantities in advance to a core conversion from high-enriched-uranium [HEU] to reduced-enrichment-uranium fuels.

With use of light-water-moderated and heavy-water-reflected annular cores constructed in the KUCA, the following effects on the temperature reactivity coefficients were investigated for the temperature range from 20°C through 70°C: (1) the reduction in fuel enrichment, (2) the fuel loading pattern, and (3) the existence of boron burnable poison [BP].

The measured data were analyzed using the SRAC system<sup>16</sup> to assess the computational technique for the temperature coefficients. For the calculation of this quantity, 3 physical processes were taken into consideration; namely, the (1) Doppler, (2) thermal expansion, and (3) thermal neutron spectral shift effects.

## EXPERIMENTAL

A schematic cross-section of the light-water-moderated and heavy-water-reflected core constructed in the KUCA is shown in Fig. 1. The core can be divided into following 7 concentric regions: the (A) central light-water, (B) inner fuel, (C) control rod, (D) outer fuel, (E) outer vessel, (F) heavy-water reflector, and (G) outside light-water regions. The outer fuel region consists of 12 fuel elements, and the inner fuel region 6 fuel elements.

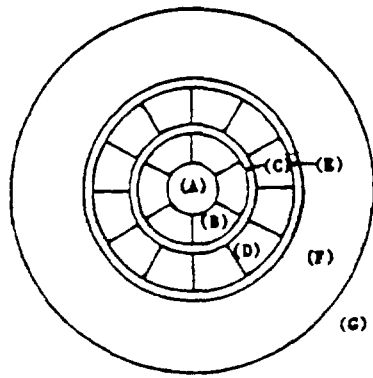
Six fuel loading patterns were employed in the present study; 4 patterns of MEU cores (see Fig. 2) and 2 patterns of HEU cores (see Fig. 3). These cores can be classified into 2 types; namely, "I" and "II". In the type "I" core, all outer fuel elements were fully loaded to its capacity with 17 fuel plates and the criticality was essentially adjusted by the number of fuel plates inserted into the inner fuel elements from the outside toward the inside in order. In the type "II" core, all inner fuel elements were fully loaded with 15 fuel plates and the criticality was adjusted by the number of fuel plates inserted into the outer fuel elements from the inside toward the outside. Therefore, the thicknesses of the central light-water region and the outer vessel region of light-water were different for the type "I" and "II". In Figs. 2 and 3, "no BP" means that there are no side-plates containing BP; "Outer BP" and "Inner BP" mean that all outer and inner side-plates contain BP, respectively.

A heater and a stirrer were installed in the heavy-water reflector in addition to 3 heaters and a stirrer installed in the dump tank from which light-water is pumped up and fed to the core tank in every operation of the KUCA. Seven thermocouples and 2 quartz-type thermometers were also installed to monitor the uniformity of the temperature as shown in Fig. 4. At several temperatures in the range from 20°C through 70°C, the excess reactivities or the subcriticalities were measured by the positive period method or the source multiplication method. The measured data of temperature dependent excess reactivities were then fitted to a quadratic equation using the method of least squares as;

$$\rho(T) = aT^2 + bT + c, \quad (1)$$

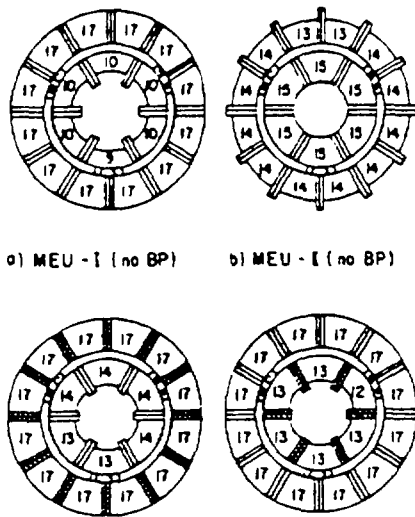
where,  $\rho(T)$  is the excess reactivity at the temperature  $T$  [°C], and  $a$ ,  $b$ , and  $c$  are the constants. Thus, the temperature coefficients  $\alpha(T)$  were determined as;

$$\alpha(T) = 2aT + b. \quad (2)$$



- (A) Central Light-Water Region
- (B) Inner Fuel Region
- (C) Control Rod Region
- (D) Outer Fuel Region
- (E) Outer Vessel Region  
(Light-water region between the outer fuel elements and the heavy-water reflector)
- (F) Heavy-Water Reflector Region
- (G) Light-Water Region Outside the Heavy-Water Reflector

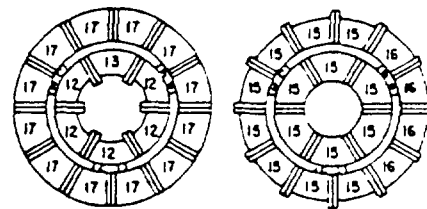
FIG. 1. Schematic cross-section of the KUCA core.



a) MEU - I (no BP)      b) MEU - I (no BP)

c) MEU - I (Outer BP)      d) MEU - I (Inner BP)

----- Side Plate Containing BP  
 Arabic Number    Number of Fuel Plates  
 C2, C3    Control Rods  
 S4    Safety Rod

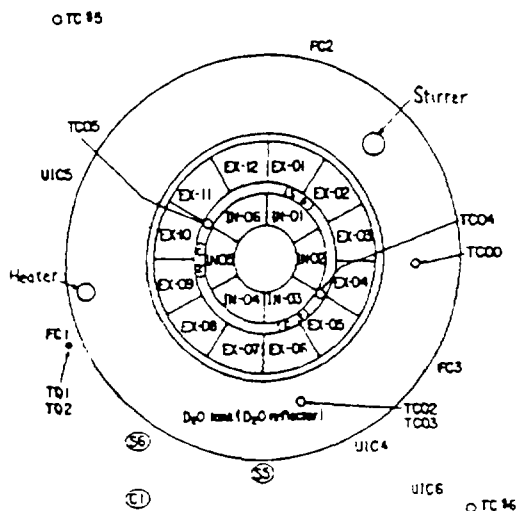


a) HEU - I (no BP)      b) HEU - I (no BP)

Arabic Number    Number of Fuel Plates  
 C2, C3    Control Rods  
 S4    Safety Rod

FIG. 2. Fuel loading patterns of MEU cores.

FIG. 3. Fuel loading pattern of HEU cores.



- IN-01-IN-06: Inner Fuel Elements
- EX-01-EX-12: Outer Fuel Elements
- C1-C3    Control Rods
- S4-S6    Safety Rods
- FC1-FC3    Fission Chambers
- UIC4-UIC6    Uncompensated Ionization Chambers
- TC#5, TC#6    Thermocouples (Stationary)
- TC00-TC06    Thermocouples
- TQ1, TQ2    Quartz-Type Thermometers

FIG. 4. Experimental arrangements.

## CALCULATIONS

The temperature effects on reactivity were calculated by the procedure shown in Fig. 5 using the SRAC system<sup>16</sup>. The effective multiplication factors were calculated at 3 temperatures (namely, 27°C, 52°C, and 77°C) for which the scattering kernels are prepared in the neutron cross section library in SRAC. In the calculation, following 3 physical processes were taken into account; the (1) Doppler, (2) thermal expansion, and (3) thermal neutron spectral shift effects.

From the public library of 107 energy groups in SRAC based on the ENDF/B-IV file<sup>17</sup>, the user library of 50 energy groups was generated. Assuming a fixed source problem, the primary cell calculations were performed by the collision probability routine in SRAC. In this step, the cell-averaged 19-group constants for the actually fueled region was obtained with approximating a curved geometry by a slab one<sup>15</sup>. Using the TWOTRAN code in SRAC, the secondary cell calculations were performed in order to take into account the neutron flux distributions in the azimuthal direction for obtaining 19-group constants of the fuel region. In this step, a curved geometry was approximated by a rectangular one and a special attention was paid to preserve the volumes of the actually fueled region and the BP layer. Therefore, by dividing a fuel element into several regions, the plural calculations were performed for the fuel region as shown in Fig. 6.

With use of the 19-group constants obtained through the above procedures, the core calculations were performed using the CITATION code in SRAC. A one-dimensional [1-D] cylindrical model was employed in this eigenvalue calculation (see Fig. 7) and the 10-group constants were generated in this step. In this step, the experimental data of reflector savings<sup>3,9</sup> were used for the vertical transverse buckling. With use of the 10-group constants, two-dimensional [2-D] R-Z calculations were performed using the CITATION code in SRAC (see Fig. 8). In order to check the difference between the 1-D and 2-D calculations, 1-D calculations using the 10-group constants were also carried out.

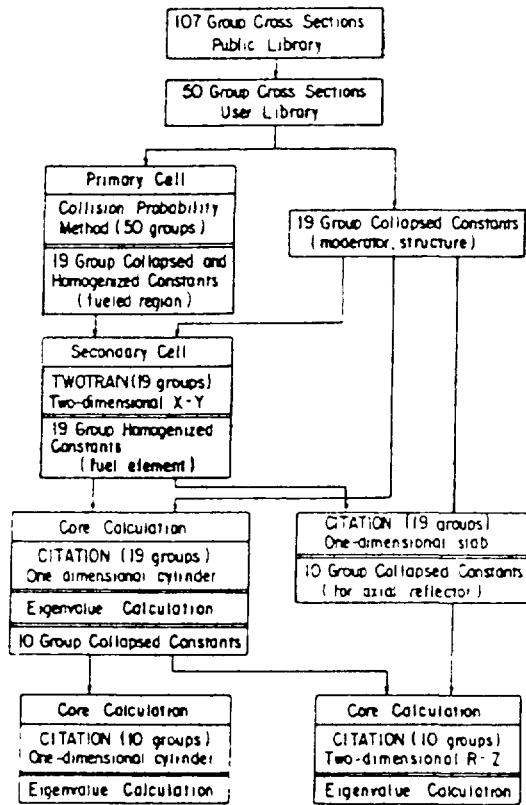


FIG. 5. Flow chart of the calculation.

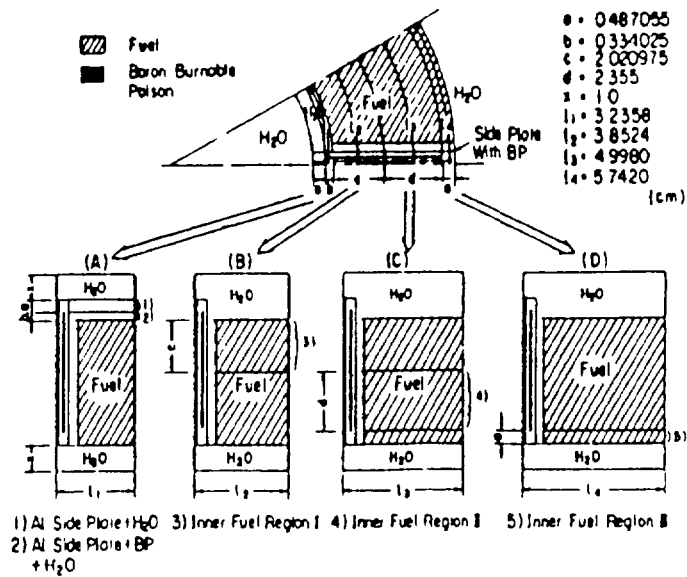


FIG. 6. Example of plural secondary cell calculations for a partially loaded inner fuel element with BP.

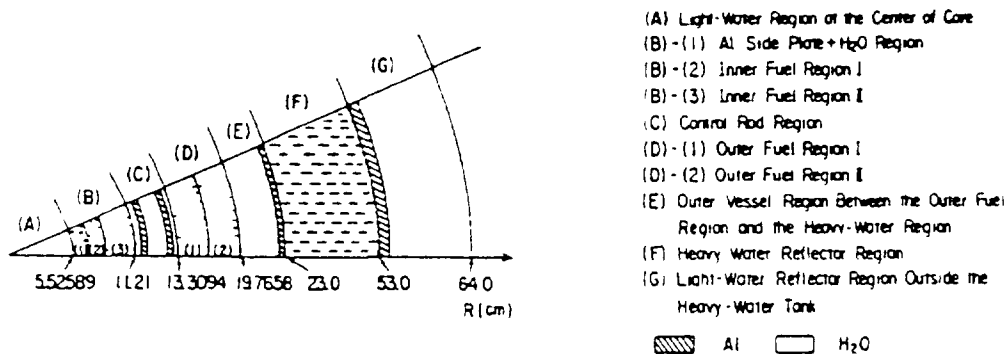


FIG. 7. 1-D calculation model for MEU-I cores.

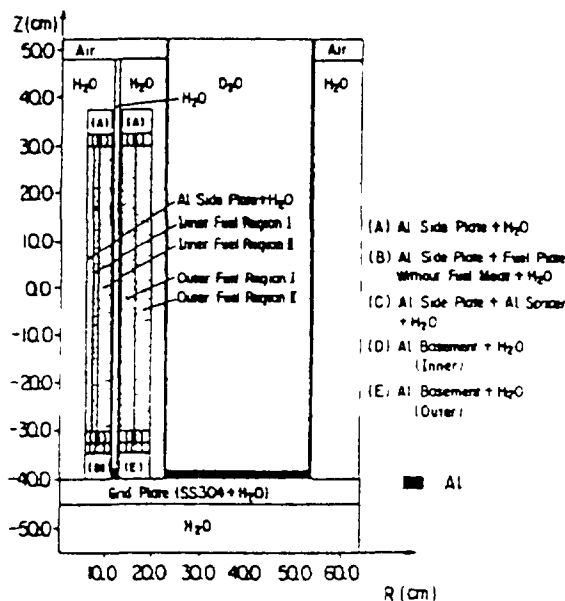


FIG. 8. 2-D calculation model for MEU-I cores.

## RESULTS AND DISCUSSION

Figure 9 shows the comparisons between the calculated and measured temperature effects on excess reactivity. Note that the calculated values are normalized to the experimental ones at 27°C. The calculations gave slightly larger effective multiplication factors than the experimental data, however, these differences were less than 3%. The 2-D calculations simulate fairly well the tendencies in temperature effect, whereas the 1-D calculations underestimate these tendencies. This can be attributed to the neglect of the positive temperature effects caused by the light-water reflectors above and below a core in the 1-D model.

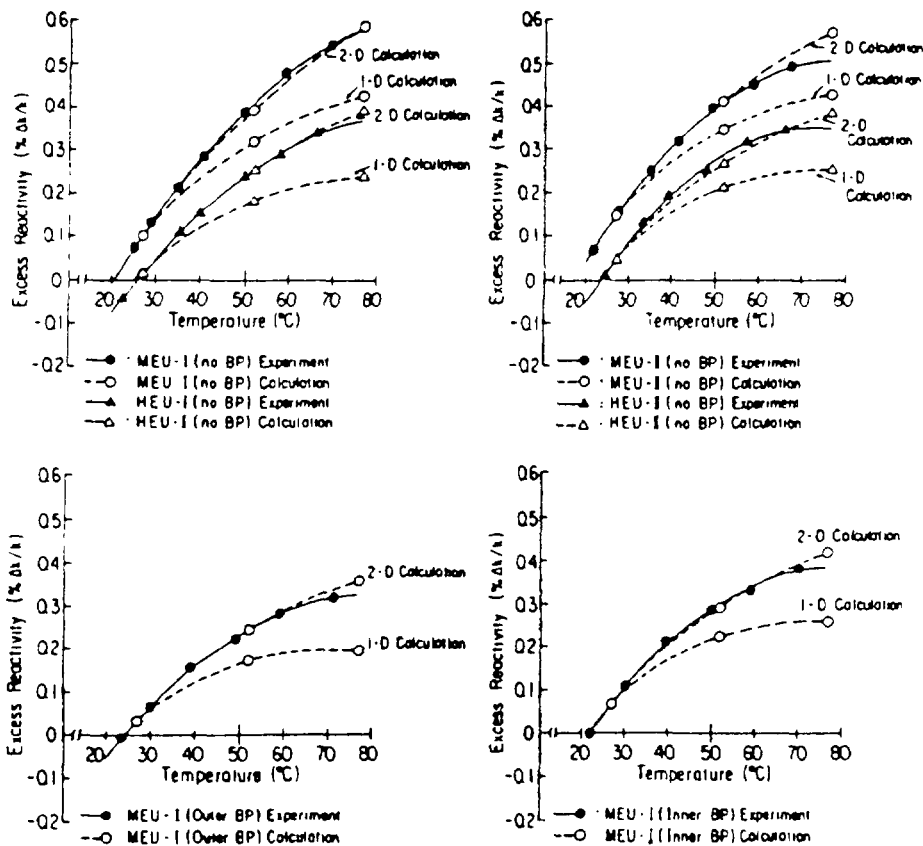


FIG. 9. Temperature effects on reactivity (the calculated results are normalized to the experimental ones at  $27^{\circ}\text{C}$ ).

Figure 10 shows the comparisons between the calculated and measured temperature coefficients of reactivity. The differences between the temperature coefficients in MEU and HEU cores are not so significant and it is considered that they depend strongly on the fuel loading patterns (see Figs. 2 and 3) as mentioned below. The calculated results approximately agree with the experimental ones, however, there exists some discrepancies between the gradients of temperature coefficients. The agreements are better in the type "I" core than in the type "II" core. This tendency was previously found in the analyses of the BP effect measurements<sup>8,13</sup>. This may be attributed to the difficulty in the generation of group constants for the inner fuel region where the neutron importance is highest and the curved geometry is most severe.

Figure 11 shows an example of the dependences of temperature effects on 3 physical processes calculated by the 1-D model. In the MEU core, the Doppler effect causes a slightly negative reactivity effect, whereas that in the HEU core is close to zero. The thermal expansion effect causes a negative reactivity effect, whereas the thermal neutron spectral shift effect causes a large positive effect which outweigh the other effects.

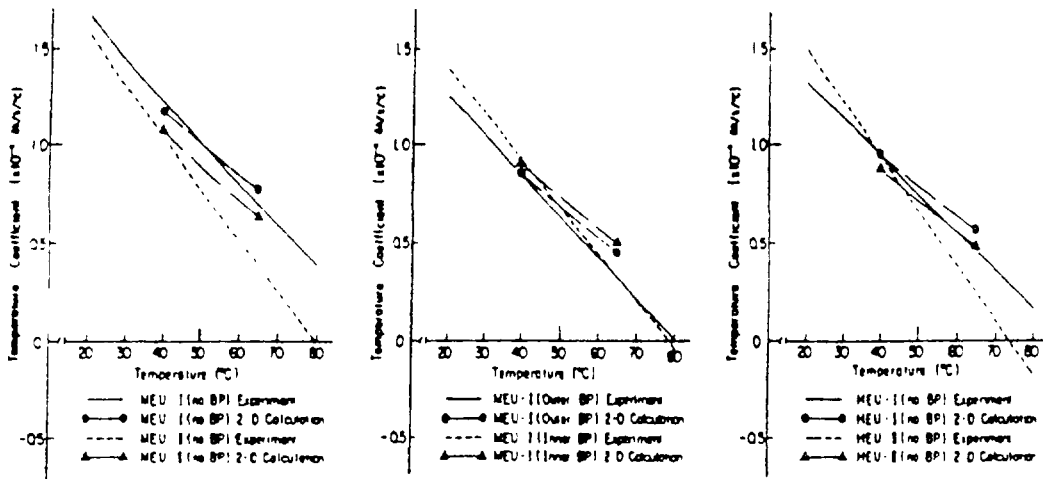


FIG. 10. Temperature coefficients of reactivity.

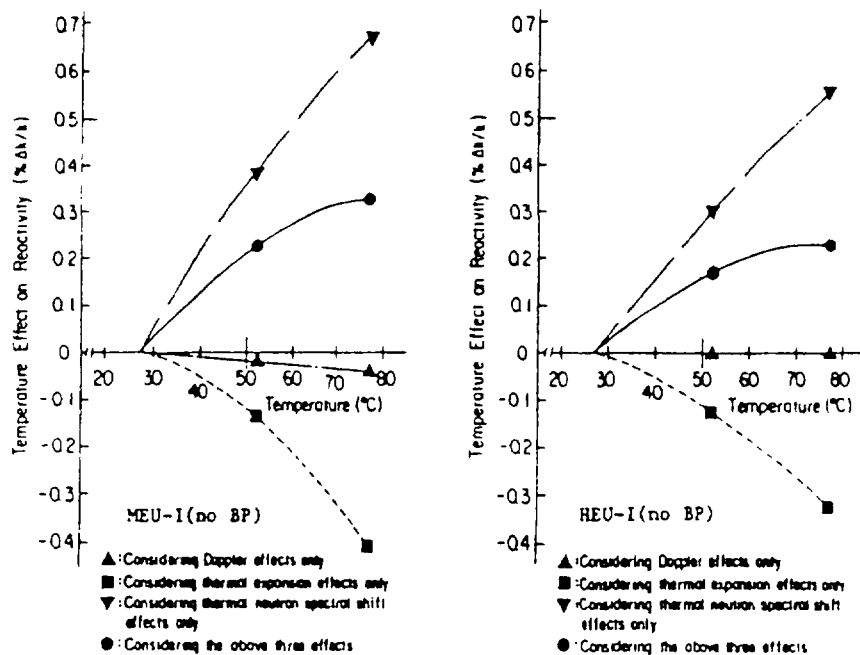


FIG. 11. Dependence of temperature effects on 3 physical processes.

Figure 12 shows the region dependent temperature effects on reactivity in the HEU cores calculated by the 1-D model. It is found that the temperature effects in the fuel regions causes negative reactivity effects and those in the heavy-water reflector are approximately zero, whereas those in the light-water regions causes positive effects. The positive temperature effects can be attributed mainly to the effects caused by the central light-water and outer vessel regions which depend strongly on the thicknesses of light-water layers.

In view of the above, the temperature effects on reactivity depend strongly on the core configurations, rather than on the fuel enrichment and the existence of BP. It is considered that

the negative temperature effects in the fuel regions are attributed mainly to the decrease in macroscopic neutron scattering cross section with the increase in temperature, and the positive temperature effects in the light-water regions are attributed to the decrease in macroscopic neutron absorption cross section.

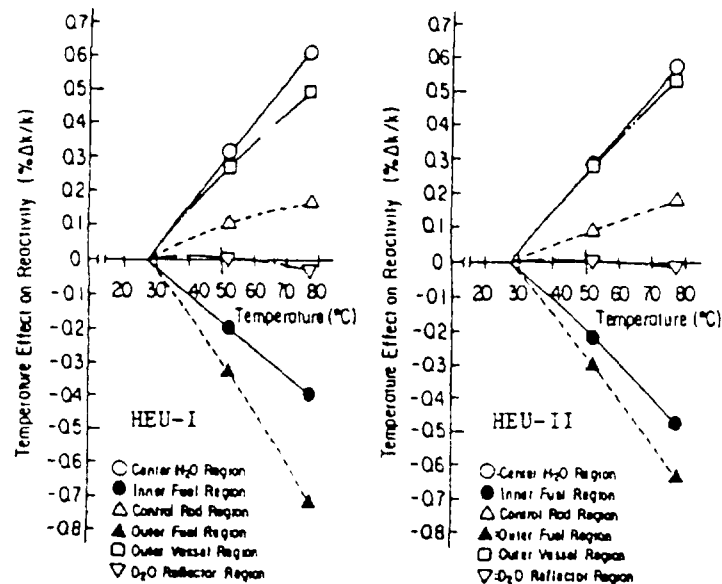


FIG. 12. Region dependent temperature effects.

#### ACKNOWLEDGEMENTS

The authors wish to express their thanks to all staff of the KUCA including Mr. Keiji Kobayashi for their generous assistance in the experiments. The calculations were performed at the Data Processing Center of Kyoto University. This study was financially supported by the Ministry of Education, Science and Culture.

#### REFERENCES

1. K. Kanda, et al., "KUCA Critical Experiments Using MEU Fuel", IAEA-SR-77/30 (1981).
2. K. Kanda, et al., "KUCA Critical Experiments Using Medium Enriched Uranium Fuel", Annu. Rep. Res. Reactor Inst., Kyoto Univ., 15, 1 (1982).
3. S. Shiroya, et al., "Measurements of Neutron Flux Distributions in a Medium Enriched Uranium Core", *ibid.*, 141 (1982).
4. K. Kanda, et al., "KUCA Critical Experiments Using MEU Fuel (II)", ANL/RERTR/TM-4 CONF-821155, 426 (1983).
5. S. Shiroya, et al., "Analysis of the KUCA MEU Experiments Using the ANL Code System", *ibid.*, 449 (1983).

6. H. Fukui, et al., "Experimental Study on the Void Reactivity Coefficient in the KUCA", Annu. Rep. Res. Reactor Inst., Kyoto Univ., 16, 1 (1983).
7. S. Shiroya, et al., "Analysis of the KUCA MEU Experiments Using the ANL Code System", *ibid.*, 17 (1983).
8. S. Shiroya, et al., "Analysis on the KUCA MEU Experiments (II), Boron Burnable-Poison Effect", JAERI-M 84-073, 369 (1984).
9. M. Hayashi, et al., "Calculation of the MEU-HEU Coupled Core in the KUCA", *ibid.*, 377 (1984).
10. K. Kanda, et al., "Experimental Study on the Void Reactivity Coefficient in the KUCA", *ibid.*, 388 (1984).
11. Y. Senda, et al., "Analysis on the Void Reactivity Measurement in the KUCA", *ibid.*, 399 (1984).
12. K. Kanda, et al., "HEU-MEU Mixed-Core Experiments in the KUCA", International Meeting on RERTR, 15-18 Oct., Argonne, USA (1984).
13. S. Shiroya, et al., "Analysis of Critical Experiments Using Medium-Enriched-Uranium Fuel in Kyoto University Critical Assembly (KUCA)", J. Nucl. Sci. Technol., 22, 507 (1985).
14. H. Fukui, et al., "Effect of Reducing Fuel Enrichment on the Void Reactivity, Part I; Experimental Study", Nucl. Technol., 70, 301 (1985).
15. Y. Senda, et al., "Effect of Reducing Fuel Enrichment on the Void Reactivity, Part II; Analytical Study", *ibid.*, 318 (1985).
16. K. Tsuchihashi, et al., SRAC: JAERI Thermal Reactor Standard Code System for Reactor Design and Analysis, JAERI 1285 (1983).
17. D. Garber, ENDF/B Summary Documentation, BNL-NCS-17541 (ENDF 201), 2nd. Edition (1975).

## Appendix H-2.7

### STUDY ON TEMPERATURE COEFFICIENT OF REACTIVITY IN KUCA LIGHT-WATER MODERATED AND REFLECTED CORE — EFFECT OF M/F RATIO AND CORE SHAPE ON THIS QUANTITY

K. KANDA, S. SHIROYA, M. MORI, T. SHIBATA

Research Reactor Institute,  
Kyoto University,  
Osaka, Japan

#### Abstract

Both the experimental and analytical studies have been performed on the temperature coefficient of reactivity in the KUCA light-water moderated and reflected core loaded with HEU fuel. The temperature effect on reactivity was measured for the range from 20°C through 70°C to investigate separately the effects of the M/F ratio and the core shape on this quantity. The results of both the eigenvalue and perturbation calculations by the SRAC code system approximately reproduced the experimental data. It was found that the contribution of the core region was negative to the temperature coefficient due to the degradation of moderation, whereas that of the reflector region was positive due to the decrease in neutron absorption. The positive contribution of the reflector region became larger as the M/F ratio became smaller and the core shape became more slender.

#### INTRODUCTION

In the last international meeting at Petten in the Netherlands, the result of study was reported on the temperature coefficients of reactivity in the highly-enriched-uranium (HEU) and medium-enriched-uranium (MEU) cores constructed in the Kyoto University Critical Assembly (KUCA).<sup>1</sup> Through this study, it was found that the difference in the core shape caused a much greater effect on this physical quantity than the other differences including the fuel enrichment.

Therefore, another experiment has been performed to investigate how the temperature coefficient of reactivity depends upon (1) the moderator-to-fuel (M/F) ratio and (2) the core shape. In the present experiment, light-water moderated and reflected rectangular-parallelepiped cores were constructed in the KUCA with use of HEU fuel, since they had simple configurations desirable to provide the benchmark data for the detailed assessment of the neutronics calculation.

The experimental data were analyzed by the SRAC code system<sup>2</sup> developed at Japan Atomic Energy Institute (JAERI). Through this analytical research, a few computational methods based on diffusion theory were examined on the validity calculating the temperature coefficient. On the basis of the above assessment, further studies were carried out (1) to separate the contribution of the core region to this physical quantity from that of the reflector region, (2) to investigate quantitatively each contribution of the nuclear features (diffusion, moderation, absorption, etc.) to this quantity, and (3) to examine each effect of the physical processes (thermal expansion, thermal neutron spectral shift, etc.) on this quantity.

## EXPERIMENTAL

An illustration of a fuel plate is shown in Fig. 1. The fuel plate had a flat shape and contained uranium-aluminum (U-Al) alloy in aluminum clad. One fuel plate contained 8.89g  $^{235}\text{U}$  and 9.55g U, which corresponded to the enrichment of 93.10%. The uranium content in the U-Al alloy was 20%, i.e. 0.59g/cc. One by one, each fuel plate was inserted between two aluminum side plates to form a fuel element.

Two types of side plates shown in Fig. 2 were used in the experiment to vary the M/F ratio ( $\text{H}/^{235}\text{U}$  atomic ratio) in the fuel region. These side plates had grooves for the fuel insertion in 4.54mm and 3.49mm pitches, which were employed to construct so called the C45 and C35 cores, respectively.

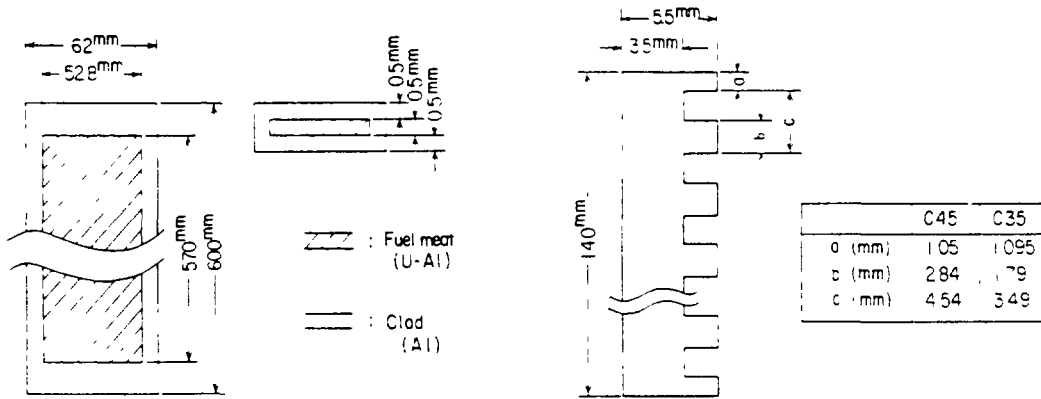


Fig. 1 Fuel Plate

Fig. 2 Side Plate

A view of a fuel element is shown in Fig. 3. The fuel elements were installed on a grid plate in the core tank, which is an aluminum tank of 1.8m in depth and 2m in diameter located at the C-core of the KUCA, with a 71mm pitch in one direction and a 142mm pitch in the other direction to form a core. The maximum of 31 and 40 fuel plates were loaded in the C45 and C35 fuel elements, where  $\text{H}/^{235}\text{U}$  atomic ratios were 315 and 212, respectively.

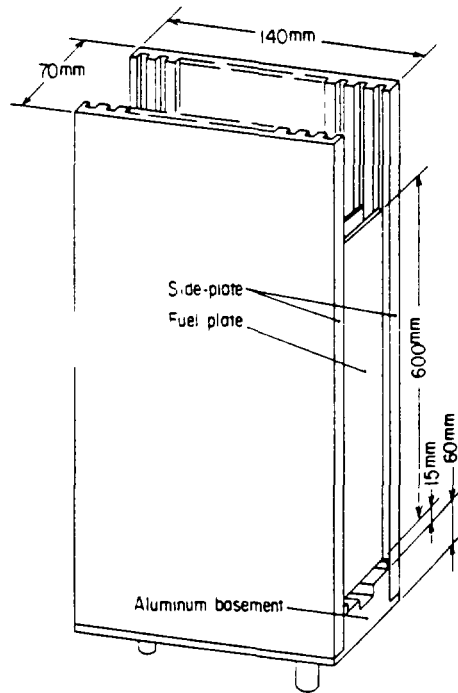
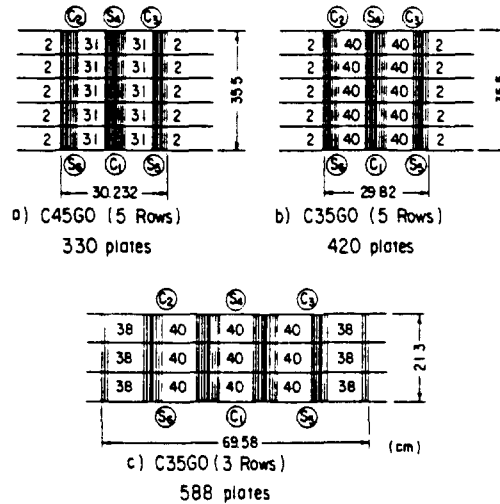


Fig. 3 Fuel Element

Three cores employed in the experiment were shown in Fig. 4. For identification, these cores were designated as the C45G0(5 Rows), C35G0(5 Rows), and C35G0(3 Rows) cores. In the above notation, G0 means that there was no light-water gap in the fuel region.



Arabic Number - Number of Fuel Plates  
C1~C3 Control Rods  
S4~S6 Safety Rods

Fig. 4 Core Designation

In the cores a) and b) shown in Fig. 4, the fuel elements were assembled in 5-row configurations. From this figure, it is clear that the longitudinal sizes of these two cores were exactly the same, and the lateral sizes of them were approximately equal with each other. Consequently, the differences in the temperature coefficients between these two cores were mainly attributed to the change in the M/F ratio. The core c) in Fig. 4 was a 3-row core constructed with the same pitch of 3.49mm as the core b). Since this core was long in the lateral direction and narrow in the longitudinal direction, the dependence of the temperature coefficient upon the core shape could be investigated through a comparison with the core b), whose shape was nearly square.

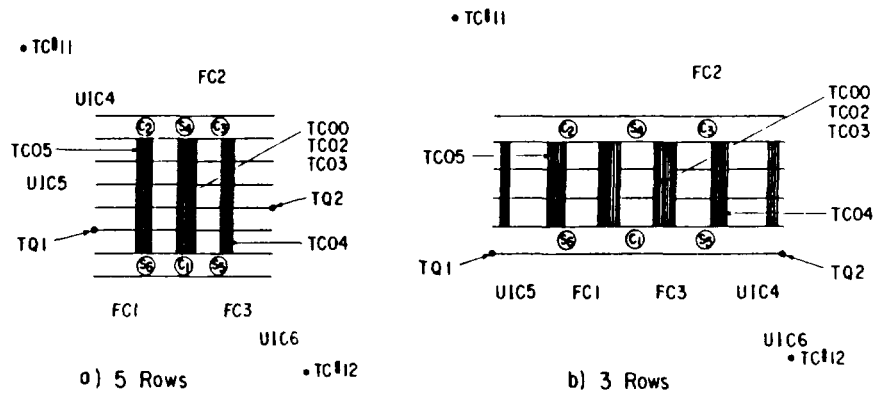
When light-water was heated up to an appropriate temperature in the range from 20°C to 70°C with the aid of heaters and a stirrer, it was fed to the C-core tank. To monitor the uniformity of temperature, 7 thermocouples and 2 quartz-type thermometers were settled in various positions as shown in Fig. 5. After the criticality was attained by adjusting the stroke of the control rod, the excess reactivity was measured by the positive period method. When the system was subcritical, the subcriticality was measured by the source multiplication method.

The measured excess reactivities were fitted to a quadratic curve by the method of least squares as;

$$\rho(T) = aT^2 + bT + c \quad (1)$$

where,  $\rho(T)$  is the excess reactivity at the temperature  $T$  [°C], and  $a$ ,  $b$ , and  $c$  are the constants. Then, the temperature coefficient  $\alpha(T)$  was obtained by differentiating Eq.(1) as;

$$\alpha(T) = 2aT + b \quad (2)$$



C1~C3 : Control Rods  
 S4~S6 : Safety Rods  
 FC1-FC3 : Fission Chambers  
 UIC4-UIC6 : Uncompensated Ionization Chambers  
 TC#11, TC#12 : Thermocouples (Stationary)  
 TC00~TC05 : Thermocouples (Stationary)  
 TQ1, TQ2 : Quartz-Type Thermometers

Thermometers	Height from the center of the fuel plate
TC#11	33.0 cm beneath
TC#12	47.0 cm above
TC00	0.0 cm
TC02	25.0 cm beneath
TC03	25.0 cm above
TC04	0.0 cm
TC05	0.0 cm
TQ1	10.0 cm above
TQ2	10.0 cm beneath

Fig. 5 Positions of Thermometers in Cores

Note here that the maximum difference was less than 1°C in temperatures measured by the 9 thermometers shown in Fig. 5. The maximum error was estimated to be  $\pm 0.005\% \Delta k/k$  for measured excess reactivities in the C-core from experience.

### CALCULATIONS

The calculations were performed by SRAC in accordance with a flow chart shown in Fig. 6. The 4-group constants for the core calculation were generated at 3 temperatures 27°C, 52°C, and 77°C, for which scattering kernels were installed in the neutron cross section library for SRAC. To calculate the temperature coefficient of reactivity, following 3 physical processes were taken into account; namely, (1) the Doppler broadening, (2) the thermal expansion, and (3) the thermal neutron spectral shift.

The cell calculations were performed by the slab geometry option of the collision probability routine in SRAC to obtain the cell-averaged 19-group constants of the core region shown in Fig. 7. Assuming a fixed source problem, the primary cell calculation was carried out with the 107-group library to obtain homogenized group constants for the actually fueled region. Next, the secondary cell calculation was performed to take into account the neutron flux distributions in the lateral direction. Thus, the collapsed constants were generated using the 107-group constants for the fueled region obtained in the primary cell calculation.

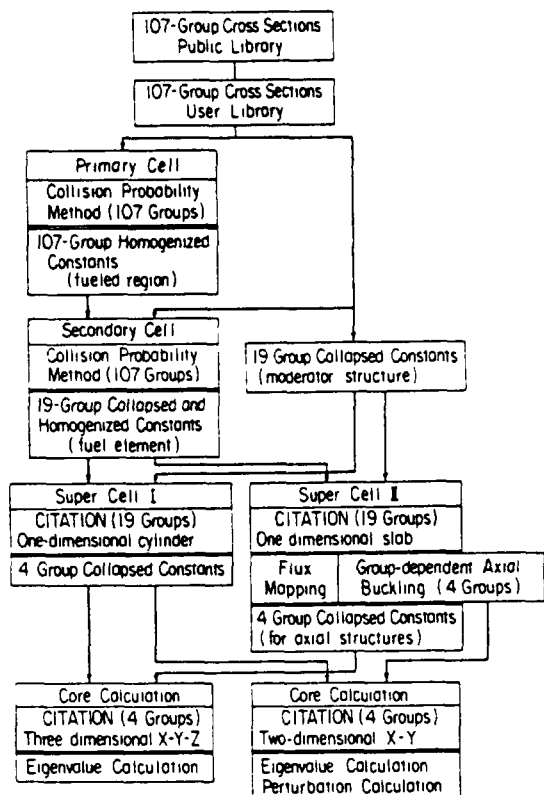


Fig. 6 Flow Chart of Calculation

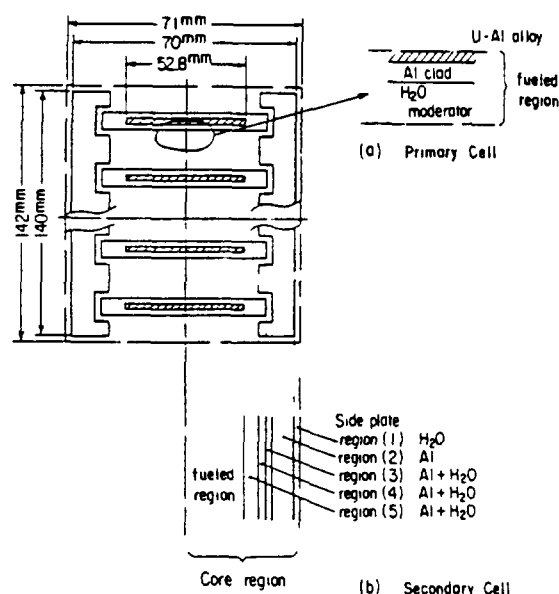


Fig. 7 Model for Cell Calculation

The super cell calculations were executed by the CITATION code installed in SRAC to obtain the 4-group constants. The super cell I calculation was performed using the 1-dimensional (1-D) cylindrical geometry option to generate the group constants of the core and reflector regions. The super cell II calculation was carried out using the 1-D slab geometry option to obtain the group constants of axial structures for 3-dimensional (3-D) calculations. The calculated axial neutron flux distributions were fitted by cosine curves to obtain the group-dependent axial bucklings at each temperature as listed in Table 1, which were employed in 2-dimensional (2-D) calculations.

Table 1 Group-Dependent Axial Buckling

Core	Temperature	Group-Dependent Axial Buckling ( $10^{-3}\text{cm}^{-2}$ )			
		Group 1	Group 2	Group 3	Group 4
C45G0	27°C	1.9088	1.9114	1.9141	1.9123
	52°C	1.8992	1.9018	1.9053	1.9036
	77°C	1.8870	1.8905	1.8940	1.8914
C35G0	27°C	1.8131	1.8182	1.8224	1.8207
	52°C	1.8020	1.8071	1.8122	1.8097
	77°C	1.7893	1.7944	1.8003	1.7969

The core calculation was performed by CITATION in SRAC to obtain the temperature coefficient of reactivity. The eigenvalue calculations were executed using both the 3-D X-Y-Z and 2-D X-Y geometry options at the three temperatures 27°C, 52°C, and 77°C. The X-Y cross sections of 3-D models are shown in Fig. 8, which were also used as 2-D models, and the X-Z cross section of a 3-D model is shown in Fig. 9. The perturbation calculations were carried out using the same 2-D models as those employed in the eigenvalue calculations on the basis of both the exact and the first order perturbation theories.

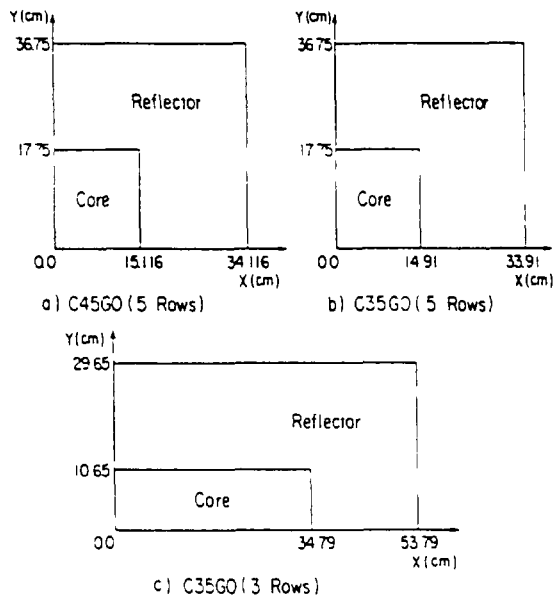


Fig. 8 X-Y Cross Section of 3-D Model for Core Calculation

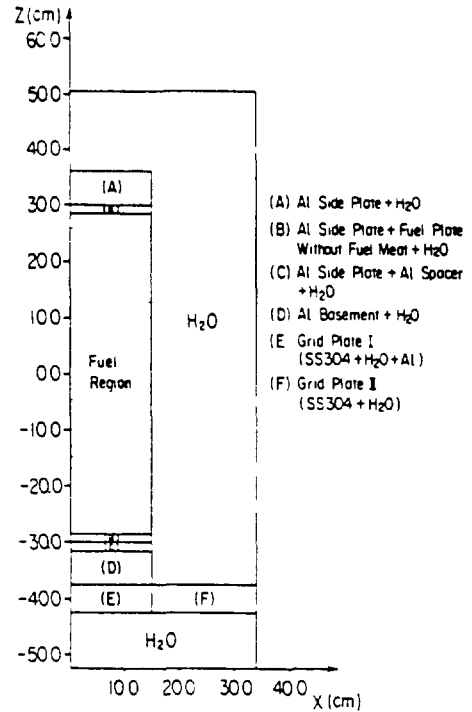


Fig. 9 X-Z Cross Section of 3-D Model for Core Calculation

## RESULTS AND DISCUSSION

Table 2 shows the calculated effective multiplication factors at 27°C in comparison with the experimental data. The calculated results agreed with the experimental data within 0.5% in the C/E ratio for both the 2-D and 3-D calculations at the three temperatures.

Figure 10 shows the temperature effects on excess reactivity in the individual cores. Note that the calculated values with 3-D models were normalized to the experimental data at 27°C. The calculated results approximately reproduced the tendency in the experimental data.

Figure 11 shows the temperature coefficient of reactivity in the individual cores. The magnitude of the negative temperature coefficient was greatest in the C45G0(5 Rows) core, the next magnitude was found in the C35G0(5 Rows) core, and the lowest was in the C35G0(3 Rows) core. The calculated results approximately agreed with the experimental data, and the agreement in the gradients of temperature coefficients was better for the 5-row cores than for the 3-row core.

Table 2 Comparison of Calculated and Measured  $k_{eff}$  at 27°C

Designation of Core	Effective Multiplication Factor $k_{eff}$			
	Experiment	Calculation	C/E Ratio	
C45G0(5 Rows)	1.0040	2-D Cal.	1.0004	0.9964
		3-D Cal.	1.0023	0.9983
C35G0(5 Rows)	1.0025	2-D Cal.	0.9997	0.9972
		3-D Cal.	1.0013	0.9988
C30G0(3 Rows)	1.0036	2-D Cal.	1.0008	0.9972
		3-D Cal.	1.0024	0.9988

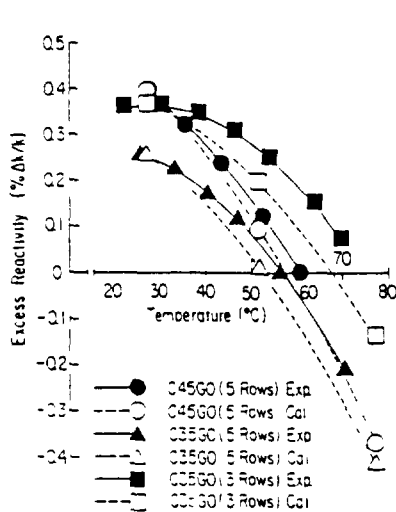


Fig. 10 Temperature Effect on Excess Reactivity

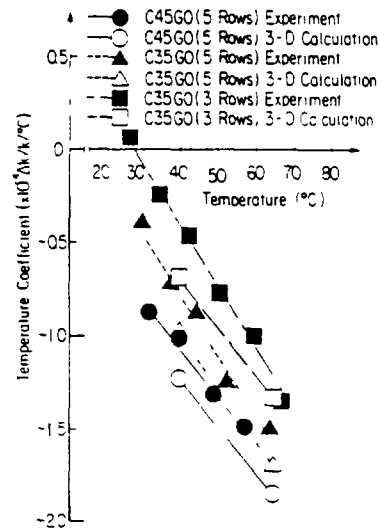


Fig. 11 Temperature Coefficient of Reactivity by 3-D Eigenvalue Method

Table 3 shows the comparison of temperature coefficients by the eigenvalue and perturbation calculations. All calculated results had slightly greater values than the experimental data, however, there was no remarkable difference in the results by any method of calculation. This indicates that both the eigenvalue and perturbation calculations can be applicable to obtain the temperature coefficient.

This table also shows that the results of 2-D and 3-D eigenvalue calculations were approximately agreed with each other. This assures the validity of the 2-D model employed in the present study. The results of the exact and the first order perturbation calculations were approximately equal with each other, however, the contribution of each region was slightly greater to the temperature coefficient by the exact perturbation method than by the first order perturbation method.

Table 3 Comparison of Calculated and Measured Temperature Coefficients

Method of Calculation		Temperature Coefficient ( $\times 10^{-4} \Delta k/k/^\circ C$ )					
		C45G0(5 Rows)		C35G0(5 Rows)		C35G0(3 Rows)	
		39.5°C	64.5°C	39.5°C	64.5°C	39.5°C	64.5°C
Eigenvalue Calculation	3-D Cal.	-1.22	-1.85	-0.98	-1.69	-0.69	-1.32
	2-D Cal.	-1.23	-1.86	-0.93	-1.71	-0.69	-1.26
Exact Perturbation Calculation	Core	-2.04	-2.67	-1.98	-2.68	-1.91	-2.51
	Reflector	0.77	0.67	0.99	0.87	1.19	1.08
	Total	-1.27	-1.99	-0.99	-1.81	-0.72	-1.43
First Order Perturbation Calculation	Core	-2.00	-2.51	-1.96	-2.56	-1.88	-2.43
	Reflector	0.73	0.56	0.95	0.75	1.14	0.93
	Total	-1.27	-1.95	-1.01	-1.82	-0.74	-1.50
Experimental Data		-1.05	-1.69	-0.77	-1.57	-0.39	-1.20

Table 4 shows the breakdown of the temperature effects on reactivity in the C35G0(5 Rows) core by the perturbation calculations. The difference between the exact and the first order perturbation methods were found mainly in the fission and absorption terms of the core region and in the absorption term of the reflector region, both of which were closely related to the change in the flux distributions of thermal neutrons rather than that of fast neutrons.

Table 4 Breakdown of Temperature Effect on Reactivity in C35G0(5 Rows) Core

Region	Component	Contribution to Reactivity ( $\% \Delta k/k$ )			
		Exact Perturbation Calculation		First Order Perturbation Calculation	
		52°C	77°C	52°C	77°C
Core	Fission	-2.33674	-4.65580	-2.28050	-4.43912
	Absorption	2.24857	4.50065	2.19849	4.31882
	Moderation	-0.34308	-0.84050	-0.34183	-0.83298
	Diffusion	-0.05447	-0.13461	-0.05560	-0.13993
	Leakage	-0.00892	-0.03425	-0.00944	-0.03682
	Total	-0.49464	-1.16450	-0.48888	-1.13003
Reflector	Absorption	0.32936	0.67954	0.32026	0.64303
	Moderation	0.01637	0.04149	0.01598	0.03884
	Diffusion	-0.09302	-0.24207	-0.09340	-0.24363
	Leakage	-0.00527	-0.01327	-0.00527	-0.01330
	Total	0.24744	0.46569	0.23757	0.42494
Whole System		-0.24720	-0.69881	-0.25131	-0.70509

Figure 12 shows the temperature coefficients calculated by the exact perturbation method. For all cores under investigation, the contributions of the core region were negative to the temperature coefficients and had negative gradients, whereas the reflector region gave approximately constant positive contributions. The sum of the above two contributions made the negative temperature coefficient having a negative gradient in total.

The negative contributions of the core region were approximately equal with each other in magnitude. As for the positive contributions of reflector region, the greatest magnitude was found in the C35G0(3 Rows) cores, the second was in the C35G0(5 Rows) core and the lowest in the C45G0(5 Rows) core. This determined the tendency in the magnitudes of total temperature coefficients in these three cores.

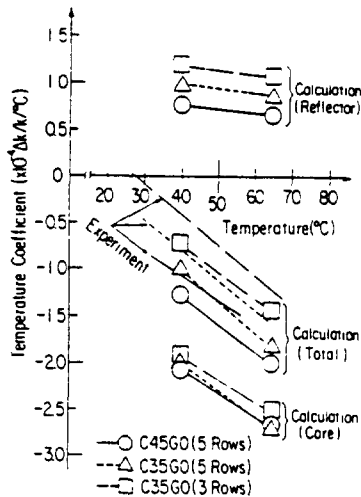


Fig. 12 Temperature Coefficient of Reactivity by Exact Perturbation Method

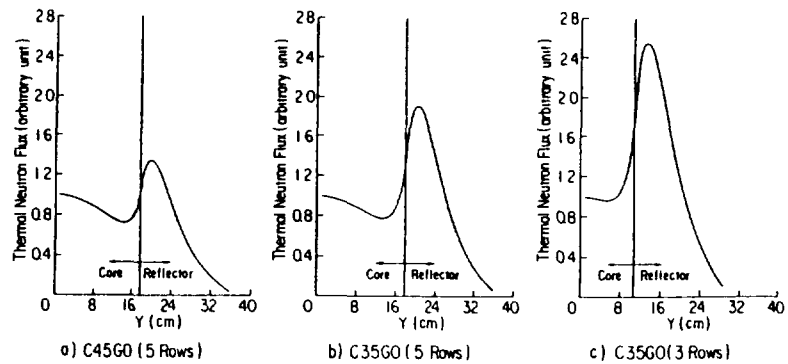


Fig. 13 Calculated Thermal Neutron Flux Distribution at 27°C

Figure 13 shows the calculated thermal neutron flux distribution in each core, which was considered to be closely related to the positive temperature coefficient in the reflector region. Note that these flux distributions were normalized to unity at the core center.

Firstly, comparing the C45 and C35 5-row cores, it is found that the flux peaking in the reflector region of the C35 core with a smaller M/F ratio was larger than that of the C45 core. Secondly, comparing the C35 5-row and 3-row cores, the flux peaking in the slender 3-row core was larger than that in the nearly square 5-row core. The reason was that the number of neutrons moderated in the reflector region became larger, when the M/F ratio became smaller and the core shape became more slender.

Figure 14 shows the contribution of each nuclear feature (diffusion, moderation, absorption, etc.) to the temperature coefficient in the C35G0(5 Rows) core by the exact perturbation calculation. In the core region, the change in the neutron absorption rate also caused the change in the fission rate, therefore, the sum of these two contributions was plotted in Fig. 14-a).

In the core region, the main contribution was due to the degradation of moderation as shown in Fig. 14-a). The negative gradient of temperature coefficients was mainly attributed to this term in the core region. The degradation of moderation was caused by the decrease in macroscopic scattering cross sections with the decrease in the atomic number density of light-water due to the thermal expansion.

In the reflector region, the absorption term was the main contributor to the temperature coefficient as shown in Fig. 14-b). The change in this term was attributed to the decrease in absorption cross sections of light-water, which was caused by both the thermal expansion and the thermal neutron spectral shift.

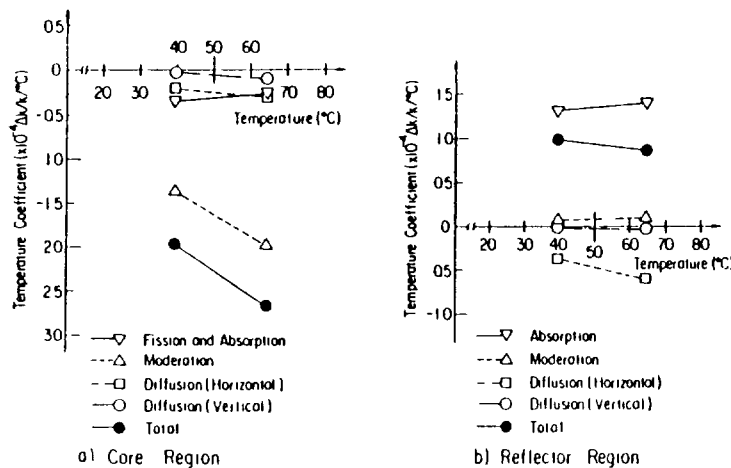


Fig. 14 Contribution of Each Nuclear Feature

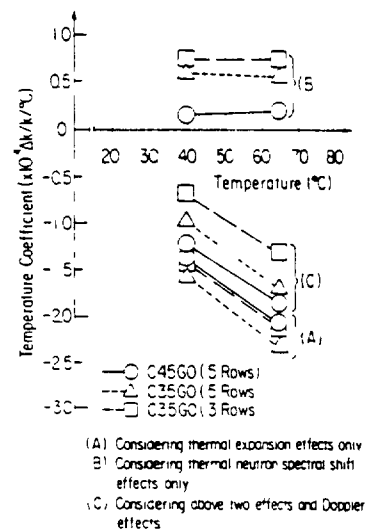


Fig. 15 Effect of Physical Processes on Reactivity

Figure 15 shows the results of the eigenvalue calculation considering two main physical processes (namely, the thermal expansion and the thermal neutron spectral shift), separately. From this figure, it is found that the thermal expansion contributed to a negative effect on reactivity for all the cores, whereas the thermal neutron spectral shift contributed to a positive one, and the overall temperature coefficients were negative. Note that the Doppler broadening effects were negligibly small on reactivity, since HEU fuel was loaded in the core.

The negative temperature coefficient caused by the thermal expansion of light-water was mainly attributed to the negative one in the core region. The thermal expansion caused the decrease in the atomic number density of light-water with the increase in temperature. This gave the negative effect on reactivity mainly by the decrease in the H/<sup>235</sup>U atomic ratio. In other words, the leakage probability of fast neutrons grew larger mainly with the decrease in macroscopic scattering cross sections of light-water.

The positive temperature coefficient caused by the thermal neutron spectral shift was mainly attributed to the positive temperature coefficient of the reflector region. The thermal neutron spectral shift caused the decrease in microscopic absorption cross sections for thermal neutrons. This caused the increase in the efficiency of neutron reflection by light-water reflector, which introduced the positive effect on reactivity in the reactor system.

## CONCLUSIONS

The results obtained through the present study are summarized as follows:

- (1) In the temperature range of 20°C up to 70°C, the temperature coefficients of reactivity were negative for all the cores under investigation. The magnitude of negative temperature coefficient was greatest in the C45G0(5 Rows) core. The next magnitude was found in the C35G0(5 Rows) core, and the lowest was in the C35G0(3 Rows) core.
- (2) The calculated effective multiplication factor agreed with the measured one within 0.5% in the C/E ratio for both the 2-D and 3-D calculations. The measured temperature effects on reactivity were approximately reproduced by both the eigenvalue and perturbation calculations.
- (3) In each core of the three, the contribution of the core region was negative to the temperature coefficient and had a negative gradient, whereas the reflector region gave an approximately constant positive contributions. The sum of these contributions made the negative temperature coefficient having a negative gradient in total.
- (4) The contribution of the reflector region became larger, as the flux peaking of thermal neutrons in reflector became larger. The flux peaking became larger, as the M/F ratio became smaller and the core shape became more slender.
- (5) In the core region, the main contribution to the temperature coefficient of reactivity was attributed to the degradation of moderation, which was caused by the decrease in macroscopic scattering cross sections due to the decrease in the atomic number density of light-water.
- (6) In the reflector region, the main contribution to the temperature coefficient was attributed to the decrease in microscopic absorption cross sections, which was caused by the increase in neutron temperature.
- (7) The results of 2-D calculations agreed well with those of 3-D calculations. This indicates that one could successfully calculate the temperature coefficient by the 2-D model, if the change in axial buckling due to the increase in reactor temperature were adequately taken into consideration.
- (8) The calculated temperature coefficients by the exact and the first order perturbation methods agreed well with each other. This indicates that, although the change in the reactor condition occurred over the whole system with the increase in reactor temperature, the first order perturbation theory could be applicable to calculate the temperature coefficient. The reasons were that the neutron flux distribution changed gently over the whole system and the negative effect on reactivity in the core region competed with the positive one in the reflector region.

## ACKNOWLEDGMENTS

The authors are grateful to Mr. Keiji Kobayashi and other staffs of the KUCA for their generous assistance in the course of experiments.

Beneficial advice and encouragement from Prof. Hiroshi Nishihara of Kyoto University, Prof. Kojiro Nishina of Nagoya University, and other members of the KUCA Technical Committee are appreciated very much.

The authors wish to thank Dr. Keichiro Tsuchihashi of JAERI, who developed the SRAC code system, for generous help on the usage of SRAC and for invaluable discussions. They are grateful to Dr. James Abbott Larrimore of GA for sending a precious copy of his doctor thesis.

A part of the present study was performed as the Cooperative Study with the JAERI titled "Verification of the SRAC Code System through the KUCA Critical Experiments".

The calculations were mainly performed at the Data Processing Center of Kyoto University and partly at the computer center of JAERI.

## REFERENCES

1. K. Kanda, S. Shiroya, M. Mori, H. Hayashi, and T. Shibata, "Study on Temperature Coefficients of HEU and MEU Cores in the KUCA", Reduced Enrichment for Research and Test Reactors, Proceedings of an International Meeting, Petten, The Netherlands, October 14-16, 1985, D. Reidel Publishing Co., Dordrecht (1986) pp. 155-164.
2. K. Tsuchihashi, Y. Ishiguro, K. Kaneko, and M. Ido, Revised SRAC Code System, JAERI 1302 (September 1986).

**CRITICAL EXPERIMENTS OF THE JMTRC MEU CORES**

*Part I*

Y. NAGAOKA, K. TAKEDA, S. SHIMAKAWA,  
S. KOIKE, R. OYAMADA

Oarai Research Establishment,  
Japan Atomic Energy Research Institute,  
Oarai-machi, Ibaraki-ken,  
Japan

**Abstract**

The JMTRC, the critical facility of the Japan Materials Testing Reactor (JMTR), went critical on August 29, 1983, with 14 medium enriched uranium (MEU, 45%) fuel elements. Experiments are now being carried out to measure the change in various reactor characteristics between the previous HEU core and the new MEU fueled core. This paper describes the results obtained thus far on critical mass, excess reactivity, control rod worths and flux distribution, including preliminary neutronics calculations for the experiments using the SRAC code.

**INTRODUCTION**

The JMTRC, a 100 W swimming pool type critical facility, has been operated as a neutronics mock-up for the JMTR (50 MW)<sup>1</sup>.

Experiments using the JMTRC and MEU (45%) fuel are being carried out in order to validate the neutronics calculation code system used for analyzing the JMTR MEU core, and to obtain nuclear characteristics for the JMTR MEU core.

Items included in the JMTRC experiment program are as follows:

For the minimum critical core,

A Critical mass

and for the full core,

B Excess reactivity

C Control rod worth

D Power calibration (Reactor noise technique)

E Space dependent mass coefficient

F  $\beta/\lambda$  (Pulsed neutron technique)

G Flux distribution and power calibration

H Shut-down margin

I Void coefficient

J Temperature coefficient (if feasible)

An application for the MEU fuel in the JMTRC was submitted to the Japanese Government in 1981. Approval of the fabrication was granted in September, 1982. Fabrication of the MEU fuel elements was performed at NUKEM in FRG, and was completed in March, 1983. The transportation of fuel elements from NUKEM to JAERI was completed in July, 1983, after the final inspections by JAERI.

The critical experiments using the MEU (45%) fuel in the JMTRC were started in August 1983. Initial criticality was achieved at 3:35 p.m. on August 29, 1983, with 14 MEU fuel elements. Items A, B, C, D, H and parts of item E and G have been finished so far.

In order to compare the MEU and HEU fuel cores, critical experiments were carried out for the HEU fuel core prior to the experiments for the MEU fuel core, with the same core configuration.

This paper describes comparison of the results of critical mass, excess reactivity, control rod worth and flux distribution, and preliminary neutronics calculations on each core.

This work is also part of the JAERI-ANL joint study concerning the RERTR program.

## GENERAL DESCRIPTION

### Core Configuration

Figure 1 shows a perspective view of the JMTRC, which is located in one of the pool wings in the JMTR containment building. The core configuration is a duplicate of the JMTR core, i.e., number and arrangement of fuel elements and control rods, the beryllium matrix etc. The core configuration for the experiments is shown in Figure 2. The fuel region consists of 7 by 5 lattice spaces, each 7.72 centimeter square. These spaces contain the 22 standard fuel elements, 5 combination fuel-poison control elements (follower fuel elements), and

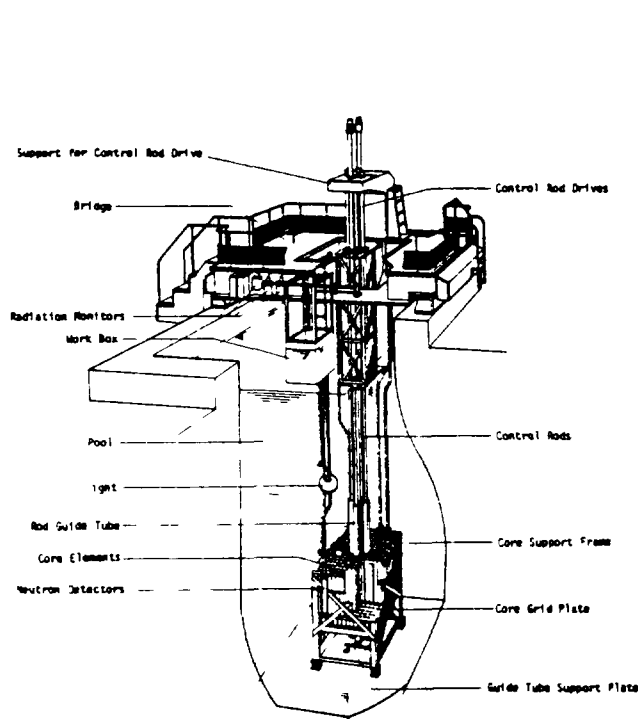


Fig. 1. The JMTRC Critical Facility.

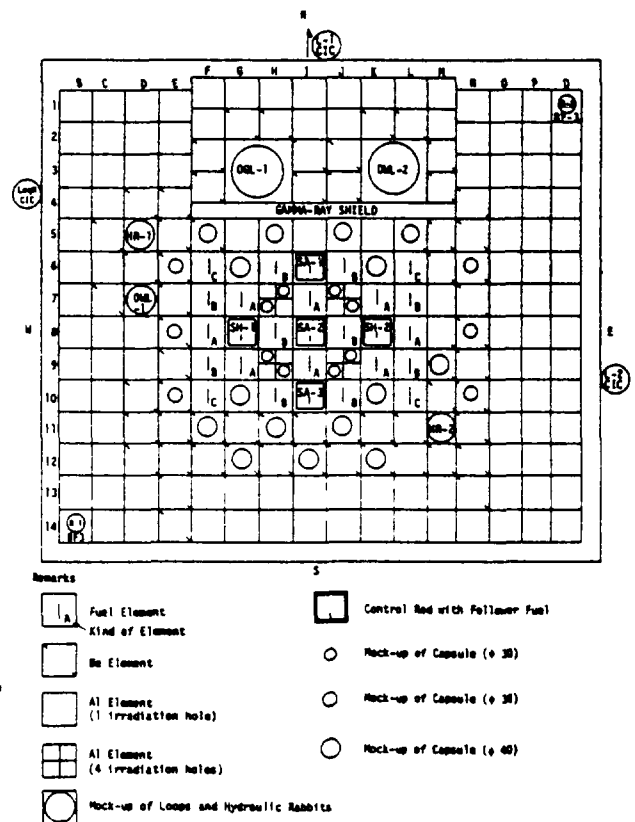


Fig. 2. Standard Core.

8 aluminum experiment holes. Surrounding the fuel region is a reflector region containing a number of beryllium and aluminum experiment holes. The core has 5 mock-up loops including two mock-ups of hydraulic rabbits. The control rods are made from borated stainless steel containing 1.6 w/o natural boron.

### Fuel Element Description

For the JMTRC experiment, 31 MEU fuel elements were fabricated without any significant change in dimensions and shape from those of the HEU fuel elements.

The  $^{235}\text{U}$  per fuel element, uranium density and number of elements fabricated are summarized in Table 1.

Table 1. MEU Fuel Element Loadings

Kind of Element	Plates per Element	Uranium Density, g/cm <sup>3</sup>	$^{235}\text{U}$ Content, g	Number Fabricated
Standard Fuel				
Element A	19	1.6	310	8
" B	19	1.4	280	10
" C	19	1.3	250	4
Special Fuel				
Element B	14-19	1.4	206-280	2
" C	14-19	1.3	184-250	2
Control Rod Fuel Section	16	1.6	205	5
			Total	31

In order to simulate the equilibrium core of the JMTR, three kinds of standard fuel elements (A, B, C) and two kind of special fuel elements (B, C) were fabricated. In the special fuel elements, the central 5 plates are removable. The standard fuel elements and the control rod fuel sections are illustrated in Attachment 1. The corresponding HEU fuel element loadings are summarized in Table 2.

Table 2. HEU Fuel Element Loadings

Kind of Element	Plates per Element	Uranium Density, g/cm <sup>3</sup>	$^{235}\text{U}$ Content, g
Standard Fuel			
Element A	19	0.7	279
" B	19	0.6	237
" C	19	0.5	195
Control Rod Fuel Section	16	0.7	195

# RESULTS

## Critical Mass

The initial critical state of the MEU fuel core was achieved with 14 standard fuel elements at 3:35 on August 29, 1983.

Figure 3 shows the initial critical core configuration in case of the MEU core, including the positions of two proportional counters, the UIC chamber, and the neutron source that were used during the approach-to-critical experiment.

The critical approach was performed by the inverse multiplication method. The standard fuel elements were loaded outwards from the core center surrounding the SA-2 control rod. Figure 4 shows the inverse multiplication curves for the MEU and HEU fuel cores. For the MEU and HEU fuel cores, the  $^{235}\text{U}$  minimum critical masses were 5077.4 g and 4746.8 g, respectively. The excess reactivities were measured to be 1.12  $\% \Delta k/k$  and 1.61  $\% \Delta k/k$  for the MEU and HEU minimum critical cores, respectively. A neutronics calculation gave excess reactivity results of 0.95  $\% \Delta k/k$  and 1.87  $\% \Delta k/k$  for the MEU and HEU fuel cores, respectively. Thus, experiment and neutronics results showed good agreement.

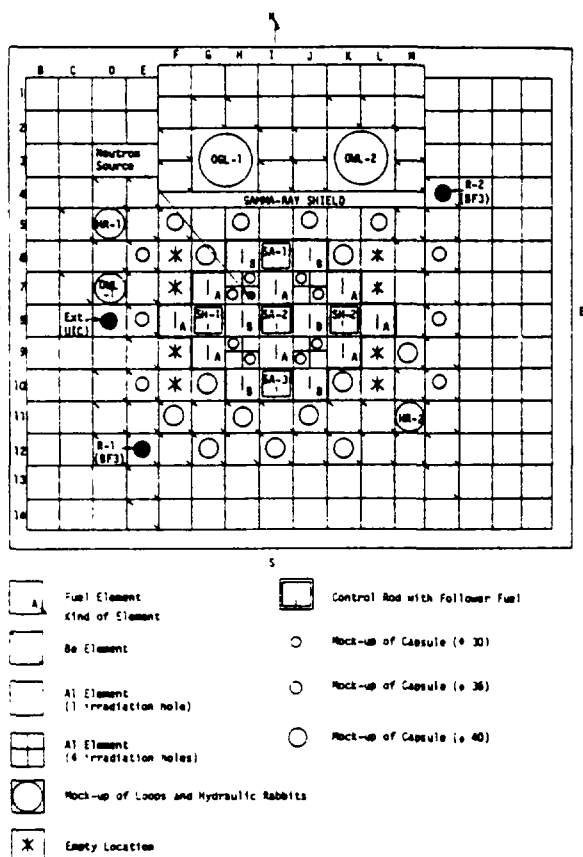


Fig. 3. Initial Critical Core.

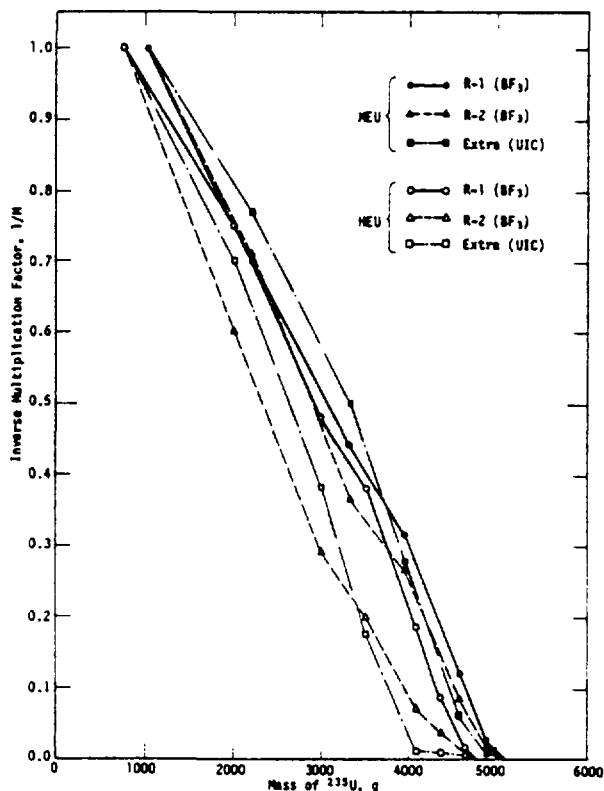


Fig. 4. Inverse Multiplication Curves.

## Rod Calibration and Excess Reactivity

An accurate calibration of the shim safety rods is most desirable in order to measure the excess reactivity available in the core. The measurements were started in the initial critical state. A fuel element was then added and the next part of the rods was calibrated. Afterwards in order to calibrate a finer stroke of the shim safety rods, a standard fuel element was replaced by a special fuel element in which a maximum of five fuel plates could be exchanged with aluminum dummy plates to reduce the  $^{235}\text{U}$  content per element. A calibration was also made on this part of stroke. This procedure was continued until the final core (22 standard fuel elements) was attained. The positive period technique was used to make the reactivity calibrations.

The differential and integral reactivity curves measured for the shim safety rods are shown in Figure 5. As can be seen in this figure, the reactivity worth in the MEU fuel core is lower and slightly sharper than in the HEU fuel core. This is attributed to the smaller thermal flux due to the larger uranium loading in the MEU fuel elements.

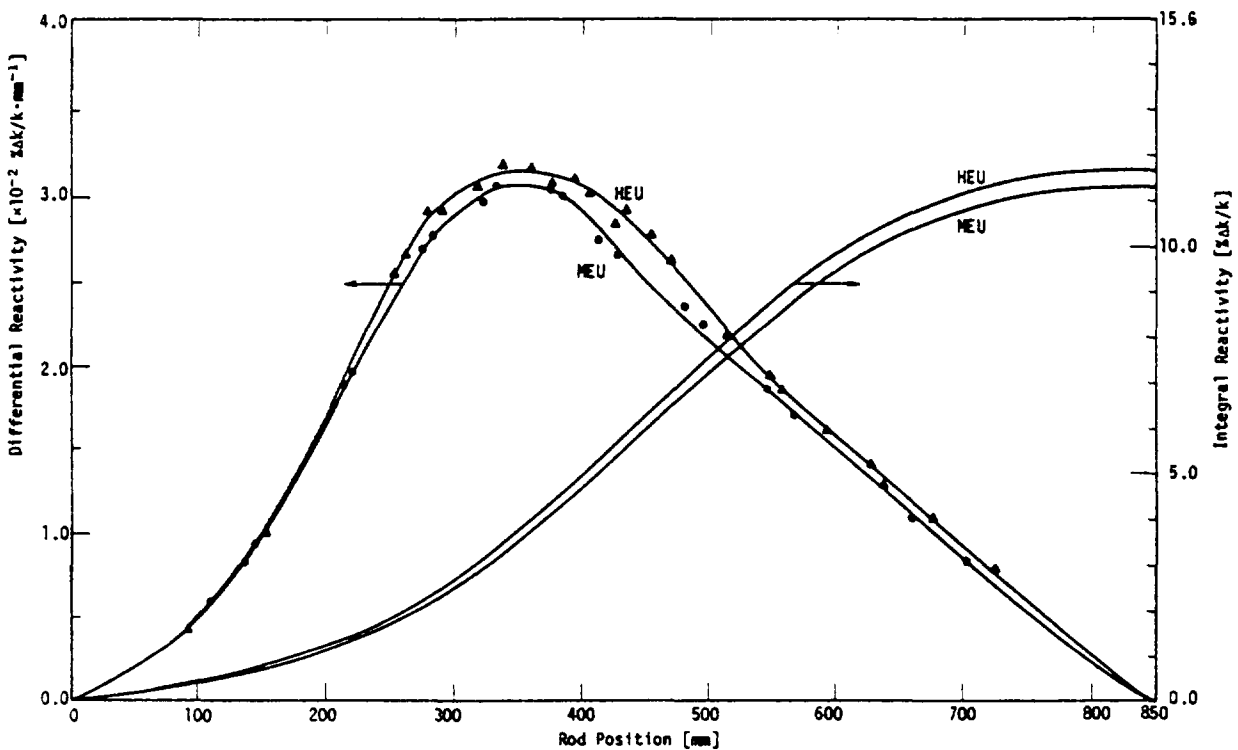


Fig. 5. Shim Safety Rods (SH-1+SH-2) Calibration Curves.

Table 3 shows the excess reactivity changes by experiments and neutronics calculations from the initial critical state to the final core configuration.

The calculations were performed using the SRAC (Standard Reactor Analysis Code)<sup>2</sup> system developed at JAERI. Four-group cross sections for each reactor cell were generated by the collision probability method. Core calculations were made using diffusion theory with the three-dimensional (XYZ) option. As shown in Table 3, calculated excess reactivity is lower than the measured one in the MEU fuel core, while higher in the HEU fuel core.

Table 3. Excess Reactivity

Number of Elements	MEU			HEU		
	Loaded U-235 (g)	Excess Reactivity Measured (% $\Delta$ k/k)	Excess Reactivity Calculated (% $\Delta$ k/k)	Loaded U-235 (g)	Excess Reactivity Measured (% $\Delta$ k/k)	Excess Reactivity Calculated (% $\Delta$ k/k)
14	5185	1.12	0.95	4629	--	--
15	5465	2.75	2.55	4866	1.61	1.87
16	5745	4.04	3.89	5103	2.91	3.23
17	6025	5.60	5.53	5340	4.56	4.92
18	6305	6.58	6.67	5577	5.63	6.09
19	6555	7.93	7.90	5772	6.95	7.27
20	6805	9.08	8.99	5967	8.05	8.33
21	7055	10.34	10.11	6162	9.28	9.42
22	7305	11.17	10.93	6357	10.04	10.23

#### Control Rod Worth

The gang rod worth of SH-1 and SH-2 (SH-1+SH-2) was obtained by integrating the gang differential reactivity curve of SH-1 and SH-2 shown in Figure 5.

On the other hand, the reactivity equivalent of the safety rods SA-1, SA-2 and SA-3 were measured simply by comparing with shim safety rods.

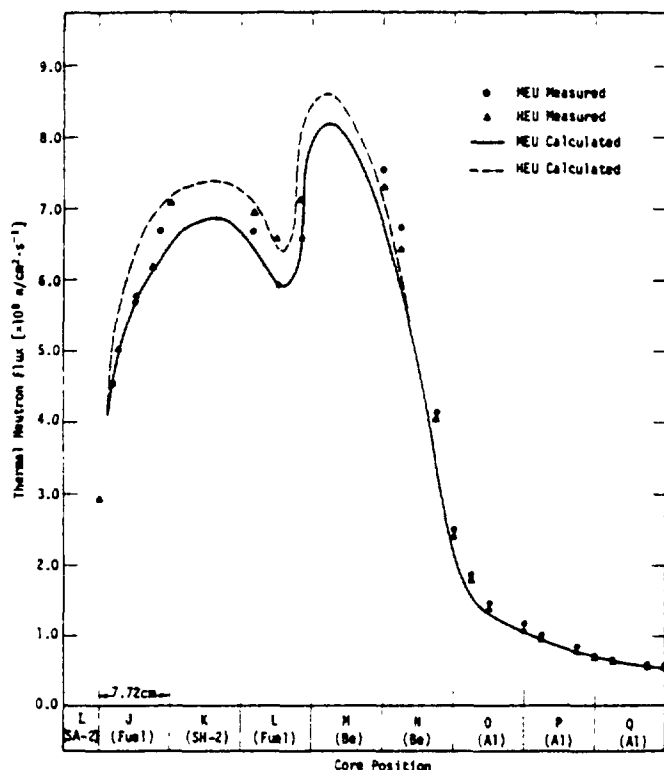
The results are shown in Table 4. As can be seen in the table, the reactivity worths for control rods SH-1, SH-2 and SA-2 in the MEU fuel core are smaller than in the HEU fuel core, while those for SA-1 and SA-3 in the MEU fuel core are larger than in the HEU fuel core. The calculated worths are in reasonable agreement with the measured worths. In the neutronics calculation, the thermal group constant for each control rod was given a value of 0.176 obtained with logarithmic differential boundary condition.

Table 4. Control Rod Worth

Rod	Measured			Calculated		
	MEU % $\Delta$ k/k	HEU % $\Delta$ k/k	$\Delta\rho$ % $\Delta$ k/k (MEU-HEU)	MEU % $\Delta$ k/k	HEU % $\Delta$ k/k	$\Delta\rho$ % $\Delta$ k/k (MEU-HEU)
SH-1 SH-2	11.30	11.72	-0.42	11.30	11.78	-0.48
SA-1	3.08	2.87	+0.21	3.19	2.99	+0.20
SA-2	5.85	6.00	-0.15	6.26	6.35	-0.09
SA-3	3.38	3.07	+0.31	3.42	3.18	+0.24

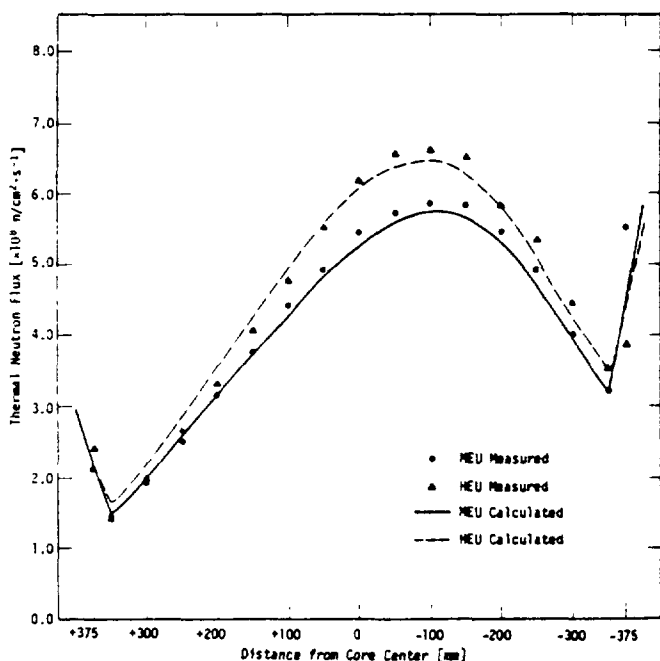
## Neutron Flux Distribution

The dysprosium foils for measuring low energy neutrons and gold foils for absolute measurements, were used for the measurement of thermal neutron flux distribution by the foil activation technique. Gold foils, with and without a cadmium cover were activated in the core. For the measurement in the fuel elements, acrylic plates on which the foils were taped, were inserted between the fuel plates. For the measurement in the reflector region, foils were taped on the surface of the elements, plugs or mock-up experiments.



The calculated neutron flux distribution was normalized at the edge of the core.

Fig. 6. The Horizontal Thermal Neutron Flux Distribution (Row 8).



The calculated neutron flux distribution was normalized at an axial position of -350 mm.

Fig. 7. The axial Thermal Neutron Flux Distribution (J-10).

The foils were irradiated for 1 hour at approximately 90 watts and taken from the core for counting. The control rod positions during the operation for irradiation of the foils were: SA-1, SA-2: up, SA-2: down, SH-1, 2: 428 mm (MEU), 504 mm (HEU).

The horizontal neutron flux distributions are shown in Figure 6. Measurements were made at an axial position of 100 mm below the mid-height of the core. Figure 6 shows the distribution along Row 8 from the core center in an easterly direction. The calculated neutron flux distribution was normalized at the edge of the core. The results of the measured thermal neutron flux distributions show a decrease by about 8 to 12 % in the fuel region in the MEU fuel core.

The axial neutron flux distributions are shown in Figure 7, for the fuel element of position J-10. The calculated neutron flux distribution was normalized at the edge of the fuel element. It can be seen that the measured neutron flux is about 11 % lower at the peak point (-100 mm from core center) in the MEU fuel core than in the HEU fuel core. The axial thermal neutron flux peaking factor (peak flux/average flux) for a fuel element at position J-10 were 1.41 and 1.48 for the MEU and HEU fuel cores, respectively.

Measured neutron flux level was normalized to the maximum power of 100 W. The reactor power was determined with activation of fission foils (93 % enriched uranium alloy), irradiated at the same time in each fuel element.

#### CONCLUSION

The MEU fueled core with the larger uranium loading, was validated by the JMTRC experiments resulting in the features as follows:

- The excess reactivity was sufficient for the JMTR cycle length with 11.17 % $\Delta$ k/k.
- The shim safety rod worth (SH-1+SH-2) is 0.42 % $\Delta$ k/k lower than in the HEU fuel core.
- The thermal neutron flux distributions are 8 to 12 % lower than in the HEU fuel core in the fuel region.
- The axial thermal neutron flux peaking factor (position J-10) were 1.41 and 1.48 for the MEU and HEU fuel cores, respectively.

The results of the neutronics calculations using the SRAC system were in fairly good agreement with experiments. More detailed analysis is underway to validate the neutronics calculation method.

#### REFERENCES

1. Division of JMTR Project, "JMTR Irradiation Handbook," JAERI-M 83-053, Oarai Research Establishment, JAERI (1983)
2. K. Tsuchihashi, H. Takano, K. Horikami, Y. Ishiguro, K. Kaneko, and T. Hara, "SRAC: JAERI Thermal Reactor Standard Code System for Reactor Design and Analysis," JAERI-1285 (Jan., 1983)



CRITICAL EXPERIMENTS OF THE JMTRC MEU CORES

Part II

S. SHIMAKAWA, Y. NAGAOKA, S. KOIKE,  
K. TAKEDA, B. KOMUKAI, R. OYAMADA  
Oarai Research Establishment,  
Japan Atomic Energy Research Institute,  
Oarai-machi, Ibaraki-ken,  
Japan

Abstract

Critical experiments in the Japan Materials Testing Reactor Critical facility (JMTRC) with medium-enrichment-uranium (MEU, 45%) fuel elements have been carried out. The purposes of the experiments are to obtain nuclear characteristics and to validate neutronics calculation performed by SRAC code system used for analyzing the JMTR MEU core.

This paper describes the results of experiments, such as reactor kinetics parameters, shut-down margin and void coefficient following the previous paper presented at RERTR meeting, 1983. The calculated results are in satisfactory agreement with the measured results. It is indicated that the changes of nuclear characteristics due to the core conversion from the HEU to the MEU core give no serious problem from the viewpoint of reactor safety.

INTRODUCTION

The Japan Materials Testing Reactor Critical facility (JMTRC), a 100 W swimming pool type critical facility and moderated and cooled by light water, has been operated as neutronics mock-up for JMTR (Japan Materials Testing Reactor, 50MW tank type).<sup>1)</sup>

Critical experiments have been carried out in the JMTRC with medium-enrichment-uranium (MEU, 45%) fuel elements. The purposes of the experiments are to obtain nuclear characteristics and to validate neutronics calculations performed by SRAC code system<sup>2)</sup> used for analyzing the JMTR MEU core. Some results of the experiments, such as critical mass, excess reactivity, control rod worths and flux distribution were presented at the international meeting of RERTR, 24-27 October, 1983, Tokai-mura.<sup>3)</sup>

This paper describes the results of the experiments such as reactor kinetics parameters  $\beta_{eff}/\lambda_p$  ( $\beta_{eff}$ : effective delayed-neutron fraction and  $\lambda_p$ : prompt-neutron life time), shut-down margin and void coefficient following the previous paper. In order to compare nuclear characteristics of the MEU and previous high-enrichment-uranium (HEU, 90%) core, the experiments were also carried out in the HEU core prior to the experiments in the MEU core with the same configuration. The validity of the neutronics calculations is confirmed by the experiments, in both the MEU and HEU core.

## CORE CONFIGURATION

The core configuration is a duplicate of the JMTR core, i.e., number and arrangement of fuel elements and control rods, the beryllium matrix etc, as shown in Figure 1. The fuel region consists of 7 by 5 lattice spaces, each 7.72 centimeter square. These spaces contain the 22 standard fuel elements, 5 control rods with follower fuel sections, and 8 aluminum experiment holes. The horizontal cross sections of MEU fuel elements are illustrated in Figure 2. Surrounding the fuel region is a reflector region containing a number of beryllium and aluminum experiment holes. The core has 5 mock-up loops including two mock-ups of hydraulic rabbits. The control rods are made from borated stainless steel containing 1.6 wt-% national boron.

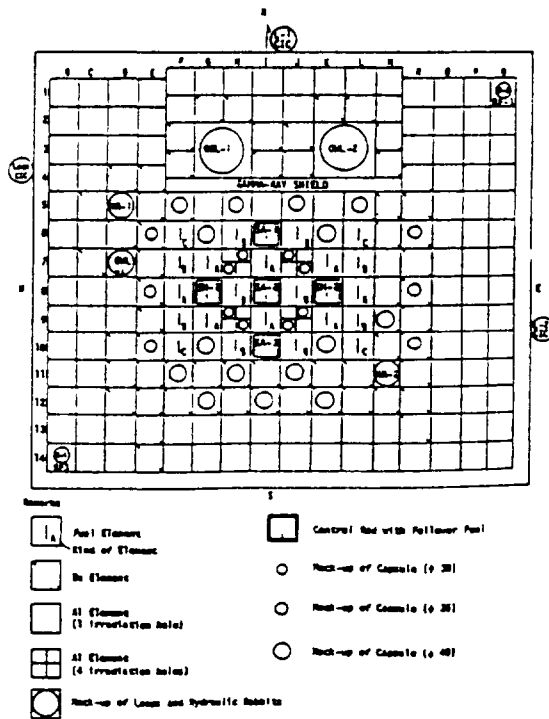


Fig. 1 JMTRC Standard Core

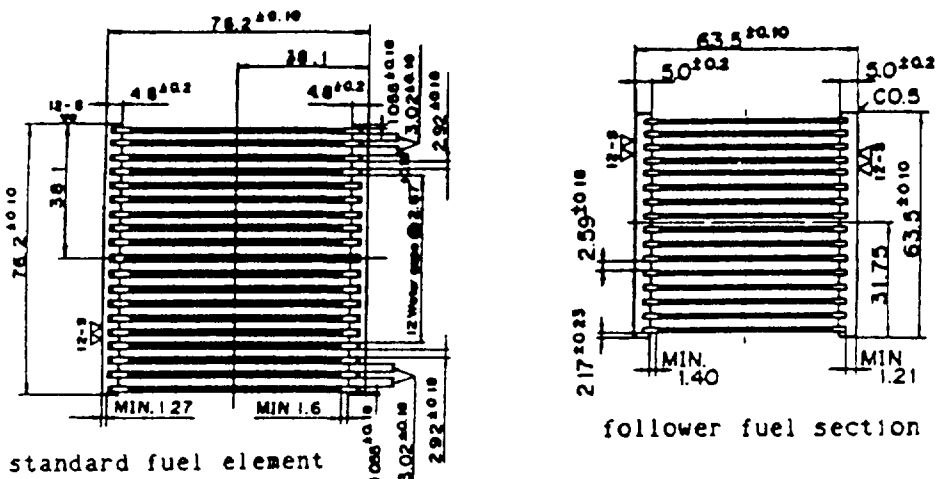


Fig. 2 Horizontal Cross Section of  
JMTRC MEU Fuel Elements

For the JMTRC experiment, 31 MEU fuel elements were fabricated without any significant change in dimensions and shapes from those of the HEU fuel elements. The uranium density of fuel elements and U-235 per element are summarized in Table 1. The JMTRC fuel elements were fabricated as three kinds of standard fuel elements (A, B, C), in order to simulate the equilibrium core of the JMTR.

Table 1. JMTRC Fuel Element Loading

Kind of Element	Plates per Element	Uranium Density, g/cm <sup>3</sup>	<sup>235</sup> U Content, g
<u>M E U</u>			
Standard fuel element A	19	1.6	310
" B	19	1.4	280
" C	19	1.3	250
Fuel follower element	16	1.6	205
<u>H E U</u>			
Standard fuel element A	19	0.7	279
" B	19	0.6	237
" C	19	0.5	195
Fuel follower element	16	0.7	195

#### REACTOR KINETICS PARAMETERS ( $\beta_{eff}/\lambda_p$ )

The kinetics parameters ( $\beta_{eff}/\lambda_p$ ) were measured by the pulsed neutron technique, as a ratio between effective delayed-neutron fraction ( $\beta_{eff}$ ) and prompt-neutron life time ( $\lambda_p$ ), i.e., prompt-neutron decay constant at critical ( $\alpha_c$ ).

The outline of the experiment system using the pulsed neutron technique is shown in Figure 3. An instantaneous pulse of neutrons, which is generated at an accelerator assembly, is injected into a subcritical core and ensuing flux of neutrons is measured by BF3 counter. And the decay constant at a subcritical ( $\alpha$ ) is defined as the time constant of a fundamental prompt-neutron mode, as shown in Figure 4. The  $\alpha$  was measured at various control rod positions. And  $\alpha_c$  was obtained by extrapolating the data of  $\alpha$  to that at the control rod position at criticality. The accelerator assembly was located at 4 lattice spaces (G-3, G-4, H-3 and H-4) in the core shown in Figure 2. The BF3 counter was set up at K-12, and the measurements were also carried out when the counter was set up at F-12, in order to check whether the data depended on counter positions in the core.

Figure 5 shows the  $\alpha$  versus control rod position from critical position. The reactor kinetics parameters ( $\beta_{eff}/\lambda_p$ ) measured are 111 sec<sup>-1</sup> in the MEU core and 103 sec<sup>-1</sup> in the HEU core. The value in the MEU core is about 7 % larger than that in the HEU core.

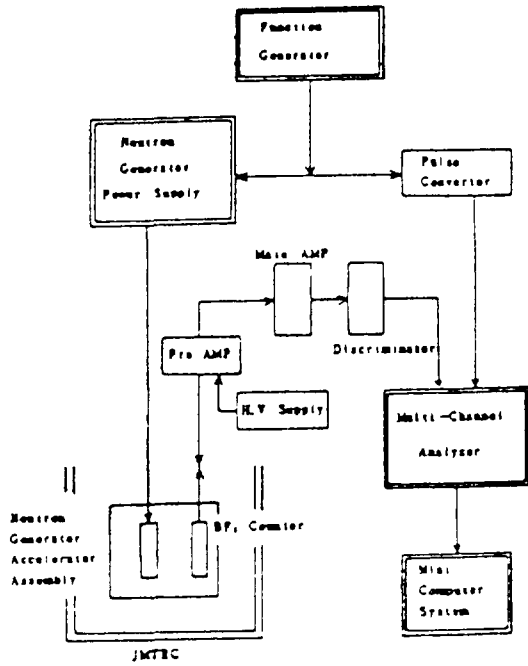


Fig. 3 Outline of Pulsed Neutron Technique System

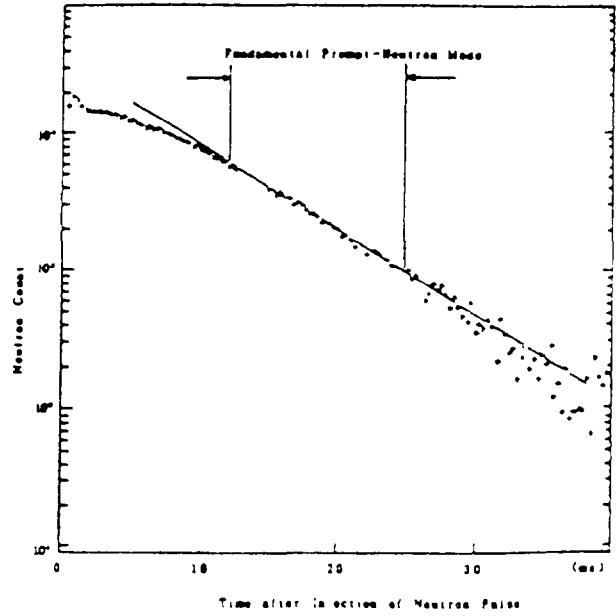


Fig. 4 Counter Response versus Time after Injection of Neutron Pulse into Subcritical Core

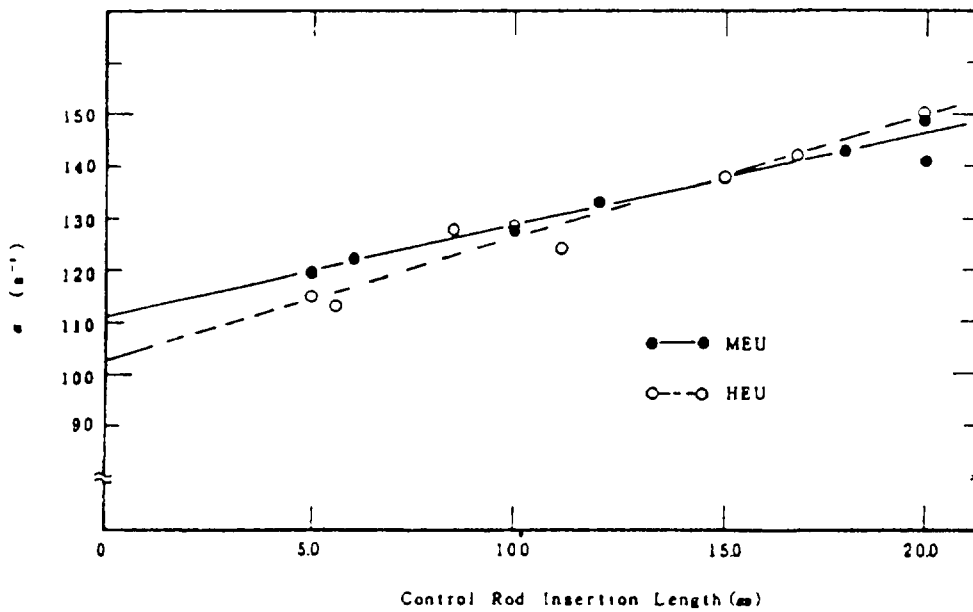


Fig. 5 Decay Constant ( $\alpha$ ) versus Control Rod Position from Critical Position

### SHUT-DOWN MARGIN

The shut-down margin was measured by two different methods : the pulsed neutron technique outlined above and the rod drop method. The measurements by the pulsed neutron technique were carried out at three different locations of the BF3 counter, i.e.,

F-12, K-12 and C-14, in the core shown in Figure 1. And the shut-down margin is determined by following equation,<sup>4)</sup>

$$\rho = (1 - \alpha/\alpha_c) / (1/\beta_{eff} - \alpha/\alpha_c)$$

where  $\rho$  is reactivity and  $\beta_{eff}$  is effective delayed-neutron fraction. On the other hand, in the measurements by the rod drop method, BF3 counters (R-1, R-2) were located at B-14 and Q-1, in the core shown in Figure 1.

The data by two methods are shown in Table 2. In the measurements of the shut-down margin, since the pulsed neutron technique is less dependent on the BF3 counter positions than the rod drop method, the pulsed neutron technique is superior than the rod drop method. Therefore the data by pulsed neutron technique have been used as evaluated data. The shut-down margins obtained are 14.0 % $\Delta$ k/k in the MEU core and 16.4 % $\Delta$ k/k in the HEU core. The margin in the MEU core is about 2 % $\Delta$ k/k smaller than in the HEU core, but is still enough as the criterion is 10 % $\Delta$ k/k in the JMTRC and the JMTR.

Table 2. Shut-Down Margin

Method & BF3 Counter Position	M E U % $\Delta$ k/k	H E U % $\Delta$ k/k	$\Delta\rho$ % $\Delta$ k/k (MEU-HEU)
Rod drop method			
B - 14	11.0	12.5	-1.5
Q - 1	13.0	15.5	-2.5
Pulsed neutron technique			
K - 12	13.7	16.8	-3.1
F - 12	13.4	16.1	-2.7
C - 14	14.7	16.4	-1.7
Average	14.0	16.4	-2.4

### VOID COEFFICIENT

In the measurement of void coefficient, the void was simulated by inserting aluminum plates into the core. It has been confirmed by the neutronics calculations that a discrepancy between aluminum and void effects is small enough to be ignored. In this experiment ten aluminum plates ( 2-mm-thick, 60-mm-width, and 840-mm-height ) were inserted vertically into water-gaps of the standard fuel element.

The results of void coefficient measured at various positions are shown in Table 3. As shown in Table 3, the locations of the fuel element with aluminum plates were symmetric with respect to the column "I" in the core shown in Figure 1. There is almost no difference in the void coefficient between the MEU and HEU core.

Table 3 Void Coefficient

Location of Fuel Elements with Aluminum Plates	M E U	H E U
	% $\Delta k/k$ /void-%	% $\Delta k/k$ /void-%
H - 8 & J - 8	$-0.97 \times 10^{-2}$	$-1.02 \times 10^{-2}$
G - 9 & K - 9	$-1.39 \times 10^{-2}$	$-1.55 \times 10^{-2}$
F - 8 & L - 8	$-1.59 \times 10^{-2}$	$-1.80 \times 10^{-2}$
F - 10 & L - 10	$-0.72 \times 10^{-2}$	$-0.68 \times 10^{-2}$
Averaged value	$-1.15 \times 10^{-2}$	$-1.22 \times 10^{-2}$

### VALIDITY OF NEUTRONICS CALCULATIONS

The neutronics calculations were performed using the SRAC code system, which was developed in Japan Atomic Energy Research Institute (JAERI). In this study, the lattice calculation to generate group constants was performed by collision probability method, and the core calculation was performed by 3-D diffusion code. The kinetic parameters,  $\beta_{eff}$  and  $\rho_p$ , were calculated by means of the perturbation theory. The group energy structures were the 4 groups (upper energy boundaries : 10 MeV, 1.0 MeV, 0.83 KeV, 0.6823 eV).

Table 4 shows the results of the measured and calculated excess reactivity, the control rod worths, the shut-down margin and the void coefficient. As shown in Table 4, the calculated excess reactivities are 0.3 % $\Delta k/k$  and 0.6 % $\Delta k/k$  higher than the measured ones in the MEU and HEU core, respectively. The calculated control rod worths agree with the measured ones within 0.4 % $\Delta k/k$  per control rod. The calculated shut-down margins are 1.3 % $\Delta k/k$  and 1.8 % $\Delta k/k$  higher than the measured ones in the MEU and HEU core, respectively. The void coefficient agrees by 0.001 % $\Delta k/k$ /void-% between the measured and the calculated values.

Table 5 shows the results of measured and calculated reactor kinetics parameters. As shown in Table 5, the calculated  $\beta_{eff}/\rho_p$  are 13-15% larger than the measured ones. And the changes of the parameters due to the core conversion from HEU to MEU fuel are about 6% decrease in the  $\rho_p$  and no significant change in the  $\beta_{eff}$ . The reason why the prompt-neutron life time is smaller in the MEU core than that in the HEU core is mainly because of increased uranium-235 loading in former core.

Table 6 shows the neutron flux changes due to the core conversion. The calculated thermal neutron flux (<0.68eV) is in satisfactory agreement with measured one, and the decrease of thermal neutron flux agrees with the measured ones within 2-5%. And the changes of calculated fast neutron flux (>1.0MeV) due to the core conversion, are almost zero in all regions.

Table 4 Calculated Excess Reactivity, Control Rod Worths, Shut-Down Margin and Void Coefficient, Comparing with Measured Ones

	M E U			H E U		
	Measured	Calculated	$\Delta\rho$ (Cal-Meas)	Measured	Calculated	$\Delta\rho$ (Cal-Meas)
Excess reactivity % $\Delta k/k$	11.2	11.5	+0.3	10.0	10.6	+0.6
Control rod worths % $\Delta k/k$						
SH-1 & SH-2	11.3	11.7	+0.6	11.7	12.5	+0.8
SA-1	3.1	2.9	-0.2	3.2	3.1	-0.1
SA-2	5.9	6.0	+0.1	6.3	6.4	+0.1
SA-3	3.4	3.2	-0.2	3.4	3.3	-0.1
Shut down margin % $\Delta k/k$	14.0	15.3	+1.3	6.4	18.2	+1.8
Void coefficient % $\Delta k/k$ / void %	-0.012	-0.013	-0.001	-0.012	-0.013	-0.001

Table 5. Calculated Kinetics Parameters, Effective Delayed-Neutron Fraction  $\beta_{eff}$  and Prompt-Neutron Life Time  $\lambda_p$ , Comparing with Measured Ones

	M E U			H E U		
	Measured	Calculated	C/M	Measured	Calculated	C/M
$\beta_{eff}/\lambda_p, \text{sec}^{-1}$	111	125	1.13	103	118	1.15
$\beta_{eff}$	-	0.00766	-	-	0.00766	-
$\lambda_p, \mu\text{sec}$	-	61.1	-	-	64.8	-

Table 6 Calculated Thermal Flux Changes by Core Conversion from HEU to MEU Fuel, Comparing with Measured Ones

	Measured	Calculated
Thermal neutron flux		
Fuel region	-8 ~ -12 %	-8 ~ -13 %
Be reflector region	-1 ~ -3 %	0 ~ -3 %
Fast neutron flux		
Fuel and Be reflector region		+2 ~ -2 %

## CONCLUSION

The MEU core with the larger uranium loading, is validated by the JMTRC experiments resulting in the feature as follows.

The reactor kinetics parameters  $\beta_{eff}/\lambda_p$  is  $112 \text{ sec}^{-1}$  in the MEU core, which is about 7% higher than in the HEU core.

The shut-down margin is  $14.0 \text{ \%}\Delta k/k$  in the MEU core, which is  $2.0\text{-}3.0\text{ \%}\Delta k/k$  smaller than that in the HEU core.

The void coefficient is  $-0.012 \text{ \%}\Delta k/k/\text{void-\%}$  in the MEU core. There is no significant difference in the void coefficient between the HEU and the MEU core.

It is indicated that the changes of nuclear characteristics due to the core conversion from the HEU to MEU core give no serious problem from the viewpoint of reactor safety.

Concerning the validity of the neutronics calculations, it is confirmed that the calculated results are in satisfactory agreement with the measured results, i.e., the differences are:  $0.3\text{-}0.6 \text{ \%}\Delta k/k$  in excess reactivity,  $0.4 \text{ \%}\Delta k/k$  in control rod worths,  $1.3\text{-}1.8 \text{ \%}\Delta k/k$  in shut-down margin,  $0.001 \text{ \%}\Delta k/k/\text{void-\%}$  in void coefficient,  $13 - 15 \text{ \%}$  in kinetics parameters and  $2 - 5 \text{ \%}$  in flux distribution.

## REFERENCES

1. Division of JMTR project, "JMTR Irradiation Handbook," JAERI-M 83-053, Oarai Research Establishment, JAERI(1983)
2. K. Tsuchihashi, H. Takano, K. Horikami, Y. Ishiguro, K. Kaneko and T. Hara, "SRAC: JAERI Thermal Reactor Standard Code System for Reactor Design and Analysis," JAERI-1285(1983)
3. Y. Nagaoka, K. Takeda, S. Shimakawa, S. Koike and R. Oyamada, "Critical Experiments of JMTRC MEU Cores," RERTR Proceeding (1983)
4. B.E. Simmon and J.S. King, Nucl. Sci. Eng. 3, P.595 (1958)

## Appendix H-4

# COMPARISON OF CALCULATIONS WITH MEASUREMENTS

### Appendix H-4.1

#### COMPARISON OF CALCULATIONS WITH MEASUREMENTS IN THE FNR FULL-CORE LEU DEMONSTRATION REACTOR

FORD NUCLEAR REACTOR/UNIVERSITY OF MICHIGAN  
Ann Arbor, Michigan

ARGONNE NATIONAL LABORATORY  
Argonne, Illinois

United States of America

#### Abstract

As part of the U.S. RERTR Program, a full core demonstration with LEU fuel began in December 1981 in the 2 MW Ford Nuclear Reactor (FNR) at the University of Michigan. This appendix compares some of the experimental data with analytical calculations based, for the most part, on three dimensional diffusion theory. The critical configuration, control rod worths, axial rhodium reaction rate profiles and thermal flux distributions have been calculated and compared with measurements.

#### I. Introduction

As part of the U.S. RERTR Program, a full-core demonstration with LEU fuel began in December 1981 in the 2 MW Ford Nuclear Reactor (FNR) at the University of Michigan. The LEU standard and control fuel elements were manufactured by NUKEM and by CERCA using specifications prepared by ANL and the University of Michigan (See Volume 2, Appendix J-4). The core went critical with 23 fuel elements on December 8, 1981.

Since that time a substantial data base of experimental results for LEU cores has been accumulated by the University of Michigan FNR staff. This appendix (Ref. 1) compares some of the experimental data with analytical calculations based, for the most part, on three-dimensional diffusion theory. The critical configuration, control rod worths, axial rhodium reaction rate profiles and thermal flux distributions have been calculated and compared with measurements.

The experiment program is still in progress and includes further measurements on a full core of LEU elements and on mixed cores of LEU and HEU elements.

#### II. The "As-Built" Fuel Element Parameters

Table 1 shows the "as-built" parameters averaged over the 20 standard fuel elements supplied by CERCA, and over the 23 standard elements and 11 control elements supplied by NUKEM. Compositions of the aluminum alloys used by both manufactures are shown in Tables 2 and 3. Table 4 shows the "as-built" fuel element data used in the ANL calculations.

### III. Critical Configuration

Figure 1 shows the FNR critical configuration with 23 fresh LEU fuel elements. The 18 plate standard FNR LEU fuel elements were fabricated by NUKEM and CERCA and contain about 167 g  $^{235}\text{U}$  per element. Control elements contain 9 fuel plates. For this critical assembly the  $^{235}\text{U}$  mass was 3512.82 g. With the shim safety rods (A, B and C) fully withdrawn and the control rod fully inserted, the excess reactivity was measured to be 0.067%. The worth of the hollow stainless steel control rod was found to be 0.383% so that the excess reactivity of the cold, clean LEU core was about 0.45%.

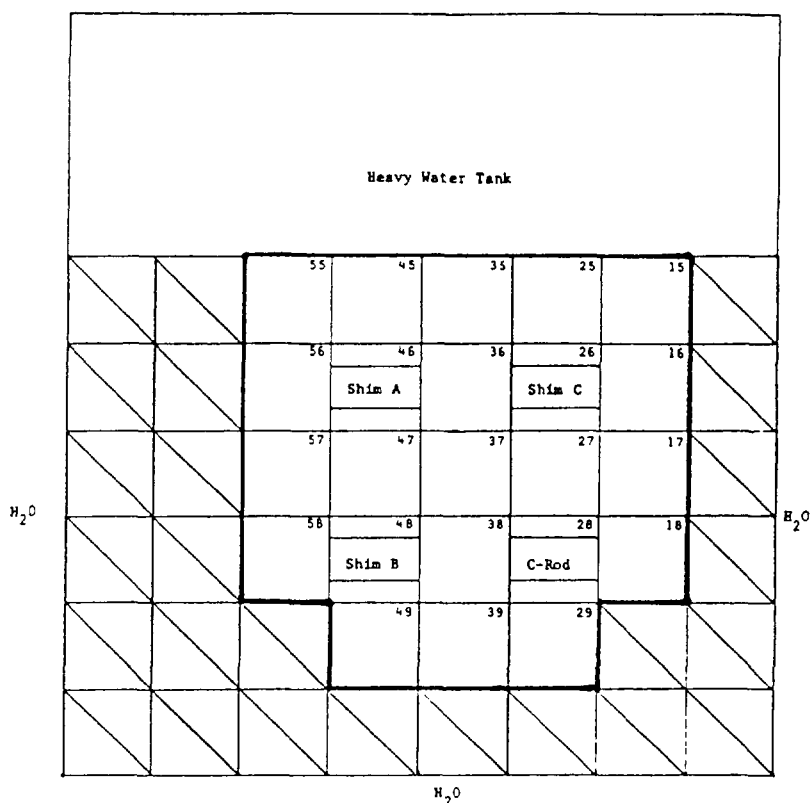


FIG. 1. FNR initial LEU critical configuration (Dec. 8, 1981).

Five-group cross sections, based on the ENDF/B Version IV data base, were generated for each reactor region by the EPRI-CELL code (Ref. 2). These multigroup cross section generation methods are described in IAEA-TECDOC-233 (Ref. 3). Table 5 shows the energy structure of the standard five-group set.

Using these cross sections, two- and three-dimensional diffusion calculations were performed to evaluate the eigenvalue for the 23-element, cold, clean LEU core. For these calculations all rods are withdrawn and each fuel element is represented by three regions -- a fuel region sandwiched between two side plate regions. Effects from the vertical H<sub>2</sub>O-filled tubes which penetrate part way into the D<sub>2</sub>O tank and from neutron leakage through the beam tubes have been ignored in these calculations. Table 6 summarizes the eigenvalues calculated from two- and three-dimensional models for both course and fine mesh structures. The XYZ fine mesh calculation gives an excess reactivity of 0.37%, 0.08% less than the 0.45% measured value. Our experience with HEU cores has been to slightly overpredict the eigenvalue, but for this LEU core we have underpredicted  $k_{eff}$ .

Table 1. "As-Built" Data for FNR Reactor LEU Fuel Elements

	NUKEM Standard Elements	CERCA Standard Elements	NUKEM Control Elements
Number of Elements	23	20	11
No. Fuel Plates	18	18	9
Fuel Meat Length, mm	600.0*	595 ± 5	600.0*
Fuel Meat Width, mm	60.0*	59.5 ± 0.1	60.0*
Fuel Meat Thickness, mm	0.779 ± 0.009	0.721 ± 0.011	0.779 ± 0.009
Water Gap, mm	2.942	2.963	2.942
Cladding Thickness, mm	0.390 ± 0.010	0.408 ± 0.012	0.390 ± 0.010
Plate Thickness, mm	1.558 ± 0.019	1.537 ± 0.009	1.558 ± 0.019
Side Plate Width, mm	79.92	80.10	79.93
Side Plate Thickness, mm	4.75	4.78	4.75
Side Plate to Side Plate Inside Dimension, mm	65.17	65.04	65.20
Fuel Plate Curvature, mm	140.0*	140.0*	140.0*
Special Guide Plate Width, mm			65.20
Special Guide Plate Thickness, mm			2.87
Fuel Meat Composition (wt%)			
Al	57.90	55.05	57.90
Fe	0.10	0.09	0.10
U	42.00*	44.86 ± 0.01	42.00*
Uranium Composition (wt%)			
<sup>233</sup> U		<0.01	
<sup>234</sup> U	0.13	0.15	0.13
<sup>235</sup> U	19.90	19.81	19.92
<sup>236</sup> U	0.17	0.22	0.14
<sup>238</sup> U	79.80	79.82	79.81
Mass <sup>235</sup> U/ Fuel Element, g (± 1%)	167.02	167.19	83.27
U Density in Fuel Meat, g/cm <sup>3</sup>	1.66 ± 0.04	1.84 ± 0.05	1.66 ± 0.04

\*Assumed Values

Table 2. Chemical Composition of CERCA Aluminum Alloys

	AG 3 N.E. Cladding and Frame	AG 3 N.E. Side Plate	UAl <sub>x</sub> -Al Fuel Meat
Density (g/cm <sup>3</sup> )	2.7	2.7	
Composition (wt%)			
Li	<0.001	<0.001	
B	<0.001	<0.001	
N			0.13
O			0.20
Mg	2.76	2.83	
Al	96.78	96.73	57.53
Si	0.12	0.11	0.05
Ti	0.01	0.01	
Cr	0.01	0.01	
Mn	0.04	0.04	
Fe	0.26	0.26	0.09
Cu	0.0039	0.0047	0.001
Zn	0.01	0.01	0.003
Cd	<0.001	<0.001	
U			42.00*

Table 3. Chemical Composition of NUKEM Aluminum Alloys

	Al-Mg-1 Cladding	Al-Mg-2 Frame	Al-Mg-Si-1 Side Plate	Al-Mg-Si-1 Guide Plate	UAl <sub>x</sub> -Al Fuel Meat
Density (g/cm <sup>3</sup> )	2.69	2.68	2.70	2.70	
Composition (wt%)					
B			0.0021		
Mg	0.895	1.95	0.74	0.72	
Al	98.66	97.53	97.26	97.44	57.875
Si	0.13	0.17	0.90	0.92	0.04
Ti		0.04	0.02	0.01	0.005
Cr	0.0055	0.01		0.01	
Mn	0.0155	0.13	0.72	0.69	
Fe	0.28	0.15	0.34	0.19	0.07
Co	0.001	0.003			
Cu	0.0045	0.005	0.01	0.01	0.004
Zn	0.006	0.01	0.01	0.01	0.006
U					42.00*

\* Assumed value.

Note: Impurities less than 10 ppm = 10 µg/g neglected.

Table 4. Data for FNR Fuel Elements Used in ANL Calculations

DIMENSIONS AND URANIUM COMPOSITION

Data for NUKEM standard and control elements listed in Table 1.

VOLUME FRACTIONS  
(Based on 81.00 mm x 77.09 mm FNR Grid Spacing)

STANDARD ELEMENT		CONTROL ELEMENT	
<u>Fueled Region</u>		<u>Fueled Region</u>	
Fuel Meat	0.1479	Fuel Meat	0.0739
Clad	0.1214	Clad	0.0607
H <sub>2</sub> O	<u>0.5090</u>	H <sub>2</sub> O	<u>0.2545</u>
	0.7783		0.3891
<u>Non-Fueled Region</u>		<u>Non-Fueled Region</u>	
H <sub>2</sub> O	0.0796	H <sub>2</sub> O	0.4191
Structure	<u>0.1421</u>	Structure	<u>0.1918</u>
	0.2217		0.6109

STANDARD ELEMENT MASSES, g

Material	<u>Fueled Region</u>			<u>Non-Fueled Region</u>		Total Mass
	<u>Fuel Meat</u>	<u>Clad</u>	<u>H<sub>2</sub>O</u>	<u>Structure</u>	<u>H<sub>2</sub>O</u>	
H <sub>2</sub> O			1901.5		297.4	2198.9
Mg		11.0		13.7		27.4
Al	1158.8	1207.3		1398.6		3764.7
Si	0.8	1.6		9.7		12.1
Cr		0.1		0.0		0.1
Mn		0.2		7.6		7.8
Fe	1.4	3.4		4.3		9.1
<sup>234</sup> U	1.1					1.1
<sup>235</sup> U	167.3*					167.3*
<sup>236</sup> U	1.4					1.4
<sup>238</sup> U	671.1					671.1
U	841.0					841.0

\*Average <sup>235</sup>U mass for 5 CERCA and 14 NUKEM standard elements chosen by FNR for the 19 standard elements in the 23 element critical core.

Table 5. Energy Boundaries of Standard Five Group Structure

<u>Group</u>	<u>Upper Energy Bound</u>
1	10.0 MeV
2	0.8208 MeV
3	5.531 keV
4	1.855 eV
5	0.625 eV

Table 6. Diffusion Theory Calculations for the FNR LEU Cold Clean Critical Configuration

<u>Model</u>	<u>Mesh in Standard Fuel Element</u>	<u>k<sub>eff</sub></u>
2D-XY	$N_x N_y = 6 \times 6$	1.00066
2D-XY	$N_x N_y = 10 \times 12$	1.00292
3D-XYZ	$N_x N_y = 6 \times 6$	1.00193
3D-XYZ	$N_x N_y = 10 \times 12$	1.00371
	Measured Value:	1.0045

#### IV. Shim Safety Rod Worths

The FNR shim safety rods are made from borated stainless steel containing 1.5 w/o natural boron. Each of the solid rods has a 3.470 cm × 5.668 cm cross section with rounded ends having a radius of curvature of 1.099 cm. They are described in Ref. 4.

To calculate the rod worths, group-dependent internal boundary conditions (defined as current-to-flux ratios) were applied at the surface of the absorber in diffusion calculations. These boundary conditions were evaluated from P<sub>1</sub> S<sub>8</sub> transport theory calculations.

Cross sections for the outer, middle and inner regions of the rod were generated by the EPRI-CELL code in cylindrical geometry. Since the rod is essentially black to thermal neutrons, the outer radius of the cylindrical rod was chosen so as to preserve the surface area of the actual rod. The outer region of the rod was 1 mm thick and the middle layer 3 mm thick.

Current-to-flux ratios were evaluated in the  $P_1 S_8$  approximation using both one-dimensional cylindrical and two-dimensional XY geometries. For each model the surface area of the shim safety rod was preserved and for the XY geometry the volume was also held constant. In both cases internal boundary conditions were evaluated at the surface of the borated steel rod. The ONEDANT transport code (Ref. 5) was used for the one-dimensional problem and TWOTRAN-II (Ref. 6) for the XY geometry. Average boundary conditions were obtained by perimeter weighting of the TWOTRAN point current-to-flux ratios. The results of these calculations are summarized in Table 7. Because of modeling deficiencies, the ONEDANT internal boundary conditions tend to be too large and the TWOTRAN values somewhat small.

Control rod worths were measured in a 27-element and a 30-element LEU core. These two core configurations are illustrated in Figs. 2a and 2b. For each of the configurations the worths of the shim safety rods were evaluated in two dimensional XY calculations using the internal boundary conditions given in Table 7. The results are summarized in Table 8 where the calculated-to-experiment (C/E) worth ratios are shown for each of the shim safety rods. Doubling the number of mesh intervals in the core would increase these C/E ratios by about 2%. The shim rod worths are reasonably well-calculated for the 27-element core, but are somewhat underpredicted for the 30-element case.

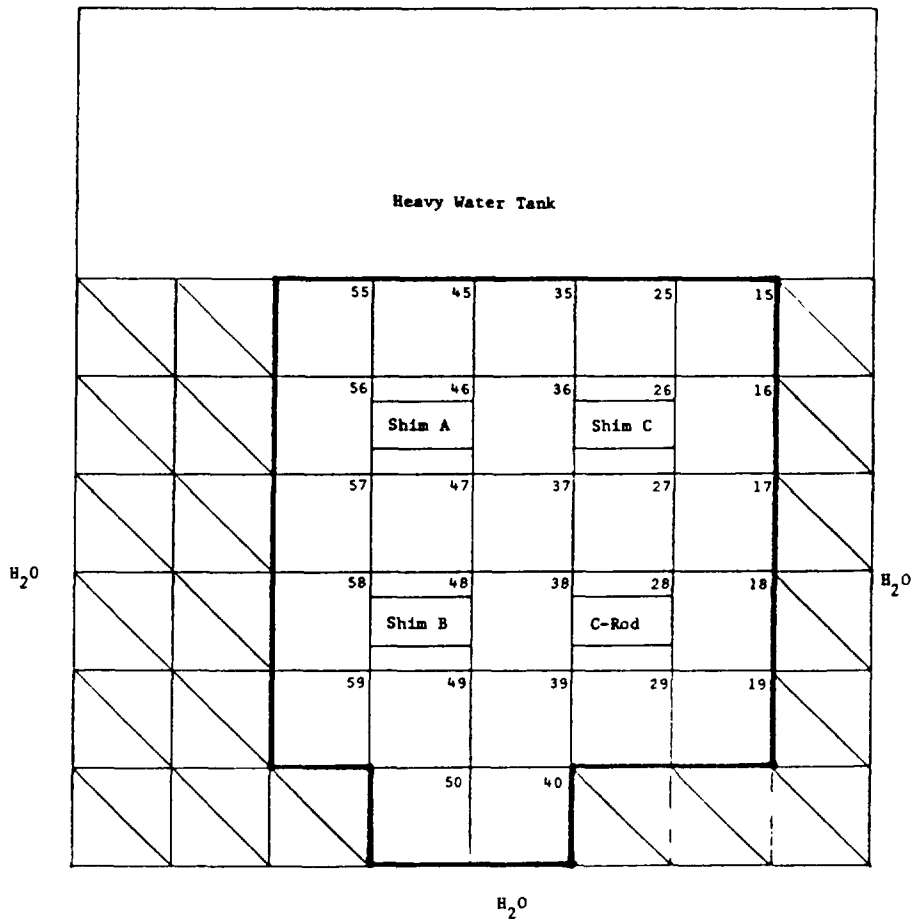


FIG. 2a. FNR 27-element LEU core for shim safety rod worth measurements.

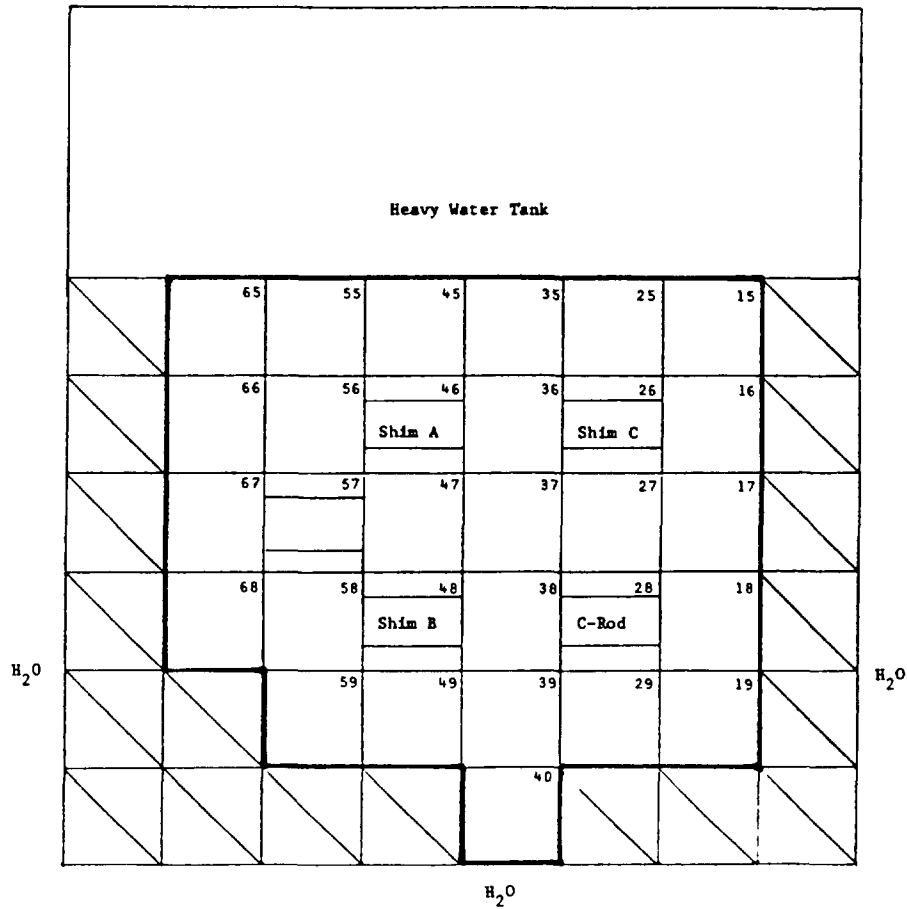


FIG. 2b. FNR 30-element LEU core for shim safety rod worth measurements.

Table 7. Group-Dependent Internal Boundary Conditions ( $-j/\phi$ )

Group	$E_u - eV$	TWOTRAN-XY ( $-j/\phi$ )	ONEDANT-R ( $-j/\phi$ )
1	10.00 + 7	2.8411 - 2	3.5206 - 2
2	8.208 + 5	-8.3937 - 3	-1.2773 - 2
3	5.531 + 3	7.9673 - 2	1.0147 - 1
4	1.855	2.4479 - 1	2.7691 - 1
5	6.249 - 1	4.1490 - 1	4.4703 - 1

Table 8. Reactivity Worths of the FNR Shim Safety Rods

<u>No. of Fuel Elements</u>	<u>Rod</u>	<u>Lattice Position</u>	<u>Exp. % <math>\Delta K/K</math></u>	<u>C/E TWOTRAN-XY</u>	<u>C/E ONEDANT-R</u>
27	A	46	2.220	0.989	1.051
27	B	48	2.320	0.974	1.035
27	C	26	2.283	0.947	1.006
30	A	46	2.642*	0.991	1.053
30	B	48	2.233*	0.943	1.003
30	C	26	2.085*	0.915	0.973

\*Estimated as 1.93 times the measured half-rod worth.

A 3D model of the FNR reactor with 27 fresh LEU fuel elements has been used to calculate the differential worth of shim safety rod A. For these calculations each fuel element was again divided into two non-fuel regions, corresponding to the side plates, and a central fuel region. A  $6 \times 6$  mesh structure in the XY plane was chosen for most fuel elements. For the control fuel elements, however, the mesh structure was  $7 \times 8$ . Axial mesh planes were separated by 2.50 cm in the core region except near the core-axial reflector interfaces where the spacing was reduced to 0.50 cm. The shim rods were represented as having a rectangular cross section whose dimensions were chosen so as to preserve the volume and surface area of the actual borated steel absorber. TWOTRAN internal boundary conditions (see Table 7) were applied at the absorber surface.

For all these 3D calculations the control rod was assumed to be withdrawn half way. Shim rods B and C were moved as a unit in such a way as to keep the reactor near critical for each step of withdrawal of shim rod A. The DIF3D code (Ref. 7), with internal boundary conditions, was used to calculate the eigenvalues corresponding to each withdrawal step and these results are summarized in Table 9. The rod position for the fully inserted rod is taken as 0.0 cm (bottom of core) and 61.27 cm for the fully withdrawn rod. Figure 3 compares the calculations with the measured differential worth of shim rod A. Note that the 3D calculation gives a total rod worth which is about 4.5% larger than that found on the basis of the 2D - XY calculation.

#### V. Comparison of ANL and University of Michigan Calculations with Measurements

From the measured excess reactivity ( $0.45\% \delta k/k$ ) and  $^{235}\text{U}$  mass (3512.82 g) of the 23 fresh LEU element configuration along with the predicted dependence of  $k_{\text{eff}}$  on the fissile mass content, critical mass estimates were made by both ANL and the University of Michigan. Two-dimensional XY diffusion calculations, based on ENDF/B-IV cross sections, were performed to simulate the actual LEU loading sequence in the "Approach to Critical" experiment. From these data the critical mass was predicted. The results are summarized in Tables 10 and 11.

Table 9. Calculated FRN Shimm Rod A Differential Worth  
in 27-Fuel-Element Core

Step	Rod A Position, cm	Rod B and C Position, cm	K-Effective	$\Delta\rho$ %	Total $\rho$ %
1	61.27 (Out)	33.12	1.002732	0.000	0.000
2	50.65	33.12	1.001214	0.151	0.151
3	40.64	33.12	0.997602	0.362	0.513
4	40.64	40.64	1.006252		
5	30.63	40.64	1.000362	0.585	1.098
6	20.63	40.64	0.993904	0.650	1.748
7	20.63	53.14	1.002876		
8	10.64	53.14	0.998774	0.410	2.158
9	0.00 (In)	53.14	0.997358	0.142	2.300

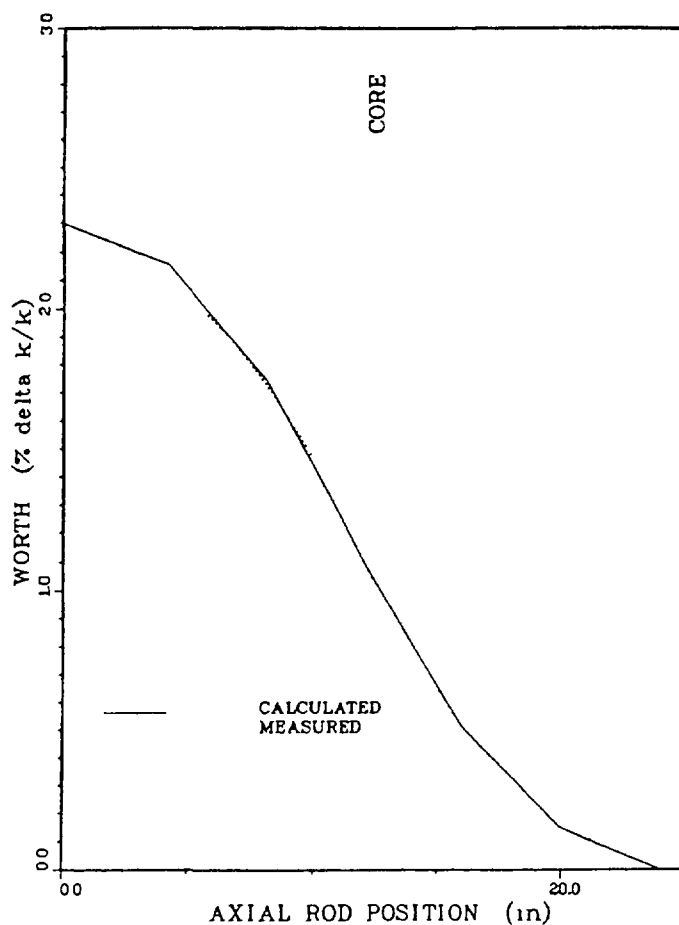


FIG. 3. FNR differential shim rod A worth,  
FEP46 with 27 LEU fuel elements

Table 10. FNR LEU Approach to Criticality  
ANL/Univeristy of Michigan Calculations

Number of Fuel Elements	ANL Calculations		Univ. of Mich. Calculations	
	$^{235}\text{U}$ Mass,g	$k_{\text{eff}}$	$^{235}\text{U}$ Mass,g	$k_{\text{eff}}$
21	3178.3	0.9762	3178.7	0.9835
22	3345.6	0.9887	3346.0	0.9926
23	3512.9	1.0011	3513.3	1.0025
24	3680.2	1.0096	3680.6	1.0097
25	3847.5	1.0178	3847.9	1.0161

Table 11. FNR Critical Mass for LEU Fuel

	Mass,g
Experiment	3436
ANL Calculation	3498
University of Michigan Calculation	3471

Table 12. FNR Control Rod Worths in Core with  
27 Fresh LEU Fuel Elements

Rod	Position	Rod Worth, % $\Delta k/k$		
		Experiment	ANL Calc.	Univ. of Mich. Calc.
A	46	2.22	2.20	2.28
B	48	2.32	2.26	2.65
C	26	2.28	2.16	2.25

Full length control rod worths for each of the shim safety rods (A, B, and C) were measured in the 27 LEU fuel element core configuration (Fig. 2a). Each rod worth was determined from a series of positive period and incremental rod worth measurements. The University of Michigan and ANL results are compared with measurements in Table 12.

## VI. Axial Rhodium Reaction Rate Distributions

Axial reaction rate distributions were measured in the FNR with a rhodium self-powered neutron detector. Figure 4 shows the core configuration of the 29 LEU fuel elements used during these measurements. A 3D model of this 29-element FNR reactor was used to calculate axial reaction rate distributions for the rhodium detector. For these calculations it was assumed that each of the shim rods was 52.58 cm withdrawn from the bottom of the core and that the control rod was withdrawn half way. Shim rods were treated using the same TWOTRAN internal boundary conditions as before (Table 7). The fuel element mesh structure discussed earlier was again used in these DIF3D calculations of the XYZ fluxes from which the rhodium reaction rate traverses were determined. Reaction rate distributions calculated with and without equilibrium xenon and samarium were found to be nearly identical.

Measured and calculated axial rhodium capture rate distributions are compared in Figs. 5-11 for fuel element positions (FEP) 15, 19, 27, 35, 39, 47 and 37 (see Fig. 4). The curves are normalized at the peak of the distributions. In general, the measured and calculated distributions agree quite well, but in all cases the calculations underpredict the peak heights in the axial reflector regions. These calculated peak heights are very sensitive to the aluminum-water volume fractions used to describe the various axial reflectors. To illustrate this, Fig. 12 shows the axial capture rate distribution in fuel element position 37 (FEP37) where the aluminum end boxes above and below the fuel plates were explicitly represented in the 3D model. Comparing this figure with the previous one shows the improved agreement in the reflector peak regions.

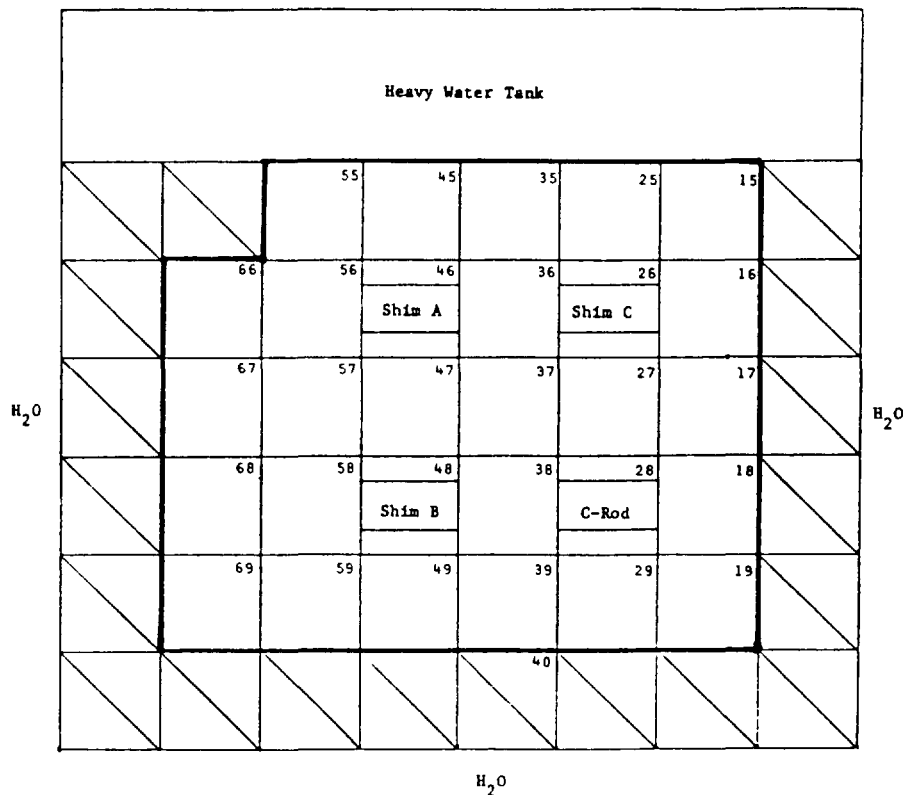


FIG 4 FNR 29-element LEU core for rhodium reaction rate axial distribution measurements

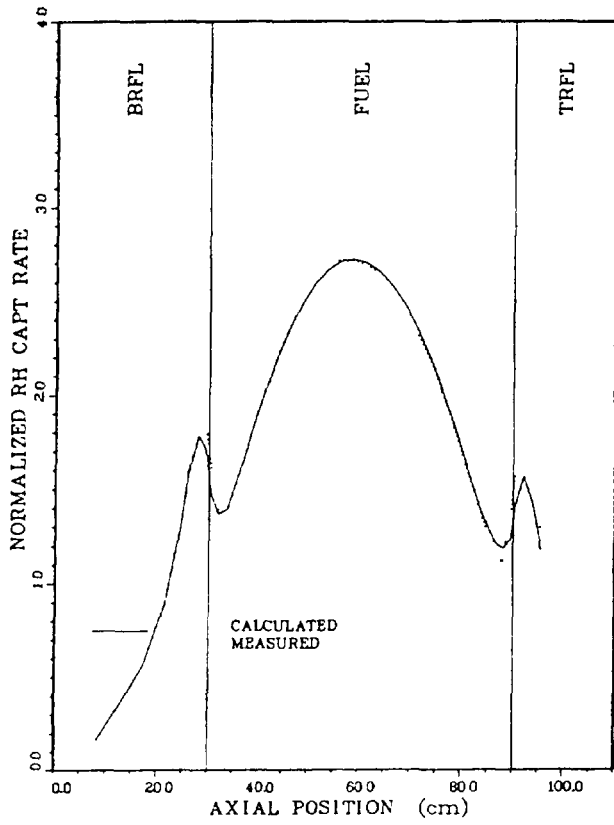


FIG. 5. Rhodium axial capture rate distribution, FEP15 in FNR with 29 LEU fuel elements.

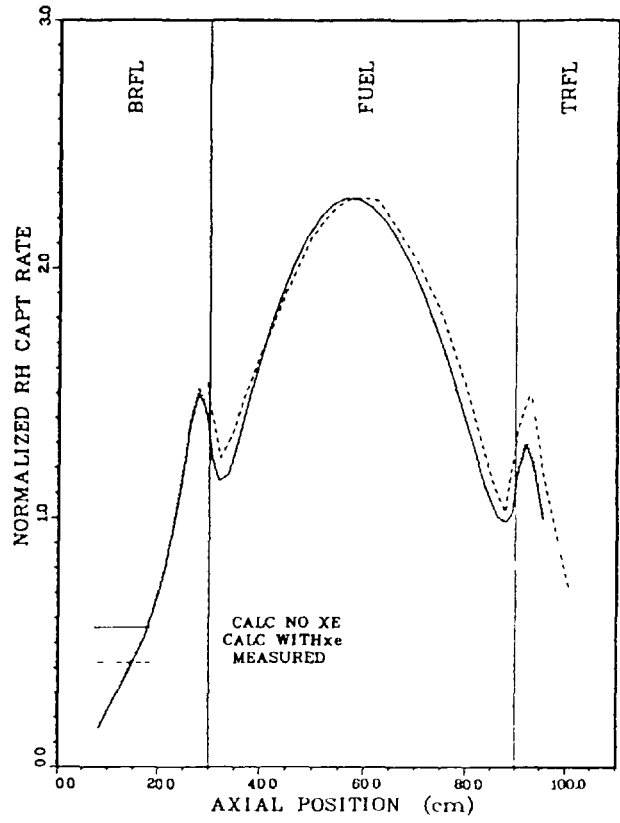


FIG. 6. Rhodium axial capture rate distributions, FEP19 in FNR with 29 LEU fuel elements.

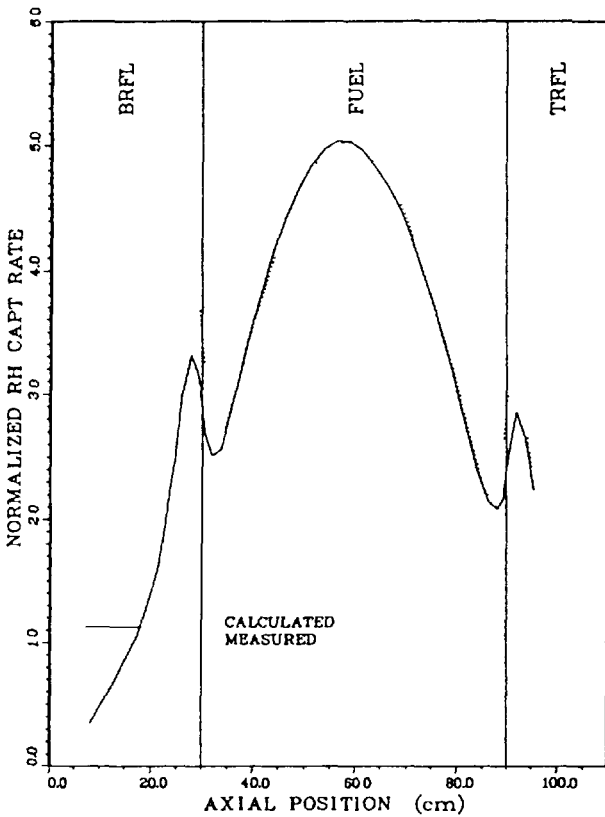


FIG. 7. Rhodium axial capture rate distributions, FEP27 in FNR with 29 LEU fuel elements.

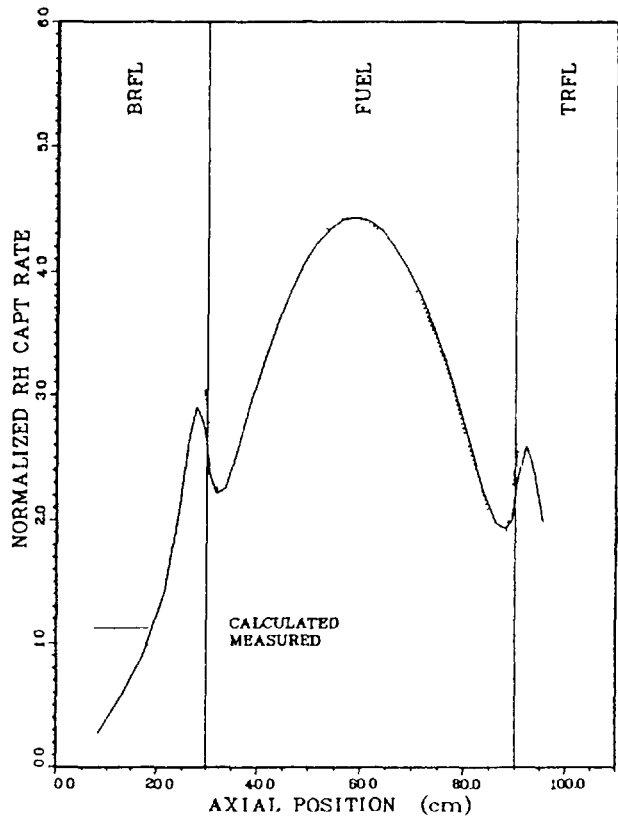


FIG. 8. Rhodium axial capture rate distributions, FEP35 in FNR with 29 LEU fuel elements.

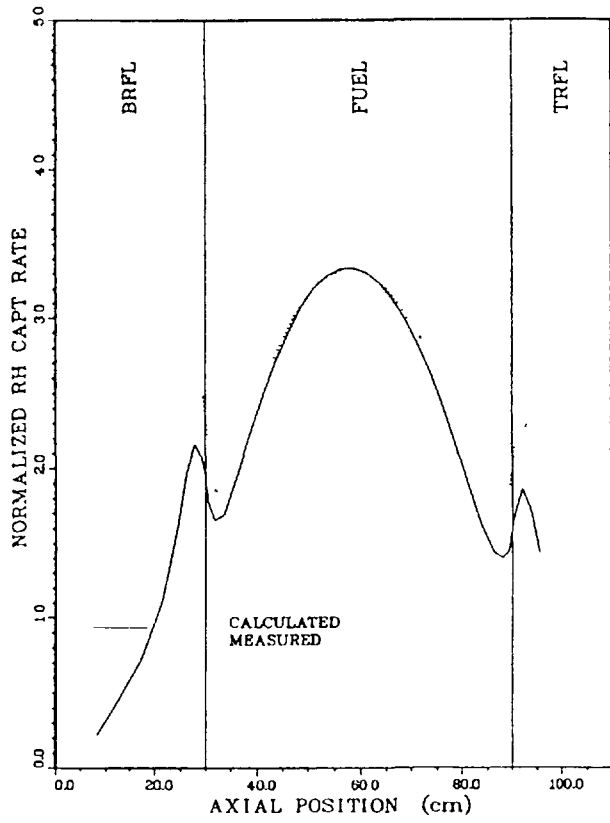


FIG. 9. Rhodium axial capture rate distributions, FEP39 in FNR with 29 LEU fuel elements.

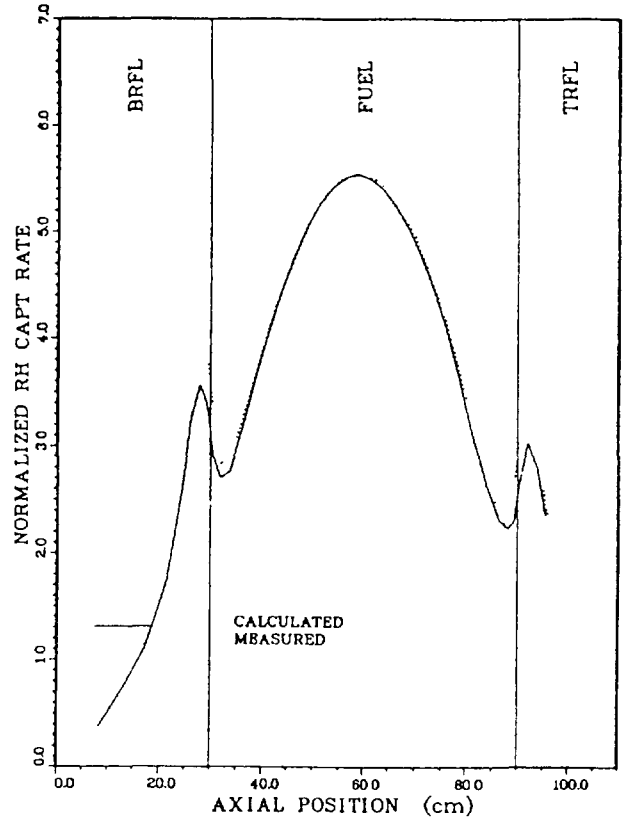


FIG. 10. Rhodium axial capture rate distributions, FEP47 in FNR with 29 LEU fuel elements.

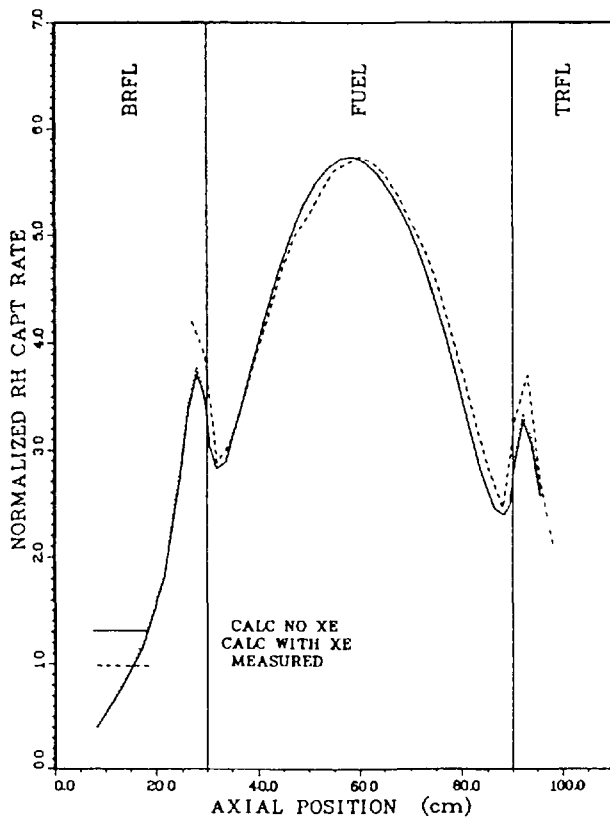


FIG. 11. Rhodium axial capture rate distributions, FEP37 in FNR with 29 LEU fuel elements.

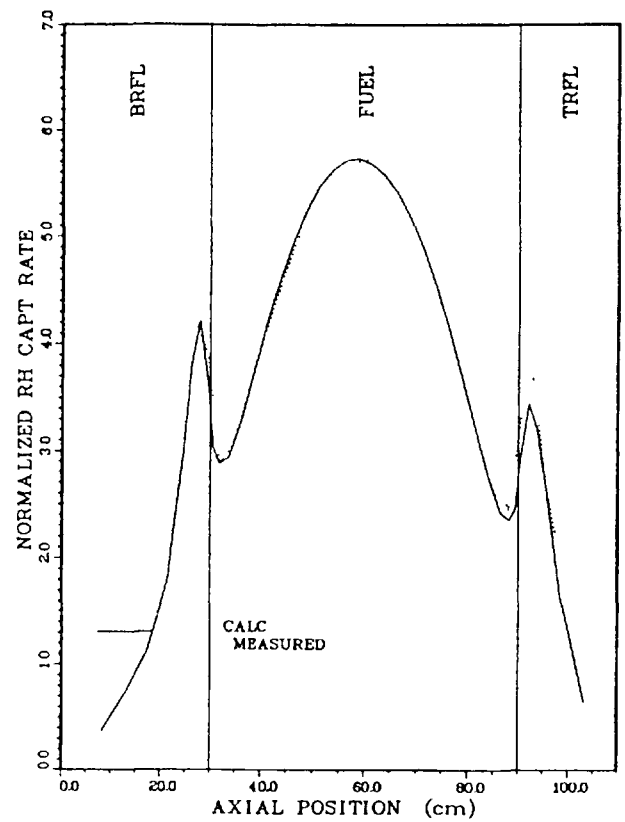


FIG. 12. Rhodium axial capture rate distributions, FEP37 in FNR with 29 LEU fuel elements.

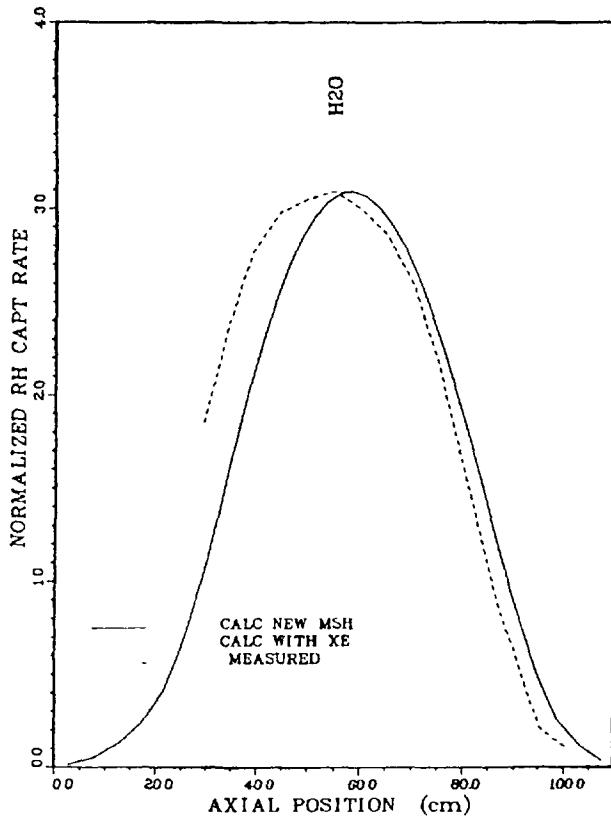


FIG. 13. Rhodium axial capture rate distributions, H2OP40-3 in FNR with 29 LEU fuel elements.

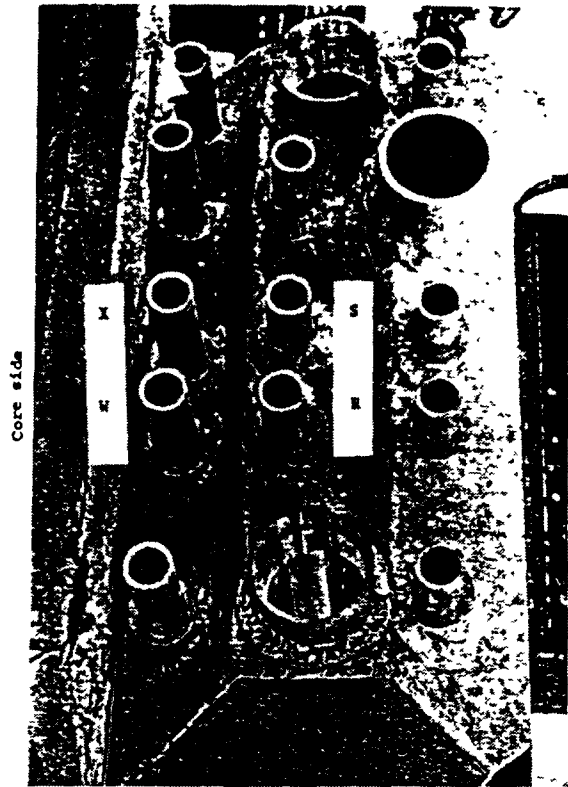


FIG. 14. View of D<sub>2</sub>O tank top from above.

The distribution in the H<sub>2</sub>O reflector (grid position 40) is shown in Fig. 13. It is seen that the measured rhodium capture rate distribution in the light water reflector is broader and shifted with respect to the calculated one.

For measurements in the heavy water reflector, 2.54 cm diameter (I.D.) vertical tubes penetrate the D<sub>2</sub>O tank to a depth of 20.32 cm below the top of the core and are filled with H<sub>2</sub>O. Figure 14, taken from Ref. 8, shows these tubes entering the top of the D<sub>2</sub>O tank and also identifies positions X, S, W and R. Rhodium capture rate distributions at locations X and S in the heavy water reflector are shown in Figs. 15 and 16. As Fig. 15 shows, the H<sub>2</sub>O-filled tubes produce additional moderation in the D<sub>2</sub>O tank, which is the reason for the discontinuity in the calculated capture rate distribution at the D<sub>2</sub>O-H<sub>2</sub>O interface at the bottom of tube X. This effect is not as evident at position S (Fig. 16) because this location is farther from the core. In the H<sub>2</sub>O region above the D<sub>2</sub>O tank the measured capture rate distribution, for some reason, does not fall off as rapidly as the calculated one.

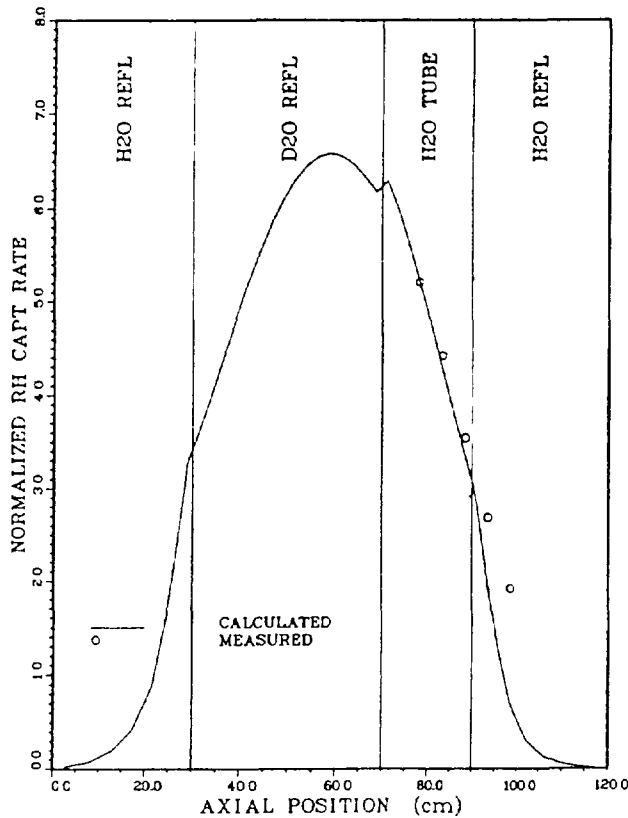


FIG. 15. Rhodium axial capture rate distribution, position X in D<sub>2</sub>O reflector tank.

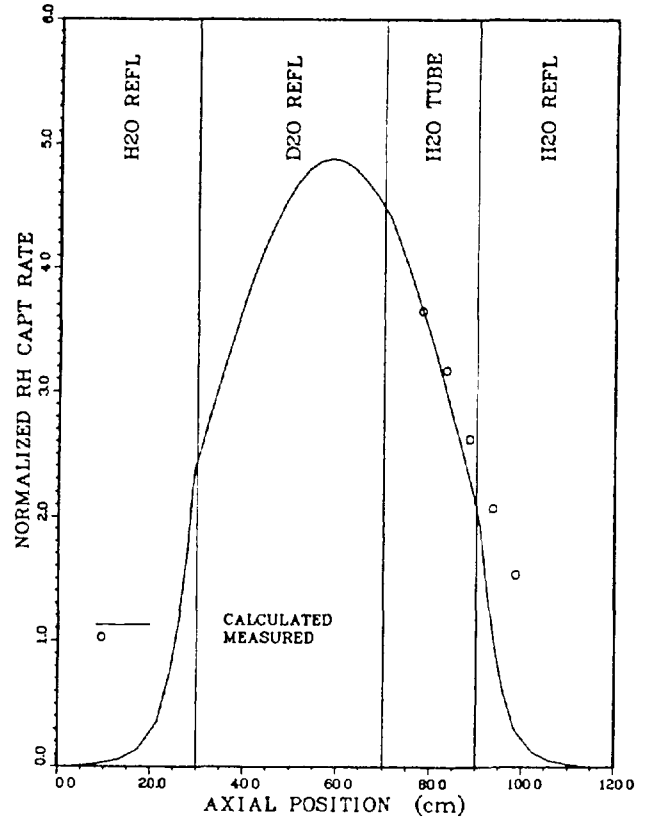


FIG. 16. Rhodium axial capture rate distribution, position S in D<sub>2</sub>O reflector tank.

## VII. Thermal Neutron Flux Distributions

The rhodium self-powered neutron detector (Ref. 8, pp.77 ff) was used to measure thermal neutron flux distributions in the 31-element LEU core. This core contains 25 standard fuel elements and 6 nine-plate control fuel elements. Using techniques already described, this core was modeled in XYZ geometry for diffusion calculations. For these calculations the control rod was withdrawn half way and the shim safety rods were banked at the 52.58 cm position. The H<sub>2</sub>O-filled tubes at positions X, S, W and R in the D<sub>2</sub>O tank (see Fig. 14) were explicitly represented in the 3D model. These tubes penetrate the heavy water tank to a depth of 20.32 cm below the top of the fuel.

Figure 17 shows the 31-element core configuration and the calculated-to-experiment (C/E) thermal flux ratios. The calculated thermal fluxes (group 5) were normalized to the measured value on the core midplane at grid position 37. In addition, measurements were made at the 1/4 and 3/4 core height positions so that the three numbers in a given grid location (Fig. 17) correspond to the C/E values at the lower, middle and upper elevations. In the 3D model these elevations correspond to axial positions for Z = 45, 60 and 75 cm. Because of access limitations, measurements in the D<sub>2</sub>O tank were made only on the Z = 78.26 cm plane. The calculated axial flux distributions were used to extrapolate the measured values at positions X, W, S and R to the core midplane and the 3/4 height position. Measurements in the H<sub>2</sub>O reflector were made at four locations in grid position 40 in order to define the thermal neutron flux peak in the reflector. The measurement at grid position 57 was in the central water hole of the 9 plate special fuel element. For most positions the C/E thermal flux ratios are within 10% of unity.

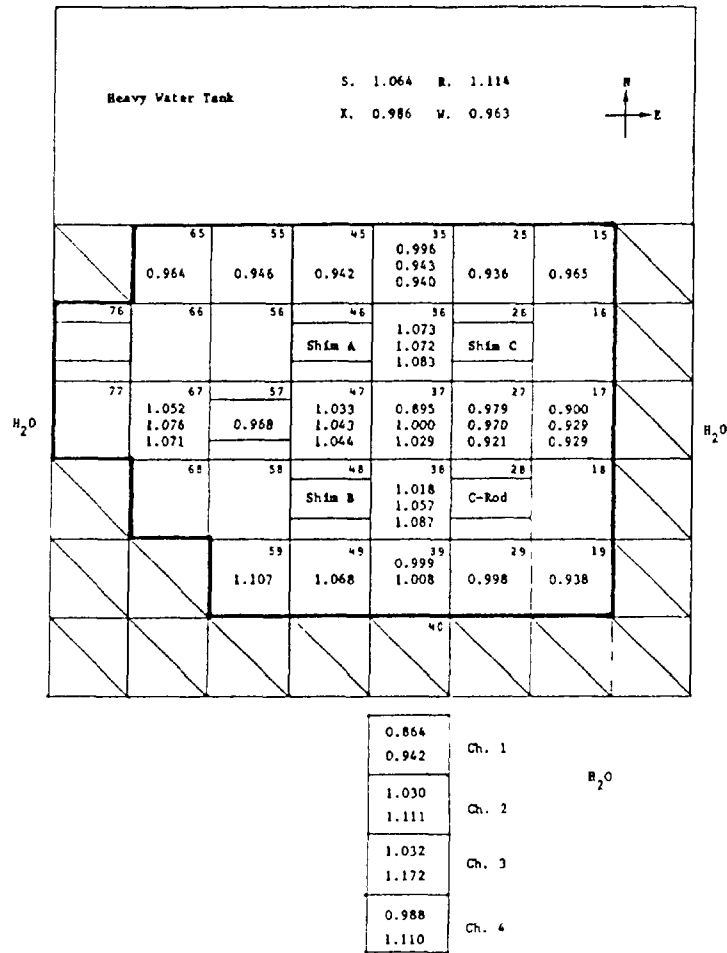


FIG. 17. Thermal neutron flux C/E ratios for the FNR 31 element LEU core.

Figure 18 shows the calculated and measured thermal neutron flux distributions in row 7. Flux peaking in the water hole associated with the special fuel element at grid position 57 and in the H<sub>2</sub>O reflector regions is clearly evident. Secondary peaks in the core correspond to the side plate regions containing Al-H<sub>2</sub>O mixtures. In general, the agreement between the calculated and measured fluxes is quite good at both the middle and upper elevations.

Figure 19 shows a North/South traverse through the middle of column 3 and then is displaced 3.81 cm to the west at the core-D<sub>2</sub>O tank interface so as to pass through positions X and S in the D<sub>2</sub>O tank. Note the flux peaking in the upper elevation distribution in the H<sub>2</sub>O-filled tube at position X (Y = 72.28 cm) in the D<sub>2</sub>O tank. The effect is much less evident at position S. No such peaking is seen in the midplane distribution since the H<sub>2</sub>O-filled tubes do not extend this deep into the D<sub>2</sub>O tank. Figure 20 shows similar curves with the upper part of the traverses displaced in the opposite direction so as to pass through positions W and R in the D<sub>2</sub>O reflector. In general, these distributions are in satisfactory agreement with the measured values.

In Figs. 17-20 the thermal fluxes are normalized to the experimental value on the midplane of position 37 and are in units of  $10^{13}$  n/cm<sup>2</sup>·s at a power of 2 MW. The 3D diffusion calculation was also done for a 2 MW power level, but the normalization required multiplying the calculated fluxes by a

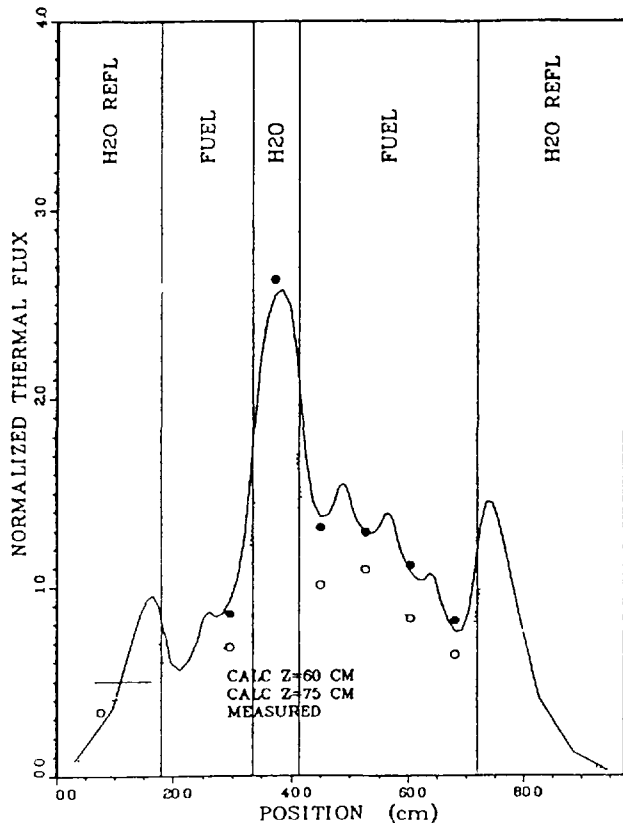


FIG. 18. Thermal flux distribution in row 7 of the FNR with 31 LEU fuel elements.

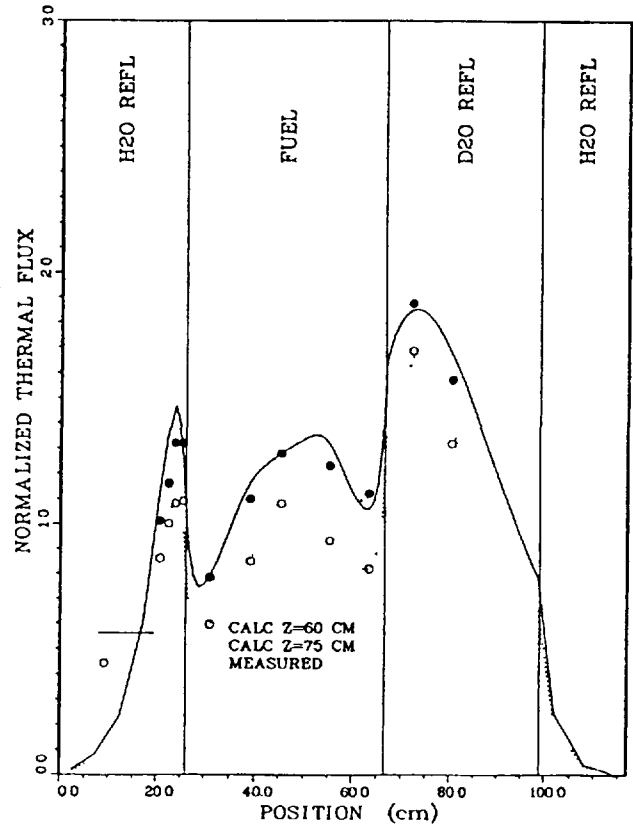


FIG. 19. Thermal flux distribution in column 3 of the FNR through D<sub>2</sub>O positions X and S.

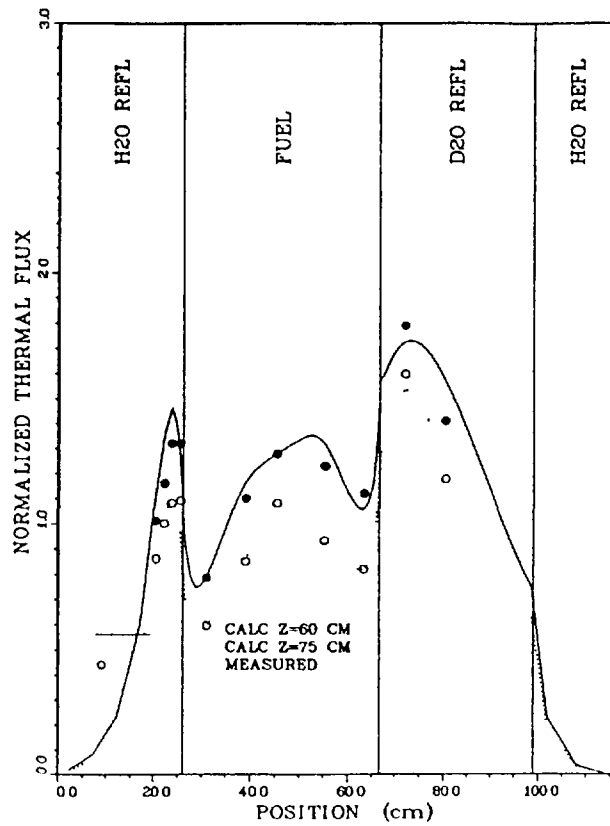


FIG. 20. Thermal flux distribution in column 3 of the FNR through D<sub>2</sub>O positions W and R.

factor of 0.646. Thus, there is a large disagreement between the measured and calculated absolute fluxes ( $C/E = 1.55$ ). This discrepancy remains to be resolved. The upper energy boundary of group 5 is 0.625 eV whereas the cadmium cutoff energy is about 0.55 eV. This difference accounts for some of the discrepancy.

#### ACKNOWLEDGEMENTS

The data upon which these comparisons are based was supplied by staff members from The University of Michigan Department of Nuclear Engineering. This cooperation is gratefully acknowledged.

#### REFERENCES

1. M. M. Bretscher and J. L. Snelgrove, "Comparison of Calculated Quantities with Measured Quantities for the LEU-Fueled Ford Nuclear Reactor," ANL/RERTR/TM-4 (1983), Proceedings of the International Meeting on Research and Test Reactor Core Conversions from HEU to LEU Fuels, Argonne National Laboratory, Argonne, Illinois, November 8-10, 1982.
2. B. A. Zolotar, et al., "EPRI-CELL Description," Advanced Recycle Methodology Program System Documentation, Part II, Chapter 5, Electric Power Research Institute (September 1977).
3. Research Reactor Core Conversion from the Use of Highly Enriched Uranium to the Use of Low Enriched Uranium Fuels Guidebook, pp. 448 ff, IAEA-TECDOC-233, (1980).
4. W. Kerr, et al., "Low Enrichment Fuel Evaluation and Analysis Program, Summary Report for the Period January 1980-December 1980," The University of Michigan Report (March 1981), Appendix C.
5. R. Douglas O'Dell, et al., "Users' Manual for ONEDANT: A Code Package for One-Dimensional, Diffusion-Accelerated, Neutral-Particle Transport," October 1980.
6. K. P. Lathrop and F. W. Brinkley, "TWOTRAN-II: An Interfaced, Exportable Version of the TWOTRAN Code for Two-Dimensional Transport," LA-4848-MS, July 1973.
7. D. R. Ferguson and K. L. Derstine, "Optimized Iteration Strategies and Data Management Considerations for Fast Reactor Finite Difference Diffusion Theory Codes," Nucl. Sci. Eng. 64, 593 (1977), and K. L. Derstine, ANL Internal Memoranda on the DIF3D Code (1977-1982).
8. W. Kerr, et al., "Low Enrichment Fuel Evaluation and Analysis Program, Summary Report for the Period January 1979 - December 1979," The University of Michigan Report (January 1980), Appendix B.

ANALYSIS OF CRITICAL EXPERIMENTS  
OF FNR LEU CORES

K. ARIGANE, K. TSUCHIHASHI

Japan Atomic Energy Research Institute,  
Tokai-mura, Naka-gun, Ibaraki-ken,  
Japan

Abstract

An analysis has been done of the critical experiments in the LEU cores of the FNR to validate the calculational method, and accuracy of the neutronic design for the core conversion of JRR-4 from HEU to LEU fuel using the JAERI SRAC code system. This report describes the calculational process, the results of calculation for the critical mass and the control rod worths, and comparisons with the experimental values. Agreement between calculated and experimental values is satisfactory.

INTRODUCTION

The core conversion of the JRR-4 from HEU fuel to LEU fuel has been prepared. To validate the calculational method and the accuracy of the neutronic design by the JAERI SRAC code system<sup>1</sup>, a series of neutronic calculations have been done for the initial LEU cores of the FNR ( Ford Nuclear Reactor at the University of Michigan ) which reached criticality in Dec 1981 as the first demonstration of the conversion from HEU to LEU. Both LEU cores of JRR-4 and FNR have somethings in common, such as a pool type reactor and use of UAlx MTR type fuel, and borated stainless steel control rods. Satisfactory results would convince us of the validity of our prediction for the LEU core of JRR-4. Several analyses for the FNR experiments have been presented<sup>2-6</sup>.

This report describes the calculational process and the results of the analysis of the critical mass and the reactivity worth of the control rods.

CALCULATIONAL METHOD

Cross Sections

The cross section data are based on ENDF/B-4 taken from the optional data libraries except the scattering law for H<sub>2</sub>O and D<sub>2</sub>O which are stored in ENDF/B-3.

The transport cross sections for P<sub>0</sub> transport calculations were calculated by the B1 approximation which correspond to the diffusion coefficient  $D = 1/(3 \Sigma_{tr})$ .

Resonance absorption of heavy nuclides was calculated by the table look-up method for  $E > 130.07$  eV, and the IR method was applied to the resonance levels in which resonance energies are located between 130.07 eV and 1.125 eV (= thermal cut off).

## Process

### Step 1 Primary Cell Calculation for a Single Fuel Plate Cell

A one dimensional plane cell composed of a fuel plate, cladding, and coolant water was assumed as shown in Fig.1. The energy group structure for the cell calculations is composed of 22 fast groups and 31 thermal groups as shown in Table 1. In this step two sets of linear equations were successively solved for (1) 22 fast groups and (2) 31 thermal groups using the collision probability method. In Table 2 we show the atomic number densities used in the cell calculations.

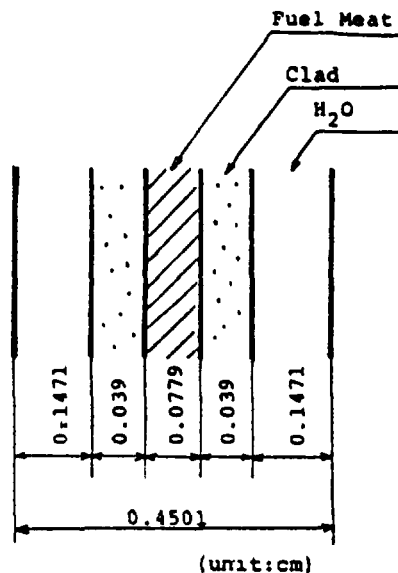


FIG 1 Cell model for fuel plate

### Step 2 Secondary Cell Calculation for an Element

A one dimensional plane cell composed of a homogenized fuel region, water gap, and side plate, as shown in Fig.2 was assumed for a standard fuel element. The same process as Step 1 was used with the same energy group structure

Another two-dimensional rectangular cell for the control element as shown in Fig 3 was assumed to have the smeared cross sections corresponding to the region surrounding the control rod. As the cell calculation is based on the assumption of the periodic array of the lattice cells, it does not reflect the actual isolated boundary condition. To mitigate this non realistic condition, we included a standard fuel region surrounding the control element in the cell.

After the cell calculation of this step, the 53 group cross sections were collapsed into the 10- ( or 3- ) group structure, also shown in Table 1, using the spectrum obtained by solving one point B1 equation with a buckling value so as to make the  $K_{eff}$  of the standard fuel element unity.

The macroscopic cross sections for non-fuel regions were calculated by the B1 approximation.

Table 1 Energy Group Structure

		Fast			Thermal
Fine	Coarse	Energy	Fine	Coarse	Energy
1	1	0.10000E+08	1	1	0.11254E+01
2		0.60653E+07	2		0.68256E+00
3		0.36788E+07	3		0.41399E+00
4		0.22313E+07	4		0.36528E+00
5	2	0.13534E+07	5		0.31961E+00
6		0.82085E+06	6		0.29792E+00
7		0.49787E+06	7		0.27699E+00
8		0.18316E+06	8	2	0.23742E+00
9	3	0.67380E+05	9		0.20090E+00
10		0.24788E+05	10		0.18378E+00
11		0.91188E+04	11		0.16743E+00
12		0.33546E+04	12		0.15183E+00
13	4	0.12341E+04	13		0.13700E+00
14		0.58295E+03	14	3	0.12293E+00
15		0.27536E+03	15		0.10963E+00
16		0.13007E+03	16		0.97080E-01
17		0.61442E+02	17		0.85397E-01
18	5	0.29023E+02	18		0.74276E-01
19		0.13710E+02	19		0.64017E-01
20		0.64760E+01	20	4	0.54520E-01
21		0.30590E+01	21		0.45785E-01
22		0.18554E+01	22		0.37813E-01
		0.11254E+01	23		0.30602E-01
			24		0.24154E-01
			25		0.18467E-01
			26	5	0.13543E-01
			27		0.93805E-02
			28		0.59804E-02
			29		0.33423E-02
			30		0.14663E-02
			31		0.35238E-03
					0.10000E-04

Energy Boundaries for 3 Group Structure

1	0.10000E+08
2	0.18316E+06
3	0.68256E+00
	0.10000E-04

Table 2 Atomic Number Density in Primary Cell (10<sup>24</sup>)

: Mixture:	Meat	: Clad	: Coolant	:
: Width	: 0.078	: 0.039	: 0.14716	:
: (cm)	:	: X 2	: X 2	:
: U-234	: 5.6078-6:	:	:	:
: U-235	: 8.4927-4:	:	:	:
: U-236	: 7.0769-6:	:	:	:
: U-238	: 3.3637-3:	:	:	:
: MG	:	: 5.9658-4:	:	:
: AL	: 5.1244-2:	: 5.9243-2:	:	:
: SI	: 3.3952-5:	: 7.4996-5:	:	:
: CR	:	: 1.7325-6:	:	:
: MN	:	: 4.568 -6:	:	:
: FE	: 2.9916-5:	: 8.1232-5:	:	:
: H	:	:	: 6.6694-2	:
: O	:	:	: 3.3347-2	:

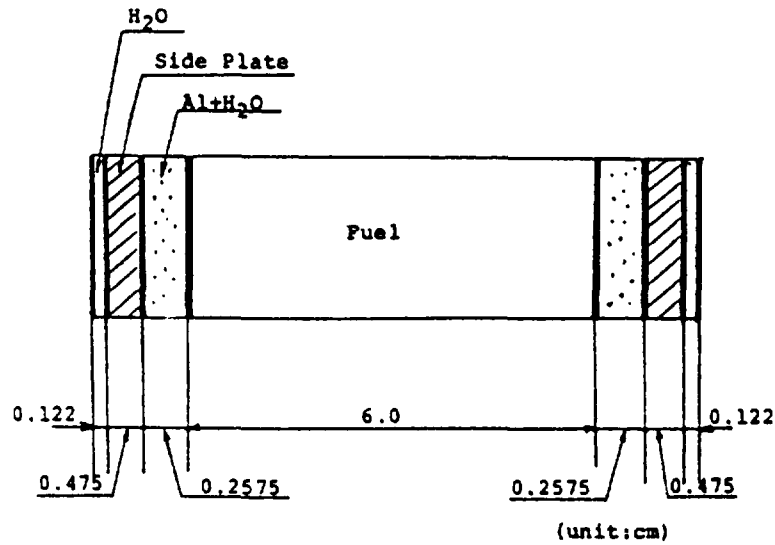


FIG. 2. Cell model for standard fuel element.

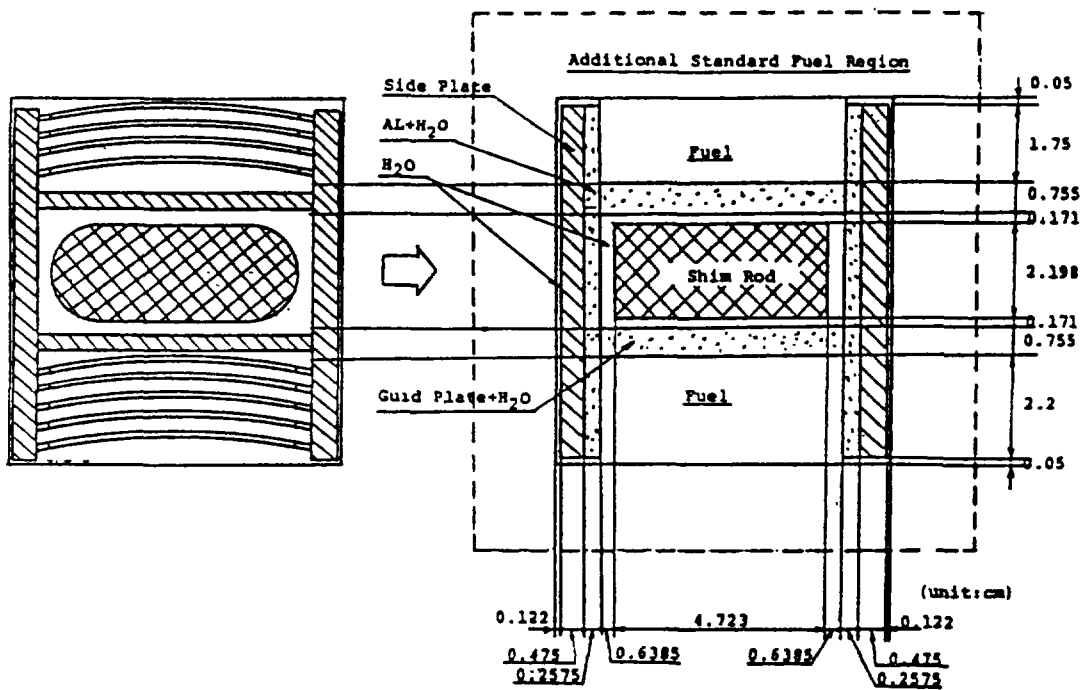


FIG. 3. Cell model for control fuel element.

### Step 3 Core Calculation for Critical Mass

The core calculations were executed by the diffusion theory code using the X-Y two-dimensional option with the 10-group structure for the clean core to get the critical mass for the geometry shown in Fig.4. To confirm the buckling value used in the X-Y two dimensional calculation, a three dimensional diffusion calculation with the 10-group structure was also done for the vertical figure as shown in Fig.5.

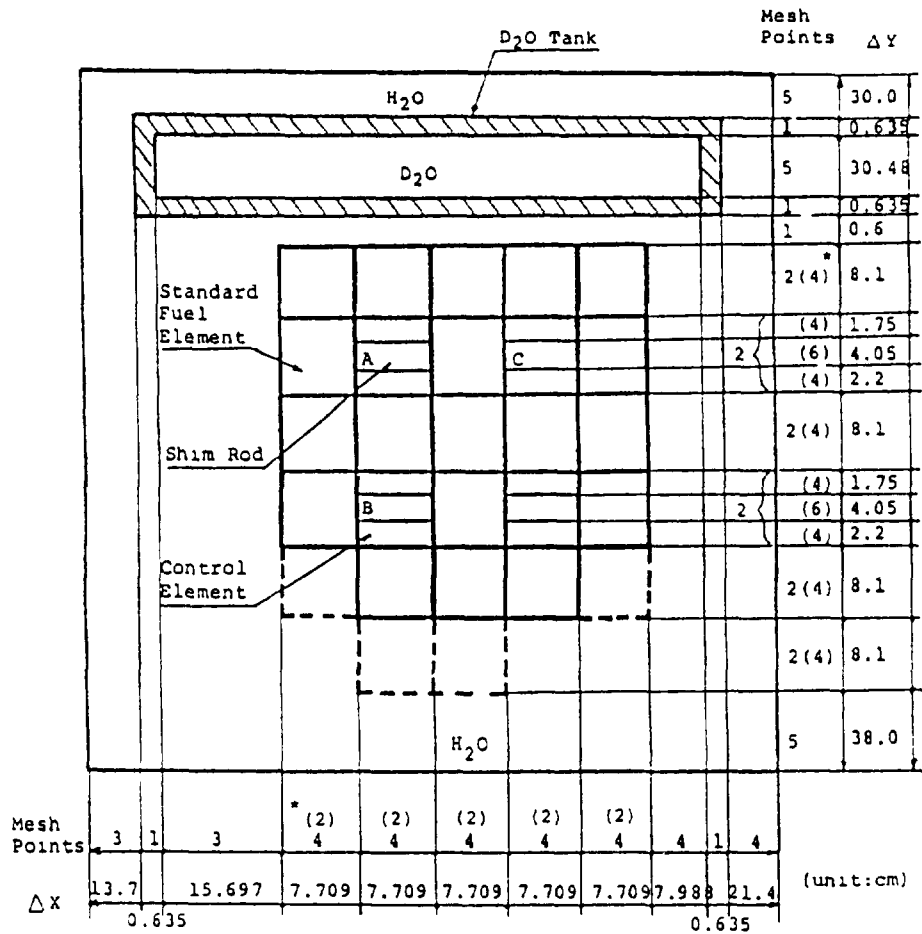


FIG. 4. Core configuration for 2-D calculation.

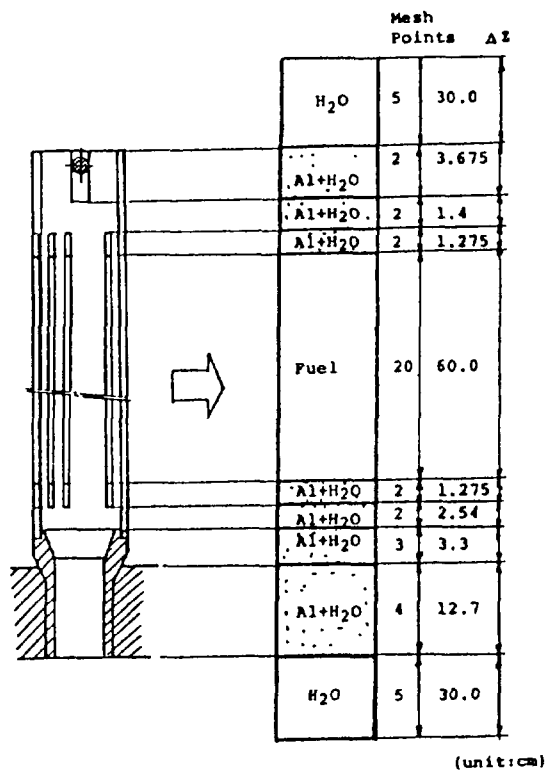


FIG. 5. Vertical model for 3-D calculation.

#### Step 4 Core Calculations for Control Rod Worth

To predict the control rod reactivity worth, the following process similar to that taken by Bretscher<sup>5</sup> was examined.

A pair of two-dimensional 10-group Sn calculations were done for 1/4 of a simplified core with and without a control rod in the central position in order to get the reactivity worth and the logarithmic derivatives around the control rod

A pair of diffusion calculations with the same conditions were done to find an adjusting factor to the derivatives for the thermal groups so that the diffusion theory calculation had the same reactivity. No derivatives were applied to the non-thermal groups as a non-absorbing reaction such as slowing-down, distorts the flux distribution. Using the derivatives described above, a series of two-dimensional diffusion calculations were done to predict the control rod worth. The disposition of the D2O tank in the northern reflector and the control rod in the excentric position of the active core forced us to use full core geometry as shown in Fig.4. Through the experience of core calculations for swimming pool type reactors, we knew the thickness of reflector could be assumed as 30 cm even though it is much thicker ( it causes an underestimate of 0.2 %  $\Delta k/k$  ).

#### Step 5 3-Group Core Calculation

Independent of the above process, a series of 3-group calculations were done for the clean core and the cores with a control rod. In such a few group calculation, the up-scattering effect is not more important, so the thermal cut off energy was chosen as 0.6825 eV. The logarithmic derivative for a black boundary was applied to the thermal group around the control rod.

#### Vertical Buckling

As the  $K_{eff}$  values by X-Y two dimensional calculations are strongly affected by the vertical buckling, we took care of how to get it. First, we calculated the material buckling by the 10-group cross sections for the standard fuel element. Next, we adjusted the radial buckling value so as to make the  $K_{eff}$  unity through a series of one dimensional 10-group diffusion calculations in the vertical direction across the top surface of the upper reflector, the standard fuel element, the grid plate, and the bottom of the lower reflector. The vertical buckling was taken as the difference of the material buckling and the radial buckling. This value seems suitable for the clean core, however, we applied it also to the core with a control rod.

The same process was taken to get the vertical buckling for the 3-group calculations

### RESULTS AND COMPARISON

#### Critical Mass

Table 3 shows the results of core calculations for the clean cores. We obtained the vertical buckling as  $0.00174 \text{ cm}^{-2}$  (  $B_m^2 = 0.00906 \text{ cm}^{-2}$  ) for the 10-group calculations and  $0.00169$  (  $B_m^2 = 0.00880 \text{ cm}^{-2}$  ) for the

3-group calculations. We see good consistency between the 10-group and 3-group calculation and also between the 2-D and the 3-D calculation. In Fig. 6 the results of the 2-D 10-group calculations are plotted together with the results by ANL and the University of Michigan. Agreement among the results of the three institutions seems good.

Table 3 Keff for Clean Core ( 23 elements loaded )

Dimension	Number of Groups	Vertical Buckling (cm <sup>-2</sup> )	K-eff	* C/E-1 (%)	** Number of Meshes
3-D	10	—	1.0063	+0.18	28x12x47
2-D	10	0.00174	1.0039	-0.06	28x12
3-D	3	—	1.0056	+0.11	28x12x47
2-D	3	0.00169	1.0039	-0.06	28x12

Note. \* Experimental Value (Ref 5,6) = 1.0045  
 at Regulating Rod Withdrawn  
 \*\* 1/2 core calculation

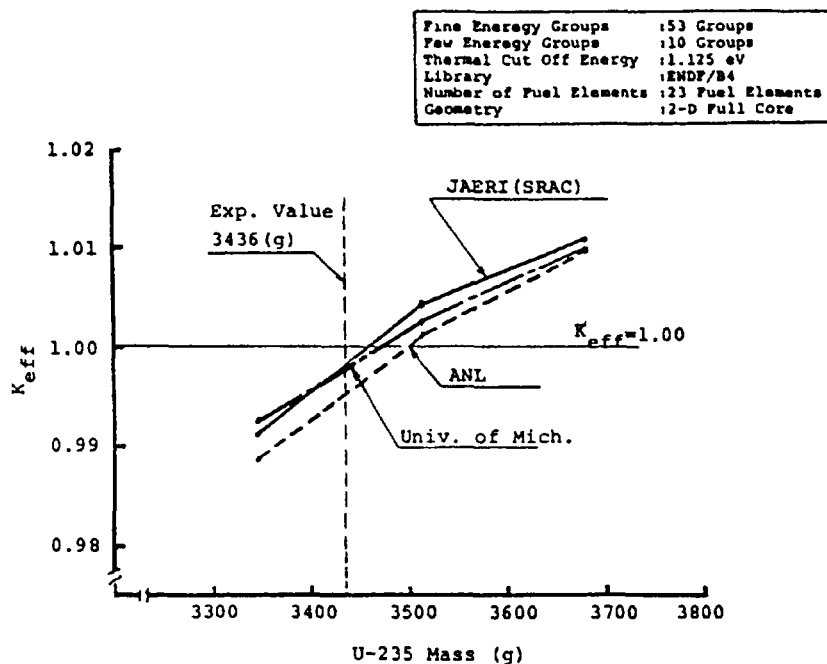


FIG. 6.  $K_{eff}$  dependent on <sup>235</sup>U mass.

### Control Rod Worth

By a pair of X-Y 10-group Sn calculations, the worth of 4.67 %  $\Delta k/k$  was obtained for the simplified core with and without a control rod in the central position. In order to have the same worth by a pair of X-Y diffusion calculations, we got an adjusting factor of 0.60 for the derivatives for the thermal groups.

The results by the 10-group full core calculations to simulate the actual rod positions are shown in Table 4 together with the experimental values. The comparison with experimental values shows an overestimate of less than 10 % of the rod worth by the 10-group calculations.

Table 4 Contro Rod Worth

Rod Position	Exp % Δk/k	10 GROUP Calc % Δk/k	Calc * C/E-1 (%)	3 GROUP Calc % Δk/k	Calc ** C/E-1 (%)
A	2.22	2.40	8.1	2.28	2.7
B	2.32	2.55	9.9	2.42	4.3
C	2.28	2.39	4.8	2.28	0.0

Note \* Logarythmic derivatives for thermal groups from TWOTRAN

\*\* Logarythmic derivative for thermal group as black boundary

In the same table, the results by the 3-group calculation using the logarithmic derivative of 0.469 are shown. We found the overestimate of less than 4.3 % by the 3-group calculations. This deviation could be minimized by setting the derivative to 0.40.

### CONCLUSION

We got satisfactory results ( 0.68 % underestimate in critical mass ) for the clean LEU core of FNR using the 10-group energy structure with the vertical buckling value obtained by a kind of buckling search.

We got consistent results between the 10-group and the 3-group calculations and also between the 2-D and 3-D calculations.

We can estimate the control rod worth to an accuracy of less than 10 % utilizing the information obtained by the two-dimensional Sn calculation for the simplified core configuration.

The better prediction for the control rod worth by the 3-group calculations with the black logarithmic derivative suggests that a borated stainless steel control rod behaves as a black body in the thermal energy region.

The overall results are so satisfactory that we may take the same calculational scheme for the JRR-4 core conversion.

### REFERENCES

- 1 'SRAC : JAERI Thermal Reactor Standard Code System for Reactor Design and Analysis', K.Tsuchihashi, H.Takano, K.Horikami, Y.Ishiguro, K.Kaneko, and T.Hara, JAERI-1285 (Jan,1983)
- 2 'Comparison of Calculations with Experiments in the FNR Full-Core LEU Demonstration Reactor' Contributed by the University of Michigan and Argonne National Laboratory to Research Reactor Core Conversion Safety and Licensing Issues, IAEA Guidebook Vol.1 (to be published)

- 3 'Low Enrichment Fuel Evaluation and Analysis Program , Summary Report for the Period January,1980-December,1980', William Kerr, University of Michigan, (Mar.1981)
- 4 'Safety Analysis Utilization of Low Enrichment Uranium (LEU) Fuel in the Ford Nuclear Reactor', Contributed by the University of Michigan to Research Reactor Core Conversion Safety and Licensing Issues, IAEA Guidebook Vol.1 (to be published)
- 5 'Comparison of Calculated Quantities with Measured Quantities for the LEU-Fueled Ford Nuclear Reactor', M.M.Bretscher and J.L. Snelgrove, International Meeting on the Research and Test Reactor Core Conversions from HEU to LEU Fuels, Argonne National Laboratory, (Nov.1982)
- 6 'Analysis of the Ford Nuclear Reactor LEU Core', J.A.Rathcopf, C.R. Drumm, W.R. Martin and J.C Lee, International Meeting on the Research and Test Reactor Core Conversions from HEU to LEU Fuels, , ANL (Nov,1982)

## Appendix H-5

# COMPARISON OF CALCULATIONS WITH MEASUREMENTS IN THE ORR WHOLE-CORE LEU DEMONSTRATION REACTOR

### Appendix H-5.1

#### ANALYTICAL SUPPORT FOR THE ORR WHOLE-CORE LEU $U_3Si_2$ -Al FUEL DEMONSTRATION

M.M. BRETSCHER  
RERTR Program,  
Argonne National Laboratory,  
Argonne, Illinois,  
United States of America

#### Abstract

Analytical methods used to analyze neutronic data from the whole-core LEU fuel demonstration in the Oak Ridge Research Reactor are briefly discussed. Calculated eigenvalues corresponding to measured critical control rod positions are presented for each core used in the gradual transition from an all HEU to an all LEU configuration. Some calculated and measured results, including  $\beta_{eff}/\ell_p$ , are compared for HEU and LEU fresh fuel criticals. Finally, the perturbing influences of the six voided beam tubes on certain core parameters are examined. For reasons yet to be determined, differential shim rod worths are not well-calculated in partially burned cores.

#### INTRODUCTION

This paper deals with analytical methods and some computational results which support the Whole Core LEU Silicide Fuel Demonstration in the Oak Ridge Research Reactor (ORR). As was discussed in the previous paper,<sup>1</sup> this demonstration began with an all HEU equilibrium core (core 174C) which was followed by a sequence of HEU/LEU mixed cores in a gradual transition toward an all LEU  $U_3Si_2$ -Al equilibrium core. Except for two HEU shim rod followers, the 30-MW ORR reactor is currently operating with an all LEU core. During this transition phase a wealth of experimental data was obtained by the ORR staff against which computational codes and methods may be benchmarked. Some of these computational/experimental comparisons will be reported here. However, comparisons between measured and calculated cobalt wire activations will be given in the next paper.<sup>2</sup>

#### CODES AND METHODS

Figure 1 shows a map of a typical HEU/LEU transition core. The HEU and LEU 19-plate fuel elements are of identical geometry as are the 15-plate shim rod (SR) fuel followers. Fresh 19 and 15-plate elements contain 340 g and 200 g  $^{235}U$ , respectively, for the  $U_3Si_2$ -Al dispersion fuel and 285 g and

167 g, respectively, for the U<sub>3</sub>O<sub>8</sub>-Al HEU case. Magnetic fusion experiments (MFE) are located in grid positions C3 and C7 and the HFED (High uranium density Fuel Element Development) miniplate irradiation facility is in E3. Radioisotopes of europium and irridium were produced in the locations shown in Fig. 1. The pressure vessel simulator and gamma shield are part of the HSST (Heavy Section Steel Technology) experiment which is normally in a retracted position at core startup until equilibrium xenon concentrations have been achieved. The EPRI-CELL code<sup>3</sup> was used to generate 5-group cross sections for each region in the reactor. For computational purposes, each fuel element was represented by a fuel (meat-clad-moderator) region and a side plate (H<sub>2</sub>O/Al) region. Burnup-dependent cross sections were calculated for both HEU and LEU fuel using EPRI-CELL. In most cases these 5-group cross sections are based on ENDF/B Version IV data.

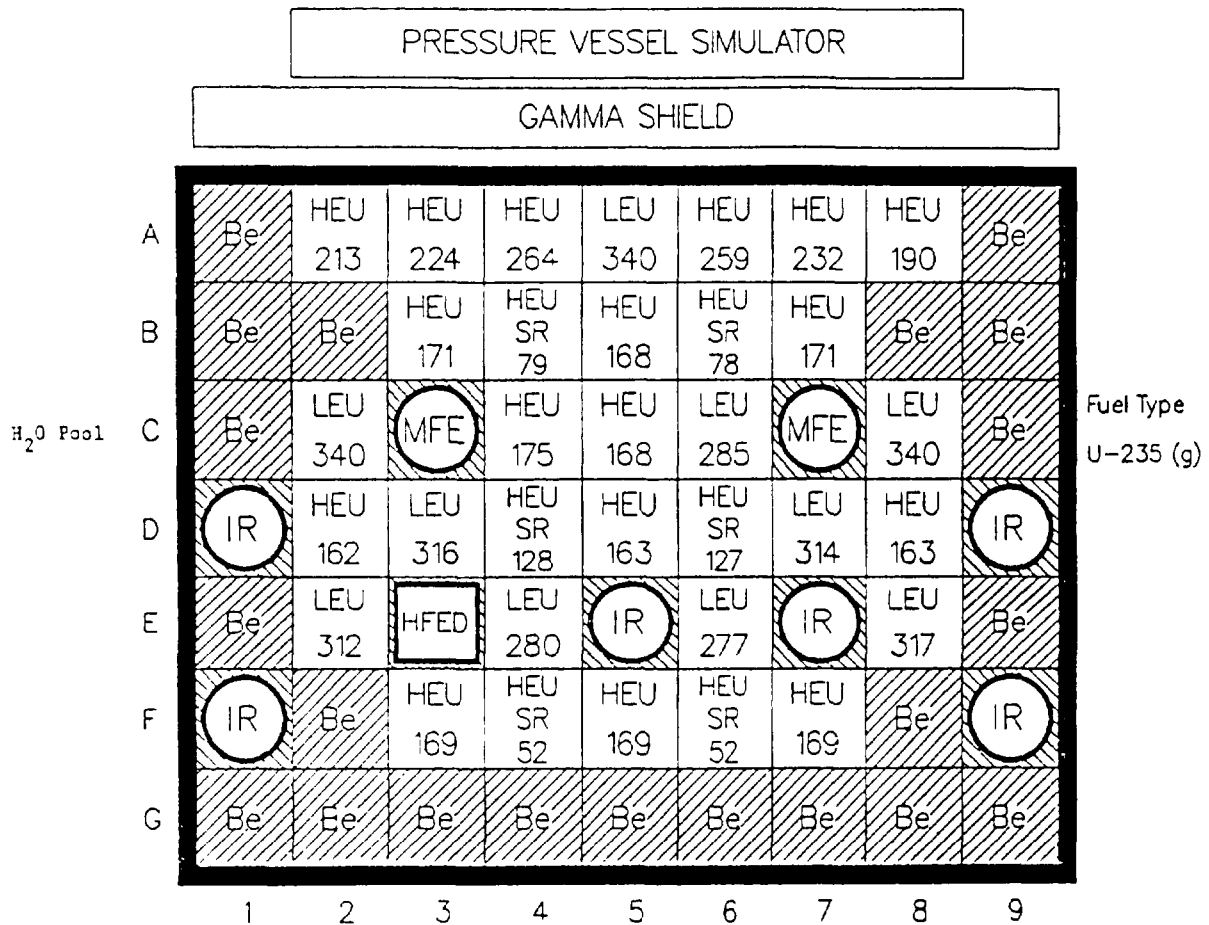


Fig. 1. ORR Cycle 175C

The burnup behavior of each fuel element in each reactor cycle was analyzed using the REBUS-3 fuel cycle analyses code.<sup>4</sup> Each of the HEU-to-LEU transition cores was analyzed by the REBUS-3 code as a non-equilibrium problem. This code allows for the use of burnup-dependent cross sections and for control rod movement during the burn cycle. In most of these calculations the burn cycle length, determined from the total MWh's of reactor operation, was divided into three equal sub intervals. Critical control rod positions at the boundaries of each of these sub intervals were determined from the recorded control rod position history and input into the REBUS problem. At each of these boundaries, or time nodes, the code determines burnup-dependent

atom densities in six axial regions of equal height for each fuel element, the eigenvalue, fuel element powers, and neutron fluxes. These calculations are based on diffusion theory for which the three-dimensional DIF3D code<sup>5</sup> is used. The buildup of neutron-induced <sup>6</sup>Li and <sup>3</sup>He poisons in the beryllium reflector, which begins with the fast neutron threshold reaction <sup>9</sup>Be(n,α)<sup>6</sup>He, are also taken into account in the REBUS-3 calculations. From numerous REBUS calculations a library of axially-dependent atom densities for partially burned fuel elements and fuel element followers has been obtained for use in subsequent calculations. These atom densities are appropriately adjusted for the shutdown decay of <sup>135</sup>I, <sup>135</sup>Xe and <sup>149</sup>Pm in the fuel elements and for the decay of <sup>3</sup>H into <sup>3</sup>He in the beryllium reflector.

The poison section of each shim rod consists of square water-filled cadmium annulus 0.040" thick, 2.30" on a side and 30.5" long. It was shown in Ref. 6 that these cadmium control elements may be represented in a diffusion calculation by using blackness-modified diffusion parameters in which the cadmium is black to group 5 neutrons ( $E_n < 0.625$  eV). In the normal operation of the ORR, shim rods F4 and F6 are fully withdrawn while the other four (B4, B6, D4, and D6) are banked together at a position to achieve criticality.

There are six evacuated beam tubes (6-7/8" ID) which leave the east side of the aluminum core box at various angles. The perturbing effect of these beam tubes on power and flux distributions within the core was investigated, in a preliminary way, using the two-dimensional transport code, TWODANT<sup>7</sup>. Just recently, three-dimensional continuous-energy VIM<sup>8</sup> Monte Carlo calculations<sup>9</sup> have been performed to study the effect of the beam tubes on certain core parameters. Some results of these calculations will be presented at the end of this report.

Calculated kinetic parameters for several ORR cores are based on ENDF/B Version V data. Beginning with REBUS-3 atom densities and flux distributions, the VARI3D code<sup>10</sup> was used to obtain  $\beta_{\text{eff}}$  and an appropriate set of  $(\lambda_1, \beta_1)$  kinetic parameters.

Numerous reactivity substitution measurements were made, relative to H<sub>2</sub>O and/or Al, for the irradiation modules, and the MFE, HFED, and HSST experiments. The worth of beryllium reflector pieces poisoned with <sup>3</sup>He and <sup>6</sup>Li was also measured relative to unirradiated beryllium. These measurements were used to show that all these facilities are reasonably well modeled in the diffusion calculations.

#### CALCULATED EIGENVALUES CORRESPONDING TO MEASURED CONTROL ROD POSITIONS AT CRITICALITY

From the control rod position data recorded throughout each burn cycle, critical rod positions at the boundaries of each subinterval of the cycle length were input into all of the REBUS-3 fuel cycle burnup calculations. The code then adjusts the control rod positions throughout the burn cycle and calculates the eigenvalue at each of these "time nodes." A small adjustment of the calculated eigenvalue is needed because the average coolant temperature is different from that at which the water cross sections were generated. For this correction a calculated temperature coefficient of

$$\alpha_T = - 1.104 \times 10^{-2} \% \frac{\delta k}{k} / ^\circ\text{F}$$

was used. Cross sections for the water coolant in the core were calculated at a temperature of 140°F which is the nearest temperature available in the cross section library to the average of the inlet and outlet coolant temperatures (~125°F). These coolant temperatures are recorded periodically throughout each operating cycle. The temperature correction to the eigenvalue amounts to a few tenths of a percent.

The eigenvalue calculations for each of the transition cores operated to date are summarized in Table I. The results in this table show that the eigenvalues are reasonably well-calculated and that the REBUS-3 code adequately accounts for the change in core reactivity due to fuel burnup. Note that no results are available for core 177C which shut down only a few days ago. The last entry in the table is also incomplete. This is the core which will be operating at the time of the ORR tour on Thursday.

Table I. Calculated Eigenvalues Corresponding to Measured Critical Rod Positions

Core	Fuel Elements <sup>a</sup>		CL in FPD's <sup>b</sup>	BOC	Calculated Eigenvalues			EOC
	HEU	LEU			1/3 CL	1/2 CL	2/3 CL	
174C	27+6	0+0	16.8402	1.0004	1.0018		1.0021	1.0021
174D	24+6	3+0	12.8451	1.0022		1.0023		1.0049
174E	24+6	3+0	10.6211	1.0043		1.0025		1.0027
174FX	20+6	7+0	0.0	0.9981				
174F	24+6	3+0	15.4290	1.0001	1.0008		1.0011	1.0020
175A	20+6	7+0	18.5178	1.0012	1.0018		1.0018	1.0012
175B	20+6	7+0	20.3036	0.9942	0.9949		0.9964	0.9972
175C	17+6	10+0	17.3544	0.9984	1.0015		1.0015	1.0020
176-AX1	13+4	14+2	0.0	1.0013				
176A	17+6	10+0	17.2238	1.0001	1.0001		1.0008	1.0029
176B	13+4	14+2	21.8612	1.0008	0.9992		1.0000	0.9984
176C	14+4	14+2	19.4343	1.0017	1.0012		1.0003	1.0011
176D	8+4	17+2	19.4449	1.0018	1.0003		1.0008	1.0027
177-AX1	4+2	21+4	0.0	1.0006				
177A	8+4	17+2	14.7716	0.9955	0.9963		0.9969	0.9988
177B	4+2	21+4	18.5173	1.0033	0.9996		0.9996	0.9997
177C	4+2	21+4						
177D	0+2	24+4						

<sup>a</sup>The notation 27+6 means there are 27 19-plate standard fuel elements in the core and 6 15-plate fuel follower elements.

<sup>b</sup>CL is the cycle length in full power days (FPD's).

It should be mentioned, however, that the results have not been corrected for the somewhat off-setting effects of neutron leakage through the six voided beam tubes and the depletion of cadmium near the bottom of the control elements. These matters are still under investigation but some preliminary findings will be presented later in this paper.

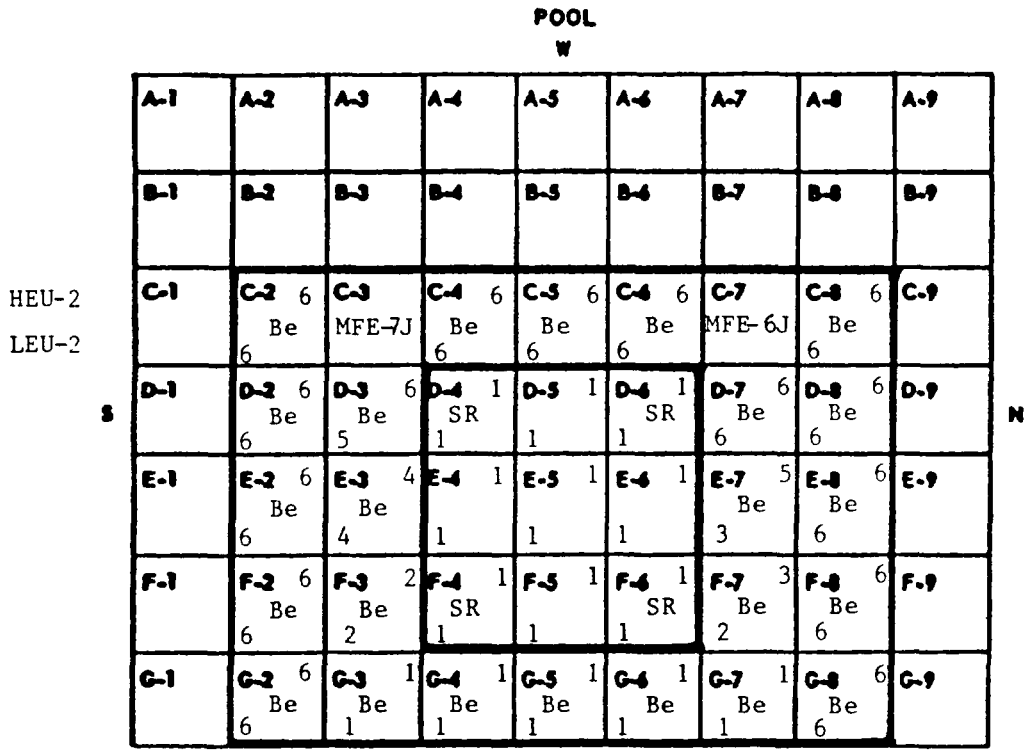
### FRESH FUEL CORES

Typical approach-to-critical measurements were made in the ORR using cores consisting of fresh HEU and LEU fuel and reflected with both water and beryllium. Figures 2 and 3 show the different core configurations and the loading steps followed in the approach-to-critical measurements. The beryllium-reflected cores consisted of a 3x3 assembly of fuel with shim rods located at each corner. Beryllium reflector pieces were added successively in the approach-to-critical studies. For these measurements all four control rods were banked together and moved as a unit. Table II gives the eigenvalue calculation corresponding to the critical banked rod position for each core configuration. For the water-reflected cores the eigenvalues are over-predicted by about 0.3% for the fresh HEU fuel and are under-predicted by about 0.7% for the fresh LEU fuel. The calculations tend to over-estimate the effect of the beryllium reflector by about 0.6%, but these results are very sensitive to the values used for the  $^6\text{Li}$  and  $^3\text{He}$  poison concentrations in the beryllium. These poison concentrations were estimated from incomplete records available for the irradiation history of each beryllium reflector element.

**POOL**  
W

	A-1	A-2	A-3	A-4	A-5	A-6	A-7	A-8	A-9
	B-1	B-2	B-3	B-4	B-5	B-6	B-7	B-8	B-9
HEU-1	C-1	C-2	C-3 MFE-7J	C-4 8	C-5 6 8	C-6 8	C-7 MFE-6J	C-8	C-9
LEU-2	D-1	D-2	D-3 6 3	D-4 1 SR 1	D-5 1	D-6 1 SR 1	D-7 6 6	D-8	D-9
S	E-1	E-2	E-3 2 2	E-4 1 1	E-5 1	E-6 1	E-7 3 5	E-8	E-9
	F-1	F-2	F-3 4 4	F-4 1 SR 1	F-5 1	F-6 1 SR 1	F-7 5 7	F-8	F-9
	G-1	G-2	G-3	G-4	G-5	G-6	G-7	G-8	G-9
									N
									E

Fig. 2. Approach-to-Critical Loading Sequence for H<sub>2</sub>O-Reflected Fresh Fuel Cores, HEU-1 and LEU-1.



**E**

Fig. 3. Approach-to-Critical Loading Sequence for Be-Reflected Fresh Fuel Cores, HEU-2 and LEU-2.

Table II. Calculated Eigenvalues Corresponding to the Measured Critical Rod Positions in Cores with Fresh Fuel

Core	Fuel	Reflector	Loading Step	Rod Bank* in.	$k_{eff}$
HEU-1	HEU	H <sub>2</sub> O	5	24.37	1.00275
HEU-1	HEU	H <sub>2</sub> O	6	17.21	1.00351
LEU-1	LEU	H <sub>2</sub> O	6	25.14	0.99485
LEU-1	LEU	H <sub>2</sub> O	7	21.33	0.99147
LEU-1	LEU	H <sub>2</sub> O	8	15.46	0.99122
HEU-2	HEU	Be	5	24.13	1.00754
HEU-2	HEU	Be	6	17.34	1.01104
LEU-2	LEU	Be	5	25.27	0.99687
LEU-2	LEU	Be	6	18.41	1.00075

\*The rod bank position is measured with respect to fully inserted rods where the 30.5 inch length of cadmium is symmetrically located about the core midplane.

Note: For loading steps not shown in this table the reactor was subcritical as shown by both experiments and calculations.

Because of the small size of these fresh cores, especially the beryllium reflected ones, the results are expected to be sensitive to core-reflector interface effects which are not properly accounted for in diffusion theory. Therefore, detailed Monte Carlo calculations are planned but no results are currently available.

Differential shim rod worths were measured in these fresh cores by the positive period technique. Table III compares measured and calculated values of the %  $\frac{\delta k}{k}/\text{in.}$  As can be seen, there is a wide scatter in the calculated-to-experimental (C/E) ratios. These discrepancies are still under investigation and some improvement may result from refined calculations. However, to-date no completely satisfactory explanation has been found for this spread in the C/E ratios. The repeatability of the experimental measurements appears to be of the order of 5-7%.

Table III. ORR Differential Rod Worths in Fresh Fuel Cores

Core	Reflector	Rod	$R_1^*$	$R_f^*$	Bank	% $\frac{\delta k}{k}/\text{in.}$		C/E
			in.	in.		Calc.	Exp.	
HEU-1	H <sub>2</sub> O	D4	12.00	12.36	20.83	0.5536	0.4936	1.122
HEU-1	H <sub>2</sub> O	D6	16.75	17.21	17.21	0.3255	0.3290	0.989
HEU-1	H <sub>2</sub> O	F4	12.00	12.26	20.03	0.4793	0.4579	1.047
LEU-1	H <sub>2</sub> O	D4	12.00	12.22	17.65	0.6154	0.6265	0.982
LEU-1	H <sub>2</sub> O	D6	14.65	15.46	15.46	0.4871	0.4991	0.976
LEU-1	H <sub>2</sub> O	F4	12.00	12.32	16.64	0.3993	0.4025	0.992
HEU-2	Be	D4	12.00	12.19	20.97	0.6312	0.5006	1.261
HEU-2	Be	D6	12.00	12.22	20.88	0.6213	0.5418	1.147
HEU-2	Be	F4	12.00	12.19	21.20	0.6806	0.5483	1.241
HEU-2	Be	F6	12.00	12.17	21.15	0.6779	0.5676	1.194
LEU-2	Be	D4	15.00	15.27	20.33	0.5257	0.5360	0.981
LEU-2	Be	D6	15.00	15.25	20.21	0.5164	0.5236	0.986
LEU-2	Be	F4	15.01	15.23	20.55	0.5905	0.5137	1.150
LEU-2	Be	F6	15.00	15.28	20.42	0.5912	0.5653	1.046

\*  $R_f - R_1$  is the step change in the rod position which produced the positive asymptotic period.

### $\beta_{\text{eff}}$ AND THE PROMPT NEUTRON LIFETIME

The ratio of the effective delayed neutron fraction to the prompt neutron lifetime,  $\beta_{\text{eff}}/\ell_p$ , was measured by J. T. Mihalczko and G. E. Ragan in several ORR cores using a two-detector cross-correlation method<sup>11</sup> to obtain the prompt neutron decay constant. To determine the calculated ratio,  $\beta_{\text{eff}}$  and  $\ell_p$  were evaluated separately. Beginning with flux distributions and burnup-dependent cross sections and atom densities from previous REBUS-3 calculations, the

VARI3D code<sup>10</sup> was used to first calculate the adjoint flux and subsequently  $\beta_{\text{eff}}$ . The code also evaluates a 6-family coalesced set of the kinetic parameters ( $\lambda_j, \beta_j$ ) from ENDF/B Version V delayed neutron data.

The prompt neutron lifetime was calculated by considering the change in the eigenvalue resulting from a uniform distribution of a purely  $1/v$  absorber throughout the entire reactor volume. The fractional change in  $k$  resulting from this perturbation is given by

$$\frac{\delta k}{k} = k \int_V [\sum_j \phi_j^* \delta \Sigma_{aj} \phi_j] dV / PD \quad (1)$$

where PD is the perturbation denominator. This result, when combined with the equation for the prompt neutron lifetime,

$$\lambda_p = k \int_V [\Sigma_j \phi_j \phi_j^* / v_j] dV / PD, \quad (2)$$

yields

$$\lambda_p = \frac{\delta k}{k} / N \sigma_{ao} v_o. \quad (3)$$

Here  $N$  is the concentration (atoms/b-cm) of the purely  $1/v$  absorber whose cross section is  $\sigma_{ao}$  when the neutron velocity is  $v_o$ . Strictly speaking, Eq. (3) is valid only in the limit as  $N \rightarrow 0$ .

This  $1/v$  insertion method was used to evaluate  $\lambda_p$  where  $^{10}\text{B}$  was chosen as the  $1/v$  absorber. At 2200 m/sec  $\sigma_{ao} (^{10}\text{B}) = 3837$  barns. Burnup-dependent infinitely dilute  $^{10}\text{B}$  cross sections were generated for spectra characteristic of each reactor region and calculations were performed for atom concentrations of  $5.0 \times 10^{-8}$  and  $2.5 \times 10^{-8}$  atoms/b-cm. Final results were obtained by extrapolation to zero  $^{10}\text{B}$  concentration. Effects from elastic and inelastic scattering and from the non- $1/v$  behavior of the  $^{10}\text{B}$  absorption cross section above about 0.3 MeV were found to have a totally negligible influence on  $\lambda_p$  evaluated by this  $^{10}\text{B}$   $1/v$  insertion method.

Results of these  $\beta_{\text{eff}}$  and  $\lambda_p$  calculations are summarized in Table IV where the ratios of the two are compared with the measured values. Although measurements were made in each of the cores indicated in Table IV, experimental results<sup>12</sup> are available only for the water-reflected fresh cores. For these two cases the calculated  $\beta_{\text{eff}}/\lambda_p$  values agree remarkably well with the measurements. A strong photoneutron source term from the beryllium reflector together with a low frequency noise problem in the measurement of the frequency-dependent cross-power spectral density function so far have made it impossible to determine  $\beta_{\text{eff}}/\lambda_p$  in the other cores. However, the results do show that  $\beta_{\text{eff}}/\lambda_p$  is smaller in these cores than in the fresh cores which is in qualitative agreement with the calculations.

Table IV.  $\beta_{eff}$  and the Prompt Neutron Lifetime

Core	Fuel Elements*		$\beta_{eff}$	$\lambda_p$ μ-sec.	$\beta_{eff}/\lambda_p$ (sec <sup>-1</sup> )		C/E
	HEU	LEU			Calc.	Exp.	
HEU-1	12+4	0+0	8.0522-3	47.8731	168.2	169.0 ± 0.9	0.9953 ± 0.0053
LEU-1	0+0	14+4	7.9796-3	41.5521	192.0	193.1 ± 0.8	0.9943 ± 0.0041
176B	13+4	14+2	7.4503-3	62.7516	118.7		
176BX2	27+6	0+0	7.4740-3	69.7233	107.2		
177AX2	4+2	21+4	7.3730-3	66.8051	110.4		

\*The notation 12 + 4 means there are 12 19-plate standard fuel elements in the core and 4 15-plate fuel follower elements.

#### ON-GOING ANALYTICAL STUDIES

##### Perturbing Influences of Voided Beam Tubes

The REBUS-3 non-equilibrium studies described earlier (Table I) do not account for the perturbing effects of the six voided beam tubes. Preliminary studies of the influence of the evacuated beam tubes on flux and power distributions in the core were made using two-dimensional XY transport theory calculations. By comparing these results with analogous XY diffusion calculations, it was found that the effect of the beam tubes could be represented approximately in a DIF3D calculation by filling the beam tubes with about 3% of normal water density. However, these XY studies suffer from the fact that they do not allow one to model the actual three-dimensional character of the beam tubes nor do they permit one to model the real angles at which the beam tubes leave the aluminum core box on the east side of the core. For these reasons beam tube effects were studied using the continuous energy, three-dimensional Monte Carlo Code, VIM<sup>9</sup>. Calculations were done for the case of voided beam tubes and for the case of the beam tubes flooded with water at normal density for core 177-AX1. Similar XYZ calculations were made with the DIF3D diffusion code where the "voided" case corresponded to water at 3% of normal density. Although comparisons between the two types of calculations are still preliminary and incomplete, some observations can be made.

1. The two types of calculations are consistent in their predictions of the amount by which the eigenvalue is lowered due to neutron leakage through the voided beam tubes relative to the flooded case.

<u>Calculation</u>	<u><math>\delta k_{eff}</math>, %</u>
VIM - Monte Carlo	-0.73 ± 0.33
DIF3D - Diffusion	-0.493

2. Within the statistics of the Monte Carlo calculations (based on 200,000 neutron histories), the voided-to-flooded ratio of the region-integrated fission rates for VIM and DIF3D agree.

<u>Row</u>	<u>Voided-to-Flooded Fission Rate Ratio</u>	
	<u>VIM-Monte Carlo</u>	<u>DIF3D</u>
A	1.032 ± 0.015	1.025
B	1.039 ± 0.017	1.021
C	1.021 ± 0.013	1.011
D	0.983 ± 0.011	1.001
E	0.978 ± 0.014	0.982
F	0.942 ± 0.011	0.950

The statistical errors correspond to one standard deviation.

3. The eigenvalues for the Monte Carlo calculations have a standard deviation of about 0.24% and are about 1.0% larger than the corresponding diffusion calculations. Before the reason for this discrepancy is understood, a detailed analyses of the results from both sets of calculations needs to be done.

Energy, position and angular coordinates for each neutron crossing the plane of the aluminum core box on the east side of the core where the beam tubes are located have been saved on a tape from the Monte Carlo calculations. From this information we plan to construct group and position-dependent reflection coefficients (albedos) for subsequent use in diffusion calculations where the beam tubes will be accounted for by means of these boundary conditions.

#### Differential and Integral Rod Worths

Differential shim rod worths ( $\% \frac{\delta k}{k}/\text{in.}$ ) are measured in the ORR by the positive period technique. This data is then integrated from the lower to the upper limit of rod movement to obtain the total rod worth. Measured and calculated differential worths for the HEU and LEU fresh cores were given in Table III. Except for the beryllium-reflected HEU core, these calculated and measured differential worths are in reasonable agreement if one takes into account repeatability errors (~5-7%) associated with the measurements. Some additional refinements in these calculations remain to be done and this may improve the C/E ratios.

For reasons which are at best only partly understood, however, calculated differential worths in the partially depleted HEU/LEU mixed cores are usually substantially larger than the measured values. This is illustrated in Table V for recent measurements made in core 177-AX1. The calculations include an approximate treatment for the perturbing effects of the voided beam tubes, the depletion of  $^{113}\text{Cd}$  in the lower sections of the cadmium poison regions (due to the irradiation of the shim rods in previous burn cycles), and the depletion of  $^{235}\text{U}$  in the fuel followers. Kinetic parameters ( $\lambda_1, \beta_1$ ) were generated for this core and used to convert measured periods to reactivities. Clearly there are effects, perhaps associated with shim rod burnups, which are not properly modeled in the calculations. In an effort to better understand this worth discrepancy we plan to do the following.

Table V. Differential Shim Rod Worths in Core 177-AX1

Rod	$R_i$ in.	$R_f$ in.	Bank in.	$k_{eff}^*$ (at $R_i$ )	C/E Worth Ratios			
					$(\lambda_1, \beta_1)$ ORR	$(\lambda_1, \beta_1)$ ANL	+ Voided B.T.'s	+ Cd Depl.
F6	12.00	12.66	16.24	0.9975	1.623	1.804	1.704	1.501
F4	12.00	12.62	16.25	0.9975				1.642
B6	12.00	12.41	16.66	0.9975				1.475
B4	11.99	12.39	16.69	0.9975				1.572
D6	6.00	6.60	19.59	0.9967				0.787
D6	12.00	12.23	17.48	0.9977				1.020
D6	18.00	18.39	15.17	0.9977				1.265
D4	12.00	12.26	17.66	0.9978				1.112

\*With the rod at the initial position,  $R_i$ , the reactor was critical. The rod was then withdrawn to  $R_f$  and the positive period measured.

Note: Prior to these measurements shim rods F4 and F6 had been irradiated for 7 burn cycles, B4 and B6 for 3 cycles, and D4 and D6 for 0 cycles.

1. Investigate the effect of the cross section mis-match between those sections of the fuel followers located in the core and the lower parts in the water reflector below the core. To date, fuel follower cross sections have been generated only for a core environment.
2. At the next shutdown period in the ORR differential worth measurements will be made using sets of both burned and fresh shim rods. This data should show whether we are able to better calculate differential worths for fresh shim rods than for burned ones.
3. Some worth measurements will be made at several power levels in order to determine the importance of the inherent neutron source term from photoneutron reactions mostly on beryllium.
4. Data will be taken to better determine repeatability errors associated with rod worth measurements.
5. The die-away curve following a rod drop will be measured in order to determine an effective set of kinetic parameters  $(\lambda_1, a_1)$ . Unfortunately, this method does not determine  $\beta_{eff}$ .

#### ACKNOWLEDGEMENTS

We at ANL are very indebted to the entire operating staff of the Oak Ridge Research Reactor for supplying us, in a very timely manner, experimental results and details for each operating core. Without such information analytical calculations would be meaningless.

## REFERENCES

1. R. W. Hobbs, M. M. Bretscher, R. J. Cornella, and J. L. Snelgrove, "The Transition Phase of the Whole-Core Demonstration at the Oak Ridge Research Reactor," these proceedings.
2. R. J. Cornella, M. M. Bretscher and R. W. Hobbs, "Comparison of Calculated and Measured Irradiated Wire Data For HEU and Mixed HEU/LEU Cores in the ORR," these proceedings.
3. B. A. Zolotar, et al., "EPRI-CELL Description," Advanced Recycle Methodology Program System Documentation, Part II, Chapter 5, Electric Power Research Institute (September 1977). EPRI-CELL code supplied to Argonne National Laboratory by Electric Power Research Institute, Palo Alto, California (1977).
4. B. J. Toppel, "A User's Guide for the REBUS-3 Fuel Cycle Analysis Capability," Argonne National Laboratory Report ANL-83-1 (March 1983).
5. K. L. Derstine, "DIF3D: A Code to Solve One, Two, and Three-Dimensional Finite-Difference Diffusion Theory Problems," Argonne National Laboratory Report ANL-82-64 (April 1984).
6. M. M. Bretscher, "Blackness Coefficients, Effective Diffusion Parameters, and Control Rod Worths for Thermal Reactors," ANL/RERTR/TM-5 (September 1984).
7. R. E. Alcouffe, F. W. Brinkley, D. R. Marr, and R. D. O'Dell, "User's Guide for TWODANT: Two-Dimensional Diffusion Accelerated Neutral Particle Discrete-Ordinates Transport Code," LA-10049-M (February 1984).
8. R. Blomquist, "VIM-A Continuous Energy Neutronics and Photon Transport Code," pp. 222-224, ANS Proceedings of Topical Meeting on Advances in Reactor Computations, Salt Lake City, Utah, March 28-31, 1983.
9. The VIM-Monte Carlo calculations were performed by R. M. Lell of ANL and are very gratefully acknowledged.
10. The VARI3D Code is under development at the Argonne National Laboratory (October 1986).
11. W. Seifritz, D. Stegemann, and W. Vath, "Two-Detector Cross-Correlation Experiments in the Fast-Thermal Argonaut Reactor (Stark)," Symposium on Neutron Noise, Waves, and Pulse Propagation, University of Florida, Feb. 14-16, 1966. USAEC CONF-660206.
12. C. E. Ragan and J. T. Mihalcz, "Prompt Neutron Decay Constant for the Oak Ridge Research Reactor with 20 wt%  $^{235}\text{U}$  Enriched Fuel," paper to be presented at the ANS Winter Meeting, Washington, D.C., Nov. 16-20, 1986.

## Appendix H-5.2

### COMPARISON OF CALCULATED AND MEASURED IRRADIATED WIRE DATA FOR HEU AND MIXED HEU/LEU CORES IN THE ORR

R.J. CORNELLA, M.M. BRETSCHER  
RERTR Program,  
Argonne National Laboratory,  
Argonne, Illinois

R.W. HOBBS  
Oak Ridge National Laboratory,  
Oak Ridge, Tennessee

United States of America

#### Abstract

Low power wire activations are being performed in the Oak Ridge Research Reactor (ORR) as part of the whole-core LEU demonstration experiments. Calculations of the demonstration cores, including simulation of the wire activations, are being performed at Argonne National Laboratory (ANL). This paper presents the results of comparisons for 293 wires from five cores and shows that, on the average, the integrated activities agree within 6%.

#### INTRODUCTION

Low power wire activation measurements are being performed in the Oak Ridge Research Reactor (ORR) during the whole-core demonstration of LEU fuel.<sup>1</sup> These measurements have the dual purpose of allowing prediction of maximum fuel power density prior to full power operation of the reactor and of providing data for comparison with results of calculations. Among the many detailed calculations of the demonstration cores being performed at Argonne National Laboratory (ANL)<sup>2</sup> are simulations of the wire activations. The purpose of this report is to describe the methods by which comparisons of calculated and measured wire data are made and to present the results obtained thus far.

#### DESCRIPTION OF METHODS

This section describes the procedures used to obtain a comparison of calculated and measured data for wires irradiated in the ORR. In part, these procedures are invoked through the use of a Fortran code which was written specifically for this application and which operates interactively within ANL's central computing environment.

## Data Generation

The calculated relative axial activity of a flux wire is inferred from the product of five-energy-group fluxes and wire cross sections. The reactor flux is obtained from a three-dimensional diffusion theory calculation of the reactor, and the wire cross sections are obtained from a one-dimensional integral transport theory cell calculation of the wire and its general environment. The relative wire activity is calculated at the center of each of the three-dimensional mesh cells of the analytical model.

The measured axial activity profile of a flux wire is determined at ORNL using a computer-controlled gamma scanning system. The data collected by this system are stored on a floppy disk which is subsequently mailed to ANL. The measured activity dataset contains, for each wire, reactor location tags and pairs of numbers corresponding to lineal wire position and associated activity. The activities, as received, are corrected for background, counting dead time and decay since irradiation. For a wire irradiated within a fuel element, the location tags give the x-y coordinates of the wire in terms of reactor row and column, water channel number, and location and distance north or south of the comb. For wires irradiated in a beryllium reflector block or in a control rod fuel follower, the x-y location is assumed to be the central coordinates of the corresponding element location.

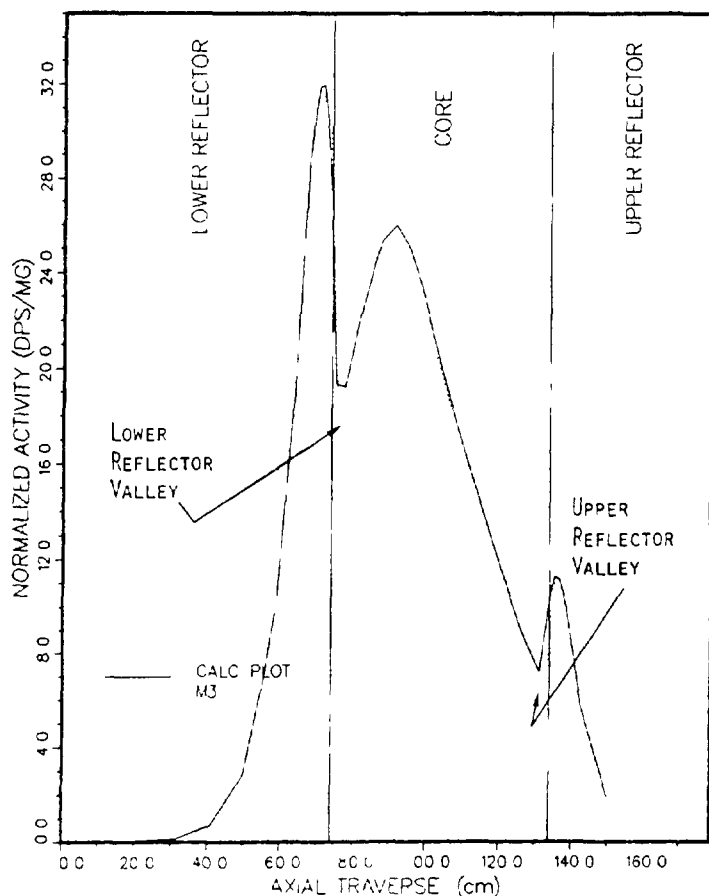
## Adjustment Of Data

The comparison of calculated and measured data for a given wire is reported in terms of a C/E ratio which is usually based upon integrated activities over the active height of the fuel. Prior to making this comparison the calculated and measured data undergo adjustment.

The measured data undergo a process of axial alignment which begins with categorization of each of the irradiated wires. A wire is categorized as qualified if it possesses the following two attributes: 1) the wire was resident in a standard fuel element during irradiation and 2) the characteristics of the wire's activity profile allow for unambiguous identification of upper and lower reflector valleys. The activity profile of each qualified wire is axially offset such that its reflector valleys are centered with respect to those of its analytical counterpart and is integrated over the active height of the fuel. The sum of all such integrals forms the numerator of a normalization constant. Figure 1 shows an aligned pair of calculated and measured activity profiles and their associated upper and lower reflector valleys.

A wire is categorized as non-qualified if it does not possess both of the above attributes. The activity profile of a non-qualified wire is axially offset so as to align its peak activity with that of its analytical counterpart. These data are neither integrated nor used in the formation of the normalization constant mentioned above.

The calculated data are integrated over the active height of the fuel at the center of all mesh cells in the x-y plane. The counterpart of a qualified wire's integral is found by linear interpolation between these analytical integrals to the coordinates of the qualified wire. The sum of these interpolated integrals forms the denominator of the normalization constant mentioned above. All of the three-dimensional mesh cell-centered data are then scaled by this normalization constant.



	M7	M8	
		M4	M6
		V1	M2
	M5	M3	
	M9	M10	

CORE LOCATION D3

- C/E (M1) = 1.03
- C/E (M2) = 0.93
- C/E (M3) = 1.05
- C/E (M4) = 1.00
- C/E (M5) = 1.00
- C/E (M6) = 0.97
- C/E (M7) = 0.91
- C/E (M8) = 0.94
- C/E (M9) = 1.02
- C/E (M10) = 1.05

Figure 1. ORR Core 176AX, Fuel Element D3 - Calculated and Measured Activity Profiles for Wire M3, Wire Locations Superimposed on X-Y Mesh Structure and the Associated C/E's.

### C/E Ratios

As indicated above, a wire's C/E ratio is usually based upon a comparison of integrated activities over the active height of the fuel. This is the case for all qualified wires. The numerator of the C/E ratio is equal to the interpolated activity integral taken from the normalized calculated data and the denominator is equal to the activity integral taken from the measured data. Due to the existence of flux gradients across the reactor fuel assemblies it is necessary to have accurate location data for the wire if meaningful C/E's are to be calculated. The standard fuel element attribute is required for qualified wires because it is only in these elements that we are certain of a wire's x-y location. The valley identification attribute is required for qualified wires in order to provide accurate parameters to the alignment algorithm and to assure that subsequent integrations are performed over the active height of the fuel.

The C/E ratio for all non-qualified wires, including those in fuel followers, is initially based upon a comparison of peak activities only. The operators of the ORR attempt to place the wire in the central water gap of the follower, however, due to the control rod's configuration, it is impossible to see where the wire finally resides. As a result, there is uncertainty in the wire's x-y location within the follower. Also, there is uncertainty in the axial location of the wires which are irradiated in beryllium reflector blocks.

After the initial C/E's are calculated it is possible to interact with the Fortran code. These interactions include viewing selected experimental and analytical data in either digital or analog form as well as offsetting and attempting integration of previously unqualified experimental data. Such interactions are generally exercised with the measured fuel follower data. If the follower data include valleys and peaks which reflect those of the corresponding calculated data then its data is axially offset to align it with the calculated data. If the subsequent integration is successful the data then becomes qualified and a C/E based upon integrals is calculated. The integration is successful if the offset wire data extends over the active height of the fuel in the follower. The analytical data used for offsetting and calculating a C/E is that corresponding to the central x-y coordinates of the follower.

### RESULTS OF COMPARISON

To date, the C/E's for 293 wires from five cores have been determined. The average magnitude by which these C/E's differ from unity and the associated standard deviation are 6.0% and 4.7%, respectively. Twenty-two of these wires were non-qualified and their corresponding statistics are 10.5% and 8.4% respectively. Generally, the wires irradiated within the interior of the core show C/E's closer to unity than those on the periphery of the core. The five cores analyzed thus far for irradiated wire C/E ratios are 174C, 174FX, 176AX, and two water reflected criticals--HEU-1 and LEU-1.

Figures 2, 3, and 4 give average C/E ratios for the 174FX, HEU-1, and LEU-1 cores, respectively. The average magnitudes by which C/E's differ from unity are 6.2%, 5.4%, and 3.9%, respectively.

ORR CORE 174FX  
AVERAGE C/E RATIOS FOR IRRADIATED WIRES

A	Be	1.04	1.01	1.02	1.10	0.96	0.95	0.98	Be	
B	Be	Be	0.96	SR	0.92	SR	0.92	Be	Be	
C	Be	1.12	MFE	1.02	0.93	1.01	MFE	1.00	Be	
D	Be	0.98	1.07	SR	0.91	SR	1.00	0.80	Be	
E	Be	1.06	HFED	0.99	IR	0.96	IR	0.98	Be	
F	Be	Be	1.11	SR	1.04	SR	1.15	Be	Be	
G	Be	Be	Be	Be	Be	Be	Be	Be	Be	
		1	2	3	4	5	6	7	8	9

Figure 2.

ORR CORE HEU-1  
AVERAGE C/E RATIOS FOR IRRADIATED WIRES

A	Water								
B	Water								
C	Water	Water	MFE	Water	0.98	Water	MFE	Water	Water
D	Water	Water	1.02	SR	1.09	SR	0.97	Water	Water
E	Water	Water	1.06	1.04	1.05	0.94	0.89	Water	Water
F	Water	Water	****	SR	1.01	SR	0.90	Water	Water
G	Water								
	1	2	3	4	5	6	7	8	9

Figure 3.

ORR CORE LEU-1  
AVERAGE C/E RATIOS FOR IRRADIATED WIRES

A	Water								
B	Water								
C	Water	Water	MFE	1.00	1.03	1.02	MFE	Water	Water
D	Water	Water	1.02	SR	1.08	SR	1.00	Water	Water
E	Water	Water	0.96	0.99	0.97	0.98	0.92	Water	Water
F	Water	Water	0.94	SR	1.12	SR	0.96	Water	Water
G	Water								
	1	2	3	4	5	6	7	8	9

Figure 4.

Figures 5 and 6 give average C/E ratios for the 174C and 176AX cores. These results show the effect of a diffusion theory modelling enhancement which is being pursued. Until recently, the analytical model of the core has not included a description of the voided beam tubes along the east side of the core. Rather, this area of the pool has been described as water (flooded beam tubes). RERTR Program staff are presently working on a model of the voided beam tubes. The status of this model is preliminary, however, it has been applied to the 174C and 176AX cores in order to investigate its affect upon irradiated wire C/E ratios. Figure 5 gives the results of two wire analyses for the 174C core. The upper-most number at each reactor location gives the average C/E ratio for the case where the beam tubes have been voided within the analytical model of the core. The lower number, given parenthetically, gives the average C/E ratio for the case where the beam tubes are assumed to be flooded with water. As indicated, the effect of the voided beam tubes is to shift the flux from east toward west with the most significant changes occurring in the G (east), F, and A rows. Although the introduction of voided beam tubes has generally improved C/E's in the G row beryllium reflector blocks, the C/E's in the F and A rows have generally been degraded. Overall, the average magnitude by which C/E's differ from unity is 0.5% smaller for the the case of flooded beam tubes (6.9%) than it is for the case of voided beam tubes (7.4%). Figure 6 gives the results of a similar study for the 176AX core. The magnitude and sign of the C/E changes in this core are essentially the same as they were in the 174C core. However, in the case of the 176AX core the average magnitude by which C/E's differ from unity is 1.2% smaller (3.7%) for the case of voided beam tubes than it is for the case of flooded beam tubes (4.9%).

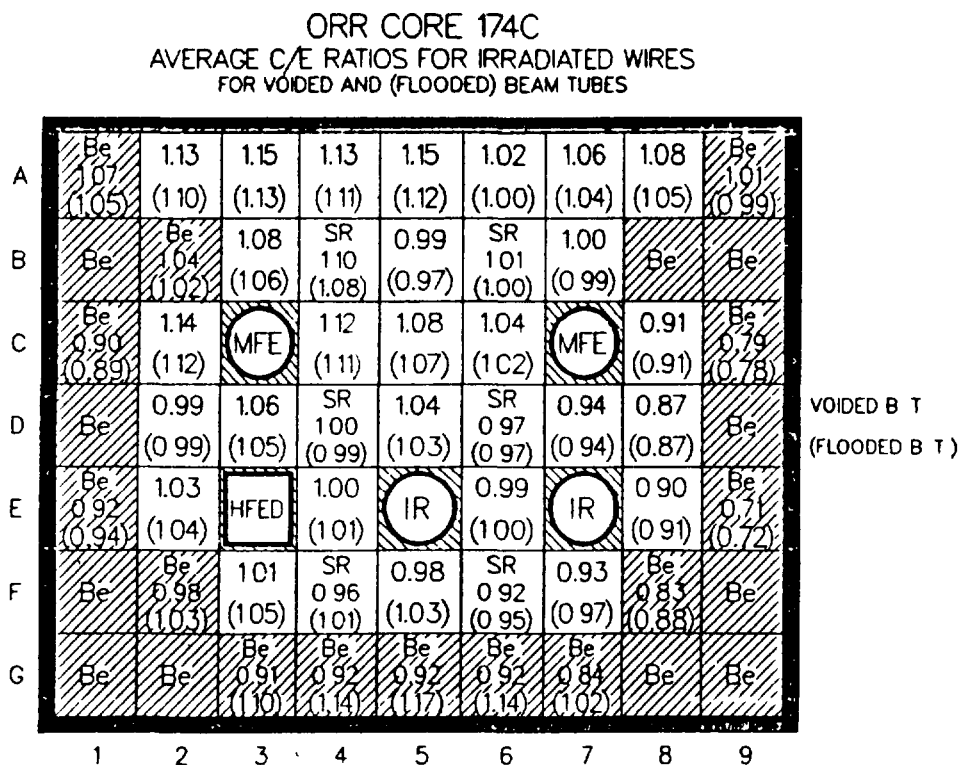


Figure 5.

ORR CORE 176AX  
 AVERAGE C/E RATIOS FOR IRRADIATED WIRES  
 FOR VOIDED AND (FLOODED) BEAM TUBES

A	Be	0.94 (0.91)	0.97 (0.94)	1.00 (0.96)	1.01 (0.97)	0.99 (0.96)	0.96 (0.93)	0.98 (0.96)	Be	
B	Be	Be	1.04 (1.04)	SR	0.97 (0.94)	SR	0.97 (0.95)	Be	Be	
C	Be	1.03 (1.02)	MFE	1.06 (1.04)	0.96 (0.95)	0.99 (0.98)	MFE	0.97 (0.96)	Be	
D	Be	0.94 (0.95)	1.00 (0.99)	SR	0.97 (0.97)	SR	1.01 (1.01)	0.96 (0.96)	Be	VOIDED B T (FLOODED B T)
E	Be	1.02 (1.05)	HFED	1.03 (1.05)	IR	1.05 (1.07)	IR	1.02 (1.05)	Be	
F	Be	Be	1.04 (1.12)	SR 0.89 (0.94)	0.96 (1.02)	SR	1.01 (1.07)	Be	Be	
G	Be	Be	Be	Be	Be 0.99 (1.25)	Be	Be	Be	Be	
		1	2	3	4	5	6	7	8	9

Figure 6.

Wires are typically loaded into the water channel of a fuel element as a two wire assembly which locates one wire near the comb (inner wire) and one wire near the side plate (outer wire). The C/E's display a trend where, for a given assembly, the inner wire's C/E is greater than the outer wire's C/E. For the 176AX core, the magnitude of this difference has a range between zero and 10% and a mean of 4%. The other four cores show a similar trend. The implication of this correlation is that the analytical model overpredicts the axially integrated flux in the center of a fuel element and underpredicts it near the side plate. This implication is generally consistent with comparisons of diffusion theory and Monte Carlo calculations performed within the RERTR Program. The consistency of this correlation also implies that the uncertainty in the experimental data is not large enough to mask this result. The upper right-hand corner of Figure 1 shows a schematic of the x-y mesh structure which was used for the analytical model of the fuel element in location D3 of the 176AX core. Superimposed upon this mesh structure are the abbreviated i.d.'s (M1, M2, ....., M10) of the ten wires which were irradiated in this fuel element. The wire pairs (M1, M2), (M3, M5), and (M4, M6) correspond to three two-wire assemblies. The C/E's shown below the schematic reflect the inner-to-outer C/E bias discussed in this paragraph.

SUMMARY

The comparison of calculated and measured irradiated wire data will continue throughout the whole-core demonstration of LEU fuel. Thus far, the activities of 293 irradiated wires have been compared with their analytical counterparts and the agreement, on the average, is within 6%. Core location-dependent biases in the agreement are being studied in order to ascertain the potential need for analytical modeling enhancements.

## REFERENCES

1. R. W. Hobbs, "The Transition Phase of the Whole-Core Demonstration at the ORR", these proceedings.
2. M. M. Bretscher, "Analytical Support for the ORR Whole-Core LEU  $U_3Si_2$ -Al Fuel Demonstration," these proceedings.

## Appendix H-6

### MEASUREMENTS AND ANALYSIS OF CRITICAL ASSEMBLIES FOR RESEARCH REACTORS WITH MIXED ENRICHMENTS

J.R. DEEN, J.L. SNELGROVE  
RERTR Program,  
Argonne National Laboratory,  
Argonne, Illinois

R.W. HOBBS  
Oak Ridge National Laboratory,  
Oak Ridge, Tennessee

United States of America

#### Abstract

A series of experiments with MEU and LEU fuel elements in the HEU-fueled Pool Critical Assembly at ORNL were performed in order to study the effects on excess reactivity and power density distributions in mixed-enrichment cores. This paper reports the results of these measurements and the subsequent validation calculations performed at ANL.

#### I. Introduction

As part of the RERTR Program whole-core demonstration in the Ford Nuclear Reactor (FNR) at the University of Michigan, data have been obtained which will allow more extensive validation of neutronics methods for whole-core calculations of an equilibrium high-enriched-uranium (HEU) core and a fresh low-enriched-uranium (LEU) core.<sup>1</sup> It is also important to validate the methods for analysis of mixed-enrichment cores, especially for those cases where one to a few lower-enriched elements with higher  $^{235}\text{U}$  content are placed in a higher-enriched core. This situation is expected to occur frequently during stepwise core conversions where one begins substituting lower-enriched elements for higher-enriched elements in the normal fuel cycle. In planning for such conversions one must be able to accurately predict the power density distribution in the lower-enriched elements in order to be able to evaluate thermal-hydraulic safety margins. It is also important to be able to predict core reactivity. A series of experiments designed to provide the data needed for these validations has been performed in the Pool Critical Assembly (PCA) at the Oak Ridge National Laboratory (ORNL). This paper reports the results of the measurements and of the subsequent validation calculations performed at ANL.

Measurements were made on approximately 20 different critical configurations in the PCA during the period June 15-26, 1981. The normal PCA fuel elements contained high-enriched uranium (HEU, 93 wt%  $^{235}\text{U}$ ) while the reduced-enrichment fuel elements, obtained for irradiation testing in the Oak Ridge Research Reactor (ORR) under the fuel demonstration activity of the RERTR Program, contained either medium-enriched uranium (MEU, 45 wt%  $^{235}\text{U}$ ) or low-enriched uranium (LEU, 19.8 wt%  $^{235}\text{U}$ ). All of the fuel elements used in these experiments were essentially fresh. The elements used were 18-plate, 140-g- $^{235}\text{U}$ , HEU PCA elements, 19-plate, 200-g- $^{235}\text{U}$  and 265-g- $^{235}\text{U}$ , HEU ORR elements,

19-plate, 282-g-<sup>235</sup>U, MEU RERTR test elements, and 13-plate, 340-g-<sup>235</sup>U, LEU RERTR test elements. In addition, four 9-plate, 70-g-<sup>235</sup>U, HEU PCA control elements were used. A complete description of the elements is presented in Tables 1 and 2. Measurements were made of critical core loadings using various combinations of HEU, MEU, and LEU fuel elements. For several of these configurations, more than one control rod insertion pattern was used in order to provide data for testing control rod worth calculations. Axial and radial fission rate traverses were made in several different cores, in as many as eight different fuel elements for a single core and in up to five different midplane positions within a single element. These measurements provided: criticality data for comparison of all-HEU cores with mixed-enrichment cores; fission density maps of all-HEU and mixed-enrichment cores, including detailed radial data for the core and individual fuel elements and axial data near and away from control rods both in the fuel zone and in the axial reflector; and partial differential worth profiles for the regulating rod and one shim rod.

Table 1. High-Enriched Fuel Element Characteristics

Parameter	Control PCA HEU	Standard PCA HEU	ORR HEU #1	ORR HEU #2
Enrichment, wt%	93	93	93	93
Fuel Meat Composition	UA1	UA1	UA1	U <sub>3</sub> O <sub>8</sub> -A1
U Density in Meat, g/cm <sup>3</sup>	0.432	0.432	0.591	0.775
<sup>235</sup> U/Plate (average), g	7.778	7.778	10.63	13.95
<sup>235</sup> U/Element, g	70.0	140.0	202.0	265.0
<sup>238</sup> U/Element, g	5.27	10.54	15.20	19.95
U Metal/Element, g	75.27	150.54	217.20	284.95
U Metal in Meat, wt%	14.72	14.72	19.24	24.78
No. of Plates/Element	9	18	19	19
Plate Length (average), cm	62.55	62.55	62.55	62.55
Plate Width (average), cm	6.655	6.655	6.655	6.655
Plate Thickness, cm	0.154	0.154	0.127*	0.127*
Meat Length, cm	60.0	60.0	60.0	60.0
Meat Width, cm	6.350	6.350	6.350	6.350
Meat Thickness, mm	0.508	0.508	0.508	0.508
Cladding Thickness, mm	0.508	0.508	0.381*	0.381*
Water Channel Thickness, cm	0.297	0.297	0.295	0.295
Width of Element, cm	7.610	7.610	7.610	7.610
Depth of Element, cm	8.049	8.049	8.047	8.047
Width of Control Rod Channel, cm	6.655	-	-	-
Depth of Control Rod Channel, cm	2.858	-	-	-

\*Cladding thickness is 0.381 mm for 17 inner plates and 0.572 mm for 2 outer plates. Consequently, the plate thickness is 1.651 mm for the 2 outer plates.

Table 2. Reduced-Enriched Fuel Element Characteristics

Parameter	MEU	LEU
Enrichment, wt%	45.0	19.75
Fuel Meat Composition	U <sub>3</sub> O <sub>8</sub> -Al	U <sub>3</sub> O <sub>8</sub> -Al
U Density in Meat, g/cm <sup>3</sup>	1.722	2.376
<sup>235</sup> U/Plate (average), g	15.0	26.2
<sup>235</sup> U/Element, g	285.0	340.6
<sup>238</sup> U/Element, g	348.3	1384.0
U Metal/Element, g	633.3	1724.6
U Metal in Meat, wt%	43.77	53.34
No. of Plates/Element	19	13
Plate Length (average), cm	62.55	62.55
Plate Width (average), cm	6.655	6.655
Plate Thickness, cm	0.127	0.226
Meat Length, cm	60.0	60.0
Meat Width, cm	6.350	6.203
Meat Thickness, mm	0.508	1.50
Clad Thickness, mm	0.381	0.381
Water Channel Thickness, cm	0.295	0.290
Width of Element, cm	7.610	7.610
Depth of Element, cm	8.047	8.047

R. W. Hobbs of ORNL directed the work at the PCA. The experiment program was designed by J. L. Snelgrove and J. R. Deen of ANL, and approved by the Operations Division at ORNL. The validation calculations were performed at ANL by J. R. Deen.

## II. PCA Core Description

The PCA is a light-water cooled, moderated, and reflected pool-type facility as shown in Fig. 1. It is located near the northwest corner of the same pool in which the 2-MW Bulk Shielding Reactor is located. The distance between the two cores is approximately 30 feet. The core consisted of a 5 × 5 array of fuel elements for most of the measurements, but for some measurements its size was reduced to 21 elements by removing the corner elements, so that five heavily-loaded, reduced-enrichment fuel elements could be loaded into the central positions of the core. A summary list of the critical core configurations is presented in Table 3. The core was operated at a power level of 50 watts so as not to burn up the fuel significantly while providing adequate counting statistics and reasonable counting times for the fission chamber measurements.

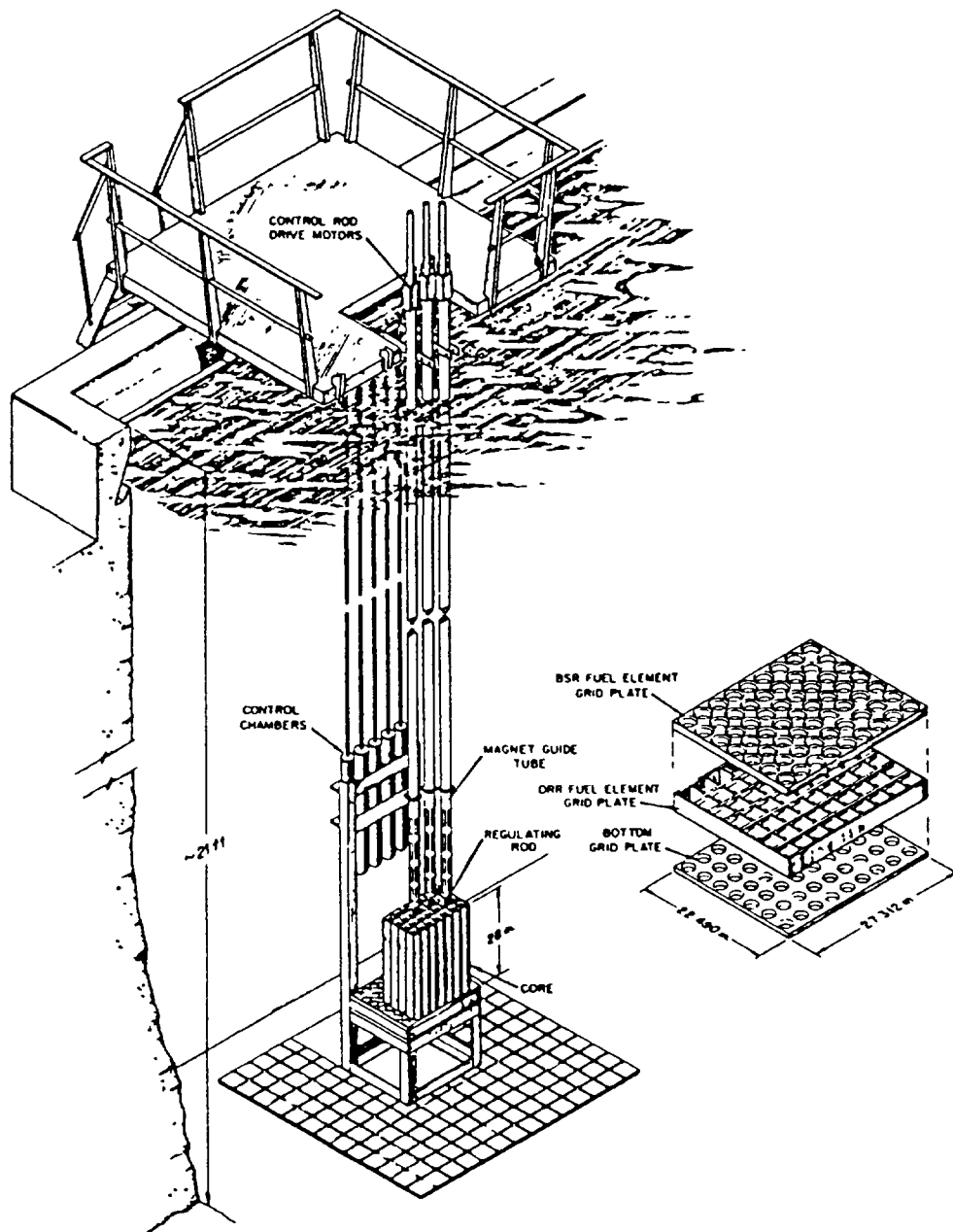


Figure 1. Pool Critical Assembly Structural Arrangement

The core is usually reflected on all four sides by practically an infinite thickness of light water. However, the PCA had previously been used for benchmark tests sponsored by the Nuclear Regulatory Commission entitled "The Computational Blind Test," which utilized the PCA Assembly Pressure Vessel Wall Benchmark Facility. Consequently, pressure vessel wall simulator materials were present on one face of the PCA as shown in Fig. 2.

The PCA is controlled by three B<sub>4</sub>C shim-safety control rods and one stainless steel (type 347) regulating rod. The control rods were located in the center of control fuel elements having aluminum guide plates on either side of the control rod as well as four fuel plates on one side and five fuel plates on the other side of the control rod. A drawing of the control element with shim rod inserted is presented in Fig. 3 and drawings of the other elements used in the measurements are presented in Figs. 4-7.

Table 3. Summary of Criticality Measurements at PCA

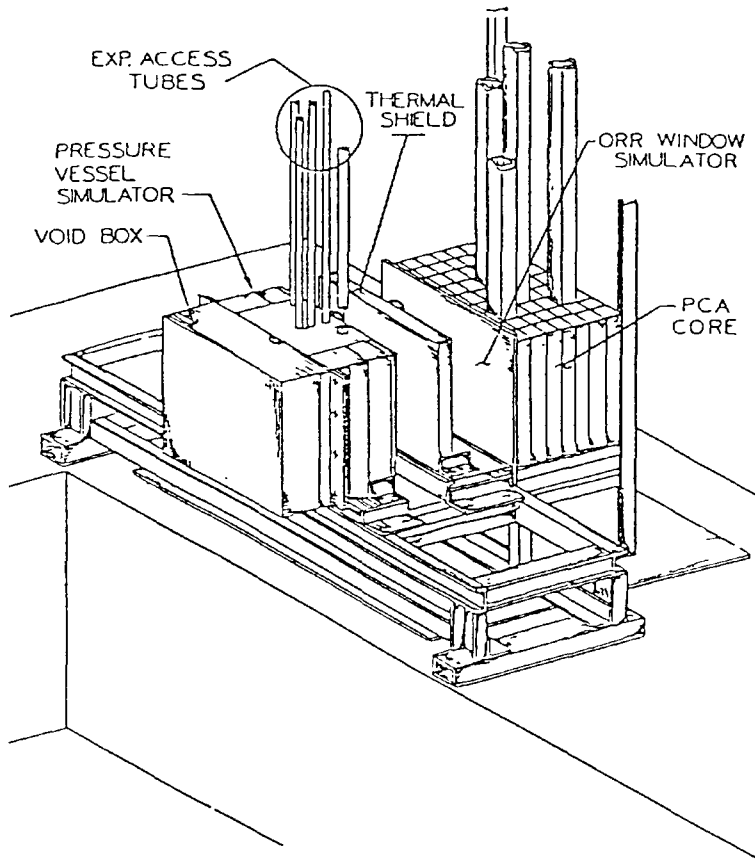
Core	# Elements	Element Location by Type ***					Corner Element Changes	Control Rod** Positions (in. withdrawn)	
		C-4	C-5	B-5	D-5	C-6		Shim Rods# 1,2,3	Regulating Rod
301	25	2	3	1	1	2	None	15.5	10.2
302	25	2	3	1	1	2	None	12.8,24.0,12.8	19.4
301	25	2	3	1	1	2	None	15.5	10.2
303	25	2	3	1	1	2	None	15.5	10.2
304	25	2	3	1	1	2	None	15.5	10.2
305	25	2	3	1	1	2	None	15.5	10.2
306	25	2	3	1	1	2	None	15.5	10.2
307	25	2	4	1	1	2	None	15.5	12.0
308	25	2	4	1	1	2	None	13.5	11.86
309	24	2	4	4	1	2	Pull A-7	14.75	12.5
310	23	2	4	4	4	2	Pull E-7	13.8	12.3
311	22	2	4	4	4	4	Pull A-3	14.4	12.0
312*	21	4	4	4	4	4	Pull E-3	15.25	10.2
313*	21	4	5	4	4	4	None	17.0	16.4
314	25	2	4	1	1	2	Replace 4 Corners	15.5	6.6
315	25	2	4	1	1	2	None	15.5	8.93
316A	25	2	5	1	1	2	None	17.0	14.0
316B	25	2	5	1	1	2	None	11.5,24.0,24.0	17.25
316C	25	2	5	1	1	2	None	24.0,16.0,16.0	10.4

\*Differential control rod worth data taken on shim rod for core #312 and regulating rod for core #313.

\*\*Control rod is fully withdrawn at 24 inches.

\*\*\*Element Classification

Type	Enrichment	<sup>235</sup> U (g/element)
1	HEU	140 ± 1
2	HEU	201 ± 2
3	HEU	265
4	MEU	282 ± 2
5	LEU	340 ± 5



PCA Pressure Vessel Wall Benchmark Facility

Figure 2. Pressure Vessel Wall Benchmark Facility

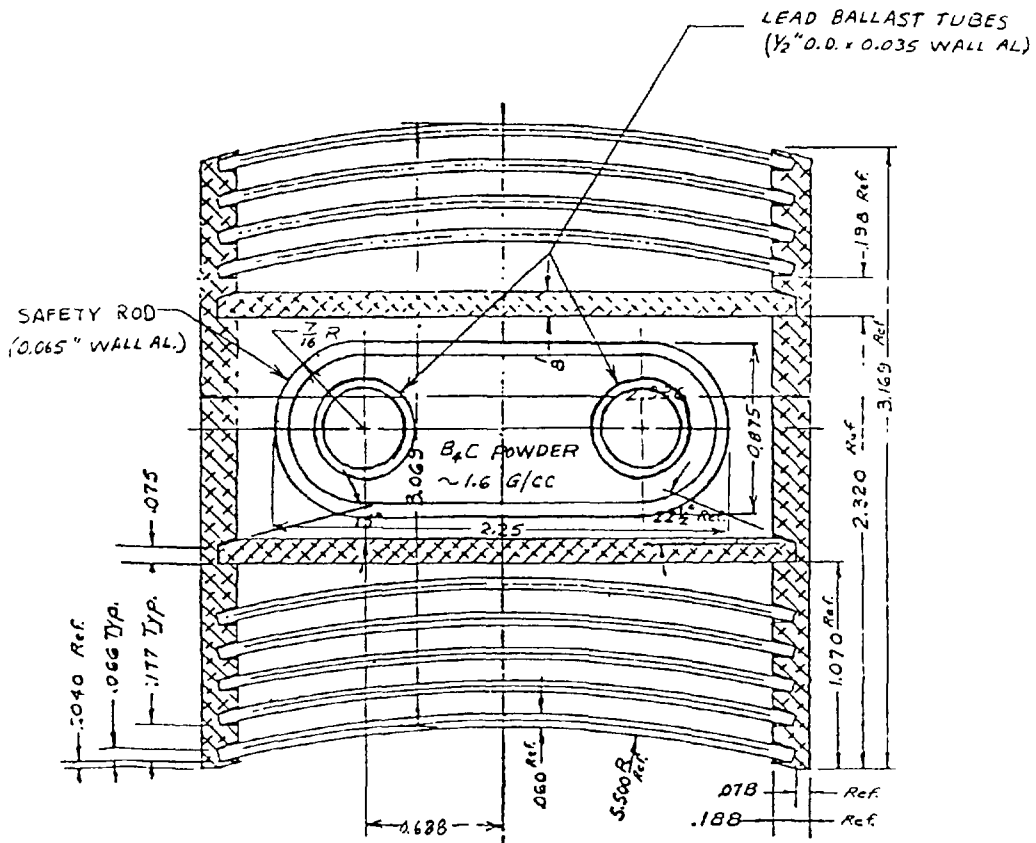
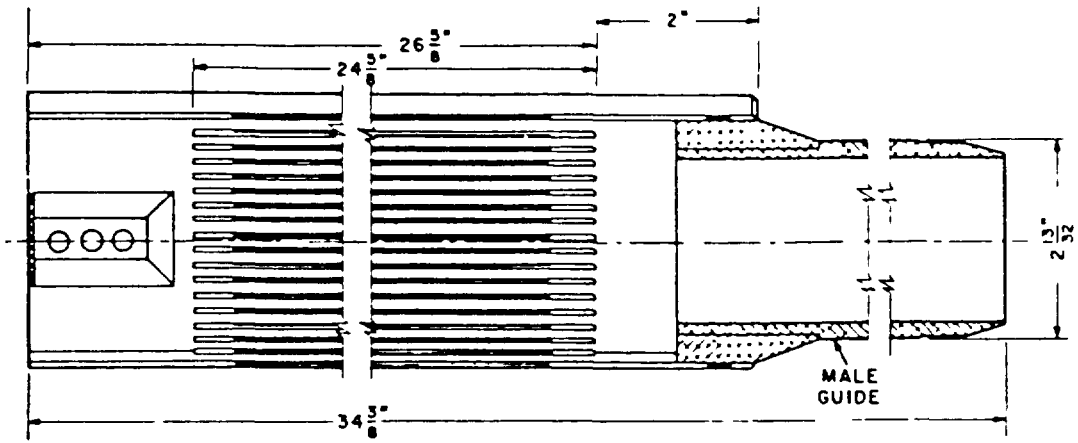


Figure 3. PCA Control Element with Safety Rod Inserted



SECTION A-A OF FUEL ELEMENT ASSEMBLY

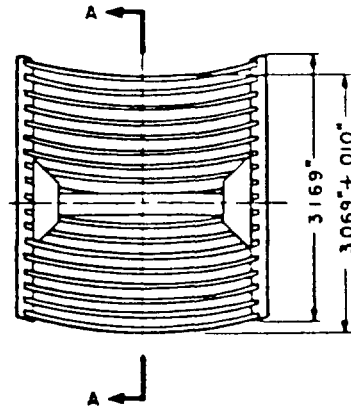
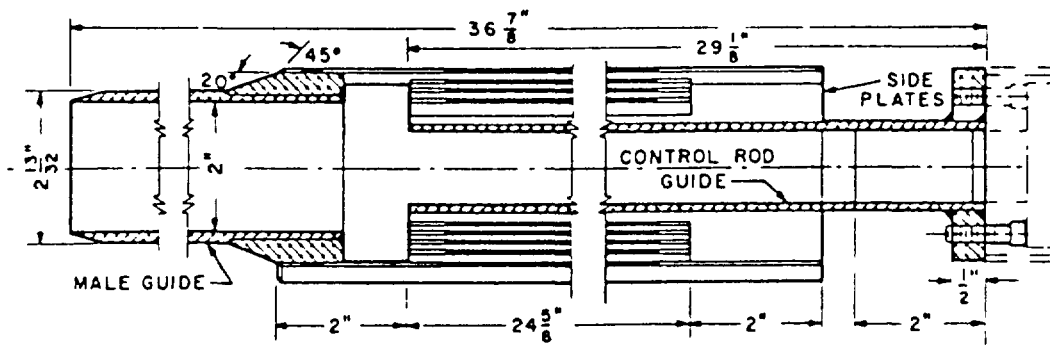
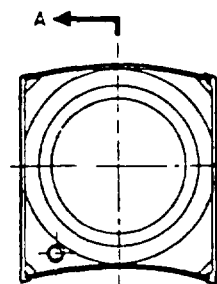


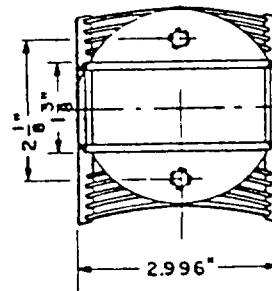
Figure 4. Standard 18-Curved-Plate HEU PCA Fuel Element



SECTION A-A OF SPECIAL FUEL ELEMENT ASSEMBLY



BOTTOM VIEW



TOP VIEW

Figure 5. Control 9-Curved-Plate HEU PCA Fuel Element

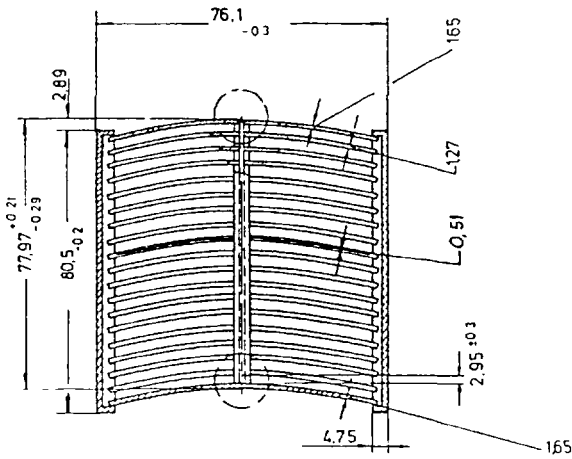


Figure 6. ORR-Type Fuel Element

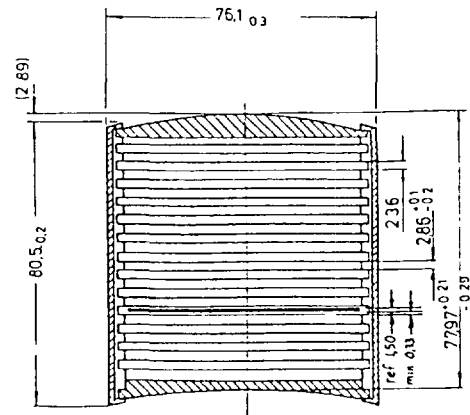


Figure 7. LEU 13-Plate Fuel Element

### III. Description of Miniature Fission Chamber and Measurement Techniques

The miniature fission chamber was located very near the tip of a semi-flexible plexiglass strip approximately 0.25 cm thick by 4 cm wide by 83 cm long. The fission chamber itself was approximately 1 cm long. The plexiglass strip was attached to a plexiglass cube approximately 5 cm on each side.

The plexiglass cube rested upon a plexiglass adapter guide when the bayonet was fully inserted into a fuel element channel. The adapter guides, shown in Figs. 8a and 8b, were attached to the top of the fuel element and rested on top of the fuel plates. There were five slots into which the plexiglass bayonet could be inserted: a central slot, two slots approximately 2.1 cm to either side in the central coolant channel, and one slot each in the fifth coolant channel to either side of the central channel. The center-to-center distance from the central channel to the fifth channel is 2.1 cm in the 19-plate element and 2.6 cm in the 13-plate element.

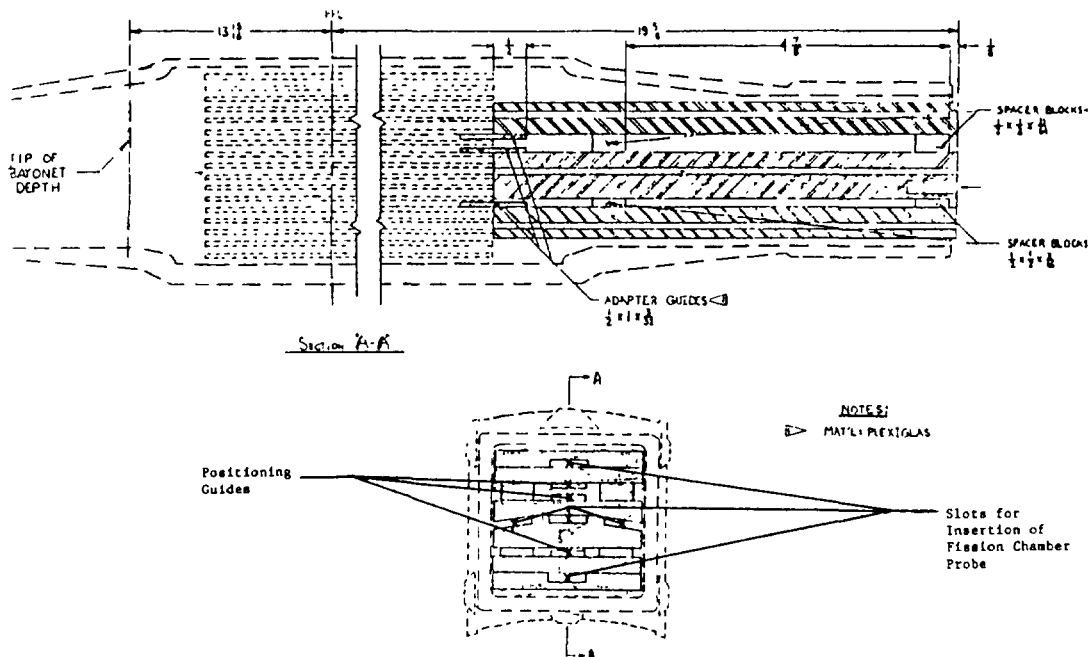


Figure 8A. Plexiglass Adapter Guide for Miniature Fission Chamber Positioned in PCA Fuel Element (all dimensions in inches)

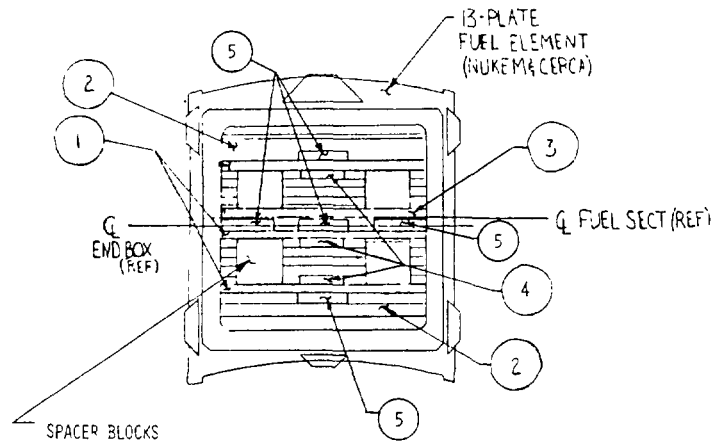


Figure 8B.

Top View of 13 Plate LEU Element with Plexiglass Adapter Guide for Miniature Fission Chamber Resting on Top of Fuel Plates

Note: Parts 1, 2, and 3 are plexiglass adapters and Part 4 is the adapter guide for locating the adapter with respect to the coolant channels. The slots for insertion of the fission chamber probe are labeled 5.

#### IV. PCA Analysis Methods

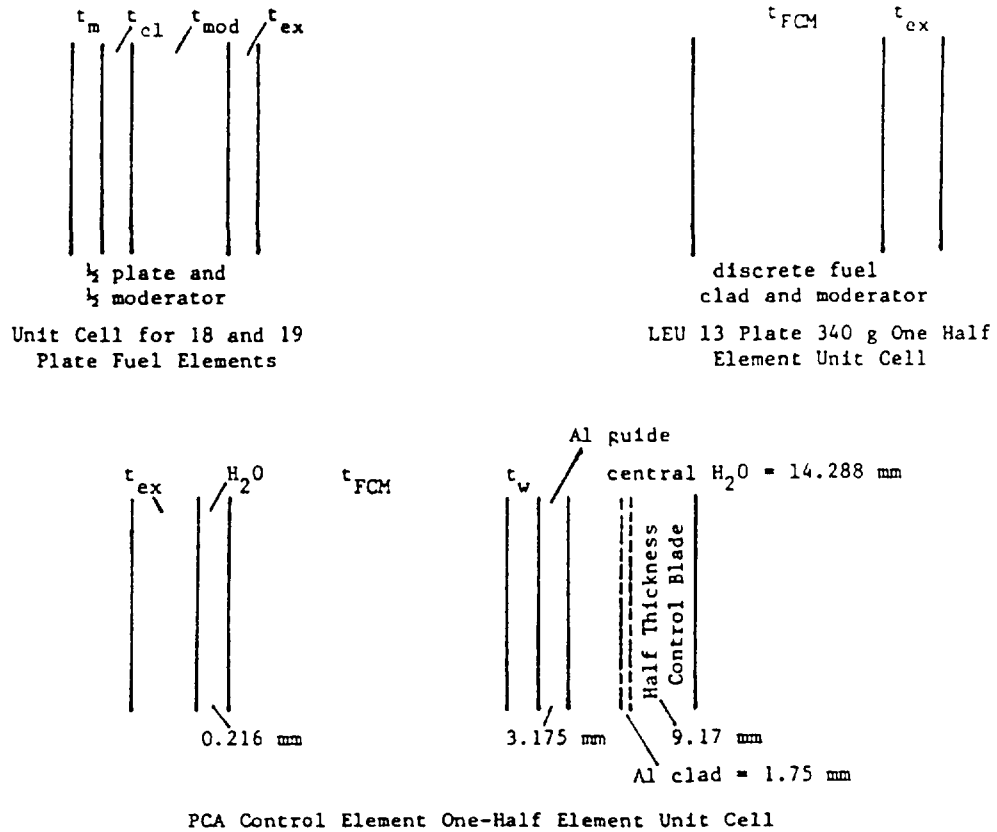
##### A. Neutron Cross Section Generation Methods

Five-broad-group neutron cross sections were generated by the ANL version of EPRI-CELL, using slab geometry.<sup>2</sup> EPRI-CELL combines a GAM-1 68-group homogeneous resonance treatment in the epithermal energy range with a 35-group, one-dimensional, integral-transport theory (THERMOS) treatment for the thermal energy range. The cross section library was based on ENDF/B IV cross section data.

Various unit cells, shown in Fig. 9, were used in order to generate cross sections dependent on the location and neutron energy spectrum of each material in the core. The most commonly used unit cell for the fuel regions consisted of a 1/2 plate thickness next to a 1/2 moderator thickness and an extra region material with a zero current boundary conditions at each boundary. The 13-plate LEU element required a more detailed 1/2-element EPRI-CELL unit cell because of rapid changes in spatial neutron spectra. The PCA control element unit cells were also represented by a 1/2 element model either with or without the control rod material present.

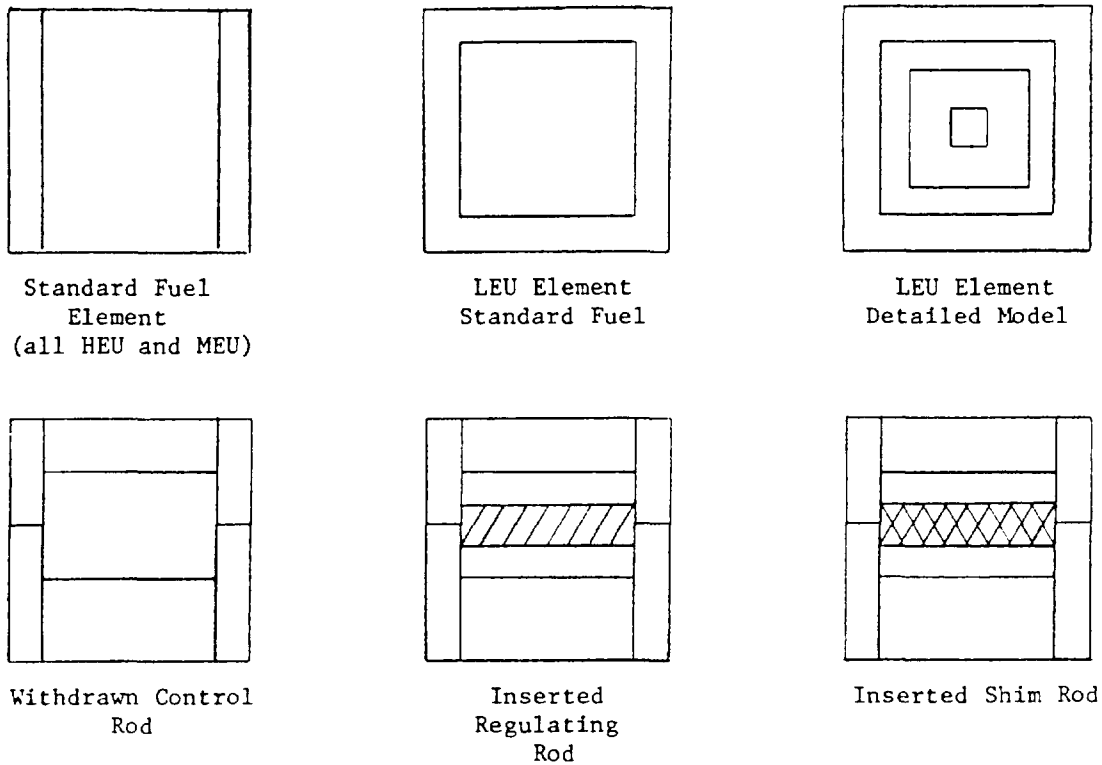
##### B. Whole Core Model

A three-dimensional diffusion-theory code, DIF3D, was used to calculate the  $k_{eff}$ 's and  $^{235}\text{U}$  fission rate distributions measured at the PCA.<sup>3</sup> Each standard fuel element was homogenized into two separate zones. The first zone was a homogenized mixture of fuel, clad, and moderator and the second was a homogenized mixture of element side plate material and water not included in the first zone. All standard elements were modelled in the same fashion except for the 13-plate 340 g LEU element. The aluminum-water mixture for that element was distributed in both the x and y directions instead of just on the two sides of the element because of the large component and location of non-fuel material. All fuel element models are shown in Fig. 10.



Description of Symbols Given Above							
Symbol	Dimension Description	Fuel Element Enrichment and <sup>235</sup> U Loading					
		HEU - 140 g	HEU - 200 g or 265 g	MEU - 282 g	LEU - 340 g	HEU Control Element - 70 g 5 plate side	4 plate side
t <sub>m</sub>	meat 1/2 thickness (mm)	0.254	0.254	0.254	1.50	0.254	0.254
t <sub>cl</sub>	clad thickness (mm)	0.508	0.401	0.401	0.380	0.508	0.508
t <sub>mod</sub>	moderator 1/2 thickness (mm)	1.486	1.473	1.473	1.450	1.486	1.486
t <sub>ex</sub>	extra region thickness (mm)	0.484	0.460	0.450	16.80	9.650	7.760
t <sub>FCM</sub>	fuel-clad-moderator zone (mm)	-	-	-	33.54	22.479	17.983
t <sub>w</sub>	gap H <sub>2</sub> O (mm)	-	-	-	-	4.699	4.064

Figure 9. EPRI-CELL Unit Cells for Cross-Section Generation



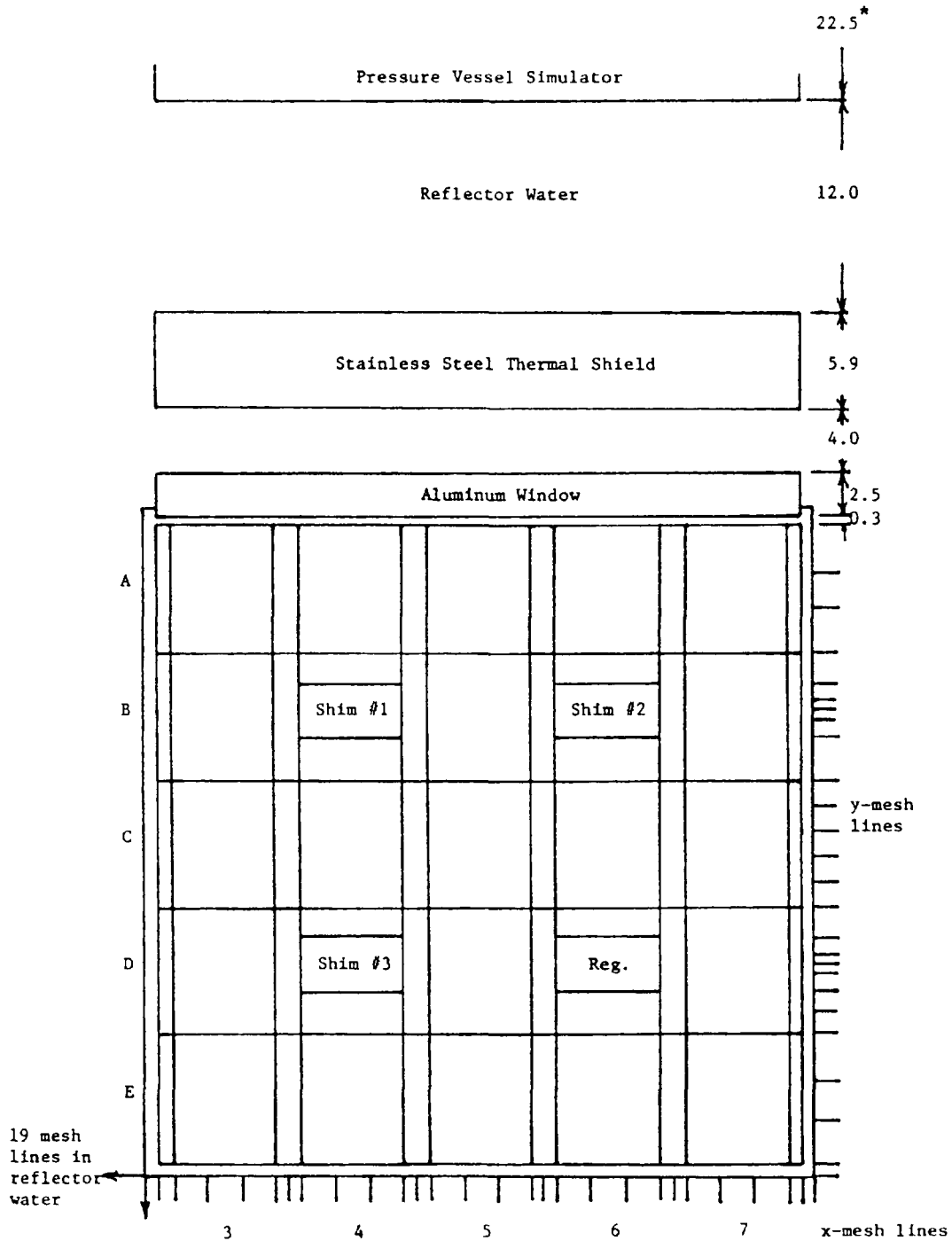
Three HEU Control Element Models

Figure 10. Fuel Element Models Used in Whole Core Calculations

Each control element was represented by using three separate material zones: one for the homogenized fuel, clad, moderator zone; one for the side plate zone; and another for the water and aluminum guide plate located in the center of the element when the control rod was fully withdrawn. When a shim control rod was inserted into the control fuel element, one region was assigned to the  $B_4C$  absorber material and another to the coolant water and guide plate surrounding the control rod. When the regulating rod was inserted into a control element, a single homogenized mixture of stainless steel absorbing material, coolant water, and guide plate aluminum was placed in the center of the control fuel element.

The XY model of the whole core calculation is shown in Fig. 11. Along the lateral surfaces of the core, a 1-cm-thick region of harder spectrum reflector water was assigned. Beyond this inner reflector water on the three water-reflected core faces, a softer-spectrum (closer to a Maxwellian distribution) water material was used for the remaining, effectively infinite, 39-cm thickness of water before a zero-flux boundary condition for all neutron groups was imposed. On the core face adjacent to the pressure vessel wall simulator facility, several different materials were located to model this experimental apparatus.

The top and bottom axial reflectors were modelled by two and four separate homogenized mixtures of water and aluminum, respectively. Locations of these axial reflector zones are presented in Fig. 12.



\* all dimensions in cm.

Figure 11. Diffusion Theory Model in X-Y Plane

Most critical configurations were calculated with a mesh of  $60 \times 60 \times 42$  for the XYZ geometry. The mesh in the XY plane allowed 18 mesh lines for the reflector on each side of the core and 24 mesh lines for calculating the core flux distribution. The axial mesh structure was much coarser than that in the XY plane due to the greater axial uniformity of the core relative to the radial. The core and both top and bottom axial reflectors required only 14 mesh lines each.

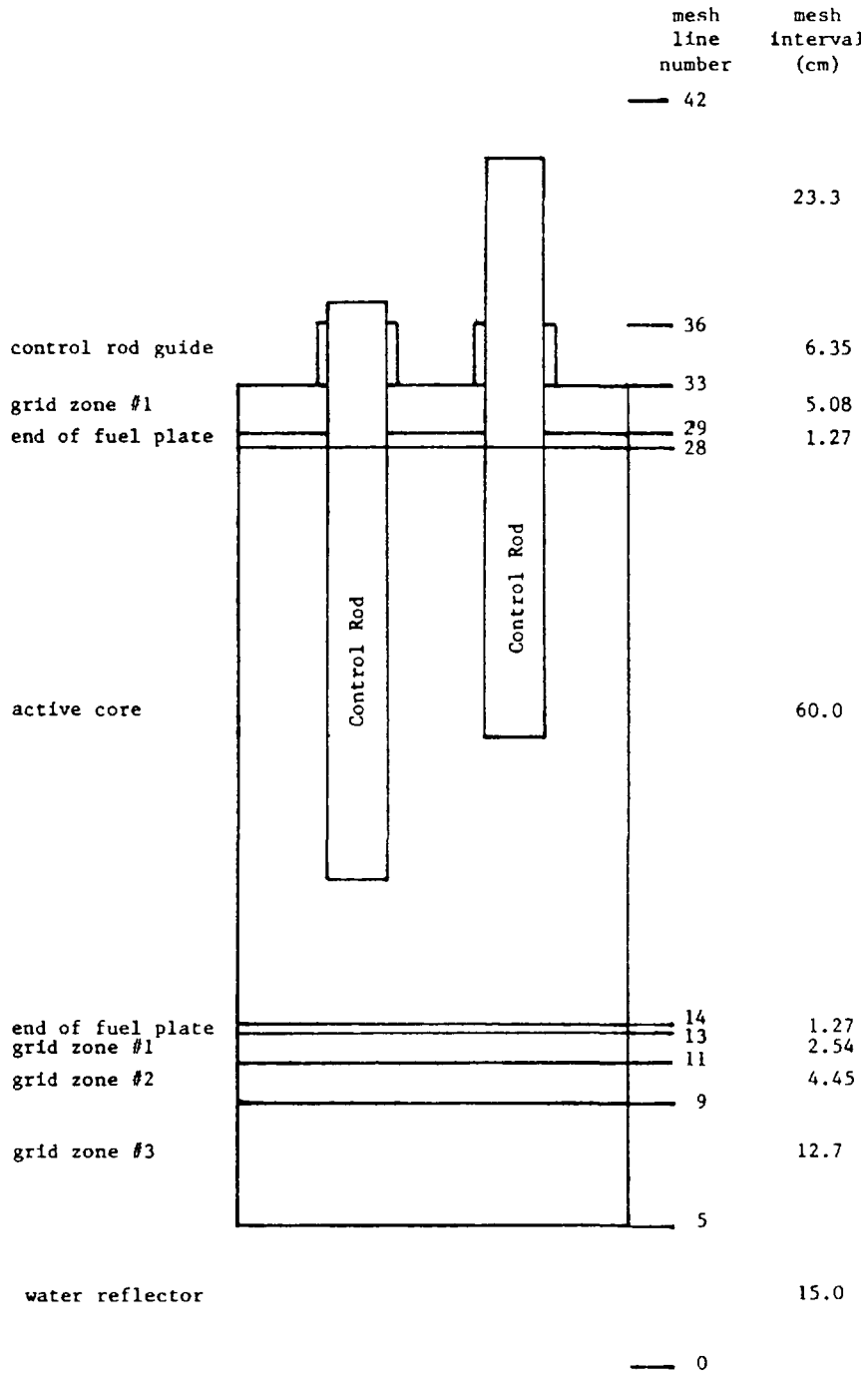


Figure 12. Diffusion Theory Model in Axial Direction

### C. Control Rod Model

The shim rods were modelled using an internal boundary condition applied at the surface of the B<sub>4</sub>C absorbing material. The internal boundary conditions are expressed in terms of group-dependent current-to-flux ratios. The current-to-flux ratios were calculated by using a VIM-Monte Carlo calculation and compared with a TWOTRAN-II transport calculation.<sup>4,5</sup> Three separate geometrical representations of the control element with the control blade fully inserted in the VIM calculations were compared with the transport model of the control element in XY and RZ geometry. The various geometrical representations in VIM were checked to determine the errors that would be made in using current-to-flux ratios from XY or RZ representations of the control rod in TWOTRAN-II.

The three VIM cases were: (a) an exact representation of the control element with curved plates and control rod as shown in Fig. 3, (b) an exact representation of the control rod with flat fuel plates in the control element, and (c) is an XY geometrical representation of the control rod and fuel plates in the control element. Each control element was surrounded by a half thickness of homogenized standard fuel element material to simulate the actual energy spectrum of neutrons leaking into the control element of the PCA core. All three cases were uniform in the axial direction and had zero current boundary conditions for all neutron groups at each outer boundary.

TWOTRAN-II was used to calculate a model identical to VIM case (c) in XY geometry as well as an RZ representation of a partially inserted cylindrical shim control rod. A P<sub>1</sub>-S<sub>8</sub> approximation was used for both transport calculations. The cross sections for TWOTRAN were obtained from EPRI-CELL.

The results of these two methods of obtaining current-to-flux ratios for use in DIF3D calculations is shown in Table 4. One may conclude that for the thermal groups 4 and 5 that there is good agreement between Monte Carlo and RZ or XY geometry P<sub>1</sub>-S<sub>8</sub> transport calculations. For group 3 the transport calculation was in error due to the inadequacy of the EPRI-CELL code in treating the spatial self-shielding of B-10 for the epithermal energies. It was found that  $\sigma_{a3}$  for B-10, which EPRI-CELL indicated was constant, actually varied from 80 b at the surface to 48 b just a few millimeters into the interior of the absorber. Therefore the VIM ( $j/\phi$ )<sub>3</sub> data were used in DIF3D calculations.

Table 4. Internal Boundary Conditions for Shim Control Rods

Energy Group	VIM-Monte Carlo Results			TWOTRAN-II Transport Theory Results	
	Exact Rod Curved Plates	Exact Rod Flat Plates	Rectangular Rod Flat Plates	Rectangular Rod Flat Plates	Cylindrical Rod Homogenized Fuel
1	*	*	*	0.01311	0.013
2	*	*	*	0.02296	0.025
3	0.2618	0.2652	0.2322	0.3316	0.362
4	0.5477	0.5502	0.5314	0.5317	0.534
5	0.5888	0.5842	0.5652	0.5479	0.544

\*Statistics from Monte Carlo calculations were not good enough to obtain reliable neutron current information.

When the net neutron current is close to zero as it is for groups 1 and 2, acceptable statistics could not be obtained from VIM without excessively large numbers of neutron histories. Therefore, the VIM  $j/\phi$  for groups 1 and 2 were not reported and the transport-calculated values were used in DIF3D. The TWOTRAN RZ calculation for an isolated control rod indicated a nearly uniform  $j/\phi$  for all groups along the entire surface except near the corners of the control rod tip, where the values decreased rapidly.

#### V. Results of Reactivity and Fission Rate Comparisons

A comparison of the measured and calculated regulating and shim differential control rod worths are presented in Tables 5 and 6. The regulating rod C/E values are closest to unity for positions near its maximum differential worth.

Table 5. Calculation of Differential Regulating Rod Worths For Core #313 Using DIF3D

Position of Regulating Rod		$\Delta k_{eff}$ (%)	$\frac{\Delta k}{k}$ cal. (%)	$\frac{\Delta k}{k}$ meas. (%)	$\frac{C}{E}$
Before Pull (Inches Withdrawn)	After Pull				
9.68	10.89	0.0473	0.0465	0.0653	0.712
10.89	12.58	0.08914	0.0875	0.0869	1.007
12.58	14.65	0.09406	0.0923	0.0919	1.004
14.65	17.34	0.07415	0.0723	0.0832	0.869

\*Note: All shim rods were held at 17.0 inches withdrawn for all regulating rod differential worth calculations. In reality, the shim rods were inserted in small increments to maintain criticality after the withdrawals of the regulating rod.

Table 6. Calculation of Differential Shim Rod Worths for Core #312 Using DIF3D

Control Rod Positions				Calculated $k_{eff}$	Calculated $\Delta k/k(\%)$	Measured $\Delta k/k(\%)$	$\frac{C}{E}$
Shim #1	Shim #2	Shim #3	Regulating (Inches Withdrawn)				
10.00	18.35	18.35	18.35	1.00728	0.0719	0.0654	1.099
10.31	18.35	18.35	18.35	1.00801			
12.00	16.40	16.40	17.2	1.00619	0.0771	0.0684	1.039
12.32	16.40	16.40	17.2	1.00691			
13.00	15.90	15.90	16.0	1.00647	0.0625	0.0650	0.962
13.31	15.90	15.90	16.0	1.00710			
14.00	15.00	15.00	17.5	1.00560	0.0711	0.0773	0.920
14.41	15.00	15.00	17.5	1.00632			
18.00	13.50	13.50	15.35	1.00475	0.0772	0.0749	1.031
18.77	13.50	13.50	15.35	1.00593			
22.00	12.80	12.80	16.9	1.00456	0.0456	0.0435	1.046
23.86	12.80	12.80	16.9	1.00502			

Table 7. Core Reactivity Comparison Using HEU, MEU and LEU Fuel Elements

Core #	Core Size (# elements)	Central Element (enr - $^{235}\text{U}$ g)	Shim #1	Control Rod Positions*** (in. withdrawn)			Calculated $k_{\text{eff}}$
				Shim #2	Shim #3	Regulating	
314	25	HEU - 265 g	15.5	15.5	15.5	6.6	1.0069
315	25	MEU - 282 g	15.5	15.5	15.5	8.9	1.0060
316A	25	LEU - 340 g	17.0	17.0	17.0	14.0	1.0071
316B	25	LEU - 340 g	11.5	24.0	24.0	17.3	1.0086
316C	25	LEU - 340 g	24.0	16.0	16.0	10.4	1.0069
312	21	MEU - 280 g*	15.25	15.25	15.25	10.2	1.0053
313	21	LEU - 340 g*	17.0	17.0	17.0	16.4	1.0059
301	25	HEU - 265 g**	15.5	15.5	15.5	10.2	1.0088
302	25	HEU - 265 g**	12.8	24.0	12.8	19.4	1.0100

\*Surrounded by four MEU 282 g fuel elements, one at each face of the central element. All HEU and MEU fuel elements have 19 curved fuel plates whereas the LEU element has 13 straight plates.

\*\*Slightly different core loading than the first all HEU core.

\*\*\*Control rod fully withdrawn at 24 inches.

The calculated differential shim rod worths were within  $\pm 10\%$  of the measured values for the range of the measured data from 10 to 24 inches withdrawn. The whole-core calculated reactivity results presented in Table 7 indicate an average  $k_{\text{eff}} = 1.0066 \pm 0.003$ . There are very small changes in whole core calculated  $k_{\text{eff}}$ 's for an all-HEU core compared to any mixed-enrichment critical core configuration. Differences of  $\Delta k_{\text{eff}} = 0.17\%$  were calculated for different critical control rod patterns as shown in core #316, which suggests some improvements are still needed to provide exact modelling of control rod worths.

All of the critical measurements were made in the order of increasing core number. Core 314 is an attempt to duplicate the previously measured results of core 301. No change was made to the calculational model in calculating these two cores except to represent the changes in the regulating rod position. Since core 314 was measured immediately before cores 315 and 316, these cores were used to report any calculational biases due to replacement of HEU fuel with MEU or LEU fuel.

The comparisons of the calculated and measured radial  $^{235}\text{U}$  fission rate distributions are presented in Figs. 13-22, 30. They are grouped as x-axis distributions along the y-axis mid-plane of the core and similarly as y-axis distributions along the x-axis mid-plane of the core. The measured and calculated distributions were all normalized to unity at the center of the central element (C-5). The largest errors in calculating relative  $^{235}\text{U}$  fission rates occurred when heavily loaded central elements were compared with neighboring 140 g-HEU elements. These sharp changes in fuel properties were predicted to within  $\pm 5\%$  except for the 340 g LEU element, for which a more detailed model was required to obtain the results shown in Figs. 17, 18, 21, and 22. The comparisons of measurement and calculation along the y-axis tend to be in slightly better agreement than along the x-axis due to the additional difficulty introduced by the effect of the spectrum softening caused by the presence of the side plates.

The only distribution that exhibits larger than ~5% error is the core #312 distribution along the x-axis. The reason for this large error is difficult to understand, especially in view of the excellent agreement along the y-axis and better agreement for other more heterogeneous cores along their x-axes.

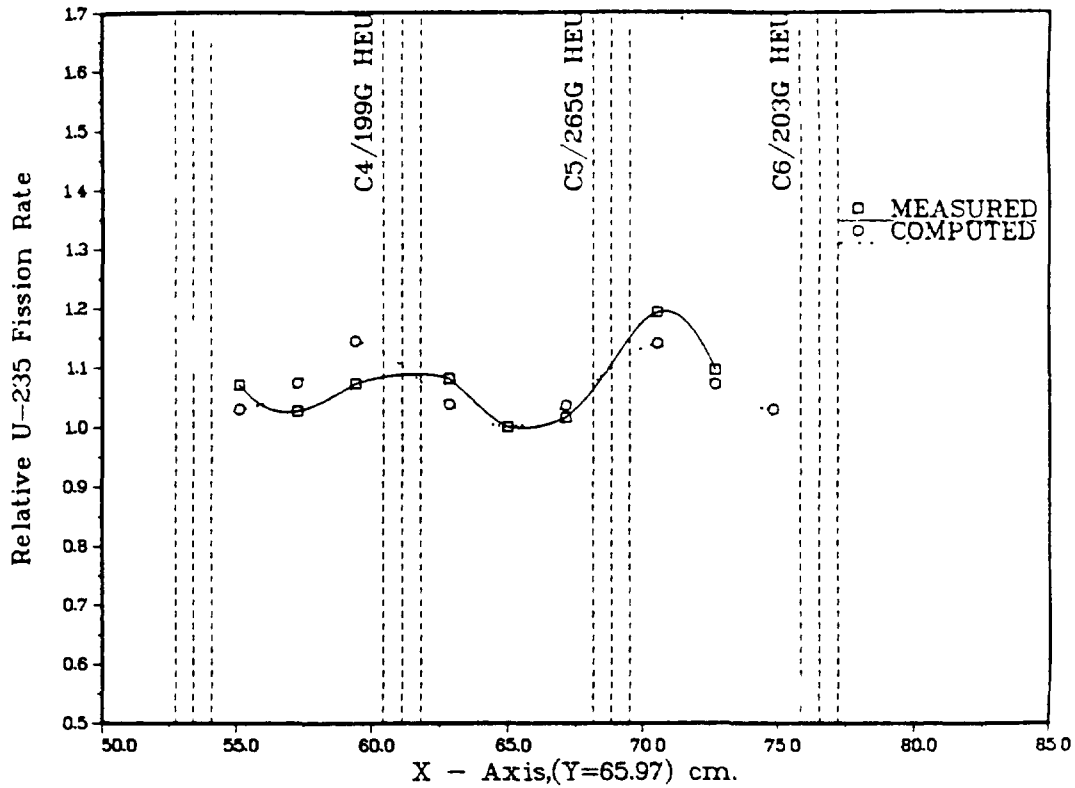


FIG. 13 PCA CORE 301 MIDPLANE FISSION RATE DISTR ALONG X-AXIS

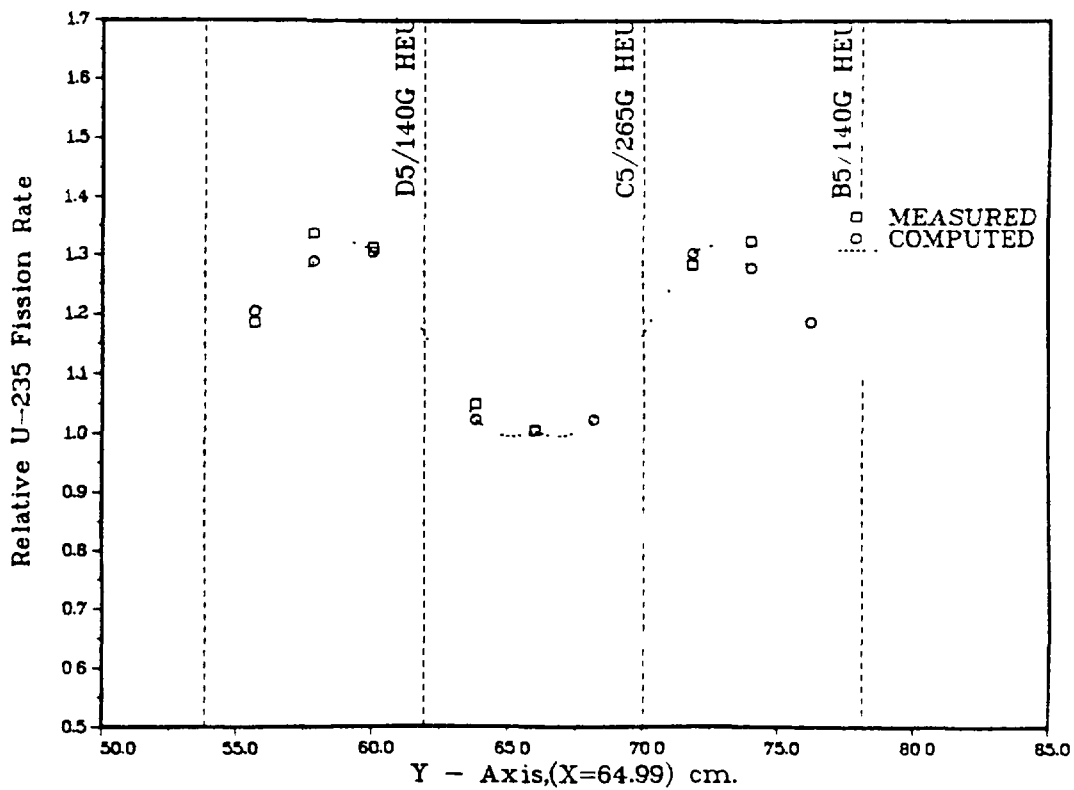


FIG. 14 PCA CORE 301 MIDPLANE FISSION RATE DISTR ALONG Y-AXIS

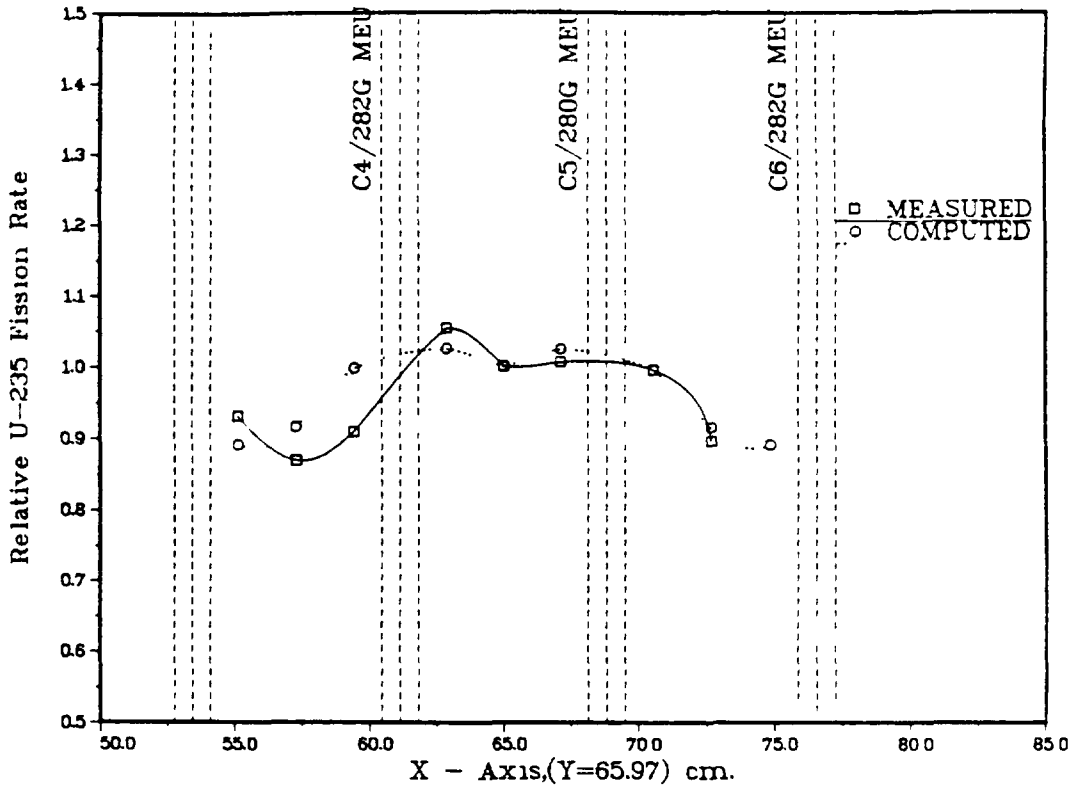


FIG. 15 PCA CORE 312 MIDPLANE FISSION RATE DISTR ALONG X-AXIS

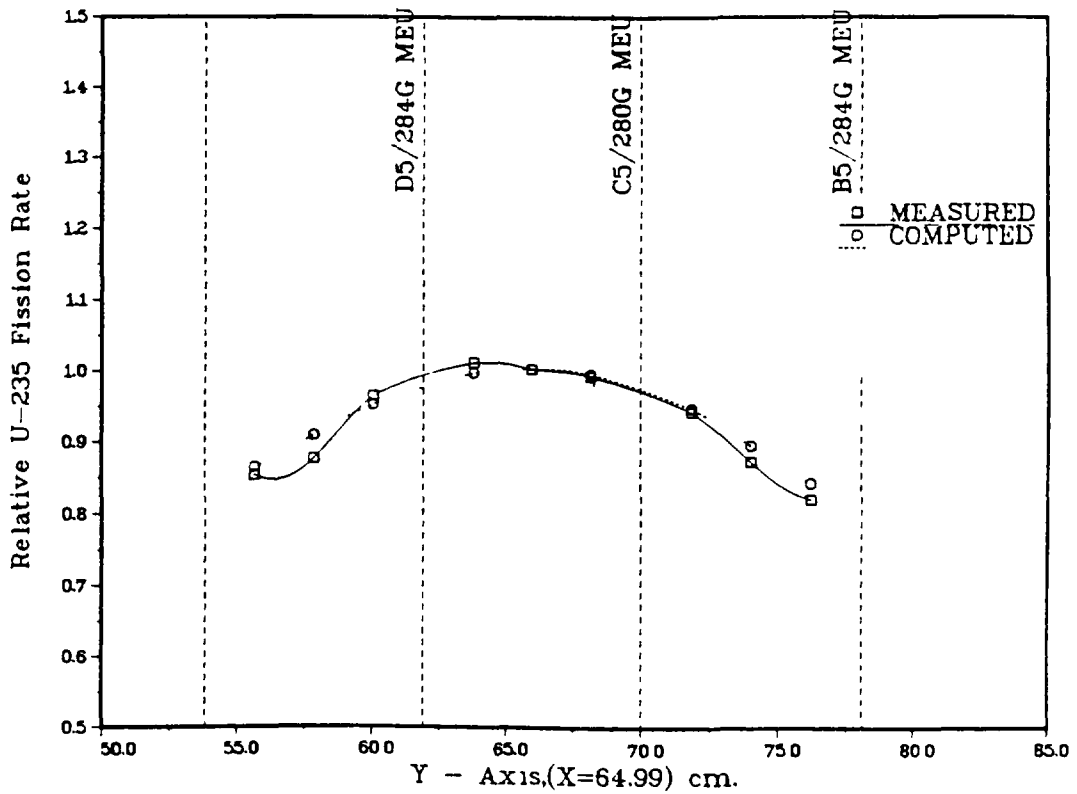


FIG. 16 PCA CORE 312 MIDPLANE FISSION RATE DISTR ALONG Y-AXIS

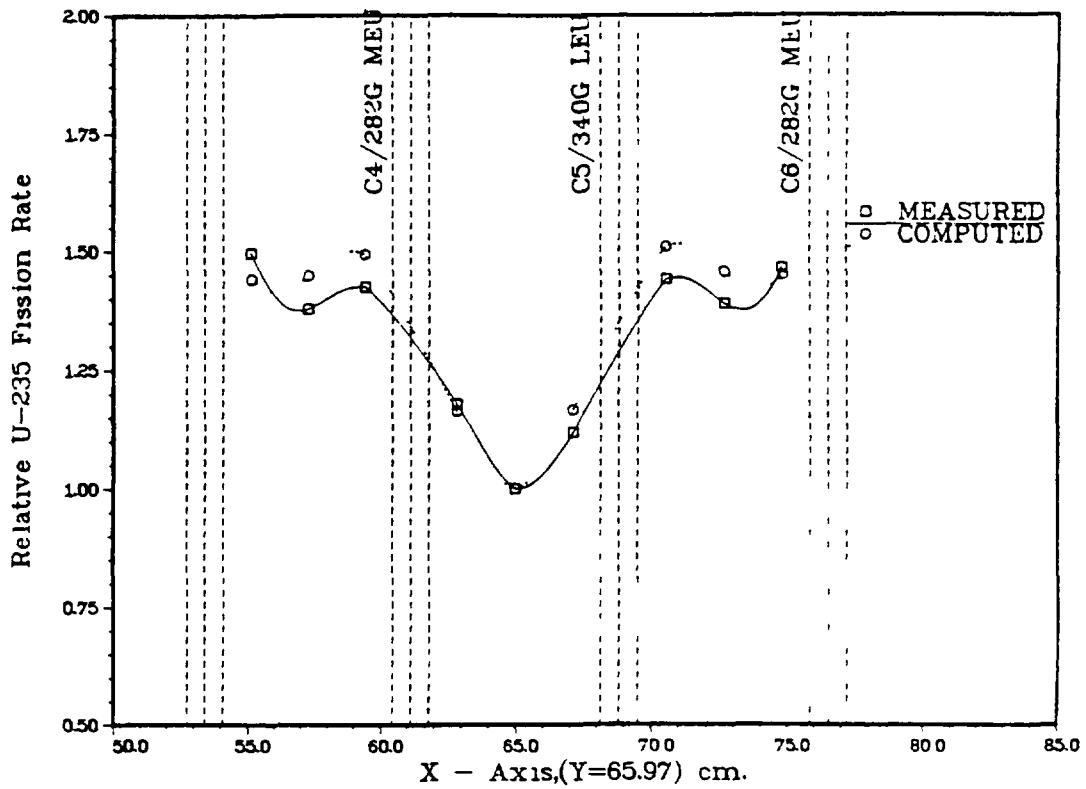


FIG. 17 PCA CORE 313 MIDPLANE FISSION RATE DISTR ALONG X-AXIS

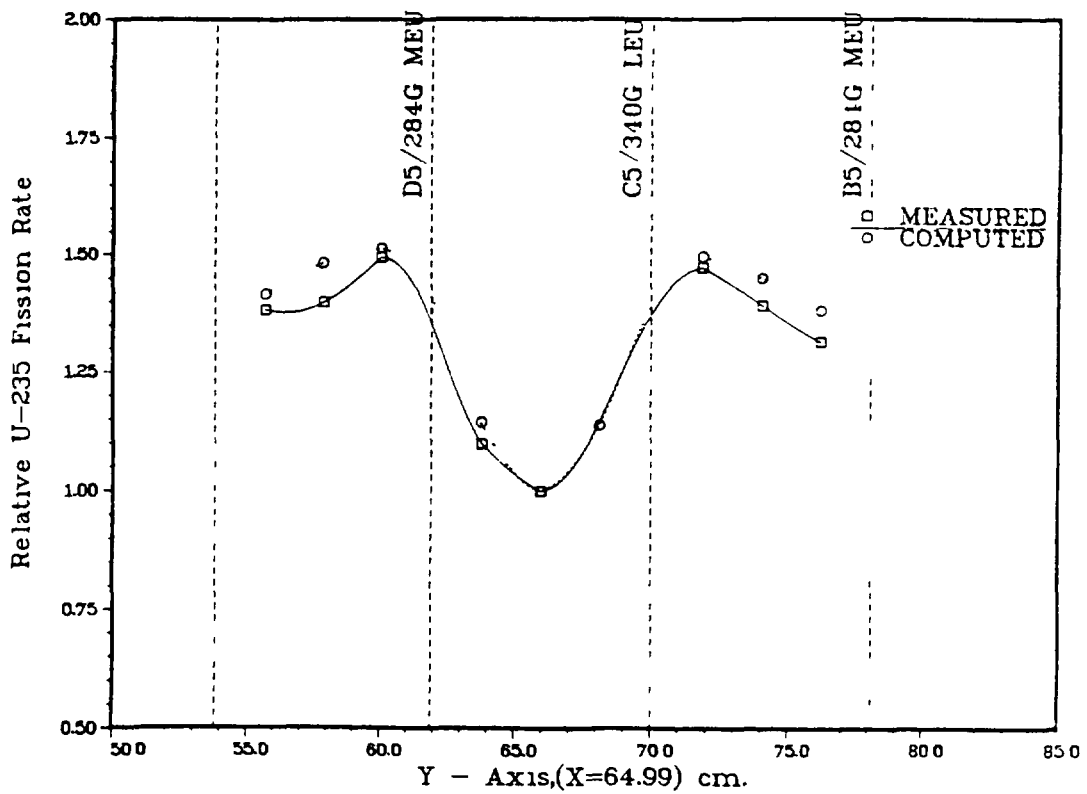


FIG. 18 PCA CORE 313 MIDPLANE FISSION RATE DISTR ALONG Y-AXIS

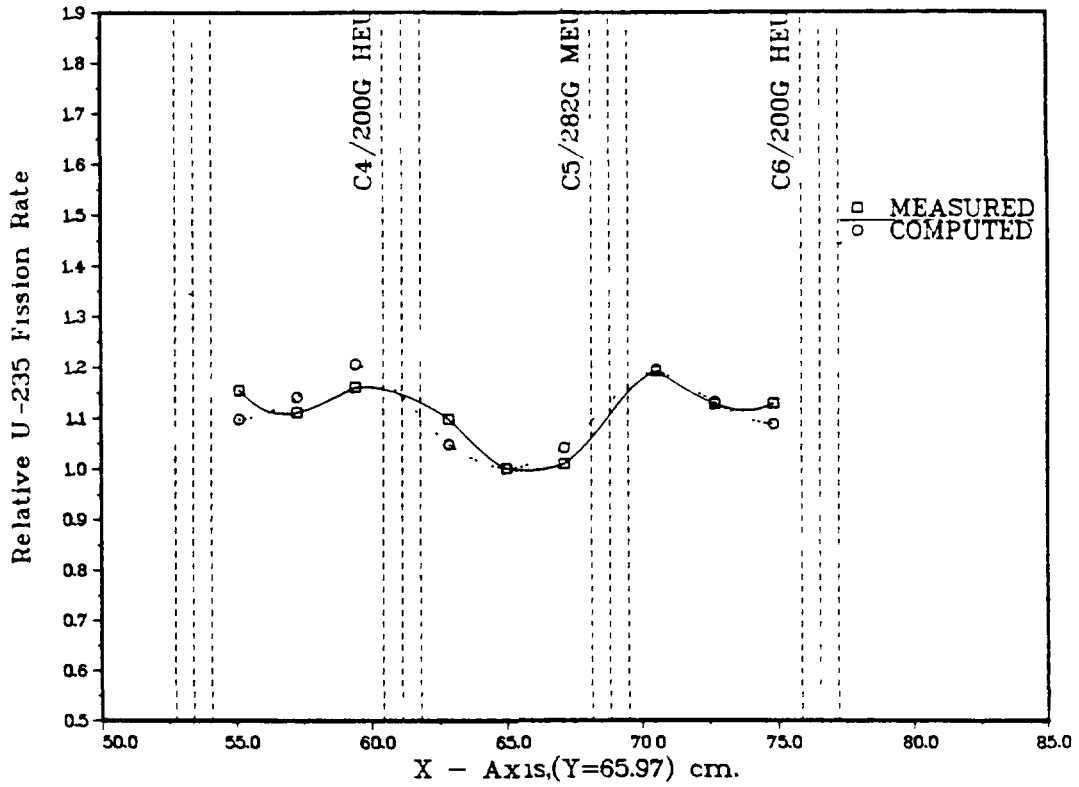


FIG. 19 PCA CORE 315 MIDPLANE FISSION RATE DISTR ALONG X-AXIS

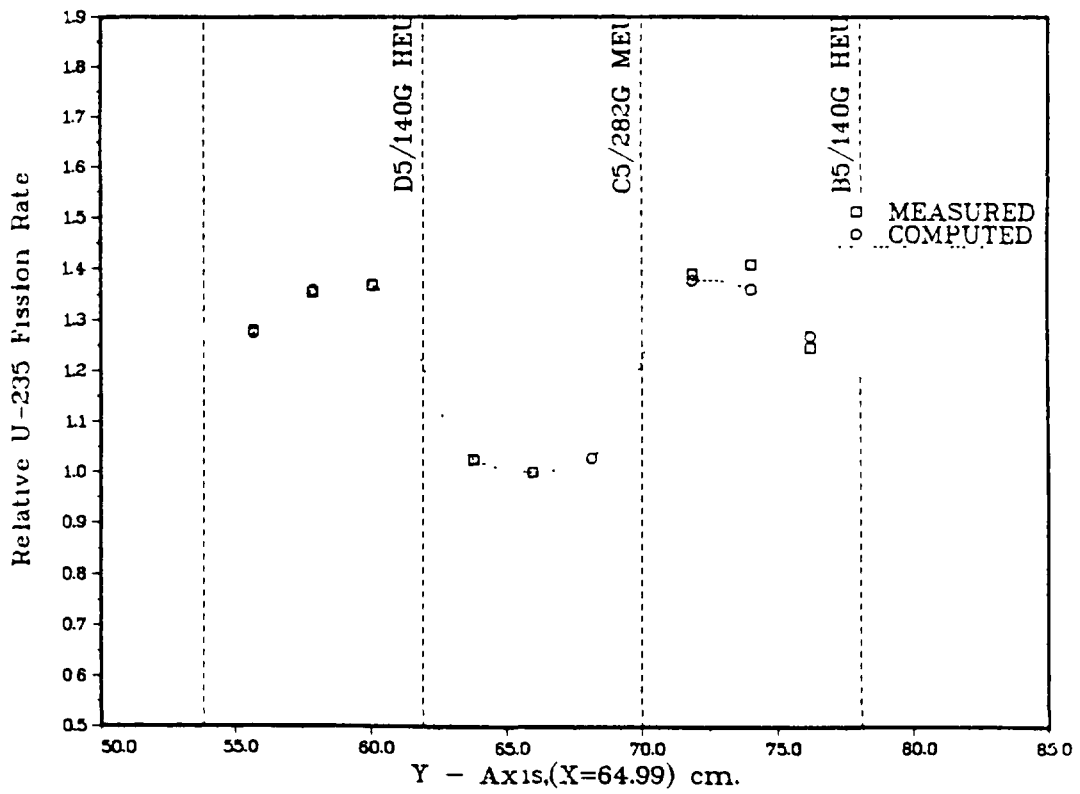


FIG. 20 PCA CORE 315 MIDPLANE FISSION RATE DISTR ALONG Y-AXIS

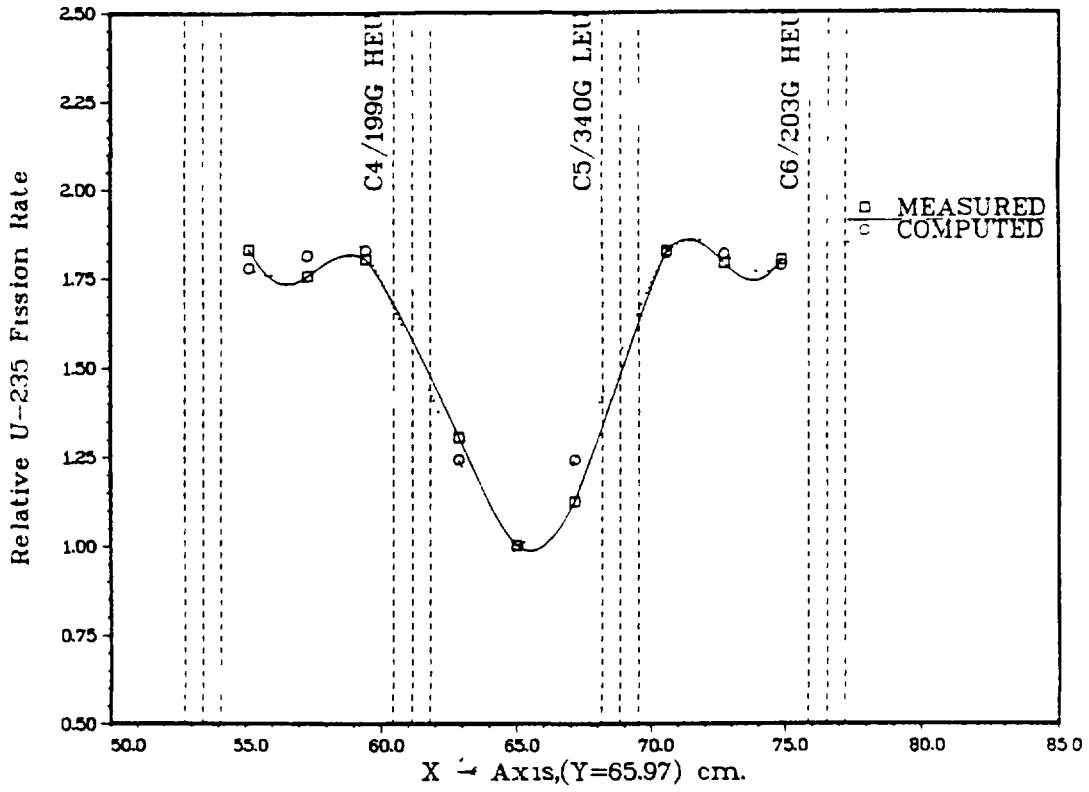


FIG. 21 PCA CORE 316 MIDPLANE FISSION RATE DISTR ALONG X-AXIS

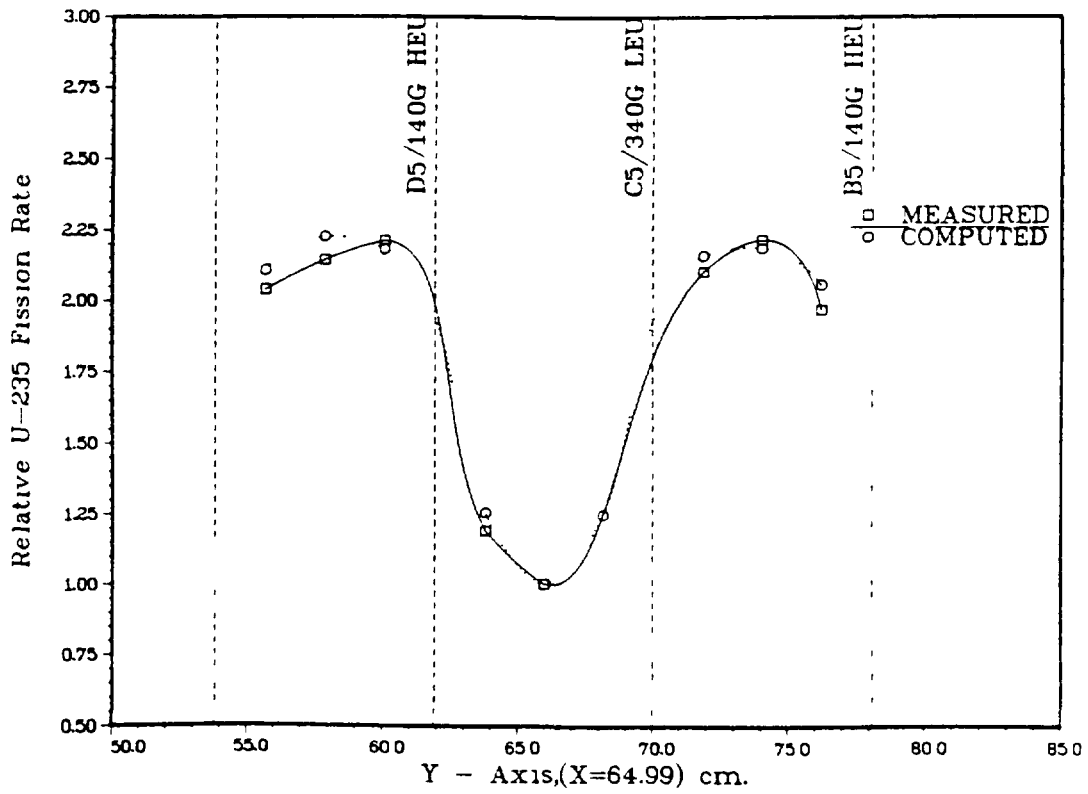


FIG. 22 PCA CORE 316 MIDPLANE FISSION RATE DISTR ALONG Y-AXIS

The relative axial  $^{235}\text{U}$  fission rate traverse comparisons were presented in Figs. 23-29. The vertical grid lines on these plots represented the upper and lower boundaries of the active fuel. The upper and lower reflector zones were located adjacent to the upper and lower active fuel boundaries. Labels are printed on the upper corner of each active fuel zone to identify the enrichment and  $^{235}\text{U}$  loading in grams/element for each figure. In the cases with neighboring inserted shim rods, the location of the top-entry shim rod tip is given by an additional grid line. The comparisons are presented in the order in which the measurements were made, i.e., by increasing core number. The calculated and measured distributions were both normalized to unity over the active fuel zone so that axial effects were completely separated from radial effects. Simpson's integration rule was used to obtain the normalized distributions from the raw measured and calculated distributions. Most axial distributions were measured in the center of the central element, although some were made in various locations in element B-5, which was located between two shim rods.

For the axial comparisons in C-5 away from shim rods, the distributions were within  $\pm 2\%$  at all points except near the reflector-fuel meat interface. These zones were more difficult to model due to the softening of the spectrum within the fuel. No attempt was made to model this effect except in the LEU element. The secondary distribution peak in the upper reflector was predicted reasonably well. Notice that the height of the peak is directly proportional to the loading of  $^{235}\text{U}$  in the fuel meat zone and thus becomes larger than the primary peak in the fuel meat zone of the LEU element distribution, as shown in Fig. 28.

For the comparisons of measurement and calculation made in the 140 g HEU element located in position B-5 between two shim rods, the agreement was not as good as in element C-5. The comparisons made to the left or right of center of B-5 appeared to be in better agreement than the one in the center of B-5, as shown in Fig. 24. The predictions of the  $^{235}\text{U}$  fission rate near or in the reflector zones was not as good as those in C-5, perhaps due to the spectral shifts introduced by the shim rods. Perhaps the best agreement and most interesting comparison of this axial series is presented in Fig. 29. Two separate comparisons are shown in this figure to illustrate the effect on the  $^{235}\text{U}$  fission rate distribution of insertion of a shim rod in a neighboring location. Both comparisons indicate very good agreement, even in the upper reflector zone. The areas of poorer agreement remained near the lower reflector - fuel meat interface and in the vicinity of the shim rod tip, where steep flux gradients are introduced. From these distributions one can conclude that to accurately calculate the effect of control rods upon the flux distribution would require further model modification, primarily in the radial planes.

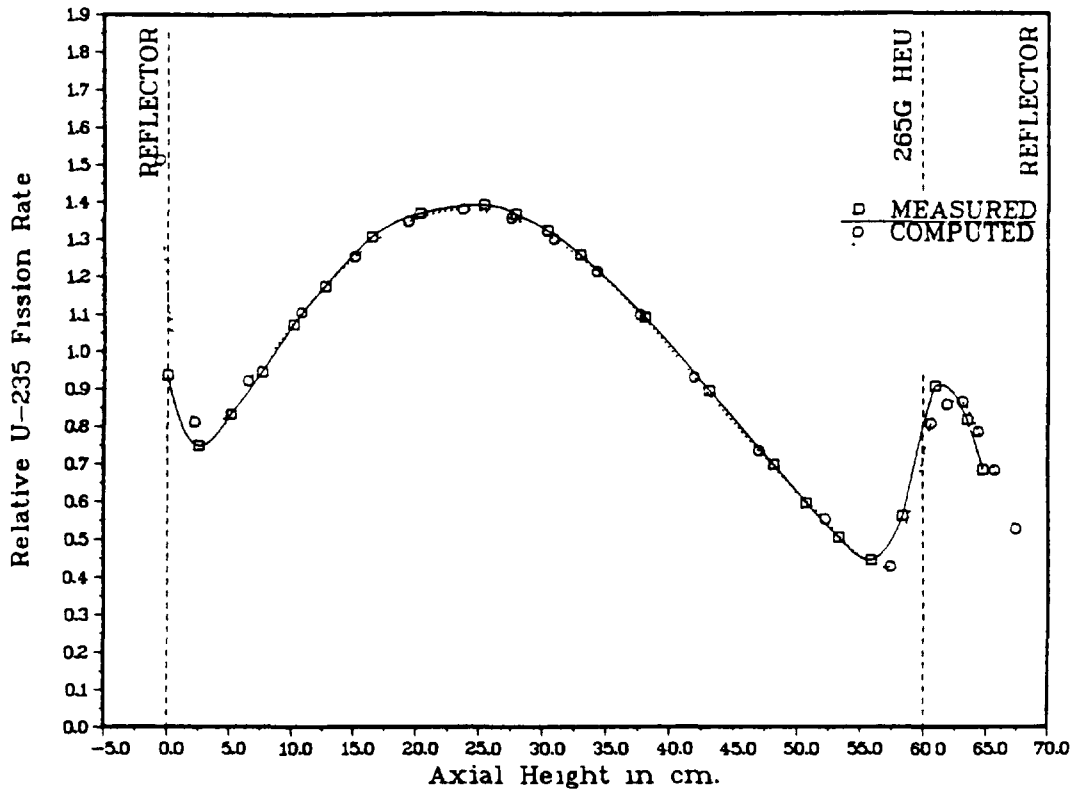


FIG. 23 PCA CORE 301 AXIAL FISSION RATE DISTR IN CENTER OF C-5

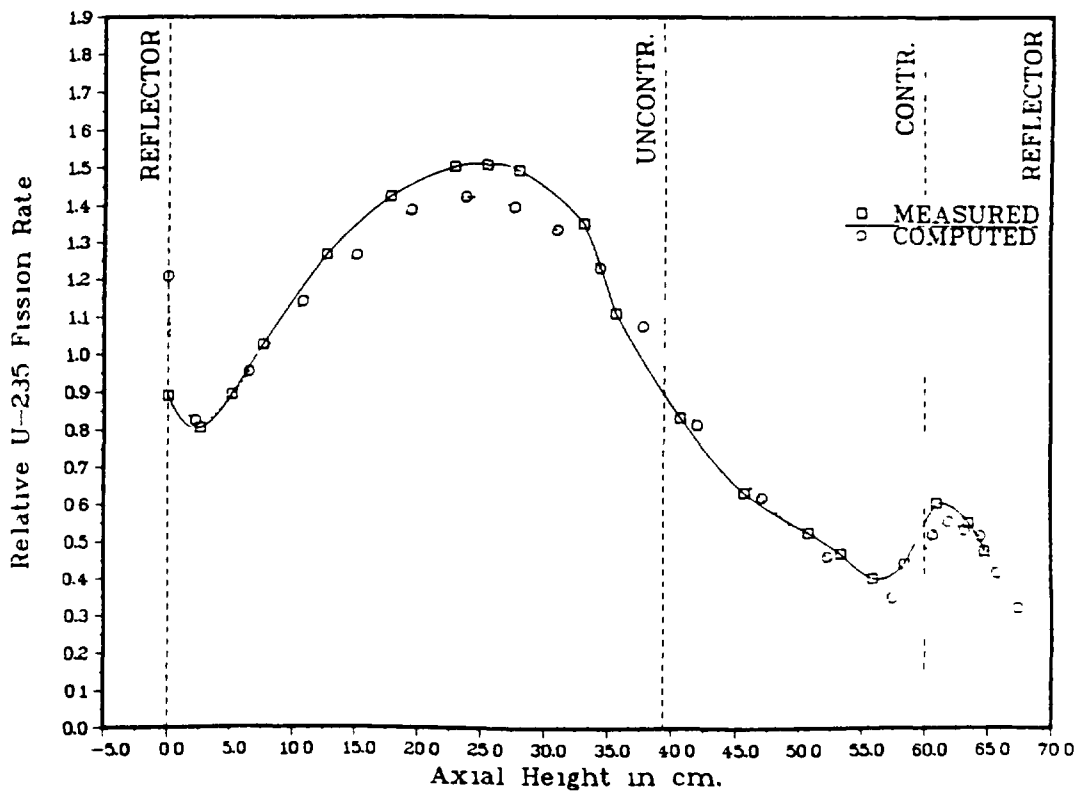


FIG. 24 PCA CORE 301 AXIAL FISSION RATE DISTR IN B-5 CNTR-140G/HEU

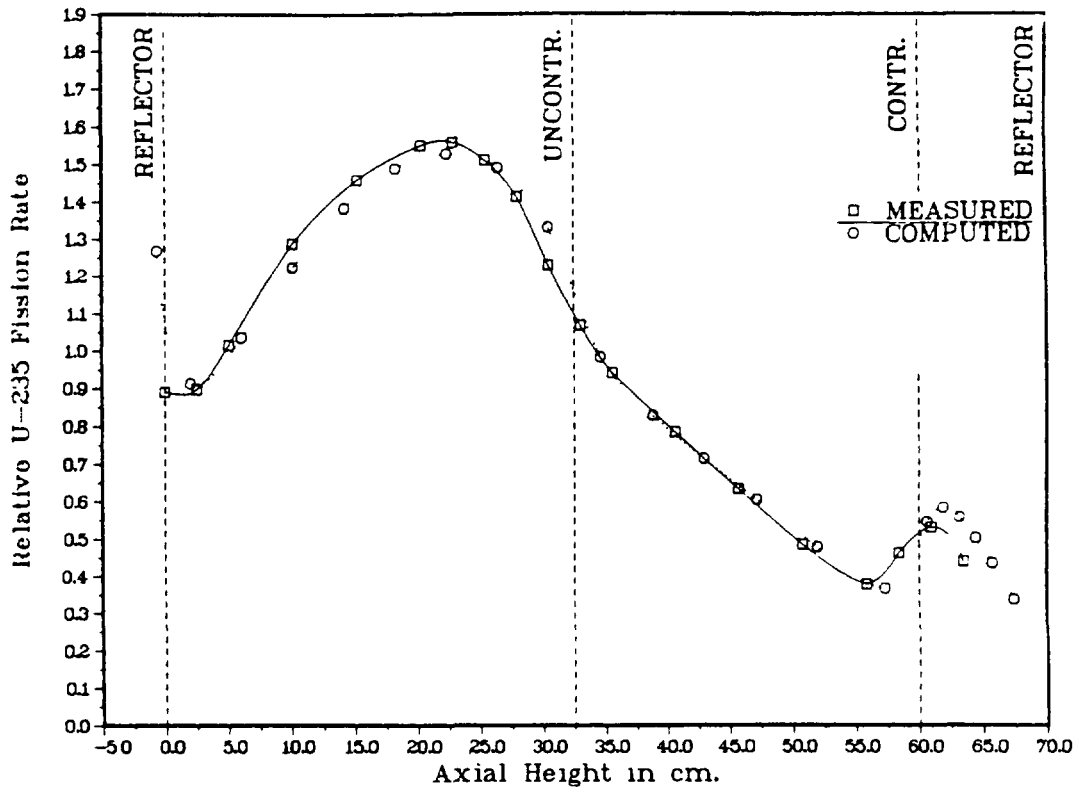


FIG. 25 PCA CORE 302 AXIAL FISSION RATE LEFT CENTER OF B-5-140G/HEU

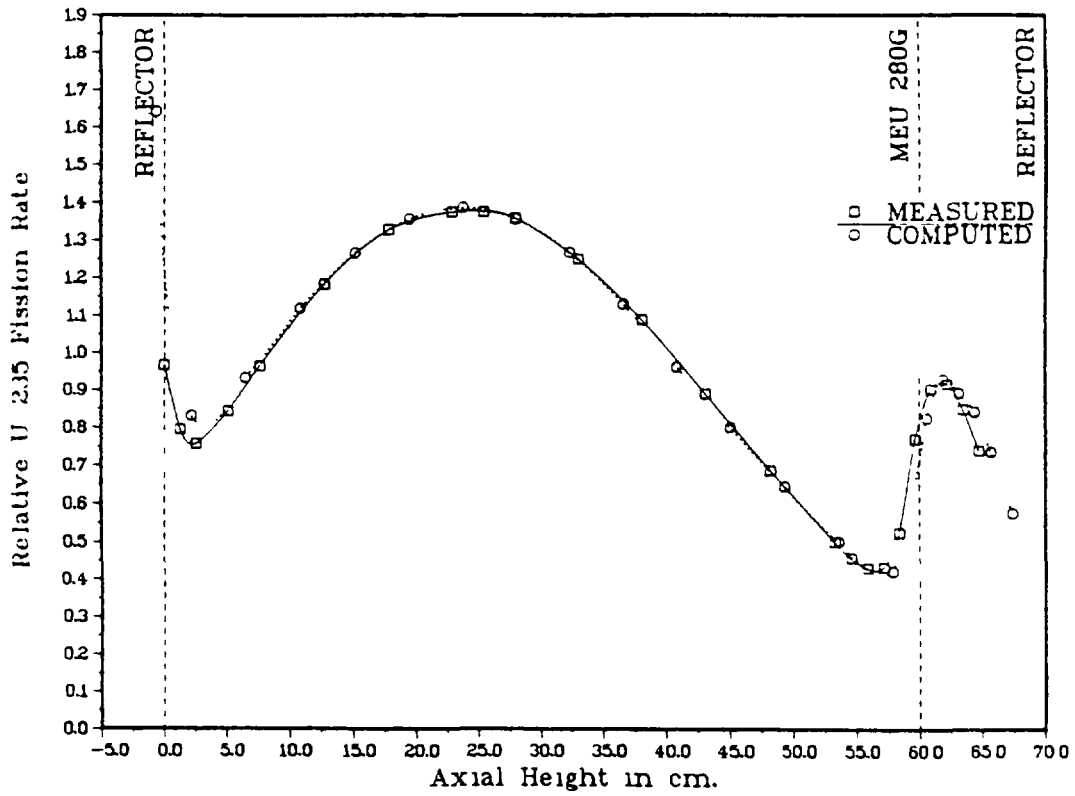


FIG. 26 PCA CORE 312 AXIAL FISSION RATE DISTR IN CENTER OF C-5

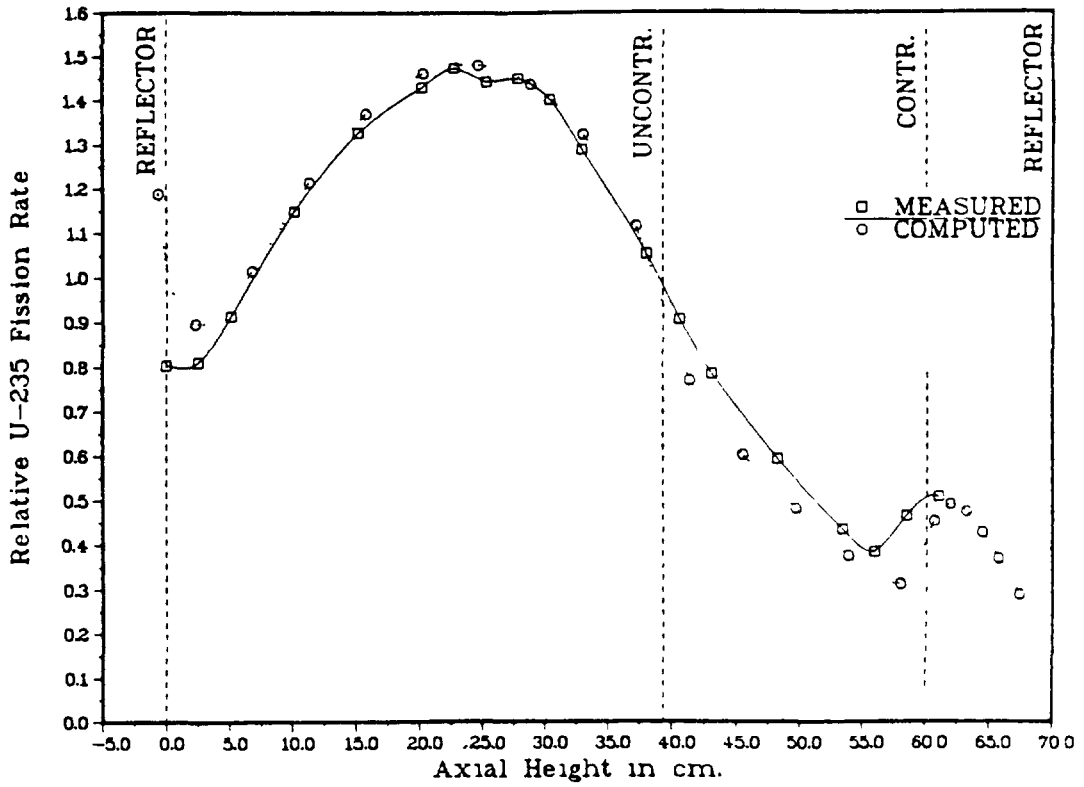


FIG. 27 PCA CORE 315 AXIAL FISSION RATE RIGHT CNTR OF B-5/140G-HEU

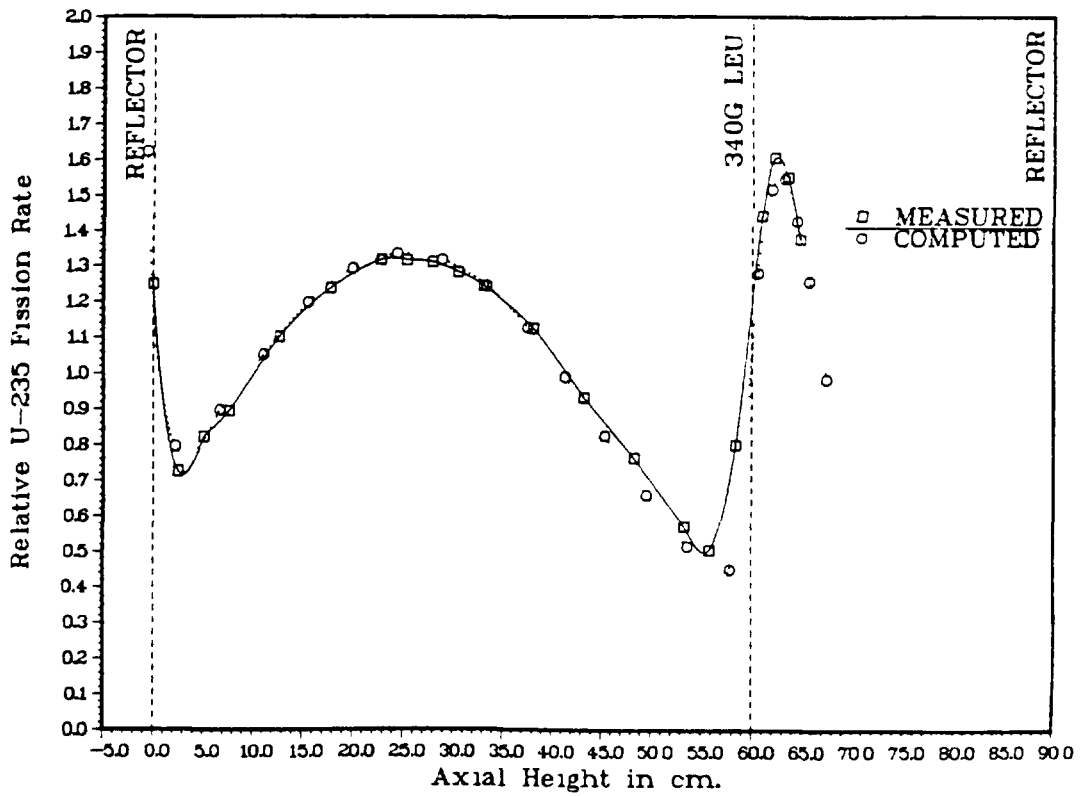


FIG. 28 PCA CORE 316 AXIAL FISSION RATE DISTR IN CENTER OF C-5

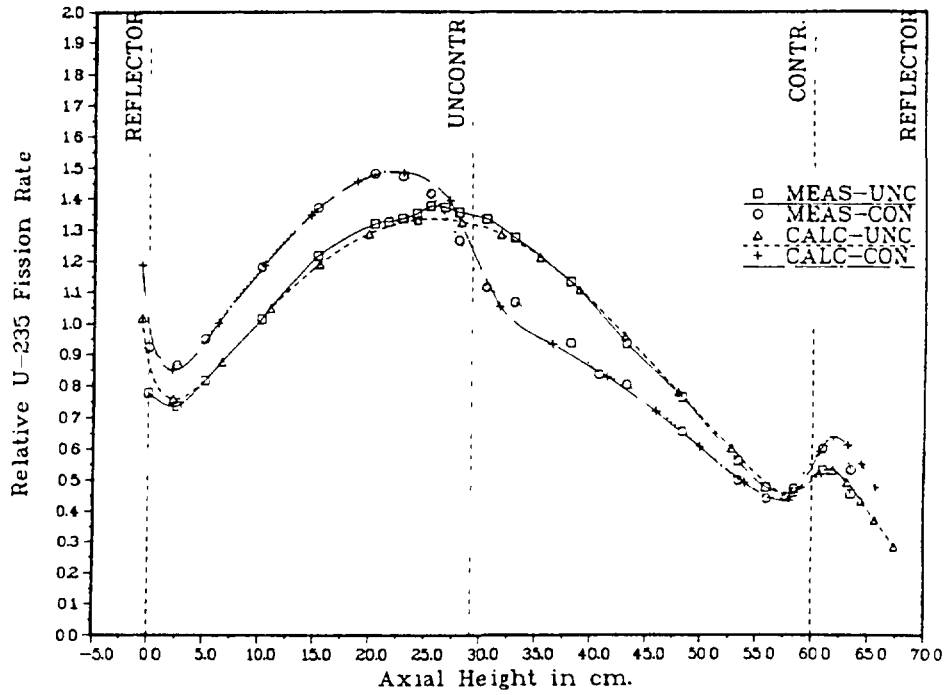


FIG. 29 PCA CORE 316 AXIAL FISS RATE LEFT CNTR OF B-5-140G/HEU

	3	4	5	6	7
A					0.587 0.602
B			1.174 1.323 1.264 1.282 1.307		
C		1.071 1.027 1.073 1.030 1.074 1.144	1.081 1.00 1.016 1.038 1.00 1.036	1.193 1.095 1.140 1.071	- 1.028
D			1.045 1.019 1.310 1.299 1.335 1.303 1.183 1.211		
E	0.568 0.629				0.638 0.633

xxx - Measured  
xxx - Calculated

Figure 30. PCA Mid-Plane U-235 Fission Rate Distribution of Core 301

## VI. Conclusions

These measurements at the PCA provided very valuable data for comparison with research reactor calculational modelling for all-fresh mixed-enrichment and all-HEU cores. These comparisons with measured data indicate the ability of the current research reactor analysis methods to predict changes in reactivity or power distribution, even under the very unusual condition of loading adjacent elements that not only differ in  $^{235}\text{U}$  content by more than a factor of two, but also in initial enrichment. The predictions of radial and axial fission rates were within an average of  $\pm 5\%$  of measured data even in fuel element positions near a shim rod. Although the calculated core  $k_{\text{eff}}$  was slightly above unity, the relative changes were consistently less than  $0.2\% \Delta k/k$  for all core configurations, including the reduction in core size by 16%. When only the central element was replaced with either an MEU or LEU element,  $<0.1\% \Delta k/k$  change in whole-core  $k_{\text{eff}}$  was calculated.

Although further model development could be done to improve the agreement with the measured data, these comparisons demonstrate that using the current research reactor analysis methods, accurate predictions of core power distributions and reactivity trends can be made for most plate-type mixed-enrichment core configurations.

## REFERENCES

1. M. M. Bretscher and J. L. Snelgrove, "Comparison of Calculated Quantities with Measured Quantities for the LEU-Fueled Ford Nuclear Reactor," International Meeting on Research and Test Reactor Core Conversions from HEU to LEU Fuels, ANL/RERTR/TM-4, (Nov. 8-10, 1982).
2. B. A. Zolotar and W. J. Eich, Advanced Recycle Methodology Program: Preliminary Specifications for a New Nuclear Computational Capability, EPRI-SR-2, (1974).
3. D. R. Ferguson and K. L. Derstine, "Optimized Iteration Strategies and Data Management Considerations for Fast Reactor Finite-Difference Diffusion Theory Codes," Nucl. Sci. Eng. 64, 593 (1977).
4. R. Blomquist, R. Lell, and E. Gelbard, "VIM - A Continuous Energy Monte Carlo Code at ANL," Proceedings of Seminar Workshop on Theory and Applications of Monte Carlo Methods, Oak Ridge, TN, RSIC, (1980).
5. K. D. Lathrop and F. W. Brinkley, "TWOTRAN-II: An Interfaced, Exportable Version of the TWOTRAN Code for Two-Dimensional Transport," LA-4848-MS, (July 1973).

COMPARISON OF CALCULATIONS AND MEASUREMENTS  
OF MEU FUEL IN THE SAPHIR REACTOR

H. WINKLER, J. ZEIS  
Eidgenössisches Institut für Reaktorforschung,  
Würenlingen, Switzerland

Abstract

In a  $4 \times 4$  core arrangement each standard element (93% enrichment  $\sim 280$  g U-235, 23 plates) has been replaced by a MEU-element with 320 g U-235, 45% enrichment. The reactivity difference has been determined over the fine control rod position. The same core configuration was calculated with the two dimensional diffusion code CODIFF in order to obtain the difference in  $k_{eff}$  resp.  $\rho$ .

1. INTRODUCTION

---

In order to check the validity of the calculations codes used for the reduced enrichment programme some reactivity measurements have been done on the SAPHIR-Reactor.

In a  $4 \times 4$  core arrangement each standard element (93% enrichment  $\sim 280$  g U-235, 23 plates) has been replaced by a MEU-element with 320 g U-235, 45% enrichment. The reactivity difference has been determined over the fine control rod position. The same core configuration was calculated with the two dimensional diffusion code CODIFF in order to obtain the difference in  $k_{eff}$  resp.  $\rho$

It is shown that the mean deviation between calculation and measurement is less than 6,5%. Thus reasonable agreement exists.

2. Core Configuration and calibration of control rods

---

Fig. 1A shows the core configuration No. 433 used for the reactivity measurements. All standard elements are fresh 23 plate MTR-elements with a content of 281 g U-235, 93% enriched, whereas the control elements are of the central rod type with 14 fuel plates and a burn up of about 20% each.

<b>Datenblatt</b> für LADUNG - Nr. 433		$P_{max}$ nom.: MW
Ladung für: <u>Reactivity Measurement MEU fuel</u>		VA-Nr.: _____

<b>LADUNGSANORDNUNG</b>	1A																																																																																																								
<table style="width: 100%; border-collapse: collapse;"> <tr><td style="width: 10%; border: 1px solid black;">Nr.</td><td style="border: 1px solid black;">Normalelement</td></tr> <tr><td style="border: 1px solid black;">Nr.</td><td style="border: 1px solid black;">Kontrollelement</td></tr> <tr><td style="border: 1px solid black;">Nr.</td><td style="border: 1px solid black;">GA-Kontrollelement</td></tr> <tr><td style="border: 1px solid black;">Be</td><td style="border: 1px solid black;">Reflektorelement</td></tr> <tr><td style="border: 1px solid black;">Q</td><td style="border: 1px solid black;">Neutronenquelle</td></tr> <tr><td style="border: 1px solid black;"> </td><td style="border: 1px solid black;"> </td></tr> <tr><td style="border: 1px solid black;"> </td><td style="border: 1px solid black;"> </td></tr> </table>	Nr.	Normalelement	Nr.	Kontrollelement	Nr.	GA-Kontrollelement	Be	Reflektorelement	Q	Neutronenquelle					<table style="width: 100%; border-collapse: collapse;"> <tr><td style="width: 20px;">1</td><td style="width: 20px;">2</td><td style="width: 20px;">3</td><td style="width: 20px;">4</td><td style="width: 20px;">5</td><td style="width: 20px;">6</td><td style="width: 20px;">7</td><td style="width: 20px;">8</td><td style="width: 20px;">9</td></tr> <tr><td>1</td><td>"</td><td></td><td></td><td></td><td></td><td></td><td></td><td></td></tr> <tr><td>2</td><td></td><td></td><td></td><td></td><td></td><td></td><td></td><td></td></tr> <tr><td>3</td><td></td><td></td><td></td><td style="text-align: center;">300</td><td style="text-align: center;">344</td><td style="text-align: center;">301</td><td style="text-align: center;">313</td><td></td></tr> <tr><td>4</td><td></td><td></td><td></td><td style="text-align: center;">341</td><td style="text-align: center;">342</td><td style="text-align: center;">343</td><td style="text-align: center;">FR</td><td></td></tr> <tr><td>5</td><td></td><td></td><td></td><td style="text-align: center;">302</td><td style="text-align: center;">345</td><td style="text-align: center;">304</td><td style="text-align: center;">323</td><td></td></tr> <tr><td>6</td><td></td><td></td><td></td><td style="text-align: center;">338</td><td style="text-align: center;">339</td><td style="text-align: center;">340</td><td style="text-align: center;">337</td><td></td></tr> <tr><td>7</td><td></td><td></td><td></td><td></td><td></td><td></td><td></td><td></td></tr> <tr><td>8</td><td></td><td></td><td></td><td></td><td></td><td></td><td></td><td></td></tr> <tr><td>9</td><td>"</td><td></td><td></td><td></td><td></td><td></td><td></td><td>"</td></tr> </table>	1	2	3	4	5	6	7	8	9	1	"								2									3				300	344	301	313		4				341	342	343	FR		5				302	345	304	323		6				338	339	340	337		7									8									9	"							"
Nr.	Normalelement																																																																																																								
Nr.	Kontrollelement																																																																																																								
Nr.	GA-Kontrollelement																																																																																																								
Be	Reflektorelement																																																																																																								
Q	Neutronenquelle																																																																																																								
1	2	3	4	5	6	7	8	9																																																																																																	
1	"																																																																																																								
2																																																																																																									
3				300	344	301	313																																																																																																		
4				341	342	343	FR																																																																																																		
5				302	345	304	323																																																																																																		
6				338	339	340	337																																																																																																		
7																																																																																																									
8																																																																																																									
9	"							"																																																																																																	
Bemerkungen:																																																																																																									

<b>LADUNGSANORDNUNG</b>	1B																																																																																																												
<table style="width: 100%; border-collapse: collapse;"> <tr><td style="width: 10%; border: 1px solid black;">Nr.</td><td style="border: 1px solid black;">Normalelement</td></tr> <tr><td style="border: 1px solid black;">Nr.</td><td style="border: 1px solid black;">Kontrollelement</td></tr> <tr><td style="border: 1px solid black;">Nr.</td><td style="border: 1px solid black;">GA-Kontrollelement</td></tr> <tr><td style="border: 1px solid black;">Be</td><td style="border: 1px solid black;">Reflektorelement</td></tr> <tr><td style="border: 1px solid black;">Q</td><td style="border: 1px solid black;">Neutronenquelle</td></tr> <tr><td style="border: 1px solid black;">7,8</td><td style="border: 1px solid black;"><math>\Delta\rho[\beta]</math></td></tr> <tr><td style="border: 1px solid black;"> </td><td style="border: 1px solid black;"> </td></tr> <tr><td style="border: 1px solid black;"> </td><td style="border: 1px solid black;"> </td></tr> </table>	Nr.	Normalelement	Nr.	Kontrollelement	Nr.	GA-Kontrollelement	Be	Reflektorelement	Q	Neutronenquelle	7,8	$\Delta\rho[\beta]$					<table style="width: 100%; border-collapse: collapse;"> <tr><td colspan="2" style="text-align: center;">Measured <math>\Delta\rho</math></td></tr> <tr><td style="width: 20px;">1</td><td style="width: 20px;">2</td><td style="width: 20px;">3</td><td style="width: 20px;">4</td><td style="width: 20px;">5</td><td style="width: 20px;">6</td><td style="width: 20px;">7</td><td style="width: 20px;">8</td><td style="width: 20px;">9</td></tr> <tr><td>1</td><td>"</td><td></td><td></td><td></td><td></td><td></td><td></td><td></td></tr> <tr><td>2</td><td></td><td></td><td></td><td></td><td></td><td></td><td></td><td></td></tr> <tr><td>3</td><td></td><td></td><td></td><td style="text-align: center;">3,7</td><td></td><td></td><td style="text-align: center;">2,0</td><td></td></tr> <tr><td>4</td><td></td><td></td><td></td><td style="text-align: center;">4,6</td><td style="text-align: center;">19,2</td><td style="text-align: center;">13,4</td><td></td><td></td></tr> <tr><td>5</td><td></td><td></td><td></td><td style="text-align: center;">15,1</td><td></td><td></td><td style="text-align: center;">7,5</td><td></td></tr> <tr><td>6</td><td></td><td></td><td></td><td style="text-align: center;">2,5</td><td style="text-align: center;">7,8</td><td style="text-align: center;">7,5</td><td style="text-align: center;">2,5</td><td></td></tr> <tr><td>7</td><td></td><td></td><td></td><td></td><td></td><td></td><td></td><td></td></tr> <tr><td>8</td><td></td><td></td><td></td><td></td><td></td><td></td><td></td><td></td></tr> <tr><td>9</td><td>"</td><td></td><td></td><td></td><td></td><td></td><td></td><td>"</td></tr> </table>	Measured $\Delta\rho$		1	2	3	4	5	6	7	8	9	1	"								2									3				3,7			2,0		4				4,6	19,2	13,4			5				15,1			7,5		6				2,5	7,8	7,5	2,5		7									8									9	"							"
Nr.	Normalelement																																																																																																												
Nr.	Kontrollelement																																																																																																												
Nr.	GA-Kontrollelement																																																																																																												
Be	Reflektorelement																																																																																																												
Q	Neutronenquelle																																																																																																												
7,8	$\Delta\rho[\beta]$																																																																																																												
Measured $\Delta\rho$																																																																																																													
1	2	3	4	5	6	7	8	9																																																																																																					
1	"																																																																																																												
2																																																																																																													
3				3,7			2,0																																																																																																						
4				4,6	19,2	13,4																																																																																																							
5				15,1			7,5																																																																																																						
6				2,5	7,8	7,5	2,5																																																																																																						
7																																																																																																													
8																																																																																																													
9	"							"																																																																																																					
Bemerkungen:																																																																																																													

<b>LADUNGSANORDNUNG</b> 433B	1C																																																																																																								
<table style="width: 100%; border-collapse: collapse;"> <tr><td style="width: 10%; border: 1px solid black;">Nr.</td><td style="border: 1px solid black;">Normalelement</td></tr> <tr><td style="border: 1px solid black;">Nr.</td><td style="border: 1px solid black;">Kontrollelement</td></tr> <tr><td style="border: 1px solid black;">Nr.</td><td style="border: 1px solid black;">GA-Kontrollelement</td></tr> <tr><td style="border: 1px solid black;">Be</td><td style="border: 1px solid black;">Reflektorelement</td></tr> <tr><td style="border: 1px solid black;">Q</td><td style="border: 1px solid black;">Neutronenquelle</td></tr> <tr><td style="border: 1px solid black;"> </td><td style="border: 1px solid black;"> </td></tr> <tr><td style="border: 1px solid black;"> </td><td style="border: 1px solid black;"> </td></tr> </table>	Nr.	Normalelement	Nr.	Kontrollelement	Nr.	GA-Kontrollelement	Be	Reflektorelement	Q	Neutronenquelle					<table style="width: 100%; border-collapse: collapse;"> <tr><td style="width: 20px;">1</td><td style="width: 20px;">2</td><td style="width: 20px;">3</td><td style="width: 20px;">4</td><td style="width: 20px;">5</td><td style="width: 20px;">6</td><td style="width: 20px;">7</td><td style="width: 20px;">8</td><td style="width: 20px;">9</td></tr> <tr><td>1</td><td>"</td><td></td><td></td><td></td><td></td><td></td><td></td><td></td></tr> <tr><td>2</td><td></td><td></td><td></td><td></td><td></td><td></td><td></td><td></td></tr> <tr><td>3</td><td></td><td></td><td></td><td style="text-align: center;">■</td><td></td><td style="text-align: center;">■</td><td></td><td></td></tr> <tr><td>4</td><td></td><td></td><td></td><td style="text-align: center;">■</td><td></td><td style="text-align: center;">■</td><td></td><td></td></tr> <tr><td>5</td><td></td><td></td><td></td><td style="text-align: center;">■</td><td></td><td style="text-align: center;">■</td><td></td><td></td></tr> <tr><td>6</td><td></td><td></td><td></td><td></td><td></td><td></td><td></td><td></td></tr> <tr><td>7</td><td></td><td></td><td></td><td></td><td></td><td></td><td></td><td></td></tr> <tr><td>8</td><td></td><td></td><td></td><td></td><td></td><td></td><td></td><td></td></tr> <tr><td>9</td><td>"</td><td></td><td></td><td></td><td></td><td></td><td></td><td>"</td></tr> </table>	1	2	3	4	5	6	7	8	9	1	"								2									3				■		■			4				■		■			5				■		■			6									7									8									9	"							"
Nr.	Normalelement																																																																																																								
Nr.	Kontrollelement																																																																																																								
Nr.	GA-Kontrollelement																																																																																																								
Be	Reflektorelement																																																																																																								
Q	Neutronenquelle																																																																																																								
1	2	3	4	5	6	7	8	9																																																																																																	
1	"																																																																																																								
2																																																																																																									
3				■		■																																																																																																			
4				■		■																																																																																																			
5				■		■																																																																																																			
6																																																																																																									
7																																																																																																									
8																																																																																																									
9	"							"																																																																																																	
Bemerkungen:																																																																																																									

Figure 1

The standard elements has been replaced successively by one MEU (45% enrichment, 320 g U-235) element.

The above described core configuration has became critical with the following rod positions:

Coarse control rod position	390 resp. 394 mm
Fine control rod position	199 resp. 141 mm.

In order to check the influence of the relatively low position of the control rods a second loading without the element on place 68 has been used (loading 433B) for control measurements. In this loading the critical rod position has been:

Coarse control rod position	650 mm (upper limit)
Fine control rod position	360 mm.

For both loadings the reactivity worth and curve of the fine control rod has been measured. The results are given in Fig. 2 and Fig. 3. Also the shut down reactivity of the coarse control rod has been determined by rod drop technique.

The rod values are:  $\rho_{390} = 11,63 \pm 0,5 \text{ \$}$   
 $\rho_{650} = 14,95 \pm 0,7 \text{ \$}$

From this a reactivity value of  $\Delta\rho = 3,3 \pm 0,8 \text{ \$}$  can be deduced for the element on place 68. (The calculations gives  $\Delta\rho = 2,03 \text{ \$}$ ).

From the reactivity curve Fig. 3 it can be determined an over-criticality of  $0.205 \text{ \$}$  for the loading 433B.

Assuming a  $\beta_{\text{eff}} = 8 \cdot 10^{-3}$  the multiplication factor will be  
 $k_{\text{eff}} = 1,00168.$

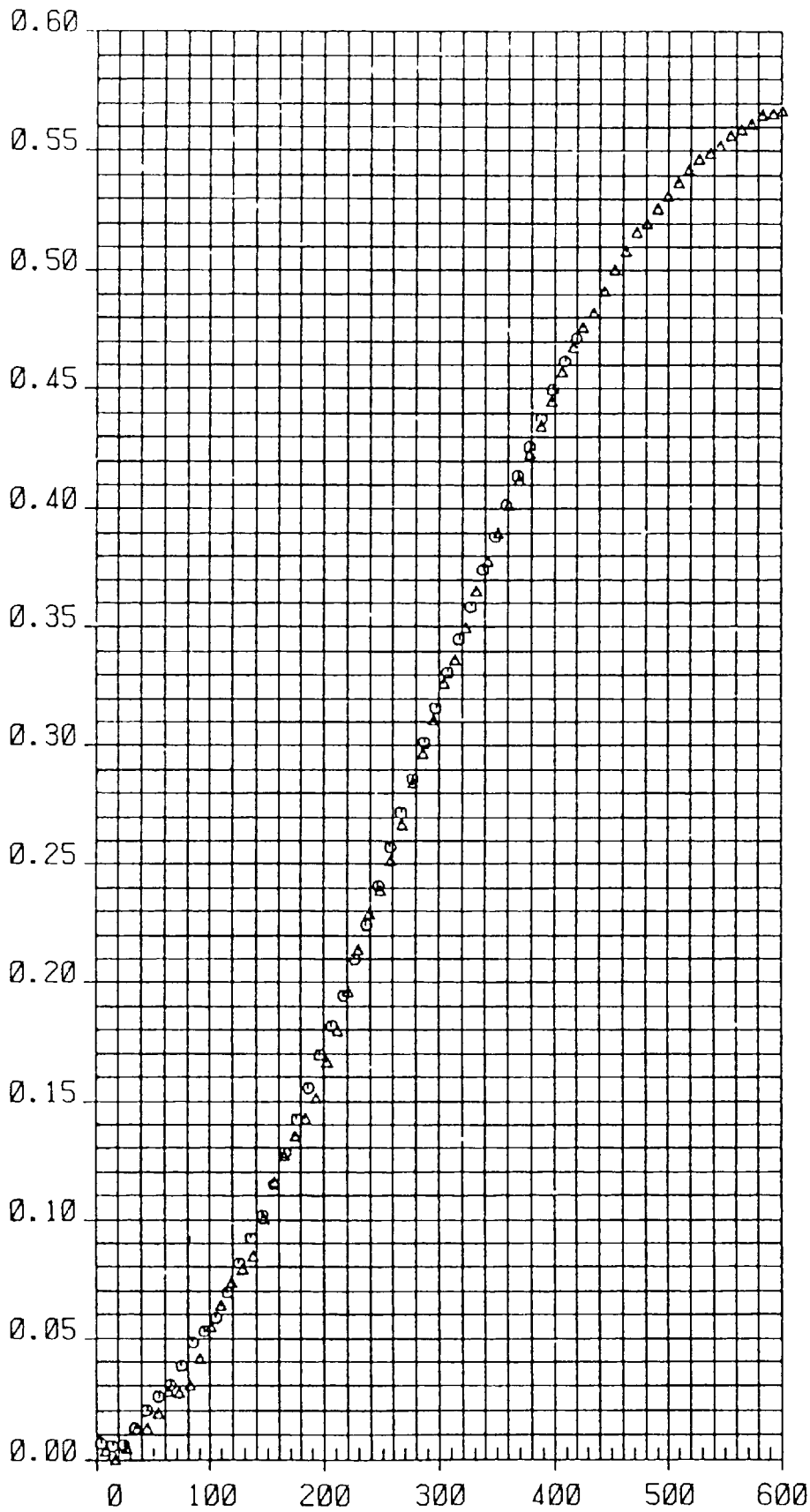
The two dimensional core calculations with the diffusion code CODIFF (Ref. 1) has given for the same loading a multiplication factor of  
 $k_{\text{eff}} = 1,03230.$

For this calculation a vertical buckling according to the BENCHMARK Problem (Ref. 2) of  $B_z^2 = 1,6943 \cdot 10^{-3} \cdot \text{cm}^{-2}$  has been used.

Comparing the two reactivity values (measured and calculated) an effective value of the vertical buckling for the standard MTR core with all control rods withdrawn can be determined to  
 $B_z^2 = 2,4 \cdot 10^{-3} \cdot \text{cm}^{-2}$  which corresponds to an extrapolated height of

$$H_{\text{extr.}} = 64,2 \text{ cm.}$$

RHO (°)



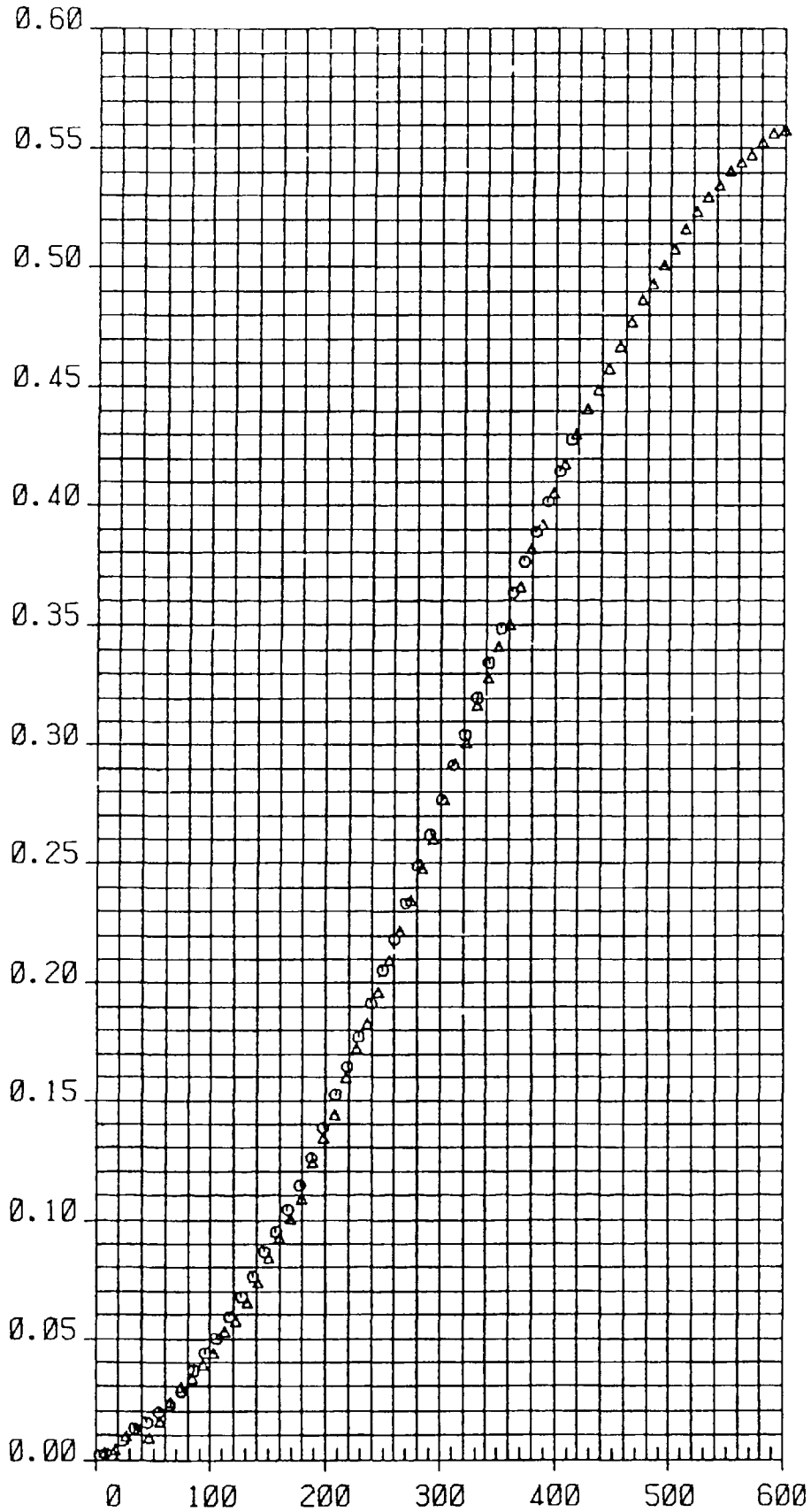
FEINREGELSTABKURVE

LADUNG 433  
MESSNUMMER 1  
LEISTUNG 10 KW  
GR - BANK 394. MM  
POSITION FC3 MP8  
ZAEHLRATE CA. 10<sup>6</sup> CPS

FR  
(MM)

Figure 2

RHO (\$)



FEINREGELSTABKURVE

LADUNG 433  
MESSNUMMER 2  
LEISTUNG 10 KW  
GR - BANK 650. MM  
POSITION FC3 MP8  
ZAEHLRATE CA.  $10^6$  CPS

FR  
(mm)

Figure 3

A recalculation of the loading 433B with this new value of  $B_z^2$  gives a multiplication factor of:

$$k_{\text{eff}} = 1,005644.$$

### 3. Measurement of the MEU-elements

The core configuration 433 contains 11 fresh HEU-standard elements (281 g U-235, 93% enriched) and 5 control elements with a small burn up.

The standard elements have been successively replaced against MEU-elements (320 g U-235, 45% enrichment) and the reactivity difference was determined over the position of the fine control rod.

For each measurement the corresponding core configuration was calculated with the two dimensional diffusion code CODIFF (Ref. 1) in order to determine  $k_{\text{eff}}$ . The vertical buckling used in the calculation is  $B_z^2 = 1,6943 \cdot 10^{-3} \cdot \text{cm}^{-2}$ .

In a second step two to three standard HEU-elements have been replaced by MEU-elements in order to check the interference effect.

Table 1 shows the results of the measurements and calculations.

### 4. Influence of rodposition

The coarse control rod position has been relatively low during the reactivity measurements.

In order to evaluate this influence a slight loading modification has been made. The element on place 68 was removed so that the reactor becomes critical with all coarse control rods in upper limit (650 mm).

In this loading (No. 433B) configuration (Fig. 1C) the 93% element on place 66 and 56 was replaced by a 45% element and recalculation of these configurations have been made.

The results of the calculations and measurements are also given in Table 1 and show no significant change in the reactivity difference.

A further test calculation were made with the adapted buckling of  $B_z^2 = 2,4 \cdot 10^{-3} \cdot \text{cm}^{-2}$ . This calculations shows that the influence on the reactivity differences is less than 2%.

Table 1: Reactivity difference of MEU fuel elements

Replaced Element	Rod position	Measured $\Delta\rho$ [ $\phi$ ]		Calculations		Coarse control rod Pos.
		total	per Element (addition)	$K_{eff}$	$\Delta\rho$ [ $\phi$ ]	
65	212		2,5	1,050441	1,8	390
67	248		7,9	1,049946	7,41	
66	248		7,9	1,049832	8,71	
56	282		13,5	1,049055	17,52	
46	329		20,0	1,048795	20,5	
36	229		3,7	1,050121	5,7	
47	285		13,4	1,049316	14,56	
45	225		4,9	1,05013	5,32	
-	196	0	0	1,05060	0	
66	203/202		7,7/7,5	1,049832	8,71	394
66+56	308	23,7	15,7			
66+56+46	478	42,1	18,4	1,046588	45,61	
56+46	381	33,2	- 8,9	1,047281	37,7	
45+56+46	426	37,5	4,3	1,046871	42,38	
66+67	251	14,6	7,1	1,049236	15,47	
-	141	0	0	1,05060	0	
	Loading 433B					650
66	422		8,1	1,032988	8,03	
56	512		16,0	1,032175	17,6	
-	360	-	0	1,033674		
All stand.	-	-	-	1.043525	80,67	

Mean value of  $\Delta\rho$  for Standard Element Positions

GP	$\Delta\rho$	Gp	$\Delta\rho$
65	2,5	68	2,5
66	7,8 $\pm$ 0,1	58	7,5
67	7,5 $\pm$ 0,5	36	3,7
56	15,1 $\pm$ 0,7	38	2,0
46	19,2 $\pm$ 1,1		
45	4,6 $\pm$ 0,4		
47	13,4		

## 5. Total reactivity loss of MEU fuel

The replacement of all standard HEU-elements in the core configuration 433 would result in a measured reactivity loss of 85,8 ¢. If the complete core including the control elements is changed against MEU-elements, then a loss in reactivity of about 1,10 \$ is expected.

The calculation of the reactivity loss due the replacement of the standard elements in this loading gives a value of  $\Delta\rho = 80,67$  ¢.

## 6. Conclusion

It has been demonstrated that the core calculation CODIFF gives reasonable results compared to the measurements. The mean difference between the calculation and the measured value can be determined from

$$\frac{\sum \frac{\Delta\rho_c}{\Delta\rho_m}}{n} = 1,065 \pm 0,013$$

( $\Delta\rho_c = \Delta\rho_{\text{calc.}}$ ;  $\Delta\rho_m = \Delta\rho_{\text{measured}}$ )

Thus the agreement between calculation and measurement is better than 7%.

## References

- Ref. 1 : J.M. Paratte, K. Foskolos, P. Grimm, C. Maeder  
TM-45-81-41, 12.10.1981  
Benützungsanleitung zum Code BOXER
- Ref. 2 : IAEA-Guide-Book TEC DOC 233, 1980

## Appendix H-8

### COMPARISONS BETWEEN CALCULATED AND MEASURED FLUX AND REACTIVITY IN HEU, MEU AND LEU FUEL ELEMENTS IN DR-3 AT RISØ

K. HAACK  
Risø National Laboratory,  
Roskilde, Denmark

#### Abstract

As part of the investigations to determine the consequences of conversion of the DR-3 reactor to lower enrichment, three MEU and three LEU fuel elements were irradiated to normal burnup (50-60%). Full axial thermal and fast neutron flux density measurements were made in the test elements and all other accessible fuel elements in the core during the test periods, and reactivity measurements were made at the loading and at the discharge of every test element. These measurements were then compared with calculations.

#### 1. Introduction

As a part of the investigations carried out to enlighten the consequences of conversion of DR 3 to lower enriched fuel, three 45% enriched (MEU) and three 20% enriched (LEU) fuel elements have been irradiated to the normal burn-up (50-60%). Full axial thermal and fast neutron flux density measurements were undertaken in the test elements and all other accessible fuel elements in the core during the test periods, and reactivity measurements were made at the loading and at the discharge of every test element.

These measurements are compared to calculations made on HEU, MEU and LEU cores by ANL and RISØ and by contributors to the benchmark calculations included in the IAEA guidebook on conversion of heavy water research reactors to lower enriched fuel.

#### 2. Measurements

The measurements are reported in appendix J-4.7 to this publication. Neutron flux density measurements were made by Ni and Co foil activation technique. The flux measurement

results are presented in graphs showing fast-to-thermal flux ratios versus  $^{235}\text{U}$  content. The reactivity measurement results are relative to HEU elements and rather uncertain, as each of them are based on two measurements, only.

### 3. Calculations

Calculations on the MEU core was done by Matos <sup>1)</sup> based on information from the DR 3 staff concerning the  $^{235}\text{U}$ -contents in realistic HEU cores and actual operation schemes.

Calculations on the LEU core was done by Matos <sup>1)</sup>, Højerup <sup>2)</sup> and contributors to the benchmark calculations <sup>3)</sup> reported in the IAEA guidebook on heavy water research reactor conversion.

In all calculations the terms "thermal" and "fast" flux are defined by the energy boundaries:

$$\begin{aligned} \text{Thermal flux } E_n &< 0.625 \text{ eV} \\ \text{Fast flux } E_n &> 5.53 \text{ keV} \end{aligned}$$

see fig. 1 which shows these boundaries in relation to the neutron spectra in a 93% enriched DR 3 fuel element, as calculated by Højerup, Risø. For comparison the fuel meat spectrum of a 20% enriched element is shown dotted.

### 4. Comparison between flux measurements and calculations

Absolute values of the measured and calculated neutron flux density values are - in the principle - incomparable, because the energy boundaries of the calculations are sharp and arbitrarily chosen. In the data treatment of the measurements, the determination of thermal flux density by Co-activation is based on Westcotts convention, which presumes a maxwellian energy distribution and also incorporate a contribution to the Co activation from the epithermal neutrons by the resonance integral; and the Ni threshold is not very sharp and furthermore a factor of  $10^3$  higher than the fast flux boundary used in the calculations.

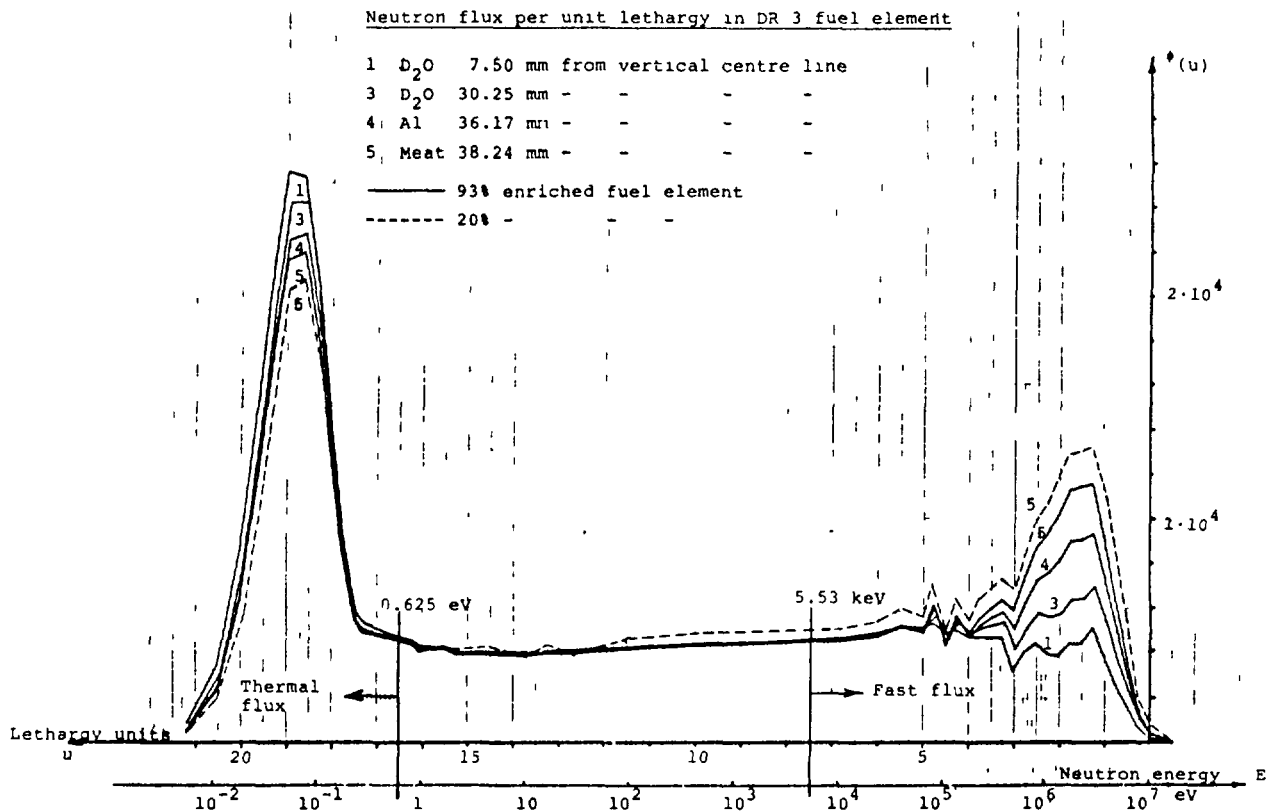


FIG. 1.

However, the most interesting figures in connection with conversion considerations are the flux changes owing to the enrichment changes. And this comparison is more appropriate, as it is relative and the errors of the absolute values are partly balanced out. Therefore the percentage changes of the fast/thermal flux ratios are given in table 1. It is seen that the calculated and measured changes  $\Delta R$  are matching fairly well.

TABLE 1.

Core position	C1			C2			Measurements
	Reference no.			Reference no.			
	2)	3)	4) x)	2)	3)	4) x)	
$C_{f,45}$	1.006			1.003			
$C_{th,45}$	0.947			0.940			
$\Delta R_{45}$	6.2%			6.7%			4.2%
$C_{f,20}$	1.016	1.018	1.015	1.007	1.028	1.020	
$C_{th,20}$	0.877	0.890	0.888	0.863	0.868	0.866	
$\Delta R_{20}$	15.8%	14.4%	14.3%	18.1%	18.4%	17.8%	13.8%

x) Mean values used.

The calculated flux ratios to be read in the references 1), 2) and 3) are the flux ratios between reduced enriched and highly enriched fuel elements:

$$C_{20} = \frac{\Phi_{20}}{\Phi_{93}} \quad \text{and} \quad C_{45} = \frac{\Phi_{45}}{\Phi_{93}} \quad \text{for fast as well as thermal neutrons.}$$

But the flux ratios needed for the comparisons are

$$R = \frac{\Phi_f}{\Phi_{th}} \quad \text{for the three enrichments, in order to find the changes}$$

of that flux ratio caused by the change in enrichment.

This flux ratio change for, par example, 45% enrichment is found as

$$\begin{aligned} \Delta R_{45} &= \frac{R_{45} - R_{93}}{R_{93}} = \frac{R_{45}}{R_{93}} - 1 = \frac{\Phi_{f,45}/\Phi_{th,45}}{\Phi_{f,93}/\Phi_{th,93}} - 1 \\ &= \frac{\Phi_{f,45}/\Phi_{f,45}}{\Phi_{th,45}/\Phi_{th,93}} - 1 = \frac{C_{f,45}}{C_{th,45}} - 1 \end{aligned}$$

A comparison between the absolute values of the calculated and measured neutron flux can be obtained by applying the activation rate instead of flux.

The activation rate obtained by the measurements is including the reaction of the total neutron spectrum on the Co foil. And so is the calculated activation rate, which is not limited to neutron energies in the defined ranges below 0.625 eV, or above 5.53 keV.

Sets of calculated and measured reaction rates are shown in table 2, for two different operation cycles. The mean values of the ratio of calculated to measured Co reaction rates don't deviate significant from 1.0, but the calculated Ni reaction rates seems to be about 10% smaller than the measured values.

TABLE 2. COMPARISON BETWEEN CALCULATED AND MEASURED REACTION RATES IN Co AND Ni

Core pos.	Co reaction rates						Ni reaction rates		
	Cycle 234			Cycle 237			Cycle 237		
	Calc.	Meas.	Calc/Meas.	Calc.	Meas.	Calc/Meas.	Calc.	Meas.	Calc/Meas.
A1	3.36 <sup>-9</sup>	2.97 <sup>-9</sup>	1.13						
A2	3.53 <sup>-9</sup>	3.40 <sup>-9</sup>	1.04						
B1	3.32 <sup>-9</sup>	3.29 <sup>-9</sup>	1.01						
B2	4.10 <sup>-9</sup>	4.06 <sup>-9</sup>	1.01						
B3	4.56 <sup>-9</sup>	4.60 <sup>-9</sup>	0.99						
B4	4.31 <sup>-9</sup>	4.21 <sup>-9</sup>	1.02						
B5	3.75 <sup>-9</sup>	3.46 <sup>-9</sup>	1.08						
C1	3.42 <sup>-9</sup>	3.25 <sup>-9</sup>	1.05	3.19 <sup>-9</sup>	3.25 <sup>-9</sup>	0.98	1.94 <sup>-12</sup>	2.27 <sup>-12</sup>	0.85
C2	4.19 <sup>-9</sup>	3.90 <sup>-9</sup>	1.07	3.98 <sup>-9</sup>	4.06 <sup>-9</sup>	0.98	2.77 <sup>-12</sup>	3.18 <sup>-12</sup>	0.87
C3	4.70 <sup>-9</sup>	4.43 <sup>-9</sup>	1.06	4.61 <sup>-9</sup>	4.80 <sup>-9</sup>	0.96	2.90 <sup>-12</sup>	3.27 <sup>-12</sup>	0.89
C6	3.17 <sup>-9</sup>	2.90 <sup>-9</sup>	1.09	3.17 <sup>-9</sup>	3.04 <sup>-9</sup>	1.04	2.09 <sup>-12</sup>	2.19 <sup>-12</sup>	0.95
D2	4.18 <sup>-9</sup>	4.36 <sup>-9</sup>	0.96						
E1	3.53 <sup>-9</sup>	3.59 <sup>-9</sup>	0.98						
E4	3.26 <sup>-9</sup>	3.00 <sup>-9</sup>	1.09						
Mean ratio			1.04			0.99			0.89
Std. dev.			0.05			0.03			0.04
Mean ratio			1.03						
Std. dev.			0.05						

The calculations were made on the very core configurations in which the measurements were carried out, and the calculated reaction rates apply to the center of the flux scan tubes, where the foils were placed for activation.

The correspondent flux values are presented in table 3, where the "Calc." columns denote the mean thermal flux (below 0.625 eV) and the maximum "fast" flux (above 5.53 KeV). The "meas." columns are the mean thermal and max. fast flux calculated from the measured activation rates by Westcotts convention and threshold detector theory, respectively.

The ratio columns show that the calculated thermal flux seem to be about 30% higher than the measured thermal flux. The calculated fast flux seem to be a factor of 2.4 higher than the measured fast flux in spite of the Ni reaction rates were slightly lower.

TABLE 3. COMPARISON BETWEEN CALCULATED AND MEASURED NEUTRON FLUX DENSITIES

Core pos.	Thermal neutron flux density						Fast neutr.flux density		
	Cycle 234			Cycle 237			Cycle 237		
	Calc.	Meas.	Calc/Meas.	Calc.	Meas.	Calc/Meas.	Calc.	Meas.	Calc/Meas.
A1	1.17	0.82	1.63						
A2	1.19	0.94	1.27						
B1	1.17	0.91	1.29						
B2	1.41	1.12	1.26						
B3	1.57	1.27	1.24						
B4	1.48	1.16	1.28						
B5	1.30	0.96	1.35						
C1	1.17	0.90	1.30						
C2	1.39	1.08	1.29	1.11	0.90	1.23	0.49	0.21	2.33
C3	1.57	1.22	1.29	1.35	1.12	1.21	0.71	0.30	2.37
C6	1.11	0.80	1.39	1.57	1.33	1.18	0.76	0.31	2.45
D2	1.43	1.21	1.18	1.09	0.84	1.30	0.53	0.21	2.52
E1	1.25	0.99	1.26						
E4	1.15	0.83	1.39						
Mean ratio			1.32			1.23			2.42
Std. dev.			0.10			0.05			0.08
Mean ratio			1.30						
Std. dev.			0.10						

All neutron fluxes are in units of  $10^{14} \text{ n cm}^{-1} \text{ s}^{-1}$

It should be pointed out here, that the thermal neutron flux values presented in the benchmark calculations <sup>3)</sup> are mean values across the fuel element and therefore only 0.92 times the thermal neutron flux values in table 3 which are the fuel element centerline values. Thus the benchmark fluxes should be in mean  $1.30 \times 0.92 = \underline{1.20 \text{ times}}$  higher than the corresponding measured fluxes would have been.

Similar considerations apply to the fast flux values, so the benchmark calculated fast fluxes should be  $1.076 \times 2.42 = \underline{2.60 \text{ times}}$  higher than the corresponding measured fluxes would have been.

As a conclusion it can be stated that owing to different energy boundaries and diverging methodology, calculated and measured flux values must deviate. With the energy boundaries

used here the calculated flux values for DR 3 should be in excess of those measured in DR 3 by factors of:

2,6 for the fast neutron flux

1,2 for the thermal neutron flux

The factors are dependant on the flux spectrum, among others things, so even with the same calculation flux boundaries, the factors will be different for various reactors.

#### 5. Comparison between calculated and measured reactivity values

The reactivity measurements in connection with the fuel element changes between the HEU, MEU and LEU elements are reported in appendix J-4.7.

The appropriate reactivity calculations have not been carried out, but the reactivity calculations on the whole core conditions at begin-of-cycle and at end-of-cycle show that further 6g will be needed in each new MEU element and about 15g in each new LEU element if conditions similar to the present HEU core should be obtained.

These figures can be checked by means of the reactivity measurements. By the measurement of the reactivity differences between HEU and MEU and between HEU and LEU in 3 of the 7 fuel element groups in which the DR 3 core can be divided, the reactivity differences in the remaining 4 groups can be estimated. This is shown in fig. 4 of appendix J-4.7. Thus the total reactivity losses by changes to full MEU and full LEU cores can be found, and by means of the fuel weight factors the  $^{235}\text{U}$  amount necessary to compensate for the losses can be found.

The results from these extrapolations were that 14g  $^{235}\text{U}$  ought to be added to each LEU element and 6g  $^{235}\text{U}$  to each MEU element, - in nice accordance to the calculated values.

## References

1. J. Matos. Enrichment Reduction Calculations for the DIDO, DR 3 and JRR-2 Reactors, ANL (USA), Appendix A in "Research Reactor Core Conversion From the Use of Highly Enriched Uranium to the Use of Low Enriched Uranium Fuels", Guidebook Addendum, Heavy Water Research Reactors, IAEA-TECDOC-324, Wien (January 1985).
2. C.F. Højerup. Enrichment Reduction Calculations for the DR 3 Reactor, Risø, Denmark, Appendix E to the Guidebook Addendum referred to above.
3. Benchmark Calculations, Appendix F to the Guidebook Addendum referred to above.
4. K.E. Beckurts, K. Wirtz, Neutron Physics, Springer Verlag, Berlin, 1964.

## Appendix H-9

### **PART I COMPARISON OF CALCULATIONS WITH MEASUREMENTS OF CONTROL ROD WORTHS IN THE HEU RA-2 REACTOR**

A. GOMEZ, A.M. LERNER, J. TESTONI, R. WALDMAN  
Comisión Nacional de Energía Atómica,  
Buenos Aires, Argentina

### **PART II USES OF THE METHOD OF COMPUTING CONTROL ROD WORTHS IN THE RA-3 REACTOR WITH HEU AND LEU FUELS**

A.M. LERNER, J. TESTONI  
Comisión Nacional de Energía Atómica,  
Buenos Aires, Argentina

#### **Abstract**

In Part I, calculations are compared with the reactivity worth of strongly absorbing materials measured in the RA-2 reactor in order to verify the calculational methods. In Part II, these methods are applied in calculating the reactivity worth of Cd control rods in the RA-3 HEU core and both Cd and Ag-In-Cd control rods in a proposed LEU core for the RA-3. The Ag-In-Cd rods are shown to have a higher reactivity worth than the Cd rods in the proposed LEU core.

## Part I

# COMPARISON OF CALCULATIONS WITH MEASUREMENTS OF CONTROL ROD WORTHS IN THE HEU RA-2 REACTOR

## 1. INTRODUCTION

The purpose of this work is having reliable calculational methods, so that they can be subsequently used in calculating low enriched fuel reactors.

This paper has two parts. In the first one some experiments are described which were performed in the RA-2 reactor; the reactivity worth of strongly absorbing materials in clean and simple configurations was measured.

In the second part, some of these experiments were calculated, and the results compared with experimental values.

## 2. MEASUREMENTS

### 2.1. Description of the experiments.

The RA-2 is a zero-power reactor located at the "Centro Atómico Constituyentes", Buenos Aires, Argentina. Its fuel elements are MTR type, of  $8.08 \times 7.7 \times 61.5 \text{ cm}^3$  size, each containing 19 plates having an average weight of 148 gr of 90% enriched uranium. In some of the fuel elements (F.E.) one or more fissionable material plates may be removed.

The initial configuration consists of 20 F.E. in a 5 x 4 arrangement, 16 of them normal ones and the remaining 4 (corresponding to the D column) with only 13 contiguous plates each. (figure 1).

The nucleus is completely reflected with light water, being the condition of infinite reflector satisfied.

The neutron detector was located within the core, inside a F.E. in which two plates were replaced by another two especially designed so as to contain the detector.

The reactivity perturbation produced by detector and special plates was measured by another detector placed outside the core; the value obtained was 0.20\$. This value was supposed constant for all the measurements.

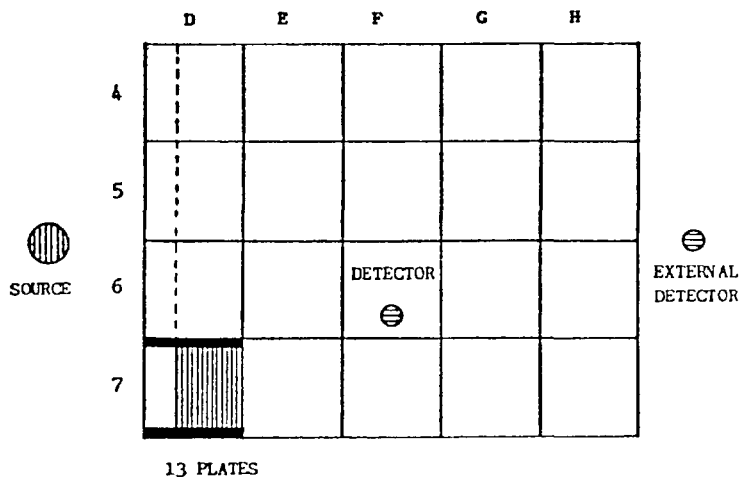


FIG. 1. RA-2 initial configuration.

The measurements were performed by means of the pulsed neutron technique, being the reactivity estimated with Gozani's method /1/.

The initial configuration was slightly subcritical (0.30\$).

Both the detector and source positions were chosen so that the spacial harmonics could be reduced and the kinetic distortion effect avoided. Statistical tests were used in order to define the adjusting channels without any harmonics.

The measuring scheme was as follows:

Two fuel plates were removed (being the vacant zone occupied by light water) and the core reactivity measured. A cadmium plate (1mm thick) was inserted in the position of one of the fuel plates removed and the measurement was repeated. The same procedures were followed with a cadmium plate in the position of the other fuel plate removed and with both fuel plates replaced by cadmium plates. The cadmium reactivity worth was then estimated as the core reactivity difference with and without absorbing material.

One of the absorbing plates was always located in position 5E3 (row 5, column E, third plate) while the other one varied along row 5.

## 2.2. Results of measurements.

Table 1 shows the values obtained for the joint reactivity of both cadmium plates as a function of the spacing between them, and the sum of each separate reactivity worth. The corresponding curves are shown in figure 2.

TABLE 1: Measured values of reactivity.

CONFIGURATION	SPACING BETWEEN PLATES (mm)	$\rho_2$ (\$)	$\rho_1 + \rho_2$ (\$)	$\rho_{12}$ (\$)
5E3 - 5E6	13	3.106 ± 0.048	5.783 ± 0.050	4.004 ± 0.150
5E3 - 5E9	25	3.532 ± 0.067	6.209 ± 0.068	5.001 ± 0.094
5E3 - 5E12	38	3.802 ± 0.059	6.479 ± 0.060	5.610 ± 0.110
5E3 - 5E15	50	4.211 ± 0.086	6.888 ± 0.087	6.188 ± 0.087
5E3 - 5F3	82	5.115 ± 0.100	7.792 ± 0.101	7.587 ± 0.083
5E3 - 5F6	95	5.197 ± 0.056	7.874 ± 0.057	7.892 ± 0.078
5E3 - 5F11	108	5.312 ± 0.088	7.989 ± 0.089	8.335 ± 0.078
5E3 - 5F17	120	5.284 ± 0.088	7.961 ± 0.089	8.413 ± 0.110
5E3 - 5G11	197	4.143 ± 0.078	6.820 ± 0.079	7.696 ± 0.085
5E3 - 5G17	222	3.390 ± 0.058	6.067 ± 0.059	6.881 ± 0.120
5E3 - 5H11	278	1.701 ± 0.032	4.378 ± 0.034	4.887 ± 0.075

Note: The reactivity value obtained for the plate in position 5E3 is  $\rho_1 = (2.677 \pm 0.013)\$$  and its distance to the center of the reactor is 121 mm.

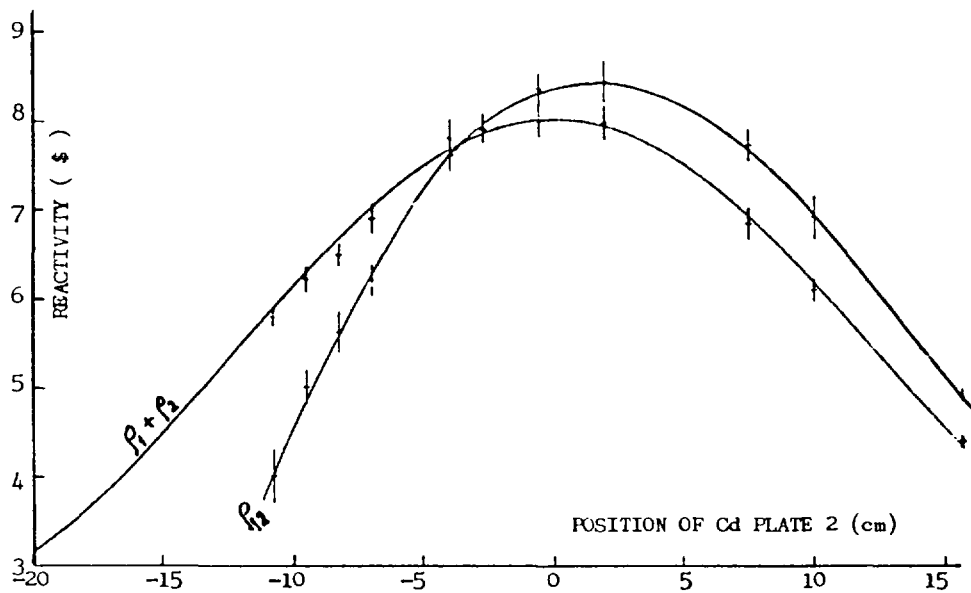


FIG. 2. Measured values of joint ( $\rho_{12}$ ) and sum of separate reactivities ( $\rho_1 + \rho_2$ ).

The values giving the sum of reactivities were adjusted by means of the function  $A \cdot \cos^2 \varphi + B$  (as given by first order perturbation theory) while the joint reactivity was represented by a smooth, continuous line. The intersection of both lines determines the position where the "shadow effect" changes sign. The separation between absorbing plates for null "shadow effect" was 9.1cm.

### 3. CALCULATIONS

#### 3.1. Computational method.

In order to calculate the reactivity worth of highly absorbing material plates in MTR fuel type reactors, a frequently used method consists in substituting the absorbing material by adequate boundary conditions on the plate's surface.

In this report some of the above mentioned experiments were calculated using this method.

The stages followed in order to perform the calculations are described in what follows.

a) Calculation of absorbing material (cadmium) cross sections with GGTC /3/ code. The condensation spectrum used was that resulting from light water moderation of U235 fission source neutrons.

Two energy group structures for transport and diffusion calculations were used, being the first of them chosen so that the cadmium absorption cross section is well described (Table 2).

b) Calculation of cell parameters for the normal fuel element, aluminum of frames and coolant in nine-group and two-group energy structures, with WIMS-D code /4/.

c) Having obtained the cadmium nine-group cross sections at the first stage and the fuel and coolant cross sections at the second one, a one-dimensional (S<sub>4</sub> - P<sub>0</sub>) transport calculation for the whole reactor was performed with ANISN code /5/, describing it along an axis normal to the plates and crossing the control element. From this third stage the boundary condition was obtained, that is to say, the current-to-flux ratio on the cadmium plate surface for the thermal group, for which cadmium absorption is considerable.

d) Having obtained the two-group cross sections at the first two stages, and the boundary conditions at the third one, three configurations of the RA-2 reactor were studied (figure 3). They differ in the position of the fuel plates substituted by absorbing material.

TABLE 2: Energy structures and its corresponding limits, chosen to describe Cd absorption cross section adequately.

$\Sigma_a$ CADMIUM ( $\text{cm}^{-1}$ )	UPPER ENERGY LIMIT	STRUCTURE OF	
		9 GR	2 GR
1.5201 E-03	10. Mev	1	
1.5271 E-02	.821 Mev	2	
1.4862 E-01	5530. ev	3	1
1.3999 E-01	4. ev	4	
9.5845 E-01	1.5 ev	5	
1.8185 E+01	.625 ev	6	
1.9519 E+02	.280 ev	7	2
1.1397 E+02	.080 ev	8	
1.5375 E+02	.020 ev	9	

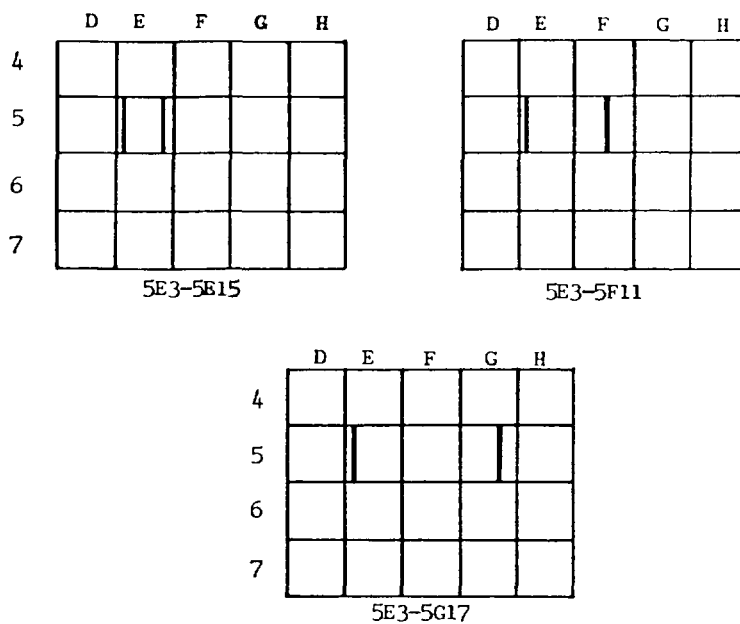


FIG. 3. Schematic RA-2 reactor: absorbing plates in three different positions.

Two-dimensional diffusion calculations were performed with EXTERMINATOR-2 code /6/. The importance of a detailed geometrical description was proved, so that in case a reduction in the computing time becomes necessary, it should rather be achieved by decreasing the number of energy groups. Having this criterion in mind, a two-group structure and a complete geometrical description (symmetry 1) were chosen.

In the reactor calculation, the absorbing material was described by giving its cross sections for the fast group and the boundary condition obtained from the transport calculation, for the thermal group.

### 3.2. Results of calculations.

Table 3 shows the results obtained. The experimental reactivity values are obtained in dollars, being thus necessary to introduce  $\beta_{eff}$ . This parameter gives the delayed neutron fraction, and it is needed to transform reactivity values from dollars to pcm.

TABLE 3: Comparison of calculated and measured reactivity values.

		CALCULATION (pcm)	EXPERIMENT (pcm)	DIFFERENCE (%)
5E3-5E15	Cd - H2O	2200	1958	12.3
	H2O- Cd	3268	3116	4.9
	Cd - Cd	4788	4579	4.6
5E3-5F11	Cd - H2O	2220	1997	11.2
	H2O- Cd	4091	3931	4.1
	Cd - Cd	6409	6168	3.9
5E3-5G17	Cd - H2O	2222	1994	11.4
	H2O- Cd	2674	2509	6.6
	Cd - Cd	5464	5092	7.3

In this report a value  $\beta_{eff} = 0.0074$  was used; it was obtained by means of the perturbation theory option of EXTERMINATOR-2 with a four-group energy structure. The delayed neutron spectrum used was suggested by Batchelor and Bonner /7/. According to which spectrum is chosen, a fluctuation of 3% in the  $\beta_{eff}$  values may be found.

Table 4 shows the dependence of the "shadow effect" with the spacing of absorbing plates. The "shadow effect" was represented by means of the non-dimensional parameter  $[p_{12} - (p_1 + p_2)] / p_{12}$ ; with this definition the comparison between calculated and measured values is not affected by the  $\beta_{eff}$  value.

Similar behaviours are observed.

It is also interesting to calculate the neutron balance, that is to say, neutrons absorbed and leaked out in each of the materials the reactor is

TABLE 4: "Shadow effect"; comparison between calculated and measured values.

CONFIGURATION	$[P_{12} - (P_1 + P_2)] / P_{12}$	
	CALCULATED	MEASURED
5E3 - 5E15	-0.14	-0.11
5E3 - 5F11	+0.02	+0.04
5E3 - 5G17	+0.10	+0.12

TABLE 5: Neutron balance.

		REFLECTOR H2O (%)	CADMIUM PLATE (%)	OTHERS (%)	TOTAL (pcm)
5E3-5E15	Cd - H2O	26.7	64.7	8.6	2210
	H2O- Cd	38.3	53.4	8.3	3277
	Cd - Cd	34.0	57.6	8.4	4797
5E3-5F11	Cd - H2O	26.7	64.9	8.4	2219
	H2O- Cd	43.2	48.8	8.0	4090
	Cd - Cd	37.8	54.0	8.2	6409
5E3-5G17	Cd - H2O	26.7	64.9	8.4	2230
	H2O- Cd	32.6	59.1	8.3	2683
	Cd - Cd	30.0	61.7	8.3	5472

made of. Table 5 shows the results of this balance. The fractions of neutrons absorbed by the reflector and the control material are shown explicitly, while axial and transversal leakages and fuel absorptions are considered together. The relative importance of reflector absorptions may be noticed.

The coincidence of calculated and measured values, within the experimental error range (a typical statistical error of 4%, and a systematic error of 3% due to the uncertainty in the  $\beta_{eff}$  value) shows that the selected calculational method results an adequate means of evaluating one or two cadmium control plates reactivity worth for highly enriched fuel reactors, being the dependence with the plates position correctly reproduced too.

It should be noted that the systematic discrepancy could be possibly associated with the error introduced by  $\beta_{eff}$  already mentioned.

#### REFERENCES

- /1/ Gozani T. - Eir Bericht N° 79 (1965).
- /2/ Difilippo F. C. et al., Nu. Sci. Eng. 51, 262 (1973).
- /3/ Chiovato O., Di Pasquantonio F., GGTC-ENEL, CNA - CPL, 1977.
- /4/ Roth M. J., Mac Dougall J.D., Kemsell P. B. "The preparation of input data for WIMS", AEEW - R538, 1967.
- /5/ Engle W. W. Jr., "A user's manual for ANISN". Oak Ridge National Laboratory, K - 1693, 1970.
- /6/ Fowler T. B., Tobias M. L., Vondy D. R.. "EXTERMINATOR-2. A FORTRAN IV code for solving multigroup neutron diffusion equations in two dimensions". ORNL - 4078, 1967.
- /7/ Tuttle R. J.- Nu. Sci. Eng. 56, 37 (1975).

## Part II

### USES OF THE METHOD OF COMPUTING CONTROL ROD WORTHS IN THE RA-3 REACTOR WITH HEU AND LEU FUELS

#### 1. INTRODUCTION

In this paper control rod worths in a realistic situation of the RA-3 reactor are calculated, and it is shown that the reactivity value of Cd plates diminishes in a LEU fuel core, as compared with the corresponding worth in the HEU fuel core. It is also shown that for the LEU fuel core it is convenient to use Ag-In-Cd control rods.

#### 2. CALCULATIONS

The reactivity worth of the pair of control rods constituting the (fork type) control element in both HEU and LEU fuel cores of the Argentine RA-3 reactor is calculated.

The method used here has already been checked with experimental values obtained from the RA-2 (HEU) reactor, and is described with some detail in /1/.

The RA-3 HEU fuel element is designed as in /1/ and its U235 load is of 195 gr. The fuel meat is an alloy of U-Al 90% enriched in U235.

In order to perform these calculations, one of the possible designs proposed for the conversion of the reactor has been chosen.

The F. E. selected has the same geometrical parameters as the HEU F.E. with a  $U_3O_8$ -Al fuel meat and a uranium density of 3.1 gr/cc (225.4 gr of U235 each F.E.).

This density was determined with the cycle length matching criterion described in /2/, by means of two independent calculations, one of them with CNEA methods, and the other one with ANL methods; the difference between them is less than 4%.

Figure 1 shows the reactor model used to obtain the reactivity worth of the pair of control plates.

In order to simplify the calculations a 27 - F.E. core surrounded by graphite elements 7.7cm thick was simulated as an equivalent square reactor. In both cases, HEU and LEU, a uniform 25% burnup was supposed.

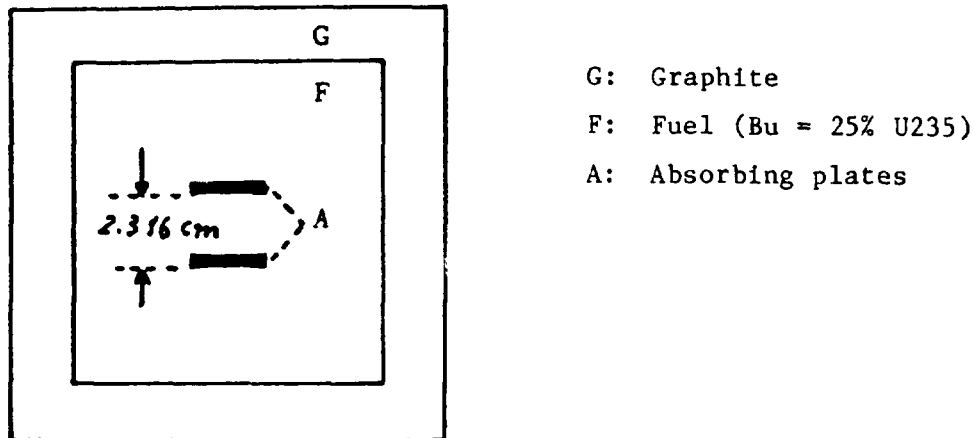


Figure 1

### 3. RESULTS

Table I contains the four different situations studied, and the corresponding results of calculations.

The first two of them show that the Cd plates lose some 12% of their reactivity value when changed from a HEU core to a LEU one.

The results obtained for the Ag-In-Cd plates corroborate the improvement this material produces, much more if its thickness is increased to 2.7 mm increasing thus the absorption due to Ag and In.

Table I

Plate material	Thickness (mm)	Core	Control rod worth of pair of plates (pcm)
Cd	1.0	HEU	4580
Cd	1.0	LEU	4026
In-Ag-Cd	1.0	LEU	4561
In-Ag-Cd	2.7	LEU	5443

On the other hand, the high reactivity values obtained for the whole set of cases is due to the fact that there is a single F.E. located at the core center.

An adequate description of both In and Ag absorption cross sections requires a more detailed energy description than the Cd one alone; in this paper an energy structure of 6 groups has been chosen for the diffusion calculation, the boundary condition for highly absorbing materials used for the last three groups.

Table II

---

Energy group structure (ev)

1.492 E+07 - 8.208 E+05

8.208 E+05 - 5.531 E+03

5.531 E+03 - 1.067 E+01

1.067 E+01 - 1.445 E+00

1.445 E+00 - 6.826 E-01

6.826 E-01 - 0

---

REFERENCES

- /1/. "Comparison of calculations with measurements in the RA-2 reactor". A. Gomez, A. M. Lerner, J. Testoni, R. Waldman. (This Appendix).
- /2/. "Research Reactor Core Conversion From the Use of Highly Enriched Uranium to the Use of Low Enriched Uranium Fuels Guidebook". IAEA - TECDOC - 233, 1980.

**MEASUREMENTS AND ANALYSIS OF CRITICAL  
EXPERIMENTS IN THE 'LA REINA' REACTOR  
USING MEDIUM ENRICHMENT URANIUM FUEL**

J. KLEIN\*, R. VENEGAS\*\*, O. MUTIS\*

\* Comisión Chilena de Energía Nuclear

\*\* Universidad de Santiago

Santiago, Chile

**Abstract**

The 5 MW La Reina reactor became critical on January 23, 1985 with 20 medium enrichment uranium fuel elements. Experiments were carried out to measure the change in critical core configuration characteristics between the previous highly enriched uranium fuel and the new medium enriched uranium fuel. This paper provides the results of measurements concerning with the critical approach, the axial flux distribution, and reflector savings and the excess reactivity, including results of neutronic calculations made for the critical experiment.

INTRODUCTION

It was estimated in 1979 that a uranium density of about  $3.7 \text{ g/cm}^3$  was required to match the cycle length of the current 80% enriched uranium (HEU) fuel for the conversion of the La Reina reactor to 20% enriched uranium fuel and no changes in the overall fuel element geometry<sup>1</sup>. However, this fuel was not available in the international marketplace.

The La Reina reactor was converted to use 45% enriched uranium (MEU) fuel elements with a uranium density of  $1.26 \text{ g/cm}^3$  with only minor changes in the design of the fuel element geometry. With the same element geometry the thermal-hydraulic characteristics of the core is virtually identical with both HEU and MEU fuels<sup>2</sup>.

The first critical state of the core using MEU fuel was achieved in January 23, 1985 with 20 fuel elements. In order to compare the MEU and HEU fuel cores, the same core configuration which reached the first criticality on October 13, 1974 was fitted using MEU fuel.

This paper shows the results of those measurements concerning with the critical approach, the axial flux distribution, the reflector savings and the excess reactivity, including results of neutronic calculations made for the critical experiment.

## GENERAL DESCRIPTION

### Reactor

The La Reina reactor is a light water-moderated, water-cooled and beryllium-reflected reactor based on the Herald reactor in operation at the UKAEA at Aldermaston. It employs flat plates MTR-type fuel. Figure 1 shows a perspective view of the La Reina reactor.

- 1 Control rod platform
- 2 Electro-magnetic clutches
- 3 Lead cell
- 4 Control rods
- 5 Reactor pool
- 6 Radial beam tubes
- 7 Tangential beam tubes
- 8 Reactor core
- 9 Ion chambers
- 10 Second pool
- 11 Delay tank
- 12 Water purification plant
- 13 Ion exchange units
- 14 Settlement tank
- 15 Filtered water tank
- 16 Deionisation plant
- 17 Pressure filter
- 18 Ventilation plant
- 19 Charcoal filter
- 20 Absolute filters
- 21 Pump room
- 22 Centrifugal pump
- 23 Heat exchanger

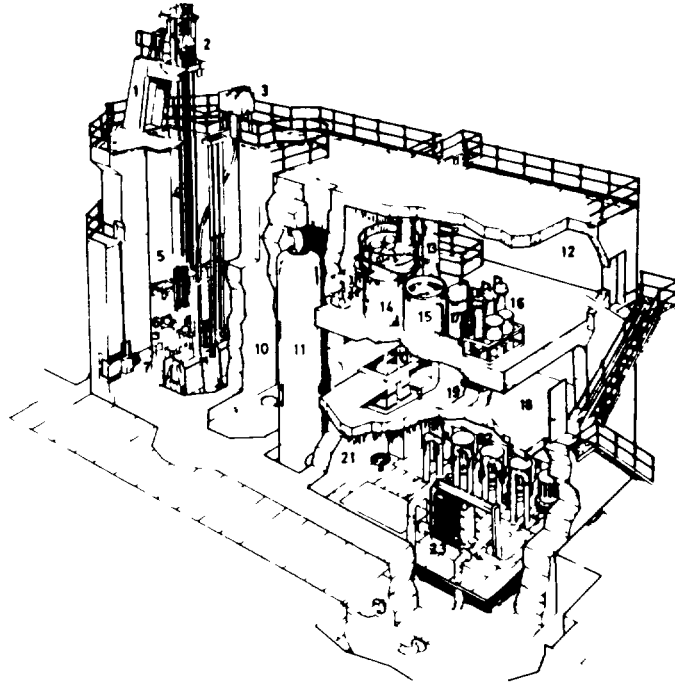


Fig. 1. La Reina Reactor Block.

The reactor core is composed of fuel elements and other special purpose elements inserted into a lattice plate made of 12 cm thick aluminium. A rectangular array of 10 x 8 holes in the lattice plate is available to suit the core elements. The arrangement of core elements can be changed to permit different experimental requirements. All core elements are similar in overall shape and have identical spigot details. Six cadmium-stainless steel control blades pass through the core in two groups of three. Slots between element rows and in the lattice plate allow the free passage of the blade absorbers.

### Fuel Element Description

Forty MEU fuel elements were framed for the La Reina reactor with only minor changes in the design of the fuel plate and no changes in the fuel element geometry. Each MEU fuel element contains 183.16 g of U-235 in sixteen fuel plates. The two outer plates contain 6.11 g of U-235 each and each of the fourteen inner plates contain 12.21 g of U-235. Fuel plates are spaced approximately 3.17 mm each other to permit the circulation of cooling water between them. The sixteen fuel plates are connected to a lower spigot fitting. The upper fitting carries two cross-members by means of which the element are to be lifted.

The upper fitting of the fuel element contains a filter grid with 85 holes, 4.76 mm diameter each, which prevents blockage of flow channels by small objects dropped into the core accidentally. If the filter grid should become blocked, cooling water will flow through lateral holes in the upper section of the fuel element from the other elements.

The fuel element is illustrated in Attachment 1 and the uranium densities and loadings for the HEU and MEU fuel elements are summarized in Table 1.

Table 1. Uranium Densities and Loadings for the HEU and MEU Fuel Elements.

Parameter	HEU	MEU
U-235 Density in Fuel Meat:		
Outer Plate, g/cm <sup>3</sup>	0.258	0.283
Inner Plate, g/cm <sup>3</sup>	0.516	0.566
U-235/Plate:		
Outer Plate, g	5.50	6.11
Inner Plate, g	11.00	12.21
Uranium Density in Fuel Meat:		
Outer Plate, g/cm <sup>3</sup>	0.322	0.630
Inner Plate, g/cm <sup>3</sup>	0.645	1.258
Uranium/Plate:		
Outer Plate, g	6.785	13.578
Inner Plate, g	13.750	27.133
U-235/Fuel Element, g	165.00	183.16

#### CORE CALCULATIONS FOR CRITICAL CONFIGURATIONS

Different cell models were prepared to generate appropriate cross sections for the different regions of the core in the standard five-group structure<sup>3</sup> commonly used at Argonne National Laboratory for MTR plate-type reactor using the WIMS-D cell code<sup>4</sup>.

The core calculations were executed by means of the EREBUS code<sup>5</sup>, a two-dimensional diffusion code, where the z leakage was approximated by an experimental axial buckling.

The results of the critical experiment, performed in October 1974 using HEU fuel, was used to evaluate the calculation methods by comparing the calculated excess reactivity value with the one experimentally measured. During the critical experiment, with all control blades withdrawn, it was found that the system was slightly subcritical with 19 HEU fuel elements (Figure 2 without the fuel element in position E9) and supercritical when the 20th element was added.

For the 19 and 20 HEU fuel element configurations, the excess reactivity was calculated using an XY model and 6.65 cm extrapolation distance<sup>6</sup>. The diffusion theory calculations gave an excess reactivity of  $-0.33\% \Delta k/k$  for the 19 fuel element configuration and  $0.79\% \Delta k/k$  for the 20 fuel element configuration.

Preliminary critical calculations were performed for the MEU fuel using the same extrapolation distance as the HEU fuel case, as an initial guess. For the 19 fuel element configuration the system was supercritical and had a calculated excess reactivity of  $0.52 \% \Delta \kappa / \kappa$ .

## EXPERIMENTAL RESULTS

### Critical Mass

The critical approach of the core was performed with the inverse multiplication method. The MEU fuel elements were loaded surrounding the A2 and B2 control blades.

Figure 2 shows the critical core configuration, including the positions of the detectors and the neutron source used during the critical approach experiment. The neutron detectors were two fission chambers and a BF3 detector, namely FC1, FC2 and BF3.

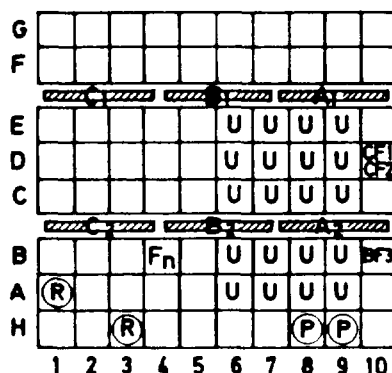


Fig. 2. Critical Configuration

Timed count rates were measured sequentially with all control blades fully inserted, fully withdrawn and at several intermediate positions prior to each fuel loading step until the critical mass was reached. The first critical state using MEU was achieved at the 7th fuel loading step. Figure 3 shows the inverse multiplication versus number of fuel elements and Figure 4 shows the inverse multiplication versus control blade positions, both obtained from the FC1 chamber.

The minimum U-235 critical mass was, for the MEU case, 3610 g while, for the HEU case, turned out to be 3240 g of U-235 as the minimum critical mass<sup>7</sup>.

### Neutron Flux Distribution

In order to determine the neutron flux distribution, foil activation technique was utilized using gold foils. All measurements were made in the fuel element using an acrylic plate, where foils were taped on, inserted in the central channel of the fuel element in position D8, Figure 2.

The axial buckling was determined from the thermal flux distribution and fitted to a cosine as shown in Figure 5. An extrapolation distance of  $\delta = 5.70 \pm 1.77$  cm was obtained for the critical configuration in which the

axial buckling of  $B_z^2 = 0.00204 \pm 0.00021 \text{ cm}^{-2}$  was measured. Using now the  $z$  leakage simulated by the axial buckling,  $B_z^2$ , experimentally determined, new calculations of critical configurations were performed. For the 19 MEU fuel element configuration an excess reactivity of  $0.06 \% \Delta\kappa/\kappa$  was obtained. The 20 fuel element configuration has an excess reactivity of  $1.12 \% \Delta\kappa/\kappa$ .

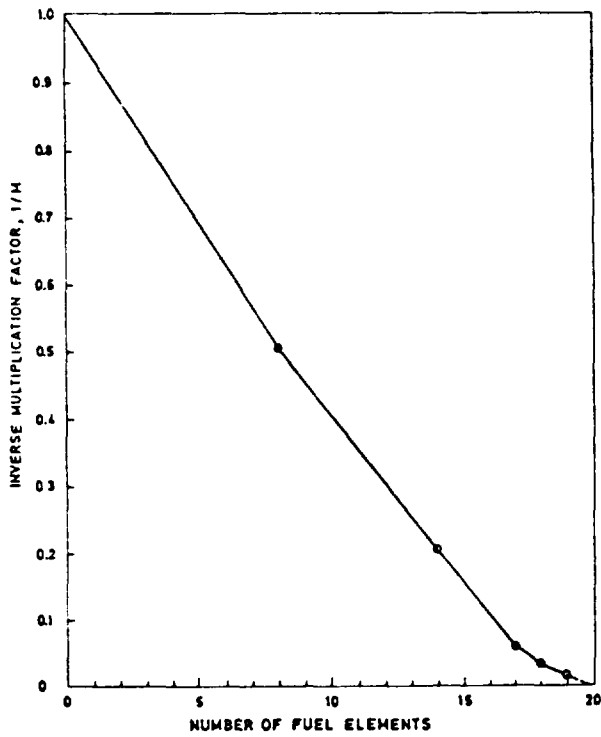


Fig. 3. Inverse Multiplication Factor as a Function of the Number of Fuel Elements.

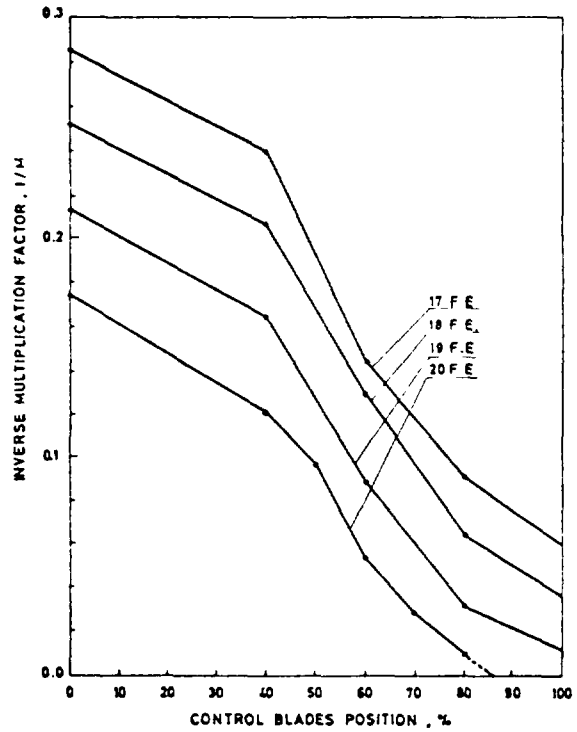


Fig. 4. Inverse Multiplication Factor as a Function of Control Blade Position.

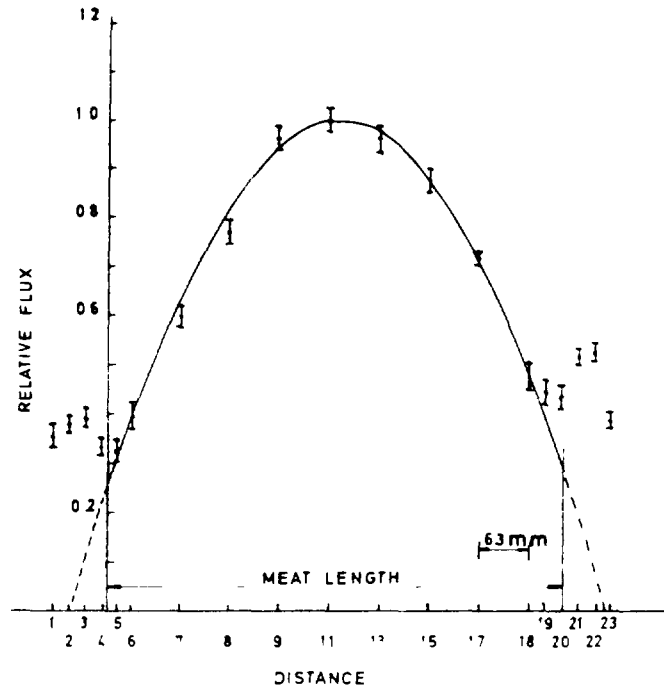


Fig. 5. Vertical Flux Distribution

## Excess Reactivity

The positive period technique was used to obtain the excess reactivity of the 20 MEU fuel element critical configuration. Measurements started together with criticality at some lower power level and with all control blades nearly at the same height. The excess reactivity of the A pair of blades were measured in six steps; however, for the B pair only three measurements steps were required. Thus, for the MEU critical configuration it was found an excess reactivity of  $0.63 \pm 0.26 \text{ \%}\Delta\kappa/\kappa$ .

## COMPARISON AND DISCUSSION

The critical state, for both HEU and MEU fuel, was achieved with 20 fuel elements. HEU critical core mass was 3300 g of U-235 and its excess reactivity was estimated approximately in  $0.77 \text{ \%}\Delta\kappa/\kappa$ ; nevertheless, MEU fueled core mass was 3663 g of U-235 and its excess reactivity was measured in  $0.63 \pm 0.26 \text{ \%}\Delta\kappa/\kappa$ .

During the critical experiment, carried out in October 1974, the reactor using HEU fuel was critical with the A control blades withdrawn up to 78.1%. Following the same loading scheme used in that critical experiment, the reactor, using MEU fuel, was now critical with the A control blades withdrawn up to 86%. In both cases the B control blades kept fully withdrawn.

The utilized calculation method allowed a good prediction of the excess reactivity for the 20 HEU fuel element critical configuration, being its value of  $0.79 \text{ \%}\Delta\kappa/\kappa$ . The experimental value for the same critical core was estimated to be  $0.77 \text{ \%}\Delta\kappa/\kappa$ . The experimental value of the excess reactivity for the 20 MEU fuel element critical core is  $0.63 \pm 0.26 \text{ \%}\Delta\kappa/\kappa$  and the calculated one is  $1.12 \text{ \%}\Delta\kappa/\kappa$ .

The experimental results demonstrated that the HEU critical configuration has a greater excess reactivity than the same critical configuration using MEU fuel, while the neutronic calculation predicts an opposite behaviour. The detailed comparison between the calculated reactivity values and those experimentally measured provides very valuable data for verification of research reactor analysis methods. As a result of the critical experiment, more detailed analysis are needed to validate the research reactor calculational modelling for the MEU cores.

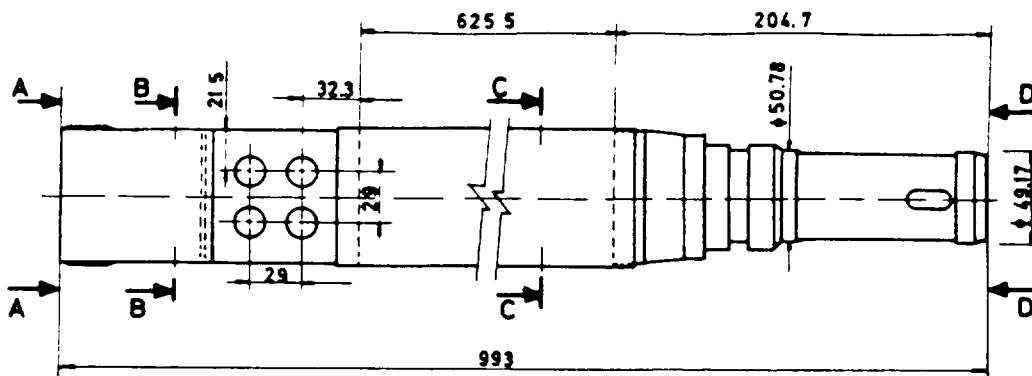
## REFERENCES

1. U. Schütt, et al ., "IAEA Technical Mission to Chile", Oct. 29 to Nov. 2, 1979.
2. J. Klein, O. Mutis, J. Medel, O. Villegas and J. Zambrano, "Neutronic and Thermal-Hydraulic Calculations for the Conversion of the 5 MW La Reina Reactor Using MEU Fuel", Proceedings of the International Meeting on Reduced Enrichment for Research and Test Reactors, 14 - 16 October 1985, Petten, The Netherlands, (1986), pp 397 - 407.
3. Guidebook on Research Reactor Core Conversion from the Use of Highly Enriched Uranium to the Use of Low Enriched Uranium Fuels, International Atomic Energy Agency, Report IAEA-TECDOC-233, (August 1980).

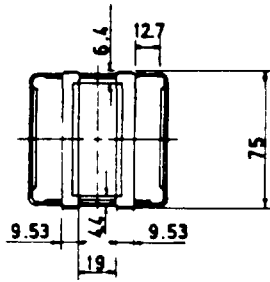
4. J.R. Askew, F.J. Fayers and P.B. Kemshell, "A General Description of the Lattice Code WIMS", Journal of the British Nuclear Energy Society, (October 1966).
5. M. Console, A. Danari and E. Salina, "EREBUS, A Multigroup Diffusion Depletion Program in Two Dimensions for the IBM-360," FN-E-38, (1967).
6. O. Mutis, "Cálculos Neutrónicos Estáticos para la Conversión del Reactor RECH-1 de Alto a Bajo Enriquecimiento en U-235", Nucleotécnica, 5, 9, (October 1985).
7. Medidas Efectuadas en las Configuraciones de 20 y 21 Elementos Combustibles. Informe N° 1, CEN La Reina, (November 1974).

Attachment 1

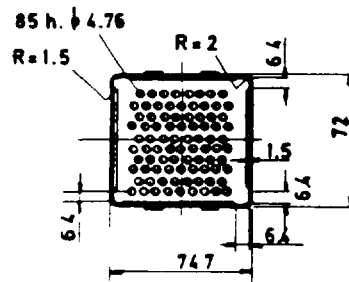
LA REINA FUEL ELEMENT



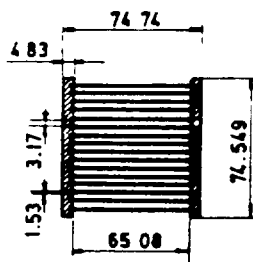
Section A-A



Section B-B



Section C-C



Section D-D

